DOCTOR OF PHILOSOPHY

An integrated meteorological / hydrological model for the Mawddach catchment, North Wales

Hall, Graham

Award date:
2008

Awarding institution:
Bangor University

Link to publication

An Integrated Meteorological /Hydrological Model for the Mawddach Catchment, North Wales

by

Graham Hall

Bachelor of Science, University of Wales, Aberystwyth
Master of Mathematics, The Open University

Volume 1

A thesis submitted for the degree of Doctor of Philosophy

Centre for Arid Zone Studies

School of the Environment and Natural Resources

Bangor University

April, 2008

Abstract

This project makes a study of meteorological and hydrological processes operating in the Mawddach river catchment of North Wales, with the objectives of recommending catchment management options to reduce the severity of flooding and to produce a design for a high resolution flood forecasting model for the catchment.

An array of rain gauges installed across the catchment has allowed the detailed mapping of rainfall distributions. Two patterns are identified, with axes of high rainfall running NW-SE and N-S respectively. Within these zones, the locations of rainfall maxima do not necessarily correspond with the highest altitude. The approach direction of weather systems and the funnelling of air flows along deep valleys appear to control rainfall distribution.

A series of flood events are examined, particularly the convective squall line storm of 3 July 2001 and the period of intense frontal rainfall of 3-4 February 2004. Modelling of rainfall is carried out using the MM5 meteorological model. It is found that frontal rainfall can be forecast to a high degree of accuracy. Convective thunderstorm events are less predictable, and different convective physics schemes within the MM5 package had differing degrees of success in forecasting the July 2001 Mawddach storm.

The catchment is an area of hard, low permeability Palaeozoic rocks. Thick deposits of glacial and periglacial materials are locally present, particularly in valleys. Experiments to monitor hillslope throughflow and runoff show that these superficial deposits play a crucial role in controlling the antecedent conditions necessary for saturation-excess flood events.

Deep blanket peat is found at a number of upland sites in the catchment. Watertable monitoring indicates that older peat has a low water storage capacity, with saturation possible within a few hours of heavy rainfall. Areas of young *Sphagnum* peat can act as regulating reservoirs for flood water, and should be conserved.

Field monitoring of river bed temperatures shows that resurgence of groundwater can occur in the deep river valleys of Coed y Brenin during storm events. However, resurgence occurs after the flood peak has passed and is not thought to influence the severity of flooding.

Flood scenarios for the town of Dolgellau are investigated, including the effects of continued gravel deposition in the River Wnion. Gravel supply should be controlled through planting of native broadleaf woodland on riverbanks of (peri)glacial materials. A flood reduction scheme is proposed, with establishment of wet woodland and creation of a flood interception basin in the lower Wnion valley.

Field monitoring of river and tidal flows at the head of the Mawddach estuary indicates no additive effect of river flood and tidal peaks. Flooding at the head of the estuary is generally caused by river flows. Further reclamation of salt marsh could worsen upstream flooding.

A new hillslope model has been written which allows for changing antecedent soil moisture conditions. The model generates a soil distribution based on the HOST (hydrology of soil types) scheme. A flood forecasting system is developed by combining the hillslope model with MM5 and existing river routing and floodplain modelling components. The system operates by a combination of parallel and distributed processing, to produce forecasts within an operationally useful timescale.

Contents

Acknowledgements

It would have been impossible to carry out this project without the help and support of many people, and in the course of the work I have made many friends – to all I offer my sincere gratitude.

I must first thank the Principal of Coleg Meirion-Dwyfor, Dolgellau, not only for allowing me to undertake the project whilst employed as a lecturer in the College but also for providing financial sponsorship. I am grateful to the staff of Coleg Meirion-Dwyfor for their interest and encouragement, and especially to Ieuan Edwards, Bryn Williams and Tony Rees for making the practical arrangements which allowed me to attend conferences and other activities related to the project. I gratefully acknowledge additional financial support from the Institute of Mathematics and its Applications.

I have been especially fortunate in receiving help with field data collection from excellent groups of students, for whom even the carrying of equipment to remote mountain locations in adverse weather conditions failed to dampen their enthusiasm: Jo Barton, Feysal Awissa, Jerome O'Connell and Simon Smith of the Bangor University MSc Water Resources course, and Osian Edwards, Richard Shaw, Sarah Johnson and Owain Williams of Coleg Meirion-Dwyfor.

Landowners within the Mawddach catchment have been generous in granting access to field locations and permission to install meteorological and hydrological monitoring equipment. I am especially indebted to: Aled Thomas of Forest Enterprise for allowing the use of sites in Coed y Brenin; Archie Jones, Alltlwyd, for access to Waen y Griafolen; and Chris Dixon, Tir Penrhos, for allowing the construction of a hillslope throughflow monitoring site.

I am grateful to the organisations who have made additional data available for the project: Environment Agency, Bangor, for providing hydrograph records for Tyddyn Gwladys and Dolgellau; Proudman Oceanographic Laboratory for Barmouth tidal data; CEH Wallingford for the digital elevation model for the catchment; and Maentwrog Hydroelectric Power Station for historical rainfall records and data for water flows in the Ardudwy leat system.

The project could not have been carried out without a range of computing applications. I owe a debt of gratitude to many software authors, some of whom I have had the pleasure of meeting but others who remain as legends, for their great technical skill and creativity. I would particularly thank the groups responsible for developing the software packages: MM5, GSTARS, MODFLOW, River2D, Mapmaker and SAGA GIS. The Portland Group were generous in allowing free use of the FORTRAN compiler.

I have been fortunate in receiving skilled technical support at various stages of the project, and gratefully acknowledge the important contributions of: Malcolm Murgatroyd, Dolgellau, for the construction of water depth monitoring equipment; Lea Anthony, Coleg Meirion-Dwyfor, for use of the College computer network; and Ade Fewings, Bangor University, for use of the Altix minicomputer.

Professor Tony Jones and Dr Tom Rippeth examined an earlier version of the thesis and made valuable suggestions for its improvement. May I extend my thanks for carrying out this task so constructively.

I have left until last to mention the two people who have made the greatest contributions to the project: my research supervisor Roger Cratchley, and my wife Margaret:

It has been the greatest of pleasure working with Roger, a scientist with extensive interests, knowledge and practical experience spanning the range of environmental sciences. I thank him for his abiding friendship and wise counsel.

Margaret has been a resolute partner in the project, willingly allowing fieldwork to take the place of more normal family activities. She has on many occasions waded in streams, dug holes and recorded data, as well as providing transport and food for the fieldwork team. Many of the photographs included in this work are hers.

Figure i. Mawddach-Wnion catchment location map

Publications related to the project:

Hall G. and Cratchley R., 2005. Modelling frontal and convective rainfall distributions over North Wales. Proceedings of the 2005 WRF/MM5 User's Workshop, National Centre for Atmospheric Research, Boulder, Colorado.

Hall G. and Cratchley R., 2005. The role of forestry in flood management in a Welsh upland catchment. Proceedings of the 45th Congress of the European Regional Science Association, Amsterdam.

Hall G. and Cratchley R., 2006. Sediment erosion, transport and sedimentation during the July 2001 Mawddach extreme flood event. In: Sediment Dynamics and the Hydromorphology of Fluvial Systems. IAHS publication 306.

Hall G. and Cratchley R., 2006. Coupling of MODFLOW with the MM5 mesoscale meteorological model for real-time input of high resolution rainfall events in a mountainous area. In: Managing Groundwater Systems. International Groundwater Modelling Center, Colorado.

Hall G. and Cratchley R., 2006. A hydrological study of Waen y Griafolen blanket bog, North Wales. Proc. International Conf. on Hydro-ecology. Carlsbad, Czech Republic.

Hall G. and Cratchley R., 2006. Hydrological Modelling Of Flood Events Around The Mawddach Estuary, North Wales. Proc. 2nd International Conf. on Estuaries and Coasts, Guangzhou, China.

Hall G. and Cratchley R., 2007. Mechanisms of flooding in the Mawddach catchment. In: Hydrology and Management of Water Resources in Celtic Countries. IAHS publication 310 (in press)

Hall G., Cratchley R. and Johnson S., 2006. The use of SAGA-GIS in an integrated meteorological/hydrological model for the Mawddach river catchment, North Wales. Gottinger Geographische Abhandlungen, 115.

Hall G., Cratchley R. and Johnson S., 2006. Integrated meteorological/hydrological modelling of the Mawddach river catchment, North Wales. Proc. British Applied Mathematics Colloquium, Keele.

List of figures

Figure **Page**

List of tables

Table **Page**

1. Introduction

1.1 Objectives of the study

The Mawddach river system drains a region of upland and mountains in the south of the Snowdonia National Park within the county of Gwynedd in Wales. The overall catchment can be divided into:

- the Mawddach sub-catchment upstream of the tidal limit, with an area of approximately 160 km^2,
- the Wnion sub-catchment upstream of the tidal limit, with an area of approximately 120 km^2,
- the sub-catchment of the tidal estuary, with an area of approximately 120 km^2.

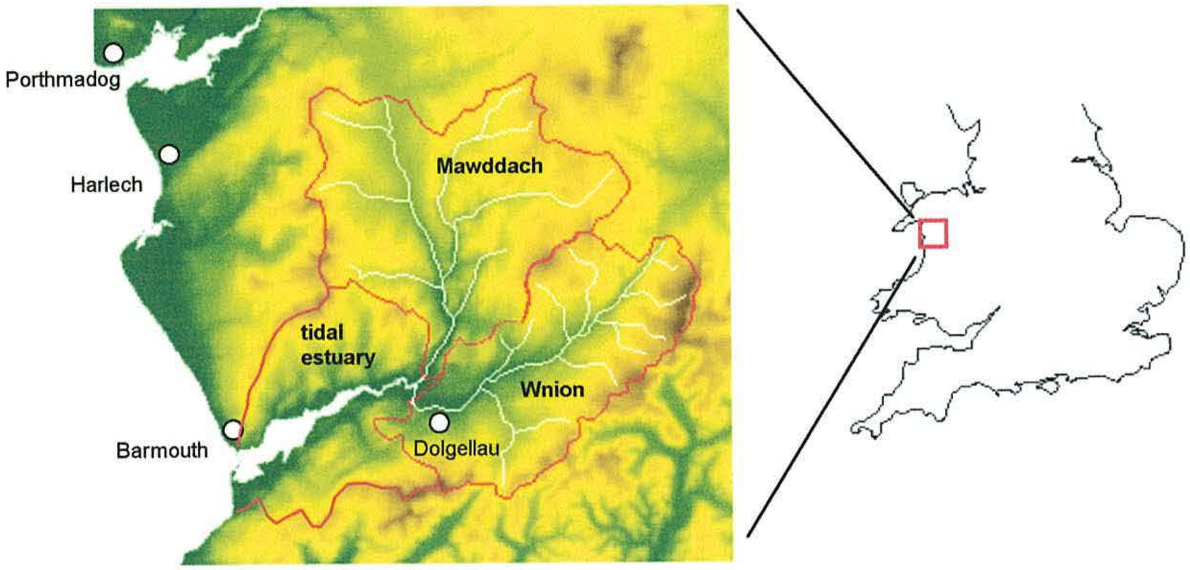

Figure 1.1 Location of the Mawddach catchment

Flooding, particularly around the town of Dolgellau, has been a problem throughout historical times (Barton, 2002). This research project has the following objectives:

- develop a realistic hydrological computer model for the Mawddach catchment based on a multi-disciplinary approach which embraces both climatic/hydrological and the various catchment characteristics,
- develop a methodology for an improved early warning system for flood prediction within the Mawddach catchment,
- identify environmental options for reduction of flood severity through land use management.

Current practice in flood forecasting

The approaches taken by the Environment Agency in flood forecasting are summarised by Moore et al. (2004).

Rainfall is determined from an array of raingauges, which around the Mawddach catchment have a spacing of approximately 10km. Alternatively, rainfall is estimated from interpretation of rainfall radar images. Computer systems are currently being developed for combining raingauge and rainfall radar data to produce improved rainfall maps during storm events. The objective of all of these approaches is to produce a catchment average rainfall value for input to a flood forecasting model.

Different hillslope-runoff and river routing models are employed to predict the effects of the observed rainfall on future river levels downstream in the catchment. Model parameters are calibrated using recorded river flows under known rainfall conditions, so that the predictive power of the model progressively improves through training. Flood warnings are issued when predictions of river depth at key locations will exceed threshold values.

The river flow forecasting period may be extended by making predictions of future rainfall over the catchment, rather than using only current observations. The movement direction and speed of the weather system is estimated, then this vector is applied to the current rainfall distribution in order to predict the location and intensity of rainfall during subsequent time intervals.

Development of an enhanced Mawddach flood forecasting system

Whilst the Environment Agency approach is a practical engineering solution for providing short term flood warnings, the system has limitations:

- Rainfall patterns over a mountainous catchment such as the Mawddach may not be adequately represented by either a widely spaced raingauge array or by low resolution rainfall radar. Localised variations in rainfall may have significant effects on hillslope runoff and river flows within particular valleys of the catchment, with consequent effects on downstream flooding.

- Weather systems may evolve rapidly during storm events, so simple spatial translation of the current rainfall pattern may not adequately predict rainfall patterns for subsequent time intervals.
- Output is restricted to the prediction of river depths at critical sites for flooding. It may be desirable to also predict the lateral extent of the floodplain to be inundated, so that more accurate warnings can be given to local residents, farmers and the emergency services.
- The approach taken in modelling only the outflow hydrographs of catchments using empirically determined model parameters gives little insight into the hydrological processes actually operating within the catchment. This limits the modelling to current experience, and gives little opportunity to predict the effects of future changes which might affect the catchment – for example: climate change, differing landuse or modifications to river channels.
- Some processes are missing from the hydrological model which may affect the location and extent of flooding in the Mawddach catchment, for example: groundwater flows, the interaction between rivers and tidal waters around the head of the estuary, and the movement of sediment in response to flood events.

This research project will investigate alternative approaches to the modelling of floods in the Mawddach catchment which could provide a longer warning period, combined with a more accurate estimation of the extent and severity of flooding. At each stage, process models will be used so that the effects of current and future catchment management practices on flooding can be evaluated.

A series of modelling components will be investigated individually, then combined into an integrated system for flood prediction (fig.1.2). An objective is to identify the key processes which are critical to flood forecasting. Equally important is the identification of processes which have only a negligible modifying effect on flooding and can safely be omitted from the final model.

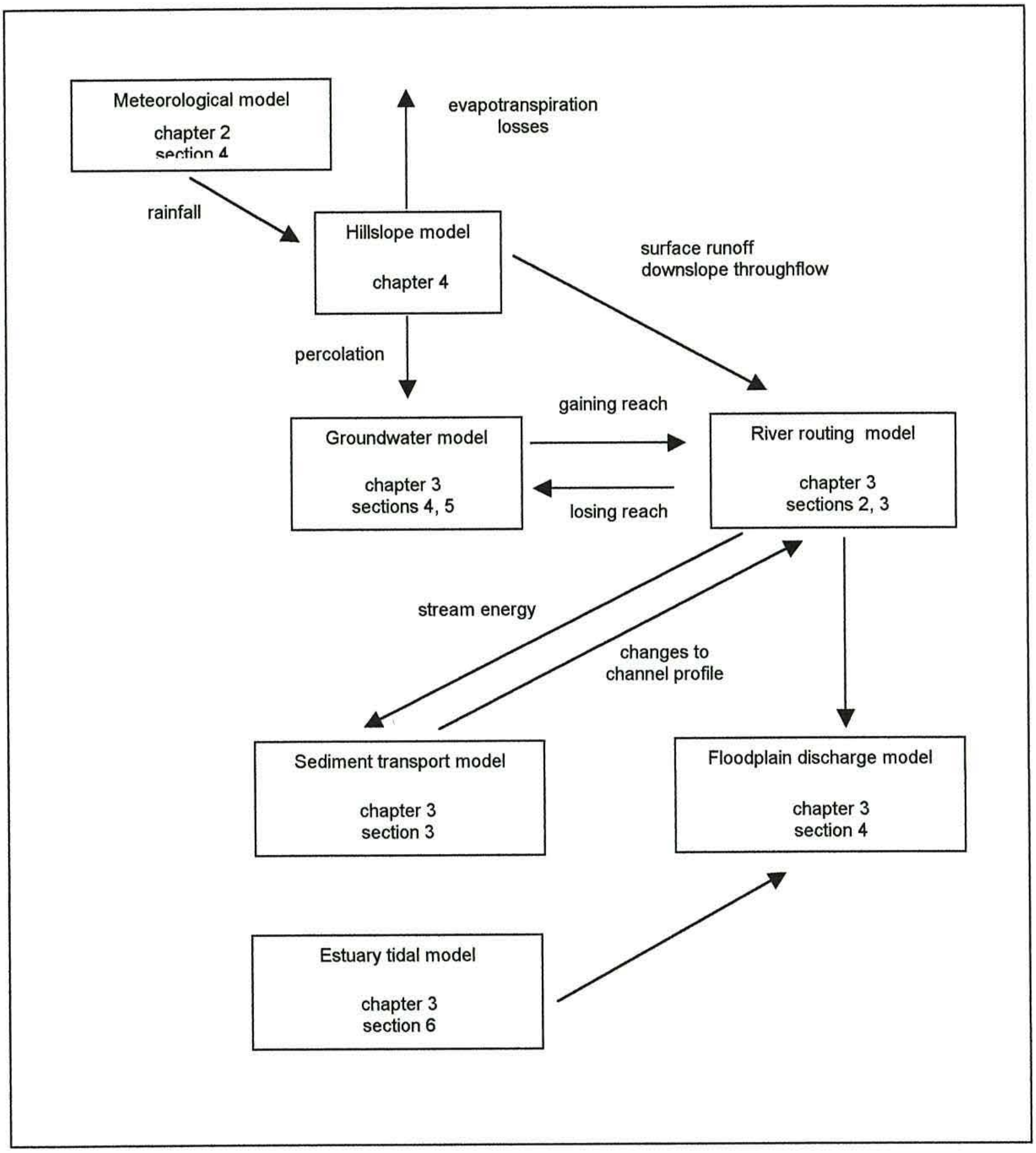

Figure 1.2: Proposed modelling components for the integrated Mawddach flood prediction system

Meteorlogical modelling is addressed first in ***Chapter 2***, followed by hydrological modelling in ***Chapter 3***. Central to the operation of the integrated system is a new hillslope runoff model which will be developed during the project – this is described and evaluated in ***Chapter 4***.

Synopsis of chapters

Flooding in the Mawddach and Wnion catchments examines historical and present day flooding, and discusses possible effects of climate change for the region.

Section 1.2 The Study Area outlines this background against which hydrological models are developed during the project. The Mawddach catchment is an upland area of diverse geology, landforms, soils and natural vegetation. Present and previous human activity within the catchment includes: agriculture, forestry, mining, and the construction of reservoirs for water supply and hydroelectric power. To some extent, all these factors influence hydrological response.

Chapter 2 Meteorology

Section 2.1 Meteorological principles outlines aspects of meteorology relevant to rainfall production over the North Wales area. Theories of midlatitude cyclone development are discussed, and the orographic effects of the mountains considered. The mechanisms of convective rainfall production are examined for thunder storms and extended squall lines.

Section 2.2 Rainfall in the Mawddach catchment reports the results of rainfall monitoring in and around the Mawddach catchment by an array of raingauges. Analyses of storms show that rainfall patterns may vary widely between events, and between adjacent valleys during the same event, depending on the approach directions of weather systems.

Section 2.3 Meteorological modelling examines the fluid dynamics approach taken in modelling the physical processes taking place at different levels of the atmosphere.

Section 2.4 The MM5 modelling system discusses underlying assumptions and mathematical formulation of the high resolution rainfall model for the Mawddach catchment. Storm events are modelled and predicted rainfall distributions are evaluated against field data. A neural network is examined as a method for improving initial rainfall forecasts. Atmospheric processes appearing during the MM5 simulations are compared to theoretical mechanisms for frontal and convective storm events.

Chapter 3 Catchment Hydrology

Section 3.1 Hydrological modelling systems discusses a conceptual model for catchment hydrological processes, and considers different approaches to modelling these processes by computer.

Section 3.2 Hillslope hydrology outlines the collection of field data for use in the calibration and evaluation of the models. The HEC-1 hillslope model is assessed for its suitability within an integrated meteorological/ hydrological model for the Mawddach.

Section 3.3 Sediment movement examines sediment processes within the river system. The valleys of the Mawddach locally have extensive infilling by poorly consolidated glacial and periglacial material. This sediment is easily eroded from riverbanks during storm events. Large volumes of sand and gravel are carried downstream, and may be redeposited within the river system or discharged into the tidal estuary.

Modelling using GSTARS software has been carried out to estimate the volumes of sediment redistributed during particular flood events. Sediment accumulation in the lower reaches of the river system and around the head of the estuary will affect river base levels, with consequences for the extent of future flooding in the area of Dolgellau.

Section 3.4 River and floodplain processes examines the flow of water once it has entered the river system. The Mawddach and its tributaries are dominantly gravel streams with steep gradients, locally flowing over bare rock or forming waterfalls. Modelling of river routing should be able to handle both subcritical and supercritical water flows.

Floodplain inundation can occur at various locations, notably the lower Wnion valley around the town of Dolgellau. Modelling is carried out to assess the likely extent of floodplain inundation in response to different catchment management strategies.

A feature of the middle courses of the Mawddach system is the alignment of river channels along major fracture zones in the bedrock. Fieldwork provides evidence of river–groundwater interaction, with water loss from river channels during dry periods and resurgence during flood events. Groundwater modelling assesses the extent of this interaction.

Section 3.5 Peat blanket bogs examines the hydrological characteristics of upland peat bogs around the headwaters of the Mawddach river system. A detailed case study has been carried out at Waen y Griafolen, a blanket bog forming the source of the Mawddach itself. Field monitoring of water table levels within the peat, geophysical and auger surveys provide parameters for a MODFLOW groundwater model. River outflows from the peat basin are assessed in relation to possible vegetation changes within the blanket bog.

Section 3.6 The Mawddach estuary considers flood processes around the head of the Mawddach estuary. Salt marsh, reed beds, water meadows and wet woodland areas are naturally flooded at certain tides, and can provide transient storage for flood water. Areas of flood land have been progressively reclaimed for agriculture by the construction of sea walls. An assessment is made of the impact of land reclamation on current and future flooding.

Chapter 4 Integrated catchment modelling

Section 4.1 Integrated meteorological-hydrological models examines the approaches taken by flood modelling systems which obtain rainfall data from meteorological modelling systems. The design is presented for a new hillslope model for use in the Mawddach catchment. This model forms an interface between the MM5 meteorological model, river routing and groundwater components.

The hillslope model is based around the computation of soil hydraulic conductivity in response to varying soil saturation, using the van Genuchten equation.

Section 4.2 The Mawddach hillslope model discusses the modular design of the hillslope program and the algorithms for water flow simulation. Kirkby wetness index, geological and land use data are used in computing soil distribution on a 50m grid, to provide hydrological parameters for hillslope infiltration, throughflow and runoff. The stages are outlined for running a model, monitoring hillslope waterflows and obtaining output hydrographs.

Section 4.3 Validation of the hillslope model presents the results of runs of the model for sub-catchments at Hermon, Pared yr Ychain and Waen y Griafolen. The physical realism of the hillslope model and the accuracy of the output generated are assessed against field data collected during storm events in the sub-catchments.

Section 4.4 Results of runs of the integrated model. The elements for an integrated meteorological/hydrological model of the Mawddach catchment which are now in place, and are brought together to create a flood forecasting system. Runs of the model have been carried out for the convective flood event of 3 July 2001 and the frontal storms of 3-4 February 2004 as a means of evaluating the system. The operation of the model in real-time forecasting mode is tested.

Chapter 5 Discussion

Section 5.1 Meteorology examines the field data collected for regional rainfall patterns and microclimate effects within the Mawddach catchment. Different approaches for rainfall forecasting are considered. There is a discussion of the future development of meteorological modelling with the introduction of the WRF modelling system.

Section 5.2 Hydrology assesses the work carried out in the Mawddach catchment to quantify the processes of hillslope runoff, river routing and floodplain overbank discharge, groundwater movement, river sediment deposition and estuary tidal flows. Sources of errors in field data collection are identified. An assessment is made of the software packages used in simulating hydrological processes during the project.

Section 5.3 Catchment modelling evaluates the integrated meteorological / hydrological system developed for flood forecasting in the Mawddach catchment.

Chapter 6 Conclusions and Recommendations

The main findings of the project are summarised. A proposal is made to reduce sediment accumulation in the lower reaches of the Wnion and Mawddach. A scheme is presented for the extension of flood plain forestry as a means of flood reduction. Conservation measures are recommended for blanket bog, salt marsh and estuary wet woodland ecosystems.

The integrated meteorological/hydrological modelling system is advocated for use as an early warning system for flooding on the Mawddach.

Flooding in the Mawddach and Wnion catchments

The Romans settled in the Mawddach region, constructing a large fort at Tomen-y-Mur near Trawsfynydd (Ellis, 1928). From Tomen-y-Mur, a road ran southwards in a straight line down the Ganllwyd valley, but before reaching Llanelltyd it turned abruptly to the east through Llanfachreth and Bont Newydd before returning to its southerly course. This diversion suggests that the Wnion valley near Dolgellau was marshy and liable to heavy frequent flooding during that period.

From the late sixteenth to the early nineteenth century, Dolgellau developed as a prosperous town based on the manufacture of woollen textiles, with abundant water power for textile mills provided by the River Aran (Rhydderch, 1976) . A 19th century illustration (fig.1.3) shows the growth of the town onto the Wnion floodplain.

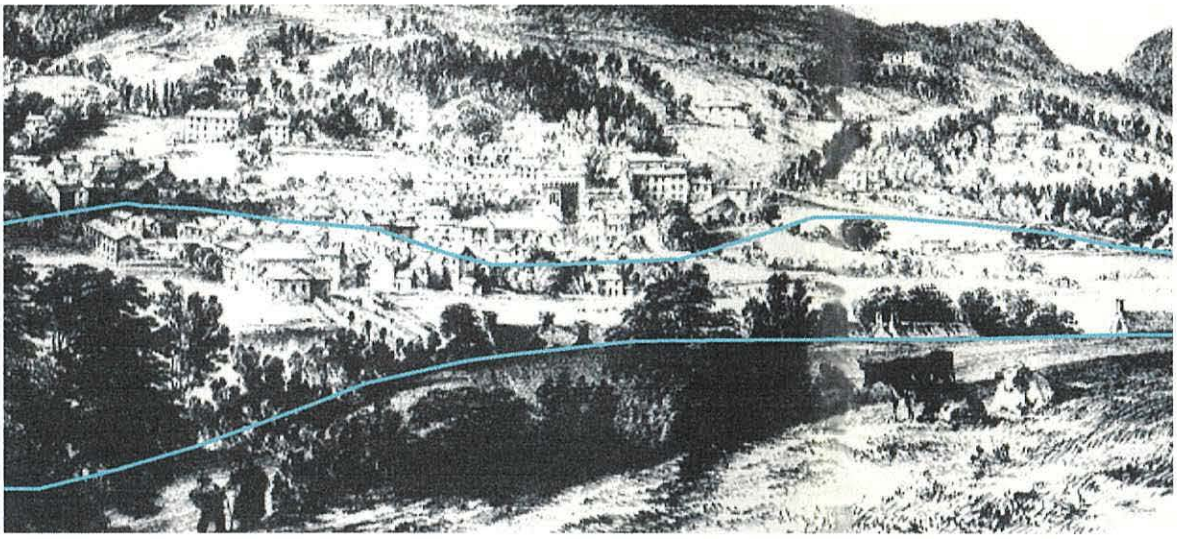

Figure 1.3: Dolgellau in the mid 1800's. The Wnion floodplain is outlined in blue. (based on an illustration from Rhydderch, 1976)

The Great Western Railway opened a line from Bala to Dolgellau in 1868, with the Cambrian Railway continuing the link from Dolgellau to Barmouth in 1869. From its inception, the railway route along the Wnion valley and the Mawddach estuary was susceptible to river and tidal flooding. A report for the Rail Safety and Standards Board (JBA Consulting, 2004) on the Impact of Scour and Flood Risk on Railway Structures cites a bridge failure on the Afon Wnion, Dolgellau, in July 1880. The Priority Rating assigned to this incident is High, based on the seriousness of damage and the frequency of flood events of similar magnitude. The exact location of the bridge is not stated, but is likely to be the structure near the tidal limit of the Wnion, west of the town, shown in fig.1.4 during flood conditions.

Figure 1.4: Disused railway bridge at the tidal limit of the River Wnion, Dolgellau. This is likely to be the site of the 1880 bridge failure.

Archive photographs illustrate a number of flood events affecting the town of Dolgellau during the 20th century. Particularly serious was the storm of September 19, 1922 when shops were flooded and extensive damage occurred to Bont Fawr, the main road bridge over the River Wnion (figs 1.5, 1.6).

Figure 1.5: Flooding in Bridge Street, Dolgellau, September 19, 1922
(photo: Richard Morgan collection)

Figure 1.6: Damage to Bont Fawr, Dolgellau, September 19, 1922.
(photo: Richard Morgan collection)

Figure 1.7: Dolgellau flood of December 12, 1964
(photo: Gwynedd County Council Archives Service)

Another serious flood (fig.1.7) on December 12, 1964 prompted the Town Council to order the construction of a one-mile flood defence wall along the River Wnion (fig.1.8). This wall has protected the town well from subsequent floods, but has come close to overtopping in recent years.

Figure 1.8: Flood defence wall alongside Bont Fawr.
Flood event of 4 February 2004.

The head of the Mawddach estuary is reached a short distance downstream from Dolgellau. Reclamation of farmland has been carried out by the construction of earth embankments around some areas of former reed beds and salt marsh, and the excavation of drainage ditches (fig.1.9).

Figure 1.9: Land reclamation at the head of the Mawddach estuary. Earth embankments are marked in red, and drainage ditches in blue.

The enclosed fields may be susceptible to both river and tidal flooding. A graphic account is provided by a Snowdonia National Park information panel alongside the estuary at Penmaenpool:

> "The fields you can see looking across towards the estuary were covered by the tide until the middle of the 19th century. Farmers transformed the land from saltings into pasture by building a wall and carrying soil onto the land by horse and cart. The wall was breached by a very high tide in 1927, carrying a farmer and his cattle into the woods above the road. The fields were not reclaimed until 1978, when the tidal defence wall was rebuilt."

The railway running along the southern shore of the estuary was regularly affected by tidal flooding, with the undermining of engineering structures occurring relatively frequently. Incidents at Arthog station (fig.1.10) are reported by Hambley, Bodlander and Southern (1991):

> "Arthog station consisted of a wooden platform and building... Severe flooding in 1927 washed away an iron bridge adjacent to the station. Its replacement withstood a similar flood in 1938 during which the stationmaster Mr W.T.Edwards clung to the ground frame levers for several hours as flood waters swirled around him. He was later able to climb onto the roof of a hut before finally being rescued by boat."

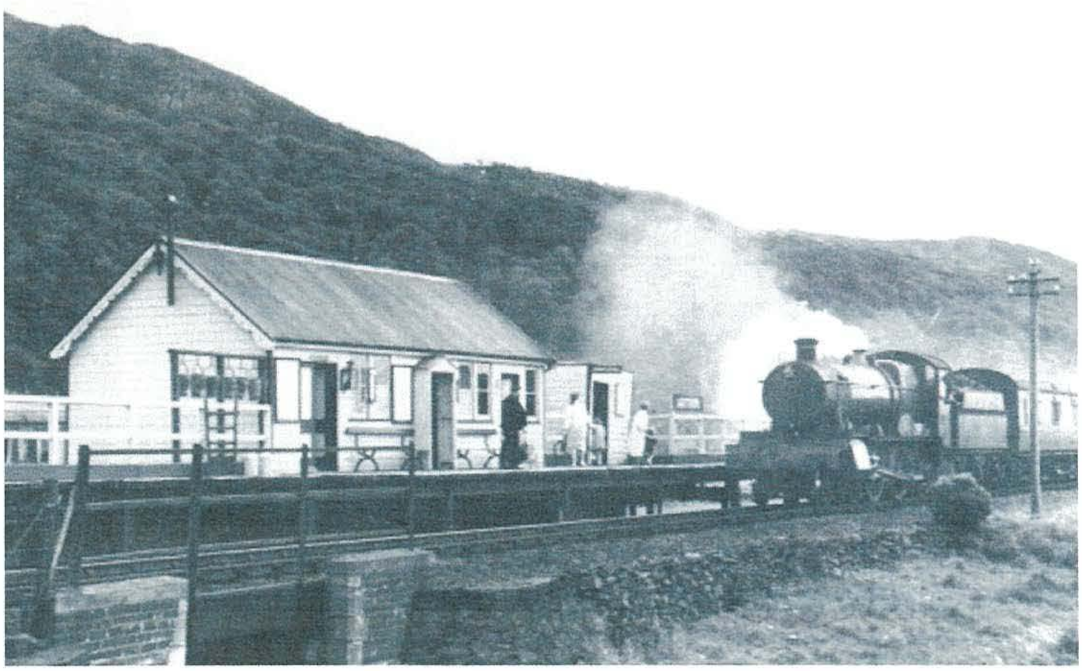

Figure 1.10: The former railway station at Arthog
(photo: Hambley, Bodlander and Southern , 1991)

The upper reaches of the Mawddach and Wnion river systems drain mountains and moorland, often in areas of impermeable rock. These streams are susceptible to a flash flood regime, with river levels rising rapidly after the onset of storm rainfall (fig.1.11).

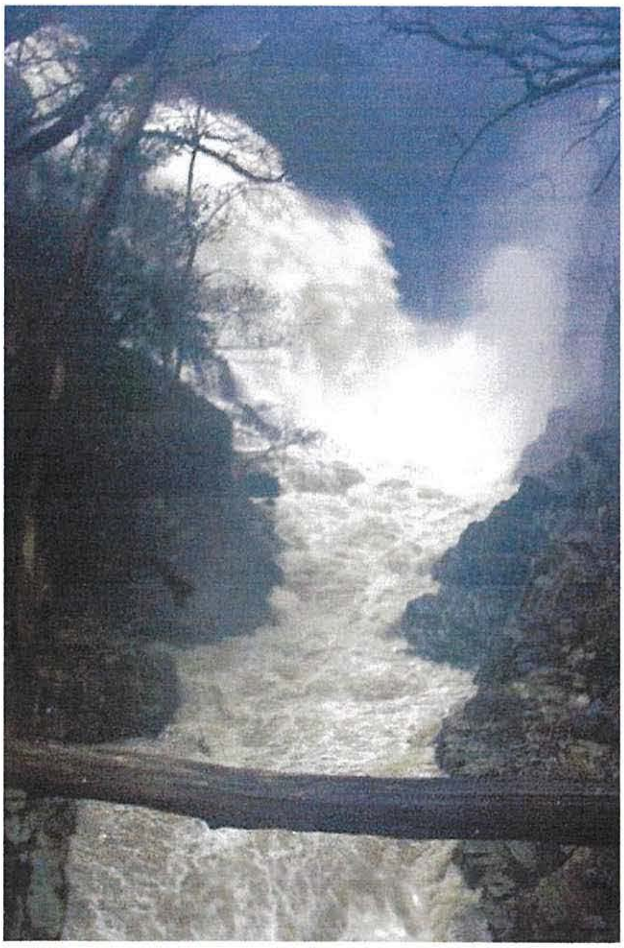

Figure 1.11:
Illustration of variations in discharge on the River Gain at Pistyll Cain.
Above: typical condition after a dry summer month.
Left: river in spate during the February 2004 flood.

The most serious flood event recorded for the upper Mawddach occurred on July 3, 2001. Up to 120mm of rain fell during a three hour period from convectional thunderstorms along a squall line (Mason, 2002). This event caused damage to buildings, washed away bridges and roads, and disrupted communications and farming activities over a wide area between Trawsfynydd, Dolgellau and Llanuwchllyn. The extent of surface runoff is shown in figs 1.12 and 1.13.

Figure 1.12: Infiltration-excess overland flow occurring during the July 2001 flood event, Cwm Prysor. The storm occurred after a hot summer's day, with extremely high intensity rainfall falling on dry ground.
photo: Robert Chilton

Figure 1.13: Flood water which disrupted traffic on the Bala to Trawsfynydd road, Cwm Prysor. July 2001 flood.
photo:
Robert Chilton

Figure 1.14: Bridge destroyed on the River Gain

Figure 1.15: Bridge damage at Abergeirw

Figure 1.16: Forestry road undermined, Coed y Brenin
photo: Robert Chilton

Figure 1.17: Bank erosion endangering buildings, Ferndale
photo: Robert Chilton

Examples of damage to infrastructure during the July 2001 flood are shown in figs 1.14 to 1.17. A total of 27 bridges were recorded by Gwynedd County Council as being damaged during the flood event, some of which were washed away completely or beyond repair.

To summarise current flood risks for the Mawddach catchment:

- Flooding can endanger livestock on farmland adjacent to rivers or the estuary.
- Flooding can lead to the undermining of roads and destruction of bridges, with potential danger to life.
- Flooding can cause damage to properties, either through direct flooding or by the undermining of foundations by river bank erosion.

Improved advance warning of flooding could allow preparations to be made by farmers, the highway authority and property owners to minimise danger and loss. Advance warnings must, however, be reliable. False alarms may lead to warnings being ignored in a real emergency. The design of an improved and reliable flood warning model for the Mawddach catchment is the first objective of this research.

Within the Mawddach catchment, flooding has occurred throughout historical times with a number of very severe events occurring during the past 100 years. A consensus of scientific opinion suggests that climate change is occurring along the Atlantic margins of western Europe, and is likely to continue in coming decades. Studies carried out for the areas of Wales (Jones et al., 2007) and Norway (Skaugen et al., 2003) both draw similar conclusions:

- a seasonal shift in rainfall patterns is occurring, with drier summers and wetter winters,
- there is no large change in total annual rainfall, but more extreme storm events are occurring due to higher available energy in the atmospheric circulatory system.
- within the overall weather patterns, large variations occur in mountainous areas due to local microclimate effects.

Figure 1.18 (right): Annual rainfall totals (mm), Trawsfynydd

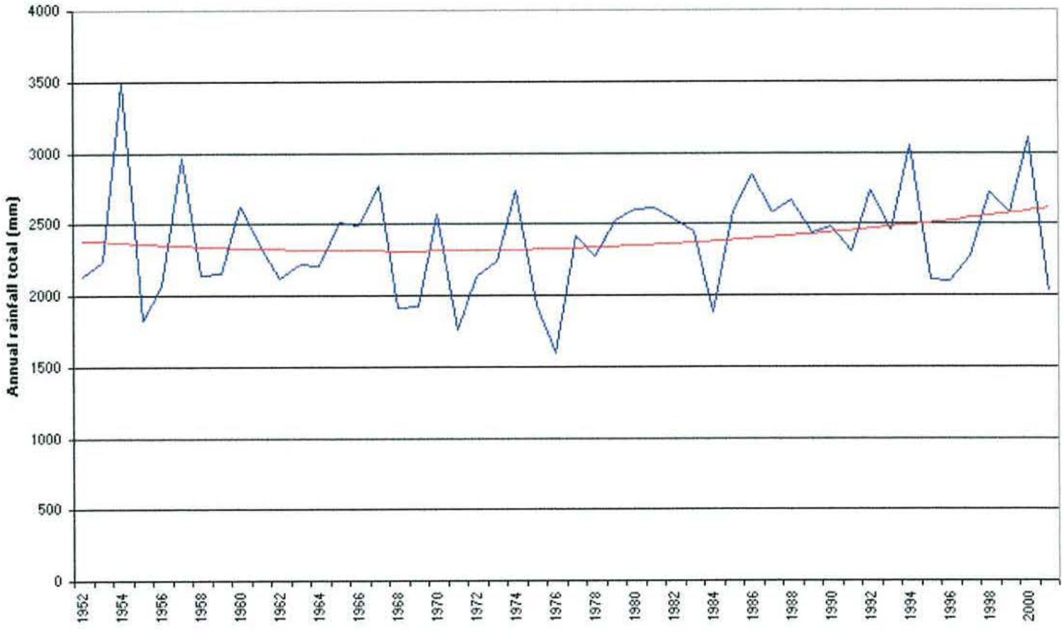

Figure 1.19 (below): Monthly rainfall totals (mm), Trawsfynydd

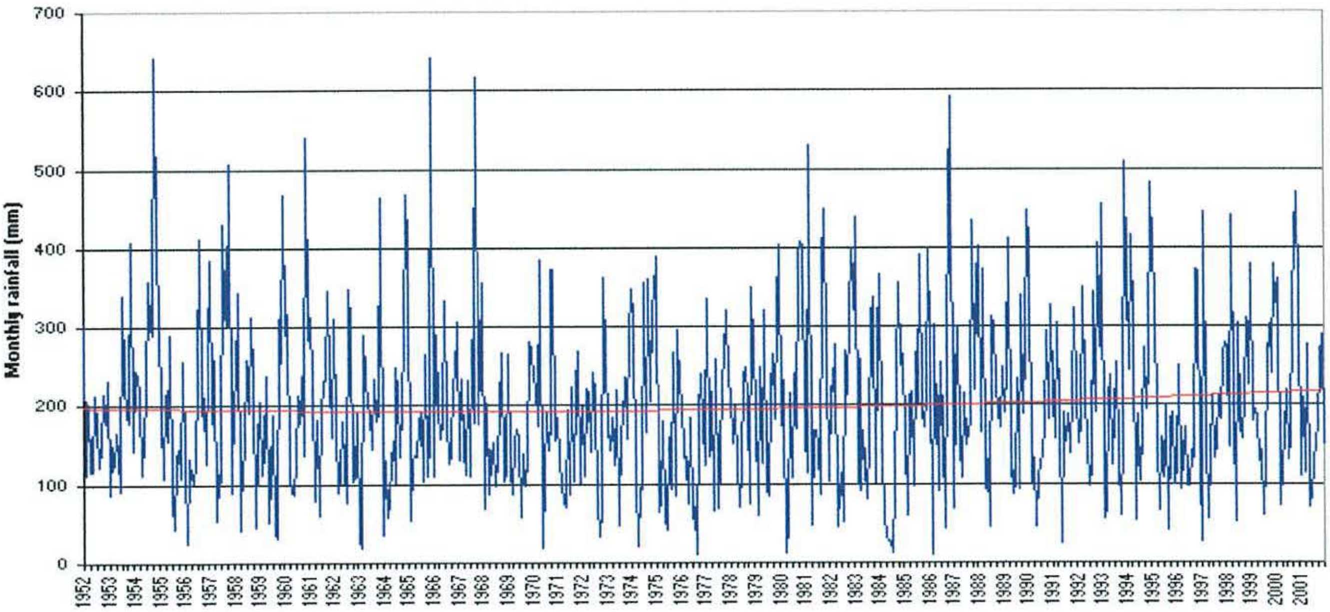

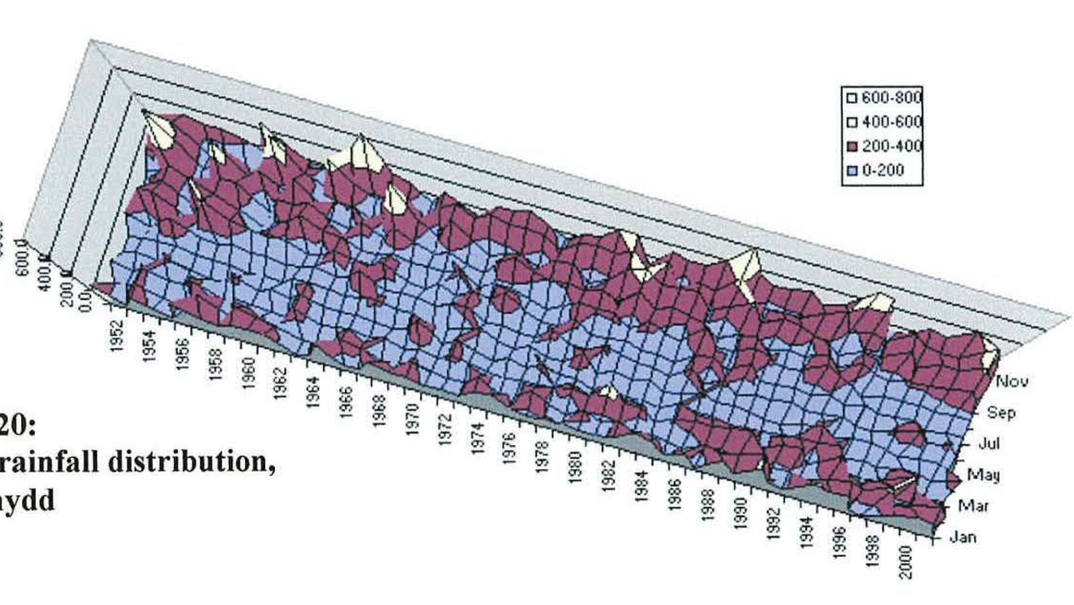

Figure 1.20: Monthly rainfall distribution, Trawsfynydd

A complicating factor is the influence of the North Atlantic Oscillation and the El Niño Southern Oscillation (Daultrey, 1996). Under certain circumstances these global circulatory effects can produce winters with particularly high precipitation in western Britain.

Rainfall data for the period 1952-2001 collected at Graig Ddu Ganol, near Trawsfynydd in the Mawddach catchment, are consistent with these conclusions

- Fig.1.18 shows considerable variation in total annual rainfall, with an upwards trend noticeable since the early 1970's.
- Fig.1.19 shows similar large variations in total monthly rainfall, with the most extreme wet months occurring in the 1950's and 1960's. However, an upwards trend in mean monthly rainfall is again observed since the early 1970's.
- Fig.1.20 suggests that a seasonal shift in rainfall pattern is occurring. Wet periods with monthly rainfall > 200mm in the 1950's typically occurred from July to January, whereas the annual wet period in the late 1990's was typically from September to March – a forwards progression of two months.

These lines of evidence suggest that the flood risk within the Mawddach catchment is likely to remain at its current high level for the present century and may increase further. Possible increases in river flows in response to global warming are addressed by Arnell (2003). Attention to long term environmental management of the catchment to minimise risk of flood generation is therefore justified. This aspect forms the second objective of the research. Two particular issues of interest locally are:

- the effects of river gravel deposition on flood risk
- the effects of forestry in controlling flood discharge.

Concern has been raised in Dolgellau at the accumulation of river gravel in the vicinity of Bont Fawr (figs 1.21-1.23). Fears have been expressed that sediment may constrict river flow through the bridge arches, leading to overtopping of the flood defence wall. Responsibility for maintaining a clear river channel lies with the Environment Agency (Environment Agency Wales, 1999) who regularly remove large quantities of gravel from the area around the bridge, but reaccumulation may occur as the result of a single flood event.

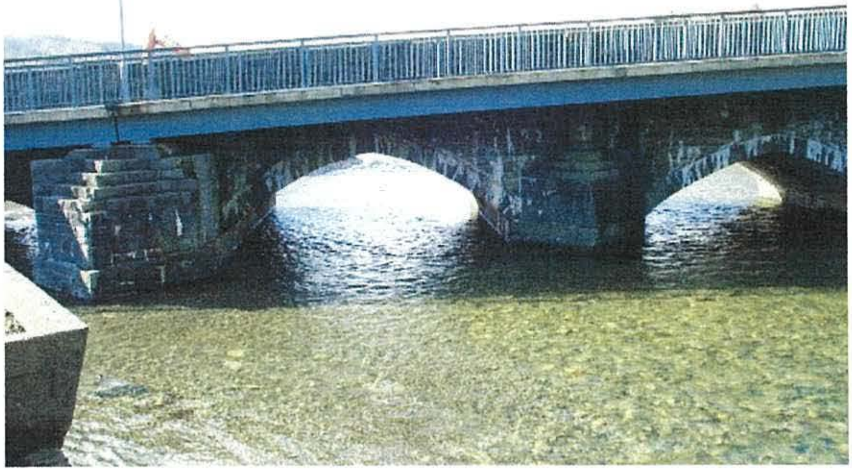

Figure 1.21: Bont Fawr, Dolgellau, after gravel clearance.

Figure 1.22: Bont Fawr, Dolgellau, showing gravel reaccumulation.

Figure 1.23: Work in progress to clear gravel from the Bont Fawr area.

Woodlands form an important component of the natural vegetation of the Mawddach catchment. Riparian broadleaf woodlands survive along many of the river courses (fig.1.24) , and wet woodland is characteristic of floodplain areas around the head of the estuary (fig.1.25). Natural woodland has been greatly augmented by the extensive forestry plantations of Coed y Brenin and the Wnion valley around Rhydymain.

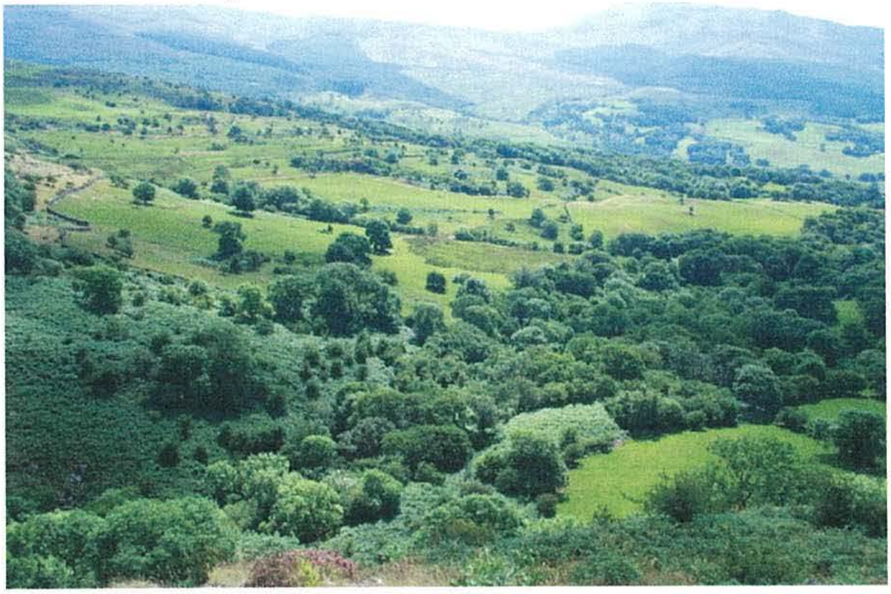

Figure 1.24: Natural riparian woodland alongside the Afon Eiddon, a tributary of the Wnion.

Figure 1.25: Wet woodland alongside the River Wnion at the head of the estuary. Photographed during the February 2004 flood event.

In recent years, interest has increased in the use of flood plain forestry as a means of flood control as an alternative to hard engineering structures (Thomas and Nisbet, 2004). This application of forestry will be examined during the modelling project.

Hypotheses

Preliminary investigation of the Mawddach catchment has revealed considerable complexity in the hydrological processes that are operating. These processes need to be considered whilst developing the conceptual model on which computer applications will be based:

- Wide variations in rainfall seem to occur across the catchment during individual storm events. These variations may not be entirely related to altitude.
- A number of river sections are aligned along major geological faults, and it is suspected that surface water - ground water interactions may occur through the fracture zones.
- Considerable thicknesses of glacial and periglacial materials infill river valleys. These materials vary greatly in hydrological properties, from low permeability clays to freely draining scree, and may have a controlling influence on infiltration and runoff during storm events.
- The headwaters of several major tributaries originate in extensive peat blanket bogs. The water storage properties of these peat deposits may have an influence on storm river discharges.
- Forestry management practices can affect hillslope runoff, and need to be considered in developing a model.
- Tidal and river interactions at the head of the estuary during flood events may influence the extent of flooding. This effect should be analysed.
- Some water is diverted out of the Mawddach catchment by a canal system to augment the water supply to the Maentwrog hydroelectric power station. The extent of this flow should be considered in the development of a water budget for the catchment.

1.2 The study area

Geology

Many of the features of the geology of North Wales can be related to a model of an ocean expansion - contraction cycle, including the patterns of sedimentation, igneous activity and tectonic events (Anderton et al., 1979).

In late Precambrian times, a change in the pattern of mantle convection led to the fracturing and separation of the North American - European continent to form an ocean basin. The line of separation of continental crust lies roughly from the Scottish border to Northern Ireland (fig.1.26). As the ocean began to open, tension in the diverging continental plates led to a series of NE-SW faults developing parallel to the continental margins. Vertical movements took place, with a block of crust sinking between the Aber-Dinlle and Church Stretton fault zones to form the Welsh Basin. Adjacent blocks were elevated as the Irish Sea landmass to the NW and the Midland platform to the SE. These fault blocks remained at or above sea level until Silurian times and are of major significance to the geology of North Wales.

The Cambrian in Wales was a period of quiet sedimentation. Sands, grits and muds were layed down in the fault bounded marine trough. Much of the coarse sediment of the Cambrian succession was provided by erosion of these bordering landmasses.

By Ordovician times the ocean basin had began to contract, with oceanic crust descending beneath Wales along a subduction zone. An important consequence of subduction was the initiation of volcanic activity from the Lake District in the north, through Snowdonia, to Pembrokeshire in the south.

Towards the end of the Ordovician period, volcanicity died out in North Wales, but normal marine sedimentation continued in the Welsh Basin until closure of the ocean was completed in the last parts of the Silurian period and the early Devonian. At this time, major compression, folding and faulting occured as the continental masses finally converged.

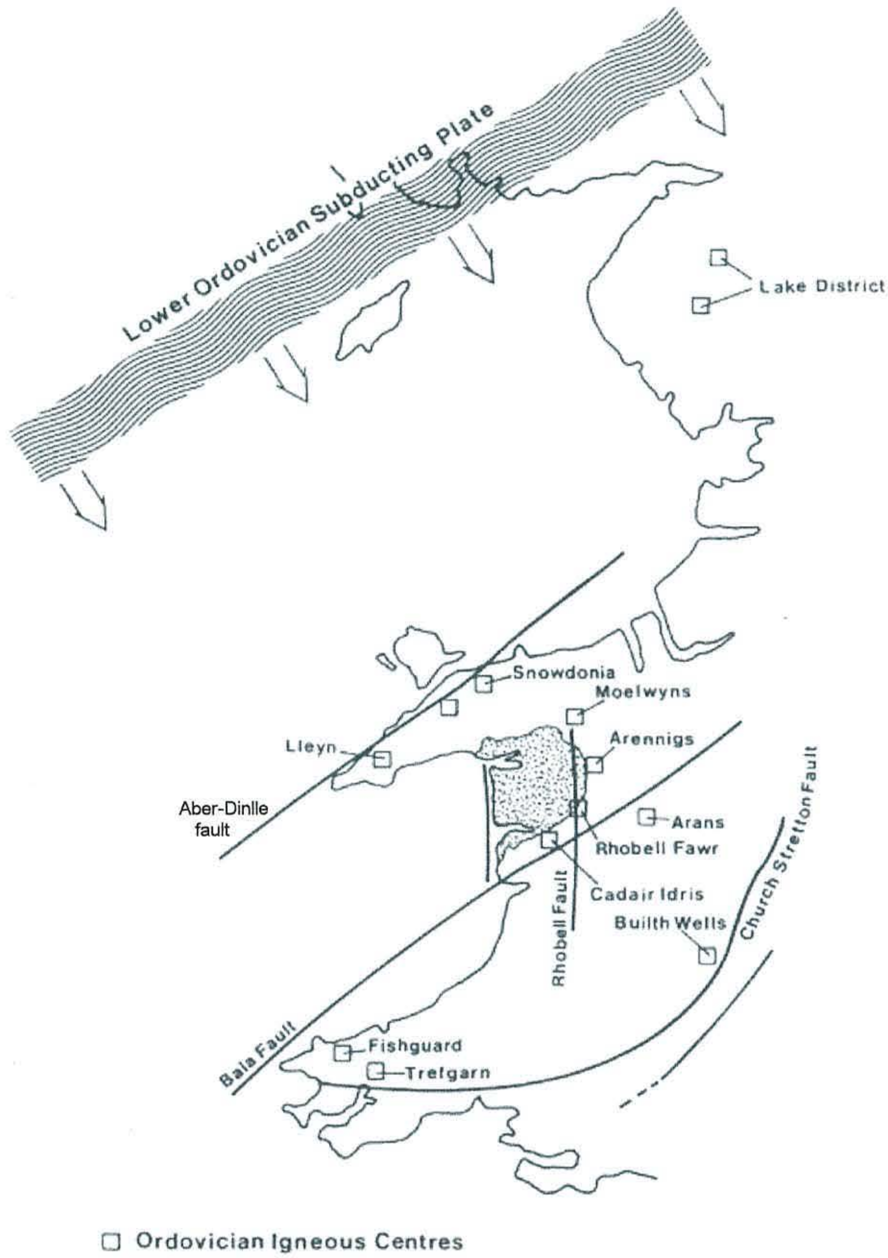

Figure 1-26: Volcanic centres and deep fracture zones related to Ordovician subduction in the Welsh Basin (after Hall, 1981)

The Mawddach catchment occupies much of the central, southern and eastern areas of a major anticlinal structure, the Harlech Dome (figs.1-27,1-28). Grits, sandstones and shales making up the Cambrian succession outcrop in the central area of the Harlech Dome (Matley and Wilson,1946). Surrounding the sedimentary outcrop is a circle of rugged mountains composed of Lower Ordovician volcanic rocks and associated igneous intrusions; these are the Moelwyn, Arennig, Aran and Cadair Idris ranges, rising to a height of around 800m.

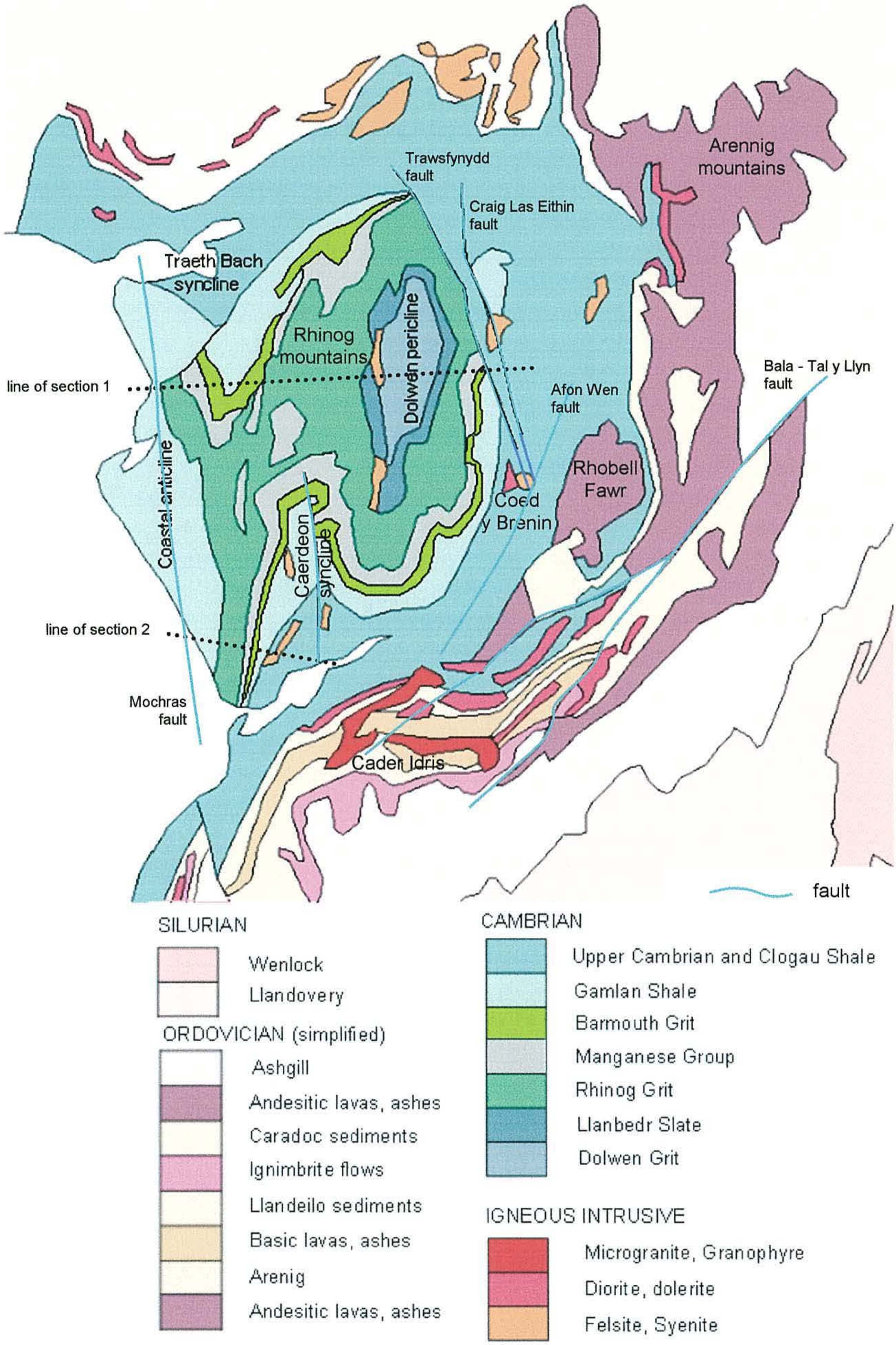

Figure 1-27: Geology of the Harlech Dome
(after Matley and Wilson, 1946; Rushton, 1974; Geological Survey, 1971)

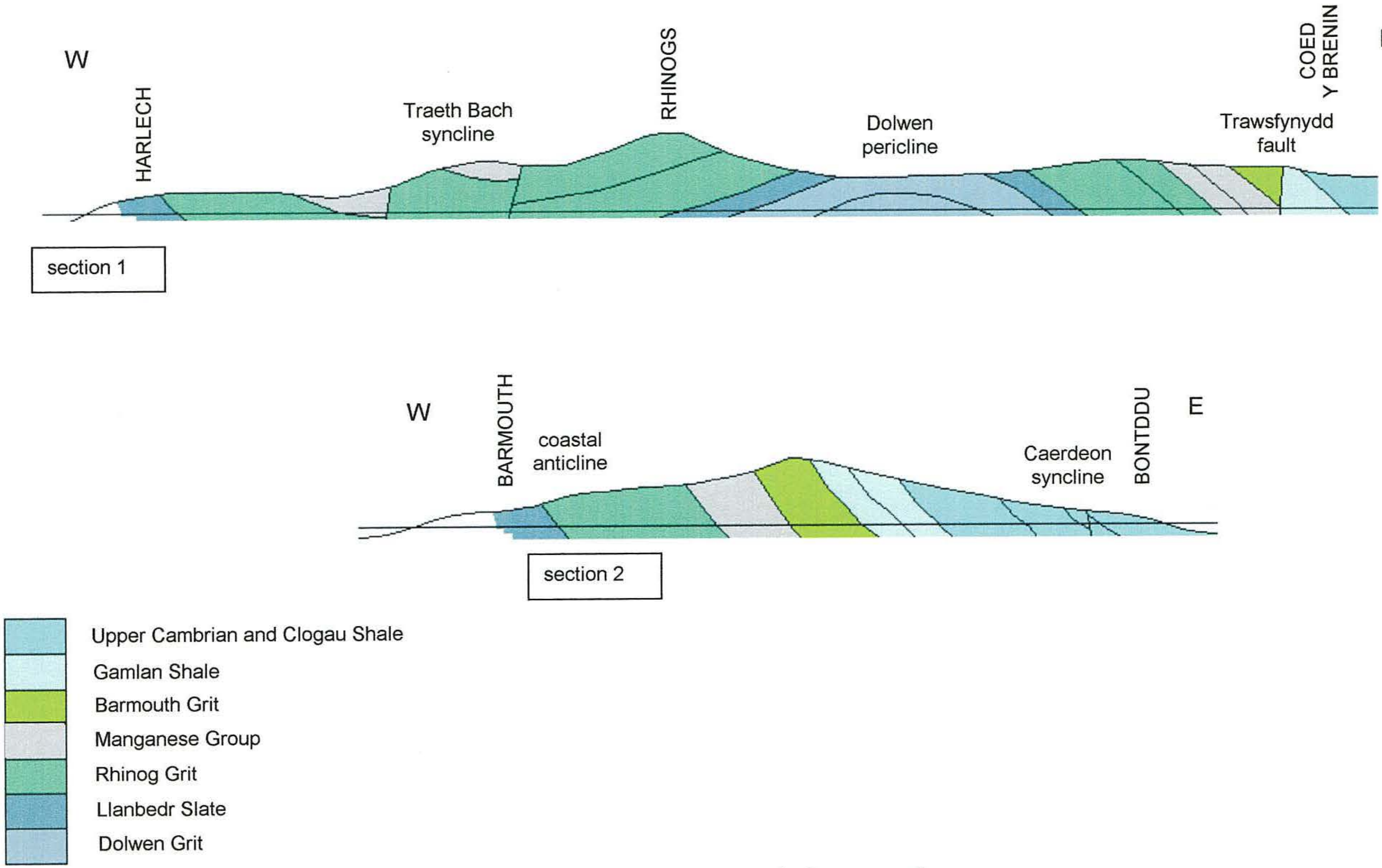

Figure 1-28: Harlech Dome geological cross sections

The lithological characteristics of Cambrian sediments in North Wales are summarised in fig.1-29 (Rushton, 1974).

The Cambrian succession in the Harlech Dome commences with the Dolwen Grit and Llanbedr Slate. These seem to indicate a period of deepening water. The Rhinog Grits represent a first phase of turbidite deposition. Coarse sediments released from the Irish Sea landmass spread across the floor of the deep water basin as a fan complex. Geological features of the Rhinog Grits are illustrated in fig.1-30.

Following the turbidite deposition, a pause in sedimentation took place, with a sequence of muds enriched in manganese accumulating on the basin floor. Near the base of this group is a bed of manganese silicate ore, which has been mined commercially in the Harlech Dome.

The subsequent deposition of the Barmouth Grits represents a return to turbidity current activity in North Wales. The geography of the Welsh Basin began to change, with the more distant Midland platform to the south-east rising above sea level whilst erosion reduced the elevation of the nearby Irish Sea landmass. By the time of the Gamlan Shale, sediment supply was predominantly from the Midland platform. Again, turbidite flows were discharged into the deep waters of the basin, but the distance of the North Wales area from the sediment source now meant that only finer shale sequences were deposited in this area. Similar conditions continued during deposition of the Clogau Shales and Maentwrog Beds (fig.1-31).

The Ffestiniog Beds of the Upper Cambrian mark another major change in the geography of the Welsh Basin. General shallowing of the water took place, and silts and shales were deposited in shallow water. Ripple marks are common on the surface of sandstone beds. In the closing stages of the Cambrian period, extensive deposits of mud were laid down in the Welsh Basin to form the Upper Cambrian Dolgellau and Tremadoc Beds.

<table>
<tr><th colspan="3">Lithostratigraphic unit</th><th>Lithology</th><th>Biostratigraphic unit</th></tr>
<tr><td colspan="3">Tremadog Slates Group</td><td>Slates and thinly bedded fine grained metasediments and siltstones (c.300m)</td><td>Tremadog</td></tr>
<tr><td rowspan="5">Mawddach Group</td><td colspan="2">Dolgellau Formation</td><td>Dark pyritous metashales and thin metasiltstones (c.50-100m)</td><td rowspan="4">Meirionydd (Upper Cambrian)</td></tr>
<tr><td colspan="2">Ffestiniog Formation</td><td>Interbedded strong metasiltstones and very fine metasandstones plus some slates (c.500m)</td></tr>
<tr><td rowspan="2">Maentwrog Formation</td><td>Penrhos Shales member</td><td>Rusty weathering dark pyritous metashales and laminated metasiltstones (c.300m)</td></tr>
<tr><td>Vigra Flags member</td><td>Interbedded grey metasiltstones, metasandstones and some metashales (c.300m)</td></tr>
<tr><td colspan="2">Clogau Formation</td><td>Predominantly dark metashales with minor metasiltstones</td><td rowspan="4">St David's</td></tr>
<tr><td colspan="3">Gamlan Formation</td><td>Thinly interbedded fine metasandstones and slates (c.250m)</td></tr>
<tr><td colspan="3">Barmouth Formation</td><td>Mainly massive greywacke sandstones (turbidite units) with intervening slates (c.200m)</td></tr>
<tr><td colspan="3">Hafotty Manganese Formation</td><td>Striped green and grey metamudstones and thin metasiltstones. Manganese bearing sandstone in lower part (c.200m)</td></tr>
</table>

Figure 1-29: Cambrian and lowest Ordovician (Tremadog) succession, after Rushton (1974)

Figure 1-30: Features of the Rhinog Grits, near Llyn Pryfed, Rhinog mountains. (Upper photograph) Rocky terraces representing individual massive grit beds. (Lower left) Conglomerate bed, composed of well rounded quartz pebbles. (Lower right) Several fining-upwards sequences from grit to sand and silt layers, representing deposition from successive turbidite flows.

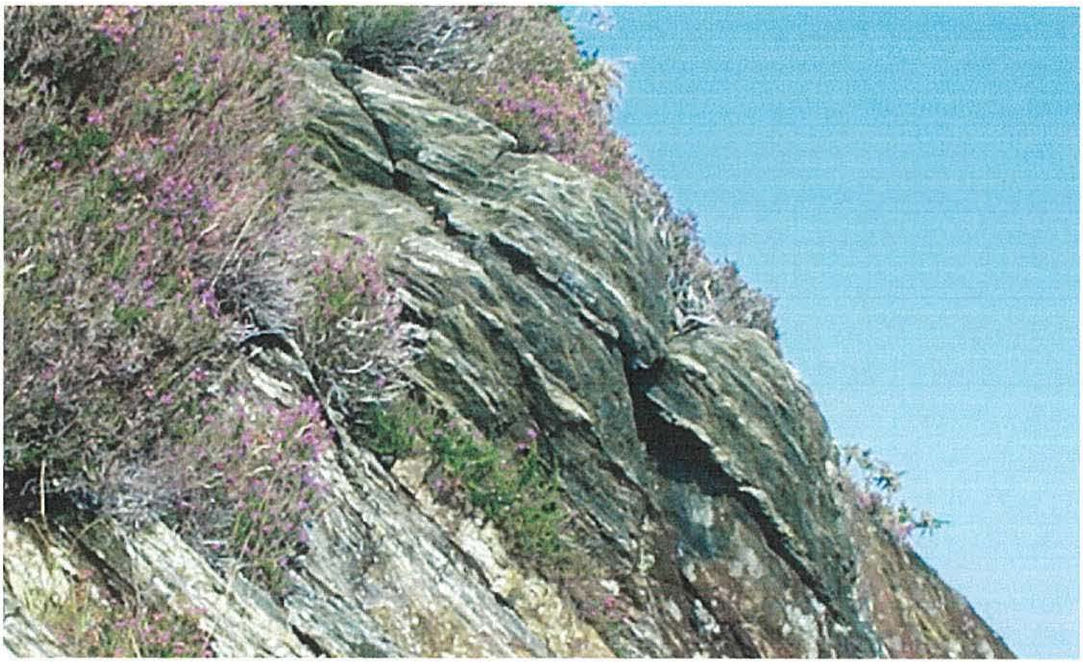

Figure 1-31: Vigra Flags member of the Maentwrog formation, Foel Ispri.

The softer sediments in the higher parts of the Cambrian succession produce less rugged scenery. Middle to Upper Cambrian rocks outcrop as the belt of hill country alongside the Mawddach estuary in the south, and the Vale of Ffestiniog in the north of the Harlech Dome, and follow the headwaters of the Mawddach inland into the Coed y Brenin forest. These outcrops produce the most productive areas of forest and agricultural land within the Mawddach catchment.

The Ordovician period saw the development of volcanic centres around the Harlech Dome (Wood, 1969) in response to the subduction of oceanic crust. Fault structures in the floor of the Welsh Basin controlled the distribution of volcanic centres around the Harlech Dome.

In late Tremadoc times, block faulting raised the central area of the Harlech Dome above sea level. Soft semi-consolidated beds of Upper Cambrian sediment were folded over the eastern edge of the fault block in the form of a monocline between Ffestiniog and Dolgellau, and erosion cut downwards into the sedimentary succession above the Dome. Rise of magma along the fault zone initiated volcanic eruptions in the area of Rhobell Fawr, with an accompanying phase of dyke and sill intrusion. At the close of the Rhobell volcanic episode the area again subsided below sea level, and marine sediments of early Ordovician age were laid down unconformably on top of the Rhobell lavas and folded Cambrian strata.

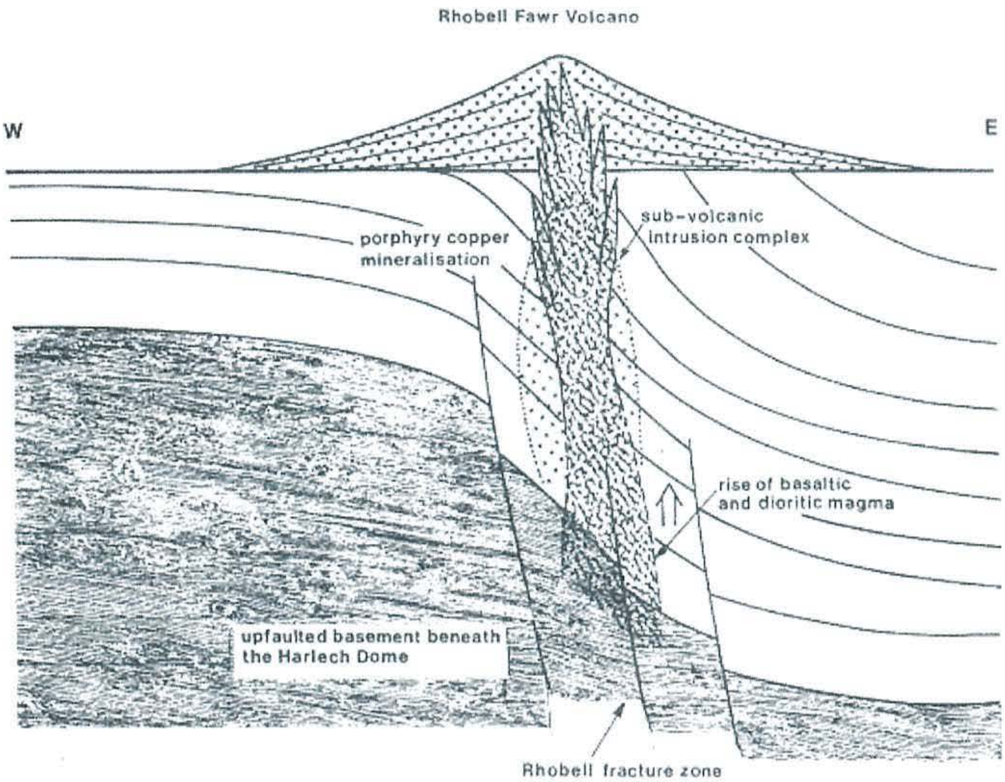

Figure 1-32: Structure of the Rhobell volcanic centre (after Kokelaar, 1977)

A feature of the Rhobell volcanic centre is disseminated copper pyrite within the sub-volcanic diorite intrusions and adjacent sediments in the Hermon area; this forms the Coed y Brenin porphyry copper deposit (Rice and Sharp, 1976). The copper was emplaced from hydrothermal fluids rising from the magma chamber beneath the volcanic centre in the late stages of crystallisation (fig.1-32). The hot hydrothermal fluids were also able to break down silicate minerals in the diorite to form clay minerals, in an analogous way to the formation of china clay around the Cornish granites. The area of copper emplacement around Hermon is now one of decomposed and easily eroded rock material with clearly visible green colouration of copper carbonate (fig.1-33).

Figure 1-33: Outcrop of decomposed diorite with disseminated copper carbonate mineralisation. Coed y Brenin porphyry copper deposit, Hermon.

Following the Rhobell volcanic episode, volcanic activity became more widespread along the southern and eastern margins of the Harlech Dome during the Ordovician period. Eruptions took place from various centres, and a thick succession of lavas, pyroclastic deposits, and interbedded marine sediments was built up, along with the emplacement of sub-volcanic and intra-volcanic intrusions. This complex succession is well exposed in the mountain ranges of Cadair Idris, the Arans, and the Arennigs. The complete volcanic succession extending from Arenig to Caradoc times is termed the Aran volcanic group (Ridgway, 1975), and has been divided into a series of nine smaller units (figs.1.34-1.36).

Craig y Llam formation	Thick and extensive rhyolitic ignimbrites deposited under sub-aerial conditions, representing a phase of widespread emergence. An eruptive vent has been identified at Mynydd Moel on Cader Idris.
Craig y Bwlch formation	Acid pyroclastics and ignimbrites layed down on emergent volcanic islands. Marine muds and water laid ashes, which may indicate subsidence below sea level after eruptions emptied the underlying magma chambers.
Pen y Gader formation	Basaltic lavas and ashes. Characteristics of both submarine eruption and accumulation on a land surface are found within the succession, suggesting deposition on and around low volcanic islands in a shallow sea area.
Nant Fridd Fawr formation	Acid ignimbrites and ashes. It may represent a localised eruption from an emergent volcanic island in the Rhobell area.
Llyn y Gafr formation	Basalt lava flows and associated ashes and muds deposited in submarine conditions, The basalts show pillow structures characteristic of eruption into water.
Cefn Hir formation	Acid ashes and coarser pyroclastic sediments. Volcanic mudflows are widespread, layed down from turbidity currents transporting loose pyroclastic debris down the submarine slope of the volcano.
Gwynant formation	Quiet sedimentation when muds were layed down on the sea bed. Occasional thin ash beds indicate continued volcanic activity.
Mynydd y Gader formation	Acid ashes and ignimbrites, deposited from pyroclastic flows under subaerial conditions. It is likely that the eruptions took place from the Rhobell igneous centre.
Pared yr Ychain formation	A sedimentary formation, composed variously of sands, mudstones and conglomerates, and represents a general submergence of the North Wales area at the beginning of the Ordovician period.

Figure 1-34: Formations within the Aran Volcanic Group

Figure 1-35: Cefn Hir volcanic mudflow, showing fragments and pebbles of rhyolite in a roughly stratified matrix of ash and mud.

Figure 1-36: Pared yr Ychain grey sandstones and mudstones.

Acid and basic magmas were erupted in alternate phases. Basic phases of volcanism were dominantly submarine. Clouds of basaltic froth would be ejected explosively from sea floor vents and would fall back to the sea bed as pyroclastic ash deposits. Quieter flows of magma would also radiate from the vents, with the hot basalt forming pillow structures on contact with the cold water. In the country rock beneath the submarine volcanoes, sheets of magma spread laterally to produce the vertical dolerite dykes (fig.1.37) or horizontal sills common in the area. Sill intrusions often follow weaker horizons of rock such as shales which would present less resistance to magma flow.

Figure 1-37: Dolerite dyke intruded through Upper Cambrian sediments, Moel Oernant

Acid magma was generated by partial melting of the granitic lower crust due to heat from basaltic magma above the subduction zone. This granitic melt would make its way upwards to a high crustal level, where it could form cylindrical intrusions or spread laterally to form domed sill-like magma chambers known as laccoliths. The space for the intruding melt was created by lifting of the overlying rocks, and phases of acid volcanicity were frequently accompanied by emergence of volcanic islands. As crystalisation of the acid melt took place, gas pressure would build-up until explosive fracturing of the magma chamber roof occurred. Lava froth would thrown into the air from the vent, to fall as pyroclastic ash or pour down the side of the volcano as a dense ignimbrite flow.

After the close of volcanic activity in the Harlech Dome, quiet deposition of marine muds continued for the remainder of Upper Ordovician times. Only occasional thin volcanic ashes from a distant source north-east of Bala appear within the sedimentary succession. Beyond the Harlech Dome area, however, major eruptions continued from centres in Snowdonia.

The varying lithologies of the Cambrian and Ordovician strata outlined above have an important effect on the hydrological response of the Mawddach catchement. Other geological factors which must be considered are folding and faulting within the region. Structurally, the Harlech Dome is more complex than its name implies. Within the encircling Ordovician outcrop occur several folds lying roughly on a north-south axis to form parts of the major structure (figs 1-27,1-28). South of Trawsfynydd reservoir is the Dolwen pericline, an anticlinal structure exposing Llanbedr Slate amid. Dolwen Grit at its core, The Rhinog mountains have the form of an escarpment, composed of resistant Rhinog Grit overlooking the western side of the pericline. Nearer the coast are two complimentary synclines; the Caerdeon syncline plunges south towards the Mawddach estuary and the Traeth Bach syncline plunges north towards the Vale of Ffestiniog. Beyond these structures, outcrops of Rhinog Grit and Llanbedr Slate form the eastern limb of the coastal anticline, which is terminated at this point by the shoreline between Porthmadog and Barmouth. Evidence from boreholes indicates that a downfaulted trough of Mesozoic sediments lies offshore in Cardigan Bay, with the N-S Mochras fault trucating the older rocks of the coastal anticline.

Faulting is very obvious on the geological map of the Harlech Dome, and has had considerable influence on the development of the landscape. The major estuaries to the north and south of the Harlech Dome have been eroded along fault zones; and the courses of several rivers, notably the Afon Wen north of Dolgellau, follow fault lines for parts of their courses. Faults in the Harlech Dome can be divided into several groups:

- Strong faults running in a general north-south direction along the inland and seaward margins of the Dome. To the east of the Dolwen pericline, these include the Trawsfynydd, Craig Las Eithin and Afon Wen faults, and in the coastal region around Harlech are the Moelfre and Mochras faults.
- Strong faults running in a general north-east to south-west direction. The principal of which is the Bala fault. These control the orientation of Wnion and Tal y Llyn valleys.

Both of these groups are related to deep fractures in the Earth's crust beneath North Wales. They were initiated as lines of weakness during plate motions associated with the opening and subduction phases of Iapetus, when they provided magma conduits for vocanic activity (fig.1-26). Once established as lines of weakness, these fractures have been reactivated at subsequent times during geological history.

- More minor and superficial are two sets of faults related to the Caledonian folding which produced the Dome in late-Silurian and Devonian times. One set radiate from the centre of the Dome, and are termed radial faults; they are well developed in the Coed y Brenin area. The second set run in arcs concentric with the dome margin, and are termed circumferential faults; these are well developed to the north of the Mawddach estuary around Bontddu. The radial and circumferential faults are of interest, as mineralisation along these fractures produced the gold bearing quartz lodes of the Harlech Dome (Gilbey, 1968).

Where a fault line has been reactivated on a number of occasions, a complex fracture zone of multiple sub-parallel failure planes can develop (fig.1-38).

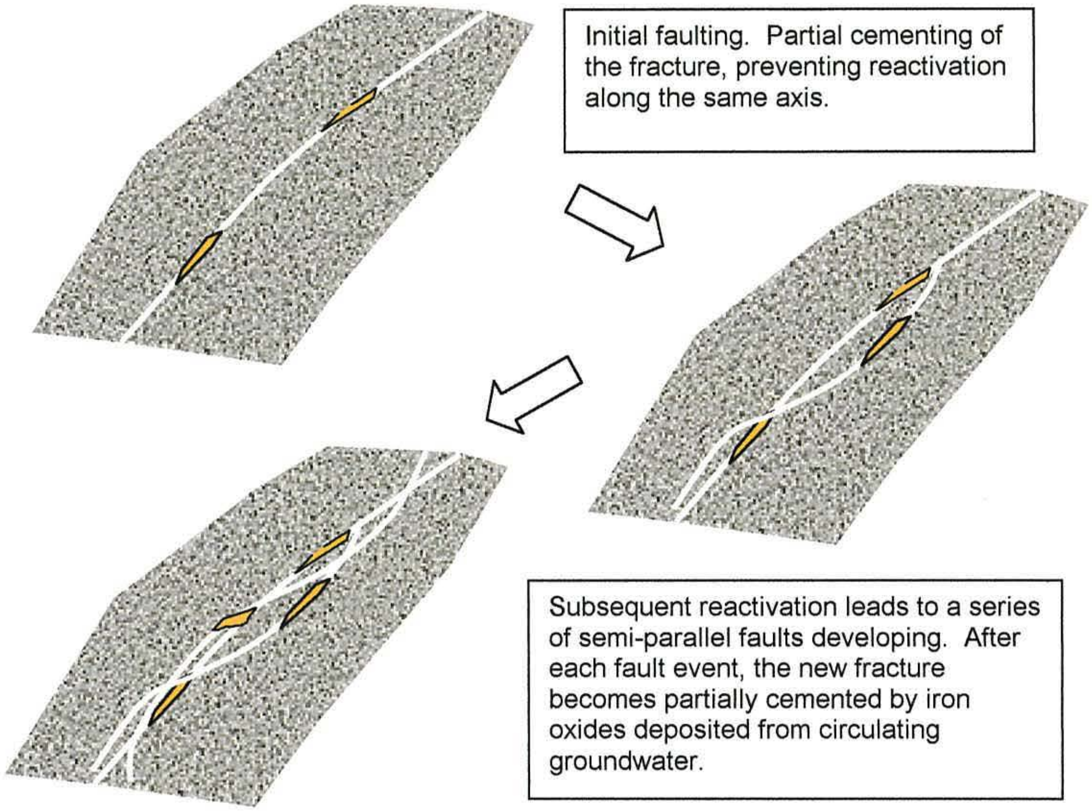

Figure 1-38: Evolution of a complex fracture zone by successive reactivation

Sections of early fault planes may become cemented by circulating ground water, so that subsequent movement takes place preferentially in softer country rock alongside. A wide zone of disrupted rock is produced, with high connectivity between fracture planes. Overall hydraulic conductivity in the fracture zone may be considerably increased in comparison to undisturbed country rock. Features of the Afon Wen fracture zone are illustrated in fig.1-39.

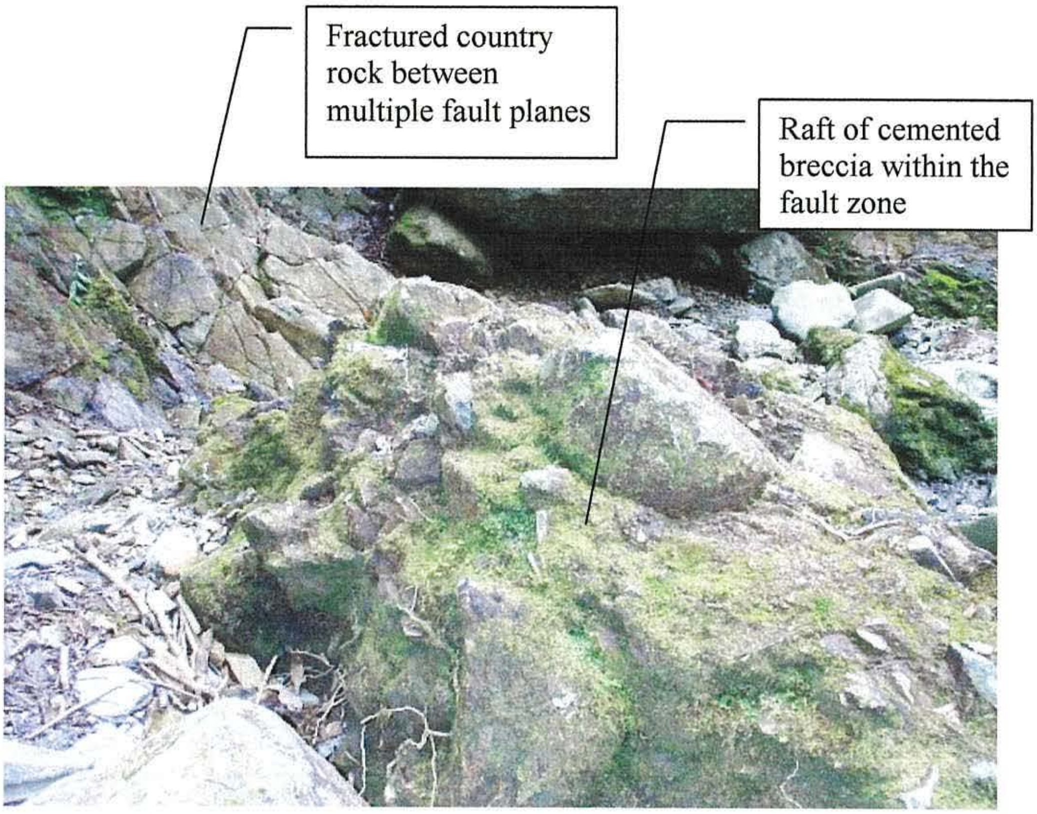

Figure 1-39: Afon Wen fracture zone, Hermon

Geomorphology

An important feature of the geomorphology of the Mawddach catchment is a well developed sequence of erosion surfaces developed in response to a pulsed uplift of North Wales during late Tertiary times. This uplift may be related to Alpine earth movements occurring to the south and east in Europe.

A prominent plateau surface extends across much of mid-Wales at an altitude of around 600m (fig.1.40). Deep valleys have been incised into this surface. The origin of the plateau surface is not known precisely, but is likely to be the result of prolonged river erosion reducing the land surface to a plain close to sea level during a period of crustal stability. Higher mountain summits such as the Brecon Beacons, Plynlimon and Cader Idris rise above this surface, and represent relict hills which were never reduced to the level of the surrounding plain.

Figure 1.40. View from Hyddgen across the Plynlimon mountain range, mid-Wales. The planar surface forming the skyline in the middle distance is a remnant of the 600m plateau. The summit of Plynlimon rises to 750m in the distance.

In the Mawddach catchment, erosional history is more complex. Miller (1946) has identified additional erosion surfaces at lower altitudes (fig.1.41).

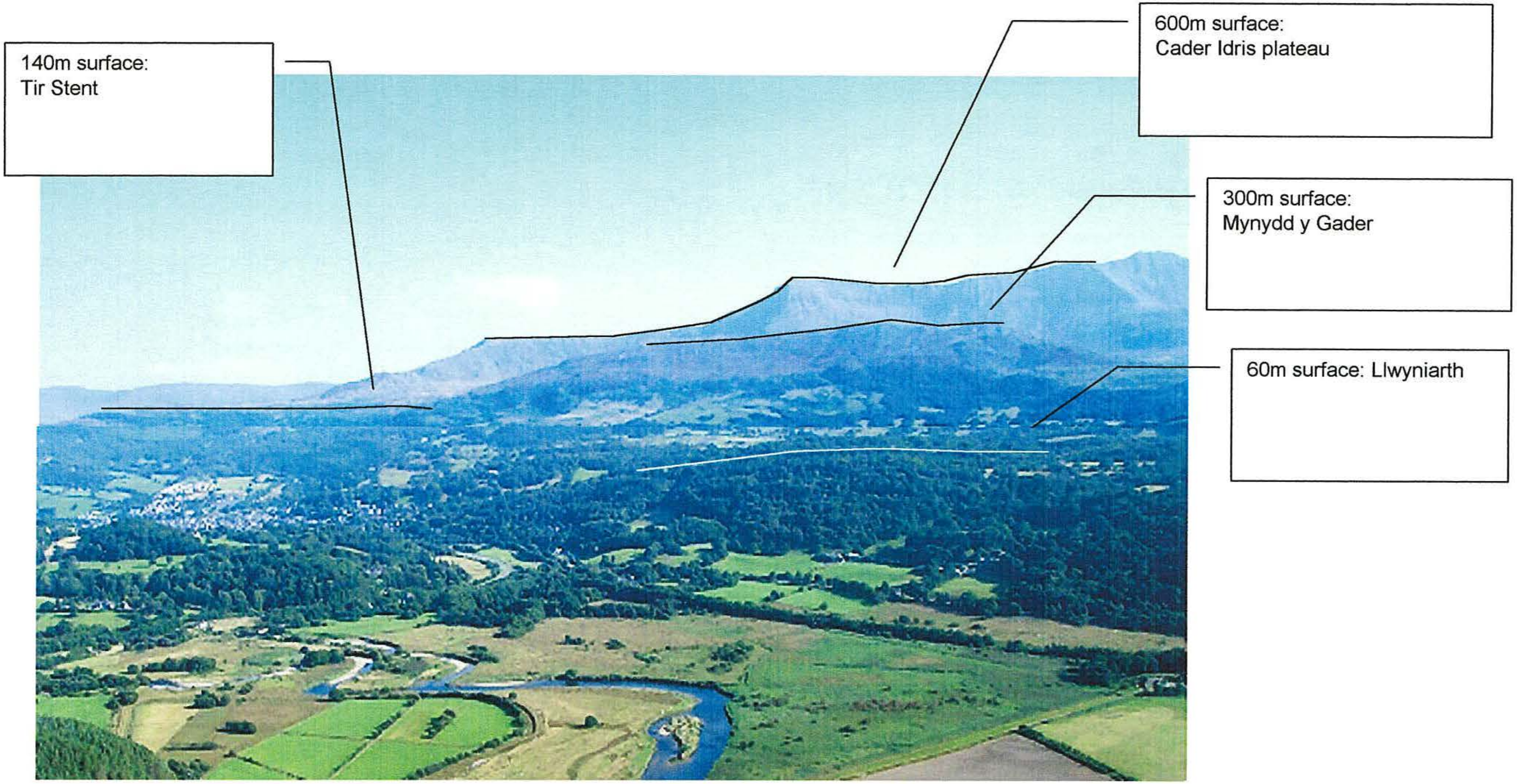

Figure 1.41. Erosion surfaces above the town of Dolgellau, looking south-east

Within the Mawddach catchment, the 600m plateau of mid-Wales is represented by the shoulders of Cader Idris, the summit of Y Garn, and the ridge of Llawlech. Initial drainage may have developed on that surface. Subsequent phases of rapid uplift, followed by periods of stability, have led to river rejuvenation and the development of polycyclic relief. Over a series of erosion cycles, major streams have become aligned to follow the outcrops of softer rocks or fault lines. Short tributaries, generally at right angles, drain the interfluve areas.

Miller named three lower erosion surfaces after localities around the Mawddach estuary where they are well developed:

- 300m surface: the Foel Ispri stage,
- 140m surface: the Rhyd Wen stage,
- 60m surface: the Ynys stage.

The origin of the surfaces is conceived as a combination of marine erosion near the coast and river erosion inland. The main north-facing scarp of Cader Idris may have originated as a sea cliff following fall of sea level to the Foel Ispri stage. Remnants of the 60m surface are prominent along the north and south shores of the Mawddach estuary (fig.1.42).

Each erosion surface may be expected to ascend as it is traced inland, following a graded river profile. Multiple rejuvenation is evident in the long profiles of the Afon Mawddach, and its main tributary the Afon Gain (fig.1.43). Graded reaches between knick points may be correlated with inland extensions of erosion surfaces of the Ynys and Foel Ispri stages.

Hayakawa and Oguchi (2006), in a study of Japanese mountain rivers, found that knickzones are more abundant in portions of rivers characterized by active erosion and rapid uplift, regardless of bedrock lithology, suggesting the dominant influence of fluvial hydraulics on location of knickzones. This finding is consistent with observations in the Mawddach catchment.

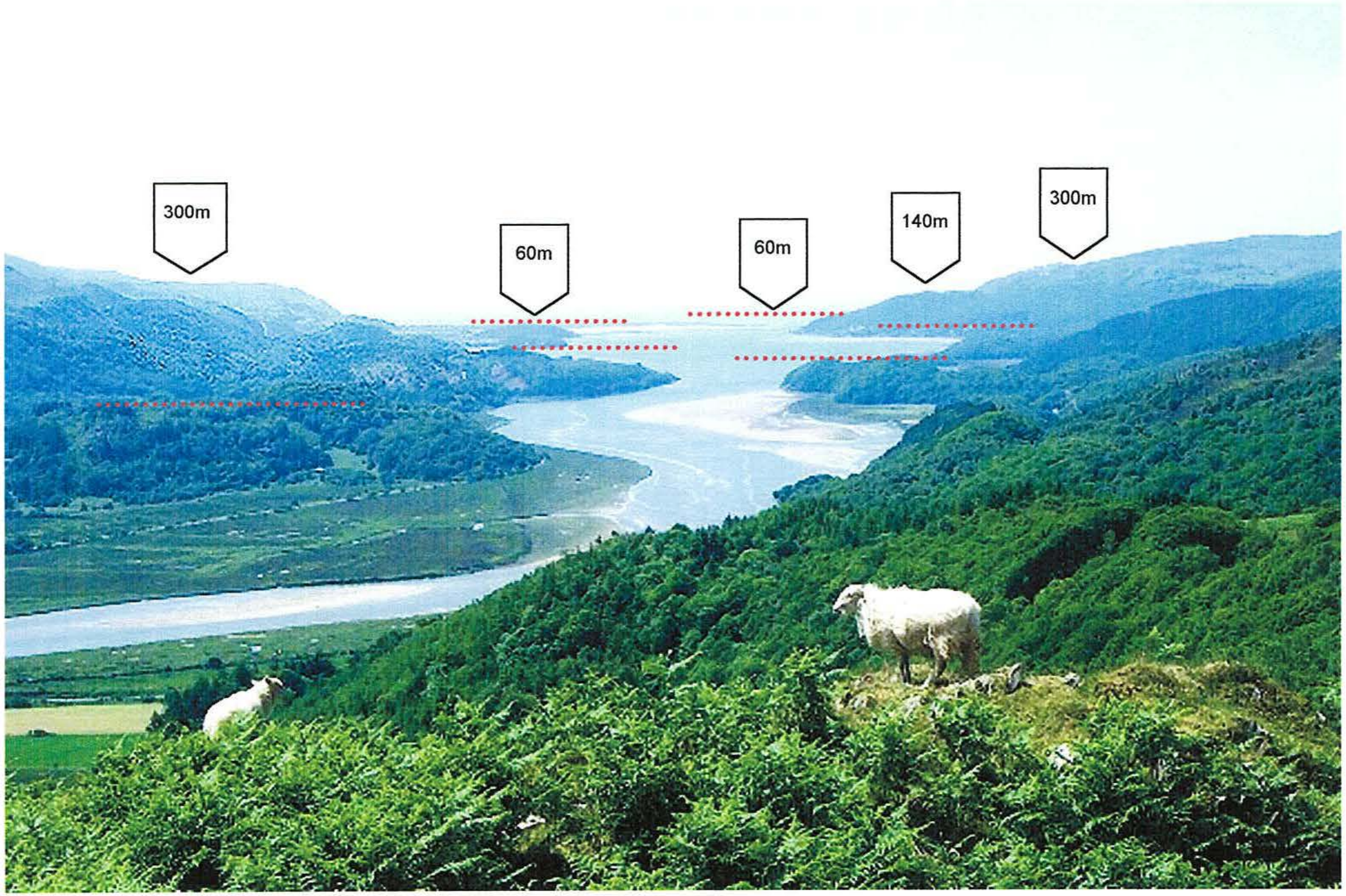

Figure 1.42. Erosion surfaces above the Mawddach estuary. Relics of the 60m surface are marked by red dotted lines.

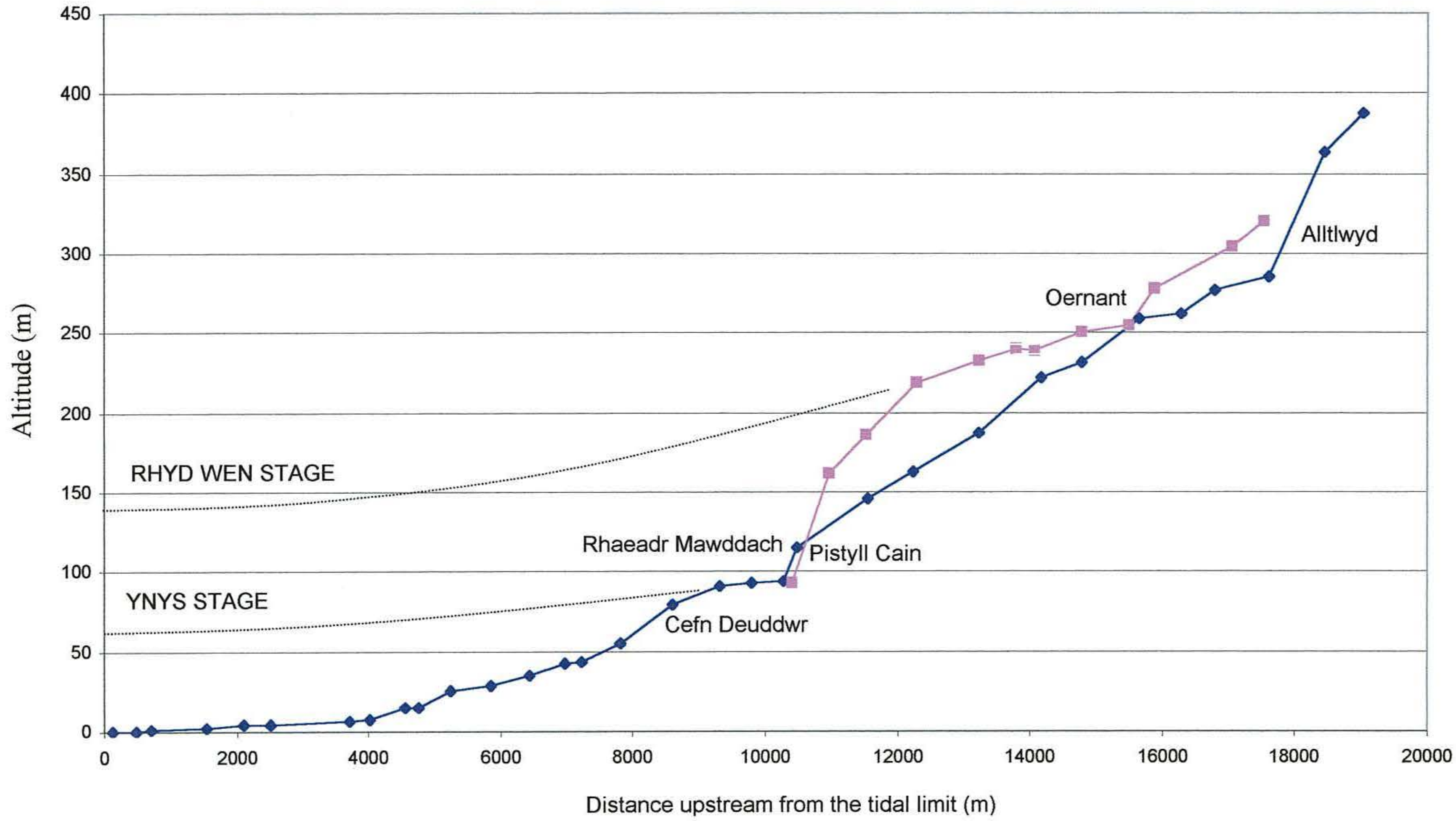

Figure 1.43. Long profiles of the Afon Mawddach (black) and Afon Gain (red). Sites of waterfalls and rapids associated with knick points are named: see fig.1.11

North Wales was extensively glaciated during Pleistocene times, and the landscape extensively modified as a result of glacial erosion, deposition, and subsequent periglacial sediment redistribution (Bowen, 1973) prior to the establishment of the present day Mawddach and Wnion catchments.

Local ice sheets developed over the Welsh mountains and flowed radially outwards (fig.1.44) during the three main stages of the Ice Age: the Wolstonian, Ipswichian and Devensian. Westwards flowing ice merged along the coast of Cardigan Bay with Irish Sea ice moving southwards from a source area in Scotland.

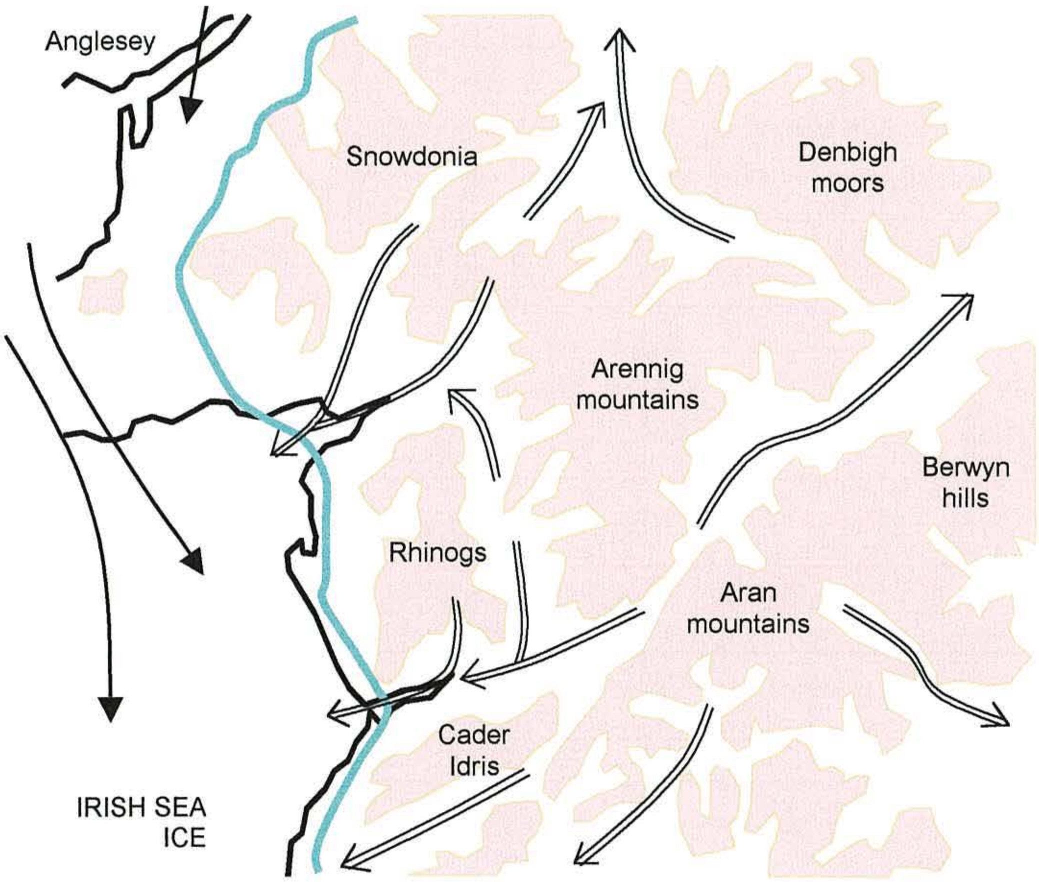

Figure 1.44. Main ice flow directions in North Wales (after Howe and Thomas, 1968)

Within the Harlech Dome region, a major ice cap was centred on the Arennig mountains, with the altitude of the ice reaching 1200m (Foster, 1968). Westwards flowing ice accumulated on the plateau surface around Trawsfynydd, from which it spilled northwards to the vale of Ffestiniog and southwards to the lower Mawddach valley. An extensive drumlin field developed around what is now Trawsfynydd reservoir. Mechanisms of drumlin formation are discussed by Price (1973).

Classical U-shaped profiles indicative of erosion by valley glaciers are shown by the lower Mawddach valley between Gelligemlyn and Llanelltyd (fig.1.45) and the lower Wnion valley between Bontnewydd and Dolgellau (fig.1.46).

Figure 1.45. The lower Mawddach valley

Figure 1.46. The lower Wnion valley

Figure 1.47. Llyn Aran

It is significant that the E-W oriented middle valley courses of the Mawddach, Gain and Afon Wen show no similar signs of glacier erosion, retaining deep V-shaped profiles, although boulder clay till is commonly present. The orientations of these valleys may have been such that they carried little ice flow in comparison to the main N-S oriented Trawsfynydd glacier.

Glacial cirque basins probably related to the late Devensian valley readvance (Watson, 1960; West, 1977) are seen along the north face of the Cader Idris escarpment. These may contain cirque lakes as at Llyn y Gader, Llyn y Gafr and Llyn Aran (fig.1.47). Cirques are also developed along the east facing escarpment of the Rhinog range above the Trawsfynydd plateau.

In the upper course of the Mawddach, features of valley glacier erosion are well developed at Allt Lwyd (fig.1.48). Downstream beyond Abergeirw, the River Mawddach descends into the steep gorge system of Coed y Brenin so it is unlikely that the main ice flow outlet from Allt Lwyd followed this route. Ice may have crossed low hills to reach the Trawsfynydd plateau directly, then merged with the main southwards ice flow towards the Mawddach estuary.

The Allt Lwyd valley is the possible site of a post glacial ribbon lake, dammed by a lobe of solifuction debris released from the steep south facing valley side. To investigate this theory, a geophysical survey was carried out in the area of the conjectured lake using the vertical electrical resistivity (VES) technique. Readings give a best fit (3% error) against a six layer model (table 1.1). Three layers with low resistivities in the range 44–196 Ω m occur at depths between 2m and 47m below the present ground surface. These resistivity values would be consistent with wet lacustrine clay, and show a sharp contrast with the high resistivity shale country rock beneath. An alternative interpretation is that one or more of the low resistivity layers represents glacial till of high clay content.

Figure 1.48. Allt Lwyd valley, looking SW. Site of the electrical resistivity sounding is marked in red.

Table 1.1. VES interpretation, Allt Lwyd

Resistivity (Ω m)	Modelled thickness (m)	Interpretation	Depth to base (m)
518	0.3	Topsoil	0.3
2015	1.8	Subsoil	2.1
149	18.9	Lake deposit	21.0
196	9.8	Lake deposit or glacial till	30.8
44	16.8	Lake deposit or glacial till	47.6
3465		Shale country rock	

It is likely that numerous additional lakes of various sizes existed within the Mawddach catchment in the immediate post-glacial period. The largest may have occupied the plateau east of the Rhinog mountain escarpment in the central area of the Harlech Dome (fig.1.49). Auger surveys have identified cream clay of probable lake origin beneath peat at both Cefn Clawdd near Trawsfynydd, and at Cefn Cam above Ganllwyd.

Figure 1.49. Site of conjectured post-glacial lake, Cefn Cam

A notable feature of the deeply incised river valleys of Coed y Brenin is a thick infill of glacial and periglacial material. The sequences are very varied in lithology, from freely draining gravel to sands, silts and clays of decreasing permeability (French, 1976; Clark and Small, 1982). Successions of up to 10m vertical extent are exposed in river cliffs in gorge sections of the Mawddach, Gain and Afon Wen.

To investigate the provenance of the sediments, grain size analysis was carried out on a series of samples from a river cliff succession at Pen Rhos in the Afon Wen valley (figs 1.50,1.51). The sediments may be divided into three groups:

- Very poorly sorted, with grain sizes reaching pebble grade or larger. Deposits falling within this group are identified as glacial till, and coarse river gravels with interstitial sand matrix.
- Very well sorted with finer grain sizes. Within this group were identified fluvial sands and silts, and a thin band of very clean, plastic yellow clay. The yellow clay is persistent downstream, and might represent lake bed material mobilised and carried down river after the failure of a glacial dam in the upper catchment.
- Materials exhibiting moderate sorting. These are interpreted as solifluction deposits, either in situ or emplaced within a short distance by river transport.

The sequence of sediments at Pen Rhos are interpreted as Boulder Clay of the Devensian valley readvance stage, overlain by periglacial deposits. The Late Devensian period has been subdivided into three Zones in North Wales (Howells et al., 1978), and it is during these Zones that the periglacial materials were produced:

- Zone I (Bølling) was a cold period after the final valley readvance. Solifluction processes would have been active at this time. Mass movement could occur on steep valley sides as periodic melting lead to saturation of the surface sediments above a permafrost horizon.
- Zone II (Allerød) was a warm period, during which larger volumes of meltwater would deposit fluvial sediments.

Zone III saw a return to cold conditions, with renewed solifluction activity.

Zone III cold period	SOLIFLUCTION
Zone II Allerød warm period	RIVER CHANNEL
	LAKE FLOOR
	FLUVIAL REDEPOSITION OF SOLIFLUCTION MATERIAL
	FLUVIAL
Zone 1 Bølling cold period	SOLIFUCTION
Devensian valley readvance	VALLEY GLACIER

1. Forest brown earth
2. Grey sandy clay
3. Iron cemented cobble band
4. Yellow clay
5. Unstratified sandy gravel
6. Fine gravelly sand
7. Silty clay
8. Sandy gravel
9. Boulder clay

Figure 1.50. River cliff deposits, Pen Rhos, Afon Wen

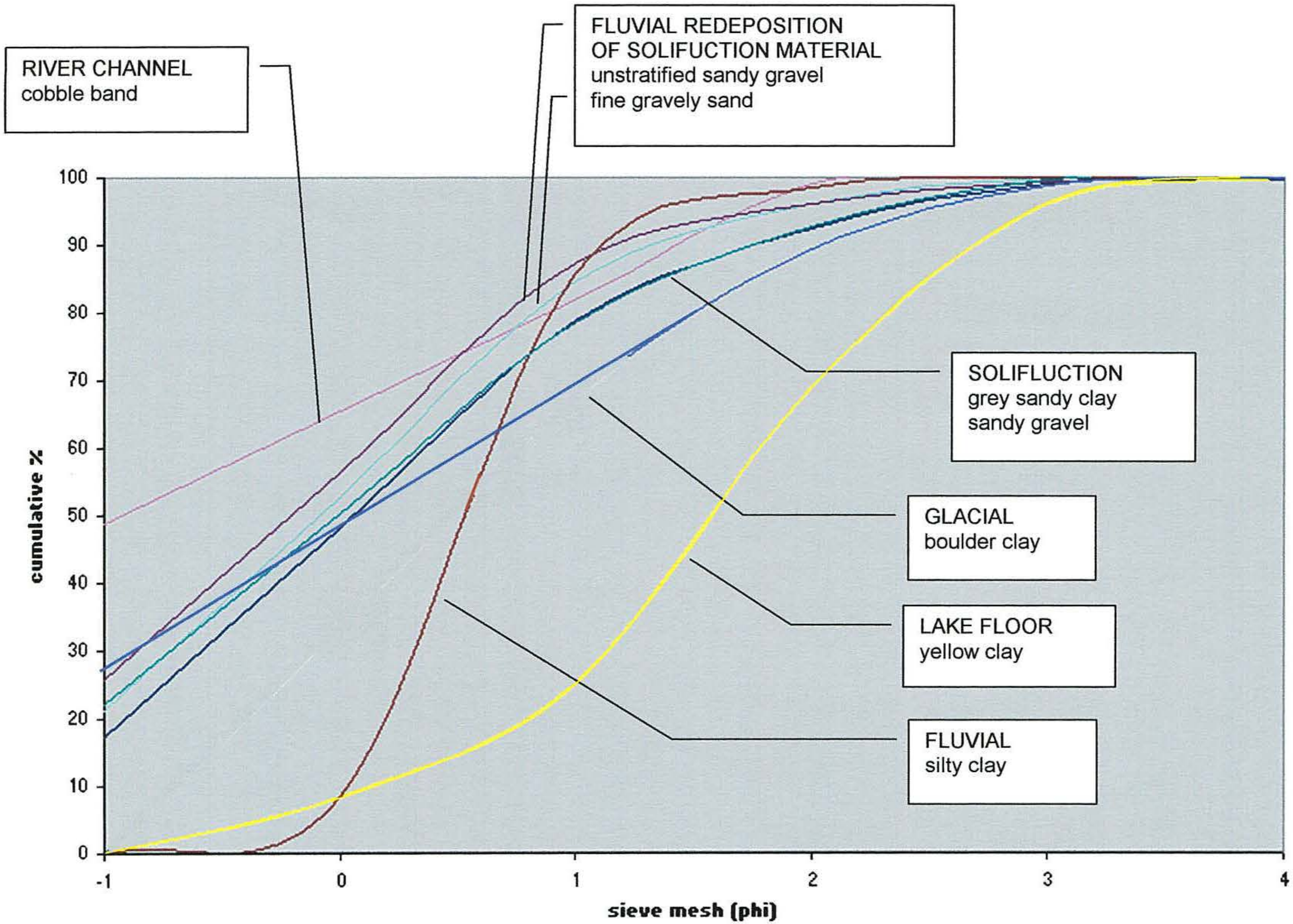

Figure 1.51. Sediment size distributions. River cliff deposits, Pen Rhos, Afon Wen.

When developing a hydrological model, the river routing function will be governed by characteristics of the river channels (Ward and Trimble, 2003). It is useful to carry out morphological classification of the river reaches within the Mawddach system. This will allow hydrological parameters to be assigned to reaches, based on measured parameters of sites with similar characteristics (Arcement G.J. and Schneider, 2003; Barnes, 1967).

Beechie et al. (2006) have considered river channel patterns and river-floodplain dynamics in forested mountain river systems of the Pacific Northwest USA. Straight channels are the least dynamic with relatively slow floodplain turnover. Braided channels are most dynamic, with floodplain turnover as low as 25 years and predominantly young floodplain surfaces. Island-braided and meandering channels have intermediate dynamics, with moderately frequent disturbances (erosion of floodplain patches) maintaining a mix of old and young surfaces. A threshold for the lateral migration of a channel occurs at a bankfull width of 15–20 m, as larger channels are deep enough to erode below the rooting zone of bank vegetation. Above this threshold, channels not confined between valley walls exhibit channel patterns distinguishable by slope and discharge, and slope–discharge domains can be used to predict channel patterns. The predicted spatial distribution of channel patterns reflects a downstream decline in channel slope, which is likely correlated with a declining ratio of bed load to suspended load.

Several morphological classification systems are available. The method chosen is that of Montgomery and Buffington (1997). This scheme has been developed for classification of mountain rivers, so it applies well to characteristics of the Mawddach drainage system.

The Montgomery and Buffington system defines seven basic categories of stream morphology, which represent in a general way a downstream sequence in response to decreasing stream gradient and increasing discharge. Reference reaches have been identified within the Mawddach-Wnion catchments which display characteristic stream morphology:

- Colluvial reach: Afon Ty Cerrig, Pared yr Ychain.

  Colluvial reaches occur as small first-order streams in the mountain headwaters of the river system. Stream gradients are typically greater than 20%, with much sediment movement occurring through debris flows from the steep valley sides (fig.1.52). Within the Mawddach catchment, colluvial reaches are associated particularly with slopes covered by Boulder Clay or periglacial deposits.

Figure 1.52. Colluvial reach. Afon Ty Cerrig at Pared yr Ychain, in the headwaters of the Afon Wnion.

- Cascade reach: Afon Ty Cerrig, Pared yr Ychain

  Cascade reaches are the next morphological type to appear as mountain rivers are followed downstream (fig.1.53). Typically they have boulder or cobble beds, and are narrowly confined by the valley sides. Slopes are in the range 10 - 30%.The large rocks within the channel are normally immobile, and are only transported during extreme flood events. More readily transported sand and fine gravel occurs within pools.

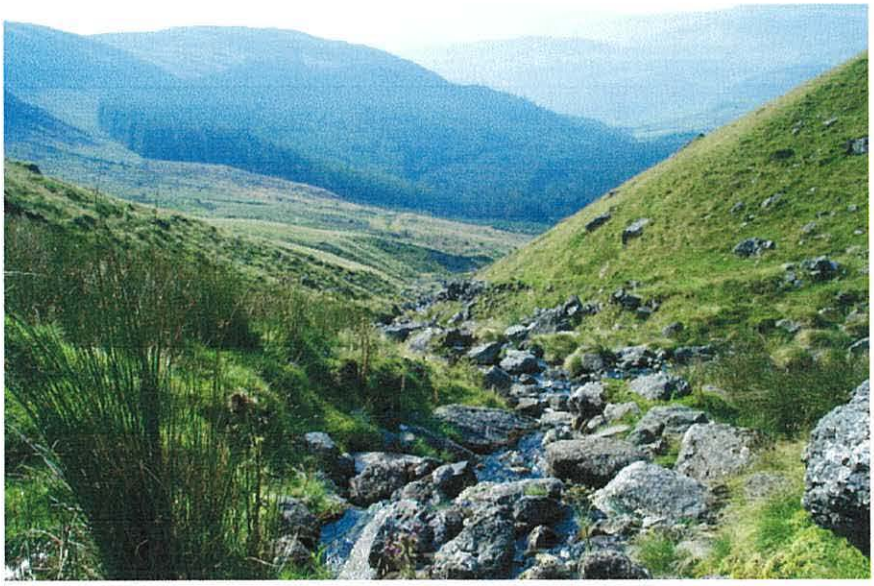

Figure 1.53. Cascade reach. Afon Ty Cerrig, Pared yr Ychain.

- Step pool reach, Afon Mynach, Tai cynheaf

  Step pool reaches appear at gradients of 3 – 10%. Longitudinal steps form most of the elevation drops, with deep pools retaining sand and gravel bedload Fig.1.54). Step pool reaches may exhibit alternating supercritical and subcritical flow conditions between the steps and pools.

Figure 1.54. Step pool reach, Afon Mynach, Tai cynheaf.

- Bedrock reach, Afon Gain near Gwynfynydd

  Bedrock reaches differ from the previous types in having no significant bed sediment present. Bedrock reaches are typically located where gradients are steep so the sediment transporting capacity of the stream greatly exceeds the sediment supply, even during normal flow conditions. Within the Mawddach catchment, bedrock reaches occur below knick points on the Afon Mawddach and Afon Gain (fig.1.55) where river rejuvenation is evident.

Figure 1.55. Bedrock reach, Afon Gain near Gwynfynydd.

- Plane bed reach: Afon Mawddach, Ty'n y Groes

  Plane bed reaches (fig.1.56) occur for gradients around 2-3%, and typically have a high bed roughness. They lack rhythmic bed forms such as steps, pools and riffles. Plane bed reaches are thought to form a transition between upstream channels where sediment movement is limited by supply, and downstream channels where sediment movement is limited by stream energy.

Figure 1.56. Plane bed reach. Afon Mawddach, Ty'n y Groes.

- Pool riffle reach: Afon Wnion west of Dolgellau

  Pool riffle reaches (fig.1.57) have a gentler gradient of around 1-2%. Pools occur at intervals of approximately 6 channel widths, with intervening shallow riffles crossing the channel. Flood plains are usually well developed.

Figure 1.57. Pool riffle reach, Afon Wnion west of Dolgellau.

- Dune ripple reach, Mawddach estuary upper basin, Penmaenpool

  Dune ripple reaches normally occur in sand bed channels with bed slopes less than 1%. These systems are very dynamic, with sediment movement occurring frequently and bedforms changing regularly. Dune ripple reaches occur in the upper basin of the Mawddach estuary, where fluvial processes are dominant.

Figure 1.58. Dune ripple reach, Mawddach estuary upper basin, Penmaenpool.

An additional category in the classification is the **forced pool reach**. This refers to step pools produced by non-fluvial processes, such as obstruction by fallen trees (fig.1.59) or the construction of weirs and fords. Wohl (2000) stresses the importance of woody debris and bank mass movement in controlling morphological changes in mountain rivers.

Figure 1.59. Fallen trees in the channel of the Afon Wen, Coed y Brenin.

Forced pool reaches are relatively rare within the Mawddach catchment, as timber obstructions in the main rivers of the Mawddach system are generally removed rapidly by the Forestry Commission, other land owners or the Environment Agency, to prevent flooding of riparian areas.

Soils

Classification

Soil type is related to a number of factors acting together at a locality (Burnham, 1980):

- the physical nature of the bedrock or glacial and periglacial deposits affecting the mechanical breakdown and input of rock material to the soil profile.
- the chemical nature of the bedrock, affecting the input of plant nutrients, especially calcium.
- relief, affecting drainage and soil movement under gravity.
- hydrological conditions which affect the amount of water passing through the soil, and hence the degree of leaching or waterlogging.
- the agricultural history of the site, affecting the characteristics of the soil horizons.

Due to the seaboard location, southerly latitude, and relatively low elevation, the Mawddach catchment experiences an oceanic rather than montane climate. Typically, there will be high precipitation, high cloud cover and humidity, and low sunshine levels. Most soils are at least seasonally wet and show reducing chemical conditions with iron present as the ferrous ion . Locally the presence of steep slopes produce well drained soils, as do scree slopes and blockfields where drainage into cavities is rapid.

Fig.1.60 illustrates the distribution of the soils in and around the Mawddach catchment, simplified from the National Soil Map (Avery B.W., 1980; Cranfield University, 2004). The principal soil types found in the Mawddach catchment are:

Ranker. Ranker soils occur where the input of mineral material from the bedrock is almost negligible. The profile shows an organic A horizon, generally as a peat mat, lying directly on the solid rock surface (C horizon). Two types are distinguished within the Mawddach catchment:

- Revidge series: peaty humic ranker occurring mainly on Rhinog grit.
- Skiddaw series: more decomposed humic ranker, mainly on resistant igneous rocks (fig.1.61A).

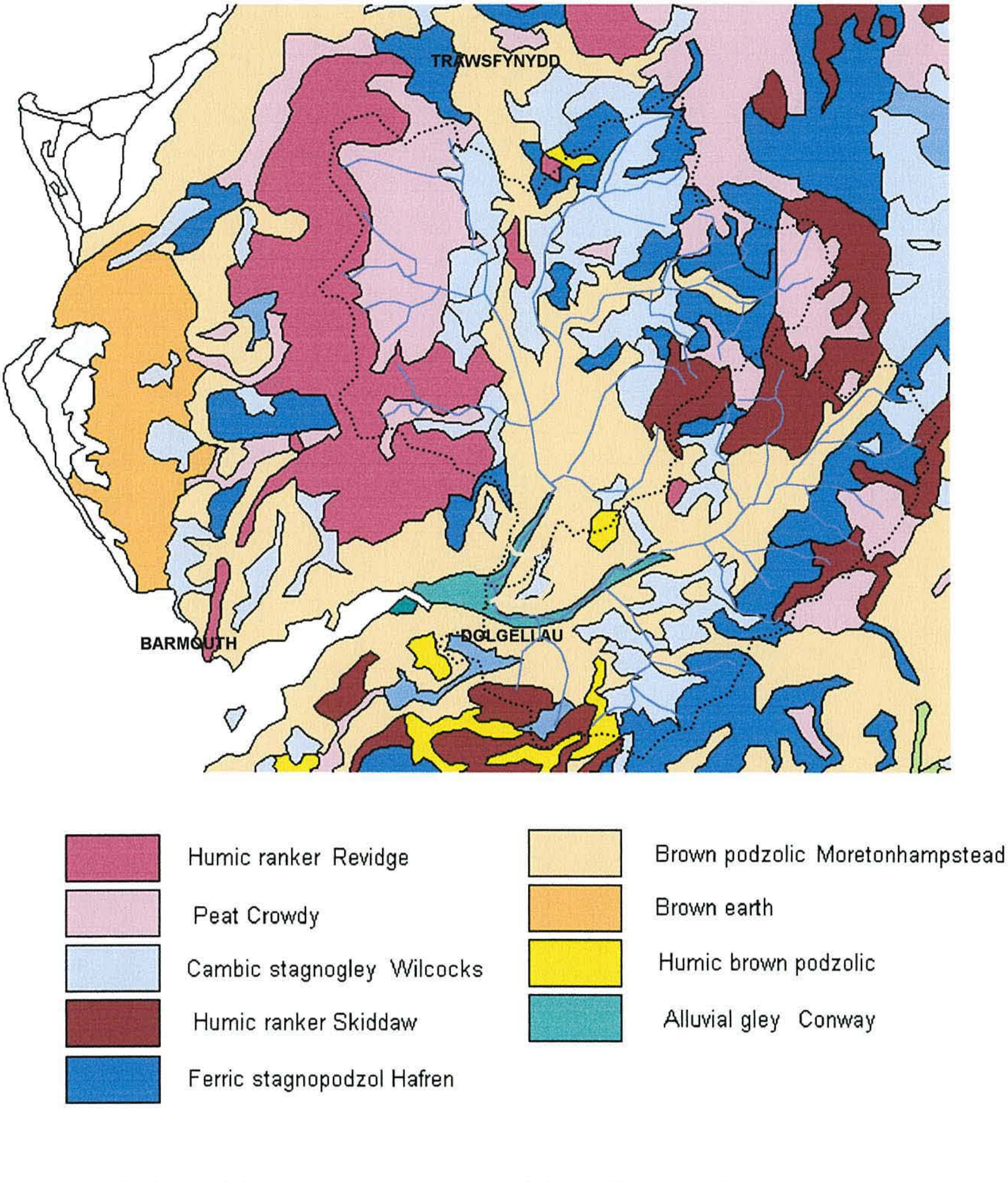

Figure 1.60. Soils of the Mawddach catchment (after Soil Survey of Great Britain)

A. Humic ranker on ignimbrite, Aran Fawddwy

B. Brown podzolic soil on diorite, Hermon

C. Stagnohumic gley on glacial till, Pared yr Ychain

D. Cambic gley on Upper Cambrian shales, Oernant

Figure 1.61. Soils of the Mawddach catchment

Brown earth. This soil type is deep, well drained and fertile. The A. horizon consists of mild humus of well-rotted plant material. Below is the B horizon composed of mineral particles, rich in iron and showing a brown colouration. The B horizon does, however, show a division into a sandy upper layer from which clay has been washed (E_b) and a lower layer where clay has accumulated (B_t); the layers are distinguished by their textures rather than colour or chemical nature. Brown earths are found in the coastal region of Ardudwy, west of the Mawddach catchment.

Podzolic soils. A podzol shows sharply contrasting soil horizons. The A horizon is dark brown or black and composed of acid humus. Below is a white or bleached horizon from which iron and other bases have been washed downwards by percolating groundwater. This removal of bases is called eluviation, and the horizon termed E_a. Below is a reddish horizon where iron has accumulated, termed the B_{fe} horizon.

If fluctuations in the water table occur during the year, the upper part of the B horizon may become aerated and an iron pan layer may form by oxidation of the accumulated iron. The C horizon consists of unaltered bedrock or glacial deposits forming the soil parent material.

The soils of the more fertile valley areas of the Mawddach catchment are brown podzolic soils, intermediate between brown earths and true podzols, showing a smaller amount of downwards leaching (fig.1.61B). A variety of brown podzolic soil with high humus content in the A horizon is found on volcanic outcrops around Cader Idris

Gley. Gley soils result from waterlogging. If water stays in the soil for a long period, the soil pores become filled and oxygen is excluded. Iron in the soil becomes reduced, giving a greenish colouration, although red mottles may be present where oxygen has been able to penetrate the soil along pores and structural cracks. Under conditions of gleying, the activity of soil microorganisms is prevented and plant material fails to decompose completely. This gives rise to peat accumulation if growth of vegetation continues fig.1.61C).

Alluvial gley soils subject to regular flooding are found in the lower valleys of the Mawddach and Wnion, and around the head of the estuary.

Cambic soils are poorly developed soils lying on bed rock at shallow depth. Where the bed rock is impermeable, gleying can occur. Cambic gley soils are found on outcrops of Cambrian shales and grits north of Coed y Brenin (fig.1.61D).

Peat soils. True peats occur in bogs and mires, where the peat reaches sufficient thickness to isolate the soil from any mineral substrate. Peat blanket bogs within the Mawddach catchment are discussed further in Chapter 3.

Hydrological characteristics of soils

The soil map above gives a general distribution, but wide variations in soil type can occur over short distances due to local conditions of slope, geology or vegetation (Pears, 1977). Typical soil sequences or *catenas* developed down hillslopes are shown in figs 1.62-1.63.

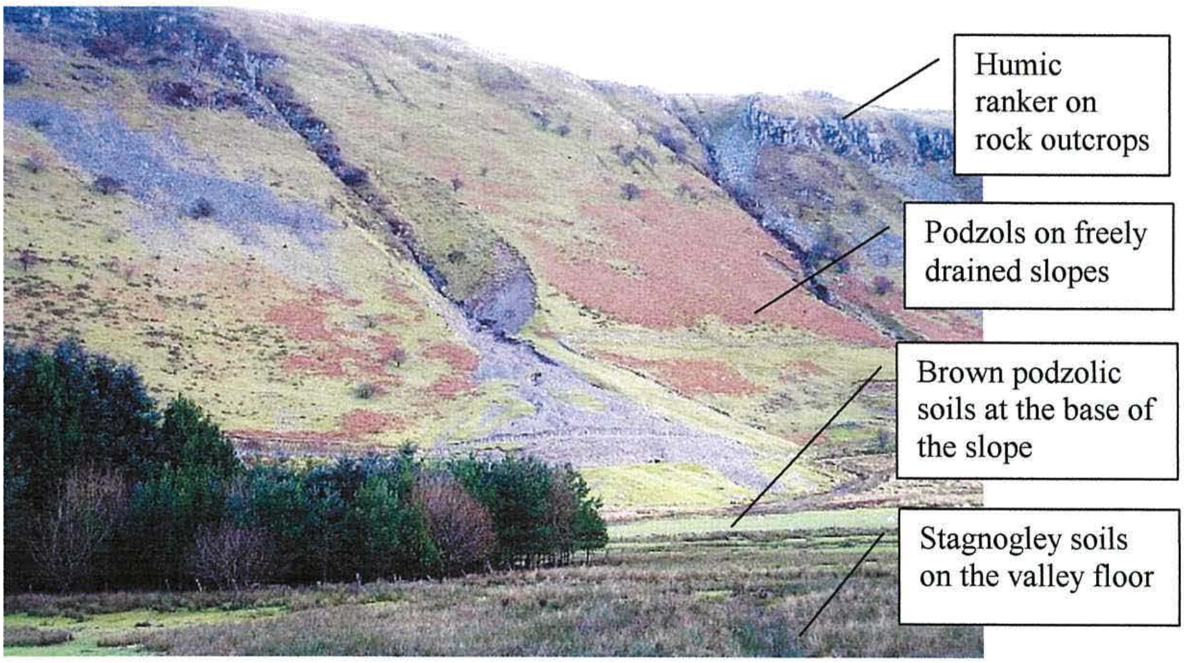

Figure 1.62. Soil catena, Allt Lwyd valley.

Ranker soils are formed on outcrops of resistant rock exposed by glacial erosion in upper mountain areas. Peaty gley podzols may develop on the gentler slopes surrounding summit plateaus where rain water runoff moves slowly towards the incised valleys.

Steeper valley slopes represent areas of rapid shallow throughflow, leading to leaching of soluble minerals and formation of podzols. Finer clay and silt particles carried down hill may accumulate on the well drained concave slopes of the valley floor to develop the thicker soil profiles of podzolic brown earths.

Flatter areas of the valley floor, especially near streams, may be subject to gleying due to a high water table for much of the year. In glaciated valleys, drainage is particularly impeded by boulder clay till or lacustrine clay deposits at shallow depth.

Gley soils of valley floors are potentially very fertile, and land drainage is commonly carried out within the Mawddach catchment to improve grass yield, both for hay and silage production and to bring forward the time in spring when grazing of the land may begin. Drainage techniques include construction of open ditches, and the installation of buried perforated plastic pipes. Agricultural modification of soil characteristics should be considered when developing a hydrological model for areas where land drainage has been carried out.

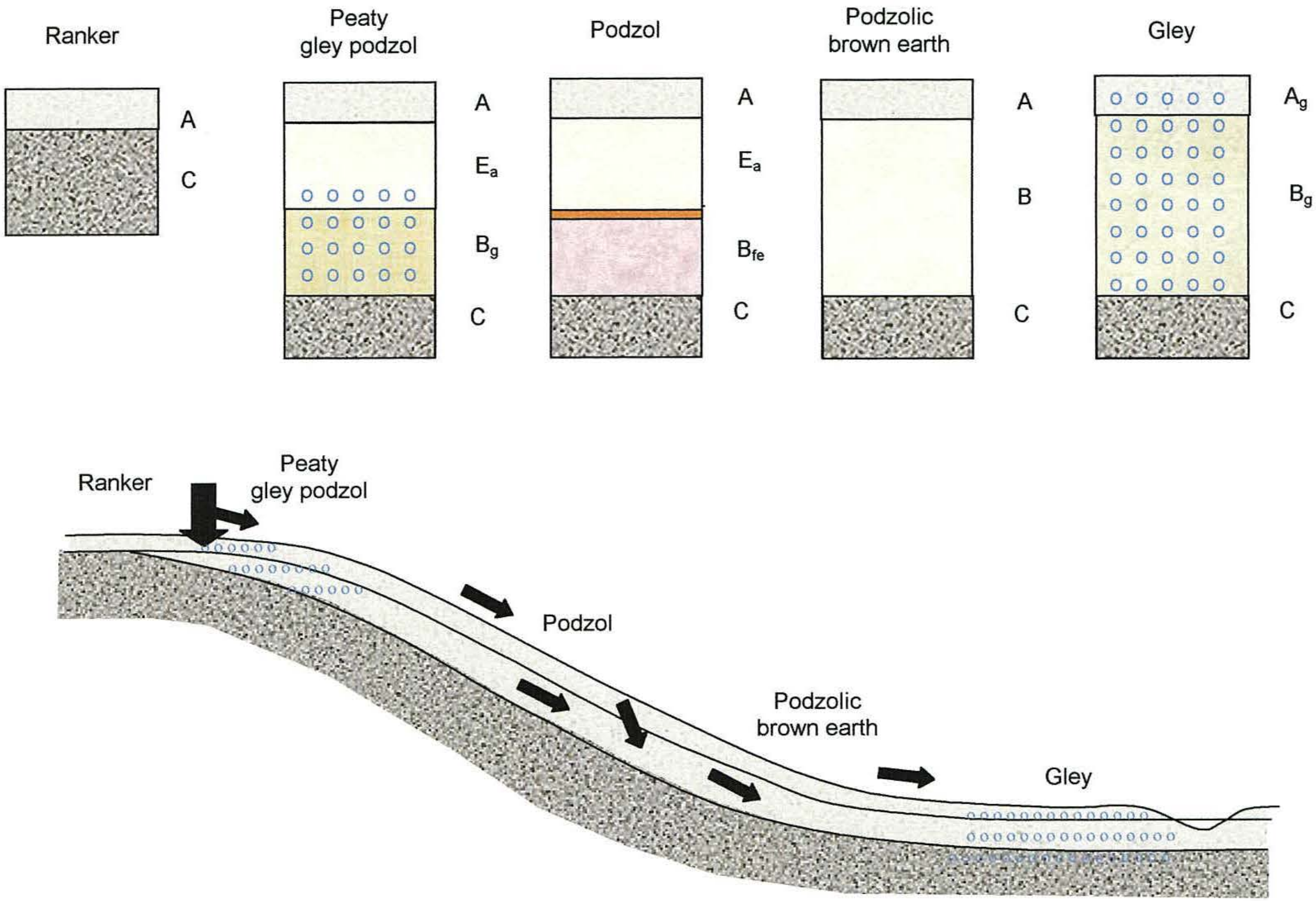

Figure 1.63. Soils in relation to slope and water movement

HOST classification scheme

The National Soil Classification system used in fig.1.60 has been developed for geographers, agriculturalists and ecologists, so does not directly address the hydrological characteristics of soils. An alternative classification known as HOST (Hydrology Of Soil Types) has been produced by the Institute of Hydrology (Boorman et al.,1995) and concerns itself primarily with the surface runoff and infiltration characteristics of soils. It is the HOST classification which has been used in the Mawddach research project.

The HOST system is based on a matrix of 11 hydrological response models identified by the letters A to K (fig.1.65). The three horizontal rows within the matrix represent the three basic hydrological pathway structures which may be present in soils:

1. Soils with a high permeability substrate in which the groundwater table is usually deep. Possible water pathways are: vertical infiltration, shallow throughflow and surface runoff. Vertical infiltration generally predominates, and surface runoff is uncommon.
2. Soils with moderate permeability substrate, so the groundwater table is generally near the surface. Possible water pathways are: addition to groundwater store, shallow throughflow and surface runoff. Shallow throughflow is predominant.
3. Soils with low permeability substrate. Possible water pathways are: slow infiltration to groundwater store, shallow throughflow and surface runoff. Shallow throughflow and surface runoff are predominant.

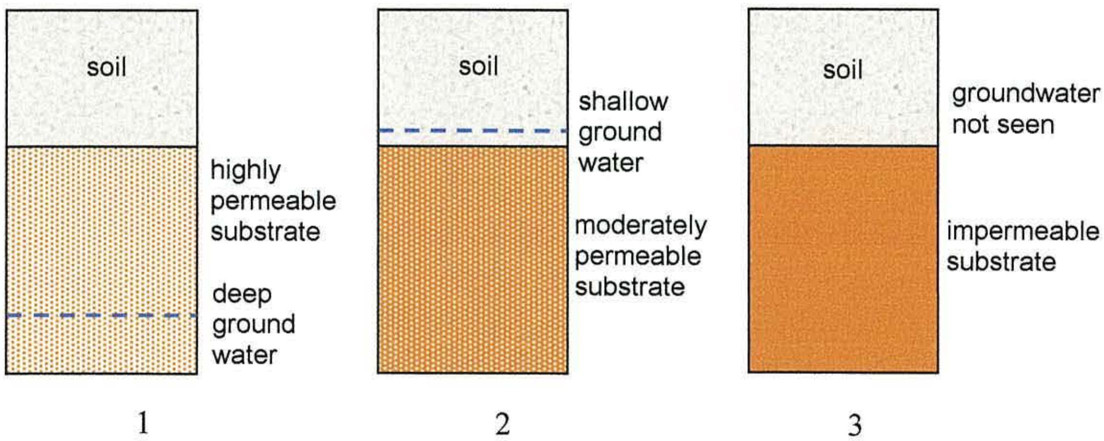

Figure 1.64. Basic hydrological classification of soils

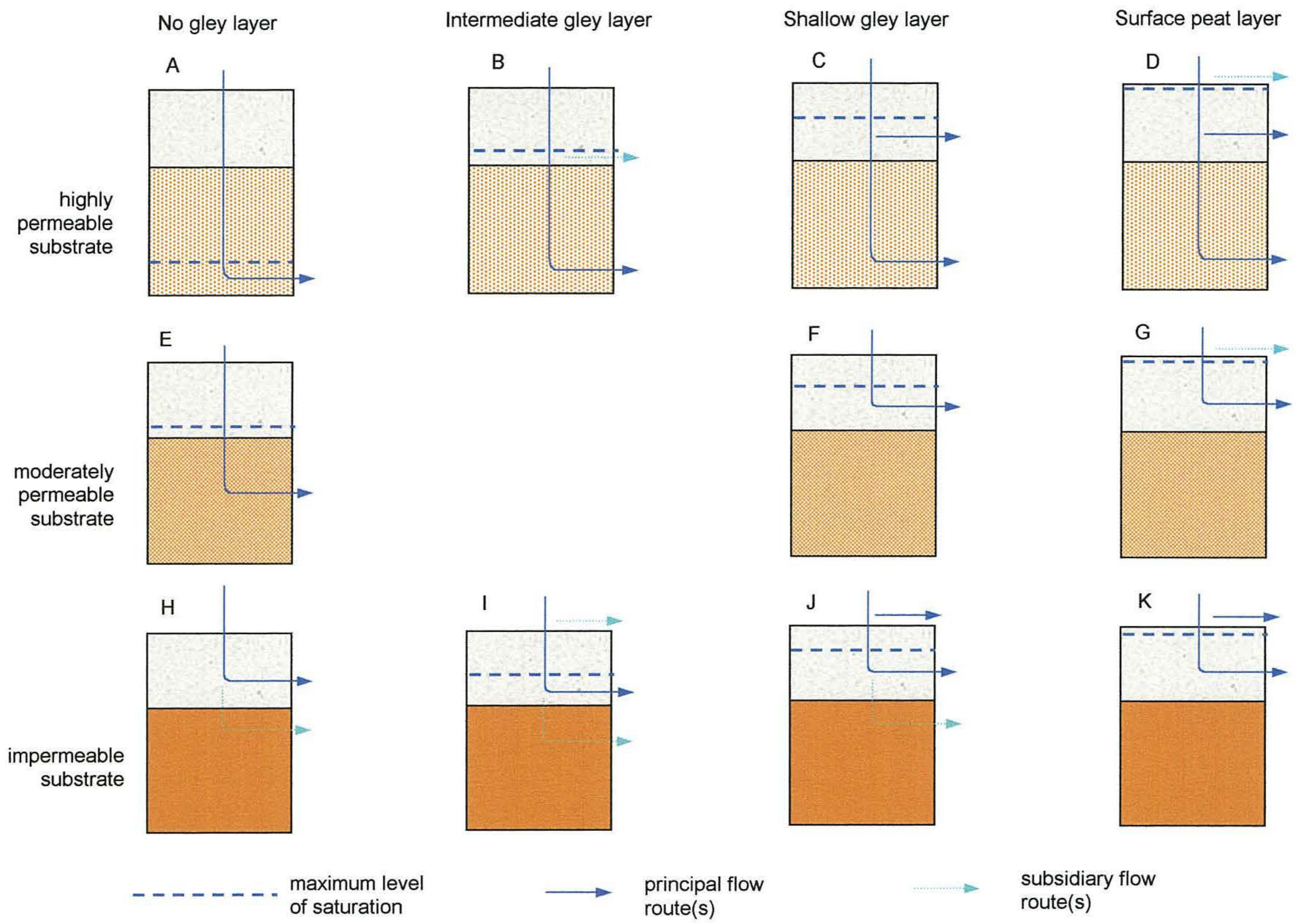

Figure 1.65. HOST hydrological response models (after Boorman, Hollis and Lilly, 1995)

The four vertical columns of the matrix of models (fig.1.65) represent progressively wetter sites within a soil catena. Column 1 contains situations with small volumes of water accumulation, allowing the level of saturation to be low in the soil profile. Columns 2 and 3 represent sites with larger volumes of water accumulation. Column 4 is the situation in which waterlogging is complete, and a surface peat layer is able to accumulate. Dominant and subsidiary water flow pathways are illustrated for the different models.

The HOST classification further subdivides the general models to distinguish a total of 29 hydrologically distinct soil classes which can be identified within Britain (fig.1.66). Only a subset of these classes is present in the Mawddach catchment.

Model A of highly permeable substrate with low water accumulation is subdivided into HOST classes 1-6 according to the substrate geology.

Integrated air capacity (IAC) is used to subdivide models F and I. This parameter is a measure of the amount of small pore space within the soil which is capable of holding water by capillary action. It is used as an indicator of saturated hydraulic conductivity for model F, and as a measure of soil water storage capacity for model I.

The HOST classification system is used in the Mawddach hillslope model as a basis for automated soil mapping and the allocation of hydrological parameters. This application is discussed in Chapter 4.

drier types intermediate wetter types

	SUBSTRATE HYDROGEOLOGY	MINERAL SOILS: Groundwater or aquifer	MINERAL SOILS: No impermeable or gleyed layer within 100cm	Impermeable layer within 100cm or gleyed layer at 40-100cm: IAC > 7.5	Impermeable layer within 100cm or gleyed layer at 40-100cm: IAC <= 7.5	Gleyed layer within 40cm: IAC < 12.5	Gleyed layer within 40cm: IAC >= 12.5	PEAT SOILS: Drained	PEAT SOILS: Undrained
permeability increases downwards	Chalk	Normally present and at >2m	1 A	13 B		14 C		15 D	
	Limestone		2						
	Weakly consolidated, macroporous, by-pass flow uncommon		3						
	Strongly consolidated, non- or slightly porous, by-pass flow common		4						
uniform permeability	Unconsolidated macroporous, by-pass flow very uncommon		5						
	Unconsolidated microporous, by-pass flow common		6						
	Unconsolidated macroporous, by-pass flow very uncommon	Normally present and at <= 2m	7 E			9	10 F	11	12 G
	Unconsolidated microporous, by-pass flow common		8						
permeability decreases downwards	Slowly permeable	No significant groundwater or aquifer	16 H	18	21 I	24 J		26 K	
	Impermeable (hard)		17	19	22			27	
	Impermeable (soft)			20	23	25			
	Eroded peat							28	
	Raw peat							29	

Figure 1.66. Hydrology of Soil Types (HOST) classification system (after Boorman, Hollis and Lilly, 1995)

Vegetation

Most upland areas in the Mawddach catchment are underlain by rocks whose character is acidic or of intermediate acidity. This, combined with a normally high rainfall, gives soils that are mainly leached and podzolic (Edgell, 1969).

Most upland pastures have been formed from ancestral oak and birch forest. Pressure on this forest area began in the Bronze Age and continued until much had been removed by the fifteenth century. Associated with this change was an increase in pastoral agriculture and in the numbers of both sheep and cattle. In the 17th and 18th centuries, sheep increased more than cattle to create sheep farming in a form and on a scale similar to today. Thus, many areas have been grazed for at least 600 years, with large scale intensive sheep farming appearing in the last 200 years.

The variation shown by the present vegetation of the uplands of the Mawddach catchment is related to two main environmental gradients, soil nutrient level and soil drainage. Vegetation classes are summarised in fig.1.67.

Bogs and mires

Impeded drainage on valley floors leads to waterlogging and gleying of soils, often accompanied by accumulation of peat where the activity of decomposing microorganisms in the soil is prevented by anaerobic conditions. Waterlogged areas can be divided into bogs, which are mainly stagnant zones of water accumulation, and mires which have a constant throughflow of groundwater carrying plant nutrients in solution. Mires are more floristically rich than bogs as they present a less chemically hostile environment (Rodwell: 1991b, 1995).

Two types of bog site are common:

- Topogenous bogs with unhumified peat occur in level basin areas where ground water accumulates.
- Ombrogenous bogs occur on gentle slopes where waterlogging results from high rainfall in conjunction with slow run-off of ground water. The peat in such sites is humified as the water table is below the surface for much of the year.

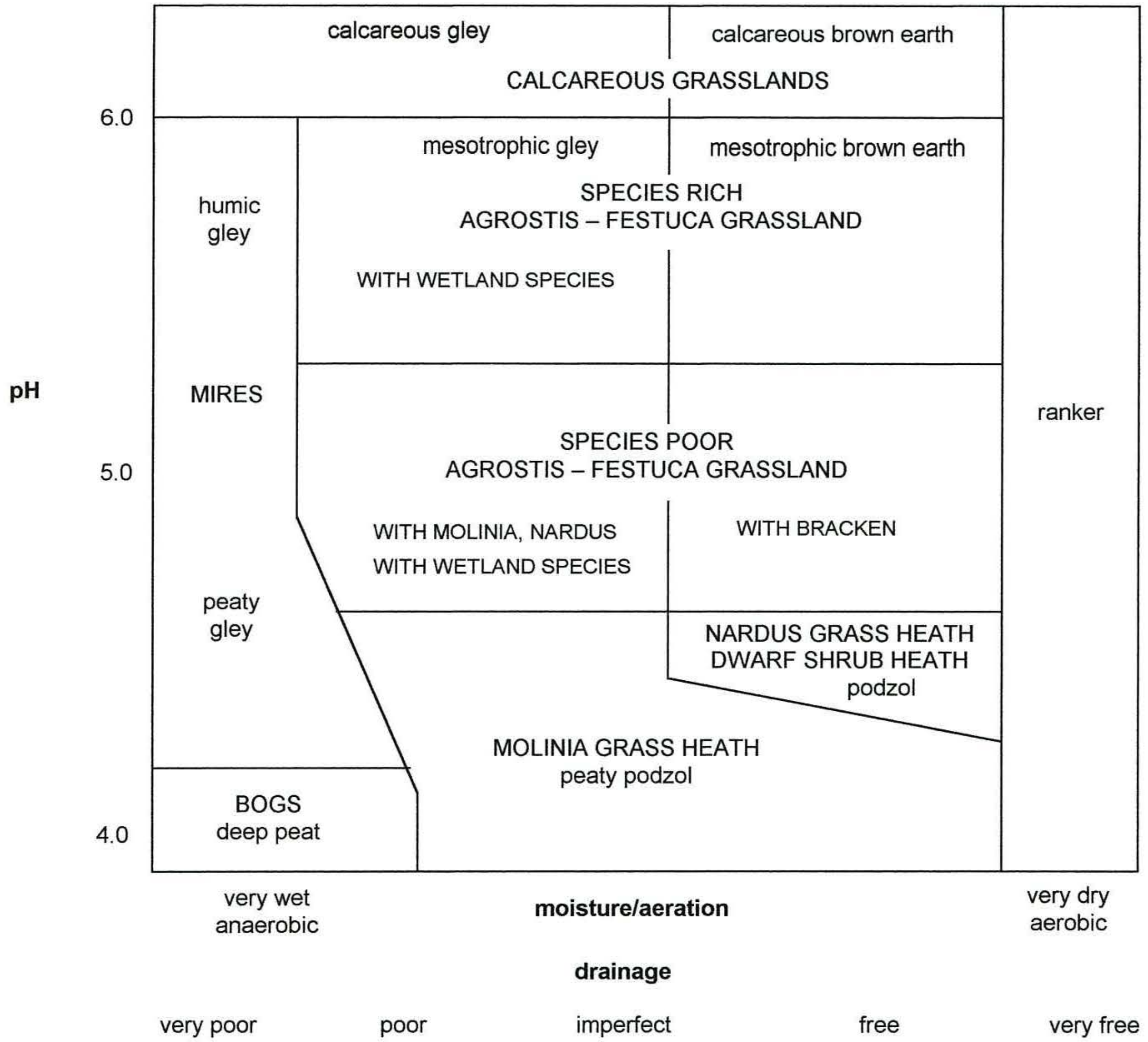

Figure 1.67. Vegetation classes in relation to soil nutrient level and drainage (after Edgell, 1969)

Topogenous bogs often occur initially around pools of open water. There will be a change in vegetation from true aquatic plants such as *Potomogeton* (pondweed) and *Nymphaea* (waterlily) to scattered plants of *Carex* and *Juncus*, and then a carpet of *Sphagnum* moss supporting *Carex rostrata* (bottle sedge). Basin sites may be covered by a community of *Sphagnum* and *Eriophorurn angustifolium* (common cotton grass) (University of Paisley, 2005).

Figure 1.68. Topogenous bog, Waen y Griafolen

Ombrogenous bogs are generally drier, and form a transition to heaths. *Eriophorum vaginatum* (hare's tail cotton grass) is often dominant, with heath dwarf shrubs in association including *Calluna, Vaccinium, Empetrum nigrum* (crowberry) and *Erica tetralix* (cross leaved heath). *Drosera*, the insectivorous sundew plant may be common.

Peat which is shallower and drier than in *Eriophorum* bogs may support a community of *Juncus squarrosus* (heath rush). *Luzula sylvatica* (woodrush) may also be important. A further species which may dominate ombrogenous sites is *Tricophorum* (deer grass).

Figure 1.69. Transition from topogenous to ombrogenous blanket bog, Waen y Griafolen.

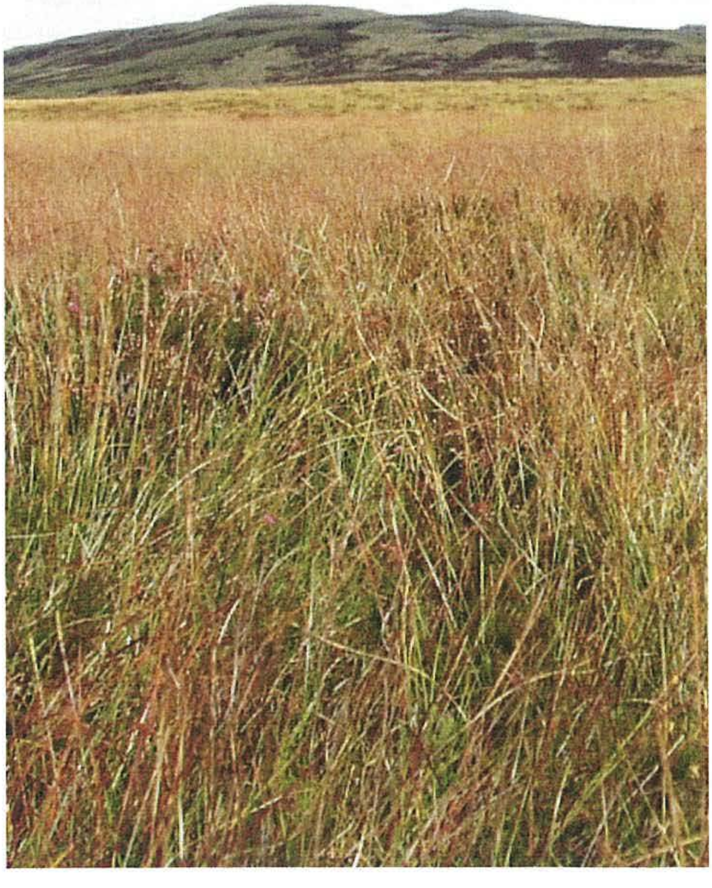

Figure 1.70. *Tricophorum* (deer grass) blanket bog, Waen y Griafolen.

Mires experience a constant throughflow of drainage water, in contrast to the more stagnant conditions of groundwater in bogs. This leads to a higher input of nutrient bases in mires, giving reduced acidity and a more favourable chemical environment for floristic diversity.

Figure 1.71.
***Carex echinata* (star sedge) mire, Llyn y Gafr, Cader Idris.**

Mires are most common on lower concave slopes which receive drainage water from the hillside above. The floristic richness of a site will depend on the rate of water flow and the geochemical nature of the surrounding area of the drainage basin. Mires range from acid sites closely resembling bogs, dominated by *Sphagnum* and *Eriophorum*, to sites with great diversity of flora including:

- *Calluna* (ling), *Erica* (cross leaved heath), *Vaccinium* (bilberry)
- grasses: *Agrostis, Festuca, Holcus, Molinia, Nardus*
- sedges and rushes: *Carex, Juncus*
- a variety of flowering plants: *Cirsium* (marsh thistle), *Galium* (heath bedstraw), *Potentilla* (tormentil), *Ranunculus* (meadow crowfoot), *Saxifraga* (starry saxifrage), *Viola* (marsh violet)
- mosses: *Hypnum, Polytrichum, Rhytidiadelphus, Sphagnum.*

Heaths

Heaths are dominated by dwarf shrubs (Rodwell: 1991b,1992). The soil is podzolic and nearly always with surface peat of pH 3.7 - 4.7. Heaths can be divided according to the dominant vegetation:

Calluna vulgaris heaths in which ling is the dominant species are widespread on well-drained scree of slope angles from 10° to 40°. In areas affected by water seepage, mosses can be important. *Hypnum cupressiforme*, however, is a moss which can dominate the ground layer even on excessively drained screes.

Figure 1.72. *Calluna* (ling) heath, Llyn Aran

On slopes of low angle where drainage is impeded, gley or pasty podzol soils develop. These support a heath vegetation dominated by *Erica tetralix* (cross-leaved heath). This damp heath can grade into bog and mire communities. Soil acidity is the factor favouring heath vegetation.

Vaccinium myrtillus (bilberry) heath is transitional between *Calluna* heath and acidic grasslands. *Vaccinium* is best developed on north-facing slopes of scree.

Figure 1.73.
***Vaccinium* heath, grading into grassland. Llyn Aran.**

Grasslands

In the upland areas of the Mawddach catchment, grasslands can be divided according to altitude into montaine and sub-montane types. These in turn are divided into communities with characteristics resulting from variations in soil moisture, soil acidity and grazing pressure (Rodwell, 1992).

- Sub-montane grasslands

  Nardus stricta grasslands (matgrass) are developed on flat plateau areas with gentle slopes where deep peat podzols and gley podzols are dominant. Wetter areas have *Viola palustris* (marsh violet) and *Cirsium palustre* (marsh thistle) present.

  Agrostis-Festuca grassland (purple moor grass - sheep's fescue) is widespread on slopes of 10° - 40° which are freely drained. The mosses *Polytrichum* and *Rhytidiadelphus* have a high cover value. *Agrostis tenuis* (brown bent) may be common.

- Montane grassland:

  Festuca-Juncus (Sheep's fescue - rush) grassland occur on the high summit plateaus where drainage is impeded.

  On drier sites, *Festuca - Cladonia* (sheep's fescue - lichen) grasslands develop.

The relationships between slope, soil type and the natural and semi-natural vegetation associations of the Mawddach uplands are summarised in fig.1.74.

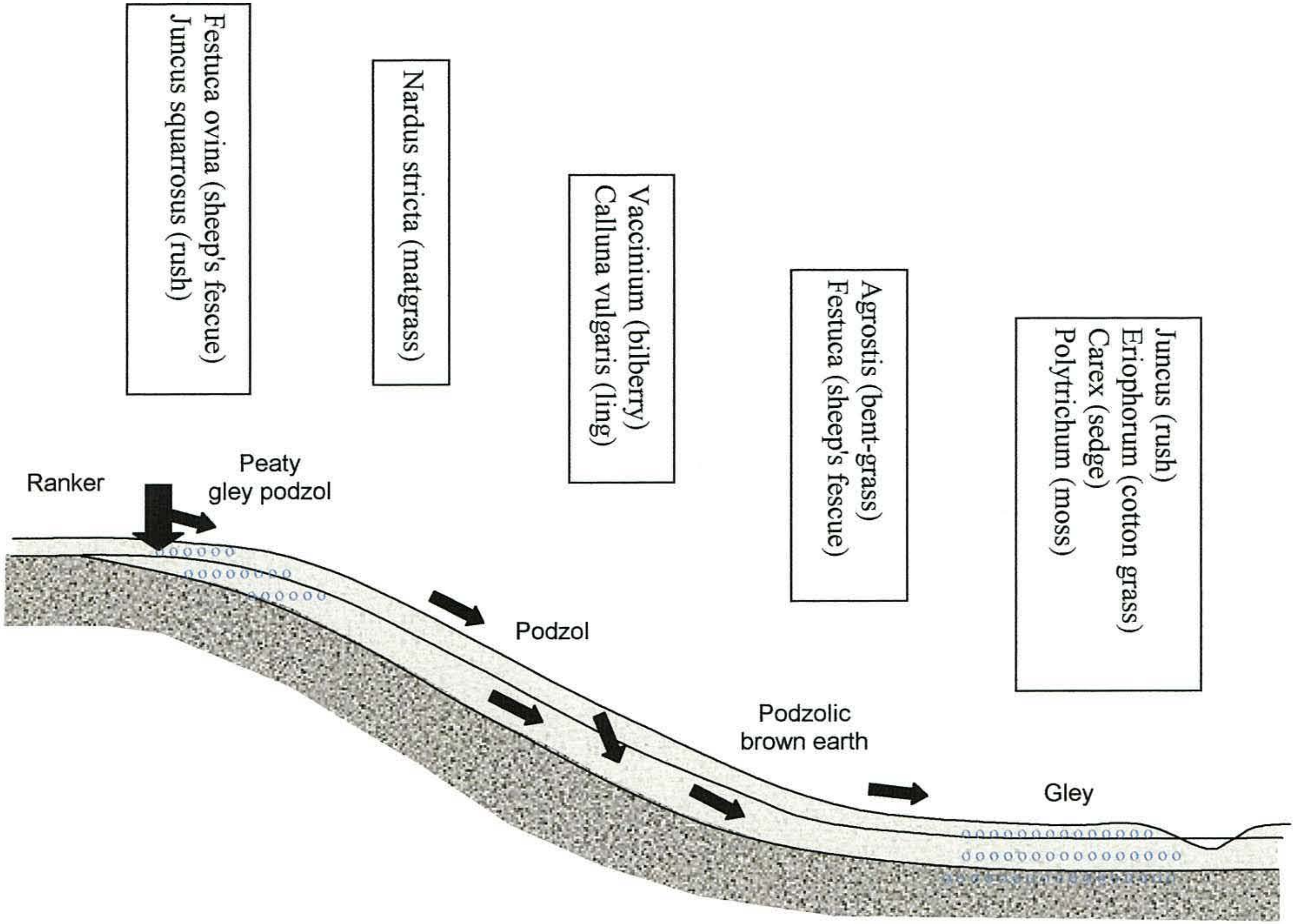

Figure 1.74. Typical vegetation associated with soil types, slope and drainage conditions

In the lower valleys of the catchment, grassland is mainly utilised for sheep and cattle grazing or production of hay and silage. Where grazing is restricted, species rich meadows can develop. Examples occur around the head of the Mawddach estuary (fig.1.75).

Figure 1.75. Species-rich water meadow in the upper basin of the Mawddach estuary, dominated by Rush, Sedge, the grasses *Agrostis* and *Deschampsia*, and a variety of flowering plants including: Clover, Marsh Thistle, Sharp Dock, Buttercup and Burnet Saxifrage.

Forestry

Relics of oak-dominated native woodlands survive in the Mawddach catchment, particularly in the gorge sections of the main rivers where their precarious sites have protected them from grazing pressures (fig.1.76). Mixed woodlands commonly occur across the riparian zones of the lower valleys, with wet woodland types dominated by willow and alder close to streams.

Commercial forestry has been developed extensively since the 1950's, establishing the conifer plantations of Coed y Brenin and the Wnion valley. In recent years, emphasis has moved from timber production towards recreational use of Coed y Brenin.

Figure 1.76: Mixed broadleaf woodland, Afon Clyweddog

Mountain bike trails around the forest are being extensively developed, in addition to encouraging use by walkers. The woodlands are increasingly being managed for their landscape and ecological value, with a move towards planting areas of broadleaves to replace conifers.

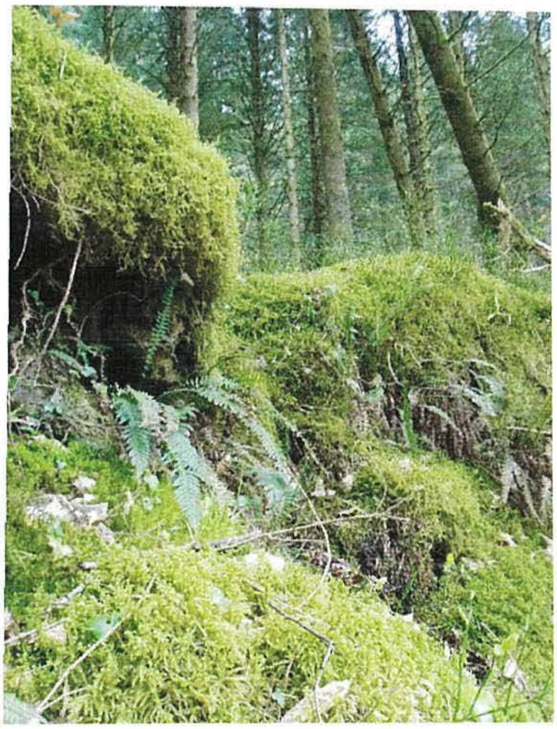

Figure 1.77:
Ground vegetation beneath a plantation of Douglas Fir, Hermon.
Mosses *Polytrichum* and *Plagiothecium* predominate.

An aspect of forestry practice which has implications for hydrological response is the age at which felling and replanting takes place. For commercial production, felling of Sitka spruce typically occurs after 34 years, with larch felled after 40 years. In areas of scenic importance, trees are being allowed to mature beyond this age, creating a higher canopy and more open forest structure. This encourages the growth of a prolific ground vegetation which may be dominated by mosses (fig.1.77).

To investigate the effects of vegetation on surface runoff production, a set of experimental sites were set up on hillslopes overlooking the village of Hermon in the Afon Wen sub-catchment. Three sites were chosen which were closely similar in slope angle and all underlain by a thick sequence of sand and gravel and clay periglacial valley infill deposits. The sites differ in land use: site 1 is a mature conifer plantation, site 2 is a clear-felled area of the same plantation, and site 3 is permanent grassland (figs 1.78-1.79).

Figure 1.78: Surface runoff experiment, Hermon. (left) Site 1 beneath mature conifer plantation. (right) Site 3 beneath permanent grassland.

Figure 1.79: Clear felled hillslope at Hermon site 2

At each site, a collecting trough for surface runoff was installed, connected by tubing to a tipping bucket gauge and data logger. Runoff was measured for storm events during a period of six months from March to September 2003. Typical results are presented in fig.1.80 and redisplayed as cumulative curves in fig.1.81.

Runoff production is significantly higher from the clear felled hillslope in comparison to the forest and grassland sites. Whilst the mature conifer plantation and grassland generate approximately equal amounts of total runoff, the cumulative curves indicate that runoff initially increases more rapidly at the grassland site with the onset of storm rainfall. In fig.1.81 this effect is first observed for the rainfall event at 18 hours, but becomes progressively more marked with the events at 28 hours and 83 hours.

It is suggested that the difference in runoff rates for the forest and grassland sites can be explained by the nature of the ground vegetation. In the case of the forest, this is composed of deep and irregular masses of moss. With the onset of storm rainfall, surface water which cannot infitrate moves downslope through the vegetation cover. Dry mosses and grasses may provide similar resistance to flow, but the soft and flexible grass cover becomes progressively less resistant to surface flow with wetting. Moss colonies have a more rigid structure and maintain their resistance to surface water flow. Fast surface runoff from grassland increases in relation to moss ground vegetation for subsequent storms within a rainfall sequence.

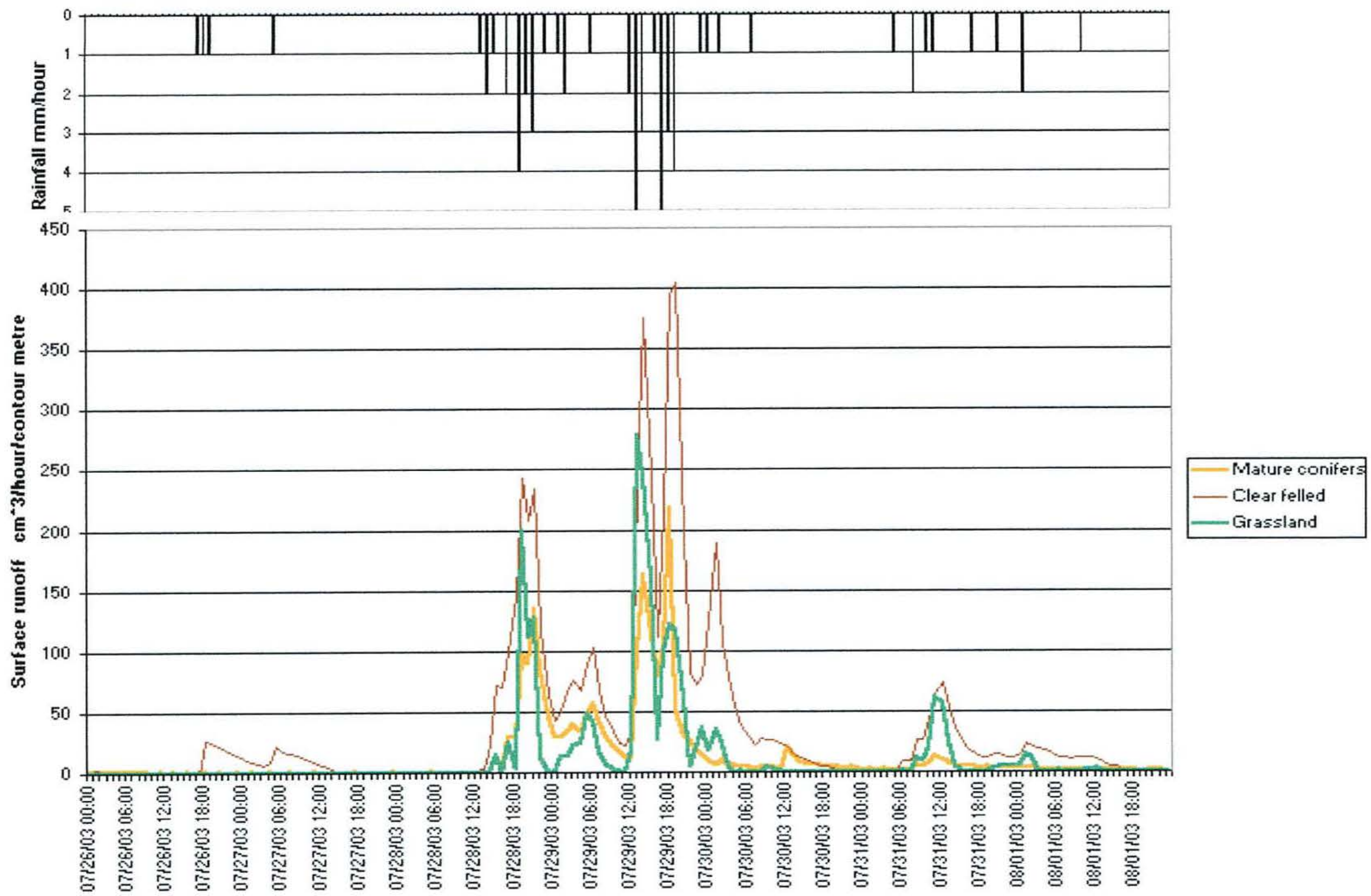

Figure 1.80: Surface runoff at experimental sites, 26 July – 1 August 2003

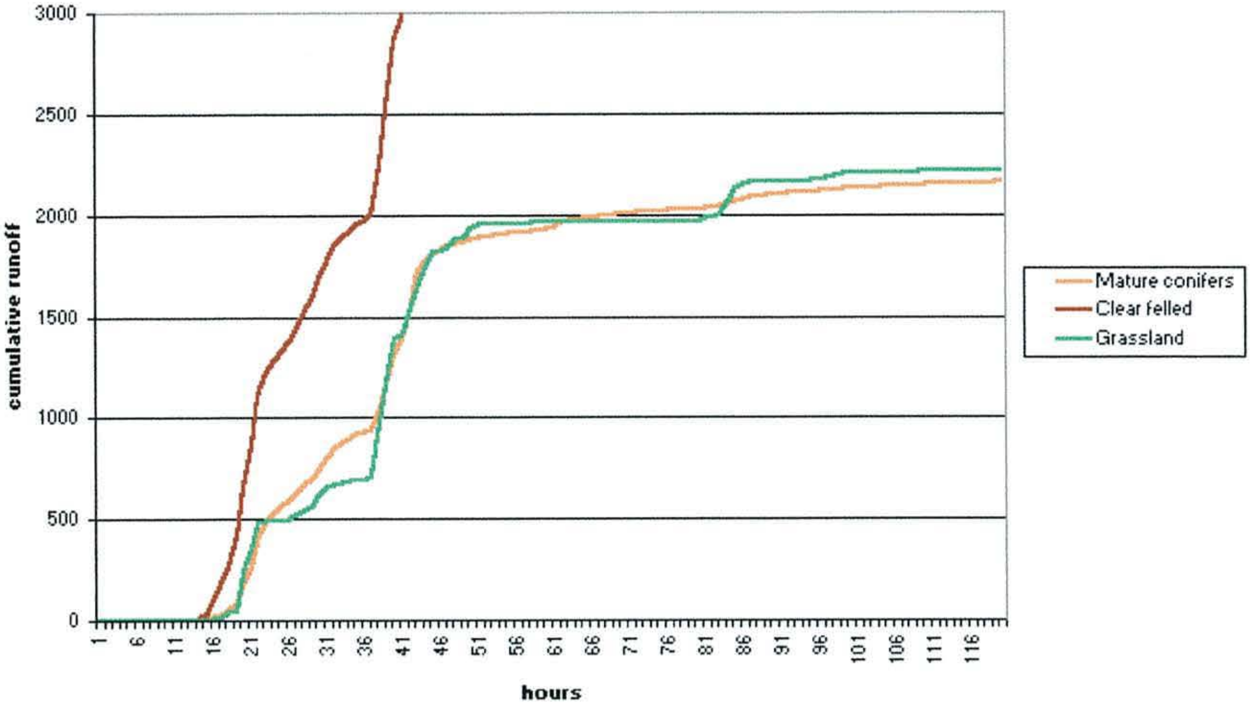

Figure 1.81: Cumulative surface runoff at experimental sites for the period 00:00h, 28 July to 00:00h, 2 August 2003

The moss cover beneath mature woodland appears to be playing a useful role in delaying surface runoff into river channels, and consequently has a moderating effect on flood peak generation downstream. It is therefore of interest to consider the conditions which encourage prolific moss growth beneath woodland in the Mawddach catchment.

A conceptual model has been developed, linking microclimate, vegetation and soil profiles developed beneath the sites (fig.1.82). Temperature and relative humidity at sites 1 and 2 have been monitored during the period of the soil runoff experiment, with example results shown in fig.1.83. Graphs of temperature are similar, but relative humidity is significantly higher within the forest, often remaining at 100% for much of the day during wet periods. The effect is to promote the growth of a prolific moss ground cover. This vegetation is able to trap slope wash sediment and adds organic material to the soil. The important role of high humidity for moss growth is discussed further by Clymo (1973).

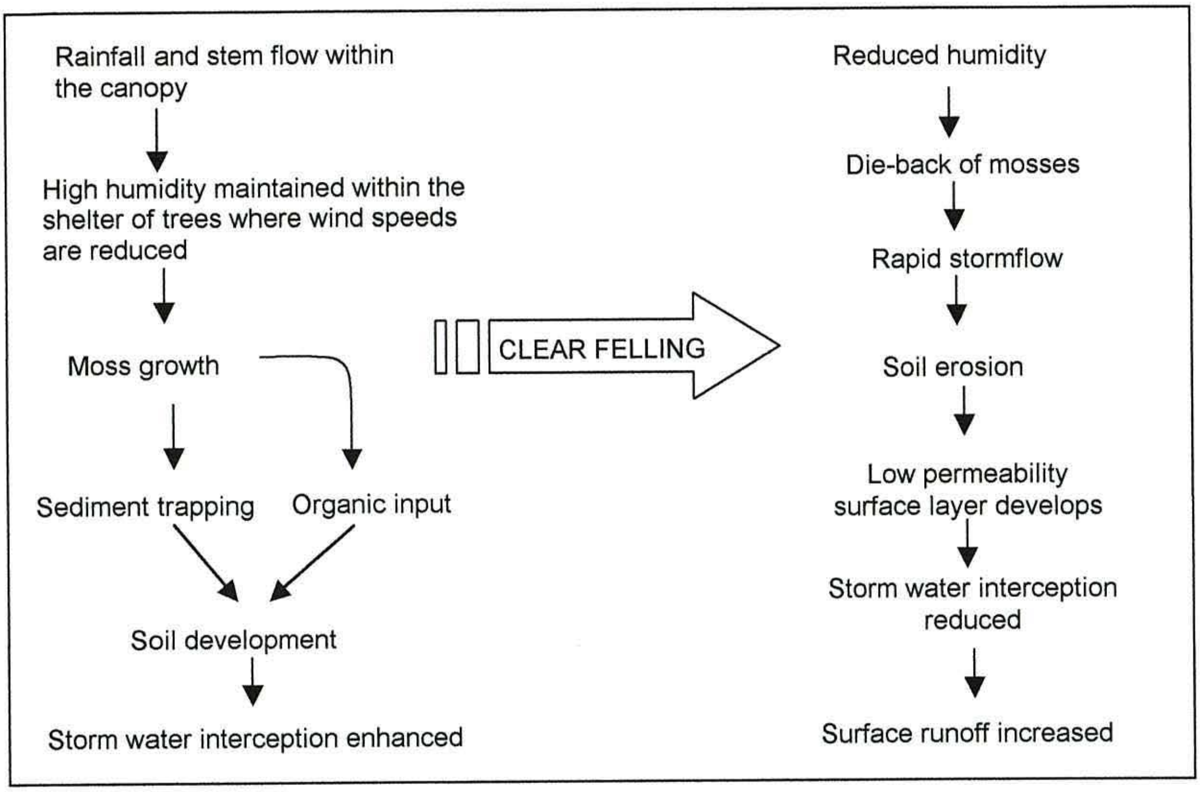

Figure 1.82: Summary of hillslope hydrology processes operating in the mature forest areas of Coed y Brenin

Figure 1.83: Humidity levels on hillslopes, measured at 50cm above the ground

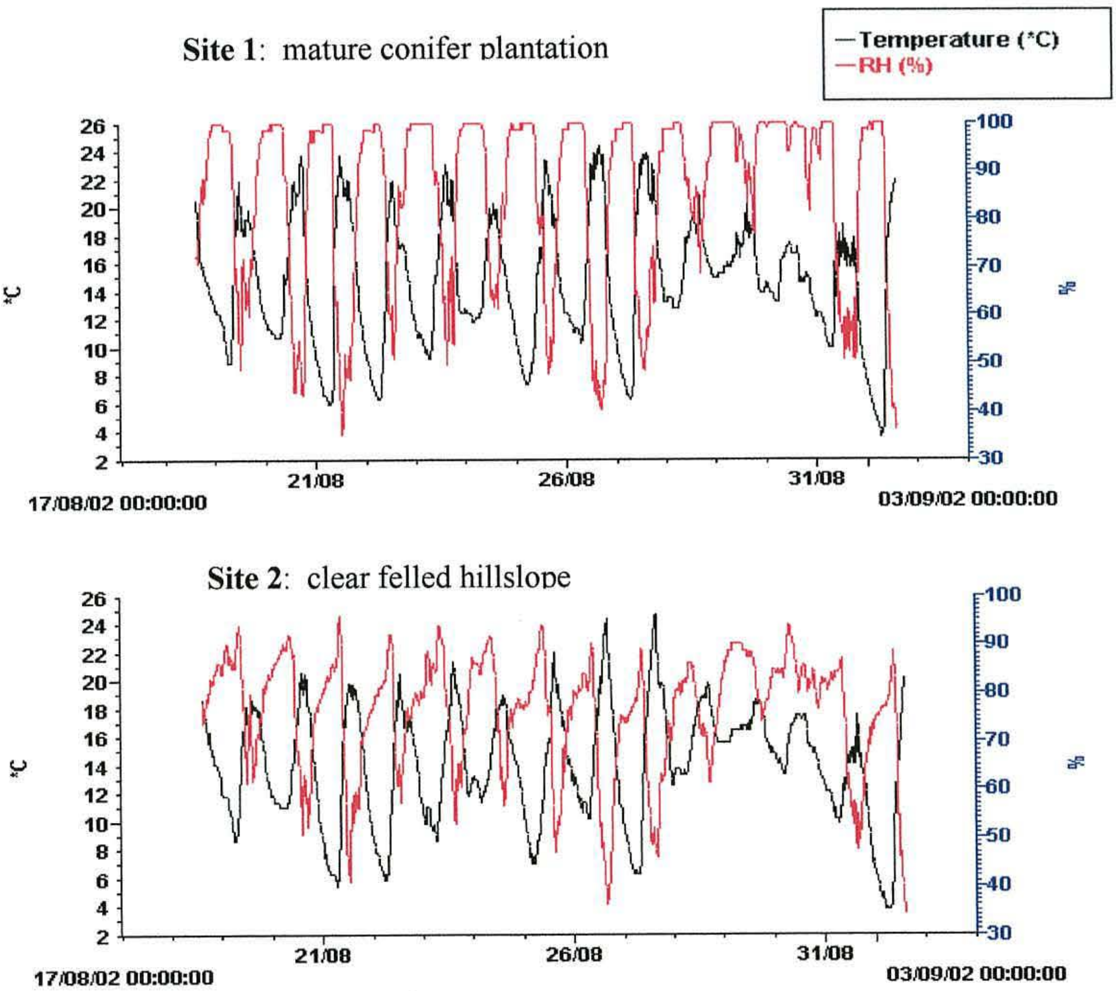

Fig. 1.84 illustrates soil profiles beneath sites 1 and 2. Over the 50 year period of forest growth, a deep soil profile of 140cm of brown earth developed at site 1. Within one year of clear felling, severe erosion removed over a metre of soil. 30cm of matted humus remains as a relatively impermeable hillslope cover.

Figure 1.84(a):
soil profile beneath forestry at site 1

Figure 1.84(b):
soil profile beneath clear felled hillslope: site 2

Soil development beneath the grassland has reached a stable profile depth of around 90cm. The limited depth in comparison to the conifer plantation may be due to less efficient trapping of downslope sediment wash by grasses.

A plot has been made of relative runoff rates for the three experimental sites, with time intervals sorted in order of increasing grassland runoff (fig.1.85). For low total runoff, the relative flow rates from the mature conifer plantation and from the clear felled hillslope can be very variable, but settle down to consistent ratios for moderate to high intensity rainfall events. Runoff is greatest from the clear felled site and least from the mature conifer site. Standardising to the runoff from grassland produces an average runoff relationship (table 1.2).

Land use	Relative runoff volume
Mature conifers	0.67
Grassland	1.0
Clear felled	2.0

Table 1.2. Relative rainfall runoff volumes from experimental sites with different land use, Hermon

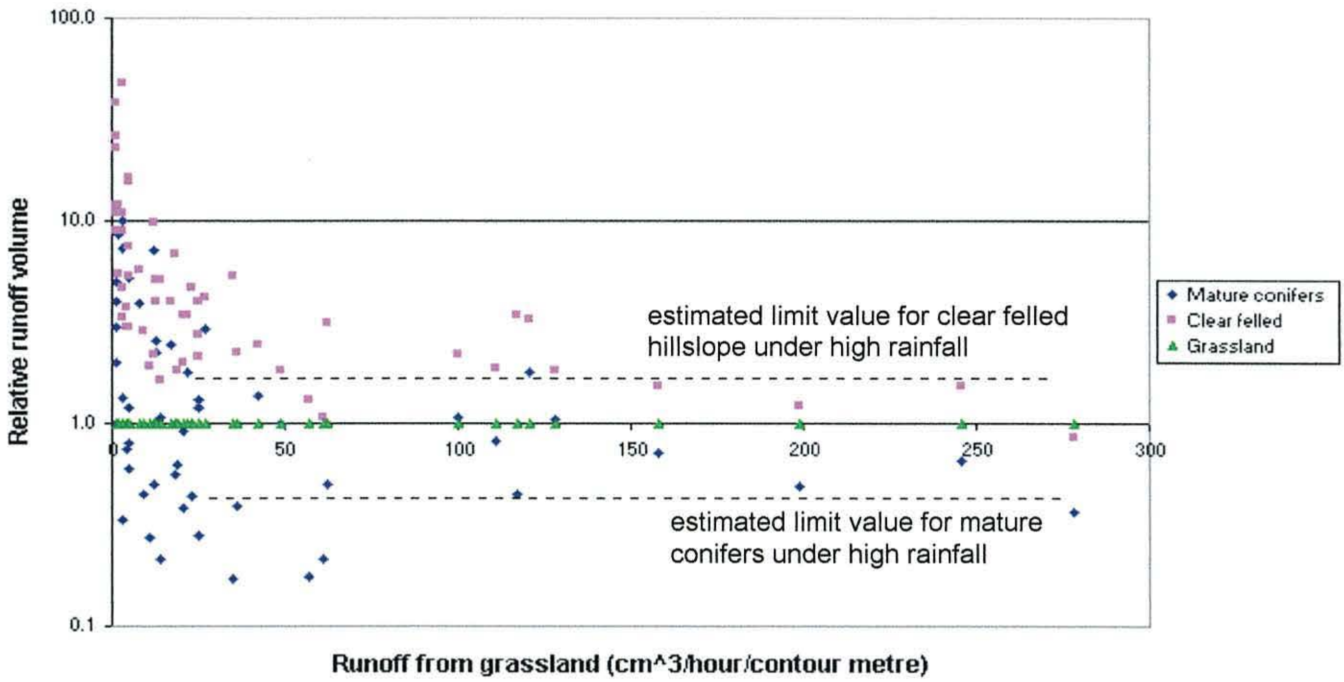

Figure 1.85: Comparative runoff rates for the three experimental sites

Within Coed y Brenin, forestry practice is moving towards continuous cover forestry with selective thinning and replanting replacing clear felling. However, extensive areas of coniferous woodland within the Mawddach catchment have been clear felled in recent years. Notable amongst these were plantations on the former Army artillery ranges in the Oernant area of the upper Afon Gain (fig.1.86). Further use of this land is hazardous due to buried unexploded munitions. Replanting with semi-natural broadleaf woodlands is planned, with wide riparian zones maintained around streams.

Figure 1.86: Clear felling of forestry plantations, Oernant

Preparing a vegetation and land use map

The hillslope hydrology models which are used in the Mawddach project require vegetation and land use data sets to be provided in both vector shape format and digital gridded format. Geographical Information System data sets of these types are available from various sources, but it was decided that a catchment vegetation and land use map should be prepared directly from field knowledge, supported by landscape photography, Ordnance Survey and Geological Survey maps, and colour air photographs at 1:25000 scale. This approach allowed greater flexibility for:

- editing land use data in response to agricultural and forestry changes within the catchment,
- developing modified data sets to investigate future land use scenarios.

The approach chosen involved two stages:

Vegetation and land use maps were prepared initially as vector shape files using the software package ***Mapmaker***. This program supports multiple layers, so that the land use map could be drawn as an overlay to an air photograph, topographic or geological map (fig.1.87). Background images in .BMP or .JPG format are registered spatially by entering Ordnance Survey grid coordinates for identified locations.

Map areas outlined as vector polygons could be assigned to land use and vegetation categories. The 17 class system of the Land Cover Map of Great Britain has been used (fig.1.88). *Mapmaker* provides convenient tools for editing; polygons may be easily merged or sub-divided, or the land use categories of polygons may be reallocated in response to land use changes in the catchment.

Vector shape files exported by Mapmaker in ArcView format are used directly in the Watershed Modelling System – HEC1 hillslope hydrology model. To use the land use map in the Mawddach integrated model, the shape file is first converted to 50m gridded data sets in ArcInfo format using ***SAGA-GIS*** software (Olaya, 2004). Very little loss of resolution occurs during the grid conversion process (fig.1.89).

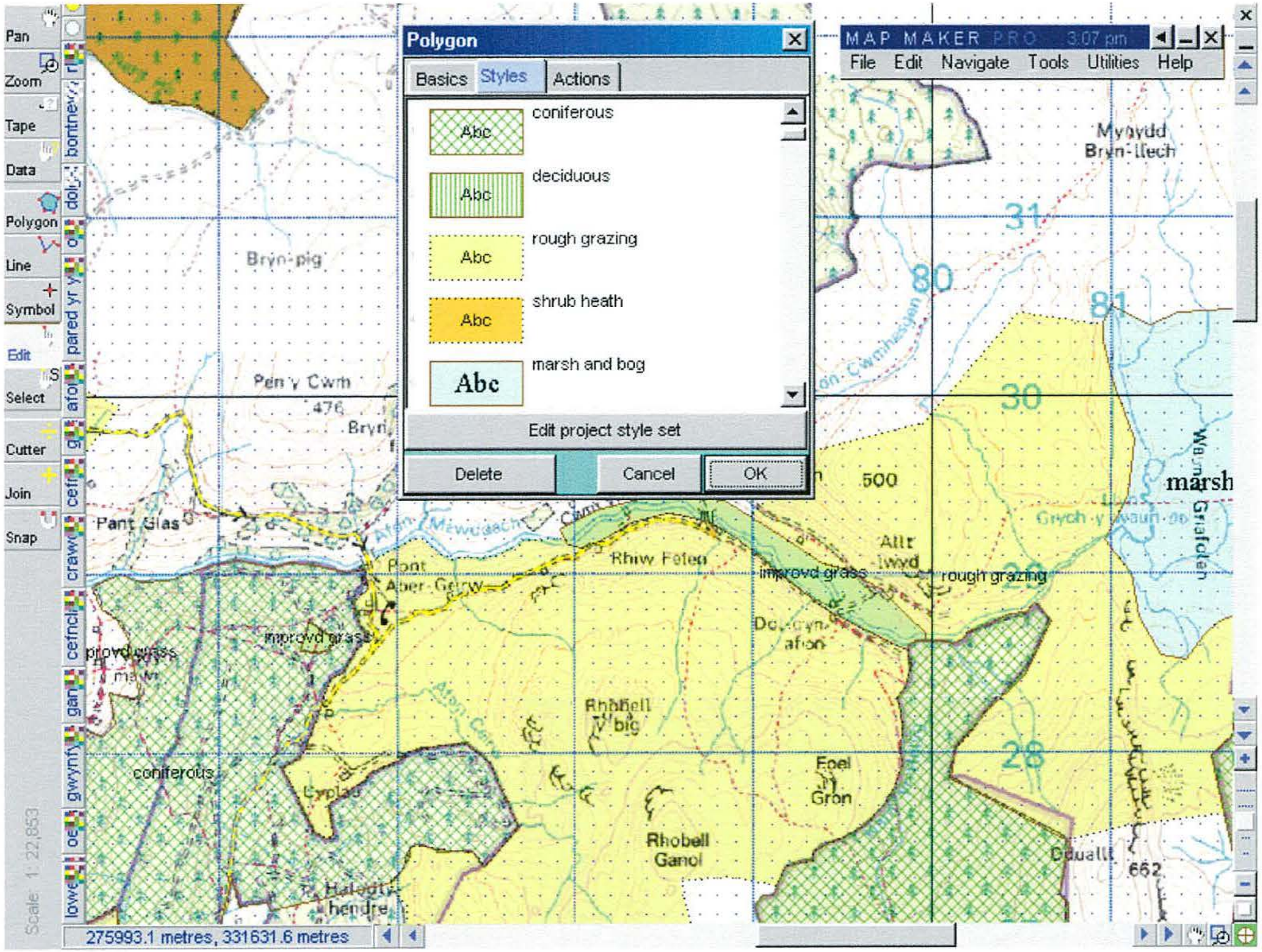

Figure 1.87: Preparation of a land use map for the Mawddach catchment using Mapmaker software

Category	Land use, vegetation
1b	Sea / Estuary
2	Inland Water
3	Beach / Mudflat / Cliffs
4	Saltmarsh
5	Rough Pasture / Grass Moor
6	Pasture / Meadow / Amenity Grass
7	Marsh / Rough Grass
8	Grass Shrub Heath
9	Shrub Heath
10	Bracken
11	Deciduous / Mixed Wood
12	Coniferous / Evergreen Woodland
13	Bog (Herbaceous)
14	Tilled (Arable Crops)
15	Suburban / Rural Development
16	Urban Development
17	Inland Bare Ground

Figure 1.88: Land Cover Categories, 17 class system
(after: Land Cover Map of Great Britain)

A simplified summary of the land use and vegetation map is shown in fig.1.90. Much of the hill land of the Mawddach and Wnion sub-catchments consists of rough grassland used for sheep grazing. Natural and semi-natural shrub heaths and blanket bogs are developed in higher mountain areas. Improved grassland is generally restricted to the lower and broader valleys and gentle hillslopes.

The extensive coniferous forest of Coed y Brenin occupies the middle course of the Mawddach, with other significant coniferous plantations on the slopes of the Rhinog and Aran mountains. Several large areas of clear felling exist at the present time. Broadleaf woodland is well developed around the lower Wnion valley, occurring as remnants of a larger area of forest. Broadleaf woodland also forms narrow riparian belts along the steep middle courses of many tributary streams, particularly where they descend in gorges incised into Tertiary erosion surfaces (cf. fig.1.76).

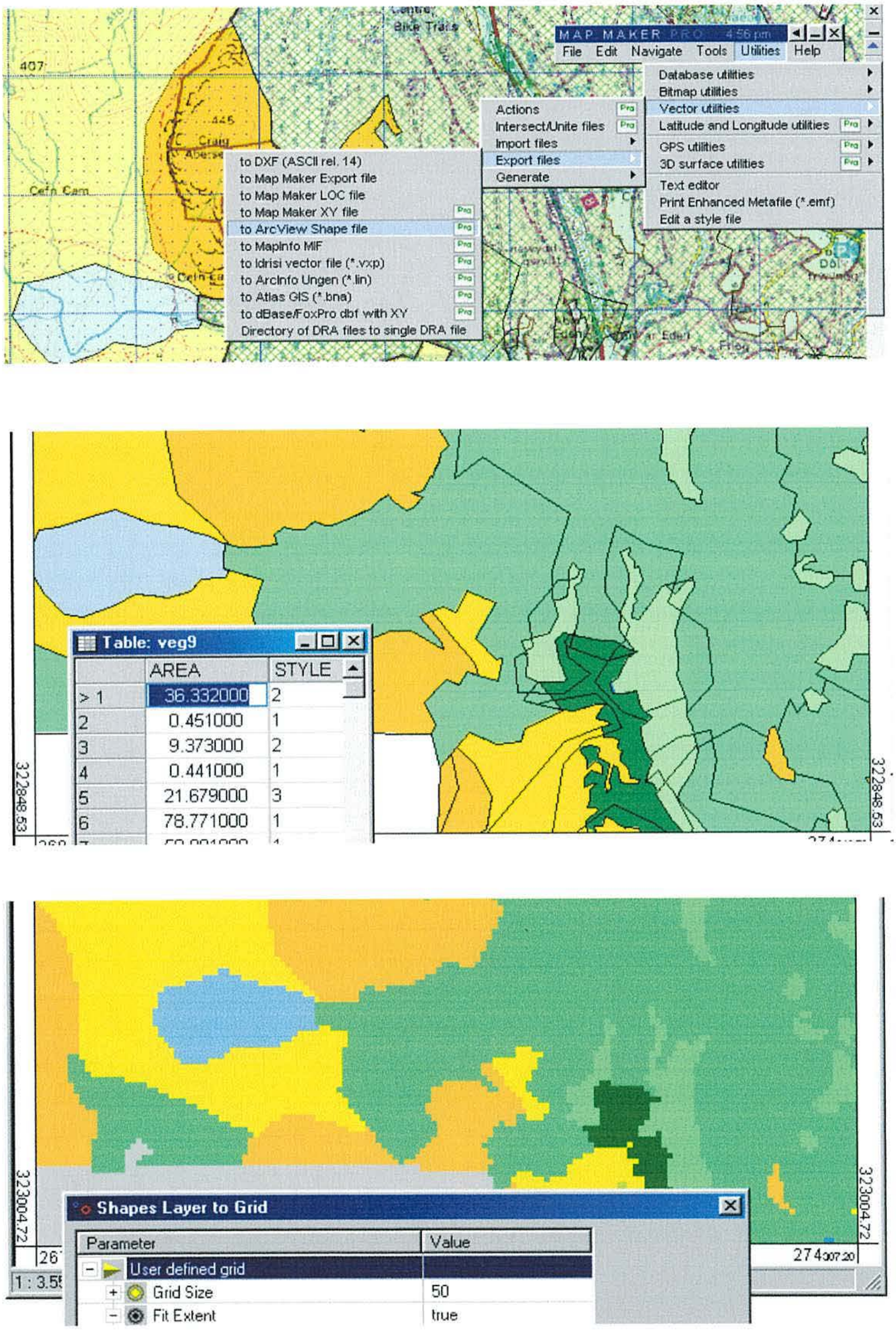

Figure 1.89: Preparation of land use data files for input to hydrological models.
Upper: conversion of Mapmaker overlay to ArcView shape file format.
Middle: shape file and corresponding database loaded into SAGA-GIS.
Lower: conversion of shape file to ArcInfo 50m gridded data using SAGA-GIS.

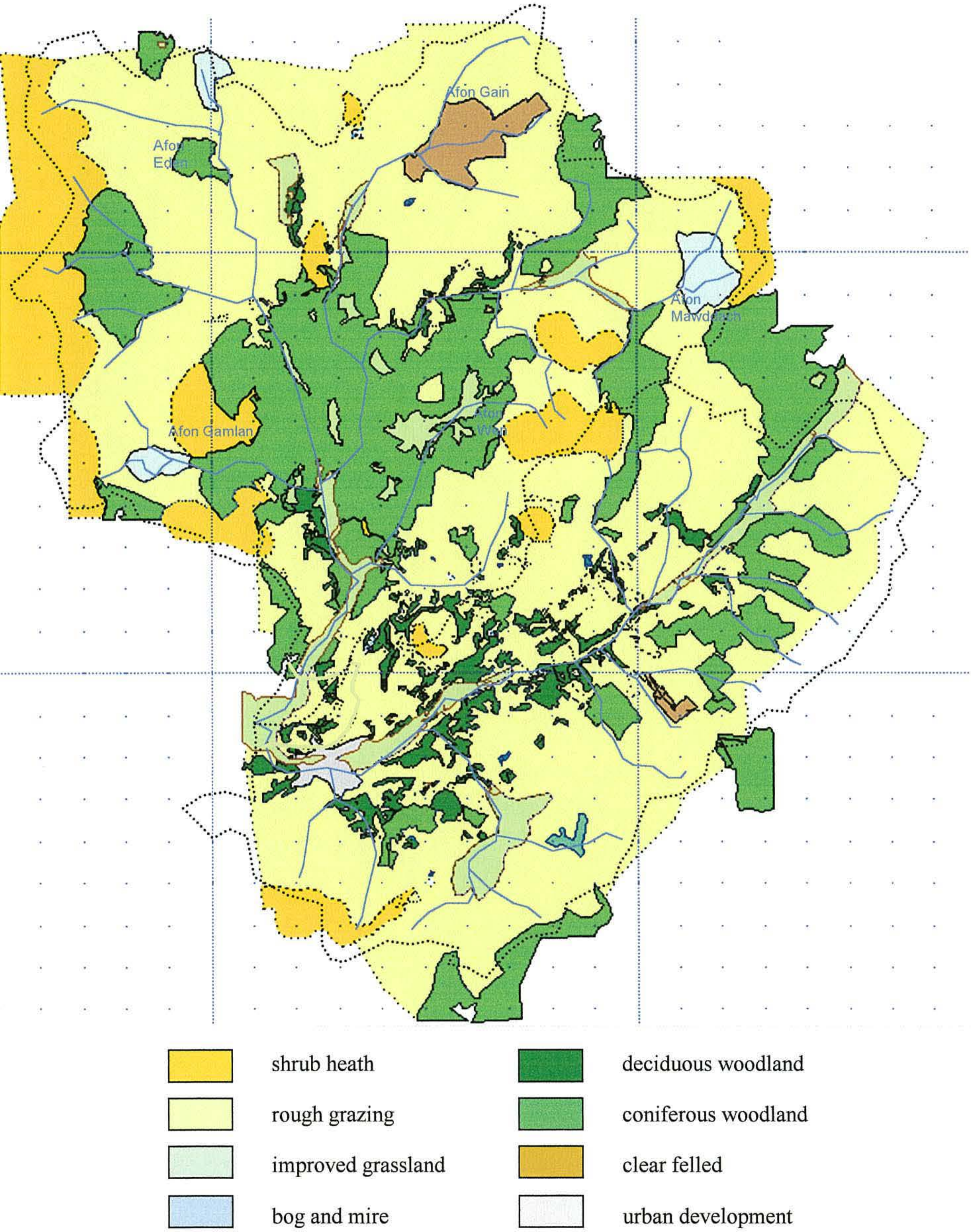

Figure 1.90: Summary of land utilisation for the Mawddach and Wnion sub-catchments

Industrial development

Metal mining

The Mawddach area is well known for metal mining, principally for gold and copper, which took place on a large industrial scale during the nineteenth and early twentieth centuries (Morrison, 1975). The Clogau and Gwynfynydd gold mines have been operated intermittently in recent years. Concerns have arisen about chemical pollution of rivers in the Mawddach catchment by drainage from mines and leakage from mineral processing operations. This issue is beyond the scope of the current modelling project. The main significance to hydrology is the presence of mine waste tips alongside rivers, where erosion during storm events can introduce large amounts of sand and gravel sediment into the river system.

Figure 1.91:
Gold mine waste tips extensively eroded during the July 2001 Mawddach flood.
(above) Gwynfynydd,
(below) Bedd y Coedwr.

In the middle course of the Afon Mawddach, extensive waste tips are present from recent mining and reprocessing at Gwynfynydd, and at the disused Bedd y Coedwr and Tyddyn Gwladys mines (fig.1.91) in the Mawddach valley within Coed y Brenin. On the Afon Wen, waste tips remain from the large Glasdir copper mine. Much sediment forming the flood plains of the lower Mawddach may have originated from mining operations over the past 150 years, when little concern was paid to environmental issues (fig. 1.92).

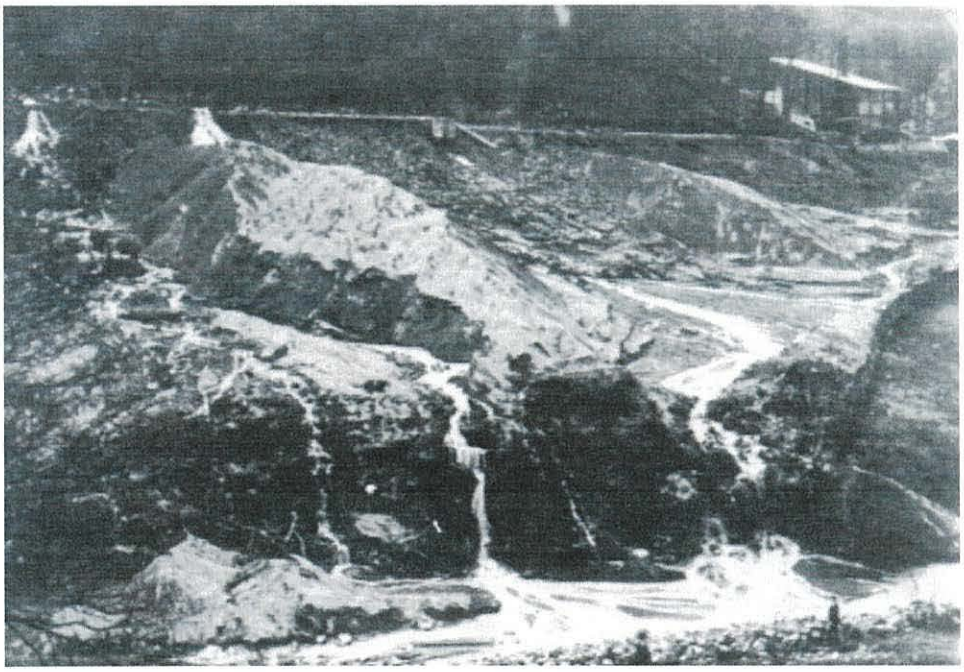

Figure 1.92: Waste tip from the ore processing mill, Glasdir, about 1900. photo: Meirionydd County Records Office.

Water supply

Two relatively small water supply reservoirs exist within the Mawddach catchment: Llyn Eithin occupies a shallow glacial basin on the slopes of Moel Oernant, and supplies the Trawsfynydd area. Llyn Cynnwch occupies a glacial basin on the interfluve between the lower Mawddach and Afon Wnion, and supplies the Dolgellau area.

Figure 1.93: Water supply reservoirs. (above) Llyn Eithin, (below) Llyn Cynnwch

Llyn Cynnwch is fed largely by groundwater from springs. Water from Llyn Cynnwch is piped to the Pen Cefn treatment works above Dolgellau. This works was re-equipped in the early 1990's. Lime is added to soften the water. The water is naturally clean, with no biological or algal contamination. Sodium hypochlorite is added as a precautionary measure. The supply for Dolgellau is gravity fed from a service reservoir at Pen Cefn. There is also a gravity supply to the main villages in the area, and down the estuary to Fairbourne.

Due to high rainfall, the levels of the two reservoirs are generally high for much of the year. In extended wet periods, the reservoirs overflow into streams. In the drought year of the 1970's there was a water shortage, so a pipeline was installed from Dolserau on the Afon Wnion to pump water up to Llyn Cynnwch. Abstraction is only permitted under Environment Agency licence when river levels are high, usually in the winter months. In practice, the pumped supply is rarely used.

The volume of water abstracted within the Mawddach catchment for domestic use can be estimated. Average per capita water use in Britain is 150 litres per day (OFWAT, 2008). The main centre of population in the Mawddach catchment is Dolgellau, with a total of 2,678 inhabitants at the 2001 census. The remaining area of the non-tidal Mawddach catchment is sparsely populated upland, so an upper limit for the total population may be taken as 5,000. Abstraction to meet the water needs of this population would be $750m^3$/day, representing a diversion of water from river flow of only $0.008m^3s^{-1}$. In a hydrological model, the amounts of water supply abstraction directly from Llyn Eithin and Llyn Cynnwch, or indirectly from the Afon Wnion, may therefore be considered negligible.

Ardudwy leat system

An engineering scheme having a significant effect on hydrology within the Mawddach catchment is the system of leats constructed to augment water supply to the Maentwrog hydro electric power station.

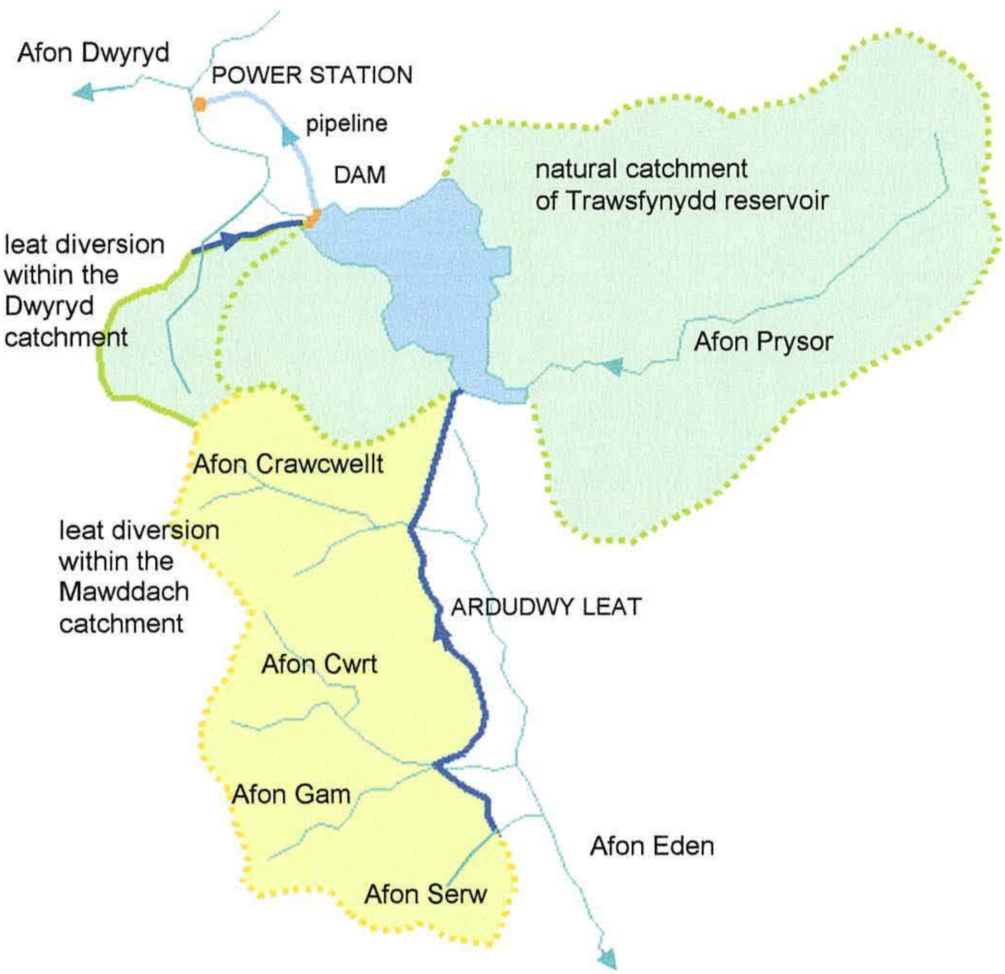

Figure 1.94: The Maentwrog hydroelectric power scheme

The purpose of the leat system is to divert water from the headwaters of three streams draining the eastern scarp of the Rhinog mountains, and carry the water into Trawsfynydd reservoir. The effect is to remove water from the Mawddach catchment and transfer it over the interfluve into the Glaslyn catchment.

Water abstraction occurs at a series of weirs, with water releases into the streams maintained at an agreed level to support fish stocks downstream.

Figure 1.95:
Cwrt weir

Figure 1.96:
Downstream discharge into the Afon Cwrt

Figure 1.97:
Ardudwy leat, between Cwrt weir and Crawcwellt weir

The Ardudwy leat which discharges into the south west corner of Trawsfynydd reservoir intercepts flows from the headwaters of the

- Afon Serw - catchment area 2.5 km^2
- Afon Gam – catchment area 6.3 km^2
- Afon Cwrt (south Crawcwellt) – catchment area 8.2 km^2
- Afon Crawcwellt (north) – catchment area 8.5 km^2

The Ardudwy leat starts at Serw weir which is 7km south of Trawsfynydd reservoir. A 1.5km underground aqueduct connects the Afon Serw and Afon Gam, and a further 300m underground aqueduct links Gam weir to the Afon Cwrt. Between Cwrt weir, Crawcwellt weir, and Trawsfynydd reservoir, the Ardudwy leat is a concrete lined open channel (fig.1.97).

At Cwrt and Crawcwellt weirs there are sluice gates that can be opened to release all the water to the natural courses of the streams or to divert all but the prescribed flow into Ardudwy leat.

The design capacity of the Ardudwy leat increases from $0.8m^3/s$ at Serw intake, to $6.0m^3/s$ near Cwrt weir, to about $8.5m^3/s$ between Crawcwellt weir and the reservoir. When flows to the leat exceed the values quoted, the excess runoff spills to the River Eden, either over the spillweirs at the four stream intakes or from one of the small overflow structures which are spaced at intervals along the length of the open section. The maximum possible inflow to Trawsfynydd reservoir from the leat is calculated to be $10m^3/s$.

The prescribed flows which must be maintained in the natural watercourses according to the North Wales Hydro Electric Power Act of 1952 are:

Afon Serw	6 litres/s
Afon Cwrt	41 litres/s
Afon Crawcwellt	248 litres/s

which amounts to a total discharge of approximately $0.3m^3/s$.

Exact data on the operation of the Ardudwy leat during individual storm events is not readily available, but longer term statistical data is available (Binnie and Partners, 1985).

The average flow into the reservoir from the Ardudwy leat over the period 1963 to 1984 has been estimated as $1.77m^3/s$. During this period, the average total inflow to the reservoir was $3.94m^3/s$, so the contribution from the Ardudwy leat is approximately 50% of the total reservoir inflow.

Maximum monthly average inflows to the reservoir during the 1963-1984 period from its whole catchment were:

Month	inflow (m^3/s)
Dec 65	13.36
Oct 68	13.19
Oct 81	10.97
Nov 77	10.67
Dec 66	10.67
Nov 82	10.56

We may assume that the Ardudwy leat contributed 50% of the total monthly flows. The leat would have been operating at approximately 70% of maximum capacity during these high rainfall months.

Considering the available data, the following rules will be used to model the sub-catchment of the Ardudwy leat:

- During low flow periods with less than $0.5m^3/s$ discharge, all water flow will be directed into the Afon Eden.

- For discharges between $0.5m^3/s$ and $12.5m^3/s$, 75% of the flow in excess of the first $0.5m^3/s$ will be directed into the Ardudwy leat and lost from the Mawddach catchment. The remaining 25% of excess flow will be directed into the Afon Eden.

- Maximum flow on the Ardudwy leat is assumed to be 9 m^3/s. Once this flow is reached, all excess will be directed into the Afon Eden as spillway overflow at the weirs.

These rules are illustrated in the graph of fig.1.98.

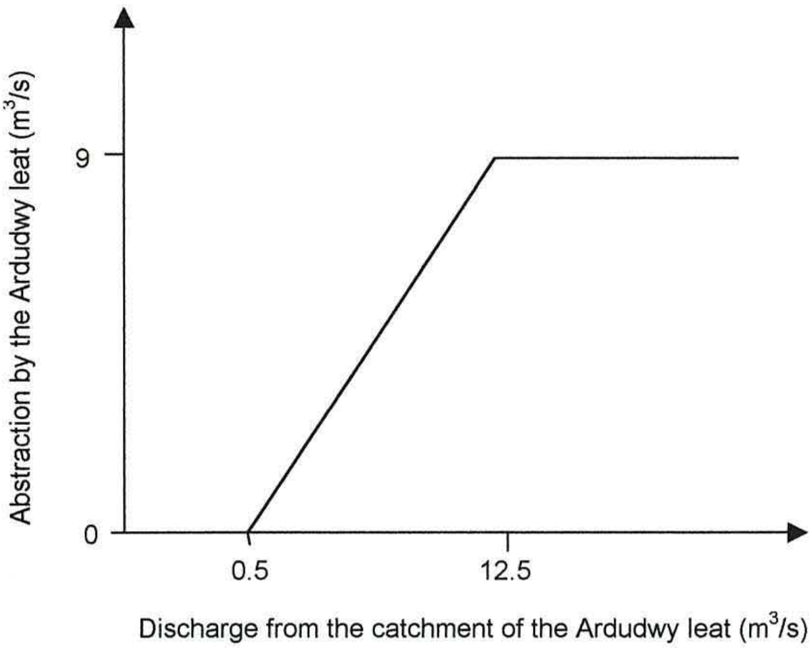

Figure 1.98: Assumed model for Ardudwy leat abstractions

Summary

The reconnaissance study carried out in the previous sections provides a conceptual basis for a hydrological model of the Mawddach catchment. The following characteristics of the catchment are considered relevant to the design of a model:

- The highest ground is formed by Cambrian grits and Ordovician volcanic rocks. Of these, the Cambrian grits generally have a higher permeability due to massive jointing. Higher mountain areas of Cambrian grit and Ordovician volcanics are covered by thin humic ranker soils.
- Less resistant sandstones, siltstones and mudstones occur in the Cambrian, particularly towards the top of the succession, and are also found interbedded with Ordovician volcanic rocks. These materials form valleys or lower ground on mountain flanks. Thin cambic soils often occur on the sedimentary outcrops, and may be gleyed due to low bed rock permeability.
- Glacial till, periglacial fluvial and solifluction deposits are common in the Mawddach catchment, particularly within deep valleys. These materials vary widely in hydrological properties. Boulder Clay impedes drainage, producing stagnohumic gley soils, whilst periglacial sands and silts encourage formation of better drained brown podzolic soils. Glacial and periglacial materials are readily eroded to provide river sediment during storm events.
- Major river valleys within the Mawddach system are aligned along geological faults. Reactivation of faults has led to zones of multiple sub-parallel fractures enclosing shattered rock. These fracture zones may facilitate river – groundwater interaction.
- Multiple phases of uplift during Tertiary times have produced a stepped landscape, with river rejuvenation and knick points evident on most main streams of the Mawddach system.
- River reaches within the Mawddach system exhibit a range of morphological characteristics within the general downstream progression of reach types: colluvial, cascade, step pool, plane bed, pool riffle, dune ripple. Classification of reaches can help in assigning appropriate hydrological parameters for river flow modelling.

- Natural vegetation within the catchment varies from bogs and mires, heaths and grasslands to broadleaf woodlands. Extensive conifer plantations are present, and some areas of grass land have been improved by drainage. Each of these vegetation zones has its own characteristic hydrological response.
- The presence of mature forest, whether broadleaf or coniferous, can lead to deepened soil profiles and reduced runoff. The development of prolific ground vegetation dominated by mosses may be important to this process.
- HOST soil classification can specify the dominant pathway(s): surface runoff, shallow throughflow, or infiltration to groundwater, at a particular hillslope site.
- The Ardudwy leat system is responsible for abstraction of water from an area of the Mawddach catchment. A model is given for abstraction rates in relation to sub-catchment runoff.
- Mining activities within the Mawddach catchment produce waste tips which are readily erodable sources of sand and gravel river sediment.

2. Meteorology

2.1 Meteorological Principles

The hydrological response of the Mawddach catchment is clearly dependent on the timing, distribution and intensity of rainfall during individual storm events, and the conditions of the ground as a result of antecedent rainfall. Aspects of meteorology affecting rainfall over western Britain are outlined in this section. An important component of the Mawddach hydrology project is the development of a rainfall model for the catchment. The setting-up and evaluation of this model will be discussed in section 2.4.

Rainfall in western Britain is mainly associated with the passage of low pressure centres termed *Mid-latitude Cyclones* or *Depressions*. To understand the air flow patterns around a low pressure centre, it is necessary to consider the effects of the Coriolis force (fig.2.2). This is an apparent force due to the rotation of the earth which deflects moving bodies towards the right in the northern hemisphere. Air will tend to move from areas of high pressure towards areas of low pressure. As air is flowing towards a low pressure centre in the northern hemisphere, it will experience Coriolis deflection to the right. This induces a spiral track towards the centre (fig.2.1a). If the pressure forces should become exactly balanced by the Coriolis force, winds will circulate in a direction perpendicular to the pressure gradient and are termed *geostrophic winds* (fig.2.1b). In the southern hemisphere the direction of rotation towards a low pressure centre is reversed to produce clockwise motion.

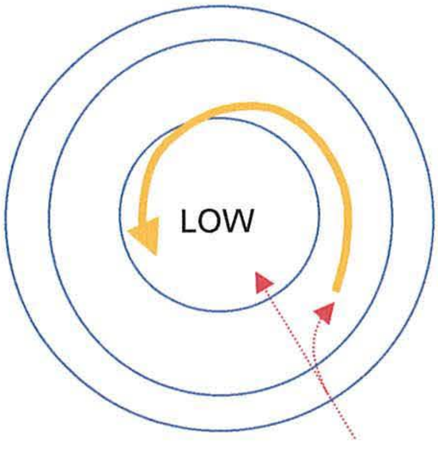

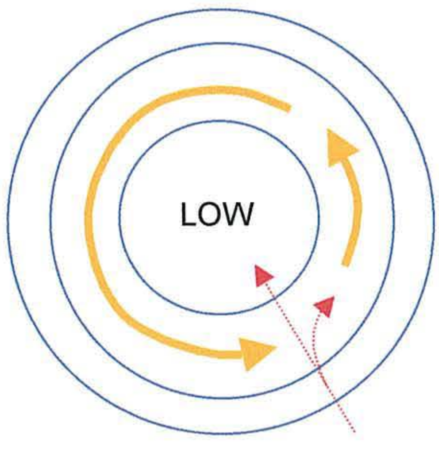

Figure 2.1a (left): Coriolis deflection of winds approaching a low pressure centre in the northern hemisphere.
Figure 2.1b (right): Geostrophic winds developed around a low pressure centre.

The Coriolis force is an apparent force experienced by a body due to the rotation of the Earth.

Imagine a body moving due south relative to a fixed frame of reference in space (a).
As the Earth rotates, the track of the body over the Earth's surface maps out a curve (b-c).

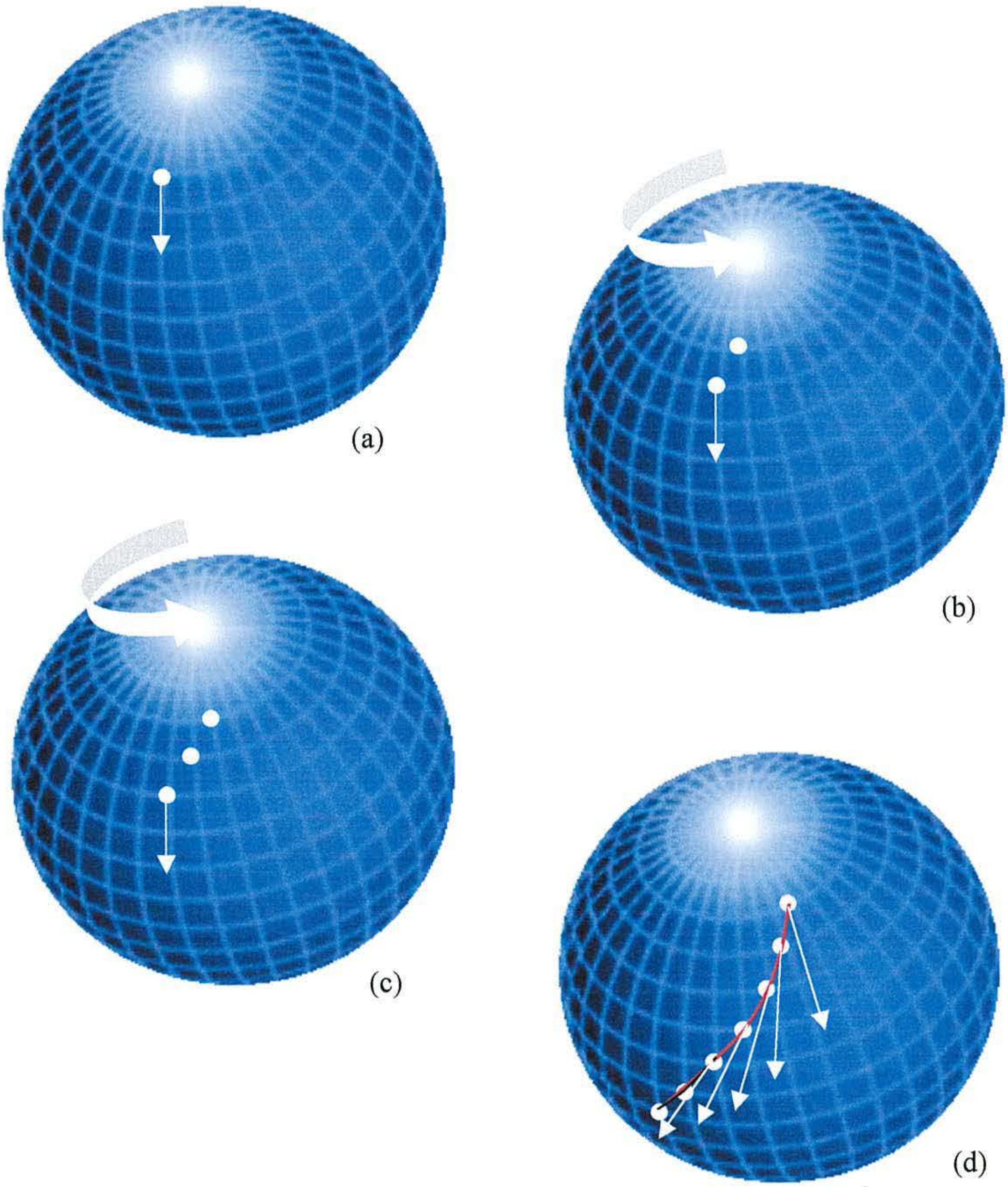

It would appear that a force was operating which was continuously accelerating the body to the right of its track (d) in the northern hemisphere, or to the left in the southern hemisphere. This apparent force is termed the **Coriolis force**.

Figure 2.2: The Coriolis effect

The satellite image of fig.2.3 shows typical cyclonic circulation about a low pressure centre in the mid-Atlantic.

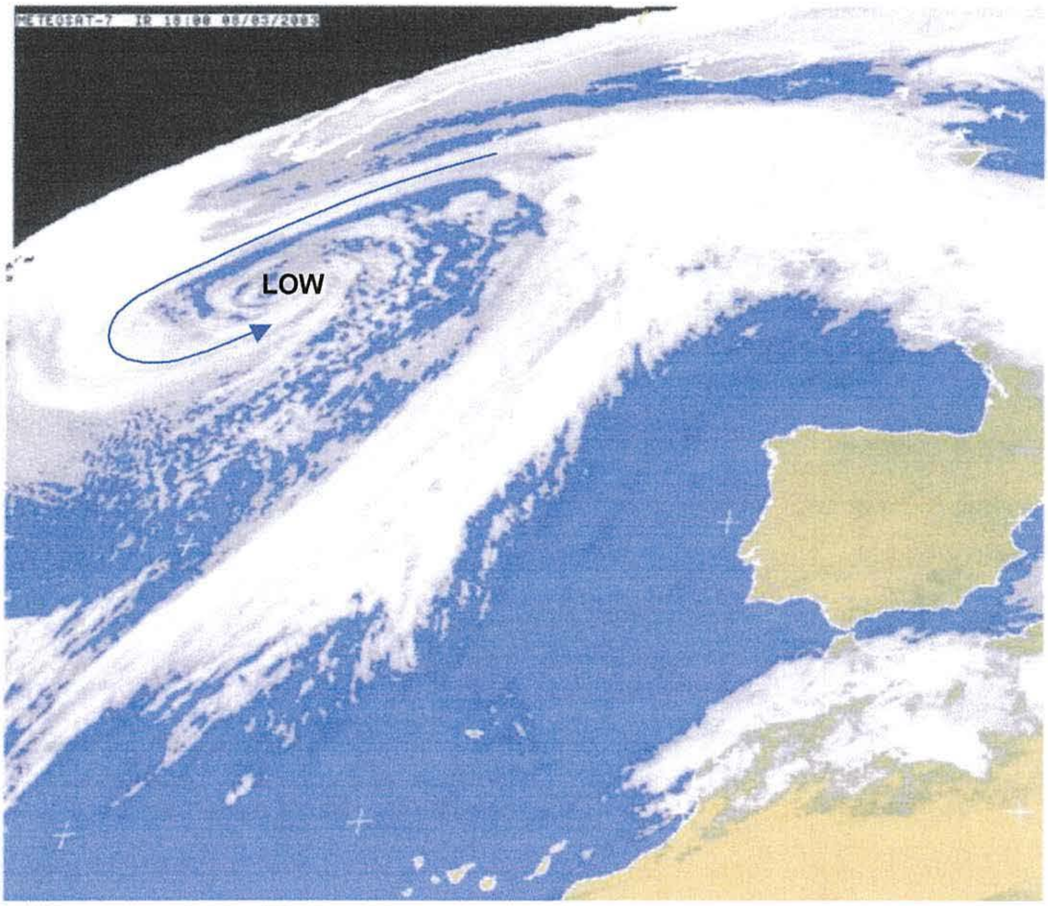

Figure 2.3: Meteosat-7 image for 18:00h, 8 March 2003.
Dundee Satellite Receiving Station

Weather processes take place within the lowest layer of the atmosphere, the *troposphere*, which varies in thickness between 8 and 17km. The circulatory system of the earth controls weather patterns; the driving force is the tendency to transfer heat from equatorial areas towards cold polar areas by the movement of air masses. A model for the large scale air motions of the planet was first proposed by Hadley in 1735, and has been progressively refined as more detailed observational data became available. A vertical section through the atmosphere of the northern hemisphere is given in fig.2.4. Within the tropical belt, large convective cells carry warm air northwards at high level, with a return flow near the surface.

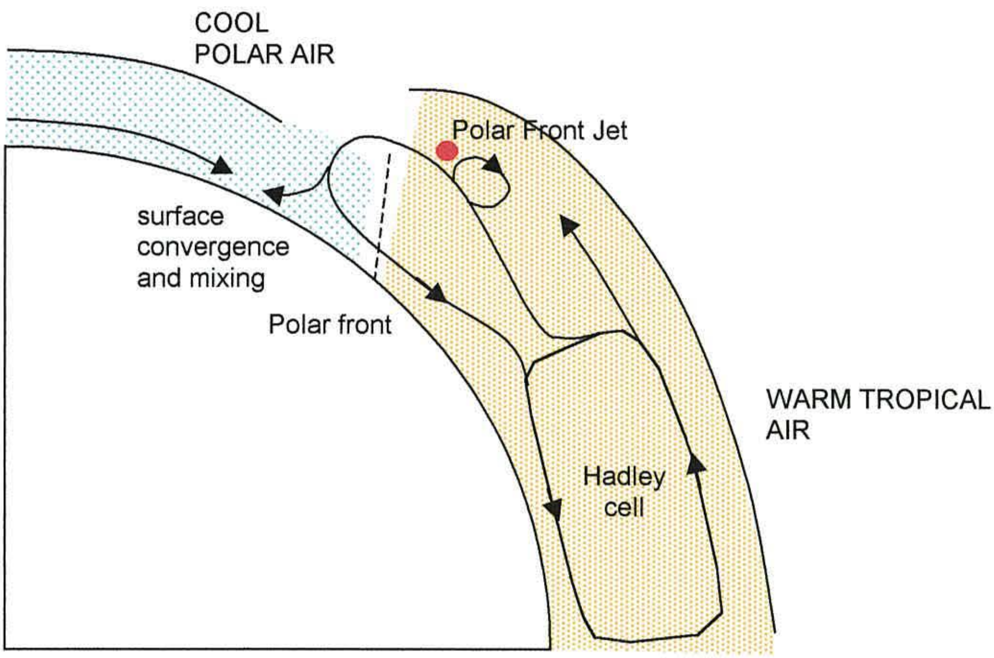

Figure 2.4: Flow of air masses in a generalised vertical section of the northern hemisphere. After Barry and Chorley 1976.

Air movements in mid-latitudes are more complex. The cold Polar air mass is separated from the warm Tropical air mass along a narrow zone called the Polar Front. Since warm air expands upwards in comparison to cold air, the troposphere is thicker for the Tropical air mass and thinner for the Polar air mass. The Polar Front is a *baroclinic* zone across which the air pressure changes rapidly. This is a result of the different thicknesses of the Polar and Tropical air columns which extend above any chosen reference level in the troposphere.

The Polar Front Jet

A high velocity channel known as the Polar Front Jet exists a short distance to the south of the Polar Front and near to the top of the troposphere. This jetstream flows from west to east across the Atlantic, with velocities reaching 250km/h. The mean winter position of the Polar Front Jet is shown in fig.2.5.

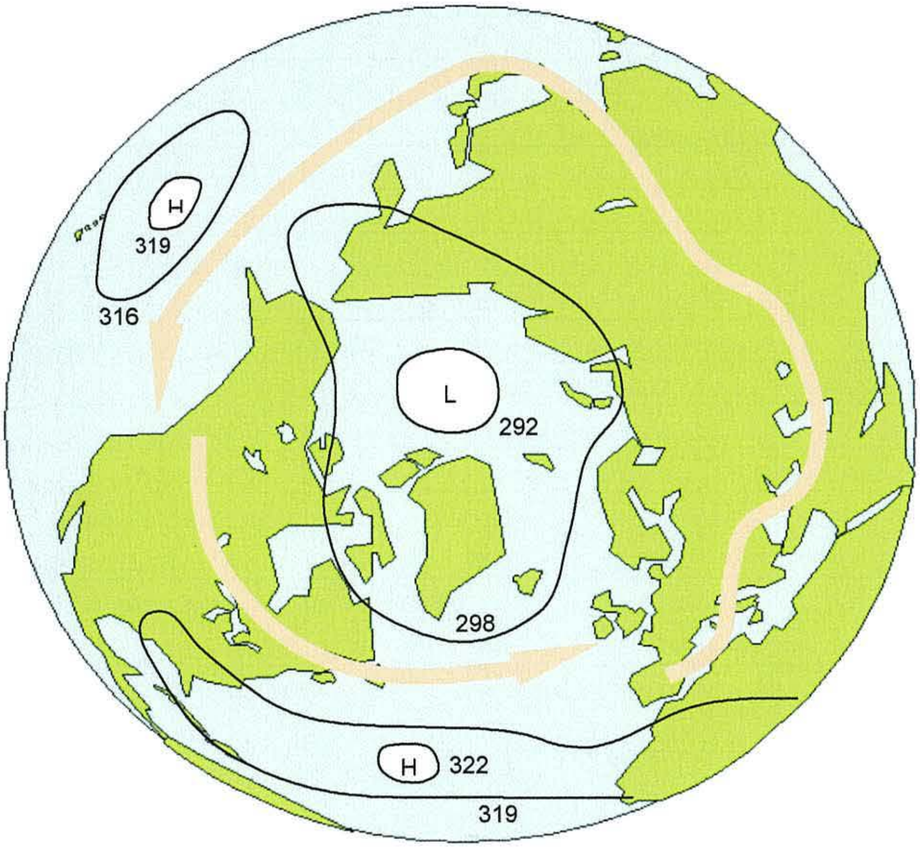

Figure 2.5: Average pressure distribution and location of the Polar jet stream: winter. Heights of 700mb surface (geopotential hectometres), after Barry and Chorley, 1976

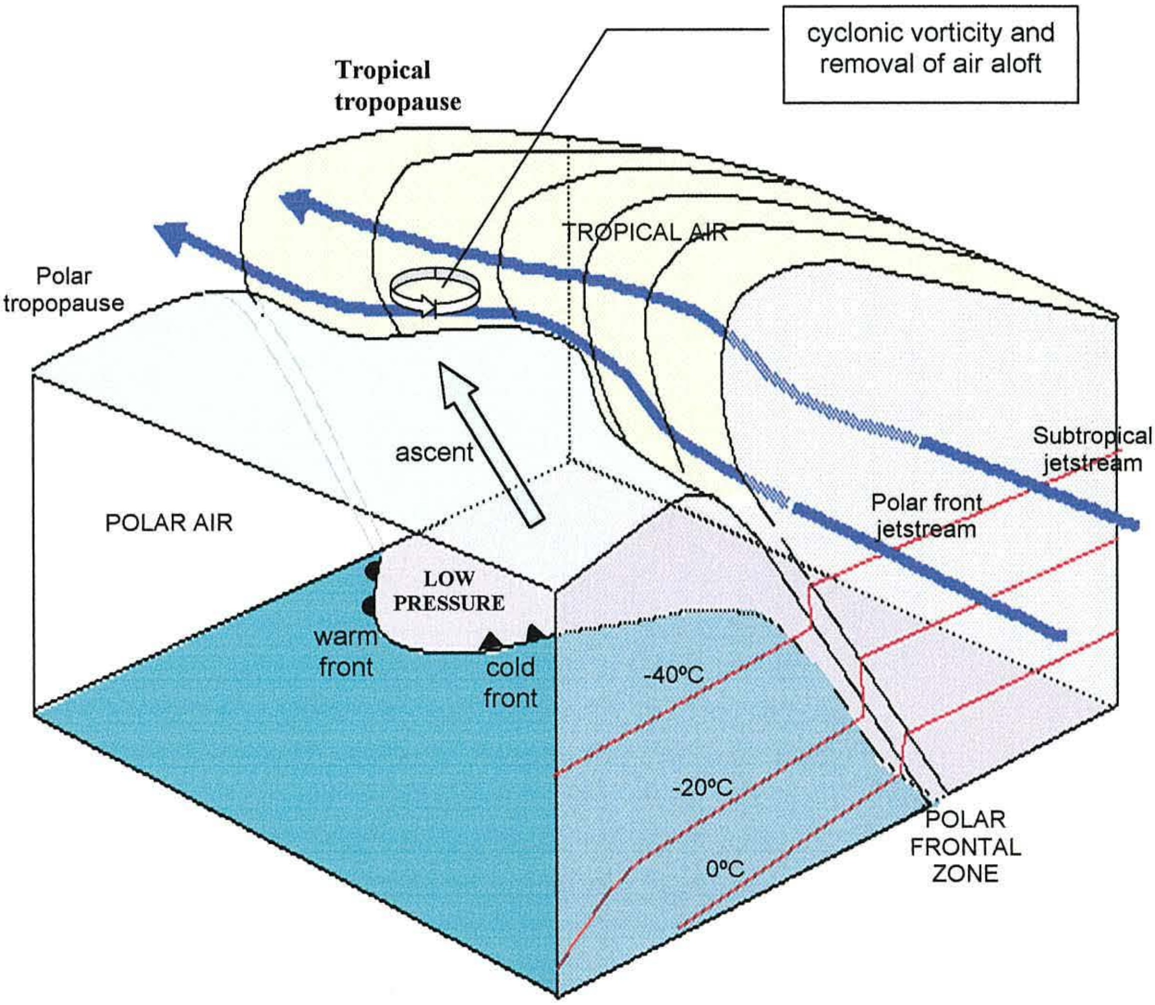

Figure 2.6: Diagramatic cross section through the Polar frontal zone of the North Atlantic

The Polar font jet stream provides a mechanism for dissipation of angular momentum, and appears to play a central role in controlling weather patterns of the North Atlantic.

Rotating bodies must obey the principle of conservation of angular momentum. For air masses, the total vorticity about a vertical axis is made up of the sum of the Coriolis force f related to the earth's spin, and vorticity ζ about a local point such as a high or low pressure centre. Overall, angular momentum is conserved. This is expressed mathematically as:

$$\frac{d(f + \varsigma)}{dt} = 0$$

If air moves poleward so that f increases, then ζ tends to decrease correspondingly, producing anticyclonic vorticity and inducing curvature of the air stream to the right. If air moves towards the equator so that f decreases, then ζ correspondingly increases, producing cyclonic vorticity and inducing curvature of the air stream to the left. This process gives rise to the large waves seen in the north Atlantic jetstream, known as Rossby waves

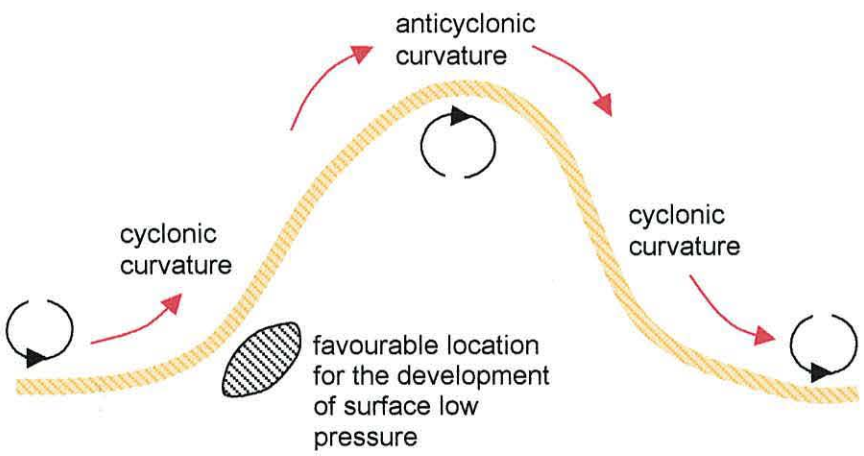

Figure 2.7: Induced vorticity along Rossby long waves.

Fig.2.6 illustrates the relationship between the jet stream pattern in the upper troposphere and the surface distribution of weather fronts. A *front* is a boundary between air masses with different physical properties. The Polar air mass is colder and generally has lower pressure. The Tropical air mass is warmer and generally has higher pressure.

A key factor in production of weather systems is the ability of cyclonic circulations in the upper troposphere to disperse air outwards. The air beneath cyclonic circulations tend to rise to compensate, forming low pressure centres at the earth's surface called *depressions.* Rising air provides the conditions necessary for condensation of atmospheric moisture and rain production. A particularly favourable location for the development of cyclonic circulations is just ahead of the Rossby wave where it penetrates furthest to the south. Anticyclonic circulations, by contrast, draw air inwards at high level. Beneath an anticyclonic circulation, the air column tends to sink, producing a high pressure centre at the earth's surface and stable, dry conditions.

The jet stream is often broken into a series of wider segments of high velocity, known as *jet streaks*, separated by narrower zones of lower velocity. It is known that low pressure centres can develop where air flows enter a jet streak from the equatorial direction (right entry sector), and where air flows leave a jet streak in the polewards direction (left exit sector). Examples are shown in fig.2.8. At this time on 11 November 2005, there were indeed low pressure frontal systems located to the west of Ireland and over Spain. These lows would be favourable for the ascent of air and production of rainfall.

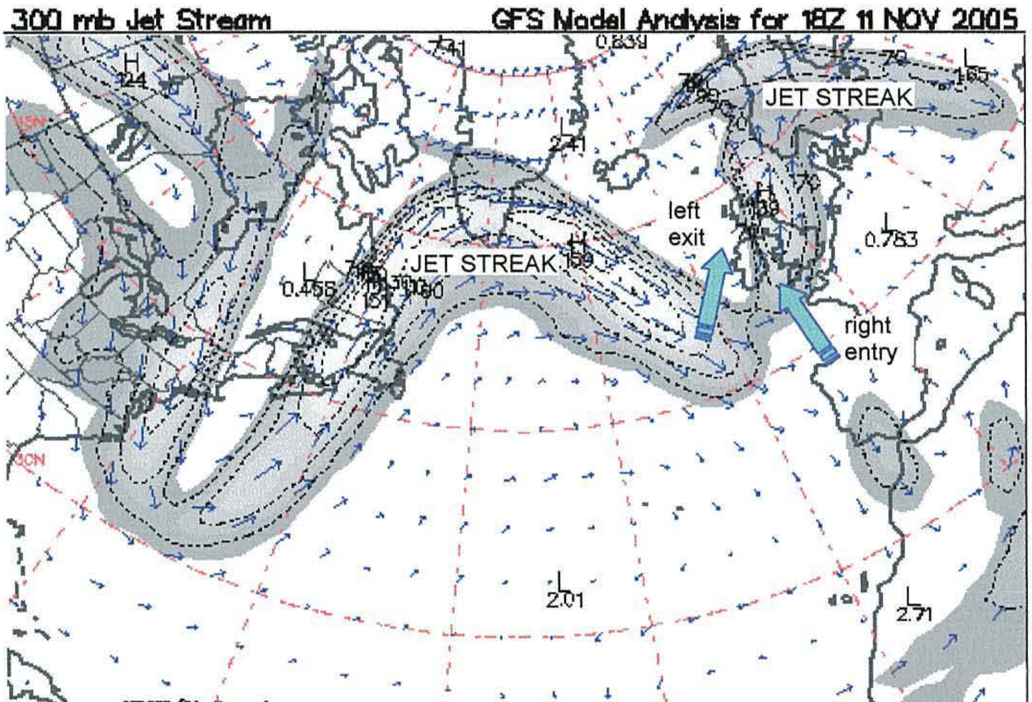

Figure 2.8: Jet stream map, identifying favourable locations for low pressure development in relation to jet streaks

The Polar jet stream is not fixed in position over the Atlantic region. A cycle of changes in the jet stream is commonly observed:

1. Commencement with a sub-linear pattern, known as a *zonal* jetstream
2. Sigmoidal waves are initiated
3. The sigmoidal waves develop with greater amplitude to form a *meridional* jetstream pattern
4. The jet stream continuity finally breaks down into a pattern of circular vortices.

The cycle will then be repeated with the formation of a new sub-linear pattern. Examples of zonal and meridional jetstream patterns during the period 24-26 October 2005 are shown in fig.2.9.

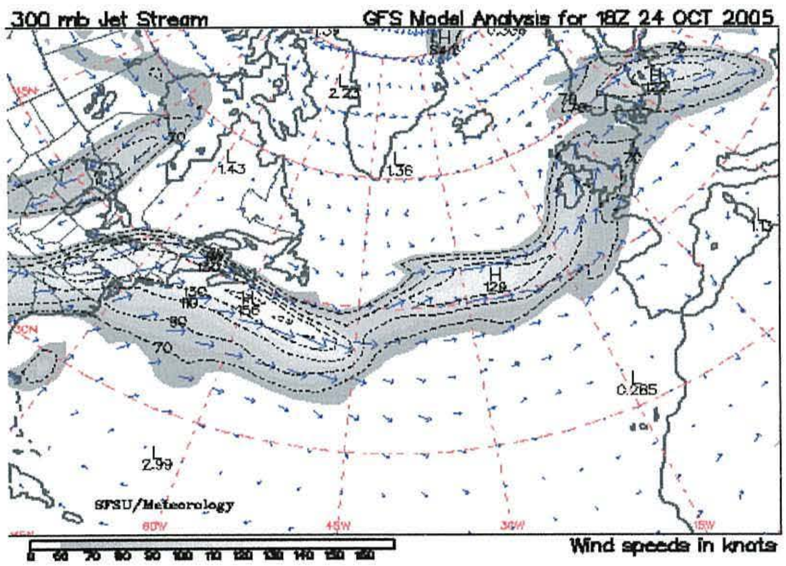

Figure 2.9(a). Zonal Polar Front Jet pattern in the Mid Atlantic, 24 October 2005

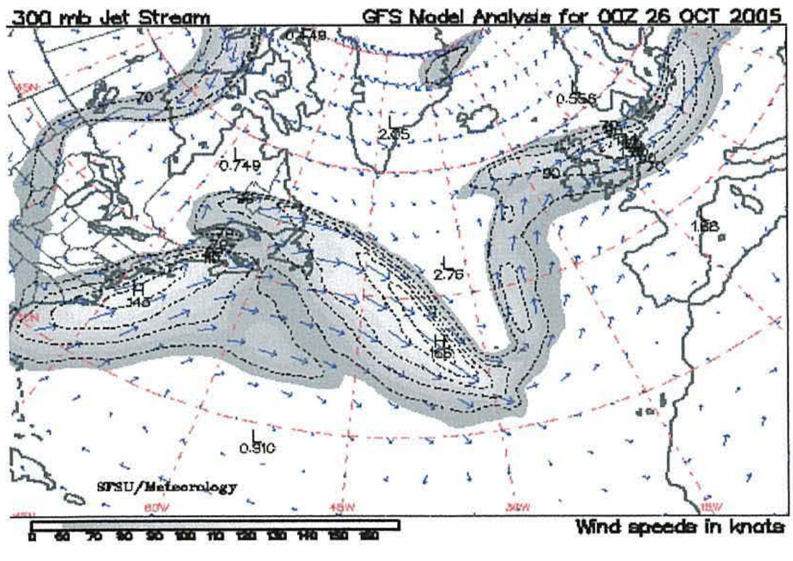

Figure 2.9(b). Meridional Polar Front Jet pattern in the Mid Atlantic, 26 October 2005

source: California Regional Weather Server

Theories of midlatitude cyclone structure

Early work in determining the structure and evolution of low pressure centres along the Polar Front was carried out by Bjerknes and Soldberg (1922). The theory, known as the *Norwegian Model*, envisages the development of a wave in the Polar Front which develops into distinct warm and cold fronts enclosing a wedge of tropical air termed the *warm sector* (fig.2.10).

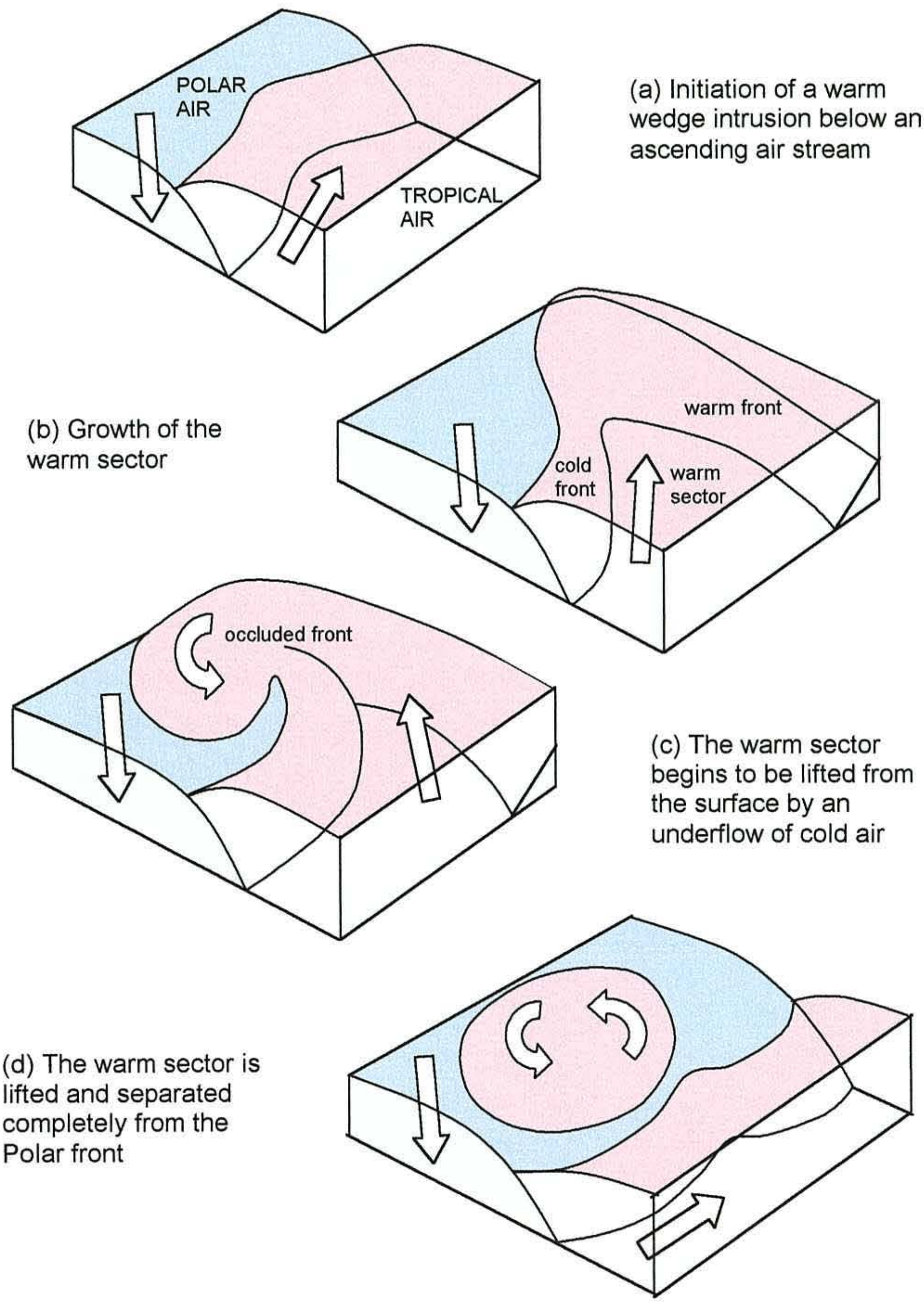

Figure 2.10: Evolution of the frontal system of a mid-latitude depression, after Barry and Chorley, 1976

A feature of the Norwegian model is that the cold front to the rear of the warm sector advances more rapidly than the warm front, and gradually overtakes the warm sector. The warm sector is progressively closed by occlusion of the cyclonic system, with warm air lifted from the ground and separated from the Polar Frontal zone.

With improved satellite imagery, it became increasingly evident that features of many cyclonic centres developed over the North Atlantic do not fit well with the Norwegian Model.

Browning and Hill (1984) identify three cases where cyclonic vortices develop in association with a Polar air mass low pressure centre:

- In the first case, the low pressure centre lies close to the Polar Front. In this situation, warm and cold fronts develop in a pattern consistent with the Norwegian model as shown in the example of fig.2.11.

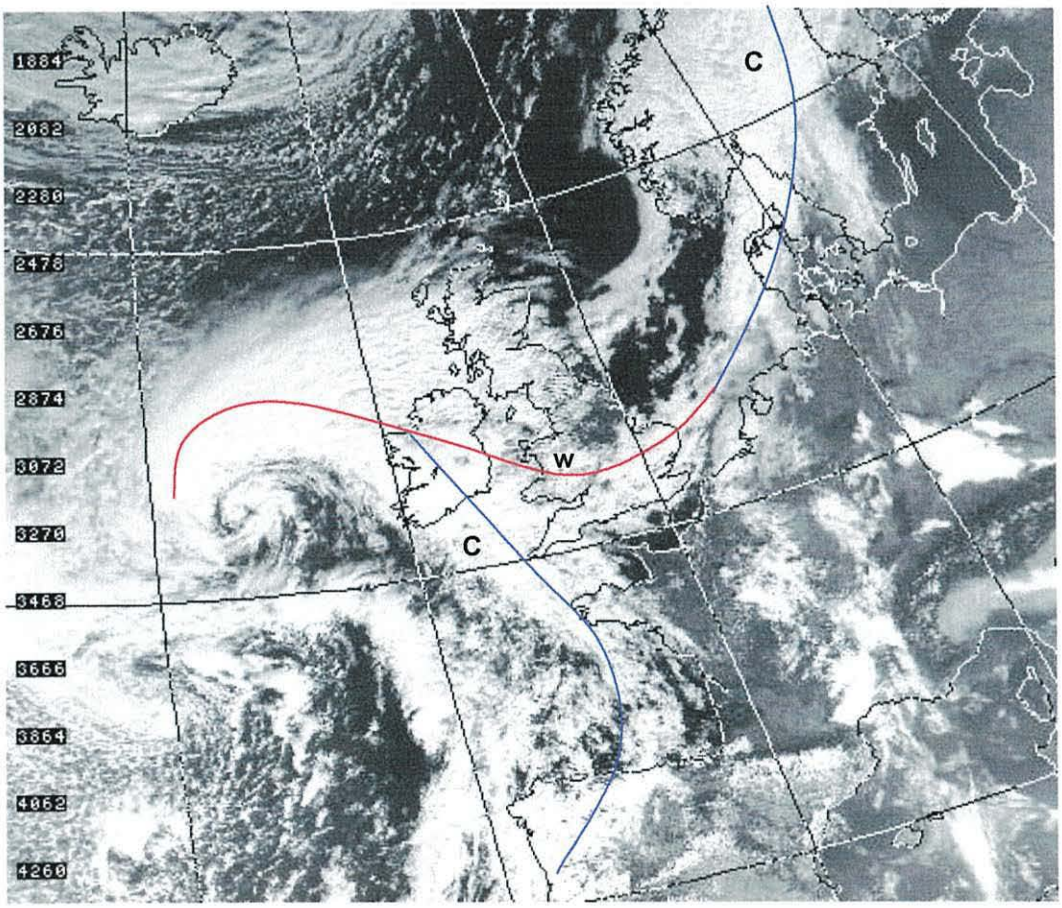

Figure 2.11: Satellite photograph for approximately mid-day on 29 October 2005, showing the development of warm-sector depression at the Polar Front (c: cold front, w: warm front). Dundee Satellite Receiving Station

- A second case is the situation where the low pressure centre lies within the Polar air mass well away from the Polar Front. No interaction occurs with the Polar Front, and an isolated vortex develops with a 'comma cloud' pattern as in the example of fig.2.12:

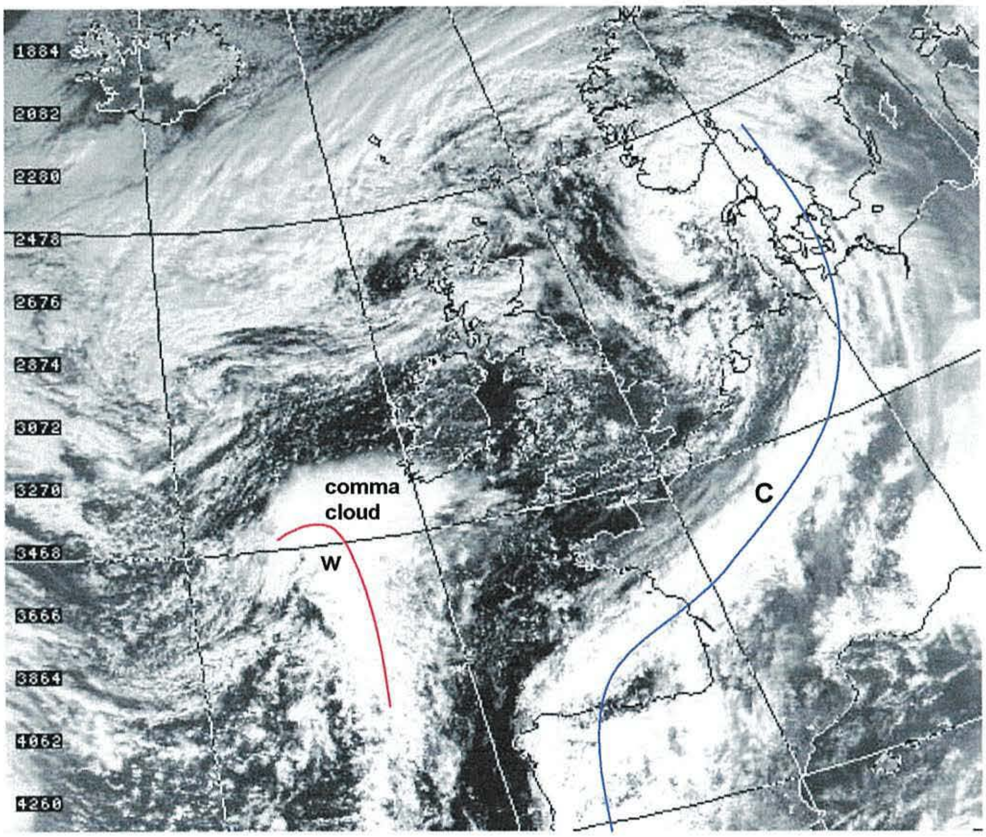

Figure 2.12: Satellite photograph for approximately mid-day on 20 October 2005 showing comma cloud development around a Polar air mass cyclonic centre. (c: cold front, w: warm front). Dundee Satellite Receiving Station

Significant to the model of Browning and Hill is the concept of the Polar air mass low pressure centre being the driving force for cyclonic convergence, uplift and air removal into the upper troposphere. Air flow within the vortex follows an ascending spiral path. Whether or not warm air from the Polar Front becomes entrained in the cyclone will depend on the proximity of initial vortex development to the surface position of the Polar Front. This mechanism is in contrast to the perceived driving force for the classical Norwegian model of cyclonogenesis. The Norwegian model assumes that the initiation and growth of wave disturbances along the Polar Front produces a warm sector intrusion, by analogy with the initiation and growth of meanders in a river.

- A third case represents an intermediate position for the low pressure centre. An initially isolated vortex draws in warm air from the Polar Front at a late stage in its development, as shown in fig.2.13.

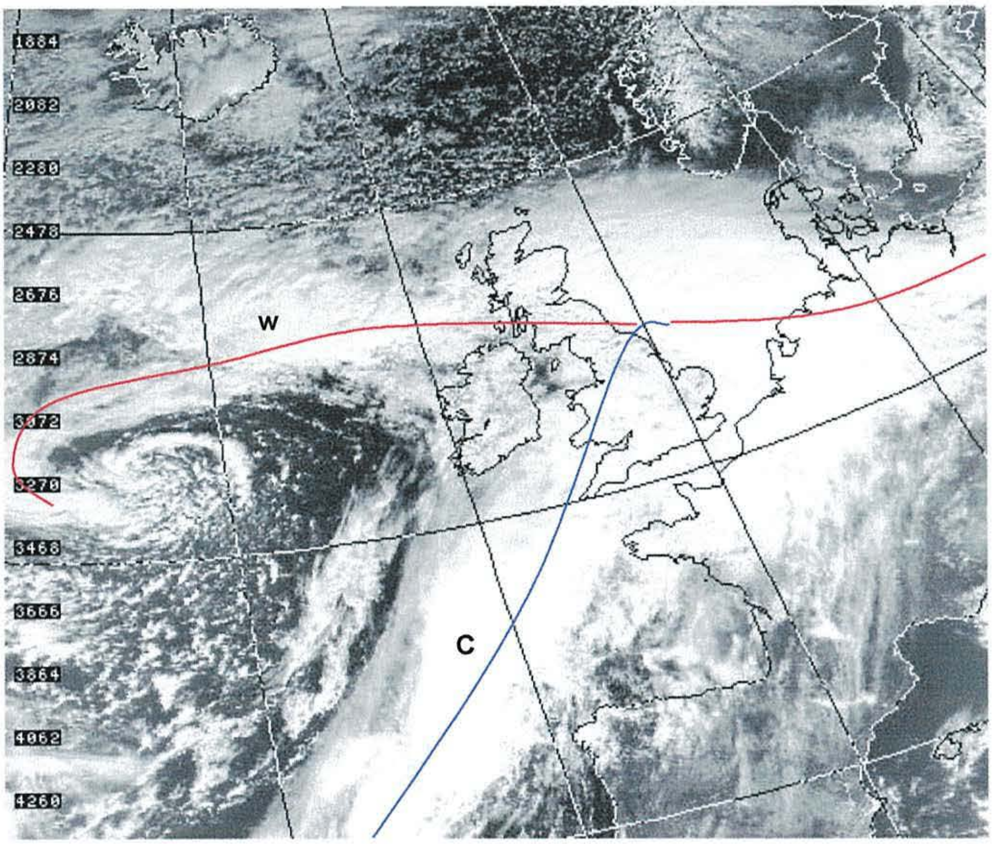

Figure 2.13: Satellite photograph for approximately mid-day on 24 October 2005, showing late stage linking of a cyclonic centre to the Polar Front. (c: cold front, w: warm front). Dundee Satellite Receiving Station

A further model for frontal system development has been developed by Shapiro and Keyser (1990). This is summarised in an illustration from their paper, reproduced here as fig.2.14. Early development of a Polar Frontal cyclone in the Shapiro-Keyser model resembles that of the Norwegian model, with formation of warm and cold fronts along a wave structure in response to a developing vortex in the Polar air mass. The cold front soon becomes detached from the warm front and remains roughly perpendicular to the warm front for much of the development sequence. This limits the closure of the warm sector. The warm front is considered to extend beyond the warm sector to form a *'T-bone'* structure, and bends back on itself towards the centre of the low pressure vortex.

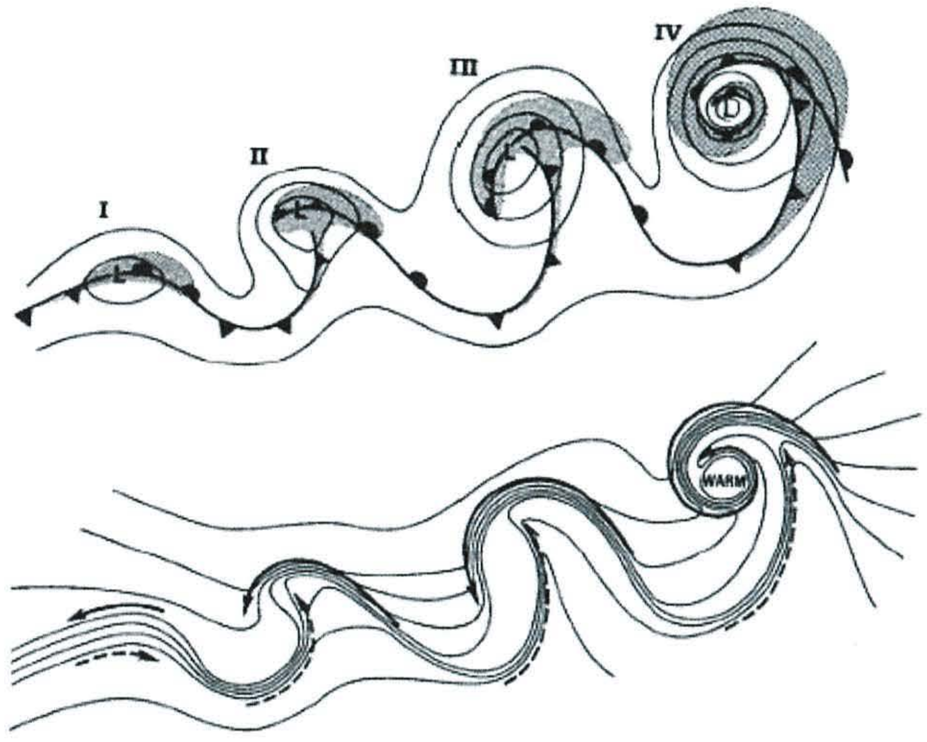

Figure 2.14: Shapiro-Keyser (1990) frontal-cyclone evolution: incipient broad-baroclinic phase (I), frontal fracture (II), bent-back front and frontal T-bone (III), and warm-core frontal seclusion (IV), Upper: sea level pressure (solid), fronts (bold), and cloud signature (shaded). Lower: temperature (solid), and cold and warm air currents (solid and dashed arrows, respectively).

A feature of the Shapiro-Keyser model is the enclosure of a cylinder of relatively warm pre-frontal air by advected cold air at the centre of the vortex – termed the *warm seclusion.* In contrast to the Norwegian model, no lifted occlusion is present. Lifted occlusions are not unknown, but are much less common than had previously been assumed. Lifted occlusions are most likely to occur over land, rather than open ocean, and may be a secondary feature induced by the land surface topography.

Thorncroft, Hoskins and McIntyre (1993) examined the air flows associated with Polar-front cyclonic centres (fig.2.15). Warm air ascends from south of the Polar front and cold air descends from north of the Polar front. Both flows are able to diverge into anti-clockwise *(cyclonic)* and clockwise *(anti-cyclonic)* rotating components. It is suggested that the Norwegian model for mid-latitude cyclone development occurs when the *anti-cyclonic* flows *A* and *D* are strong, whereas the Keyser-Shapiro model is followed when the *cyclonic* flows *B* and *C* dominate.

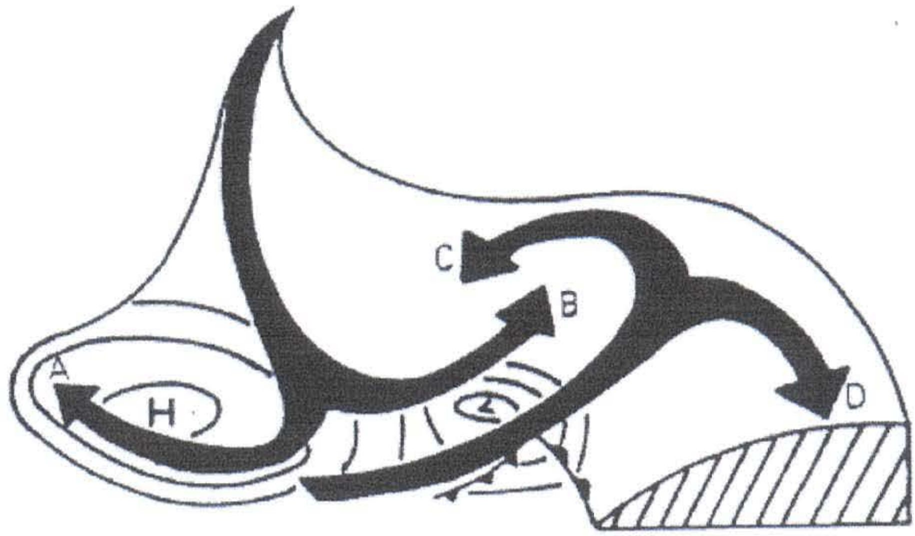

Figure 2.15: Three-dimensional diagram looking northwards, illustrating the air flows associated with a cyclonic centre and trailing high pressure region. Warm air ascends from the warm sector and may diverge as flows C and D. Cold Polar air descends southwards and may diverge as flows A and B. (After: Thorncroft, Hoskins and McIntyre,1993)

Schultz, Keyser and Bosart (1998), and Schultz and Wernli (2001), have been able to make a further link between the various theoretical models by showing that the pattern of mid-latitude cyclone development can be related to upper air flow patterns. The *jet streaks* of the Polar Jetstream exhibit divergent air flows in left-hand exit regions and convergent air flows in right-hand exit regions. When a cyclonic centre comes under the influence of jet stream divergence, it tends to develop with a Norwegian pattern of fronts. However, if it comes under the influence of jet stream convergence then its development follows the Keyser-Shapiro pattern.

The example charts for 29 October 2005 (fig.2.16) illustrate a mid-latitude cyclone tracking north eastwards towards Britain. This is under the influence of the divergent flow in the left exit zone of the overlying jet streak, and is developing a Norwegian structure of occluded front:

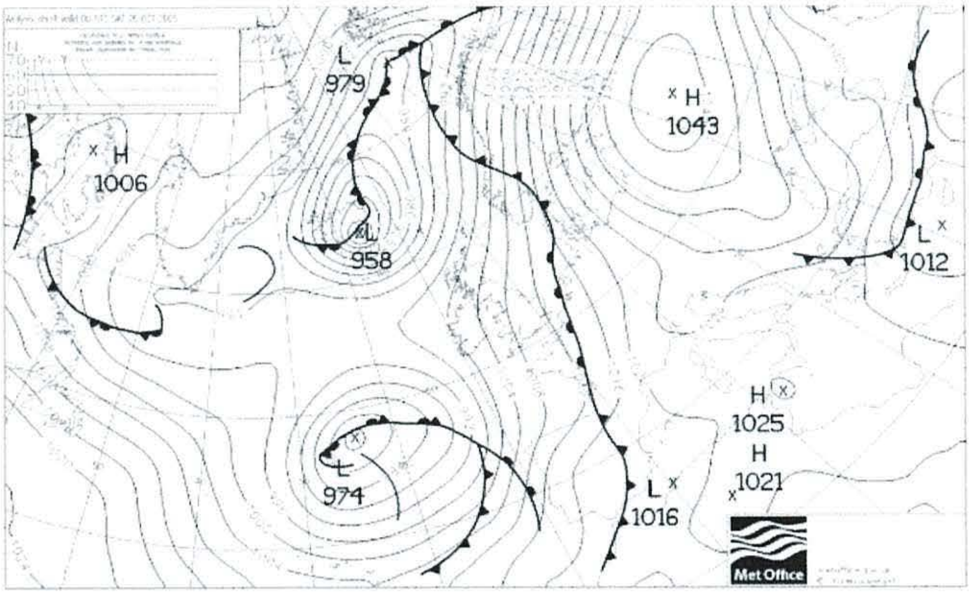

Figure 2.16(a): Synoptic chart for 00:00h 29 October 2005. Source: Wetterzentrale.

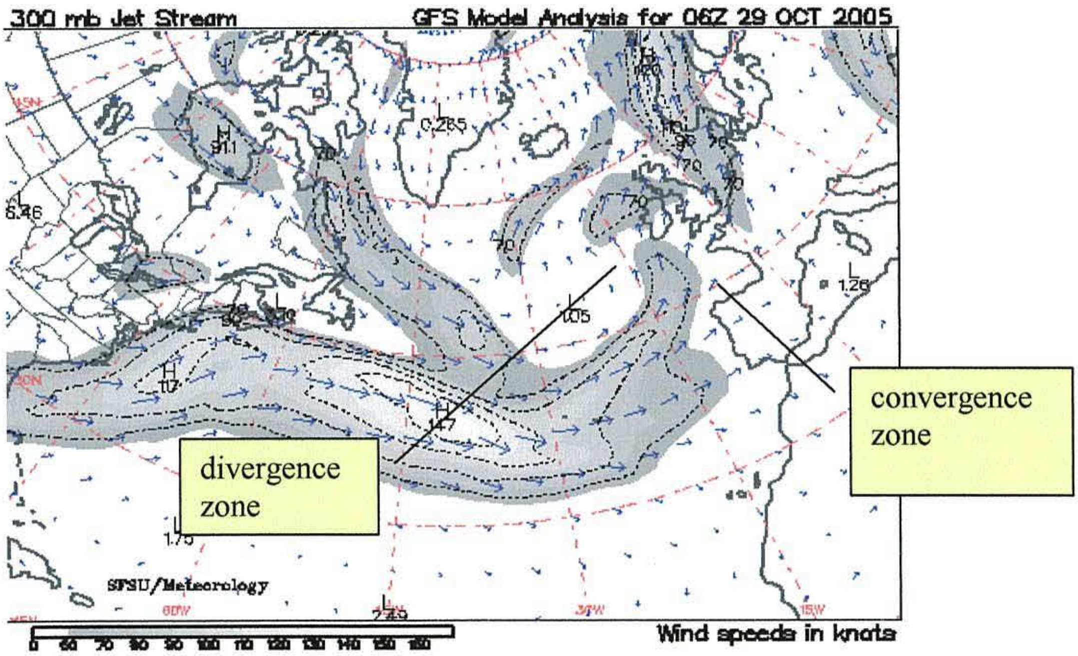

Figure 2.16(b): Jetstream map for 06:00h 29 October 2005. Source: California Regional Weather Server

Rainfall patterns associated with Polar Front cyclones

Considerable interest has been focussed on the mechanisms of rainfall generation within extratropical cyclones, leading to the 'conveyor' model of Harold (1973). In this model, it is assumed that upwards displacement of warm air by the advancing cold front leads to convective instability. This is promoted by a mid-altitude flow of colder air crossing the warm sector, which maintains potential instability conditions as the warm air rises along an inclined surface termed the *conveyor* (fig.2.17). Initially the conveyor rises parallel to the cold front, but after crossing the warm front at mid-altitude it may swing round to join the flow direction of the high-level jet stream. A counter-current of cold air descends ahead of the warm front. This model, based on field data from rainfall radar and radiosonde balloon ascents, is consistent with the rainfall and air current patterns of the Shapiro-Keyser cyclone model (cf. fig.2.14).

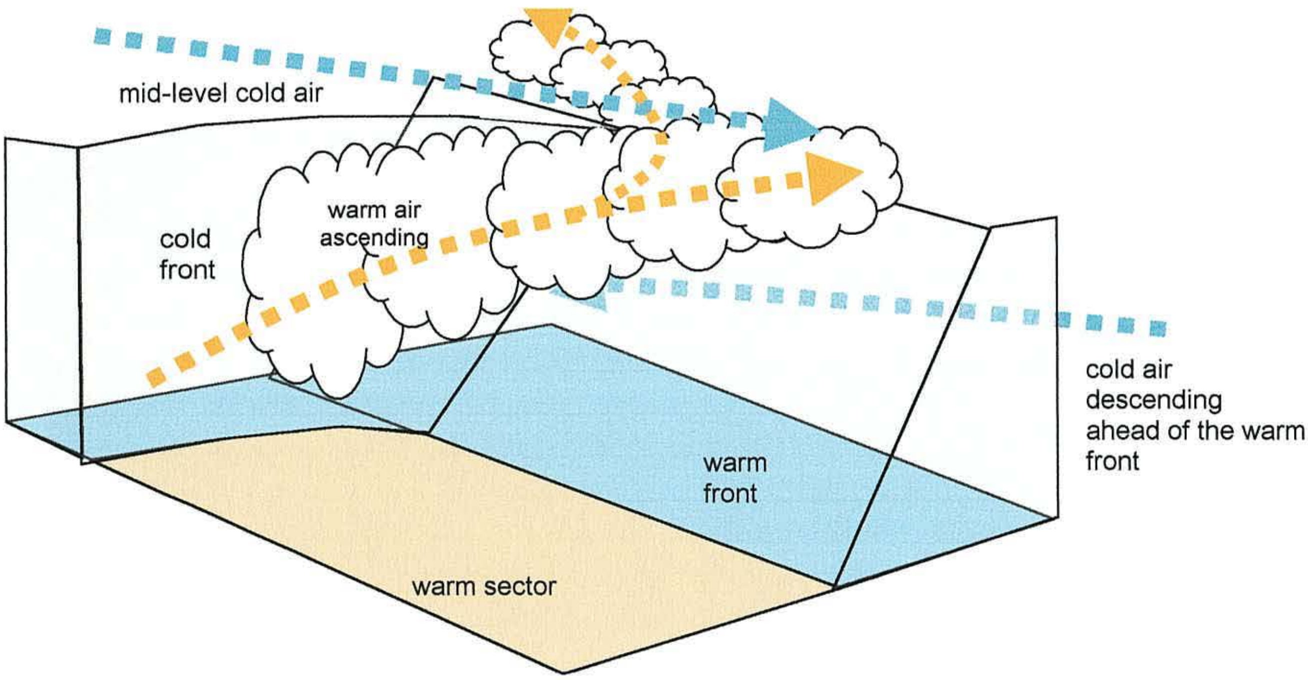

Figure 2.17: Ascent of warm air conveyor within a frontal system

A figure from the paper of Harold (1973) is reproduced here as fig.2.18. Values of θ_w shown in the diagram refer to *wet bulb potential temperature*. This is a measure of the temperature that an air parcel would take if brought to sea level without transfer of heat energy to or from the surrounding environment. Potential temperature is a useful concept, as it allows the comparison of temperatures of air masses without the additional complication of computing temperature changes due to expansion or contraction during ascent or descent. It provides a measure of the relative quantities of thermal energy at different positions within a weather system.

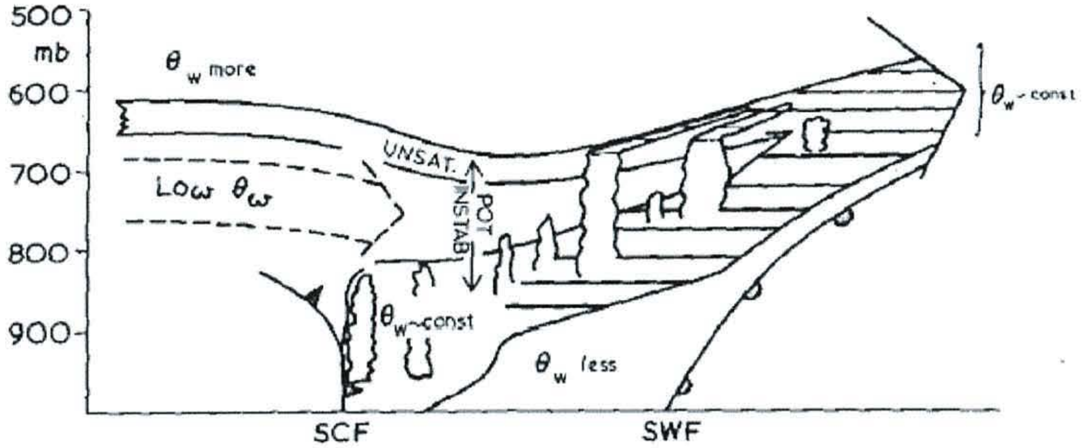

Figure 2.18: Schematic representation of the flows in the region of the cold front. Hatching denotes layer cloud and convective overturning is depicted by the cumuli form shapes. Two initially separate flows, with lower θ_w between, mix to produce a lapse of near constant θ_w above the warm frontal zone. Figure and caption reproduced from Harold (1973).

Browning, Hardman, Harold and Pardoe (1973) present a study of a frontal rainfall event over the Scilly Isles on 18 January 1971 which was intensively monitored by a combination of ground observations, rainfall radar, aircraft data collection and radiosonde balloon ascents. This generated an extremely detailed three dimensional model of the frontal system and associated rainfall as it approached Cornwall from the Atlantic. A series of rainbands were mapped, running parallel to the cold front and merging into a zone of uniform precipitation ahead of the advancing surface warm front (fig.2.19). These rainbands are seen as zones of convective uplift above the ascending warm sector conveyor. The intervening rain-free zones may represent the return flows of the convection cells, where descending air is warmed and re-evaporation of moisture takes place. The cause of the convective instability was again identified as a tongue of cold air over-running warm sector moist air ahead of the cold front (fig.2.20).

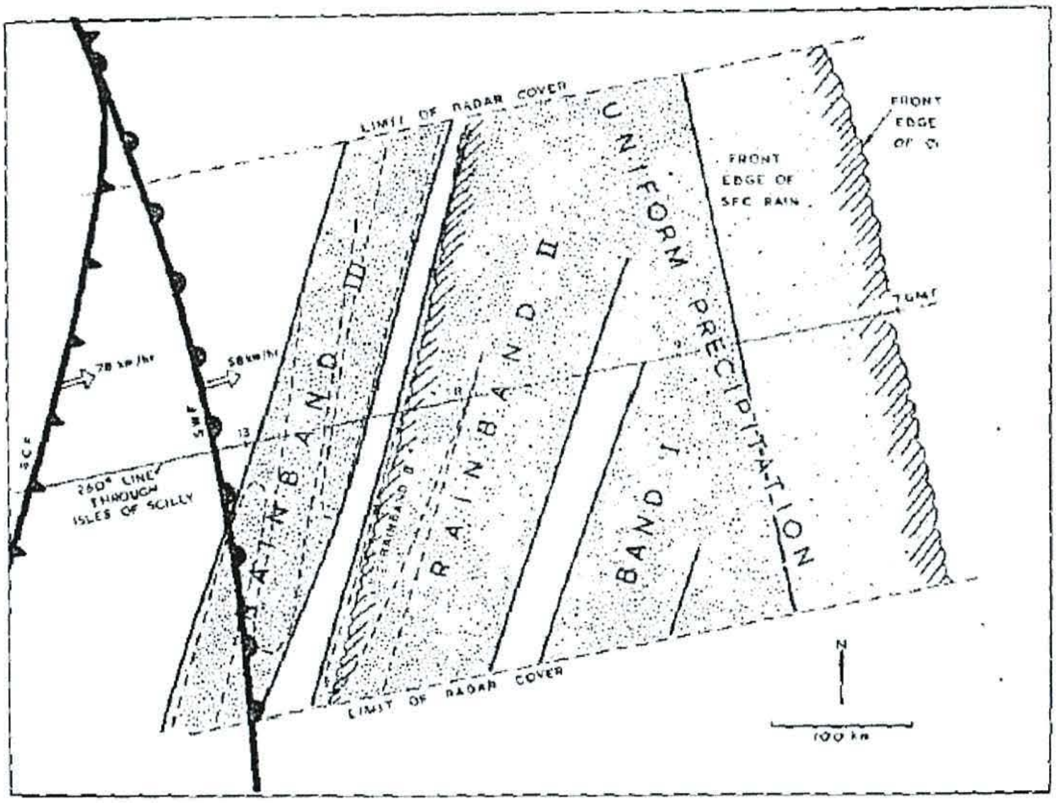

Figure 2.19: Schematic distribution of precipitation [above the Scilly Isles for the rainfall event of 18 January 1971]. The extent of surface rain is shown stippled. The further extent of precipitation aloft is lightly stippled. The leading and rear edges of the dense high-level cirrus canopy is indicated by hatched shading. Figure and caption reproduced from Browning, Hardman, Harold and Pardoe (1973).

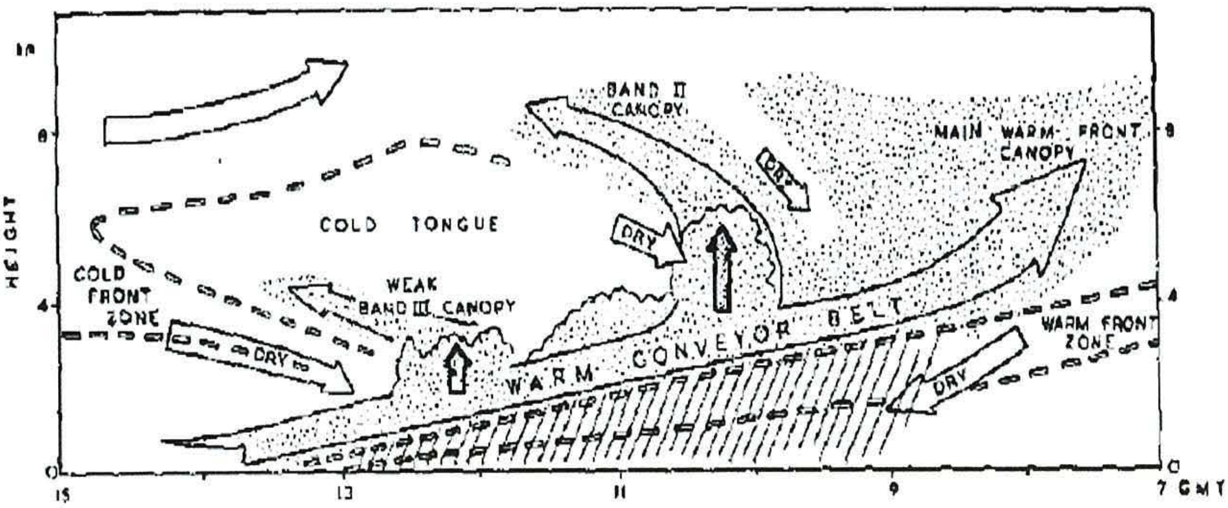

Figure 2.20: Schematic time-height cross-section representing some of the principal features of the convective rainbands on 18 January 1971. Cloud areas are stippled. Figure and caption reproduced from Browning, Hardman, Harold and Pardoe (1973).

Browning and Hill (1985) give a model for the relative positions and orientations of the Polar Front jet stream at high altitude, and the lower level ascending warm air conveyor associated with a cyclonic low pressure centre situated within the Polar air mass (fig.2.21):

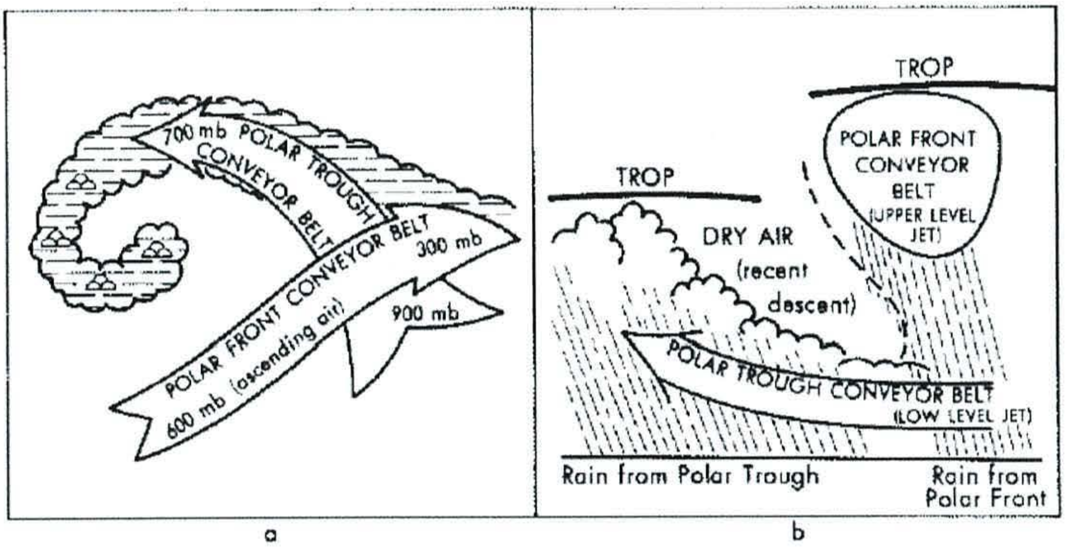

Figure 2.21: Conceptual model showing intersecting polar trough conveyor belt and polar front conveyor belt: (a) plan view, (b) vertical section along axis of polar trough. Figure and caption reproduced from Browning and Hill (1985).

An example of the approach of a cold front to the coast of Cardigan Bay is illustrated in fig.2.22. A middle-altitude conveyor flows northwards, with a well developed cumulo-stratus cloud layer indicating condensation from moist ascending air. Convective instability is producing rounded cloud tops. At higher altitude the conveyor will swing eastwards to join the track of the jet stream, picked out here by trails of cirrus ice cloud.

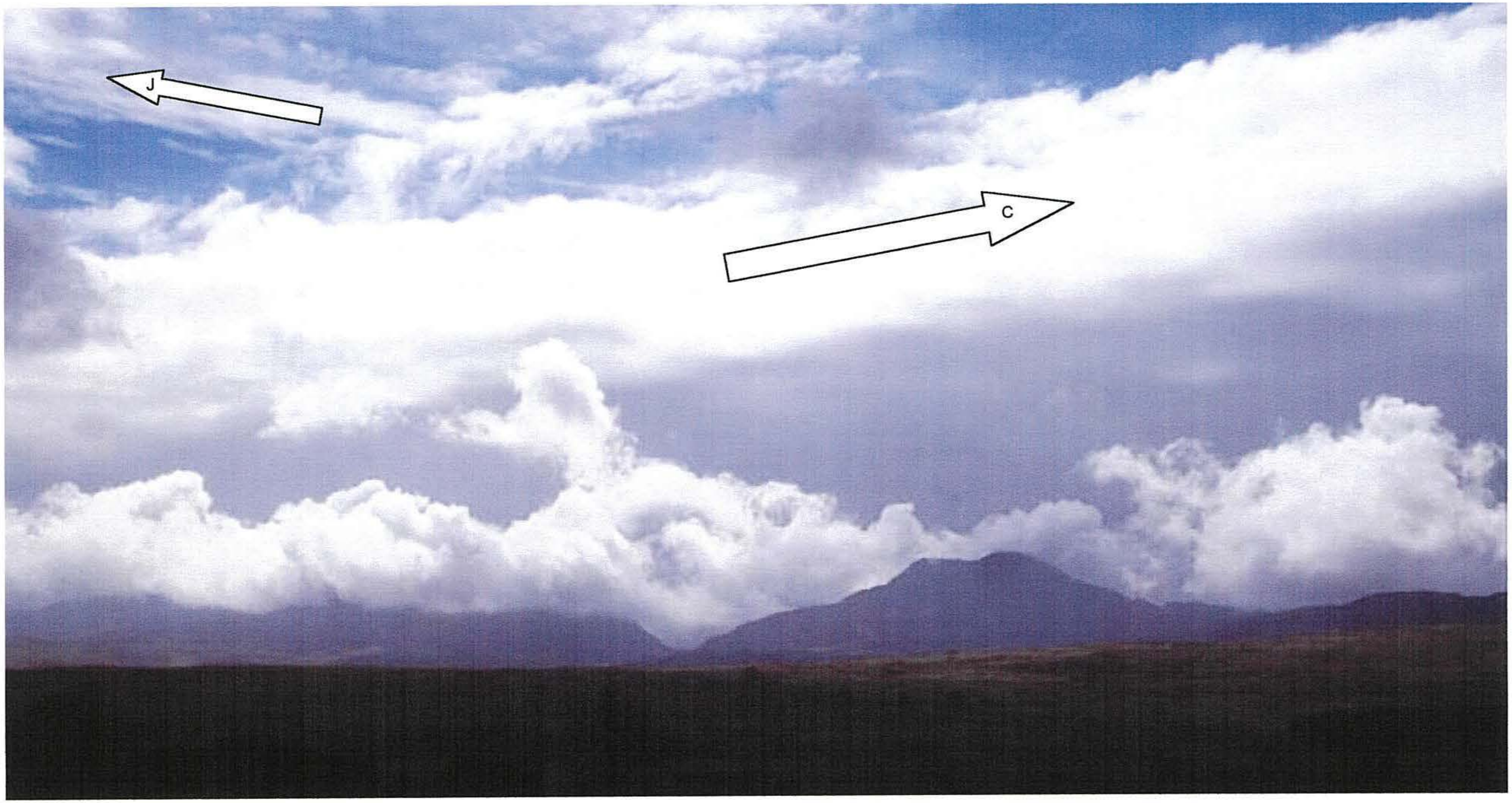

Figure 2.22: Cold front approaching the Rhinog mountains.
C: mid-altitude conveyor J: high-altitude jet stream. Photo: John Mason

Orographic effects on rainfall

The production of rainfall discussed so far has been on a regional scale, controlled by the location of synoptic features such as the jet stream, low pressure centres and frontal systems. For detailed prediction of rainfall over an upland catchment such as the Mawddach, modification of rainfall patterns by smaller mesoscale processes must be considered.

The lowest 1000m of the troposphere is termed the planetary boundary layer. Localised effects are produced in this zone, including frictional drag from vegetation, deflection of winds around hills, convection from ground heated by solar radiation, or convection from warm sea water. These effects need to be considered in a high resolution meteorological model.

Fluid dynamic processes for airflow over hills are discussed by Raupach and Finnigan (1997). They identify three air flow regions:

- *Inner region* on the upflow side of a hill where the air flow pattern is influenced by both a pressure gradient due to the hill obstruction, and also a frictional effect due to the land surface.
- *Outer region* forming the higher air layer on the upflow side of the hill, where only pressure effects are experienced.
- *Wake region* on the downflow side of the hill where turbulence may occur as a result of flow separation.

Barry (1992) discusses the factors which affect whether an air flow ascends over a hill obstruction or is deflected around the obstruction (fig.2.23). The critical height h_c at which a streamline within the airflow is deflected *around* a hill rather than *over* it is given by the equation:

$$h_c = H(1 - F)$$

where H is the height of the hill.
F is the Froude number in the range [0,1] which represents a ratio of viscous forces to gravitational forces. In the case of air flow approaching a hill, this may be interpreted as the ratio of the kinetic energy of the air flow to the potential energy needed to rise over the hill.

There are two limiting cases:

- For fast moving air approaching a low hill, the Froude number will be close to 1, resulting in h_c near to zero. Almost the full depth of the airflow down to ground level will be able to surmount the hill.

- Slowly moving air approaching a high barrier will generate a Froude number close to zero. The critical height h_c will be approximately equal to the height of the hill, H. Almost the entire airflow below the hill summit will be deflected around the obstruction.

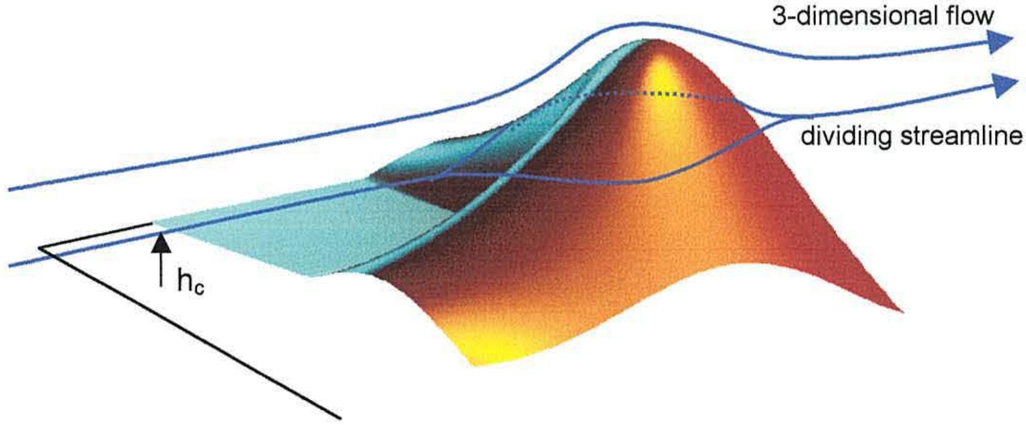

Figure 2.23: Flow paths around an isolated hill of height H

Airflow ascent over mountains can lead to cooling and condensation. If the air mass is in a stable buoyancy state, it may descend again beyond the mountain barrier and reabsorption of water vapour can occur. This situation is illustrated in fig.2.24, where a stable air flow is generating cloud as it streams north-westwards over the Aran mountains.

Figure 2.24: stable air flow generating cloud as it streams north-westwards over the Aran mountains

Chen and Lin (2003) have carried out modelling to investigate precipitation associated with unstable airflow over mountains. They identify different cases in which rainfall may occur upstream of the mountain summit, over the mountain summit itself, or over the downstream slopes. Critical factors are: the air flow velocity which affects rate of forced ascent and cooling, and the convective available potential energy (CAPE) of the air mass which affects the rate of free ascent after upwards displacement.

If atmospheric conditions are neutral in their buoyancy effect, a series of standing waves known as *lee waves* can be generated downstream of the mountain barrier. The waves are maintained by air circulation in rotors above the ground surface (fig.2.25).

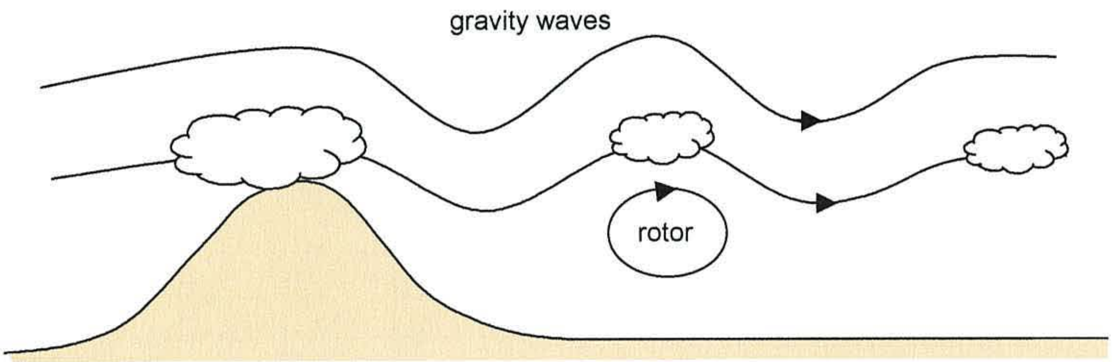

Figure 2.25: Development of lee waves (after Barry and Chorley, 1976)

Galvin and Owens (2006) have presented a satellite photograph showing the development of lee waves over the British mountains on 25 February 2006 (reproduced in fig.2.26). Lines of cloud developed in response to a stable airflow from the east. Lee wave clouds appear where the airflow crosses the northern Pennines towards the Lake District, and cloud ridges of longer wavelength can also be seen over Wales.

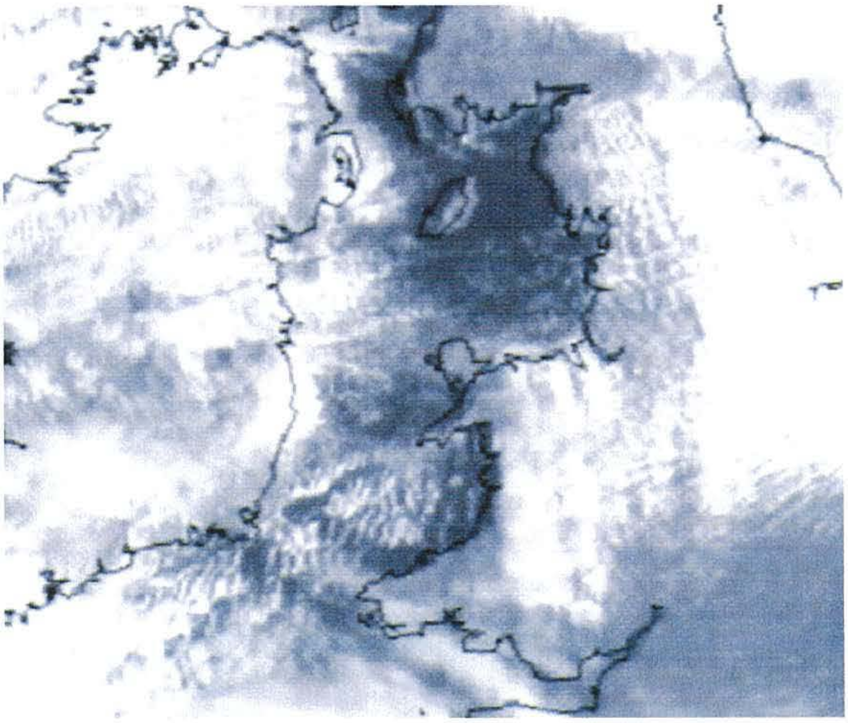

Figure 2.26: Development of lee waves over the Welsh mountains and the Lake District on 25 February 2006. From Galvin and Owens (2006)

Where atmospheric conditions are unstable, or neutral in their buoyancy effects, air given an upwards motion by passage over a mountain barrier may continue to rise. Condensation may lead to growth of water droplets within cloud, and the release of rainfall.

Garvert, Colle and Mass (2005) collected data from aircraft and radar to show that gravity waves over the Cascade Mountains of Oregon produced enhanced rainfall in the vicinity of narrow mountain ridges. The authors went on to simulate the storm events using the MM5 meteorological model and found that rainfall was increased by 20% in comparison to a smooth slope model without localised gravity wave forcing.

Rainfall generation over mountains may occur by a two stage process termed the *seeder-feeder* mechanism (Sibley, 2005). Cloud layering is commonly present over mountains during rainfall events, with low level orographic cloud formed by advection over the mountain barrier and higher level cloud produced by uplift along a warm air conveyor. This situation is illustrated in the photograph of the Rhinog mountains in fig.2.22. Small diameter rain droplets descend from the upper *seeder* cloud, then accrete further moisture as they pass through the lower *feeder* cloud. The resulting rainfall may be two or more times the intensity of frontal rainfall alone. Strong low level winds ahead of the front may advect the falling raindrops some distance beyond the mountain barrier, so that the location of maximum rainfall does not correspond exactly with the area of highest surface altitude (fig.2.27).

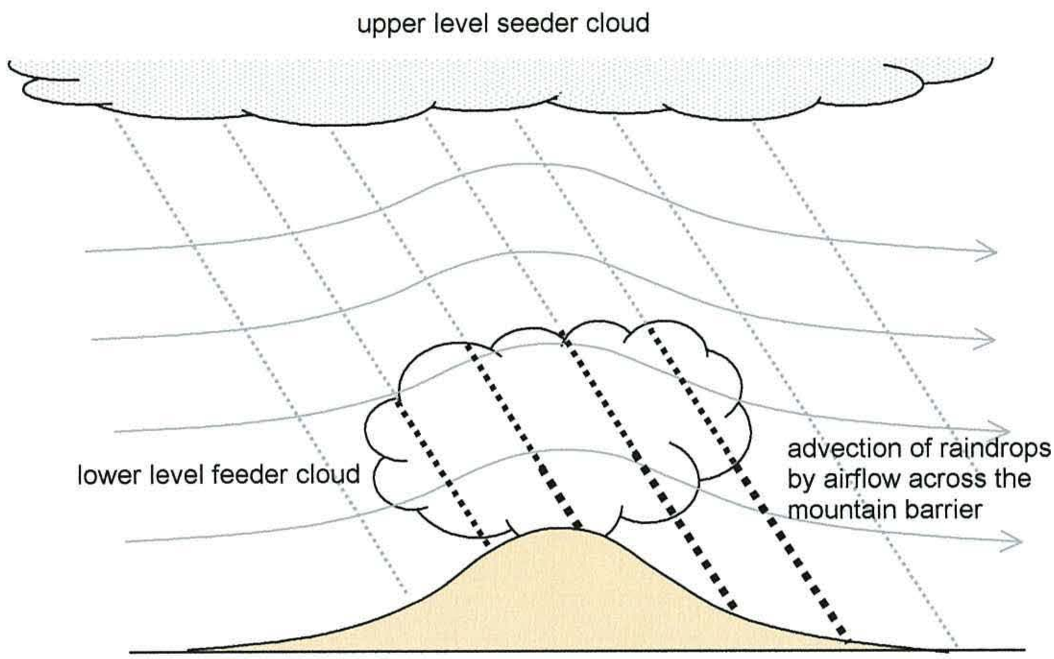

Figure 2.27: Seeder-feeder mechanism for rainfall generation

Bader and Roach (1977) develop formulae for estimating the amount of water vapour washed out by droplets falling through low level orographically produced cloud.

Convective storms

The most intense storm events recorded in the Mawddach catchment are associated with extremely unstable warm air masses undergoing convective uplift. Where a rising air parcel continues to be warmer than the surrounding air, uplift can extend to great altitude. Atmospheric temperatures near the tropopause are well below the freezing point of water so ice crystals separate by freezing, rather than the condensation of water droplets. Cool, descending counter-currents can develop in clouds of great vertical extent, leading to convective cycling and the accretion of ice crystals into larger hail particles. In the process, static electrical charges can be separated and conditions develop for the discharge of lightening. A typical thunder cloud structure is illustrated in fig.2.28. Particular features often present are an upper cloud extension, termed an *anvil*, close to the tropopause, and a low level cloud development ahead of the main convective structure, termed a *roll cloud* or *shelf cloud*. A *gust front* may occur below the leading edge of the thunder cloud, with high winds of varying direction causing damage at the ground surface. Precipitation typically commences as hail, with a progression to heavy rain as the storm advances.

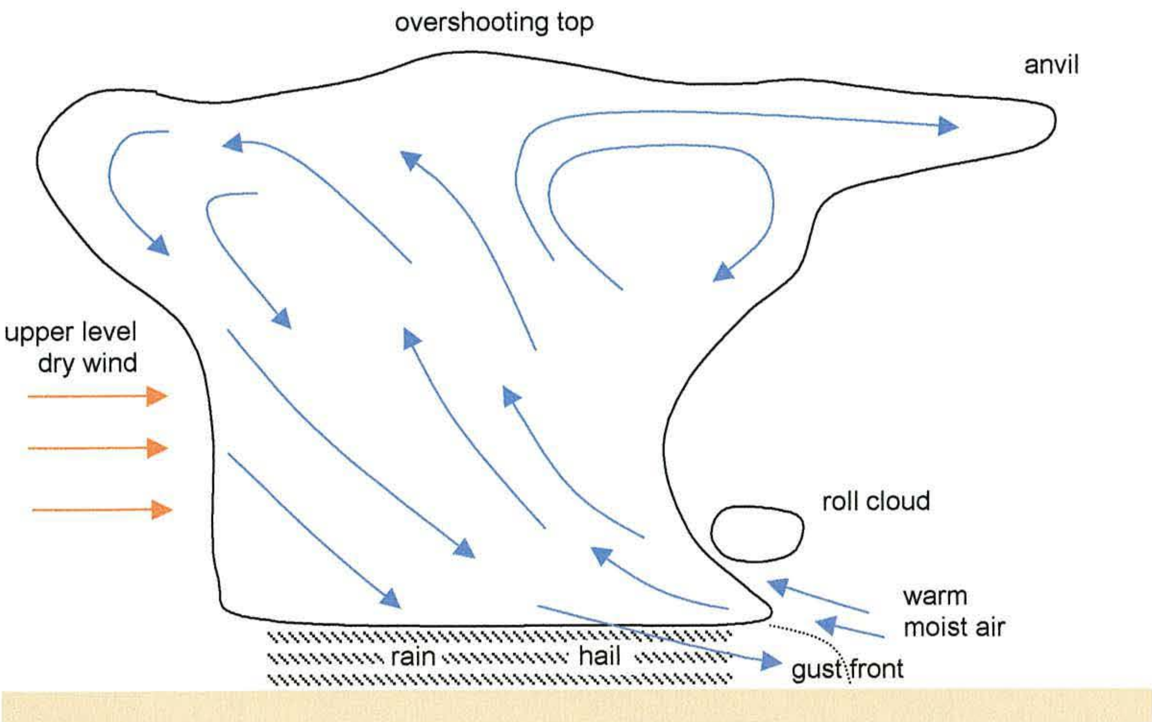

Figure 2.28: Structure of a typical thunder cloud (after Short, 2006)

Squall line structure

Thunder clouds may develop in isolation, but the most destructive storms occur when a line of thunder clouds are formed in association with a synoptic scale front. This structure is known as a *squall line* (National Weather Service, 2005). The storm of 3 July 2001 which caused widespread damage in the Mawddach catchment was of this type.

A section of squall line over the Midwest of USA is shown in the rainfall radar image fig.2.29 (National Weather Service, 2005). Red colour shading indicates zones of maximum rainfall intensity. Embedded within the squall line is a *bow echo* structure – a curved line of thunderstorms associated with strong vertical convection. Cold air is drawn in at the rear of the bow, forming an inflow notch of lower rainfall intensity. The most powerful thunderstorm activity is often just to the north of the bow apex, with the development of strong cyclonic vortices carrying warm air aloft.

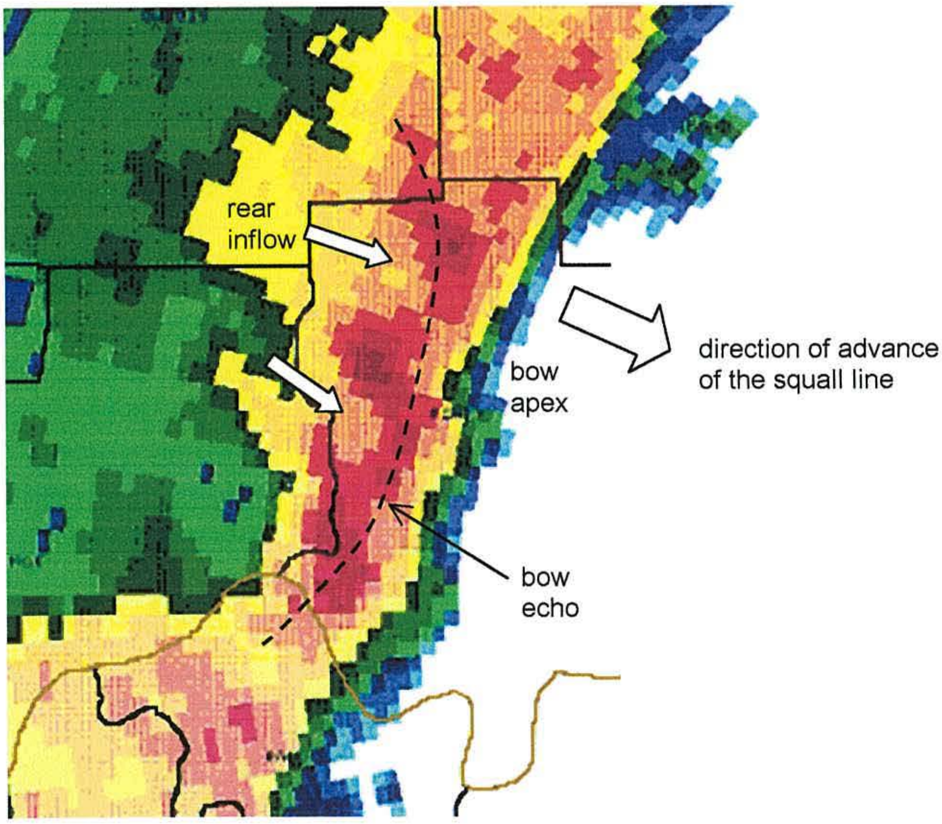

Figure 2.29: Rainfall radar image of a squall line over Kentucky
source: US National Weather Service

The leading edge of the squall line generally produces a sharp rainfall boundary. There may, however, be a large area of stratiform precipitation extending to the rear of the main rainfall band due to high level air flow from the front to the rear of the squall line.

Several theories have been proposed for the development of thunderstorm squall lines ahead of a cold front, and may variously account for different storm events. The cold front may push forward, so that cold air aloft intrudes above warmer air near the ground. This situation leads to severe instability. Intrusion of a cold air wedge at ground level ahead of the main front can impart an upwards motion to the warm air mass, which will lead to continued convective uplift if instability is present. Subsiding cold air behind the squall line can complete the return flow for the convective cell and drive further uplift (fig.2.30).

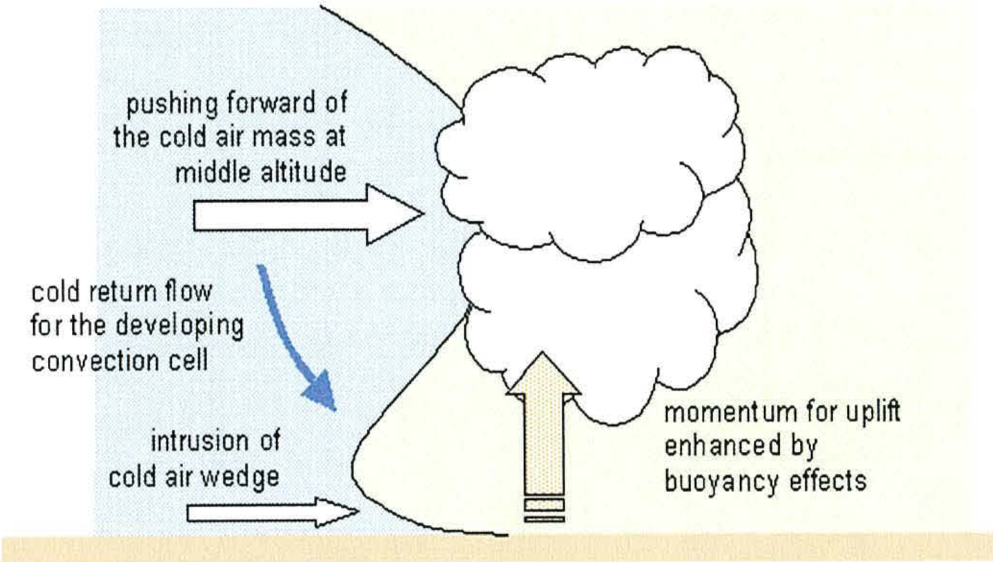

Figure 2.30: Convective uplift ahead of a cold front.

Mechanisms for squall line development have been examined in detail by Fovell and Tan (1998, 2000), illustrated here as fig.2.31:

> A body of air sufficiently warmer than its surroundings can begin to ascend through buoyancy forces. The ascending air body compresses the air above itself, causing an increase in pressure. Pressure is relieved by the

establishment of contercurrents flowing downwards around the margins of the ascending air body. In this way a convective cell is established (fig. 2.31a).

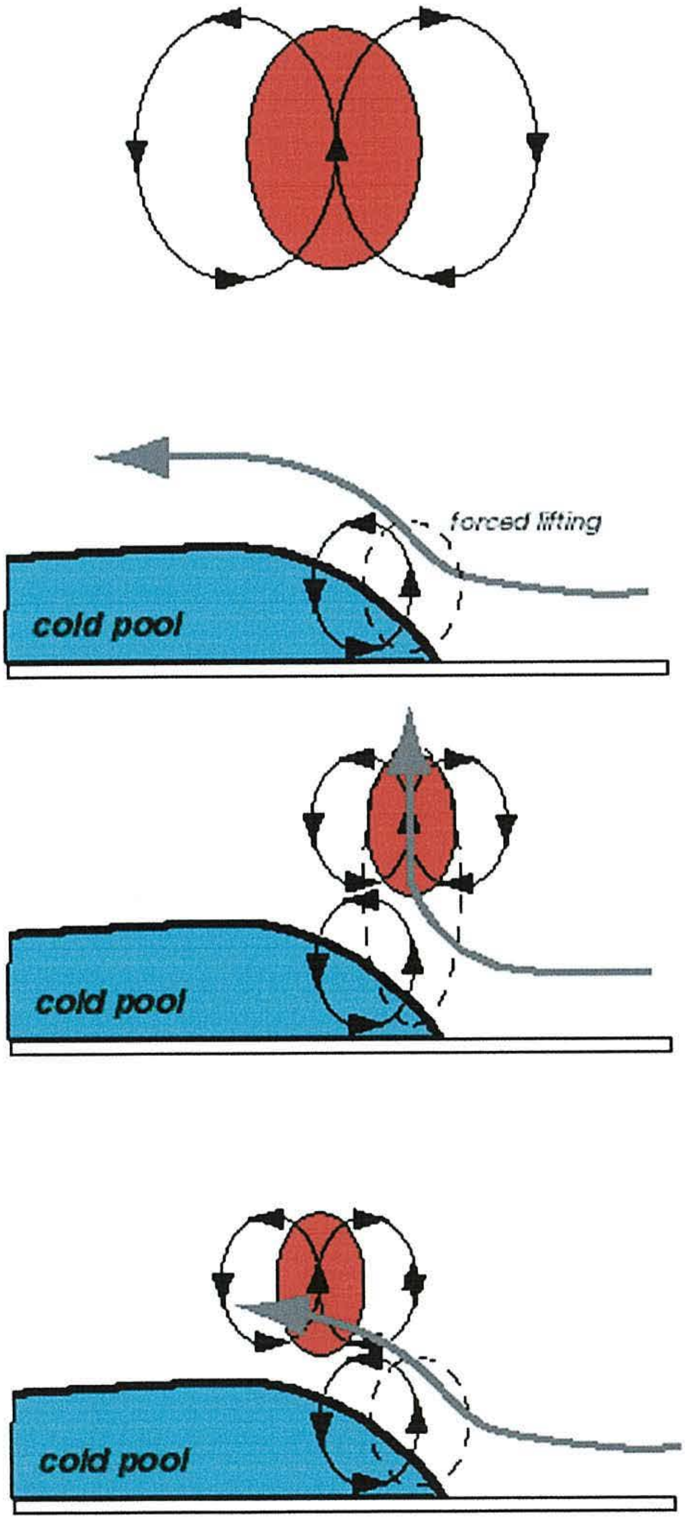

Figure 2.31: Diagrammatic representation of convective processes at a squall line. After: Fovell and Tan, 1998.

Fovell and Tan assume convective activity at a squall line is initiated by the extension of a tongue of cold air at ground level ahead of a cold front. This advancing cold pool displaces warm moist air upwards. An asymmetric convection is established, with a countercurrent of cooler air descending rearwards into the cold tongue (fig. 2.31b).

If sufficent instability is present, bodies of warm air may begin to rise at the front of the cold tongue (fig. 2.31c). Interaction with the low level circulation causes the convective cells to be advected backwards above the cold pool at the same time as they are developing in vertical extent (fig. 2.31d). Cold air begins to enter the lower parts of the convection cell, and a point is reached where convective instability is removed. This results in the final fragmentation of the convection cell and upwards motion ceases.

The theory developed by Fovell and Tan (1998, 2000) can explain many charcteristics of squall lines, including: their position some tens of kilometers ahead of an advancing cold front, their narrow lateral extent, and the well developed flow of cold decending air at the rear. The authors have tested their theory by field observations and detailed modelling. An example model sequence is shown in fig.2.32. This figure combines displays of potential temperature (shown by shading, with dashed contours for a negative temparature zone representing the low level cold pool), and vertical air velocities (shown by solid contours for upwards motion and dotted contours for downwards motion).

Frame A illustrated the initiation of convective activity in a body of warm air displaced upwards by the advancing.

In frames B and C, the convection cell is advected backwards above the cold tongue and reaches maturity. The cell develops to a great vertical height, and shows a strong downwards countercurrent at the rear. Rainfall would be intense at this stage due to convective cooling and condensation within the ascending air flow.

In frame D, cold air at mid-troposphere levels is mixing with the decending air flow and stabilising the convective cell. Temperatures begin to fall and the cell fragments, bringing convective activity to a close. Simultaneously, however, a new convective cell is initiated at the forward edge of the cold tongue and the sequence begins again.

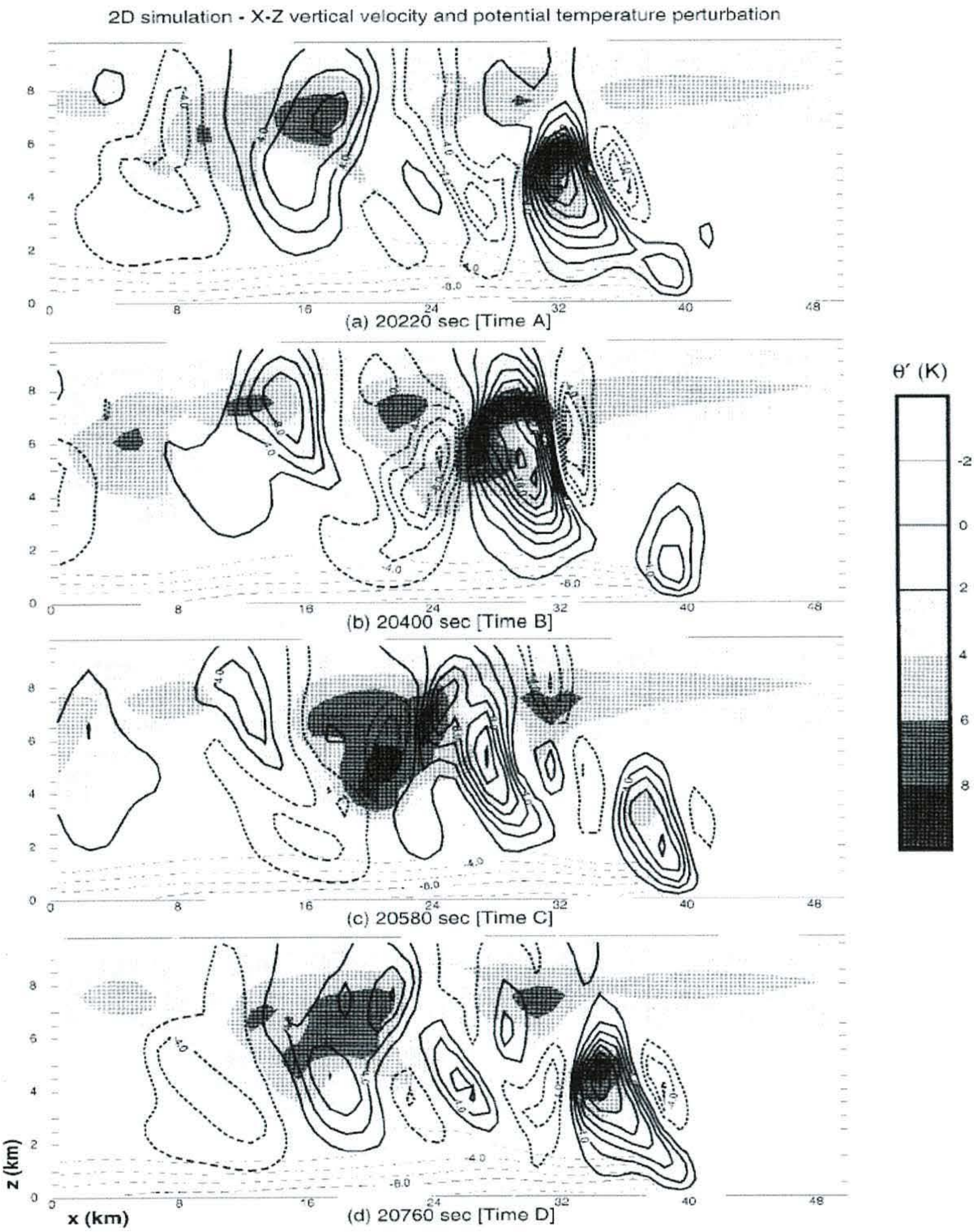

Figure 2.32: Example modelling sequence showing a cycle of convective cell development within a squall line. From: Fovell and Tan (1998).

Summary

- Most rainfall in North Wales is associated with mid-latitude cyclones which have crossed the Atlantic.
- Cyclones move eastwards roughly following the track of the Polar Front and its associated Jet Stream.
- Cyclones may also develop in isolation within the Polar air mass north of the Polar Front.
- Cyclones associated with the Polar Front have two main development patterns. Cyclones following the Norwegian model evolve to produce an occlusion of warm air undercut and lifted from the surface by cold Polar air. Cyclones following the Shapiro-Keyser model evolve to produce a cylindrical warm-core seclusion surrounded by colder air.
- Linking between a cyclone and the overlying Polar jetsteam can determine whether development will follow the Norwegian or Shapiro-Keyser model.
- Rainfall associated with a mid-latitude cyclone is produced by ascending air flow within the warm sector, termed the 'conveyor' and marked by cloud development.
- On making landfall, mid-latitude cyclones may encounter mountains which promote rainfall by forcing the uplift of moist air to the level of condensation.
- Mountains may induce gravity waves in neutrally stable air, or may initiate the continued uplift of unstable air.
- Raindrops originating from high cloud layers may grow by accretion of water vapour during their descent through low level cloud, known as the *seeder-feeder* mechanism.
- Some of the most severe floods in North Wales are caused by convective processes, where unstable warm moist air rises to produce thunderstorms.
- Thunderclouds may align along a cold front to produce a squall line. The squall line may remain almost stationary for a period, with convective cells repeatedly growing and decaying along its length.
- All of the processes listed above need to be incorporated in a successful rainfall prediction model for the Mawddach catchment. It will be shown below that the MM5 meteorological model can represent all these processes to a high degree of accuracy, with the possible exception of some convective thunderstorm events.

2.2 Rainfall in the Mawddach catchment

Rainfall monitoring

Rainfall distribution is clearly an important controlling factor for catchment hydrological response. Field investigations were carried out to determine the extent to which rainfall distribution patterns varied across the Mawddach catchment:

- during individual storm events
- between different storm events

At the commencement of the project, a small number of raingauge stations were operated in and around the Mawddach catchment by the Environment Agency:

	Grid reference
Ffestiniog	716433
Arenig	839391
Drws y Nant	849269
Rhydymain	797238
Llyn Cynnwch	736204

Data from these stations has been used in studies of the 3 July 2001 Mawddach flood event (Barton, 2002).

Figure 2.33: Weather station at Coleg Meirion-Dwyfor, Dolgellau

To improve the coverage of meteorological data for the catchment, additional stations have been added: Automatic weather stations have been installed at Coleg Meirion-Dwyfor in Dolgellau (fig.2.33) and Aran Hall School, Rhydymain. These provide readings of temperature at 10 minute intervals, 10 minute averaged wind speed and direction, and tipping bucket raingauge event data.

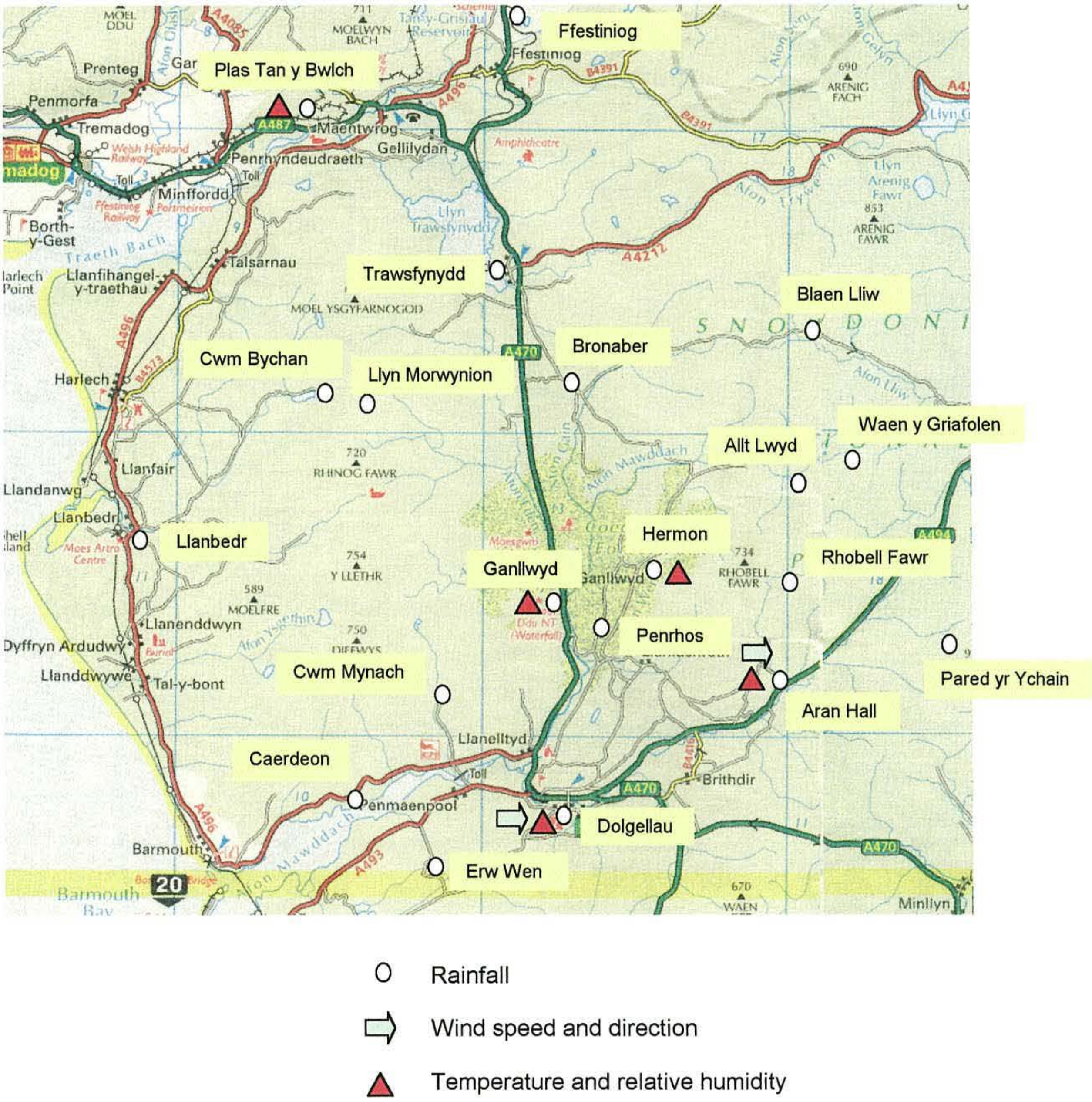

Figure 2.34: Meteorological recording sites

A pattern of 18 automatic rain gauges has been established across the Mawddach catchment and adjoining areas. The gauges are of the tipping bucket type, with event signals sent to an electronic data logger. Sites were chosen to fill gaps in the existing coverage, particularly for mountain terrain (fig.2.35). The distribution of additional recording sites in shown in figure 2.34.

Figure 2.35(a). Pared yr Ychain raingauge site, Aran mountains.

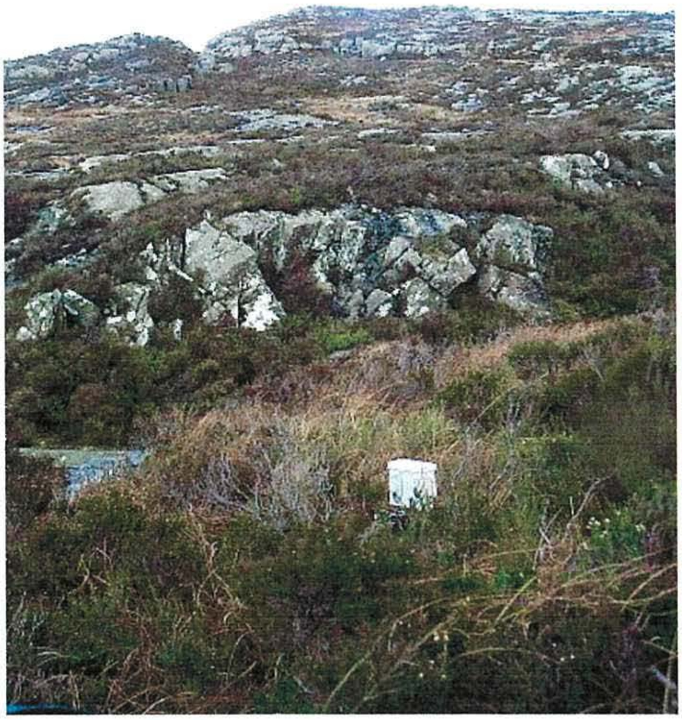

Figure 2.35(b). Llyn Morwynion raingauge site, Rhinog mountains.

Classification of rainfall patterns

Data was collected from the raingauge array for 28 storm events during the period August 2002 to February 2004. A 'storm event' was defined as a 24 hour period during which at least 15mm of rainfall was recorded by a raingauge within the Mawddach catchment. An isohyet map was plotted for each storm event. Meteorological Office synoptic charts were also obtained. Prevailing wind directions during all the storm events were from the westerly or southerly quadrants.

Examination of the set of iohyet maps revealed three principal rainfall distribution patterns. These have been termed rainfall distribution **Types A1, A2** and **B**. Every frontal storm event recorded during the project conformed to one or other of these three basic patterns. It should be noted, however, that convective thunderstorm activity shows more randomness and cannot be assigned to an A-B pattern.

Rainfall distribution Type A1

Rainfall is concentrated in the area of Coed y Brenin and Rhobell Fawr, giving a single zone of maximum rainfall near the centre of the catchment. Isohyets appear as ellipses extended on a WNW – ESE axis.

A typical storm event of type A1 occurred on **8 November 2002**. Isohyet patterns for the storm are illustrated in fig.2.36.

Synoptic charts for the period 8-9 November 2002 are given in fig.2.37. The area of low pressure A remains stationary to the south east of Greenland, whilst low B tracks from the north of Scotland towards the Dutch coast. Early in the morning of 8 November a wedge of warm air is drawn towards low B, creating a depression with warm and cold front structure.

Local meteorologocal charts for Wales for the period 11:00h to 14:00h, 8 November, are given in fig.2.38. The warm front crosses the Mawddach catchment around 11:00h with a N-S orientation, followed around 13:30h by the cold front with orientation NNE-SSW. Low level wind directions within the warm sector have an average orientation between westerly and west-south-westerly.

Heavy rainfall commences as the warm front approaches, with maxima below and to the rear of the front where a warm air conveyor will be ascending with the west-south-westerly air flow. Rainfall is concentrated in the central area of the catchment, with local maxima in the areas of the mountains Diffwys and Rhobell Fawr.

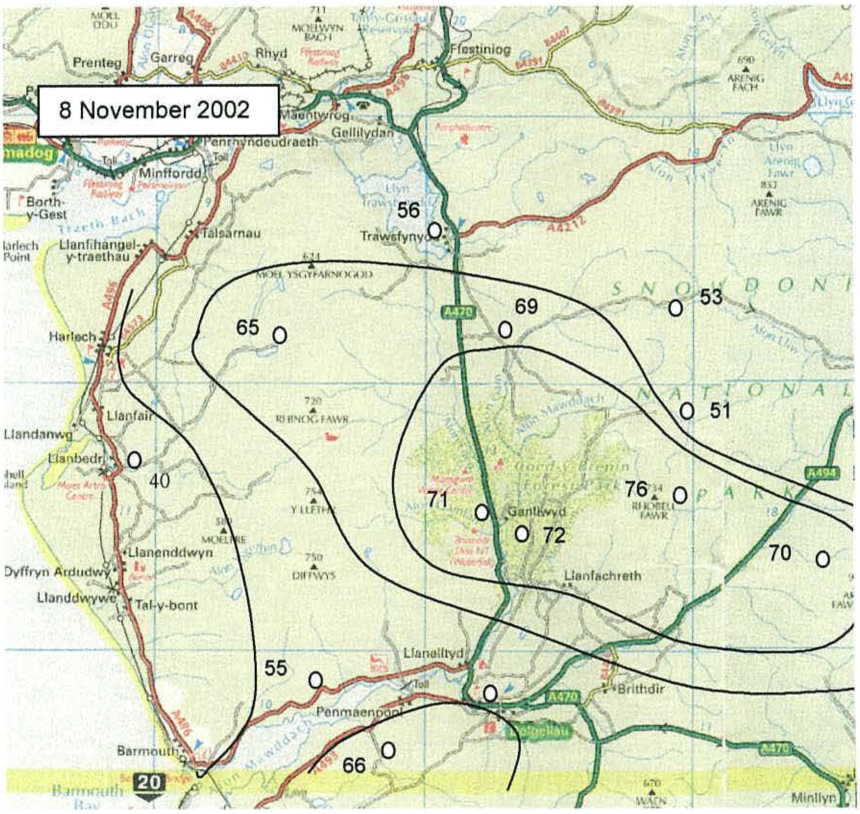

Figure 2.36: Type A1 rainfall distribution pattern. Total storm rainfall isohyets, 8 November 2002

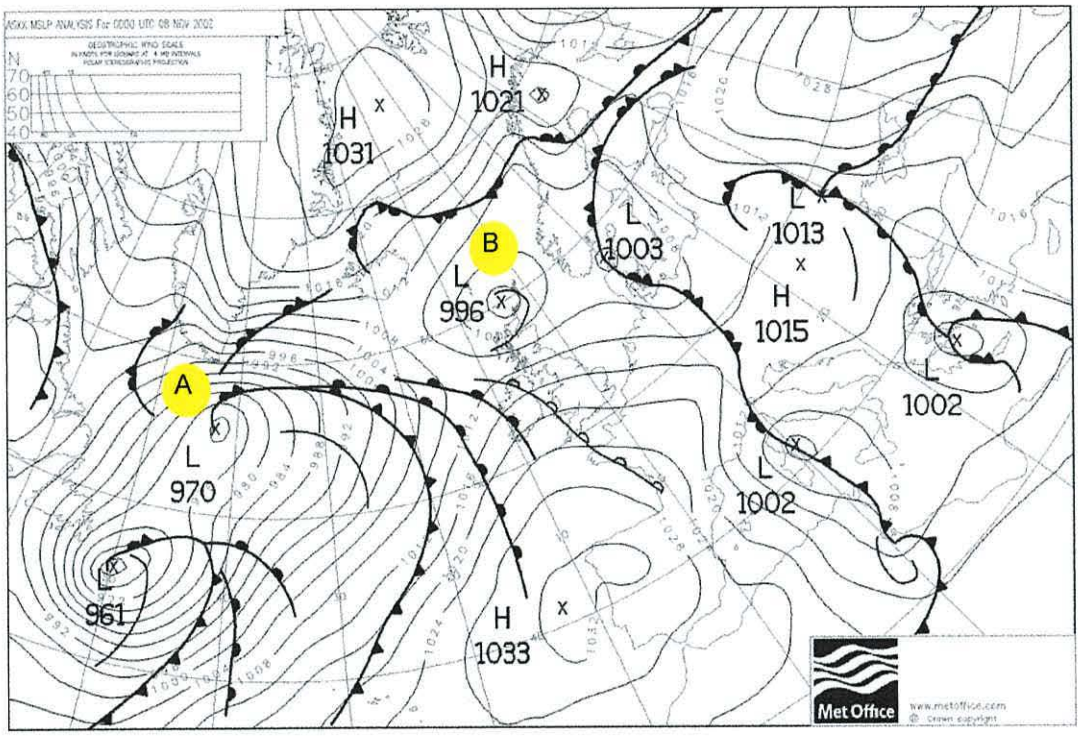

Figure 2.37(a) . Synoptic chart, 00:00h 8 November 2002

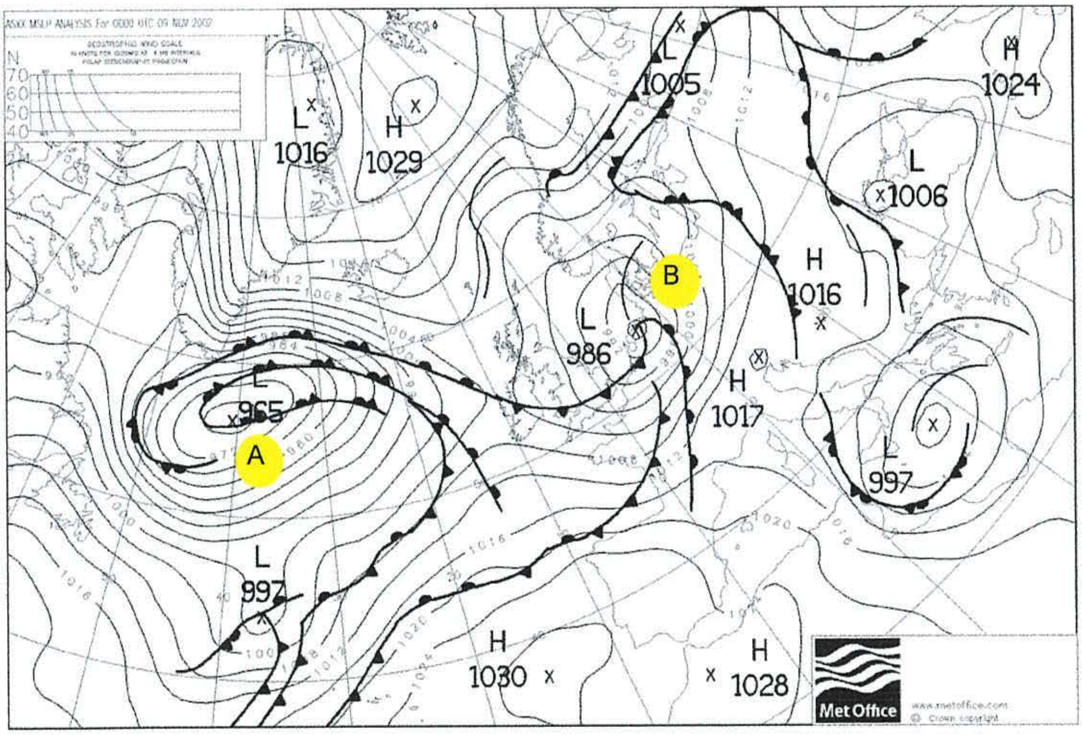

Figure 2.37(b) . Synoptic chart, 00:00h 9 November 2002

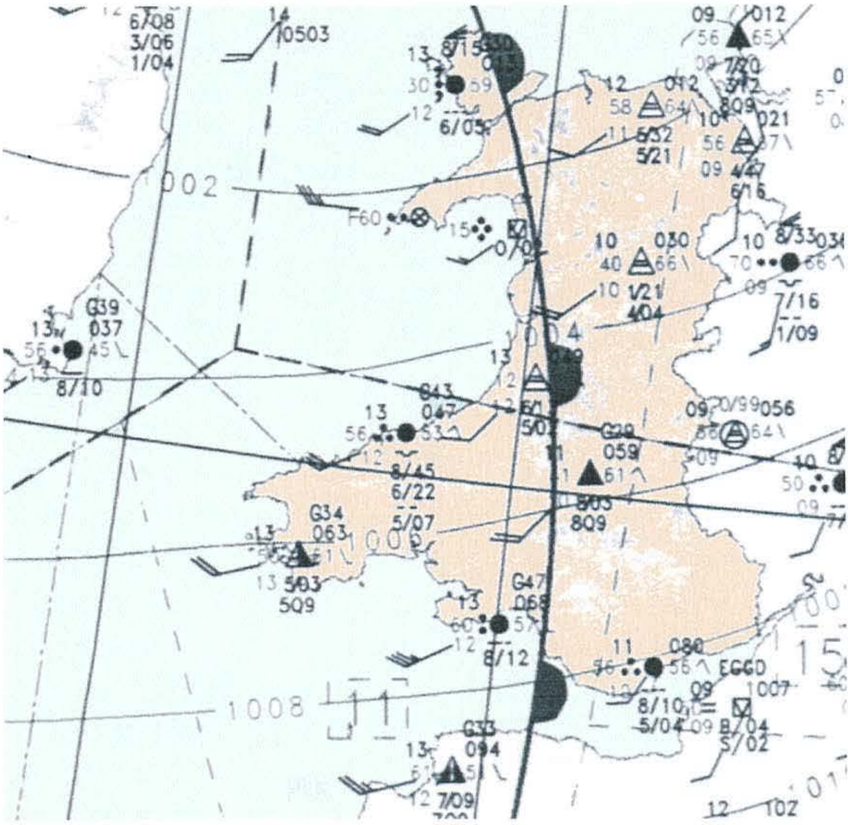

Figure 2.38(a). Regional meteorological chart: 11:00h 8 November 2002

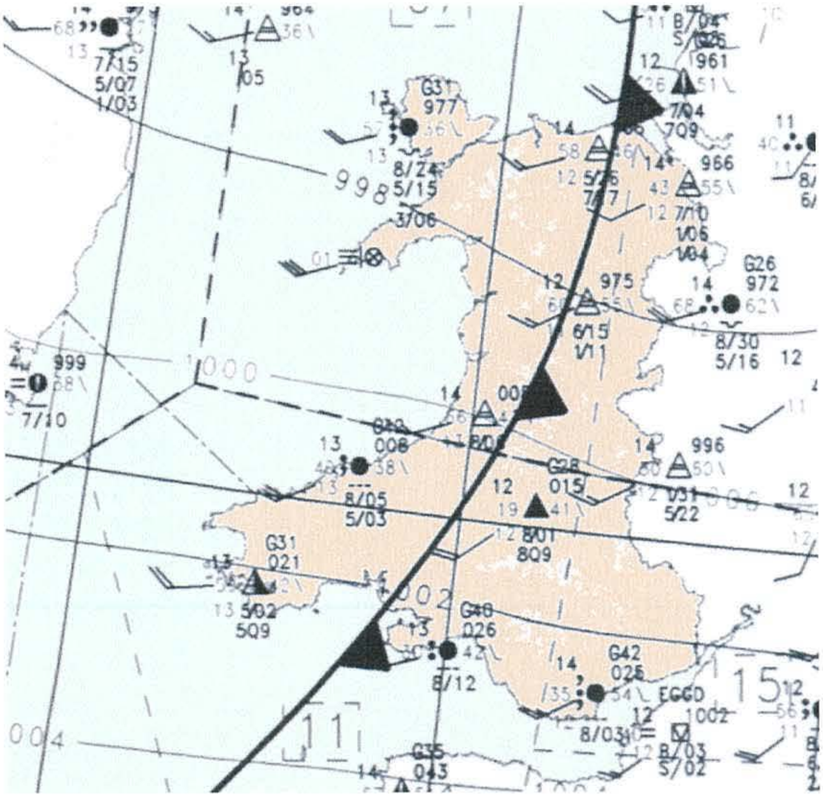

Figure 2.38(b). Regional meteorological chart: 14:00h 8 November 2002

The dominant regional airflow direction on 8 November is aligned with the Mawddach estuary(fig.2.39). It is conjectured that the mid altitude warm airmass in the conveyor ascends over Rhinog Fawr, Diffwys and Rhobell Fawr, initiating precipitation above these mountains. Low level airflows are forced to rise at the valley heads in Coed y Brenin, leading to saturation and condensation. Rainfall enhancement by the seeder-feeder mechanism occurs where rain drops descend through this saturated valley air, concentrating the maximum rainfall in the centre of the catchment.

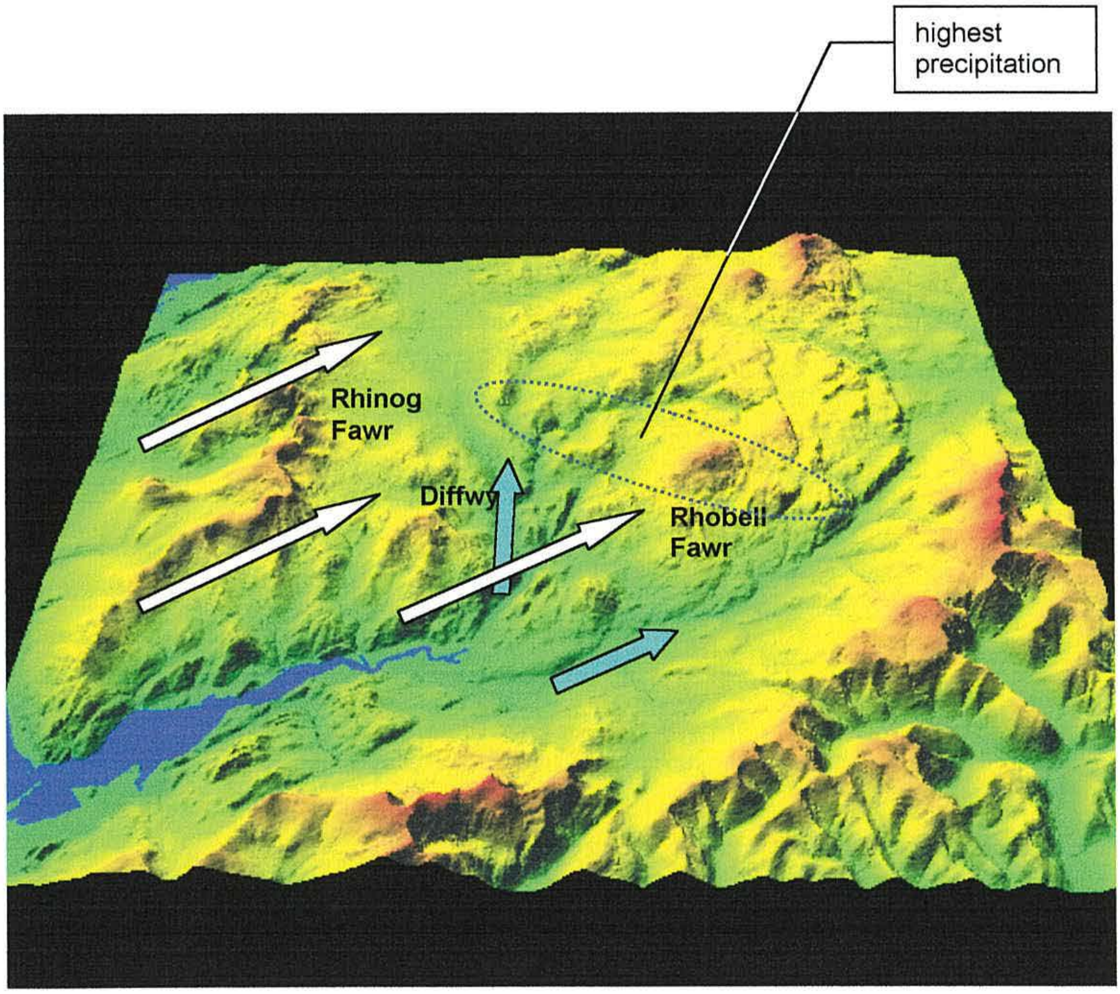

Figure 2.39: Airflow directions across the Mawddach catchment, 8 November 2002. Key to arrows: white: middle atmospheric level, blue: valley airflows.

Rainfall distribution Type A2

Type A2 is a variant on type A1 where rainfall distribution now shows two maxima, one in the area of the Trawsfynydd plateau and the other in the area of Pared yr Ychain in the Aran mountains. Isohyets show a band of high rainfall oriented NW – SE connecting the two zones of rainfall maxima.

A typical storm event of type A2 occurred on **29 December 2002**. Isohyet patterns are shown in fig.2.40.

Synoptic charts for 28-30 December 2002 are given in fig.2.41. During this period there is a slowly moving low A tracking eastwards in the mid Altantic. A depression associated with this low is partly occluded, with surface warm and cold fronts present beyond point C. An older partly-occluded depression at B is tracking eastwards from Scotland to Scandinavia.

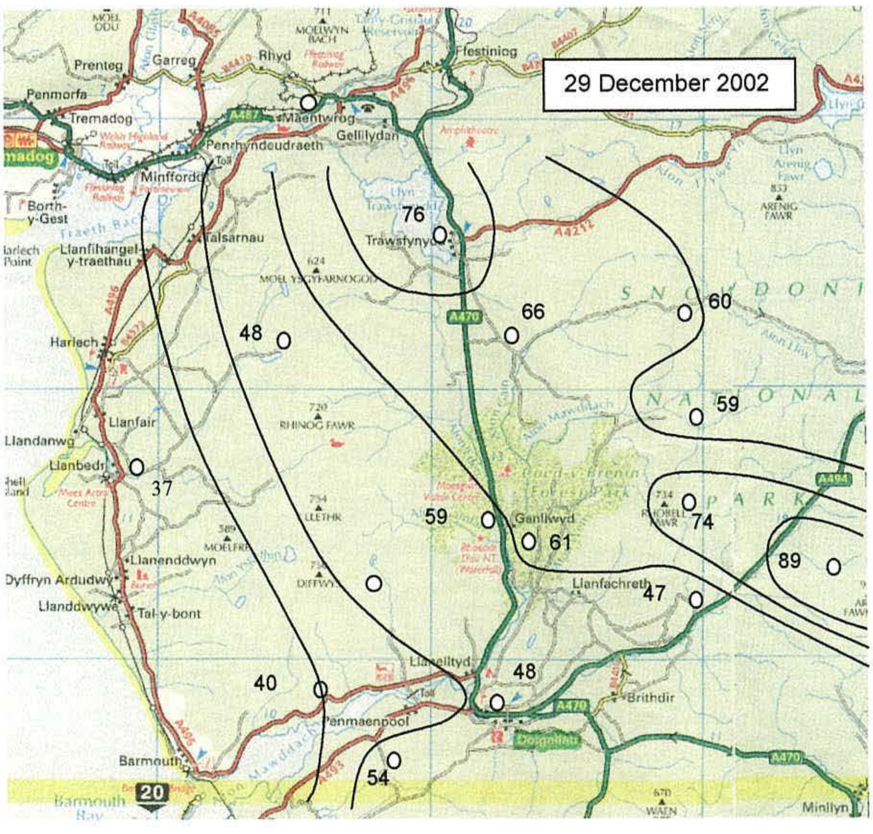

Figure 2.40: Type A2 rainfall distribution pattern. Isohyets show total storm rainfall, 29 December 2002

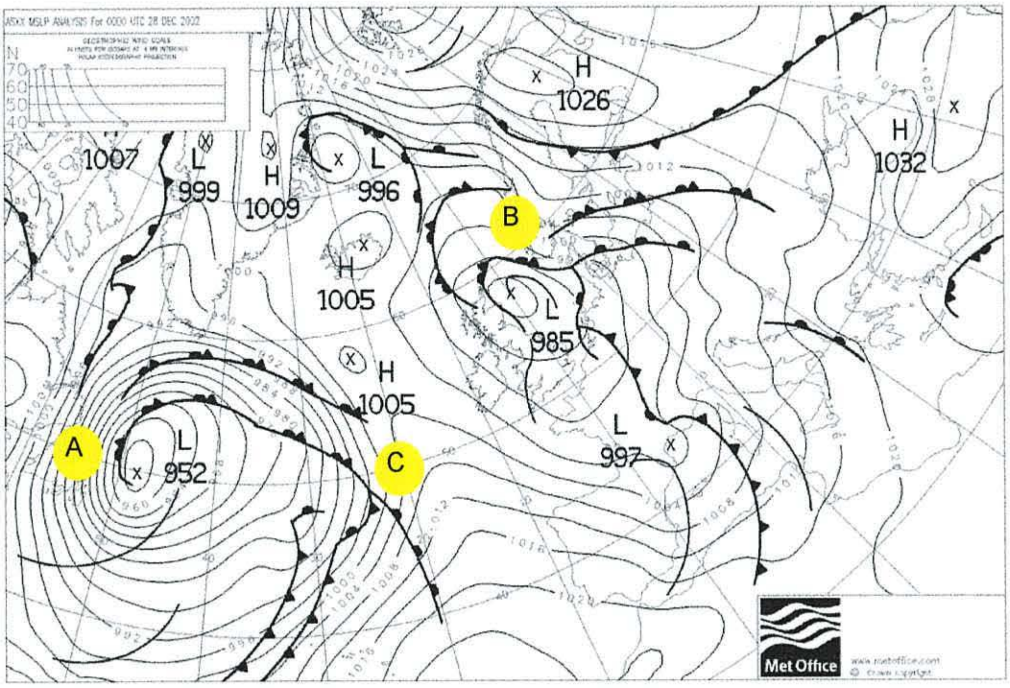

Figure 2.41(a). Synoptic chart, 0:00h 28 December 2002

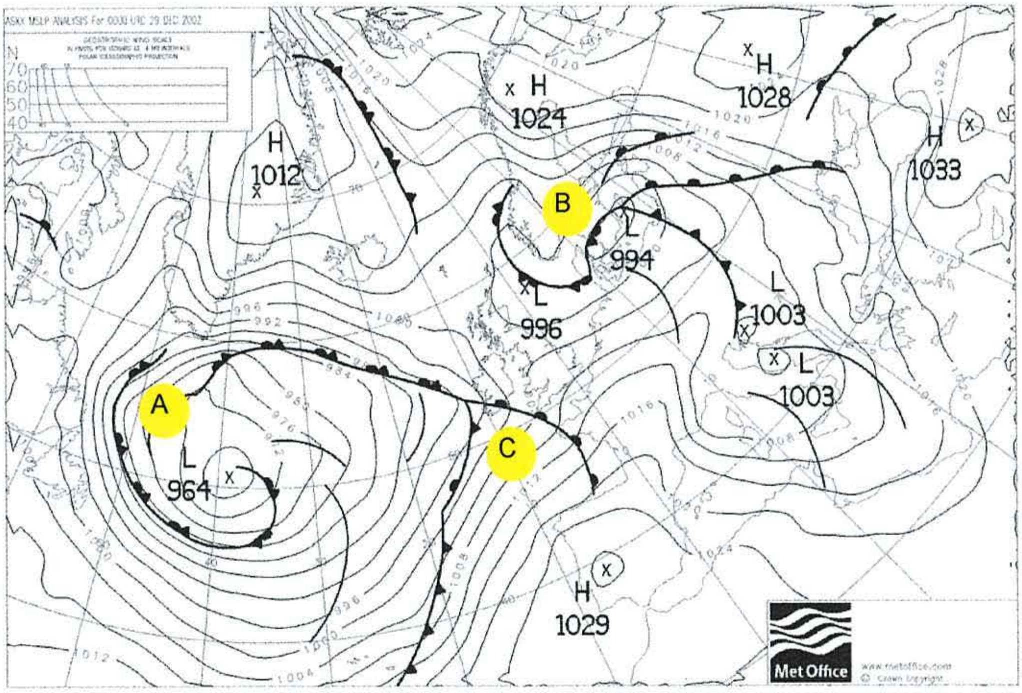

Figure 2.41(b). Synoptic chart, 0:00h 29 December 2002

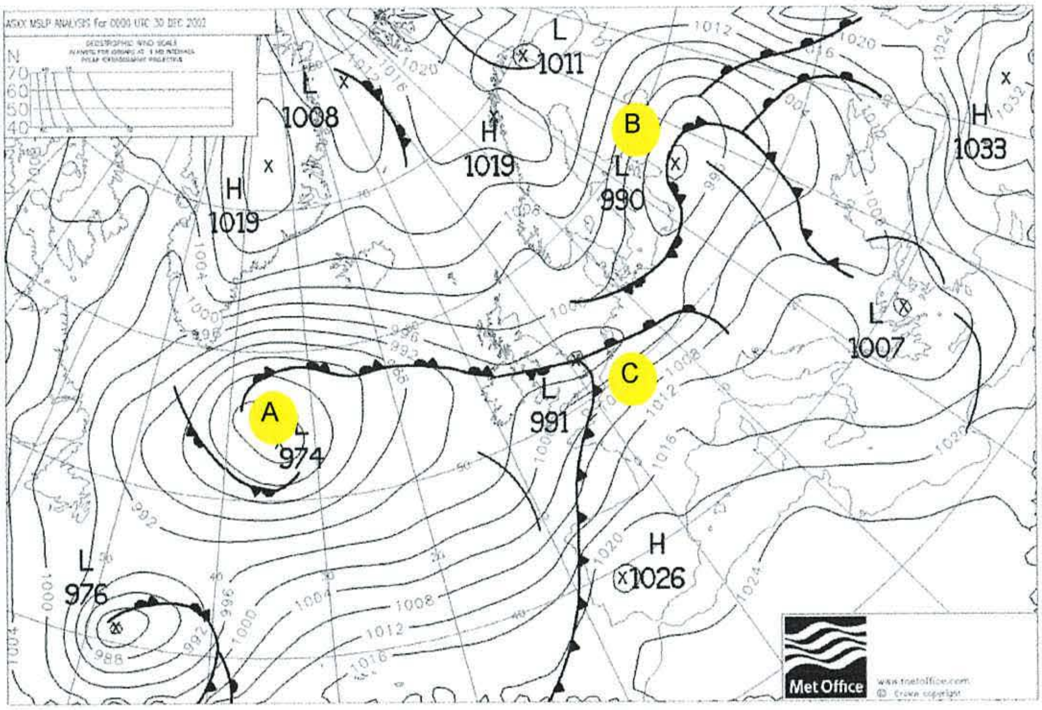

Figure 2.41(c). Synoptic chart, 0:00h 30 December 2002

Regional charts for the period 10:00h to 16:00h on 29 December are given in fig.2.42. The warm front close to point C crosses the Mawddach catchment at 12:00h with a NW-SE orientation. Within the warm sector, winds are from the south-west. The cold front is slow moving and crosses the Mawddach catchment during the evening of 29 December.

Rainfall totals for 29 December are given in fig.2.38. Substantial rainfall occurs around mid-day, below and behind the warm front where a warm air conveyor is ascending towards the NE. Rainfall continues through the afternoon, up to the time that the cold front passes.

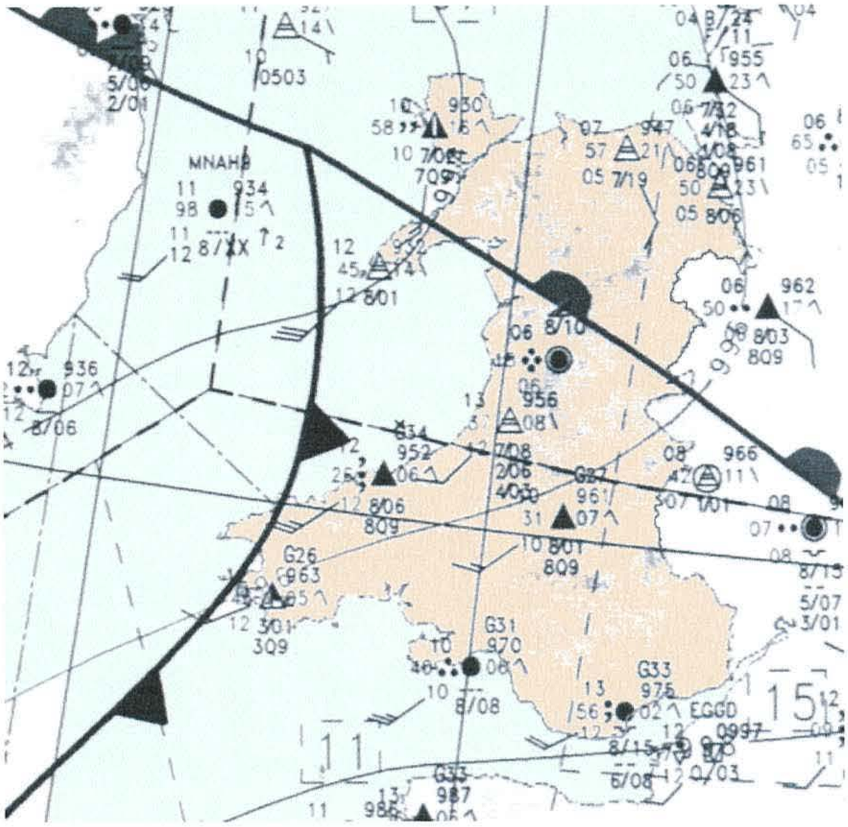

Figure 2.42(a). Regional meteorological chart: 12:00h 29 December 2002

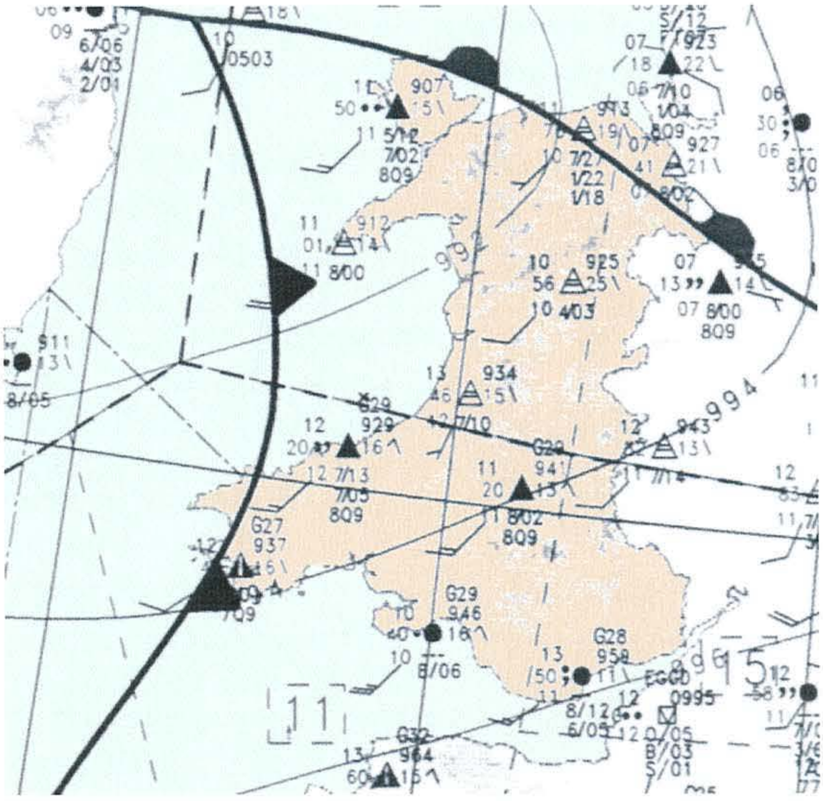

Figure 2.42(b). Regional meteorological chart: 16:00h 29 December 2002

The orientation of winds on 29 December is illustrated in fig.2.43. It is conjectured that the mid altitude warm airmass in the conveyor ascends over Rhinog Fawrand Aran Fawddwy, initiating precipitation above these mountains. Low level airflows follow the deep Mawddach and Wnion valleys and are forced to rise at the valley heads, leading to saturation and condensation. Rainfall enhancement by the seeder-feeder mechanism occurs where rain drops descend through this saturated valley air, concentrating the maximum rainfall in the areas of Trawsfynydd and Pared yr Ychain.

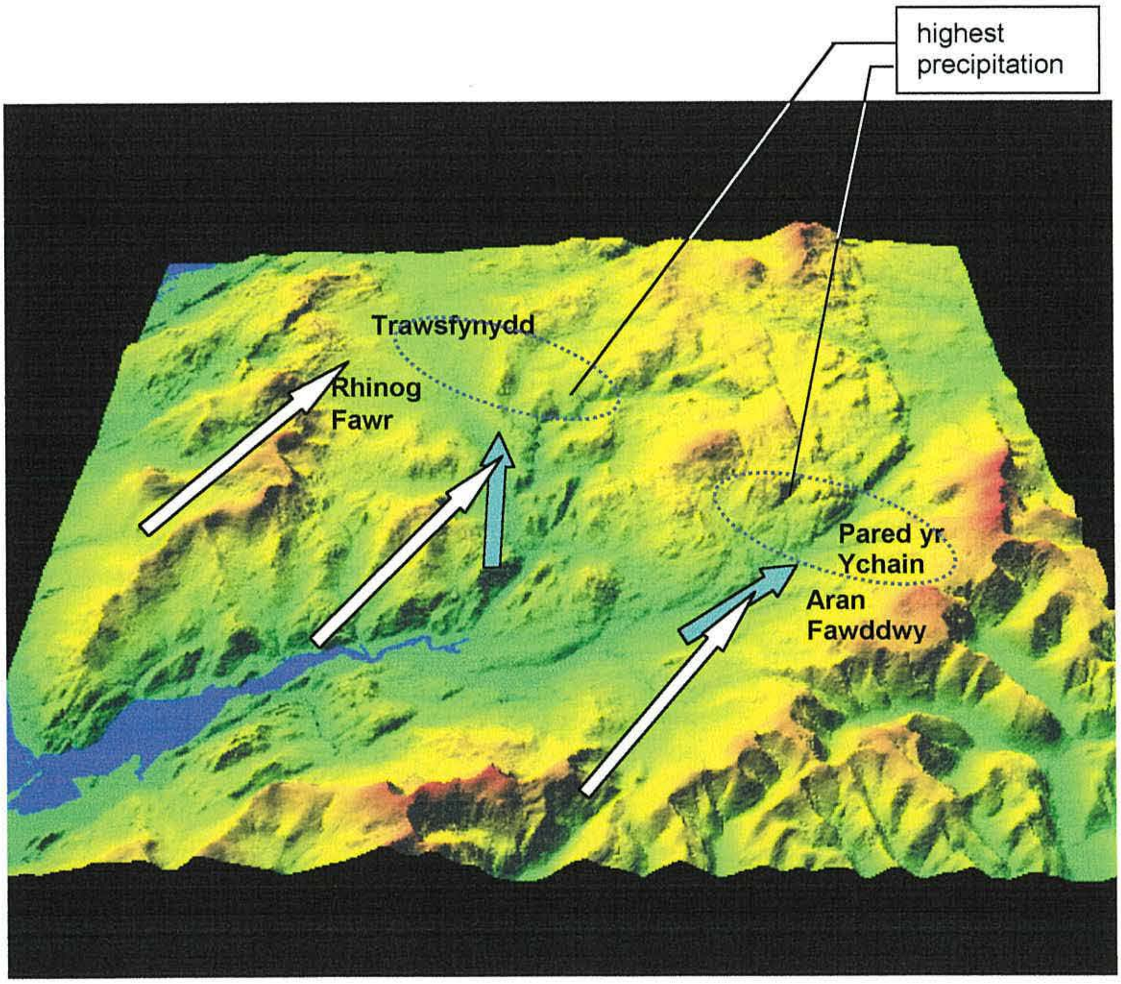

Figure 2.43: Airflow directions across the Mawddach catchment, 29 December 2002. Key to arrows: white: middle atmospheric level, blue: valley airflows.

Rainfall distribution Type B

Rainfall is concentrated in a band following the axis of the Rhinog mountains from the Mawddach estuary in the south to the Vale of Ffestiniog in the north. Rainfall declines inland.

A typical storm event of type B occurred on **22 May 2003**. Isohyet patterns are shown in fig.2.44.

Synoptic charts for 22-23 May 2003 are given in fig.2.45. At this time, a low pressure centre at A is occluding in the area of Greenland. To the east, a low pressure centre B is tracking in from the mid-Atlantic towards the north of Scotland. Associate with centre B is a complex front separating cold Polar air to the north from the warm Tropical airmass to the south. The front shows oscillation, with warm air pushing northwards in some sectors and cold air pushing southwards in others. During 22 May this front sweeps southwards across Wales.

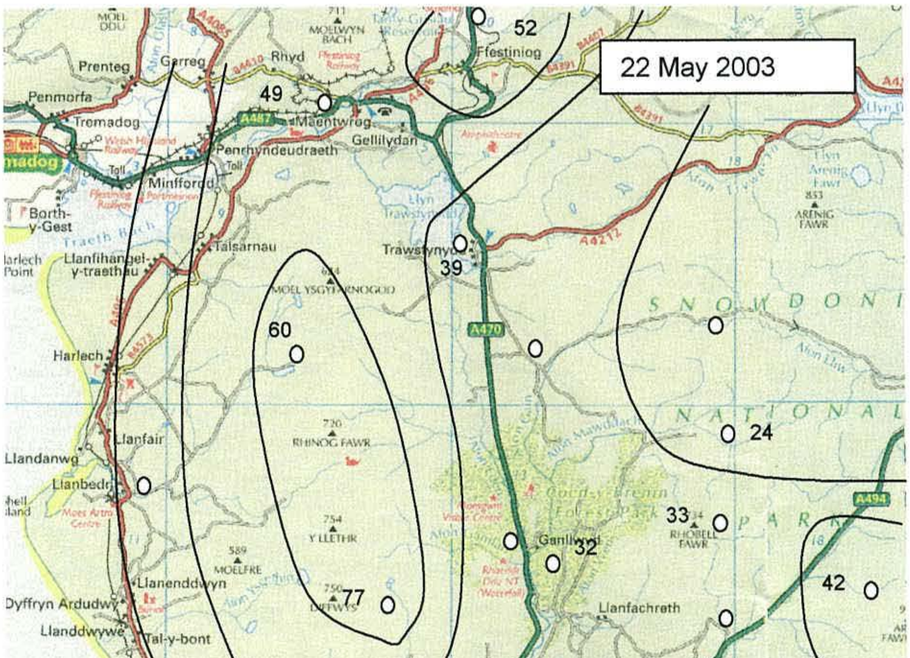

Figure 2.44: Type B rainfall distribution pattern. Isohyets show total storm rainfall, 22 May 2003

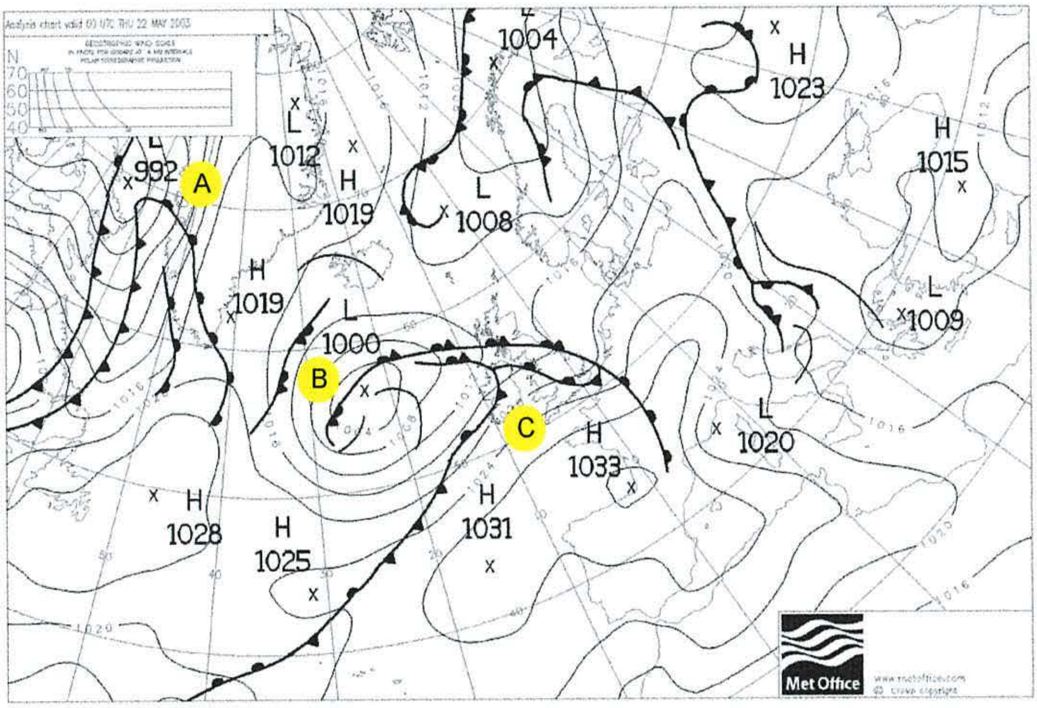

Figure 2.45(a). Synoptic chart, 00:00h 22 May 2003

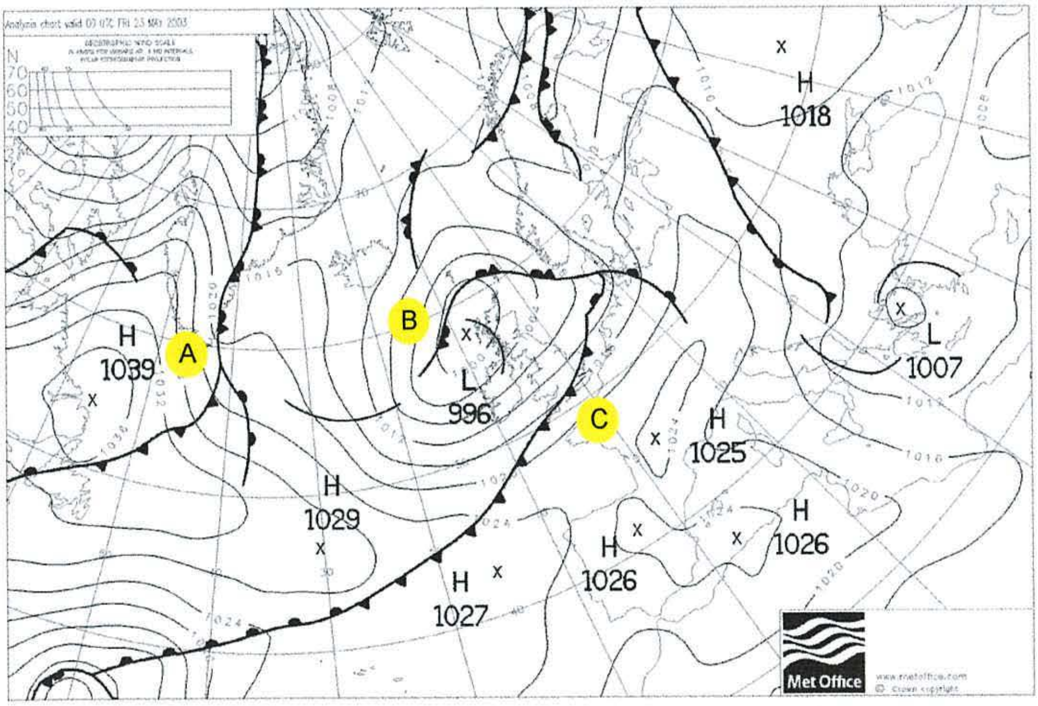

Figure 2.45(b). Synoptic chart, 00:00h 23 May 2003

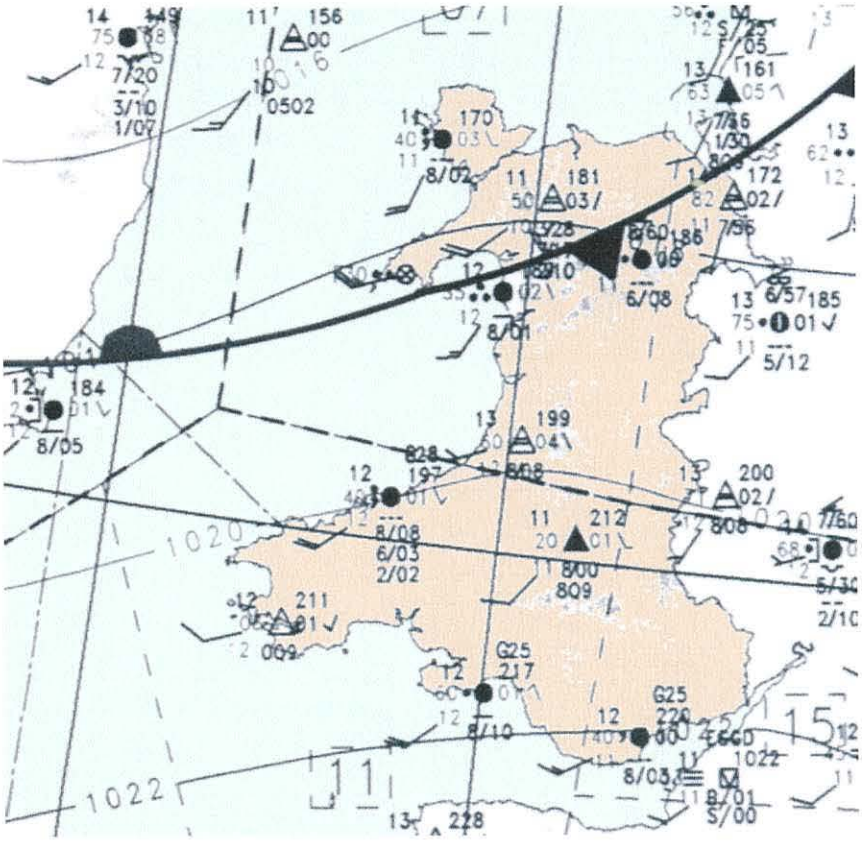

Figure 2.46(a). Regional meteorological chart: 07:00h 22 May 2003

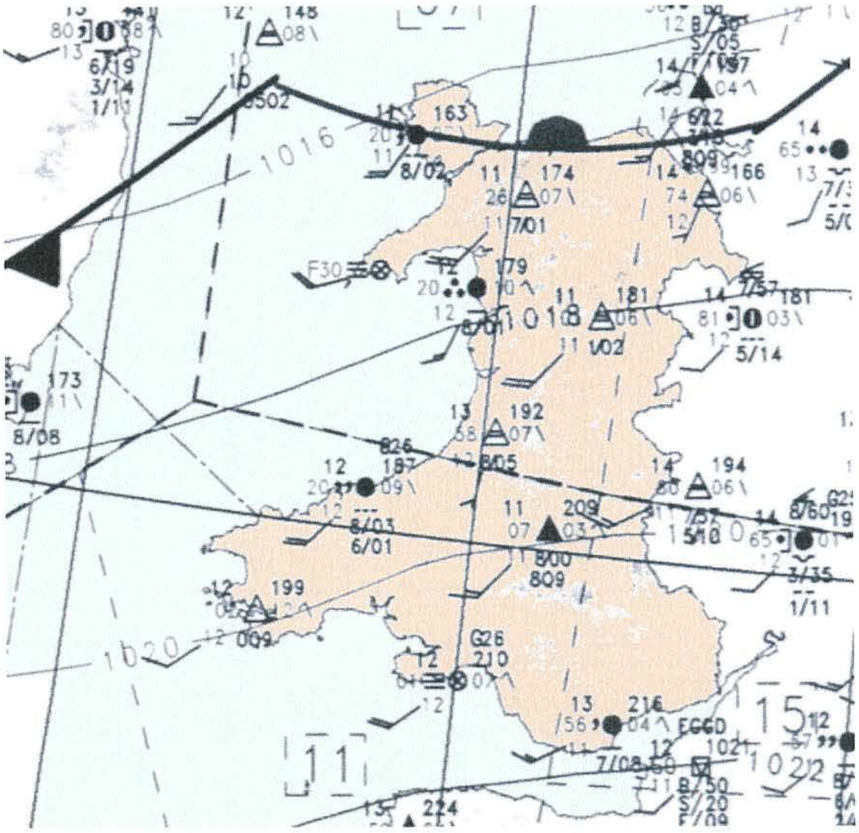

Figure 2.46(b). Regional meteorological chart: 10:00h 22 May 2003

The motion of the oscillating front is seen more clearly in the regional chart, fig.2.46. The front line is moving southwards across the Mawddach catchment at 07:00h, but pushes northwards again to reach Anglesey by late morning. Warm air is being drawn northwards towards the low pressure centre in a conveyor ascending above the surface front.

The orientation of winds on 22 May is illustrated in fig.2.47. It is conjectured that winds from the south-south-west encounter the mountain masses of the Rhinogs and Arans, and forced ascent causes precipitation. Rainfall is largely concentrated along the north-south axis of the Rhinogs, with a subsidiary maximum in the area of Pared yr Ychain to the north of the Aran ridge. Type B precipitation patterns are purely orographic, with no appreciable valley air interraction affecting rainfall intensity.

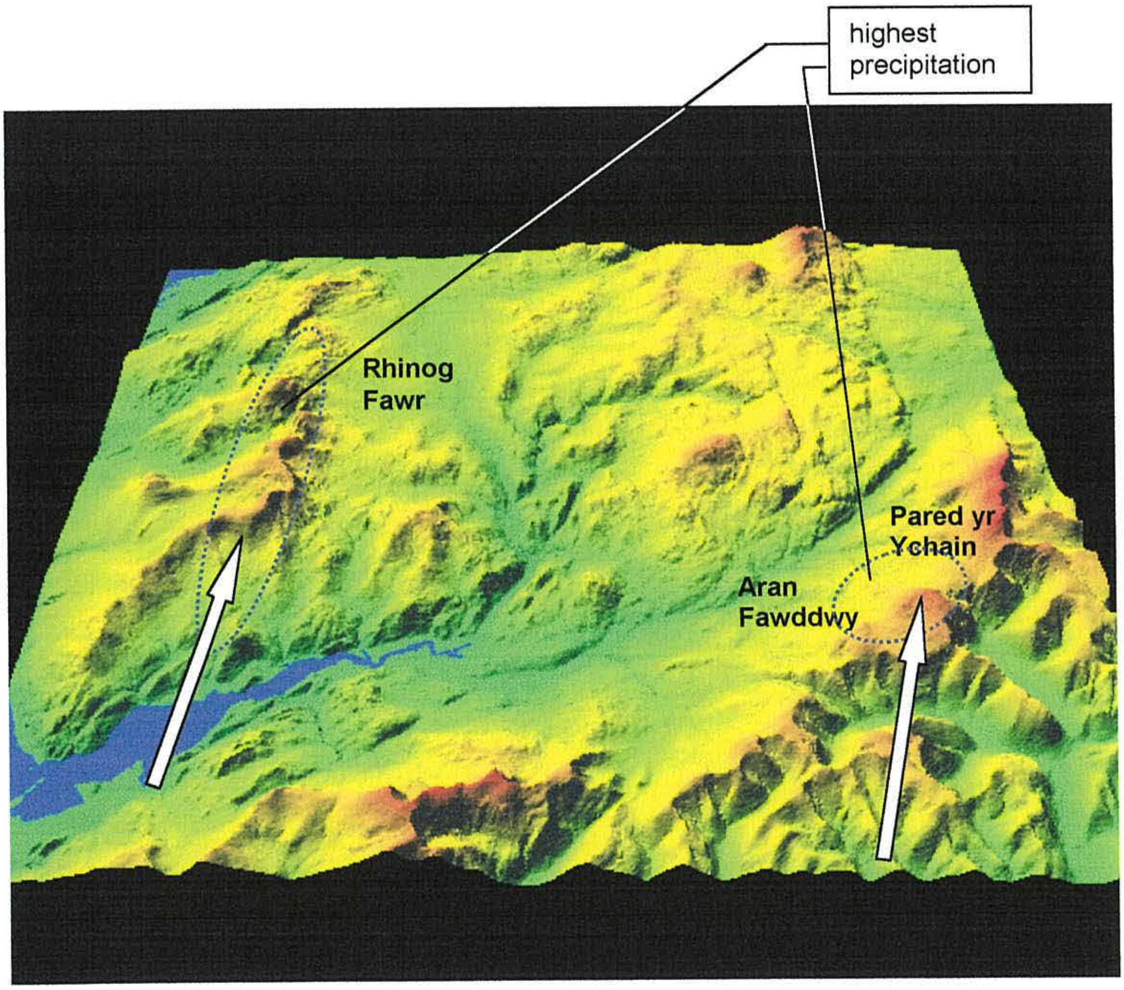

Figure 2.47: Airflow directions across the Mawddach catchment, 22 May 2003

The extended rainfall period of 2-4 February 2004

During the first week of February 2004, the Mawddach catchment experienced flooding of exceptional severity, with farmland around the head of the Mawddach estuary submerged for several days and road communication disrupted (fig.2.49). The flooding was the result of a prolonged period of heavy rainfall, during which large areas of the catchment became saturated and runoff progressively increased. Flooding during this period was widespread throughout Snowdonia:

> *"The early part of February 2004 brought heavy rainfall to North Wales. The effect of this, falling on already sodden ground, led to very serious flooding particularly in the Conwy Valley around Llanrwst. The Conwy Valley railway line suffered very badly with serious damage to the line between Tal y Cafn and Betws y Coed. Repairs to the line were extensive and it was not reopened until 22nd May 2004."* (Sallery, 2005)

Figure 2.48: Flood damage to the Conwy Valley railway line near Betws y Coed 4 February 2004. photo: Dave Sallery

The February 2004 flood event has been analysed by Sibley (2005). It will be used as a test case in the evaluation of hydrological models for the Mawddach catchment.

Figure 2.49: Flooding around Llanelltyd at the head of the Mawddach estuary, 4 February 2004

The origins of the flood event can be ascribed to a period of nearly a week in which the jet stream remained stable above the British Isles (fig.2.50). During this time a series of depressions formed in the mid-Atlantic and tracked north eastwards below the jet stream, carrying a sequence of fronts across North Wales.

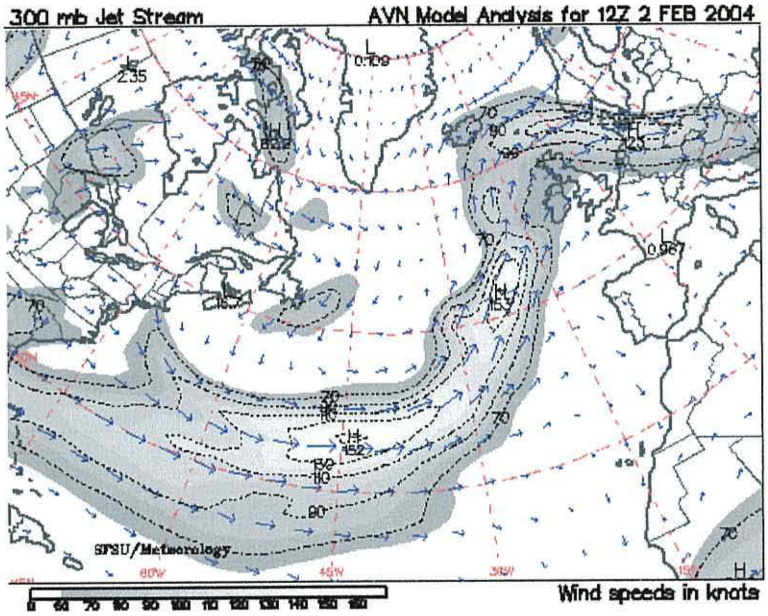

Figure 2.50(a).
Jet stream map for 12:00h, 2 February 2004

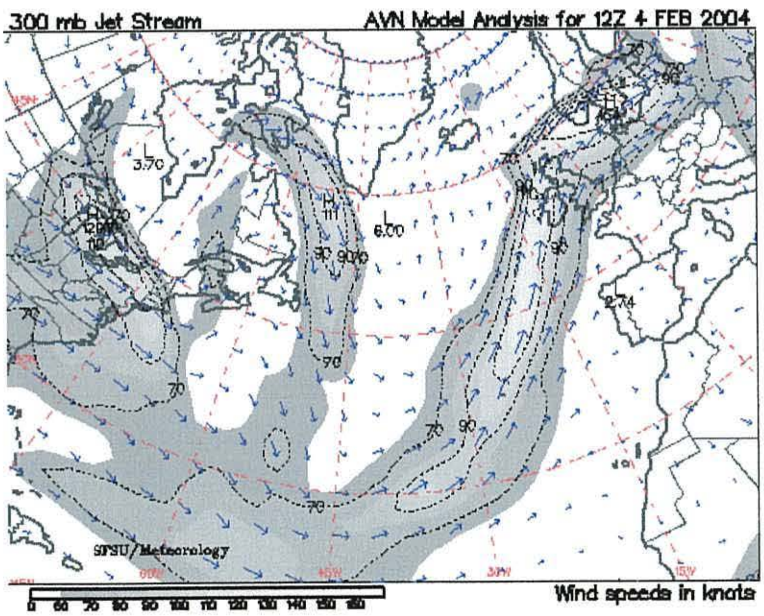

Figure 2.50(b).
Jet stream map for 12:00h, 4 February 2004

Synoptic charts for the period 00:00h 3 February to 00:00h 5 February are given in fig.2.51. Fast moving low D clears Britain during 2 February, with a cold front associated with low C moving north-westwards across Wales during that day. On 3 February this front pushes slowly southwards to cross Wales for a second time.

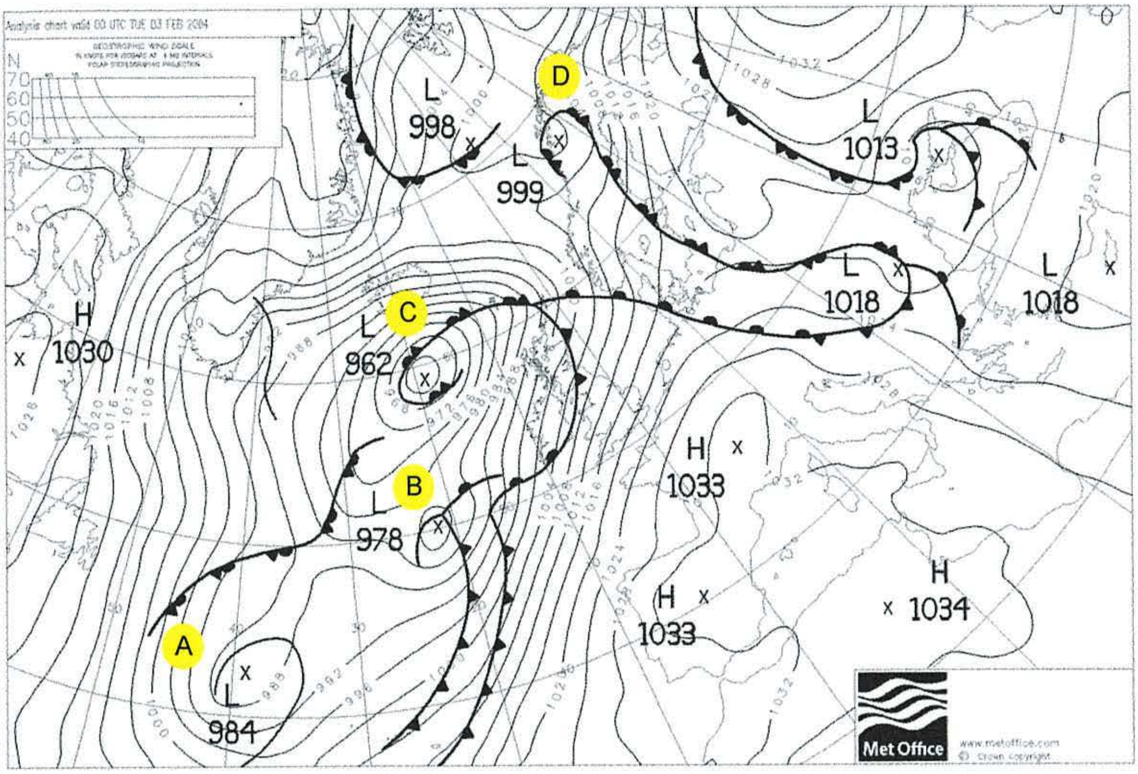

Figure 2.51(a). Synoptic chart for 00:00h, 3 February 2004

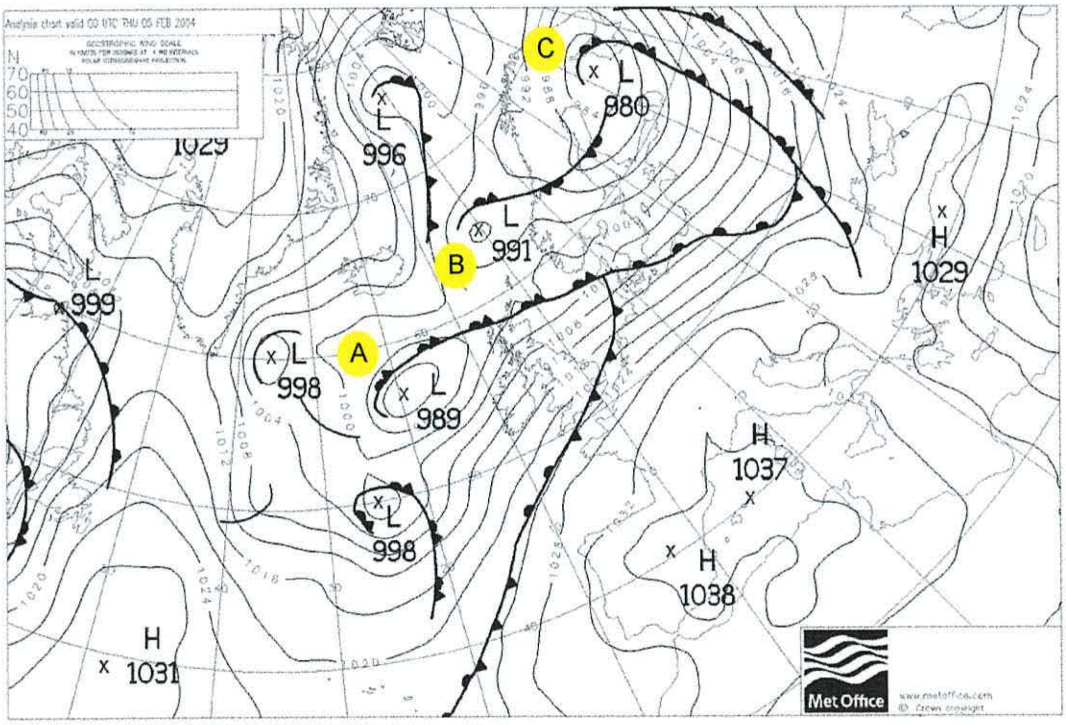

Figure 2.51(b). Synoptic chart for 00:00h, 5 February 2004

Frontal system C at 00:00h on 3 February and frontal system A at 00:00h on 5 February both show the characteristics of the Shapiro-Keyser cyclone model. The warm and cold fronts are near-perpendicular, and extensions of the warm fronts curve around seclusions (see fig.2.14).

Rainfall during the period 2-4 February predominantly followed patterns A1 and A2, with an axis of high rainfall intensity crossing the Mawddach catchment from north-west to south-east (fig.2.52).

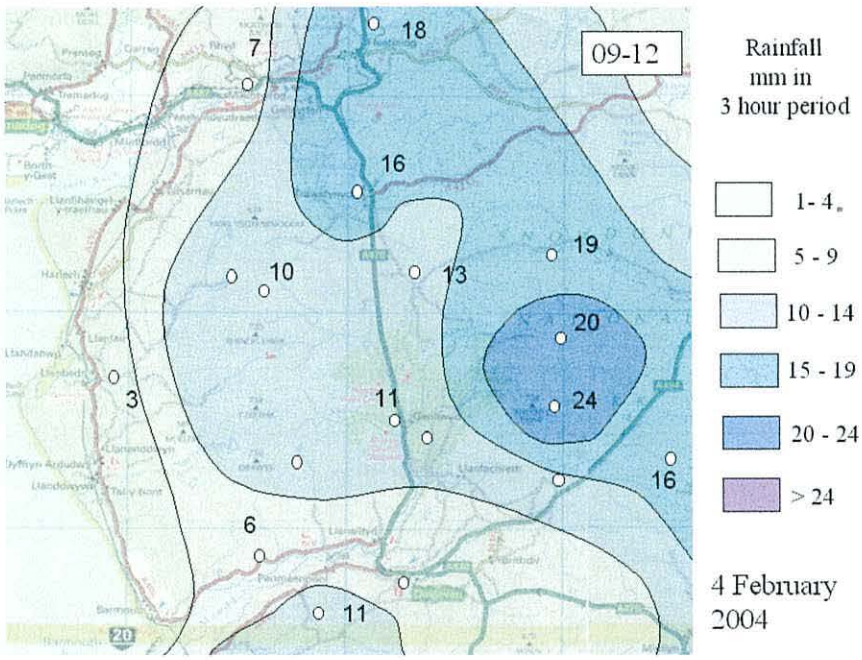

Figure 2.52. Typical rainfall pattern during the 2-4 February 2004 rainfall event: 3 hour rainfall total(mm) for the period 09:00h to 12:00h, 4 February.

A feature of the storm event is the extreme enhancement of rainfall totals inland, in comparison to coastal locations. This feature was also observed further north in Snowdonia, and is illustrated by Sibley (2005) in rainfall graphs contrasting the inland site of Capel Curig with the coastal site of Aberdaron (fig.2.53). Sibley suggests mechanisms for the rainfall enhancement:

Uplift of warm moist air occurred in a conveyor ahead of the cold front along the west coast of Wales. Cloud associated with the conveyor is seen in the satellite photograph for 13:40h, 4 February 2004 (fig.2.54).

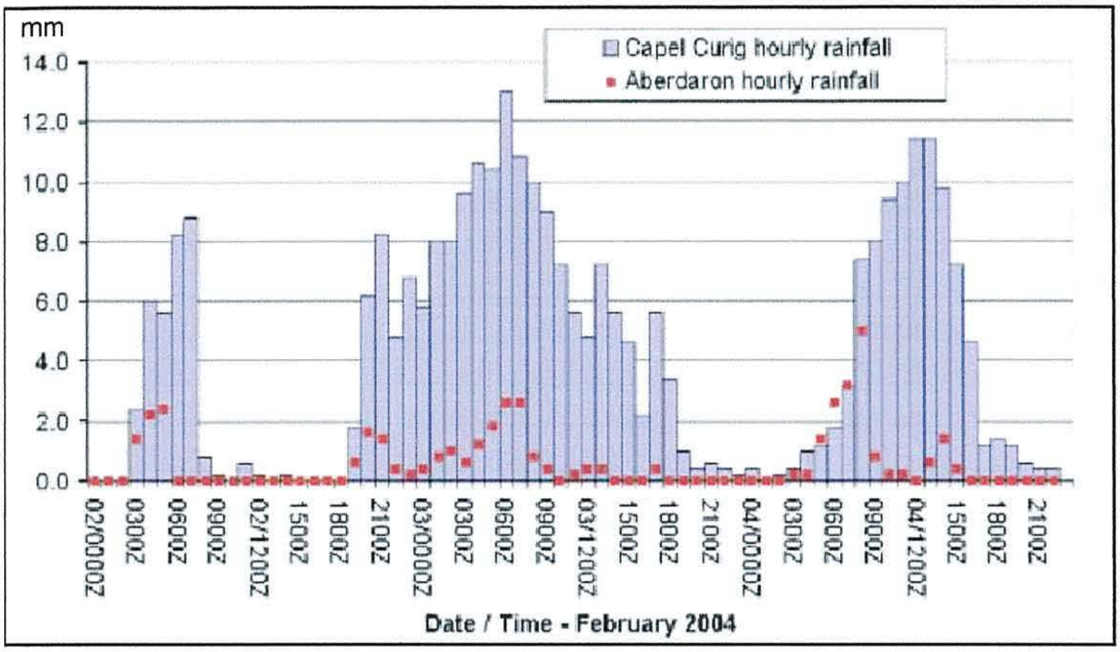

Figure 2.53. Comparison of rainfall at inland (Capel Curig) and coastal (Aberdaron) sites during the 2-4 February 2004 storm event. Reproduced from Sibley(2005)

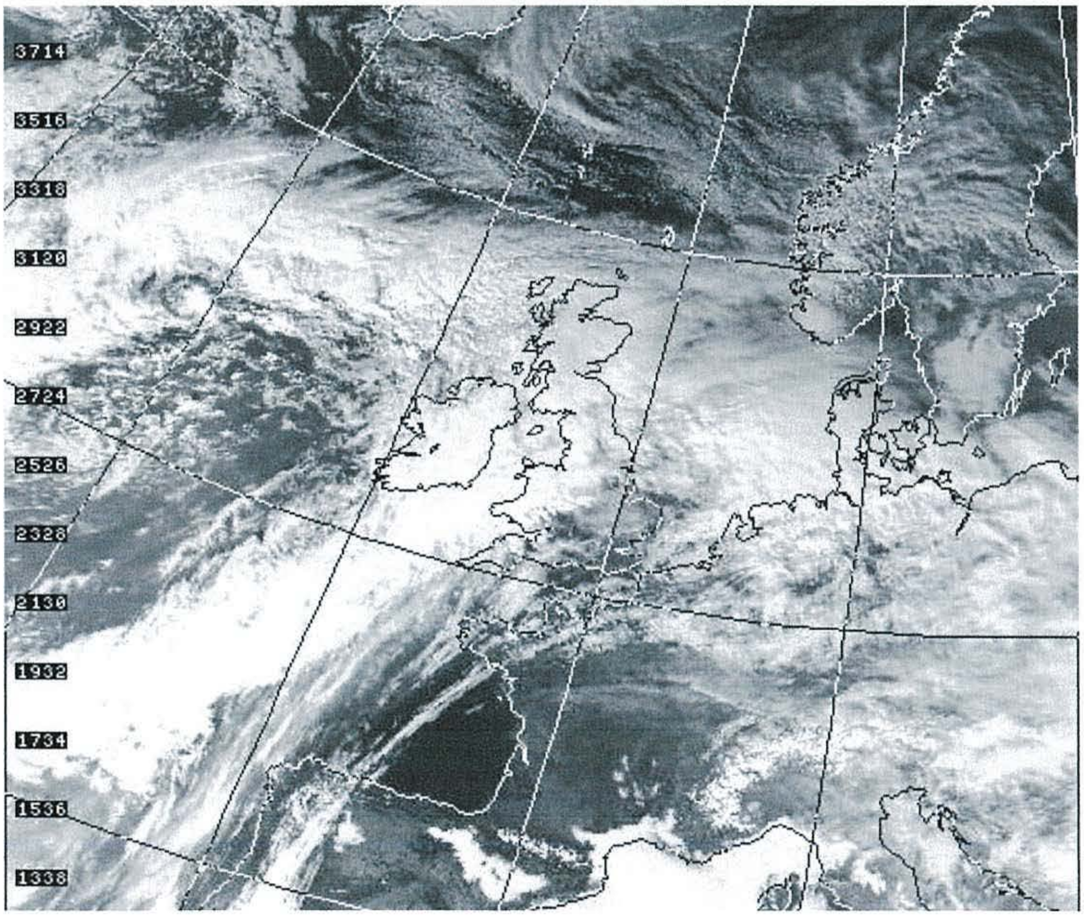

Figure 2.54. Satellite image (visible range), 13:40h on 4 February 2004.
Dundee satellite receiving station

Air within the warm sector was unseasonally warm, with a wet bulb potential temperature of 12^0-14^0C. This allowed the air mass to carry an unusually large amount of moisture, and provided thermal instability which assisted ascent within the conveyor.

The seeder-feeder mechanism of rainfall enhancement is considered by Sibley (2005) to have produced approximately 6-7mm h^{-1} additional rainfall over the mountains of Snowdonia at the peak of the February 2004 storm event, in comparison to the coastal area. This is consistent with evidence from the Mawddach catchment. Hill et al. (1981), in a study of rainfall in South Wales, have calculated that 80% of rainfall enhancement occurs in the lowest 1.5km of the troposphere, as rain from the upper cloud layer falls through orographic cloud covering hills and mountains.

Gravity mountain waves, unconstrained upwards, can produce the uplift required for seeder cloud formation (see figs 2.25-2.27). A strong low level jet at an altitude of approximately 1.5km was identified by Sibley (2005) in the tephigram of a balloon ascent from Aberporth at 06:00h on 3 February. This south westerly jet, reaching 80 knots, would carry seeder drops well inland below the warm air conveyor and orographic clouds of the coastal mountains.

July 2001 exceptional rainfall event

Effects of the storm of 3 July 2001 over the Mawddach catchment are described in Chapter 1. This was the most destructive storm in living memory. Flood waters destroyed or seriously damaged bridges built before the 19th century, so this storm may represent more that a 200-years maximal event. The 3 July 2001 storm occurred within a violent squall line. The pattern of the storm was unique, and did not conform to the normal Type A or B patterns of frontal rainfall in the catchment.

Features of the storm are recorded in the photographs of figs 2.55-2.56, with roll clouds developed ahead of the storm front, and intense convective activity producing great vertical development of thunder clouds. At the height of the storm, electrical activity was intense, with lightening strikes occurring with a frequency greater than one per minute.

Figure 2.57 shows the synoptic situation under which the squall line developed. A cold front associated with low A separated cold Polar air from very warm and convectively unstable air within the warm sector. Uplift began well ahead of the cold front, in association with an upper trough of low pressure air which promoted convective activity. It is conjectured that upper air was being removed along this north-south line by high level cyclonic circulation. The trough position is shown in the regional charts of fig.2.59, advancing slowly inland during the evening of 3 July.

Rainfall maps for the 3 July storm have been constructed from limited data (fig.2.60). The 1-hour readings from a ring of five raingauge sites around the periphery of the Mawddach catchment have been augmented by a hypothetical modelled raingauge for Oernant, approximately 5km to the ESE of Trawsfynydd, where field evidence suggests that the storm reached its maximum intensity. Derivation of the modelled data will be discussed in section 2.4. The rainfall maps suggest a very narrow band of high intensity rainfall crossed the catchment in the period between 18:00h and 20:00h, accounting for the majority of the storm damage through rapid infiltration-excess runoff directly into watercourses.

Figure 2.55: July 3 storm over the Mawddach catchment, showing roll or shelf cloud ahead of the main body of the storm (photo: John Mason)

Figure 2.56: Cloud base of the July 3 storm over the Mawddach catchment (photo: John Mason)

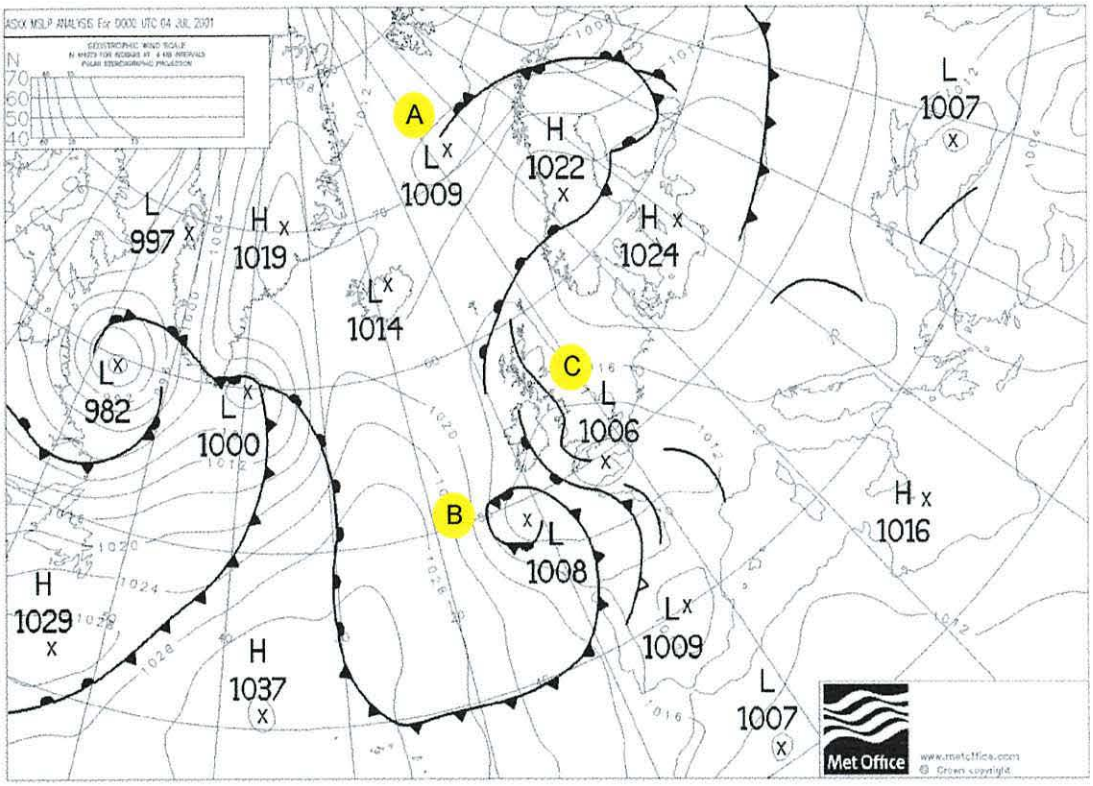

Figure 2.57: Synoptic chart for 00:00h, 4 July 2001

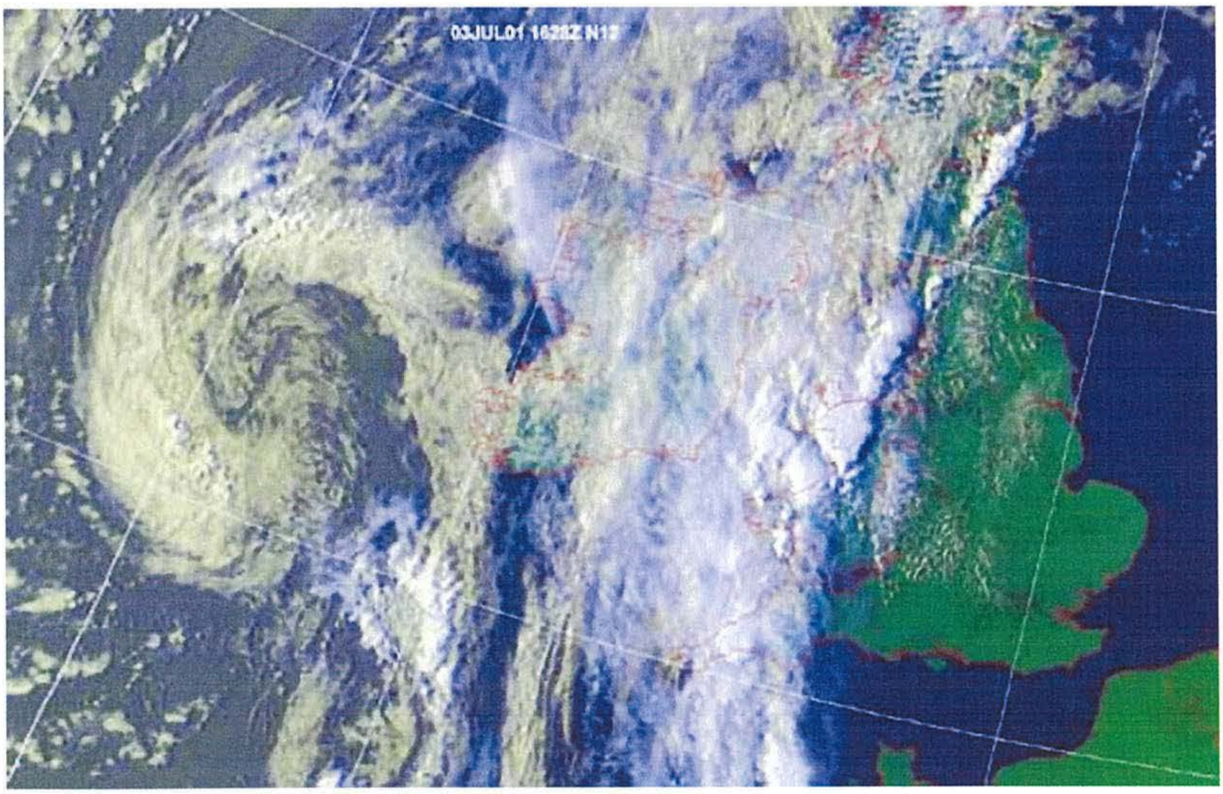

Figure 2.58: Visible satellite image, 16:30h 3 July 2001 (courtesy of Bernard Burton)

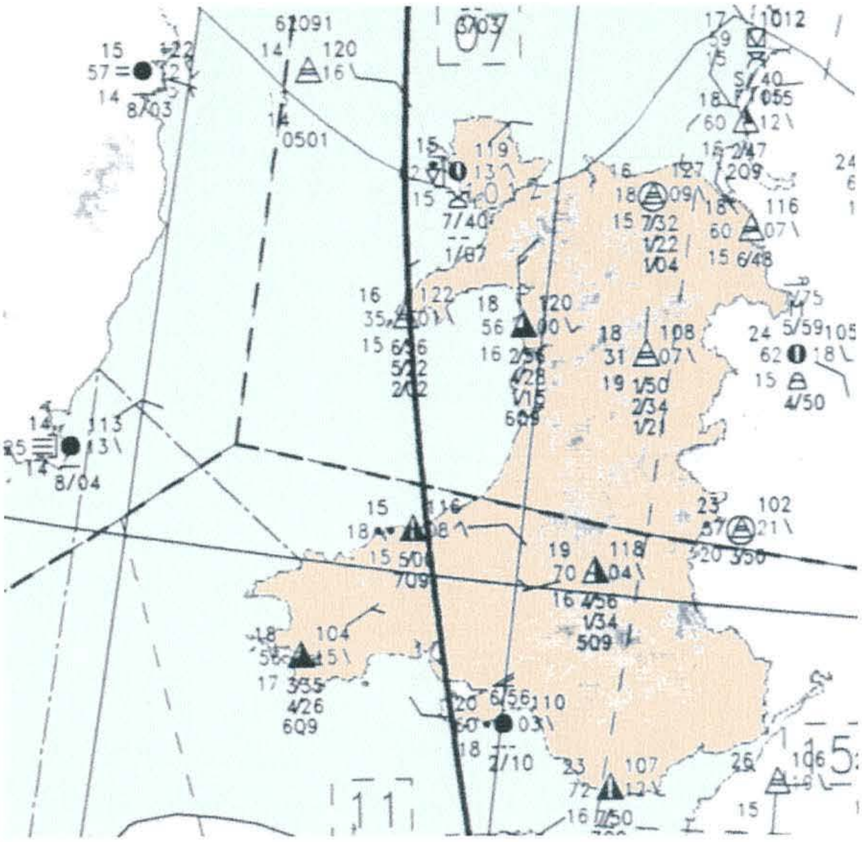

Figure 2.59(a). Regional chart for 19:00h 3 July 2001

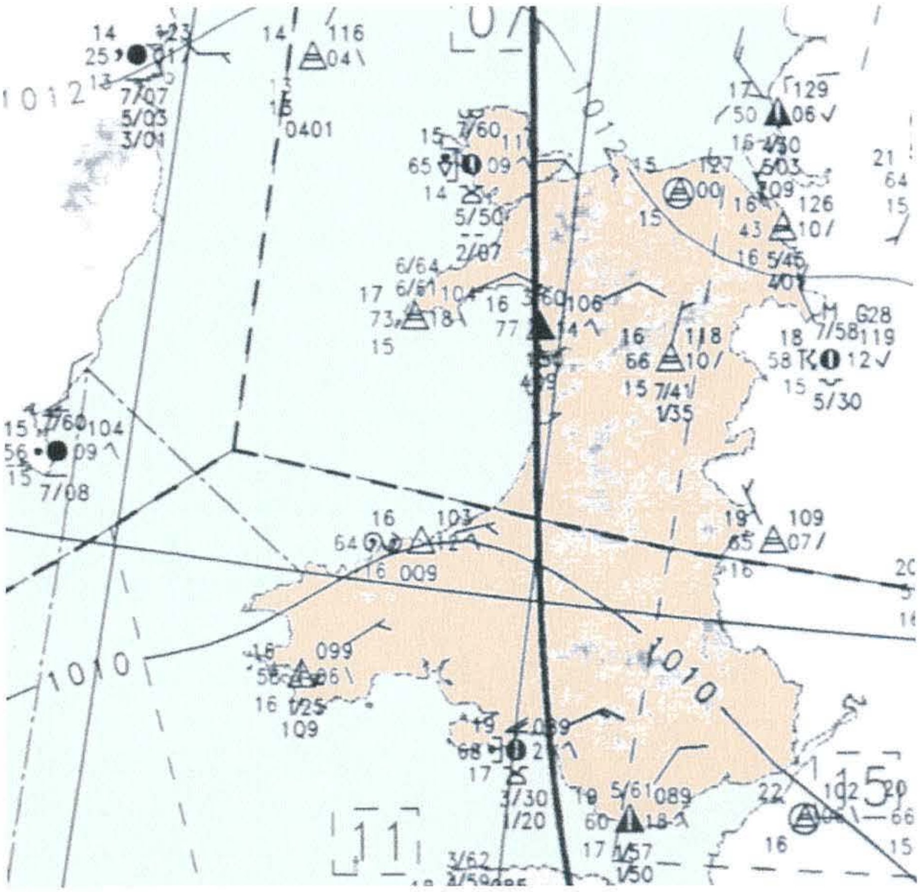

Figure 2.59(b). Regional chart for 22:00h 3 July 2001

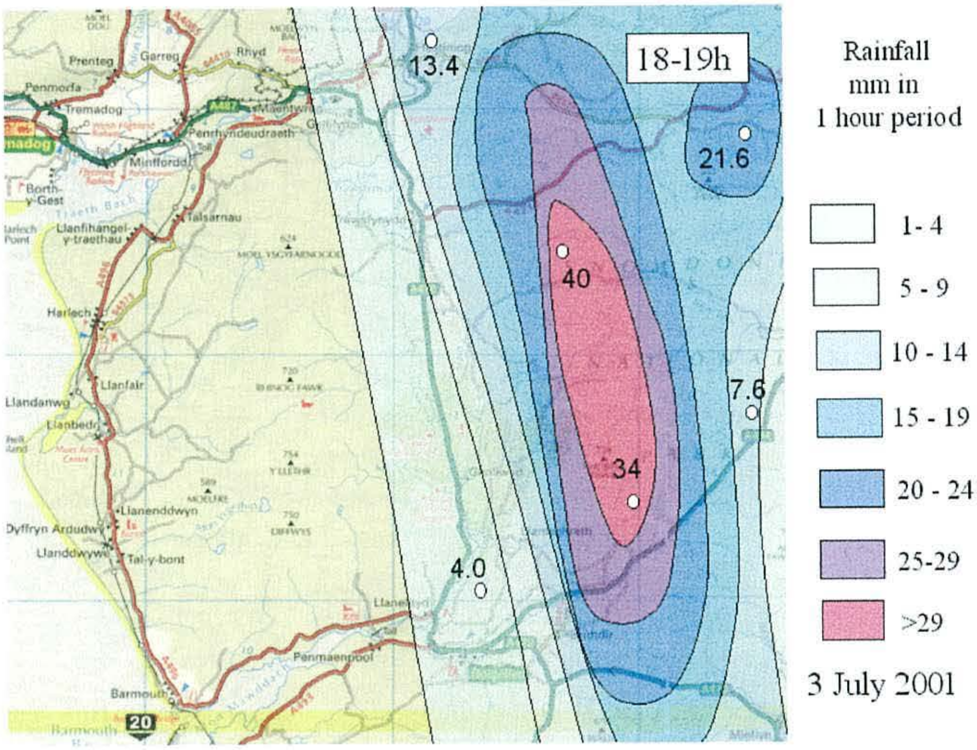

Figure 2.60(a). Rainfall total for the period 18:00h to 19:00h, 3 July 2001.

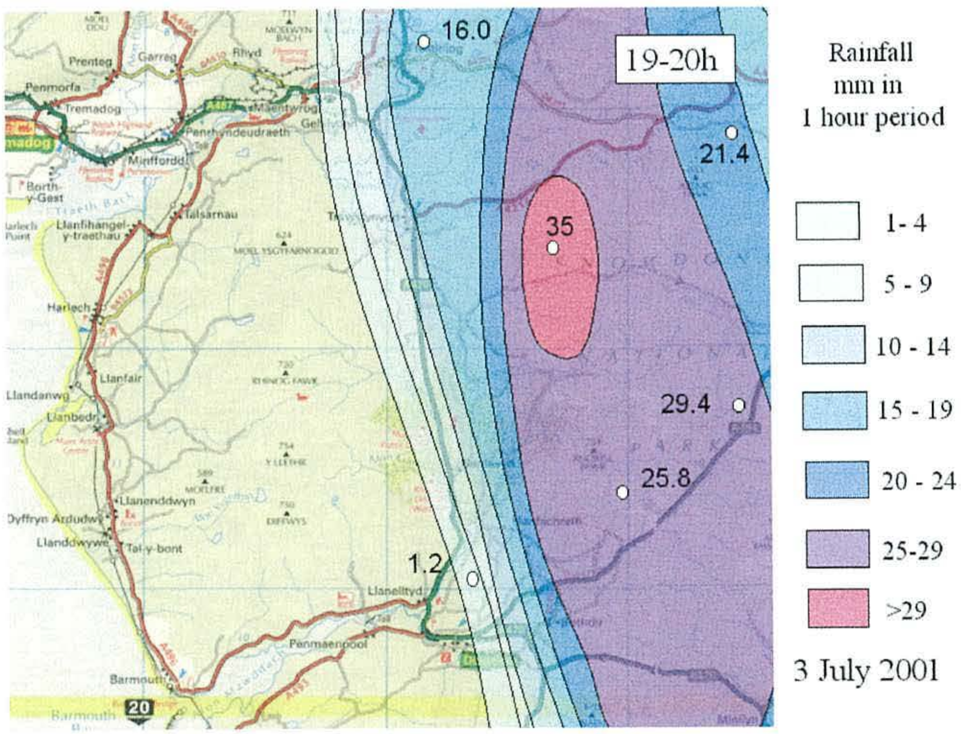

Figure 2.60(b). Rainfall total for the period 19:00h to 20:00h, 3 July 2001.

Summary

- The great majority of storm events in the Mawddach catchment are associated with frontal systems.
- Three distinct rainfall distribution patterns have been identified for storms within the Mawddach catchment, and have been termed Types A1, A2 and B.
- In the Type A1 pattern, a zone of high rainfall crosses the Mawddach catchment on a diagonal axis from Trawsfynydd in the NW to Pared yr Ychain in the SE. A single rainfall maximum occurs in the centre of the catchment, around Coed y Brenin and Rhobell Fawr. This pattern is associated with a dominantly west-south-westerly airflow.
- In the Type A2 variant, rainfall maxima are located at the two ends of the axis of high rainfall from Trawsfynydd to Pared yr Ychain . This pattern is associated with a dominantly south-westerly airflow.
- In the Type B pattern, a zone of high rainfall is oriented north-south along the line of the Rhinog mountain range. This pattern is associated with a dominantly south-south-westerly airflow.
- Dominant wind directions may be linked to the orientation of warm fronts. Type A1 rainfall patterns are typically produced by N-S oriented warm fronts. Type A2 patterns are typically produced by NW-SE oriented warm fronts. Type B patterns are typically produced by W-E oriented warm fronts.
- During an individual rainfall event, the orientation of a front may change as it crosses the Mawddach catchment, leading to a change in rainfall pattern between the early and late stages of the rainfall event.
- Within an individual storm event, total rainfall may differ by a factor of four or more between different locations within the Mawddach catchment. Zones of highest rainfall do not generally correspond with the highest ground.
- The most extreme and destructive storm event experienced in the catchment occurred in association with a low pressure trough in the upper air which promoted uplift of large volumes of air ahead of a cold front, forming a squall line.

2.3 Meteorological modelling

The derivation of mathematical models for meteorology is presented by Jacobson (1999) and Grell, Dudhia and Stauffer (1995).

Meteorological models may cover the whole globe for world climate modelling, or may be restricted to particular areas for weather forecasting or research. Models focussing on particular areas are known as *mesoscale models.* A mesoscale meteorological model uses an outer domain which links to the global weather circulatory pattern, and one or more high resolution inner domains covering areas of special interest (fig.2.61).

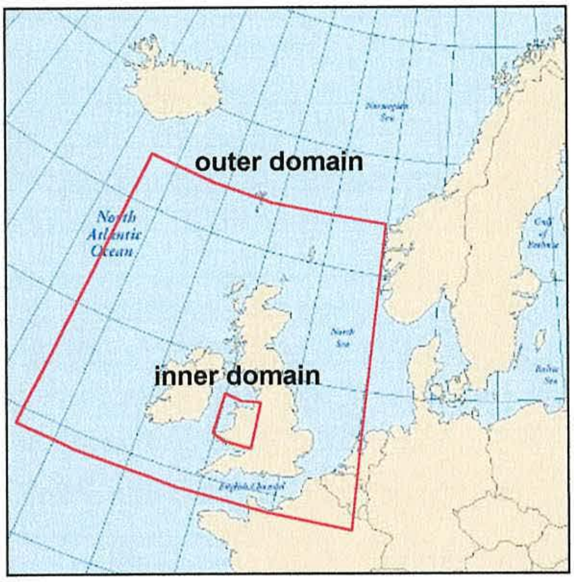

Figure 2.61: Nested mesoscale domains

The outer domains of mesoscale models often extend for more than 1000km, so the curvature of the Earth cannot be ignored when calculating distances. Models are usually represented by the Spherical Polar Coordinate system (fig.2.62).

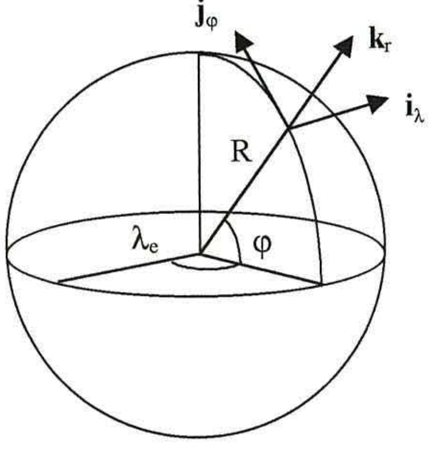

Figure 2.62: Spherical Polar Coordinates

The spherical polar system uses lambda (λ_e) to represent longitude, and phi (φ) to represent latitude. The radius of the Earth (R_e) is also required for the calculation of distances on the Earth's surface.

The inner domain of a mesoscale model can operate with a horizontal grid spacing of 1km or less, and will take into account local factors such as topography, soil types and vegetation cover which can influence surface air temperatures and wind vectors.

The model must represent processes taking place in the lower part of the atmosphere, the *troposphere*, up to an altitude of around 10km and air pressure of 250mb. This region would typically be modelled by between 20 and 30 atmospheric layers. Problems can arise if horizontal layers are employed, as these may intersect the ground surface topography and increase the complexity of calculations. An alternative approach using ground-following coordinates is generally used, in which each layer boundary represents a fixed fraction of the pressure difference between the ground surface and the top surface of the model. This is known as the sigma-pressure (σ) coordinate system (fig.2.63).

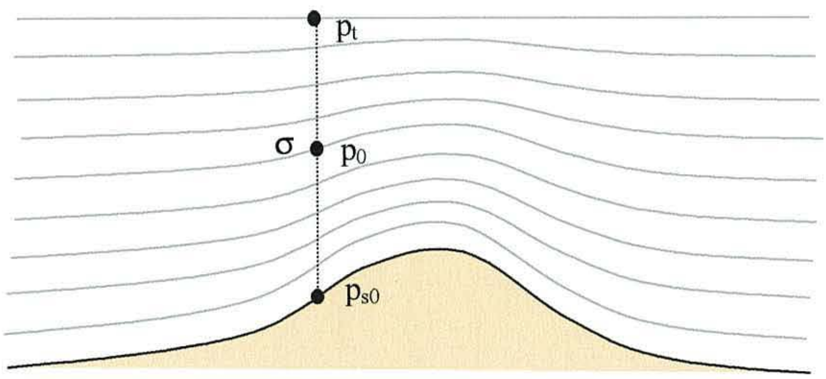

Figure 2.63: Sigma-pressure coordinate system

The sigma value at any point may be calculated using the relation:

$$\sigma = \frac{(p_0 - p_t)}{(p_{s0} - p_t)}$$

p_0	local pressure
p_{s0}	ground surface pressure
p_t	model top surface pressure

A complexity of meteorological models in comparison to hydrological models is that air is compressible, whereas water is normally considered to be incompressible. Dry air behaves as a close approximation to the Ideal Gas Law:

$$p = \frac{nRT}{V}$$

where:		
	p	pressure
	n	moles of gas
	R	universal gas constant
	T	absolute temperature

Pressure naturally varies with altitude. An air parcel at any point in the atmosphere will be subject to the weight of the overlying column of air, which increases towards the ground surface (fig.2.64).

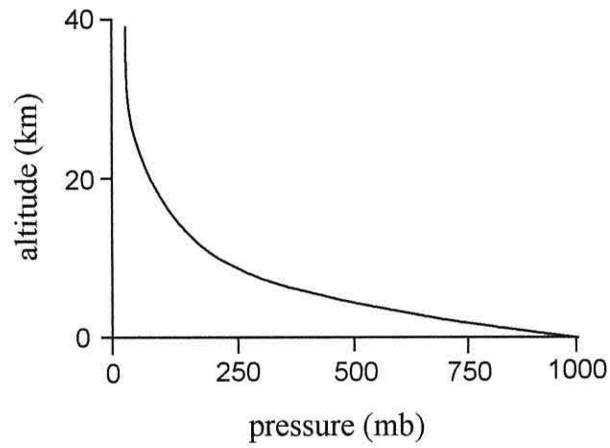

Figure 2.64: Pressure distribution in the lower atmosphere

The relationship between altitude and pressure is given by the hydrostatic equation:

$$\frac{\partial p}{\partial z} = -\rho g$$

where:		
	g	acceleration due to gravity
	ρ	density of air
	p	air pressure
	z	altitude

Meteorological models covering large areas at low resolution often make a simplifying assumption that the atmosphere remains in vertical equilibrium according to the hydrostatic equation. This assumption is realistic provided that horizontal air motions predominate (fig.2.65a).

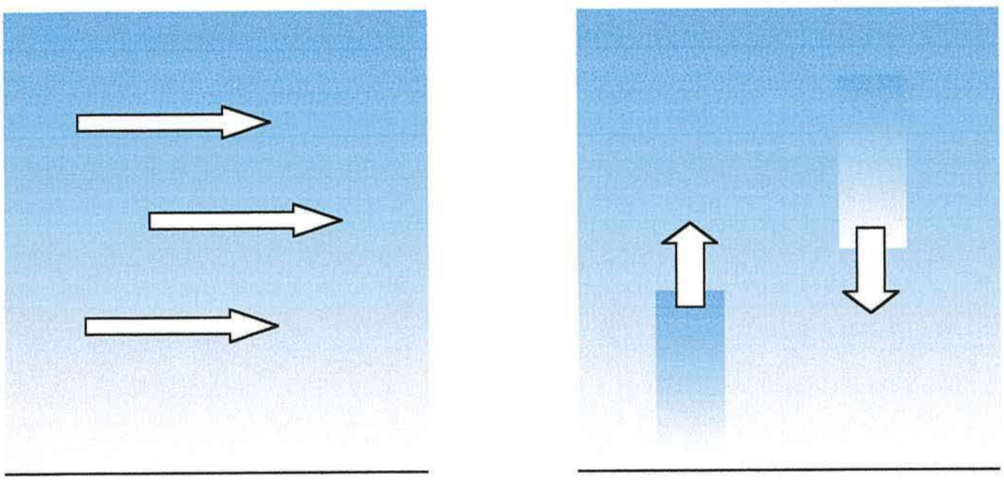

(a) hydrostatic model (b) non-hydrostatic model

Figure 2.65: Pressure distributions in meteorological models

For high resolution models of small areas, vertical air motions due to convection may be important. Heating or cooling of air parcels may lead to pressure and density variance from the surrounding stable atmosphere. In this case, the model must allow for non-hydrostatic pressure distributions (fig.2.65b).

A fundamental principle of atmospheric models is the conservation of air mass, described by the differential equation:

$$\frac{\partial N}{\partial t} = -\frac{\partial(uN)}{\partial x} - \frac{\partial(vN)}{\partial y} - \frac{\partial(wN)}{\partial z}$$

where N is the mass of air; u,v and w are velocities in the cartesian directions x,y and z; t is time.

Meteorological model development begins with the equations of atmospheric physics:

- hydrostatic equation
- continuity equation
- thermodynamic energy equation
- momentum equation

which form the basis for a simple dry air model. Jacobson (1999) provides an outline modelling scheme (fig.2.66). These equations are discussed further in section 2.4.

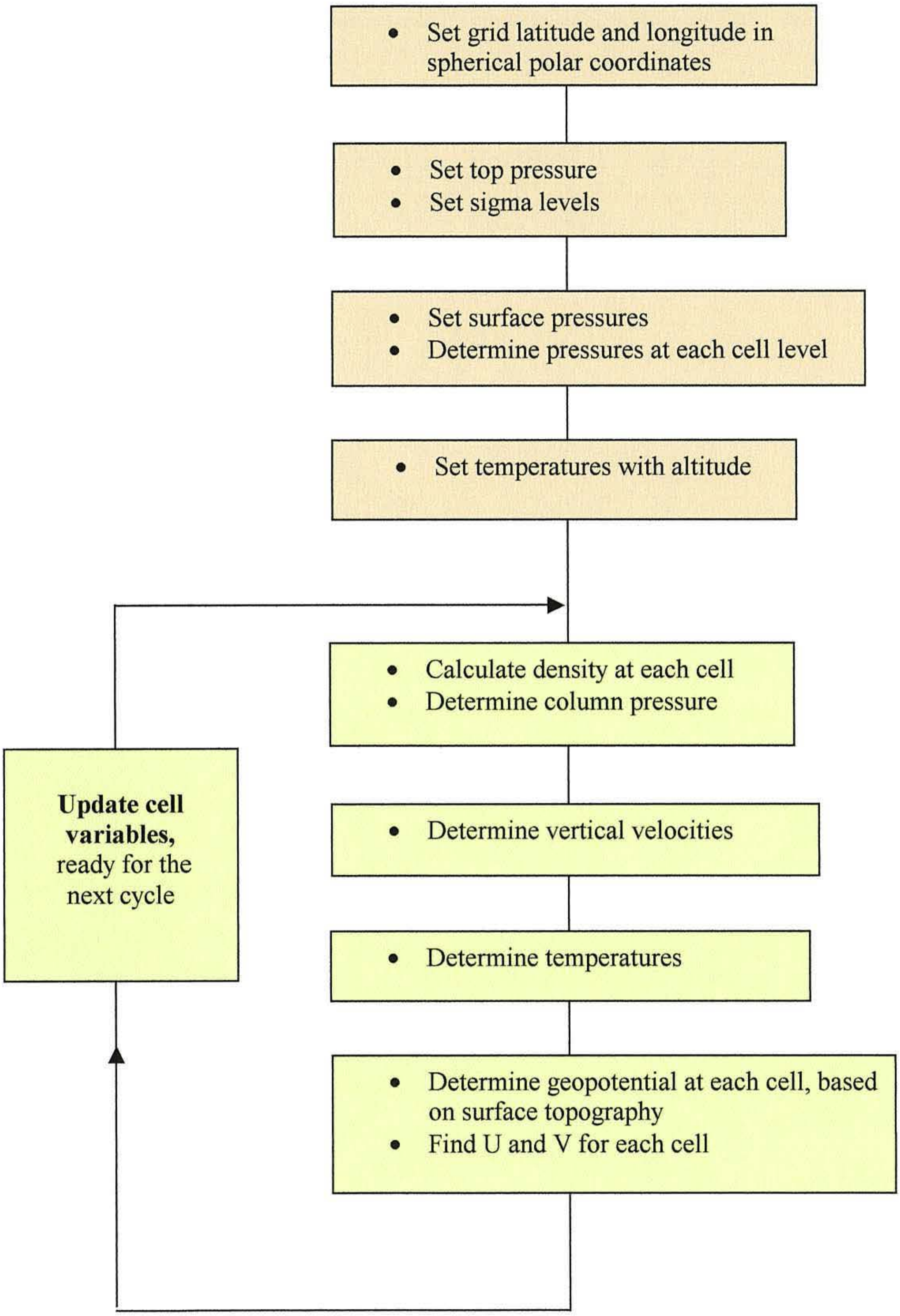

Figure 2.66: Jacobson scheme for a simple dry air meteorological model

The model is initialised by setting up a horizontal grid to cover the desired area, bounded by lines of latitude and longitude on the Earth's surface. The top atmospheric level for the model is chosen – typically this would be at 10km, and sigma levels are set between the top level and the ground surface topography.

Initial air pressures for the boundary cells of the grid are specified, with the top level of the model having a constant pressure of around 250mb throughout the simulation. Pressures are interpolated to each model cell for the start of the run. Temperatures of boundary cells are similarly initialised and interpolated to the interior cells.

The main loop of the model, shown in yellow in fig.2.66, repeats for each time interval during the simulation:

At the start of a time step, the air densities for each cell are determined, and used to calculate pressures in each cell according to the overlying air column mass.

Vertical air velocities are calculated for each cell, depending on pressure deviation from hydrostatic equilibrium and air viscosity forces. Air temperatures are determined for each cell, according to the Ideal Gas Law.

The geopotential for each cell is calculated. This is a measure of the gravitational potential energy of the air within the cell, and varies with altitude. This factor must be considered when sigma levels are used, since the altitude of a sigma layer boundary may vary across the model area according to the underlying topography.

It is now possible to calculate the horizontal velocity vectors for air within the cell, taking into account gravity, pressure gradient, Coriolis and viscosity forces. Pressure, temperature, horizontal and vertical velocity values can be updated for each model cell, and the cycle repeated for the next time interval.

Anthes and Warner (1978) develop a mathematical treatment of the Earth's physical boundary layer, and the modelling of precipitation by convective cloud processes. These aspects will be discussed further in section 2.4 in the context of the MM5 meteorological model.

Using atmospheric soundings

Rainfall production is generally the result of cooling and condensation of water vapour as air rises. Water droplets may initially form from saturated air in contact with airborn particles such as dust, smoke or salt crystals, then grow by accretion within a cloud (Barry and Chorley, 1976). Field evidence of air conditions and the likelihood of cloud formation can be obtained from the ascents of weather balloons through the troposphere. Instruments are carried which measure air temperature and moisture content, relaying this information back to the ground station along with the balloon altitude and geographical location. From this data, it is also possible to determine wind speed and direction at different altitudes during the ascent.

Data collected from balloon ascents, termed *soundings*, are generally plotted on pressure-temperature charts termed *tephigrams,* named from the mathematical symbols T used for temperature and ϕ(phi) used for pressure. An example is given in fig.2.67 and its interpretation is explained below. Atmospheric soundings provide

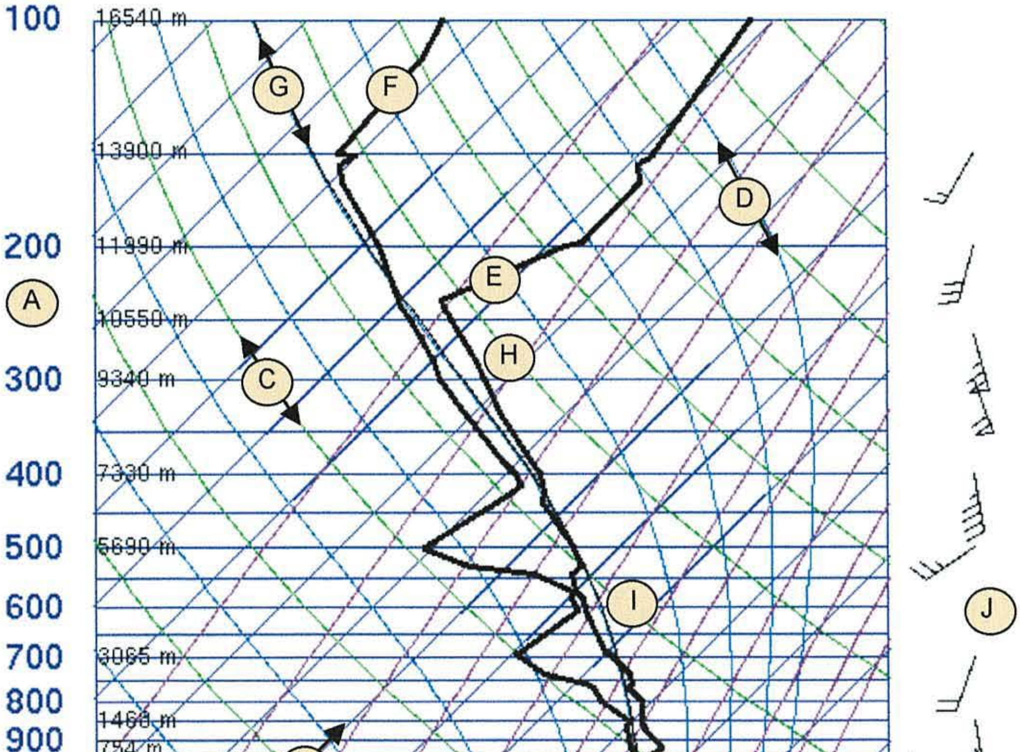

Figure 2.67: An example Tephigram

input data for the meteorological model described in Section 2.4. After a run of the model, synthetic tephigrams can be plotted for a sequence of locations or times to demonstrate the atmospheric conditions produced during the simulation.
Key to features of the tephigram:

A: The vertical axis represents altitude, shown as pressure (mb) and height (m) scales.

B: The horizontal axis represents temperature in degrees Celsius. Lines of constant temperature are shown in blue, running upwards towards to right. For this reason, tephigrams are also known as *skew-T* plots.

C: Green lines curving upwards to the left, termed *dry adiabats*, represent the pressure-temperature paths which would be followed by parcels of dry air rising through the atmosphere.

D: More steeply curving blue lines, termed *moist adiabats*, represent the pressure-temperature paths which would be followed by parcels of saturated air from which water vapour was condensing during rise through the atmosphere.

E: The right-hand thick graph line represents the dry bulb air temperatures recorded during the balloon ascent.

F: The left-hand thick graph line represents the wet bulb air temperatures recorded during the ascent. The horizontal distance between the two graph lines relates to the saturation state of the air. Where the lines are close together, the air is near saturation and condensation, cloud formation and rainfall are likely. Where the lines are far apart, the air is drier and condensation is unlikely.

G: This curving black line represents the ascent path that a parcel of air would follow if it began to rise from the ground at the point of release of the balloon. This is known as the *parcel lapse rate*. The path line initially follows a dry adiabat curve to the point where condensation begins, then follows a saturated adiabat for the remainder of the ascent.

H: The relative positions of the parcel lapse rate line and the dry bulb temperature line give information on the stability of the air. If the parcel lapse rate line is furthest to the left, as at the level of H, then the air is stable. A rising parcel will be colder and denser than the surrounding air, so has no tendency to continue its upward motion.

I: Where the dry bulb temperature line is to the left of the parcel lapse rate line, as at the level of I, the air is unstable. A rising parcel will be warmer and less dense than the surrounding air, so continues to rise buoyantly.

J: Symbols to the right of the graph represent the compass orientation of winds at different levels during the balloon ascent. Barbs on the arrows are an indication of wind speed.

Balloon ascent data is valuable for understanding atmospheric conditions and relating these to weather patterns. The use of atmospheric data can be demonstrated for an example rainfall event of 24 October 2005:

Fig.2.68 shows rainfall distributions for 00:00h and 12:00h on 24 October 2005. A rain band moves across Ireland and the mainland of Britain as a warm front advances. Uplift to the NW along a warm air conveyor is responsible for the precipitation. Data from radiosonde balloon ascents at 00:00h and 12:00h are available for the stations Camborne, Castor Bay and Nottingham.

Data for 00:00h are plotted as tephigrams in fig.2.69. The closeness of the dry bulb and wet bulb lines up to 3 000m is a good indicator of rainfall occurring. Air at Castor Bay and Nottingham is stable, with the dry bulb temperature graph to the right of the parcel lapse rate curve for much of the ascent. Removal of air by cyclonic vorticity is the driving force for ascent, rather than natural buoyancy of the air. Marked changes in wind direction within the lower 3 000m for these stations is an indicator of the vorticity.

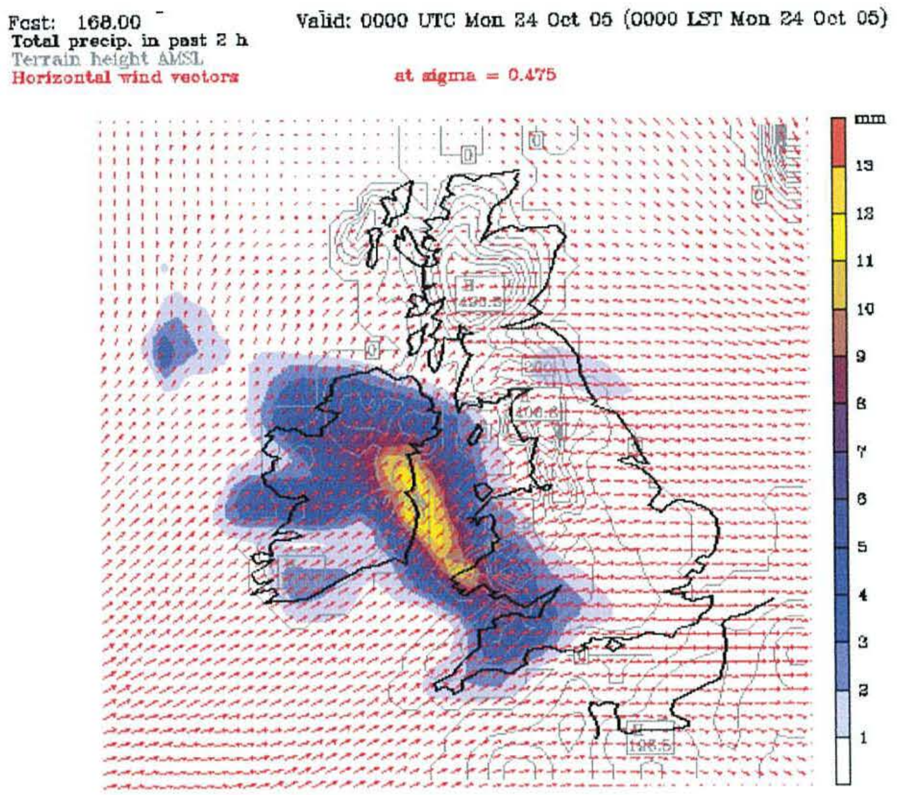

Figure 2.68(a). Modelled two-hour rainfall total for 00:00h, 24 October 2005

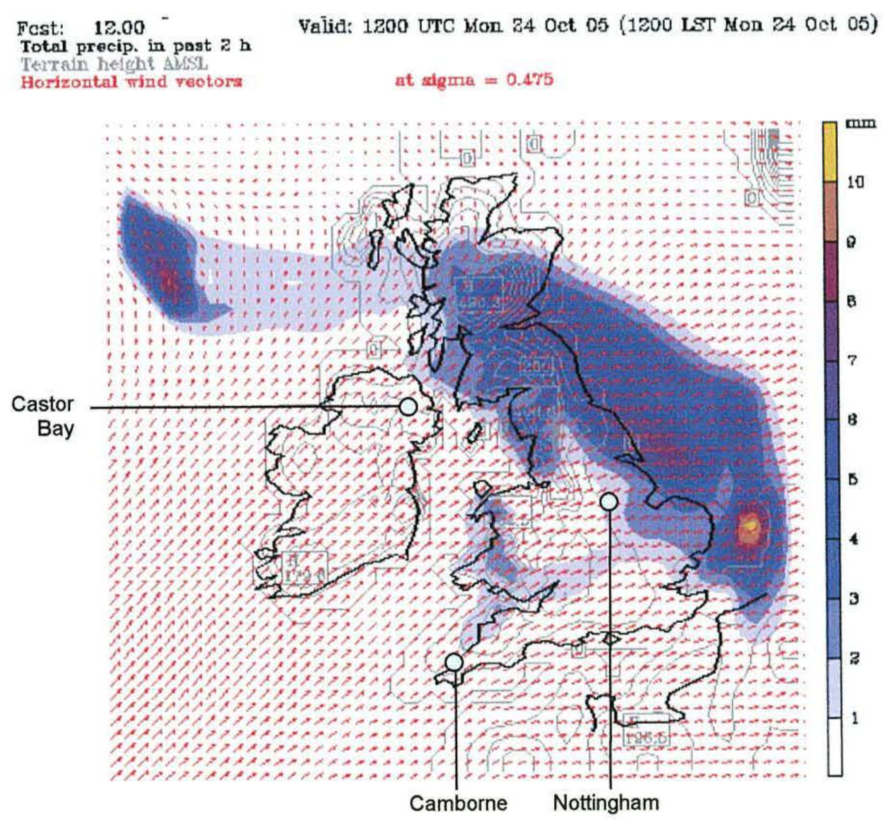

Figure 2.68(b). Modelled two-hour rainfall total for 12:00h, 24 October 2005

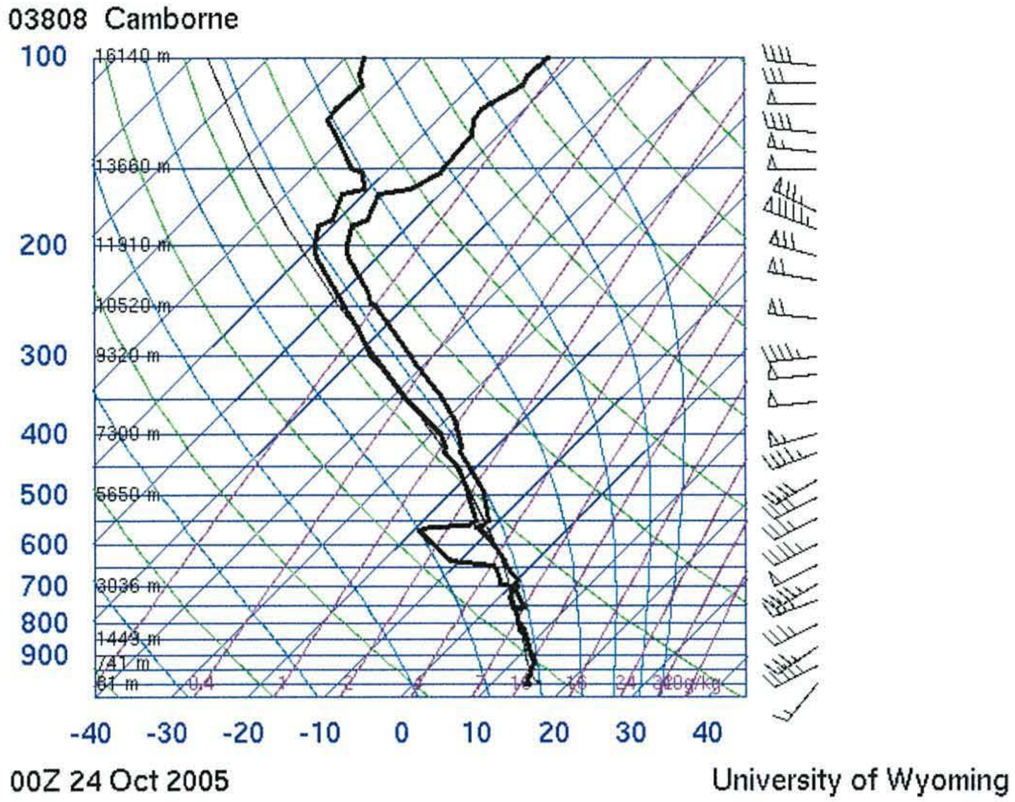

Figure 2.69(a). Actual atmospheric profile for Camborne, 00:00h 24 October 2006

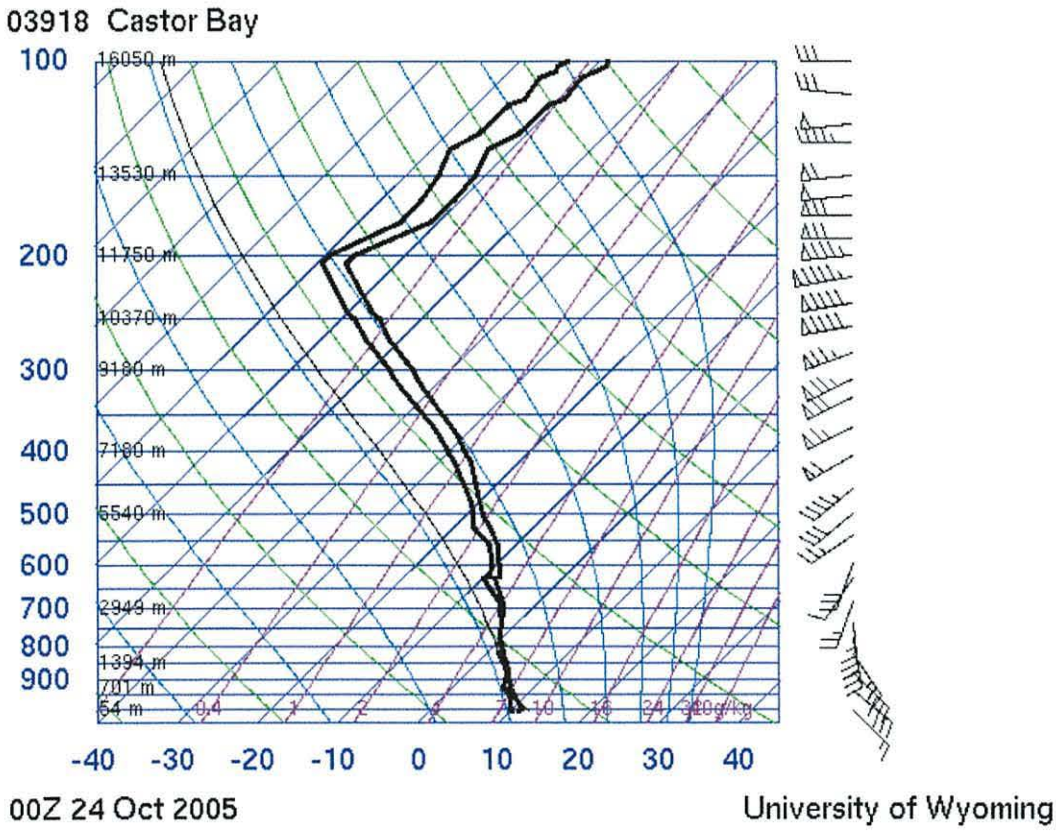

Figure 2.69(b). Actual atmospheric profile for Castor Bay, 00:00h 24 October 2006

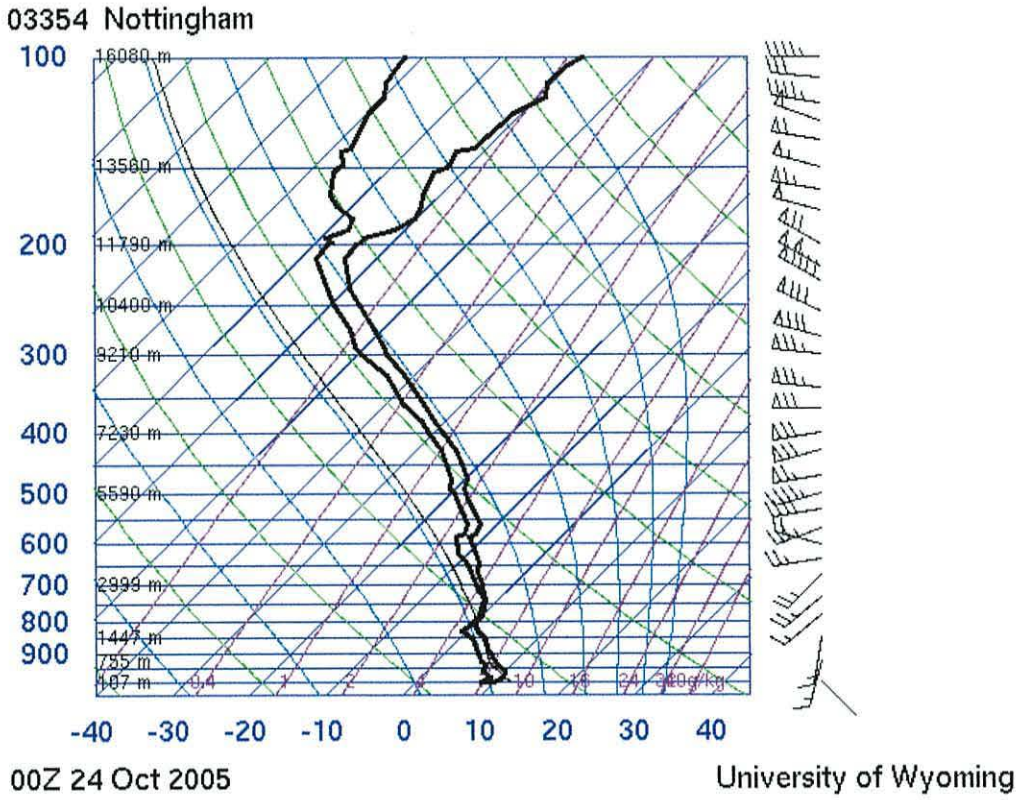

Figure 2.69(c). Actual atmospheric profile for Nottingham, 00:00h 24 October 2006

This example of frontal rainfall may be contrasted with the squall line convective event responsible for flooding in the Mawddach catchment in July 2001.

Tephigrams for Camborne over the period 12:00h, 3 July 2001, to 00:00h, 4 July 2001, are presented in figure 2.70. The profiles show strong instability at altitudes between 3000m and 5000m for the afternoon and evening of 3 July, with the dry bulb trace lying to the left of the parcel lapse rate curve. Features of instability have been highlighted in red on the graphs.

Statistical information about the state of the atmosphere is computed during the analysis of balloon ascent data, and is shown to the right of the tephigram. Of particular interest in this case is the amount of *convective available potential energy* (CAPE) recorded from the profile, which is a measure of the tendency of the air to

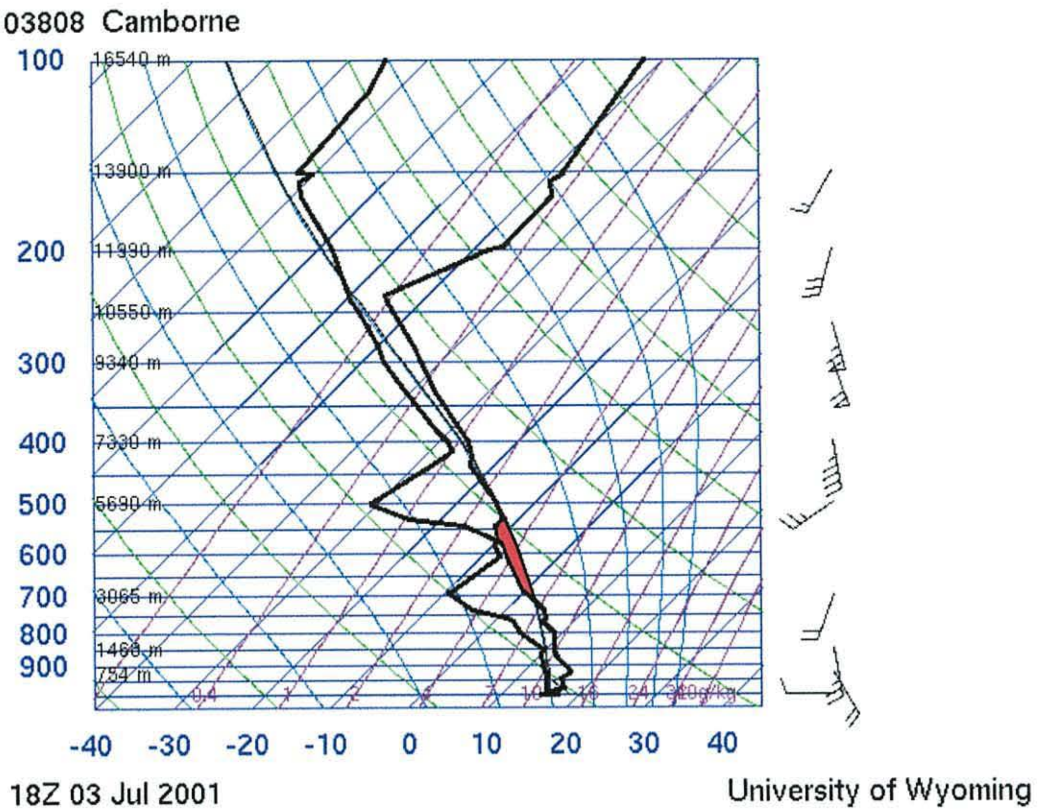

Figure 2.70(a). Atmospheric profile for Camborne, 18:00h 3 July 2001

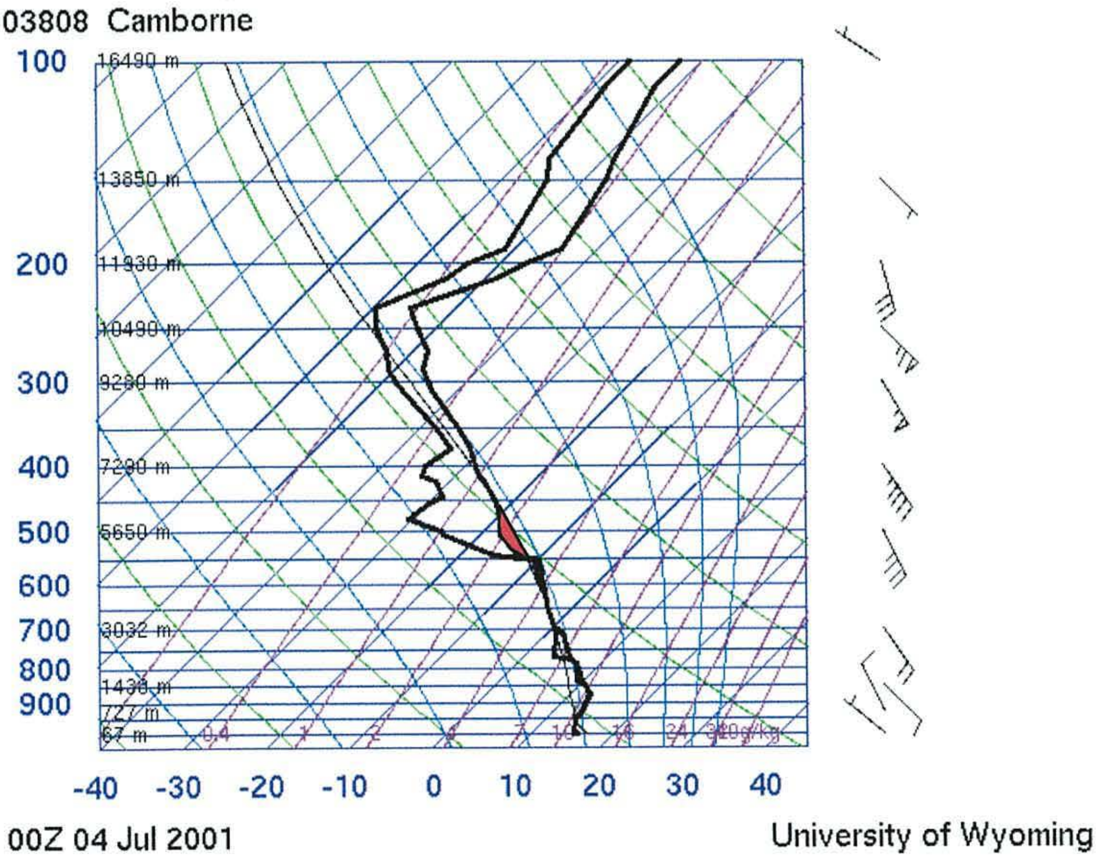

Figure 2.70(b). Atmospheric profile for Camborne, 00:00h 4 July 2001

undergo upwards convective motion. The appearance of any positive value for CAPE is an indicator that thunderstorm activity is possible.

Atmospheric soundings are of considerable value in providing data for calibration of meteorological models. They can provide important data on atmospheric motion and moisture content which may in turn be used in calculating the location, timing and intensity of rainfall events.

Summary

- Meteorological modelling may be carried out on a variety of scales. Models focussing on particular regions are known as mesoscale models.
- Models often consist of a set of nested domains, with each providing boundary conditions for a higher resolution domain which it encloses.
- Meteorological models usually cover a sufficient area that the curvature of the Earth must be taken into account when calculating horizontal coordinates.
- The sigma-coordinate system has been devised to simplify the modelling of atmospheric layers above undulating surface topography. Sigma levels represent specified fractions of the total pressure interval between the ground and the upper model surface at an altitude of typically 10km.
- Simple models may make an approximation of hydrostatic pressure distribution upwards through the atmosphere. More accurate models incorporating convection processes must allow for a non-hydrostatic pressure distribution.
- Models are initialised with temperature and pressure values at a series of sigma levels for a grid of points covering the outer domain.
- The model is run iteratively to generate horizontal and vertical air velocities, pressures and temperatures for each grid point over a series of time steps.
- Values for moisture content are added for each cell, and processes of condensation and precipitation can be simulated to produce rainfall forecasts.
- Temperature, pressure and moisture content data for initialising and updating the model may be obtained from balloon soundings in addition to ground stations.

2.4 The MM5 modelling system

Investigations have been carried out to determine whether a meteorological model could realistically predict rainfall patterns over the Mawddach catchment for the example storm events described in section 2.1. The system chosen is the MM5 Mesoscale Model, developed over a number of years by Richard Anthes at Pennsylvania State University (Anthes and Warner, 1978) and subsequently by the National Center for Atmospheric Research in Boulder, Colorado (Grell, Dudhia and Stauffer, 1995). The system is now a robust and reliable code for solving a wide range of meteorological problems.

Weather simulations require initial and boundary conditions to be supplied, in the form of land and sea surface characteristics for the study region, and gridded meteorological data at the start and subsequent time intervals during the run. Suitable global meteorological data sets are provided by the US National Center for Environmental Protection (NCEP). This gridded data specifies sea level pressure at surface grid points, and

- wind speed and direction
- temperature
- relative humidity
- geopotential height (approximately the altitude)

at the surface and at atmospheric levels where the pressure is 1 000, 850, 700, 500, 400, 300, 250, 200, 150 and 100mb.
This data is generated from observations by land stations, ships, aircraft and balloon ascents worldwide. Data sets are issued in electronic format at 6-hourly intervals, both as records of actual readings, and as advance forecasts of probable atmospheric conditions.

The task of MM5 is to take the gridded sets of land surface and air parameters, and simulate a likely sequence of weather phenomena occurring in the study region over the next time period of 6 or 12 hours. Modelling will include the patterns of winds, and vertical air movements leading to condensation. Distribution and intensity of rainfall and snowfall can be mapped. Specialist applications of MM5 are to predict the likely occurrence and tracks of electrical storms and tornados, or to predict the dispersal patterns of airborne pollutants from events such as forest fires.

MM5 is a modular system, made up from a series of software packages written mainly in the language FORTRAN 90 (fig.2.71). The programs can be run under a Unix operating system on a mainframe computer, or under Linux on a microcomputer. Modern high speed microcomputers are capable of carrying out a 1 day weather simulation on a 1km resolution grid within 3 hours of processing time. A 12-processor minicomputer using parallel processing is able to achieve a 1 day simulation in less than 1 hour.

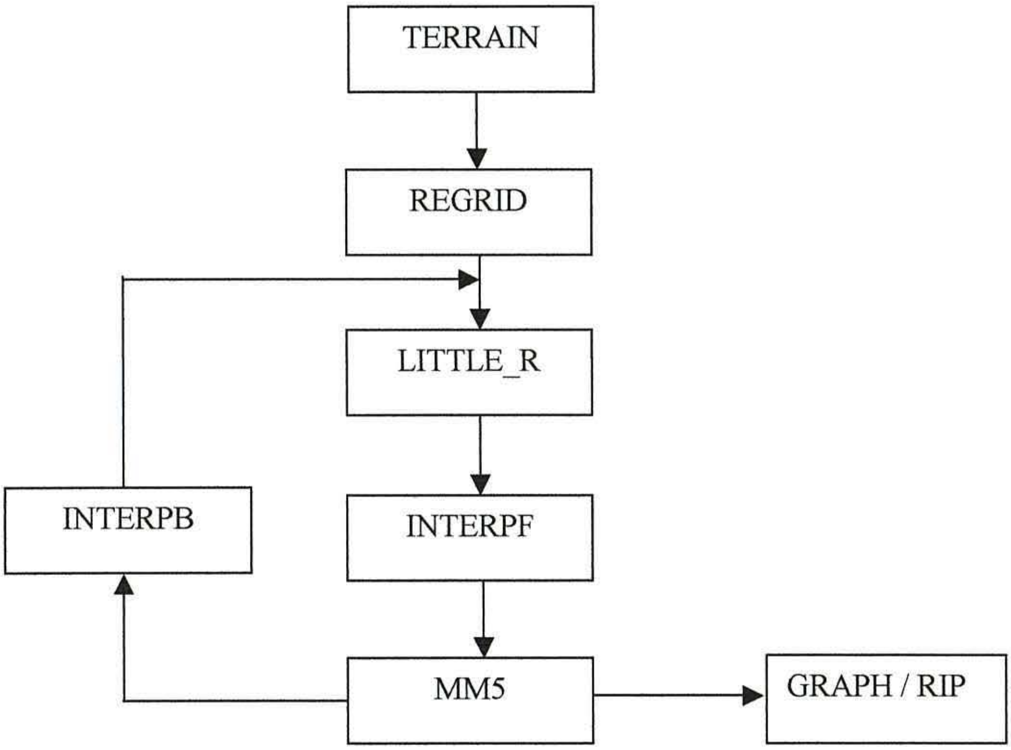

Figure 2.71: The principal modules of the MM5 modelling system

TERRAIN module

The setting up of a meteorological model begins with the TERRAIN module. It is usual to establish a series of nested domains, which will capture large synoptic weather patterns and apply these as local boundary conditions for a mesoscale area of interest. The MM5 model for the Mawddach catchment uses five domains, illustrated in fig.2.72:

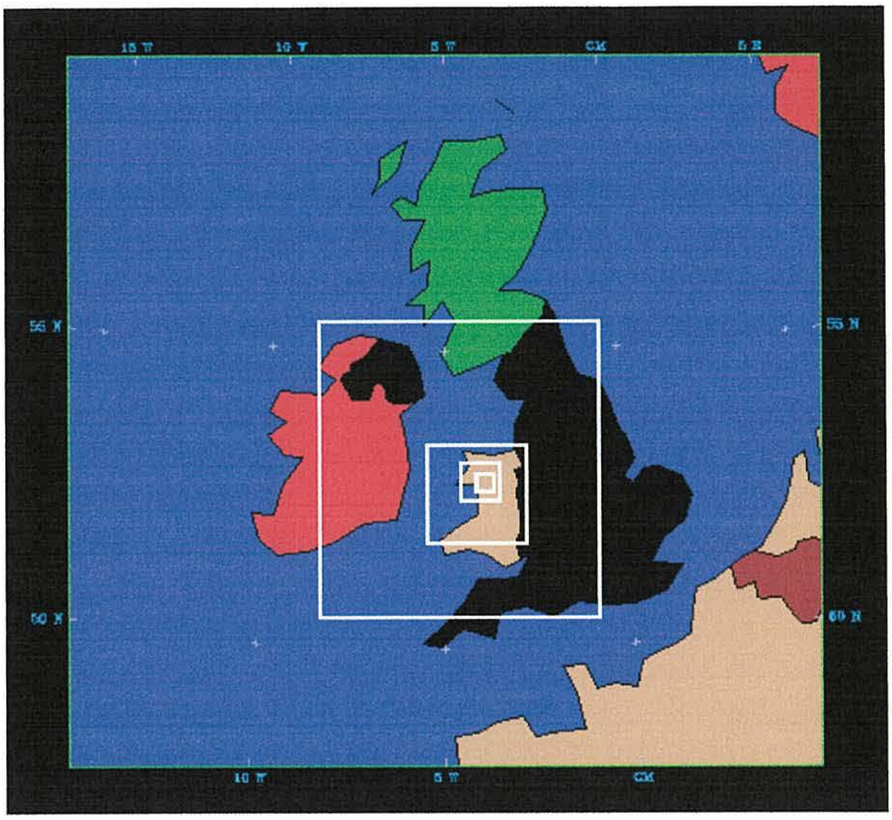

Domain	Region	Grid resolution (km)	Grid columns	Grid rows
1	British Isles	27	52	49
2	Irish Sea	9	58	61
3	Wales	3	61	61
4	Gwynedd	1	70	70
5	Mawddach	0.33	91	91

Figure 2.72: Nested domains for the Mawddach meteorological model

The TERRAIN module creates land surface boundary condition files for each of the domains, to allow the modelling of processes within the planetary boundary layer (PBL). The PBL makes up approximately the lowest 1 000m of the troposphere, and is the zone in which large scale weather patterns may be modified by properties of the land or sea surfaces over which the airflows move.

A series of data sets with global coverage have been provided by the National Center for Atmospheric Research in conjunction with the US Geological Survey, for use in initialising MM5 domains. These are listed in Table 2.1, and are illustrated for the Mawddach catchment in figures 2.73-2.77.

Data set	Provided by	Resolution	Illustrated by:
Terrain height	USGS	30sec (~1km)	fig.2.69
Land use and vegetation	USGS Simple Biosphere model	30sec (~1km)	fig.2.70
Monthly vegetation fraction	NOAA Advanced Very High Resolution Radiometer	10min (~20km)	fig.2.71
Soil data	U N Food and Agriculture Organisation	30sec (~1km)	fig.2.72
Deep soil temperature	European Center for Medium range Weather Forecasting	10min (~20km)	fig.2.73

Table 2.1: Data sets used to initialise the Mawddach PBL model

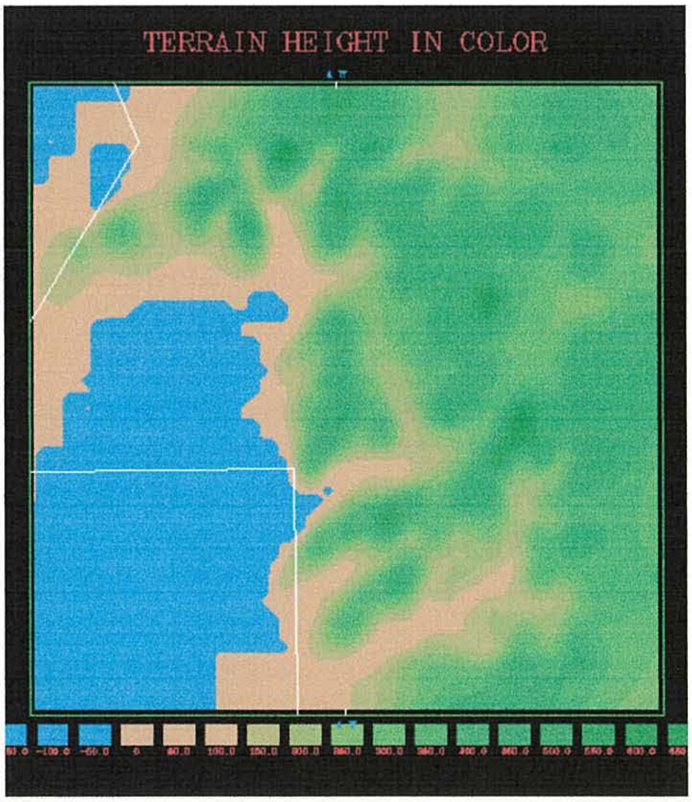

Figure 2.73: Terrain height data for the Mawddach model

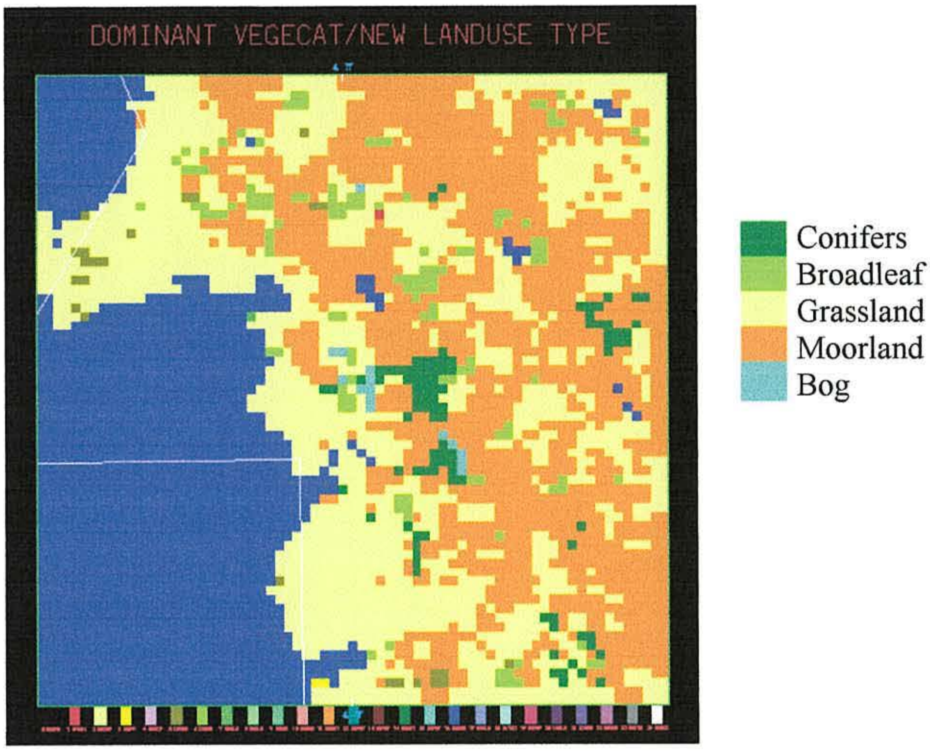

Figure 2.74: Land use classification for the Mawddach model

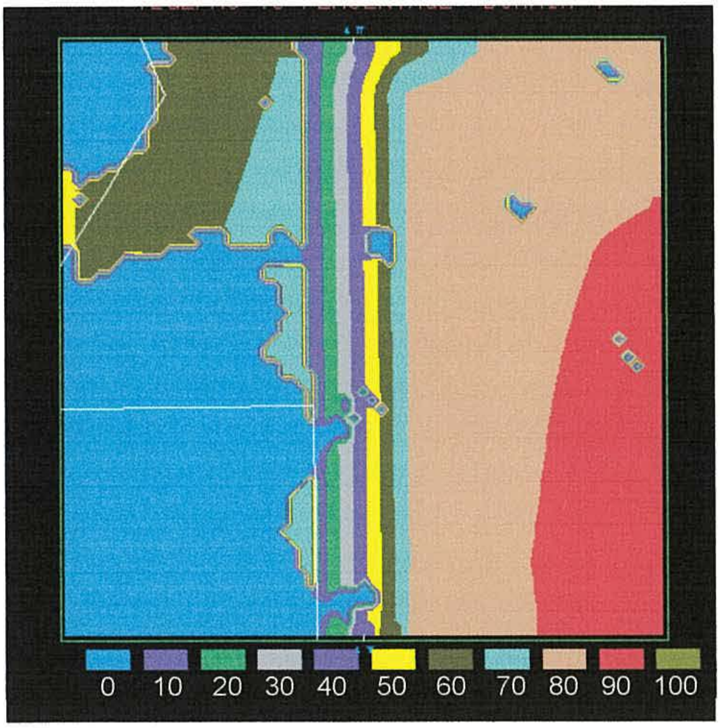

Figure 2.75: Monthly vegetation fraction for the Mawddach model – October, representing an estimate of the percentage of ground covered by vegetation.

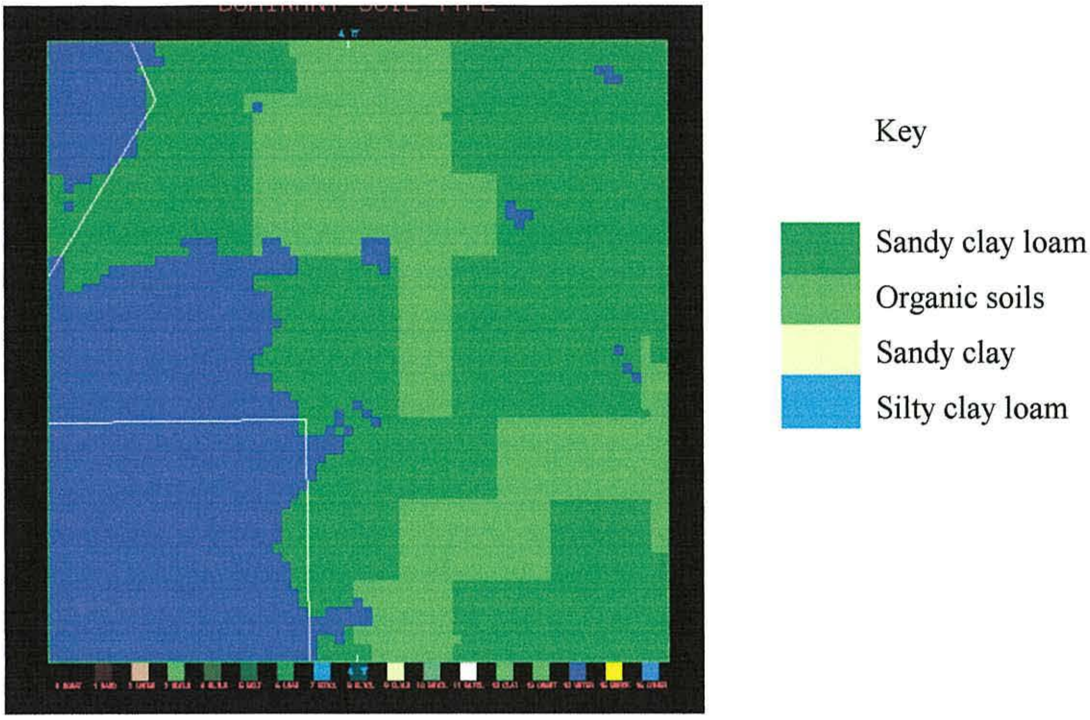

Figure 2.76: Dominant soil type for the Mawddach model

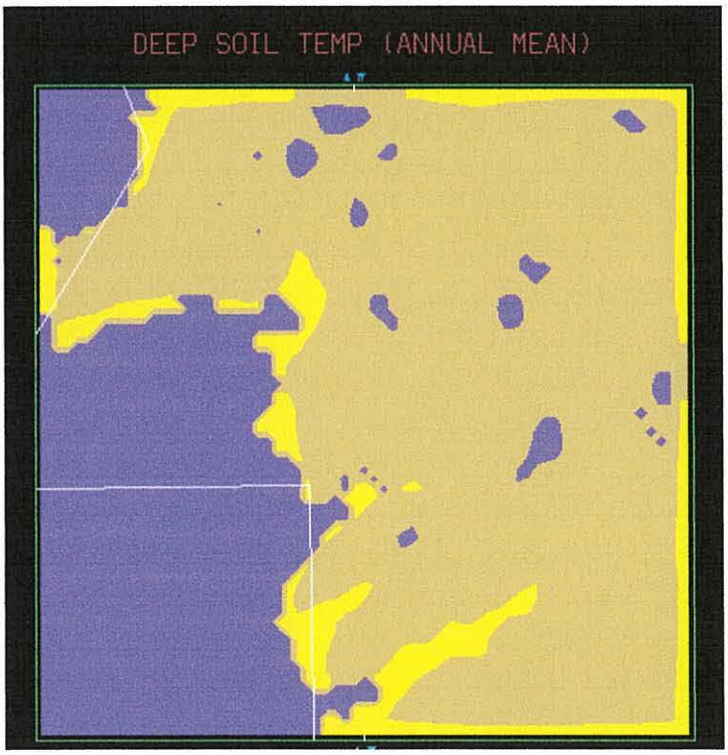

Figure 2.77: Mean annual deep soil temperature for the Mawddach model

REGRID module

The second module of the MM5 system is REGRID. Meteorological models usually involve significant sections of the globe for the outer model domains. Land surface and meteorological data are provided for latitude and longitude points, and this data has to be projected onto a horizontal grid for use in the model.

The length of east-west arc representing 1 degree of longitude will vary according to distance from the equator. This variation must be taken into consideration so that the mass of air moving through the model is conserved.

For modelling middle latitudes, the gridded latitude-longitude data is first plotted in Lambert Projection. The advantage of this projection is in preserving the shapes of small areas exactly. The map scale may, however, vary slightly from point to point and it is necessary to apply a correction factor **m** in the model to allow for this (Calvert, 2005).

Geometrically, the Lambert Projection represents the transfer of the earth's surface onto a cone which just touches the globe at some latitude φ (fig.2.78). When the cone is unwrapped, it forms a sector of a circle which does not quite meet at the edges (fig.2.79).

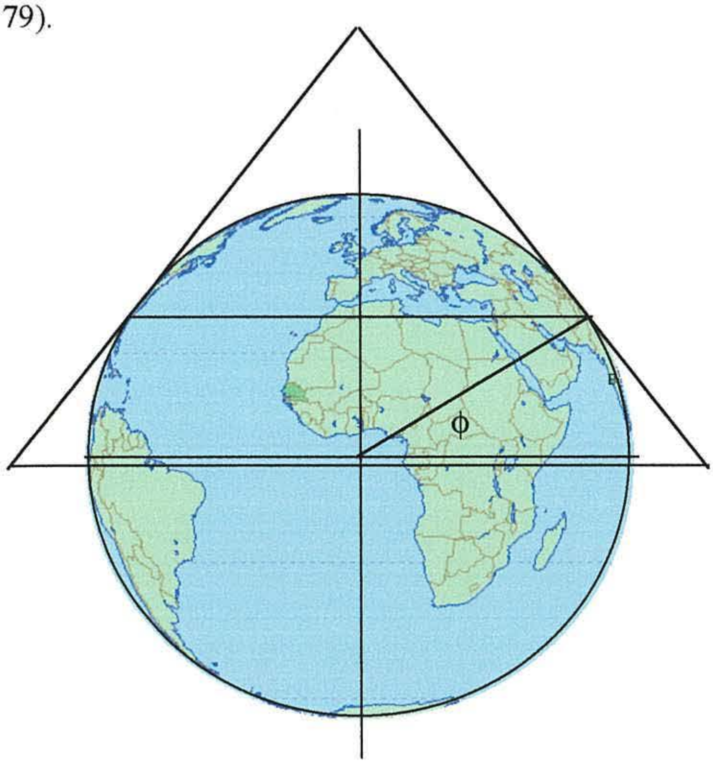

Figure 2.78: Method of generating the Lambert Projection

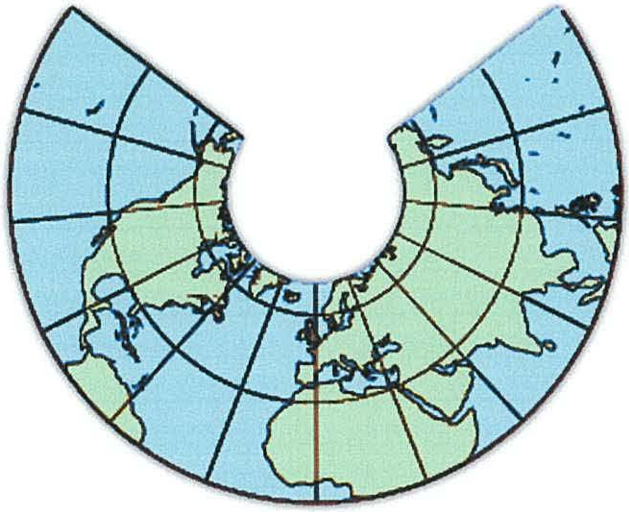

Figure 2.79: Lambert Projection onto a plane surface

In a Lambert map, the parallels of latitude are represented by concentric circles. The map has two standard parallels where the scale is unity. The Lambert conformal grid is true at latitudes 30^0 and 60^0 N, so the map scale factor is given by **m** =1 at these latitudes.

$$\mathbf{m} = \frac{\text{distance on grid}}{\text{actual distance on earth}}$$

For any other latitude ϕ, the map scale factor can be calculated from:

$$m = \frac{\sin\psi_1}{\sin\phi}\left[\frac{\tan\phi/2}{\tan\psi_1/2}\right]^{0.716}$$

where: $\psi_1 = 30^0$

Latitude-longitude data can then be transferred to corresponding positions on a rectangular grid for use in the MM5 model (fig.2.80):

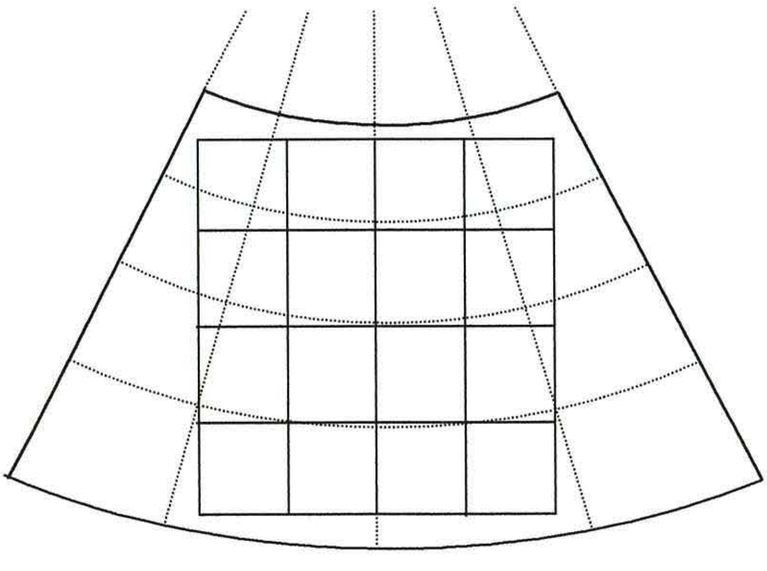

Figure 2.80: Mapping of data from a Lambert Projection to a rectangular grid

LITTLE_R module

The LITTLE_R module allows the incorporation of additional meteorological data to improve the accuracy or resolution of the original gridded input set. This new data may have come from surface observations or radiosonde balloon ascents carried out in a research area, or the interpretation of remote sensing data from satellites or radar. LITTLE_R adjusts surrounding readings according to the confidence level which the user wishes to place on the new data.

INTERPF module

The purpose of INTERPF is to convert the gridded data from pressure levels into a form which is simpler for the model to process. S*igma levels* are defined to represent intervals between the ground surface and the horizontal top surface of the model (fig.2.81). Sigma pressure levels are defined according to the equation:

$$\sigma = \frac{(p - p_t)}{(p_s - p_t)}$$

where p is the pressure at level σ, p_s is the surface pressure and p_t is the pressure at the top of the model at the same horizontal grid location. The sigma levels have values range from 0 at the model top to 1 at the earth's surface. Appropriate vertical intervals are chosen, with closer spacing near the ground where accurate calculation of meteorological variables will be most critical for the model. The Mawddach model uses 23 levels.

Sigma levels are numbered downwards, starting with K=1 at the model top surface. During runs of the MM5 model, some variables are calculated for the sigma surfaces, whilst others are calculated at the half-level positions between sigma levels (fig.2.77):

Sigma surfaces

Vertical air velocity, Pressure gradient

Half-levels

Horizontal air velocity, Temperature, Pressure, Relative humidity

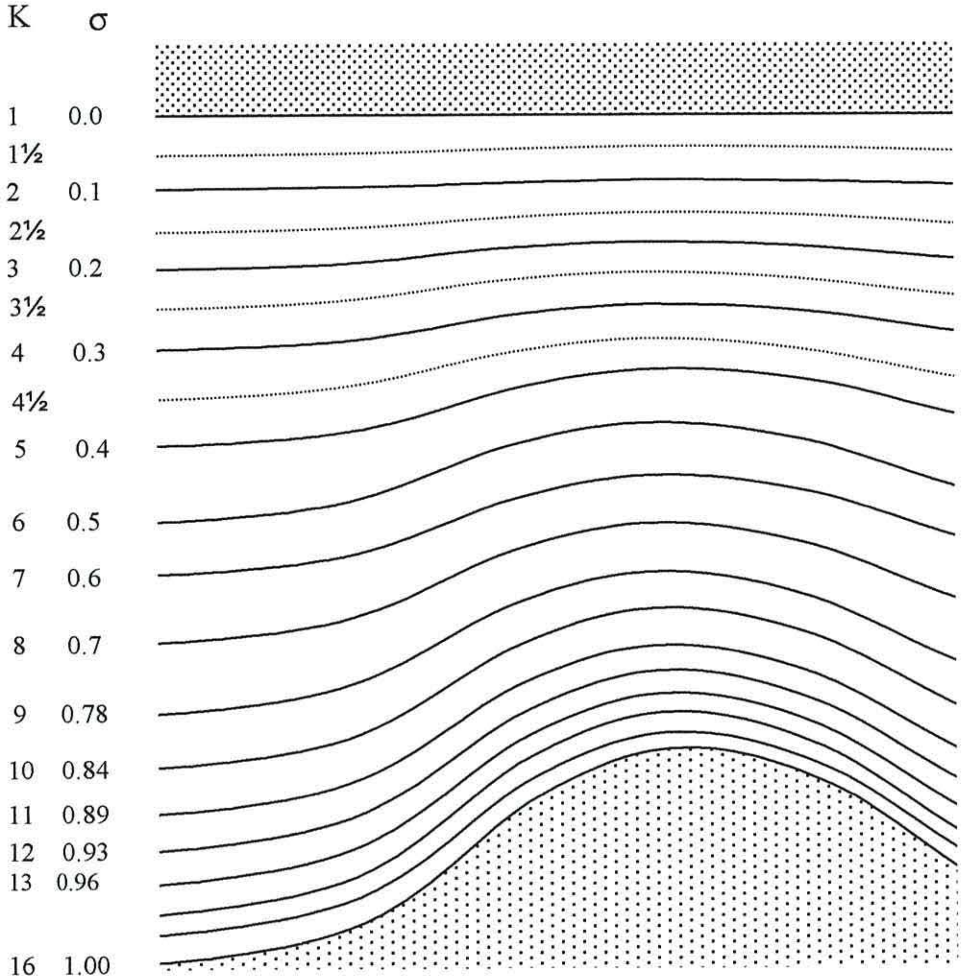

Figure 2.81: An example of sigma levels defined in a meteorological model

The meteorological model is run by the MM5 module, using the data set for initial and boundary conditions prepared by the previous modules.

Much of the mathematical formulation of meteorological models is based on the advection equation. This is demonstrated in fig.2.82 for the case of a smoke plume, but the principle is applicable to the transport of other physical properties such as temperature and pressure. The equation:

$$\frac{dN}{dt} = \frac{\partial N}{\partial t} + (v \cdot \nabla)N$$

or its three-dimensional expanded form:

$$\frac{dN}{dt} = \frac{\partial N}{\partial t} + u\frac{\partial N}{\partial x} + v\frac{\partial N}{\partial y} + w\frac{\partial N}{\partial x}$$

states that the rate of change of a property N depends on two factors:

- the rate at which the property is varying in the source region, which provides a base value
- the rate at which the base value varies as the point of measurement moves away from the source.

There is an assumption that the rates of change remain steady whilst the calculation is being made. In practice, this means that variations to the state of the system occur on a relatively long time scale compared to the time steps of the model. Typically an MM5 model recalculates for each 60sec. time step during the simulation.

The **continuity equation for air**, the **thermodynamic energy equation,** the **equation of state,** and the **momentum equations** make up the set of equations of atmospheric dynamics which form the core of the MM5 model. The significance of these functions is outlined on the following pages.

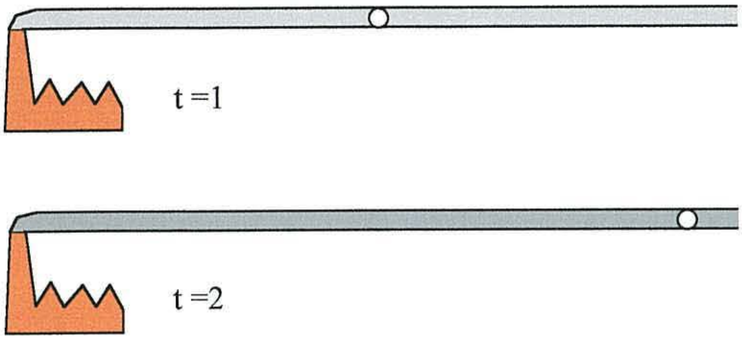

Concentration is constant with distance from the source at any time instant, but gradually changes with time.

The concentrations recorded at the moving sample point depend only on changes with time.

$$\frac{dN}{dt} = \frac{\partial N}{\partial t}$$

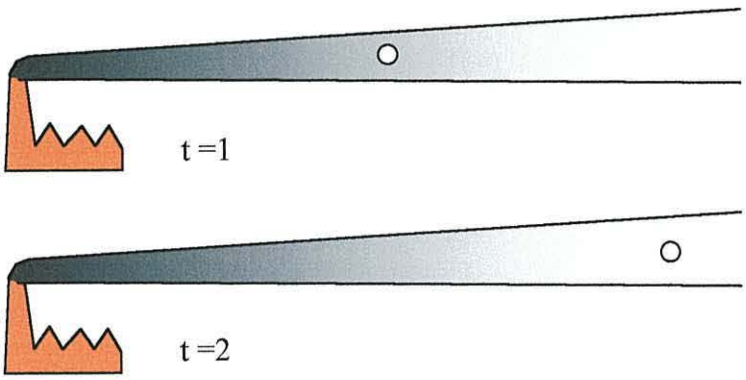

Concentration varies with distance from the source at any time instant, but the distribution remains constant with time.

The concentrations recorded at the moving sample point depend only on the rate at which the concentration varies with position, and the velocity of the moving point.

$$\frac{dN}{dt} = u\frac{\partial N}{\partial x}$$

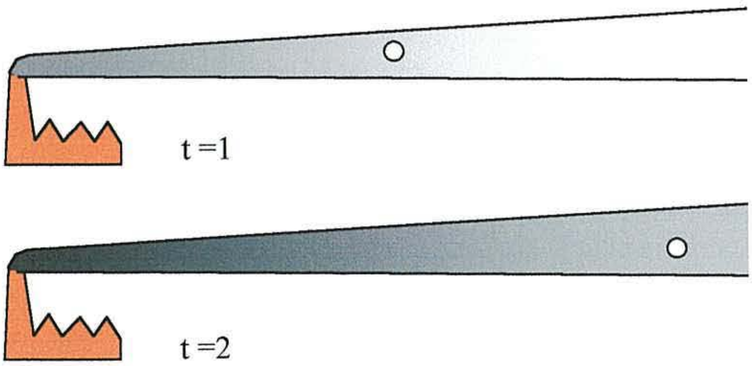

Concentration varies with distance from the source at any time instant, but the distribution also varies with time.

The concentrations recorded at the moving sample point depend on both the changes with time at a fixed point, and the rate at which the concentration varies with position at a fixed time.

$$\frac{dN}{dt} = \frac{\partial N}{\partial t} + u\frac{\partial N}{\partial x}$$

or for three coordinates:

$$\frac{dN}{dt} = \frac{\partial N}{\partial t} + (\mathbf{v} \cdot \nabla)N$$

Figure 2.82: The advection equation.

Equation of state

It is important to predict changes in temperature which accompany changes in pressure and volume, for example when an air mass expands as it rises to an altitude where atmospheric pressure is lower. The relationship between amount of gas, its pressure, volume and temperature is given by the Ideal gas law:

$$p = \frac{nRT}{V}$$

where p is pressure, n is the mass of gas, T is temperature, V is volume, and R is the Universal gas constant.

Thermodynamic energy equation

The First law of thermodynamics relates change in temperature of a gas to the energy transfer between the gas and its environment and the work done on or by the gas:

$$dQ = dU + dW$$

where dQ is the energy transferred, dU is the change in internal energy of the gas, and dW is work done. When the gas expands, work is done by the gas:

$$dW = \frac{p\ dV}{M} = p\ d\alpha$$

where M is the mass, V the volume and p the pressure.

$$\alpha = \frac{V}{M} = \frac{1}{\rho}$$

where α is the volume of a unit mass of air, known as the *specific volume,* which is the reciprocal of the density.

The change in internal energy of an air body is the change in temperature multiplied by the energy required to change its temperature by one degree:

$$dU = \left(\frac{\partial Q}{\partial T}\right) dT = c_v dT$$

where c_v is the specific heat of moist air at constant volume. This varies with the amount of water vapour in the air.

These results can be combined to give the First law of thermodynamics for the atmosphere:

$$dQ = c_v dT + p\ d\alpha$$

In an ***adiabatic*** process, no energy is transferred between the air parcel and its surroundings, so dQ = 0. The temperature of the parcel changes because of pressure variation as it ascends or descends. A rising parcel of air expands and cools, or a descending parcel of air compresses and warms according to the relation:

$$c_v dT = -p d\alpha$$

Continuity equation

An essential property of a meteorological model is that mass is conserved as air parcels move through the modelled region; mass is neither created nor destroyed. Continuity equations are a formulation of the requirements for conservation of mass.

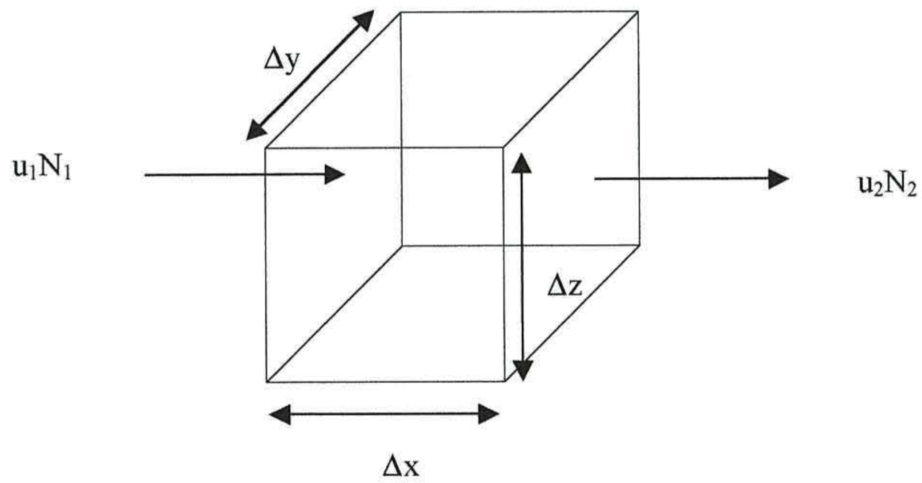

Fig 2.83: Gas flow through a cell

Fig.2.83 illustrates a cell through which a gas is passing in the x-direction. N represents gas concentration and u represents velocity. The rate of change of concentration of the gas within the cell must equal the difference between the inflow and outflow quantities of gas, as measured by the product of concentration N and flow rate u at the cell boundaries. It can be shown that:

$$\frac{\partial N}{\partial t} = -\frac{\partial (uN)}{\partial x}$$

Expanding to three dimensions:

$$\frac{\partial N}{\partial t} = -\frac{\partial(uN)}{\partial x} - \frac{\partial(uN)}{\partial y} - \frac{\partial(uN)}{\partial z} = -\nabla \cdot (\mathbf{v}N)$$

Momentum equations

In addition to mass, a model must ensure that momentum is conserved during air motions. The Momentum equation is used to predict wind velocity, and must balance the various forces which might act on an air body to affect its movement. These forces include: the *local acceleration*, the earth's *centrifugal force*, the apparent *Coriolis force, gravitational force, pressure-gradient force, viscous force* and *turbulent-flux divergence.*

When considering forces related to the motion of the earth, it is convenient to use spherical polar coordinates in preference to the normal cartesian coordinate system. The nomenclature for spherical polar coordinates is given in fig.2.84.

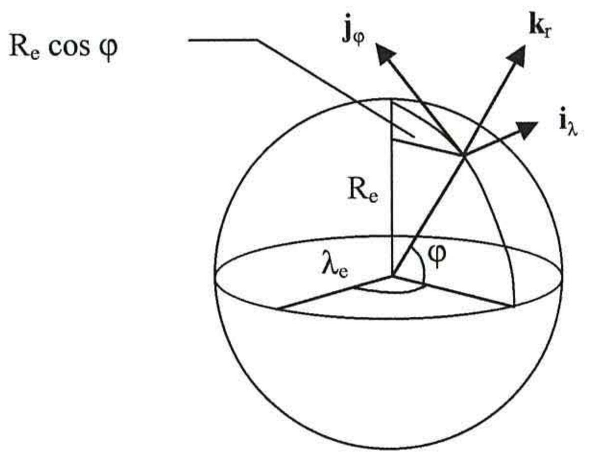

Figure 2.84: Spherical polar coordinates

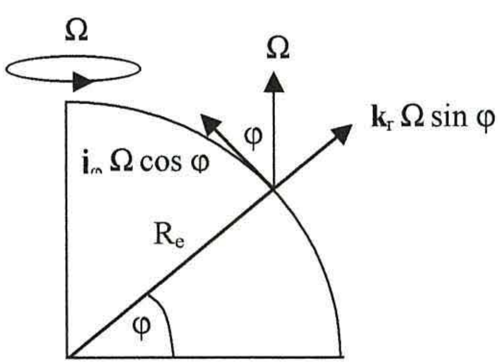

Figure 2.85: Components of the earth's angular velocity

The angular velocity Ω of the earth is 7.292 x 10^{-5} radians s^{-1}. The components of the earth's angular velocity parellel and perpendicular to the surface are shown in fig.2.85, where φ is the latitude.

The ***Coriolis force*** deflects moving bodies towards the right in the northern hemisphere. It can be shown that the Coriolis acceleration is given by

$$\mathbf{a}_c = 2\mathbf{\Omega} \times \mathbf{v}$$

as twice the vector cross product of the earth's angular velocity with the local velocity of the body. There is no Coriolis force on a body which is stationary with respect to the earth's surface.

The ***centrifugal force*** is given by

$$\mathbf{a}_r = \mathbf{\Omega} \times (\mathbf{\Omega} \times \mathbf{R}_e)$$

where R_e is the radius vector of the earth. The effect of the double vector cross product is to determine the force direction as outwards from the earth's surface in a direction perpendicular to the axis of rotation.

From a reference frame fixed on the earth's surface, a momentum equation can be derived which relates local acceleration $\mathbf{a}_l$ to other accelerations and forces acting on an air mass:

$$\mathbf{a}_l + \mathbf{a}_c + \mathbf{a}_r = \frac{1}{M_a}\left(\mathbf{F}_g + \mathbf{F}_p + \mathbf{F}_v\right)$$

where $\mathbf{a}_c$ is the Coriolis acceleration, $\mathbf{a}_r$ is the centrifugal acceleration, $\mathbf{F}_g$ is the gravitational force, $\mathbf{F}_p$ is the pressure force, and $\mathbf{F}_v$ is the viscous force.

The ***local acceleration*** is given by the advection equation (fig.2.82) as:

$$\mathbf{a}_l = \frac{d\mathbf{v}}{dt} = \frac{\partial \mathbf{v}}{\partial t} + (\mathbf{v} \cdot \nabla)\mathbf{v}$$

The local acceleration of an air parcel equals the acceleration at a fixed source point plus a variation in local acceleration due to a velocity flux gradient along the line of motion.

The ***Gravitational force*** is given by:

$$\frac{F_g}{M_a} = \frac{GM_e}{R_e^2}$$

where M_e and M_a are the masses of the earth and the air mass respectively, R_e is the radius of the earth, and G is the gravitational constant.

The ***Pressure-gradient force*** is:

$$\frac{F_p}{M_a} = -\frac{1}{\rho_a}\nabla p_a = -\frac{1}{\rho_a}\left(\mathbf{i}\frac{\partial p_a}{\partial x} + \mathbf{j}\frac{\partial p_a}{\partial y} + \mathbf{k}\frac{\partial p_a}{\partial z}\right)$$

where ρ_a is air density. This expression specifies the rate of change of pressure in terms of components along the three cartesian axes.

The ***Viscous force*** is a measure of the resistance to motion of an air mass over the ground surface. The change of wind velocity with height ($\partial u/\partial z$) is known as the *wind shear*. This can produce a shear stress τ given by:

$$\tau = \eta \frac{\partial u}{\partial z}$$

where η is the dynamic viscosity of air.

Turbulent flux divergence occurs in first 300m above the ground where wind speeds may increase logarithmically with height and wind shear is strongly developed. Turbulence consists of many eddies of different sizes operating together. Eddies are created downwind of obstacles as turbulent wakes. Surface heating can also create thermal turbulence. Flux turbulence can be formulated as:

$$\frac{F_t}{M_a} = -\frac{1}{\rho_a}(\nabla \cdot \rho_a \mathbf{K}_m \nabla)\mathbf{v}$$

where **K** is the eddy diffusion coefficient tensor. The turbulence force opposing air motion is thus a function of the air flow velocity.

Combining the expressions for accelerations and forces gives the three **Momentum equations** in the cartesian directions. Ignoring the viscous force which is small in comparison to other terms:

$$\frac{du}{dt} = \frac{\partial u}{\partial t} + u\frac{\partial u}{\partial x} + v\frac{\partial u}{\partial y} + w\frac{\partial u}{\partial z} = fv - \frac{1}{\rho_a}\frac{\partial p_a}{\partial x} + \frac{1}{\rho_a}$$
$$\times\left[\frac{\partial}{\partial x}\left(\rho_a K_{m,xx}\frac{\partial u}{\partial x}\right) + \frac{\partial}{\partial y}\left(\rho_a K_{m,yx}\frac{\partial u}{\partial y}\right) + \frac{\partial}{\partial z}\left(\rho_a K_{m,zx}\frac{\partial u}{\partial z}\right)\right]$$

$$\frac{dv}{dt} = \frac{\partial v}{\partial t} + u\frac{\partial v}{\partial x} + v\frac{\partial v}{\partial y} + w\frac{\partial v}{\partial z} = -fu - \frac{1}{\rho_a}\frac{\partial p_a}{\partial y} + \frac{1}{\rho_a}$$
$$\times\left[\frac{\partial}{\partial x}\left(\rho_a K_{m,xy}\frac{\partial v}{\partial x}\right) + \frac{\partial}{\partial y}\left(\rho_a K_{m,yy}\frac{\partial v}{\partial y}\right) + \frac{\partial}{\partial z}\left(\rho_a K_{m,zy}\frac{\partial v}{\partial z}\right)\right]$$

$$\frac{dw}{dt} = \frac{\partial w}{\partial t} + u\frac{\partial w}{\partial x} + v\frac{\partial w}{\partial y} + w\frac{\partial w}{\partial z} = -g - \frac{1}{\rho_a}\frac{\partial p_a}{\partial z} + \frac{1}{\rho_a}$$
$$\times\left[\frac{\partial}{\partial x}\left(\rho_a K_{m,xz}\frac{\partial w}{\partial x}\right) + \frac{\partial}{\partial y}\left(\rho_a K_{m,yz}\frac{\partial w}{\partial y}\right) + \frac{\partial}{\partial z}\left(\rho_a K_{m,zz}\frac{\partial w}{\partial z}\right)\right]$$

This completes the description of the **continuity equation for air**, the **thermodynamic energy equation,** the **equation of state,** and the **momentum equations,** which form the basis for the MM5 model core.

A central function of the MM5 model in its hydrological application is the determination of rainfall rates on a high resolution grid scale. Moisture and precipitation are handled by the determination of three mixing ratios:

Water vapour mixing ratio

$$\frac{\partial p^* q_v}{\partial t} = -m^2\left[\frac{\partial p^* u q_v / m}{\partial x} + \frac{\partial p^* u q_v / m}{\partial y}\right] - \frac{\partial p^* q_v \dot{\sigma}}{\partial \sigma} + \delta_{nh} q_v DIV$$
$$+ p^*\left(-P_{RE} - P_{CON} - P_{II} - P_{ID}\right) + D_{qv}$$

Cloud water mixing ratio

$$\frac{\partial p^* q_c}{\partial t} = -m^2\left[\frac{\partial p^* uq_c/m}{\partial x} + \frac{\partial p^* uq_c/m}{\partial y}\right] - \frac{\partial p^* q_c\dot{\sigma}}{\partial \sigma} + \delta_{nh} q_c DIV$$
$$+ p^*\left(P_{ID} + P_{II} - P_{RC} - P_{RA} + P_{CON}\right) + D_{qc}$$

Rain water mixing ratio

$$\frac{\partial p^* q_r}{\partial t} = -m^2\left[\frac{\partial p^* uq_r/m}{\partial x} + \frac{\partial p^* uq_r/m}{\partial y}\right] - \frac{\partial p^* q_r\dot{\sigma}}{\partial \sigma} + \delta_{nh} q_r DIV$$
$$- \frac{\partial V_f \rho g q_r}{\partial \sigma} + p^*(P_{RE} + P_{RC} + P_{RA}) + D_{qr}$$

These equations include a range of physical processes involving water phase conversion:

P_{RE} is evaporation of rain drops,
P_{CON} is condensation of water vapour,
P_{II} is initiation of ice crystals,
P_{ID} is deposition of vapour onto ice crystals,
P_{RC} is conversion of cloud drops to rain drops,
P_{RA} is accretion of cloud drops by rain drops.

The basic model provides for condensation whenever relative humidity reaches 100%, with subsequent production of raindrops and fallout under gravity. The model successfully handles seeder-feeder mechanisms, where raindrops produced in high cloud layers fall through lower saturated air and increase their volume. Advection of raindrops during descent to the ground surface is also handled correctly.

Rain accretion rate is calculated from

$$P_{RA} = \frac{1}{4}\pi\rho a q_c E N_0 \frac{\Gamma(3+b)}{\lambda^{3+b}}$$

where parameter **a** has a value of 842.99 for rain or 11.72 for snow, parameter **b** has a value of 0.8 for rain or 0.41 for snow, and Γ is the gamma- function. The parameter $N_0 = 8 \times 10^6$ for rain, 2×10^7 for snow. q_c is the cloud water mixing ratio.

The fall speed of rain is calculated from

$$V_f = a\frac{\Gamma(4+b)}{6}\lambda^{-b}$$

where

$$\lambda = \left(\frac{\pi N_0 \rho_w}{\rho q_r}\right)^{1/4}$$

Modelling of thunderstorm events where vertical motions are dominant presents a greater modelling challenge. MM5 offers a series of cumulus parameterisation schemes to model rainfall generation. The principle of cumulus parameterisation is that convective motion can take place on a scale smaller than a model grid cell. Whilst the mean relative humidity within a cell may not reach 100%, there may be zones within the cell where water vapour is concentrated and condensation may occur (figure 2.86). Condensation will produce rainfall, but also releases latent heat which can drive upward convection.

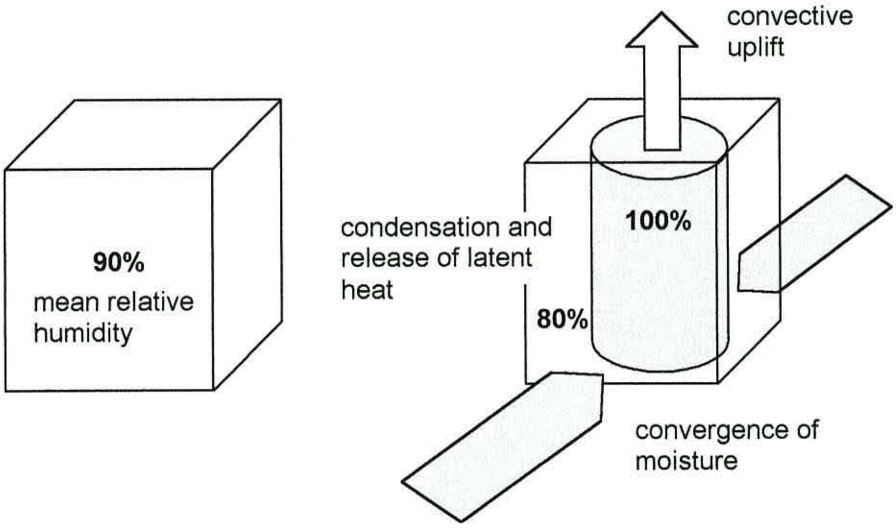

Figure 2.86: Principles of the Anthes-Kuo cumulus parameterisation scheme

The simplest cumulus parameterisation is the Anthes-Kuo scheme (Anthes, 1976; Kuo and Raymond, 1980). The is based on an analysis of water vapour flux in the zone of convection (fig.2.87). An algorithm estimates the rate of convergence of moisture M_t at the boundaries of a grid call using:

$$M_t = -\frac{1}{g}\int_0^{p_s} \nabla \cdot \overline{\mathbf{V}q}\, dp$$

where p_s is surface pressure, $\overline{\mathbf{V}}$ is mean horizontal air velocity, $\overline{q}$ is mean specific humidity and g is gravity force. If moisture convergence is above a threshold value of 3×10^{-5} kg m^{-2} s^{-1} then the temperatures for grid cells in the overlying vertical air column are checked to determine if convection is possible.

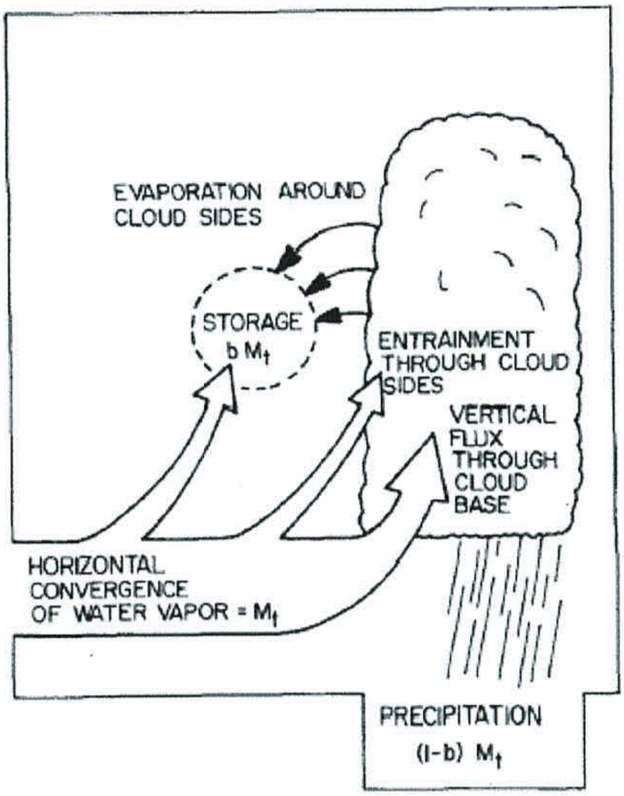

Figure 2.87: Schematic diagram showing moisture cycle in a column which contains convection. Figure and caption from: Anthes, 1977

The base and top level of cloud is then determined. Convection is assumed if the cloud depth is greater than a critical value $\Delta\sigma \geq 0.3$.

Vertical air motion is computed from:

$$\frac{dw^2/2}{dz} = \frac{gB}{(1+\alpha)} - gQ_{lw} - \mu w^2$$

where: w is vertical air velocity, B is buoyancy, $\alpha = 0.5$ is a compensating factor to allow for non-hydrostatic pressure perturbations, Q_{lw} is total liquid water as the ratio of mass of water to mass of air, and μ is the rate of entrainment of air from the environment around the convection cell. This equation shows that vertical ascent velocity in a convecting cloud is related to buoyancy of the air parcel, but counteracted by the weight of liquid water being carried upwards and by the amount of entrained air which reduces the contrast in physical properties between the cloud and its surrounding air mass. The buoyancy term is given by:

$$B = \frac{T_v - T_{ve}}{T_{ve}}$$

where T_v is the virtual temperature of the convective updraft at a particular pressure level within the cloud, and T_{ve} is the virtual temperature of the surrounding airmass at the same pressure level.

A theoretical temperature function within the convecting column is used to calculate condensation and rainfall production. It is found from atmospheric soundings that convective heating often has a parabolic shape with a maximum in the upper half of the cloud (fig.2.88).

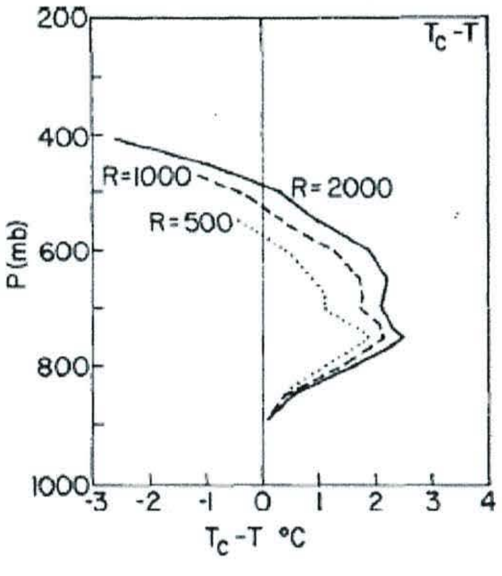

Figure 2.88: Vertical profile of (T_c–T) in three clouds of radii 500, 1000 and 2000m. The environment sounding was that for Pittsburgh, Pa., 1200 GMT 25 May 1976. Figure and caption from: Anthes, 1977

Tc: cloud virtual temperature
T: environment virtual temperature

The water vapour mixing ratio within cells is reduced to compensate for rainfall production, and the temperature is increased to allow for latent heat released during condensation.

An alternative convective scheme within the MM5 system is Grell cumulus parameterisation. This is a more sophisticated scheme in which individual clouds are modelled, along with the mechanisms of rainfall generation within them (figure 2.89).

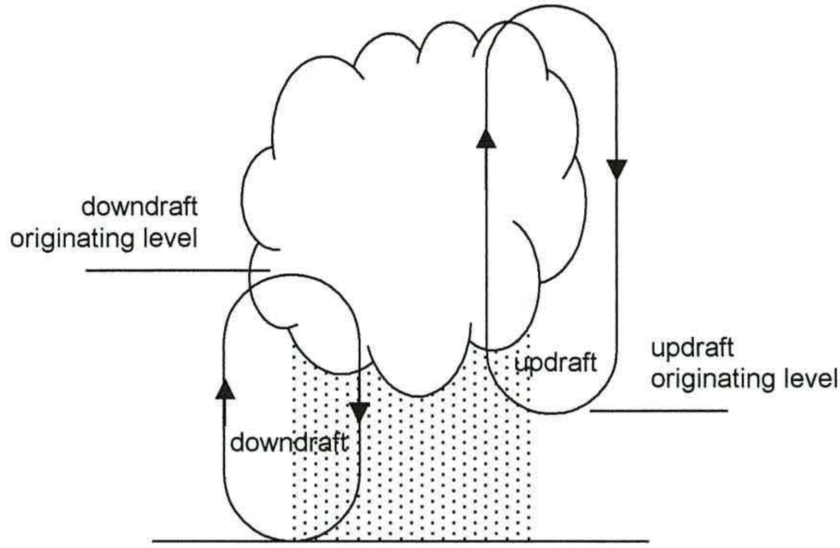

Figure 2.89: Air movements within a cloud, modelled by the Grell cumulus scheme. After: Grell, Dudhia and Stauffer (1995)

In the Grell scheme, clouds are modelled as two steady-state circulations, caused by an updraft and a downdraft. There is no entrainment of environmental air into the cloud except at the top and bottom of the circulations.

Warming occurs through condensation from ascending saturated air as it cools, but evaporation and re-absorption of water vapour can take place in descending air as it warms adiabatically. An energy budget balances these effects, with rainfall being generated from cloud water which escapes reabsorption.

Configuring and running the MM5 model

Running the MM5 module involves several stages:

- The input files from the TERRAIN and INTERPF modules are placed in a directory where they can be accessed by the MM5 program.
- An MM5 program is built specially for the current run. When creating this program, it is necessary to specify the number of nested domains which will be modelled, and the type of computer system in use.
- A file of options is created, which will be accessed by the program while it is running. This file specifies a range of parameters including: details of the domain grid sizes, choices of cumulus schemes and planetary boundary layer schemes, and options for the complexity with which phase changes between water vapour, liquid water and ice crystals will be handled when modelling cloud microphysics.
- The MM5 program is run. This generates a series of output files for chosen time intervals, representing conditions within each of the nested domains. A finite difference scheme is used within MM5 to model the progression of pressure, momentum and temperature across the modelling domain. At intervals, new observational values for these parameters will be supplied to the outer boundary. Cells within the outer rows of the model will then be progressively nudged towards the boundary values, to avoid the model diverging from observations over an extended simulation period.

GRAPH, RIP and VIS5D modules

Once a run is completed, several modules are available for producing graphical output from the domain data files:

- GRAPH is a simple plotting program for line drawings, which generates maps, cross sections and skew-T plots.
- RIP is a more flexible package which produces colour shaded images (Stoelinga, 2003). This has been used for most MM5 example data displayed in this chapter.
- VIS5D produces three-dimensional solid images, and may be used to display patterns of cloud and rainfall using isosurfaces.

Methods for creating graphical output with these packages are outlined in Appendix 4.

INTERPB module

The INTERPB module can convert MM5 output files from sigma coordinates back to pressure level (mb) data. This provides a facility for repeating the modelling cycle after addition of further meteorological observations through the LITTLE_R module.

Frontal rainfall events

Testing of the MM5 system has been carried out using a simulation of 6 hour forecasting mode. Global gridded data is updated at 6 hour intervals by US National Centre for Environmental Protection (NCEP) and distributed to forecasters via the Internet FTP service.

The MM5 model was run for the example storms presented in Chapter 2.2:

- 8 November 2002
- 29 December 2002
- 22 May 2003
- 2-4 February 2004

using data files which would have been available 6 hours in advance. Results from the model could then be evaluated against the raingauge data recorded in the catchment during the actual storm event. The objectives of the test were:

- to determine whether the high resolution 1km grid MM5 model was able to distinguish the Types A and B rainfall patterns observed over the Mawddach catchment,
- to determine whether the rainfall intensities predicted were consistent with gauge readings.

In examining the rainfall distribution maps which follow, it should be appreciated that the raingauge distribution across the Mawddach catchment is still relatively sparse for a mountain area liable to microclimate effects. The field maps were prepared from raingauge data before modelling was carried out. They represent only one interpretation of the rainfall distribution, and in some cases substantial changes to the positions of isohyets could be made to improve correspondence with the MM5 results whilst still remaining consistent with observations. Absolutely accurate field data on a 1km grid scale is not currently available for full evaluation of the rainfall forecast model.

In the following sections, predicted rainfall totals for 3-hour periods are compared with rain gauge data collected for the same periods during the storm events:

8 November 2002

A sequence of MM5 3-hour rainfall simulations for 8 November 2002 are shown in fig.2.90, with raingauge data covering the same periods for comparison.

The 03h – 06h simulation correctly identifies a type B rainfall pattern along the axis of the Rhinog mountain range, but also predicts high rainfall (9.69mm) over the Arennig mountains. There is some uncertainty about the actual rainfall pattern in the Arennig area as no gauges were present on the upper mountain slopes.

The 06h – 09h simulation shows rainfall becoming widespread across the Mawddach catchment, with maximums of approximately 10mm along the Rhinog range. A rainfall high of 11.5mm recorded for Cader Idris is beyond the geographical limit of the raingauge array, so there is uncertainty about true rainfall totals in this area.

The 09h – 12h simulation shows the rainfall axis moving eastwards to Coed y Brenin, although maximums of around 14mm are lower than the gauge readings of 21-23mm in this area. A maximum is again predicted over the ungauged summit of Cader Idris where verification is not available.

The 12h – 15h simulation correctly demonstrates a shift to a type A rainfall distribution extending inland across the catchment. Insufficient gauge data is available to verify the maximum of 17.92mm near the southern end of the Rhinog range. A predicted maximum of around 12mm in the vicinity of Rhobell Fawr and Pared yr Ychain is, however, considerably lower than the observed totals of 20-28mm.

The MM5 rainfall simulation for the 8 November 2002 storm event has reproduced approximately correct patterns of precipitation over the Mawddach catchment, although rainfall predictions are significantly lower than observed rainfall totals for some time periods at inland locations.

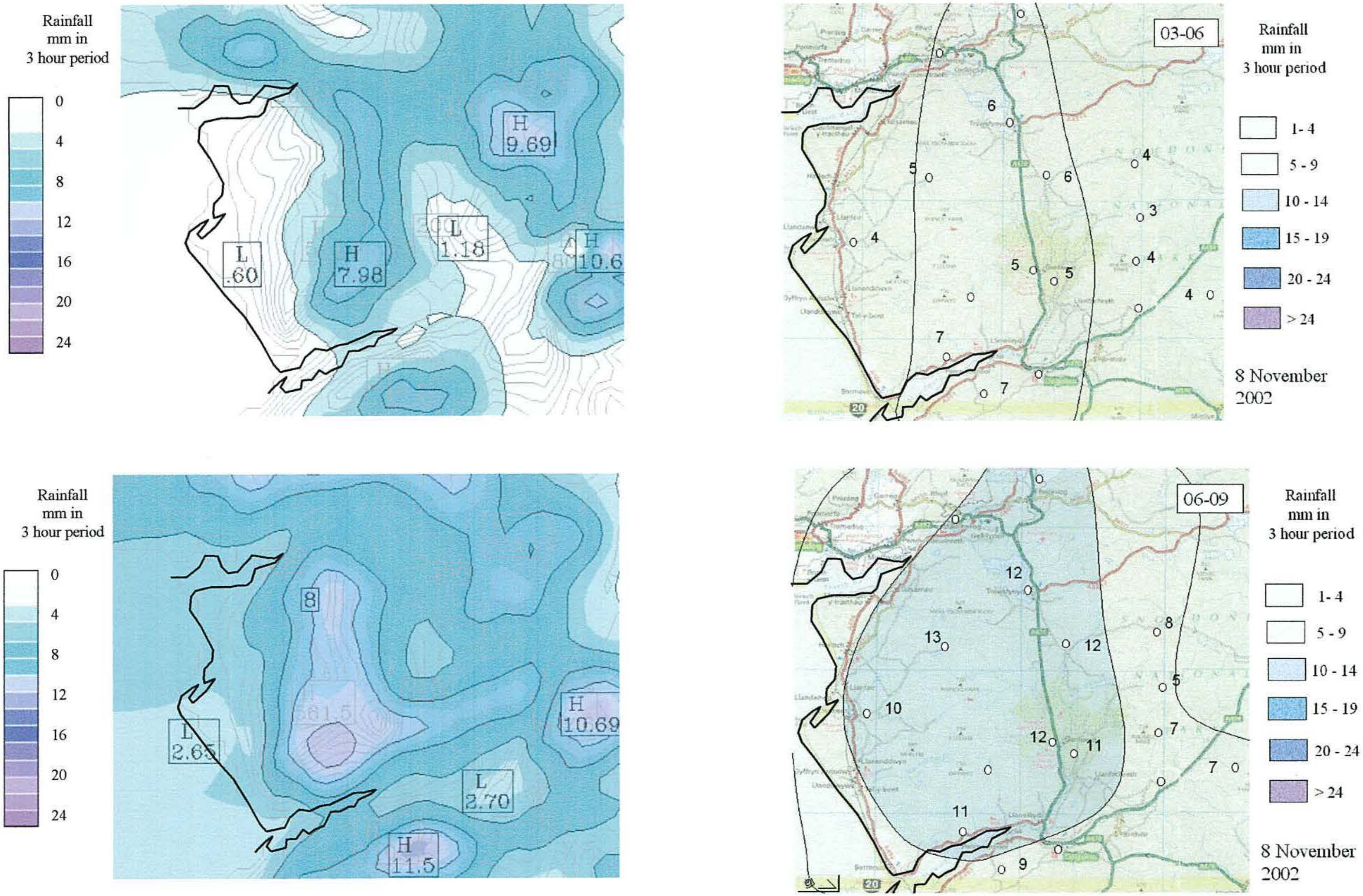

Figure 2.90: MM5 3-hour rainfall simulations (left) and 3-hour raingauge totals (right):
Above: 03:00h – 06:00h, 8 November 2002 Below: 06:00h – 09:00h, 8 November 2002

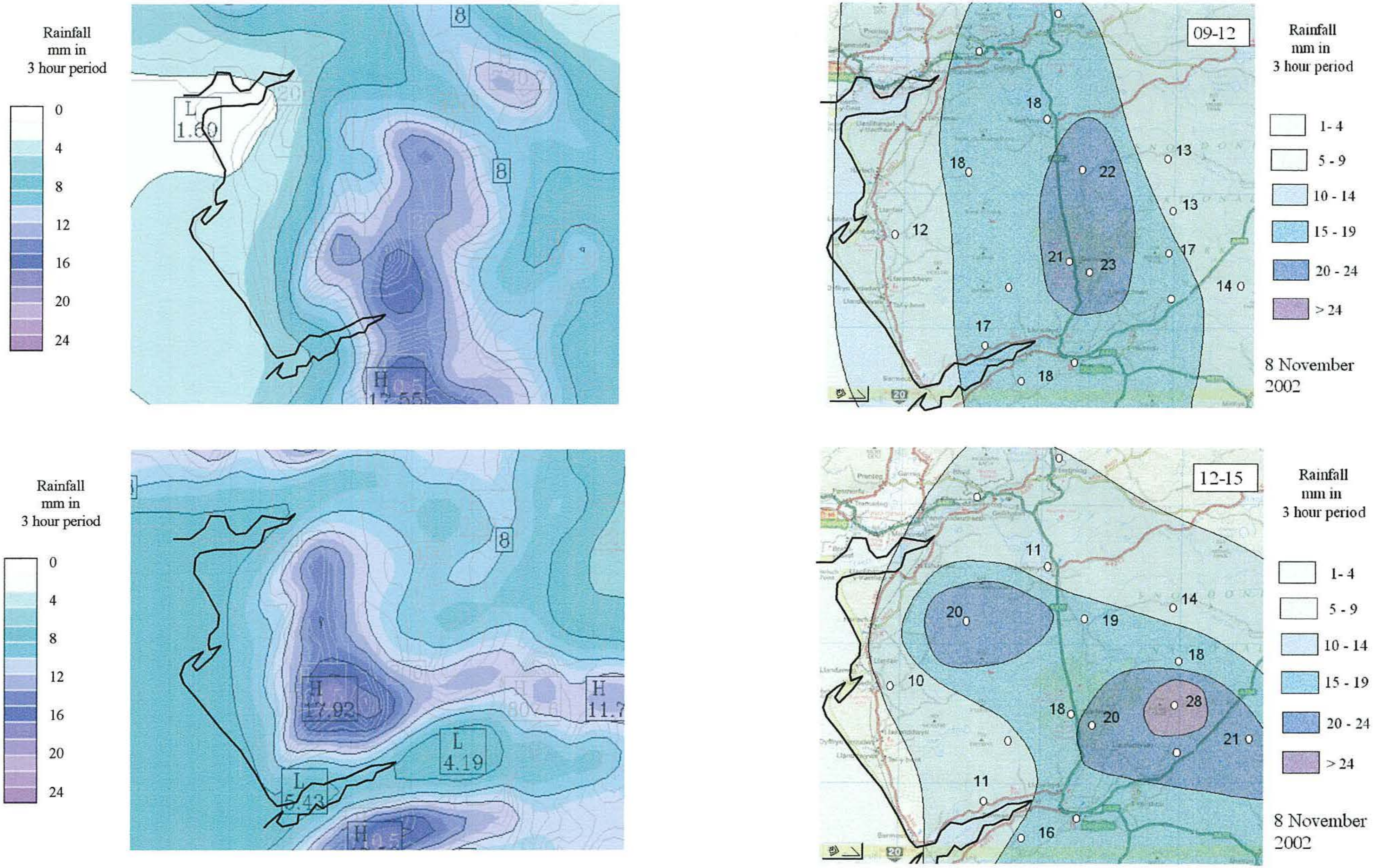

Figure 2.90(cont.) MM5 3-hour rainfall simulations (left) and 3-hour raingauge totals (right):
Above: 09:00h – 12:00h, 8 November 2002 Below: 12:00h – 15:00h, 8 November 2002

29 December 2002

MM5 3-hour rainfall simulations and 3-hour raingauge totals for 29 December 2002 are shown in fig.2.91.

The 06h – 09h simulation correctly identifies a broad band of rainfall across the catchment. A maximum of 11.56mm at the southern end of the Rhinog range is consistent with the limited raingauge data available. A zone of high rainfall is predicted for the Aran ridge along the southern margins of the Mawddach catchment, which agrees with the 11mm gauge reading at Pared yr Ychain. Insufficient data is available to verify the south western continuation of this high rainfall zone.

The 09h – 12h simulation predicts an intensification of rainfall across the whole catchment, with a maximum on the inland slopes of the Rhinog mountains. This is broadly in agreement with the rain gauge data. The exact rainfall total at the southern end of the Rhinog range is uncertain due to lack of recordings.

The 15h – 18h simulation shows an inland rainfall maximum of 18.14mm at Pared yr Ychain which is close to the observed total of 20mm. A rainfall maximum is aligned north-south along the Rhinog range, but a lack of raingauge data prevents verification of the prediction. The observed total of 18mm at Trawsfynydd is roughly consistent with the simulated value of 15mm at this point.

The 18h – 21h simulation is roughly in agreement with the observed data. A type A pattern is generated, with maxima in the areas of Trawsfynydd and Pared yr Ychain. A low rainfall zone between these maxima appears in the simulation, but was not observed in the field data where a more consistent band of high rainfall crosses the catchment.

As in the previous case of 8 November 2002, the 29 December 2002 simulation produces rainfall patterns which are largely consistent with field observations. Some local variance occurs, particularly in the central area of the catchment for some time intervals. Predicted rainfall totals are, however, closer to observed values than in the November case and no significant underestimation of inland rainfall occurs.

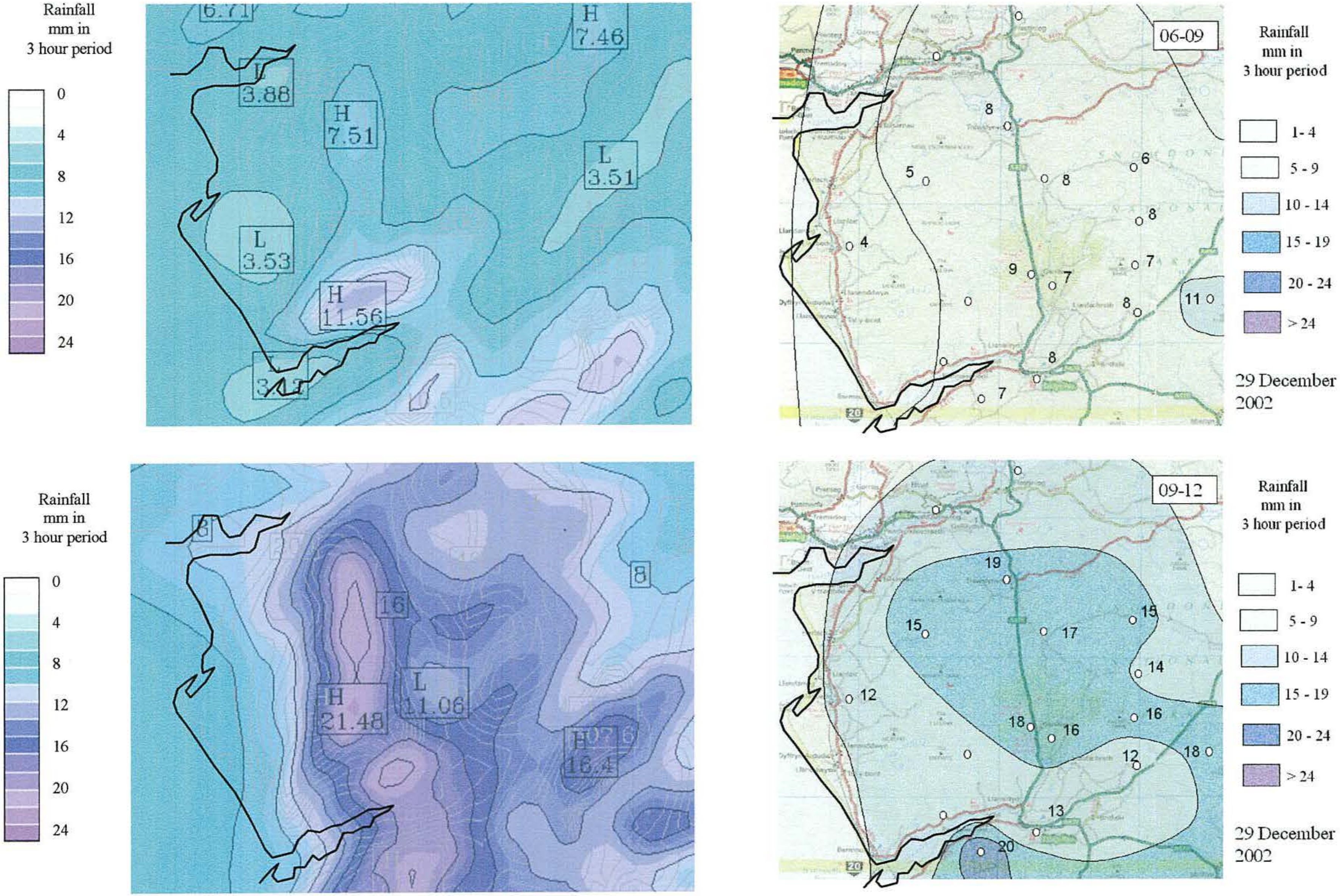

Figure 2.91: MM5 3-hour rainfall simulations (left) and 3-hour raingauge totals (right):
Above: 06:00h – 09:00h, 29 December 2002 Below: 09:00h – 12:00h, 29 December 2002

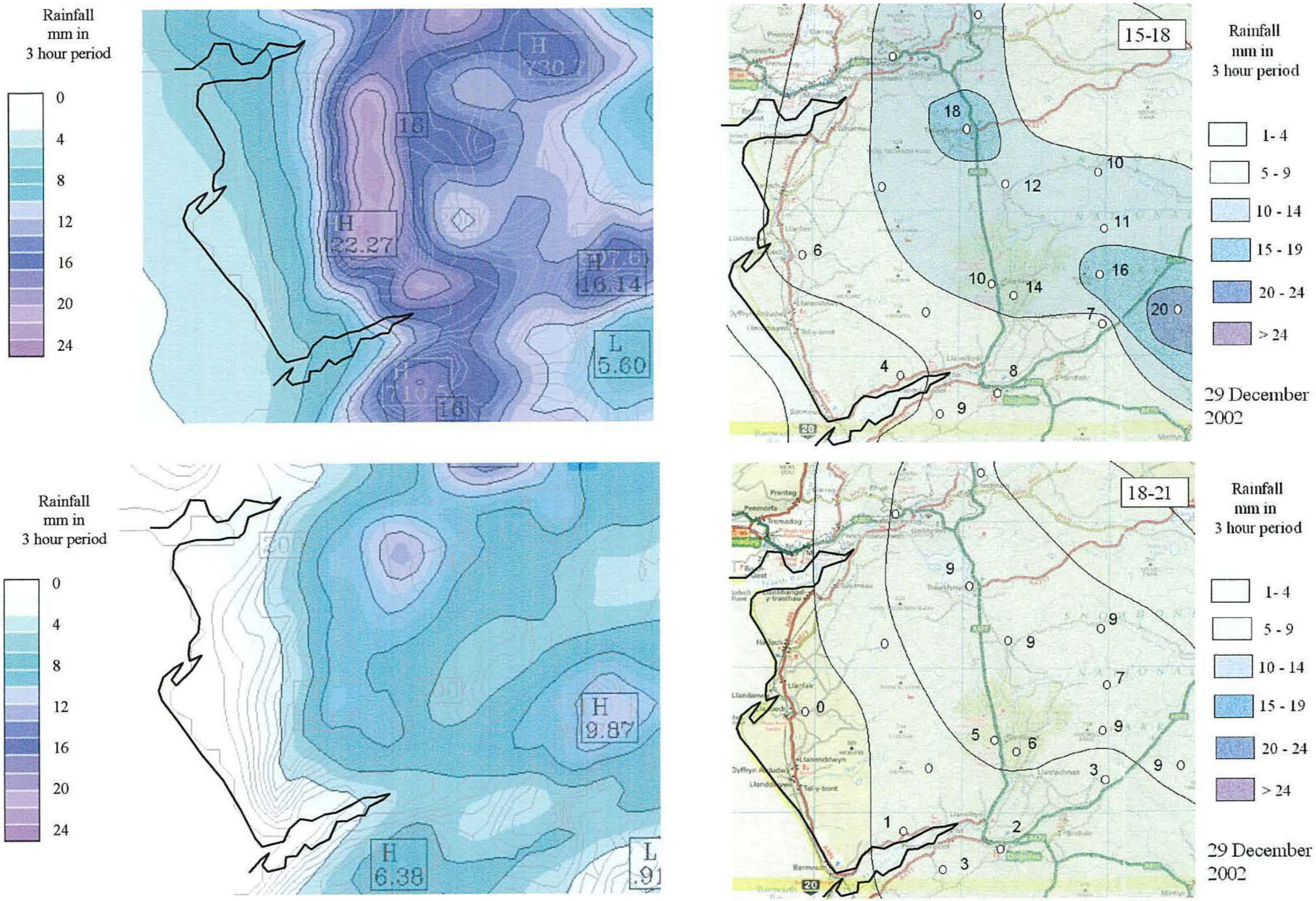

Figure 2.91 (cont.) MM5 3-hour rainfall simulations (left) and 3-hour raingauge totals (right):
Above: 15:00h – 18:00h, 29 December 2002 Below: 18:00h – 21:00h, 29 December 2002

22 May 2003

MM5 3-hour rainfall simulations and 3-hour raingauge totals for 22 May 2003 are shown in fig.2.92.

The 03h-06h simulation identifies the commencement of widespread rainfall. Values of approximately 5mm across much of the Mawddach catchment are a little higher than recorded values of 2-4mm. A zone of higher rainfall intensity over the southern Rhinog mountains is consistent with gauge readings, though a second rainfall high of 7.94mm in the Pared yr Ychain area was not recorded in the field. A rainfall total of 8mm is, however, recorded for Pared yr Ychain during the following 3-hour period which is not reflected in the simulated rainfall pattern. This seems to be an instance of the model rainfall timing being a little earlier than actually occurred.

The 06h-09h simulation correctly positions a type B pattern of high rainfall over the Rhinog mountain range, with a 3-hour maximum of 23.37mm close to the highest gauge reading of 26mm. A southwards extension of the high rainfall zone over Cader Idris cannot be verified due to lack of gauge data.

The 12h-15h simulation shows transition to a type A rainfall pattern, with the zone of high rainfall intensity extending inland across the catchment to the Pared yr Ychain area. 3-hour rainfall values are approximately in agreement with gauge readings: a modelled maximum of 26.38mm in the southern Rhinog range is close to the observed maximum of 30mm, and both the model and field data give maximums around 17mm at Pared yr Ychain. Some minor differences in detail occur around Coed y Brenin in the central area of the catchment.

The 15h-18h simulation indicates a decline in rainfall towards the end of the storm event, though not as rapid a reduction as observed from gauge readings. There again appears to be some discrepancy in timing, in the order of one hour, between the model and actual rainfall.

The MM5 simulation for the 22 May 2003 storm event has been quite successful in identifying the main patterns and intensities of rainfall across the Mawddach catchment.

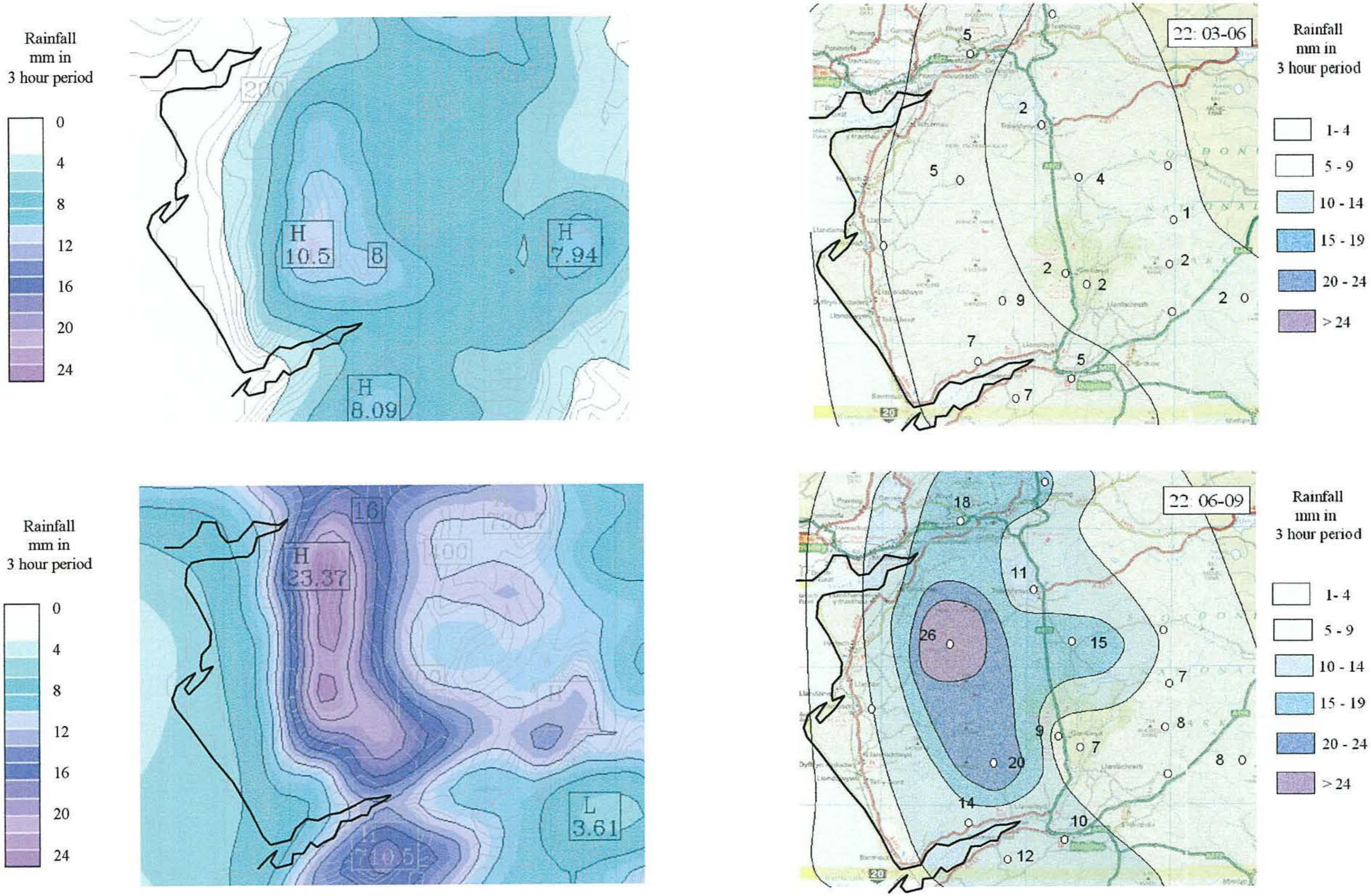

Figure 2.92: MM5 3-hour rainfall simulations (left) and 3-hour raingauge totals (right):
Above: 03:00h – 06:00h, 22 May 2003 Below: 06:00h – 09:00h, 22 May 2003

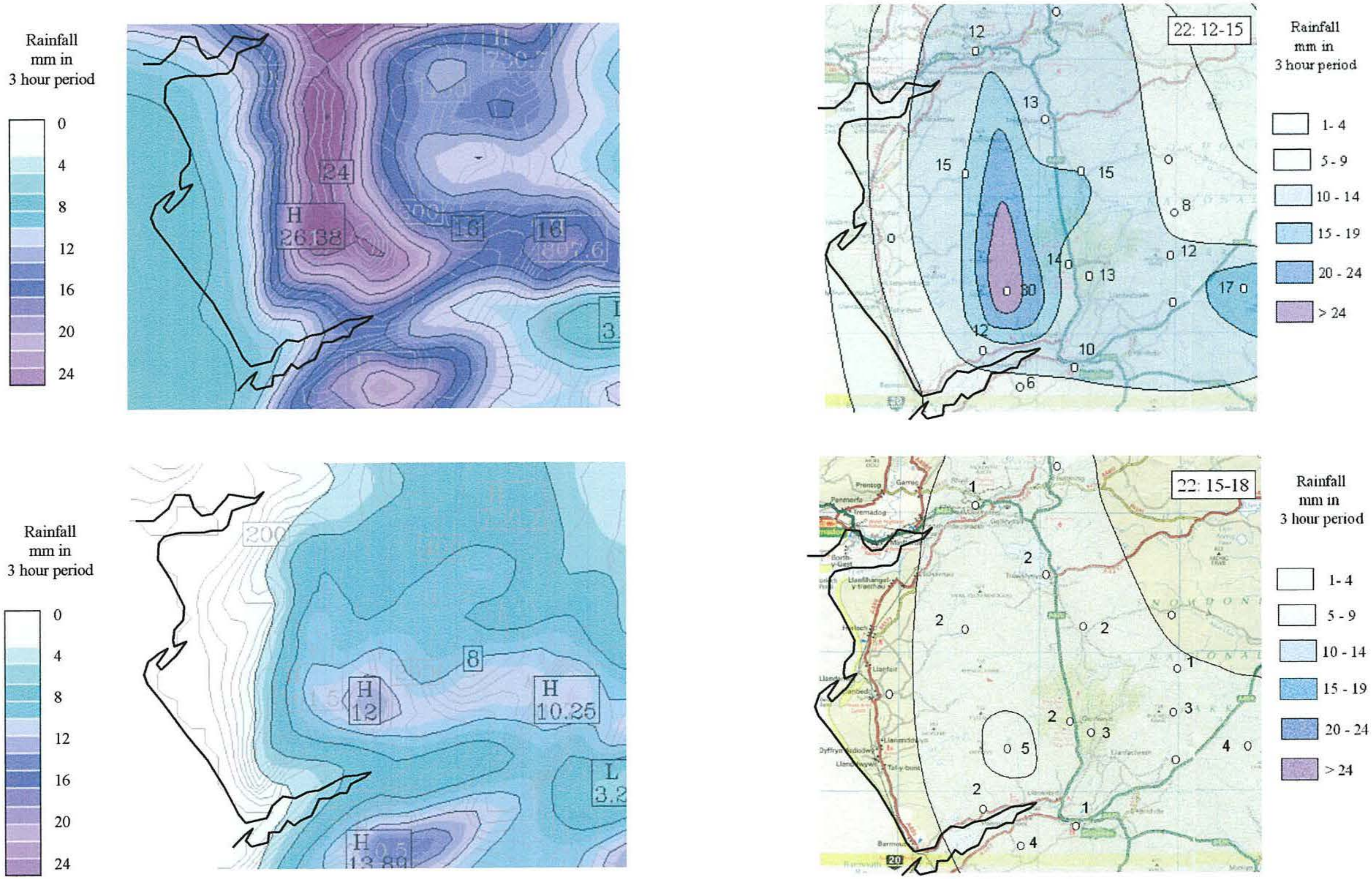

Figure 2.92(cont.) MM5 3-hour rainfall simulations (left) and 3-hour raingauge totals (right):
Above: 12:00h – 15:00h, 22 May 2003 Below: 15:00h – 18:00h, 22 May 2003

2-4 February 2004

The Mawddach catchment was subjected to major flooding during the period 2-4 February 2004. An MM5 rainfall simulation of this event will be used as input for evaluation of the integrated hydrological model in Chapter 4.

The February 2-4 rainfall simulation is illustrated in fig.2.94. For much of the period, conveyors of ascending warm moist air were generating rainfall over the Mawddach catchment. Output from the MM5 model has been examined by plotting three-dimensional images with the post-processor program Vis5D (Hibbard and Kellum, 2005). An example is shown in fig.2.93 which illustrates zones of high cloud mixing ratio (yellow) and high rainfall mixing ratio (blue). This shows well the development of stratiform cloud inland from Cardigan Bay, with downwards enhancement of rainfall over the Mawddach catchment through the seeder-feeder mechanism.

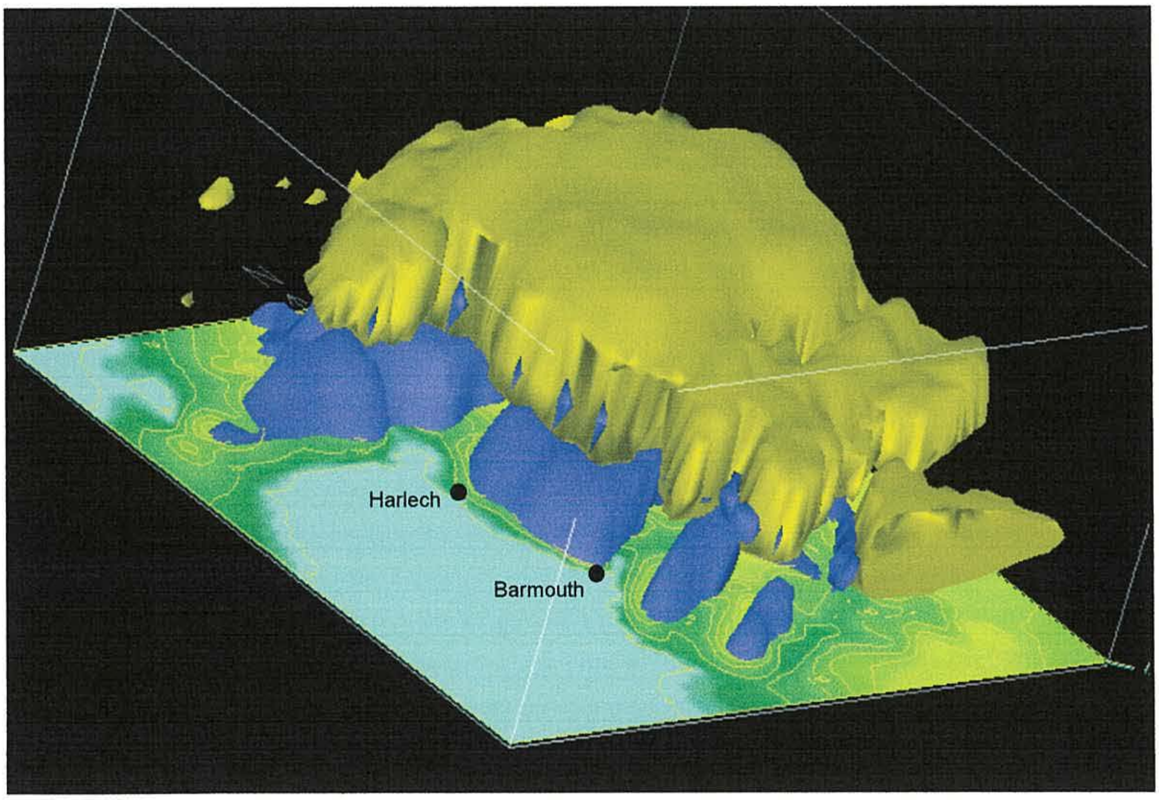

Figure 2.93: Zones of mixing ratios >0.4 for cloud (yellow) and rainfall (blue), 06:00h, 3 February 2004.

The MM5 simulation period 03h-06h on 2 February shows correctly a type A rainfall pattern extending across the catchment. A maximum 3-hour rainfall prediction of 16.81mm is close to the 18mm gauge reading in the southern Rhinog mountains.

Continuation of rainfall in the period 00h-03h on 3 February shows a simulated total of 20.65mm in the Arennig mountains and 19.51mm at Pared yr Ychain. These totals are higher than observations, although the distribution of rainfall across the catchment is similar to the actual rainfall pattern.

Rainfall simulations for the three periods covering 03h to 12h on 3 February are in reasonable agreement with raingauge records. A zone of low rainfall is predicted along the Wnion valley, and can be seen as a thinning of the stratiform cloud in the Vis5D plot of fig.2.93. This low rainfall zone is consistent with the limited raingauge data available for the Wnion valley.

Rainfall continued on 4 February, to reach a maximum intensity during the period 12h-15h which was concentrated inland of the Rhinog mountains as a type A distribution across the Mawddach catchment. This distribution is reasonably represented by the simulation. An axis of low rainfall along the Mawddach estuary and Wnion valley is again predicted, and would be consistent with the limited raingauge readings available.

For the 2-4 February 2006 storm period, the MM5 simulation is in reasonable agreement with raingauge data. The patterns of rainfall across the Mawddach catchment have been plausibly predicted, although some simulated rainfall totals are greater than actual recordings from raingauges.

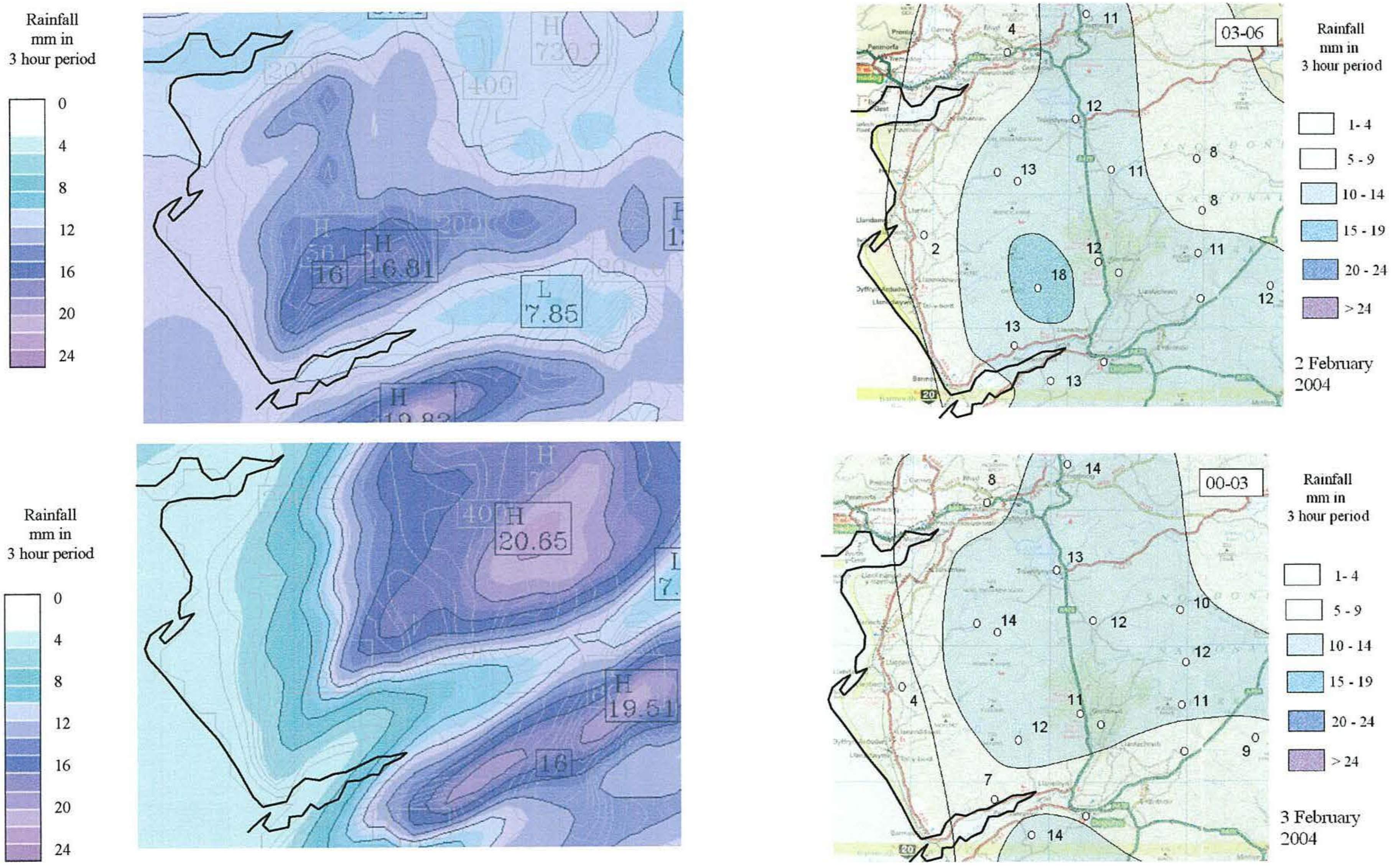

Figure 2.94: MM5 3-hour rainfall simulations (left) and 3-hour raingauge totals (right):
Above: 03:00h – 06:00h, 2 February 2004   Below: 00:00h – 03:00h, 3 February 2004

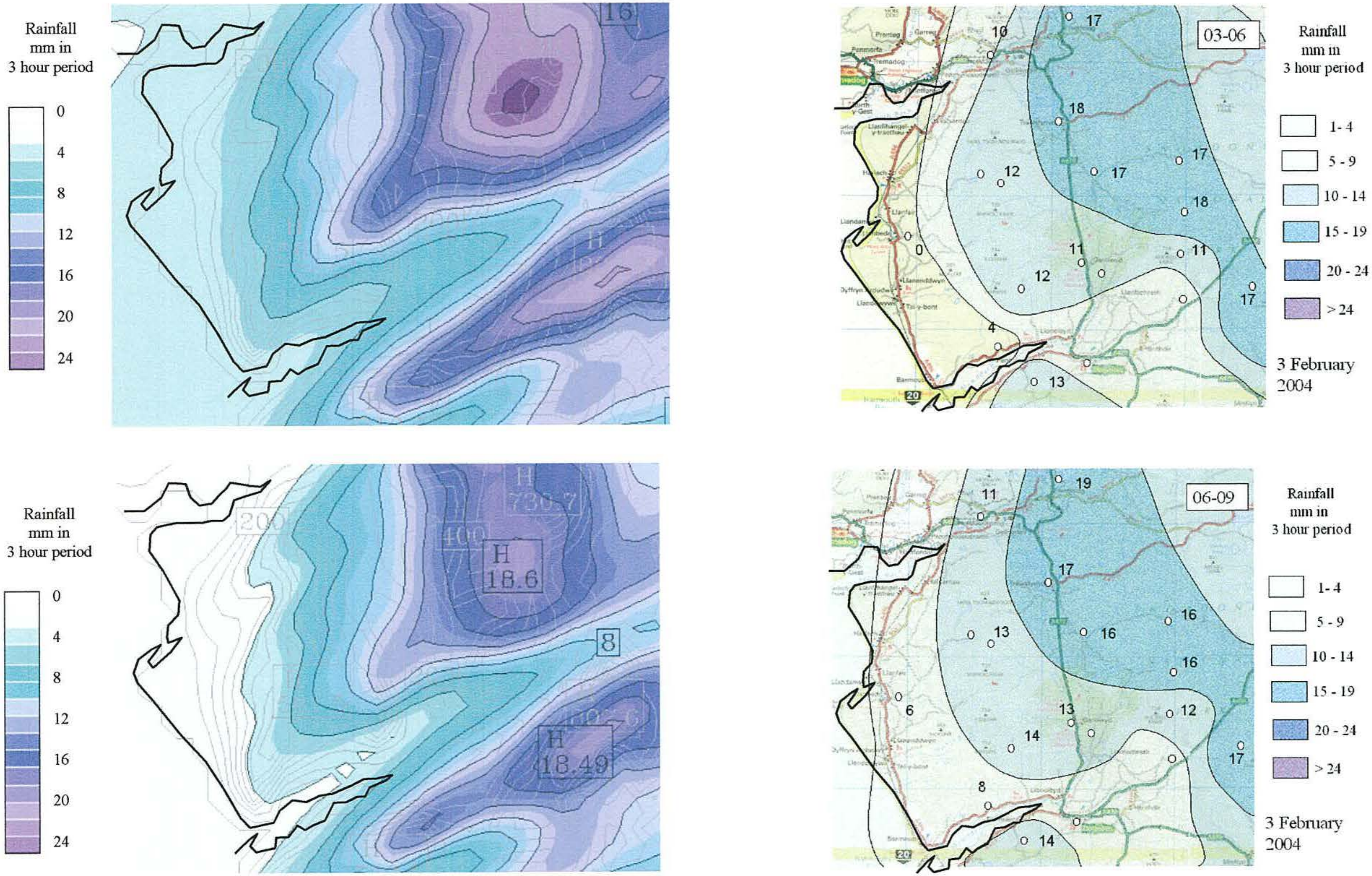

Figure 2.94 (cont.) MM5 3-hour rainfall simulations (left) and 3-hour raingauge totals (right):
Above: 03:00h – 06:00h, 3 February 2004 Below: 06:00h – 09:00h, 3 February 2004

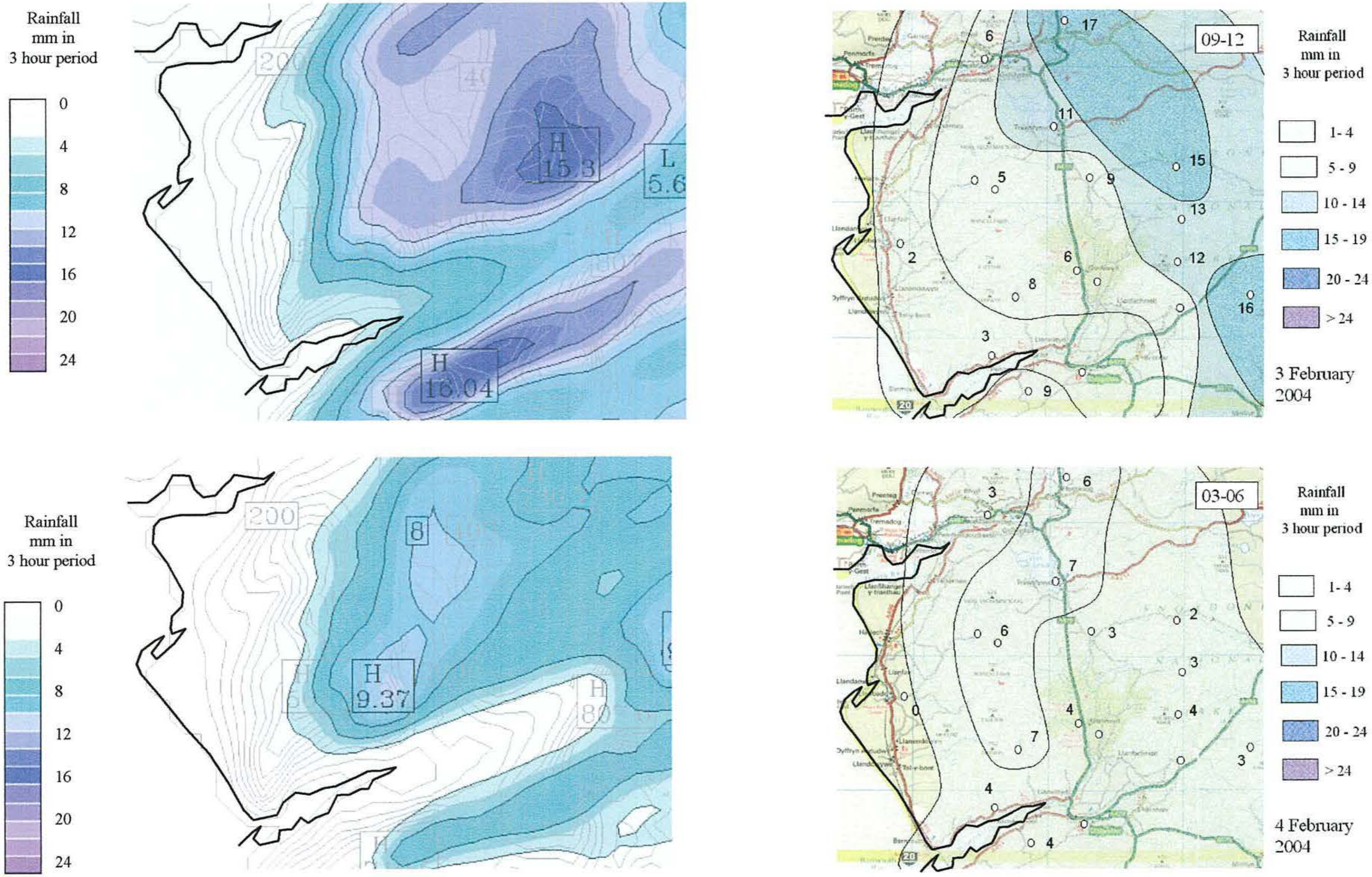

Figure 2.94 (cont.) MM5 3-hour rainfall simulations (left) and 3-hour raingauge totals (right):
Above: 09:00h – 12:00h, 3 February 2004 Below: 03:00h – 06:00h, 4 February 2004

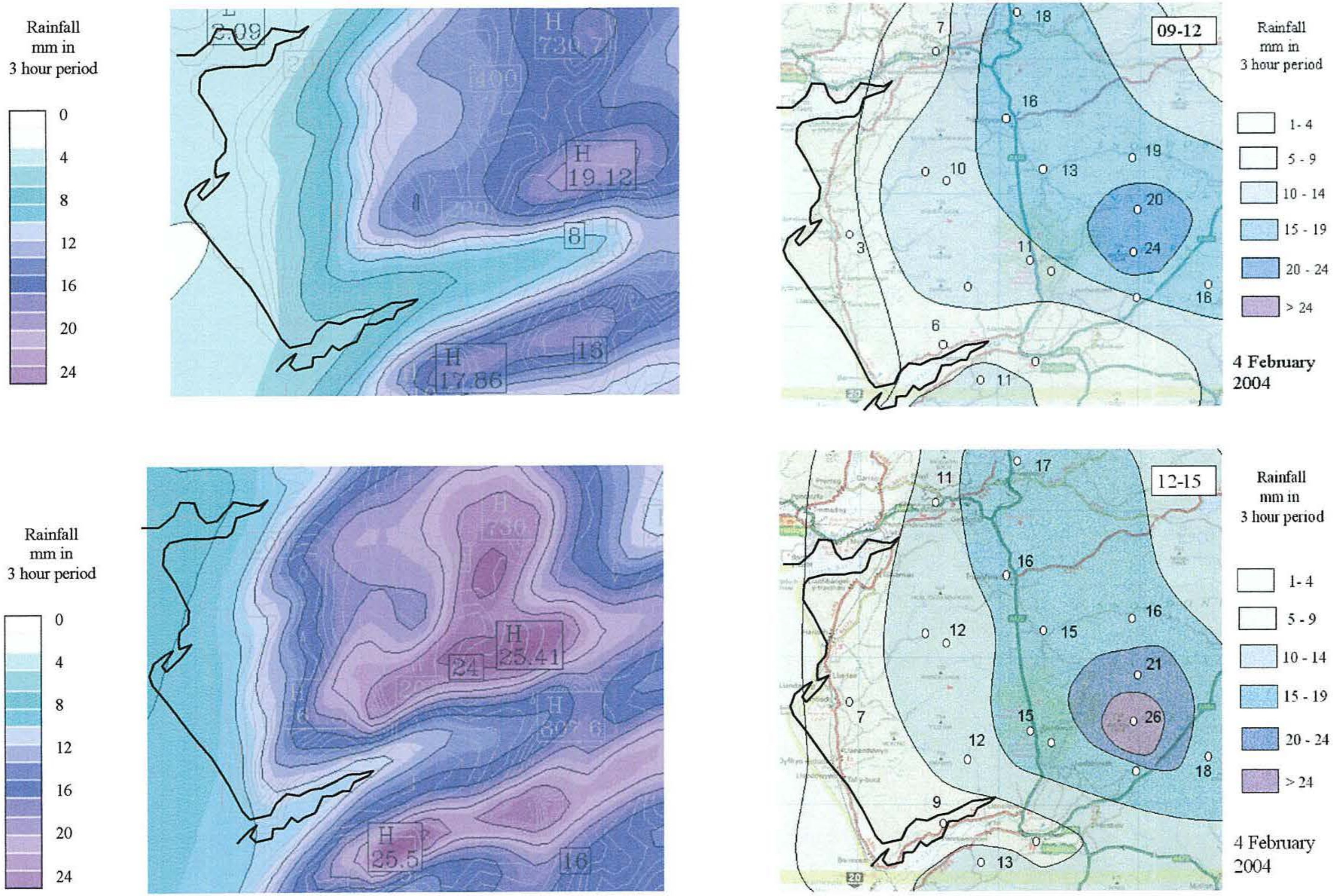

**Figure 2.94 (cont.) MM5 3-hour rainfall simulations (left) and 3-hour raingauge totals (right):
Above: 09:00h – 12:00h, 4 February 2004 Below: 12:00h – 15:00h, 4 February 2004**

Statistical analysis

To obtain a quantitative comparison of simulation results for different storm events, a spreadsheet analysis has been carried out (fig.2.95). For each raingauge site and time period, the actual rainfall total is shown in the left column and the MM5 prediction to the right. Where the raingauge site lies on the boundary of two or more 1km MM5 grid squares, the MM5 value closest to the gauge reading is taken.

> A ***mean absolute difference*** between raingauge readings and MM5 predictions averaged over all sites is calculated. This is an error value determined as a simple unsigned difference between pairs of values with no consideration as to which is larger.
>
> A ***mean signed difference*** is also calculated as an average for all sites. This records differences between individual pairs of values as either positive or negative, allowing an overestimate at one site to offset an underestimate at another site.

These two measures allow a ***% absolute deviation*** and a ***% signed deviation*** to be calculated:

> For a highly heterogeneous catchment where the pattern of rainfall is critical to hydrological response, the prediction error in stormwater flow may be close to the % absolute deviation.
>
> For a homogeneous catchment where only total rainfall and not distribution pattern is critical, the prediction error in stormwater flow may be close to the % signed deviation.

In practice, the error in predicting stormwater volume is likely to lie between the % absolute deviation and the % signed deviation. The predicted storm volumes using the MM5 system are likely to be within 15% of actual flows for the storm events of 29 December 2002 and 2-4 February 2004, and within 25% for the event of 22 May 2003. Lower accuracy of 35% calculated for the event of 8 November 2002 may be due to a more restricted raingauge array operating at that time, which failed to record key aspects of the rainfall pattern for comparison with the simulation results.

		Llanbedr		Cwm Bychan		Caerdeon		Erw Wen		Cwm Mynach		Ganllwyd		Tir Penrhos		Trawsfynydd		Bronaber		Aran Hall		Rhobell Fawr		Allt Lwyd		Blaen Lliw		Pared yr Ychain		Dolgellau		Absolute total difference	Signed total difference	Stations	Mean absolute difference	Mean signed difference	Total recorded rainfall	Mean absolute difference (mm/h)	% absolute deviation	% signed deviation	Rainfall pattern
08-Nov-02	03-06	4	1	5	4	7	5	7	4			5	5	5	3	6	6	6	5			4	4	3	3	4	6	4	6			16	8	12	1.3	0.7	60				
	06-09	10	4	13	9	11	9	9	6			12	9	11	9	12	8	12	5			7	7	5	5	8	7	7	8			33	31	12	2.8	2.6	117				
	09-12	12	4	18	8	17	9	18	13			21	14	23	13	18	11	22	17			17	9	13	9	13	10	14	7			82	82	12	6.8	6.8	206				
	12-15	10	9	20	14	11	11	16	12			18	12	20	11	11	9	19	9			28	12	18	9	14	7	21	12			79	79	12	6.6	6.6	206				
																																						1.5	35.7	34.0	A1
29-Dec-02	06-09	4	4	5	6			7	6			9	7	7	7	8	5	8	6	8	5	7	4	8	5	6	6	11	7	8	8	22	20	13	1.7	1.5	96				
	09-12	12	8	15	16			20	16			18	14	16	14	19	14	17	14	12	13	16	13	14	13	15	13	18	16	13	18	37	23	13	2.8	1.8	205				
	15-18	6	4			4	7	9	10			10	12	14	12	18	16	12	14	7	12	16	14	11	11	10	10	20	14	8	14	33	-5	13	2.5	0.4	145				
	18-21	0	0			1	2	3	3			5	4	6	4	9	10	9	7	3	6	9	6	7	6	9	6	9	10	2	3	19	5	13	1.5	0.4	72				
																																						0.7	21.4	8.3	A2
22-May-03	03-06			5	5	7	4	7	4	9	10	2	6	2	6	2	5	4	5			2	4	1	4			2	7	5	5	29	-17	12	2.4	-1.4	48				
	06-09			26	22	14	10	12	14	20	19	9	13	7	13	11	13	15	10			8	12	7	10			8	10	10	10	37	-9	12	3.1	-0.8	147				
	12-15			15	20	12	12	6	16	30	26	14	18	13	18	13	17	15	13			12	14	8	14			17	16	10	12	45	-31	12	3.8	-2.6	165				
	15-18			2	2	2	2	4	4	5	6	2	7	3	7	2	3	2	5			3	6	1	5			4	6	1	4	26	-26	12	2.2	-2.2	31				
																																						1.0	35.0	21.2	B
02-Feb-04	03-06	2	7	13	12	13	11	13	11	18	17	12	13			12	11	11	10			11	12	8	10	8	9	12	10			20	0	12	1.7	0.0	133				
03-Feb-04	00-03	4	3	14	8	7	3	14	12	12	10	11	12			13	15	12	17			11	9	12	14	10	19	9	16			43	-9	12	3.6	-0.8	129				
	03-06	0	3	12	6	4	3	13	8	12	8	11	8			18	11	17	18			11	8	18	16	17	21	17	19			41	21	12	3.4	1.8	150				
	06-09	6	1	13	4	8	4	14	8	14	6	13	8			17	10	16	14			12	14	16	14	16	16	17	16			51	47	12	4.3	3.9	162				
	09-12	2	1	5	3	3	2	9	6	8	7	6	10			11	12	9	11			12	9	13	14	15	14	16	12			24	8	12	2.0	0.7	109				
04-Feb-04	03-06	0	0	6	2	4	1	4	1	7	8	4	7			7	6	3	8			4	4	3	5	2	6	3	5			28	-6	12	2.3	-0.5	47				
	09-12	3	3	10	5	6	3	11	6	10	11	11	13			16	12	13	12			24	18	20	18	19	15	16	12			37	31	12	3.1	2.6	159				
	12-15	7	9	12	15	9	10	13	14	12	16	15	20			16	19	15	18			26	22	21	22	16	18	18	16			31	-19	12	2.6	-1.6	180				A1/
																																						1.0	25.7	6.8	A2

Figure 2.95: Analysis of errors in rainfall prediction using the MM5 model.

Comparison of MM5 model predictions with observed storm rainfall was carried out by the Spearman rank test using the method of Chalmers and Parker (1986). This test compares the distributions of readings in the two data sets when sorted into order of size. A high correlation coefficient value close to 1 would indicate that MM5 had very closely predicted the spatial pattern of the rainfall distribution, although the test does not indicate whether the actual rainfall intensity was correctly predicted. A coefficient value of 0 would indicate that MM5 had predicted a distribution pattern with no apparent similarity to the true distribution. A negative correlation coefficient would suggest that MM5 had predicted high rainfall in areas where the rainfall was actually low, and *vice-versa*.

Scatter graphs and Spearman correlation coefficient values for the four example storms are given in figs 2.96-2.100.

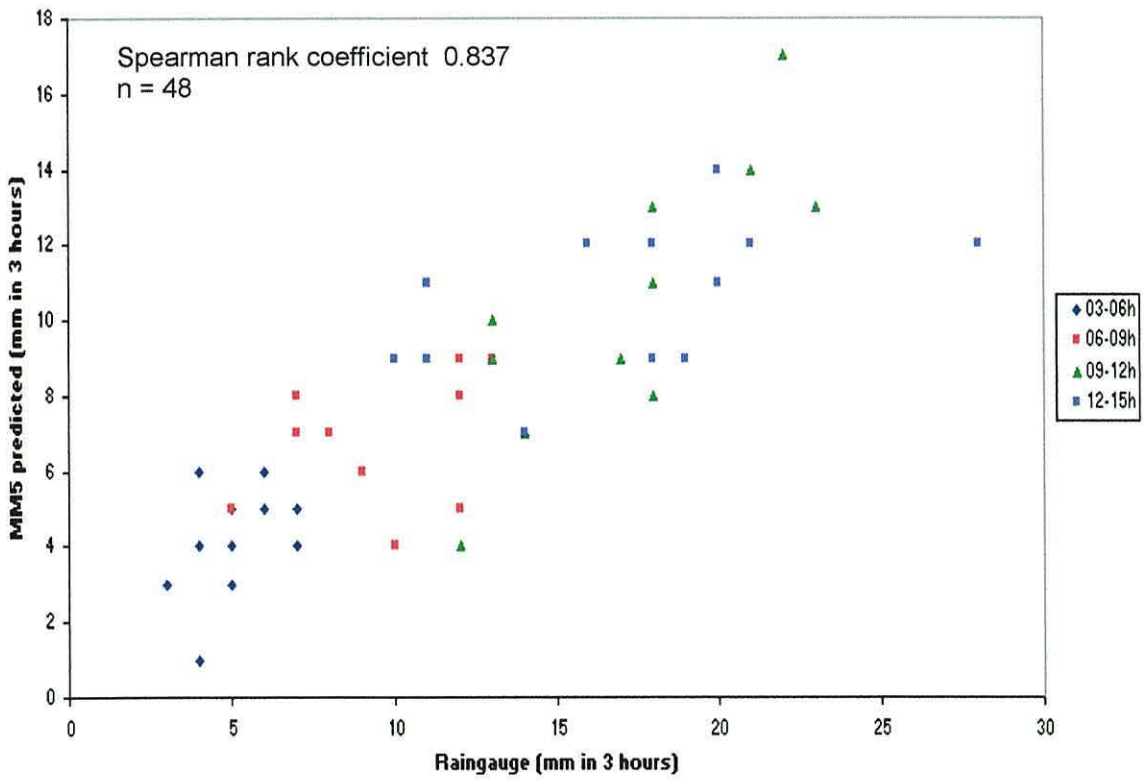

Figure 2.96: Storm event of 8 November 2002. Determination of Spearman rank correlation coefficient for MM5 rainfall forecast and observed rainfall

The highest correlation of 0.99 is obtained for the Type B storm event of 22 May 2003. High correlations above 0.8 are obtained for the Type A storms of 8 November and 29 December 2002.

The storm sequence of 3-4 February 2004 has been analysed as two rainfall events. A low correlation of 0.65 was obtained for rainfall on 3 February, with a higher correlation of 0.87 for 4 February. During the storm sequence the rainfall across the catchment changed from an initial Type A pattern, towards a more dominantly Type B pattern.

The results of the Spearman rank test need to be considered alongside the analysis of percentage deviation of rainfall totals (fig.2.95). Some tentative conclusions can be drawn.

The different degree of correlation for Type A and Type B rainfall events is a further indicator that these patterns are produced by physically different mechanisms of rainfall generation, modelled with different degrees of success by MM5.

MM5 is best able to predict Type B rainfall patterns, generated by a simple orographic mechanism. Type A patterns involve a more complex interaction between rising valley air flows and middle level saturated air.

Despite the very accurate prediction of spatial pattern for the 22 May Type B rainfall event, reference to fig.2.95 indicates that the total rainfall was underestimated by some 25%. Pattern correlation was poorer for the Type A rainfall events of 29 December 2002 and 3-4 February 2004, but total rainfall was estimated more accurately to around 15% in these cases.

The overall conclusions from analysis of the example storm events is that MM5 can adequately predict rainfall for frontal storm events over the Mawddach catchment. Where inaccuracies exist, they may be in spatial pattern or in total rainfall. The inaccuracies seem to be linked to limitations in the modelling of rainfall processes, particularly the production of orographic rainfall and rainfall enhancement by the seeder-feeder mechanism above deep valleys. These would be useful topics for further research and improvement of the MM5 program code.

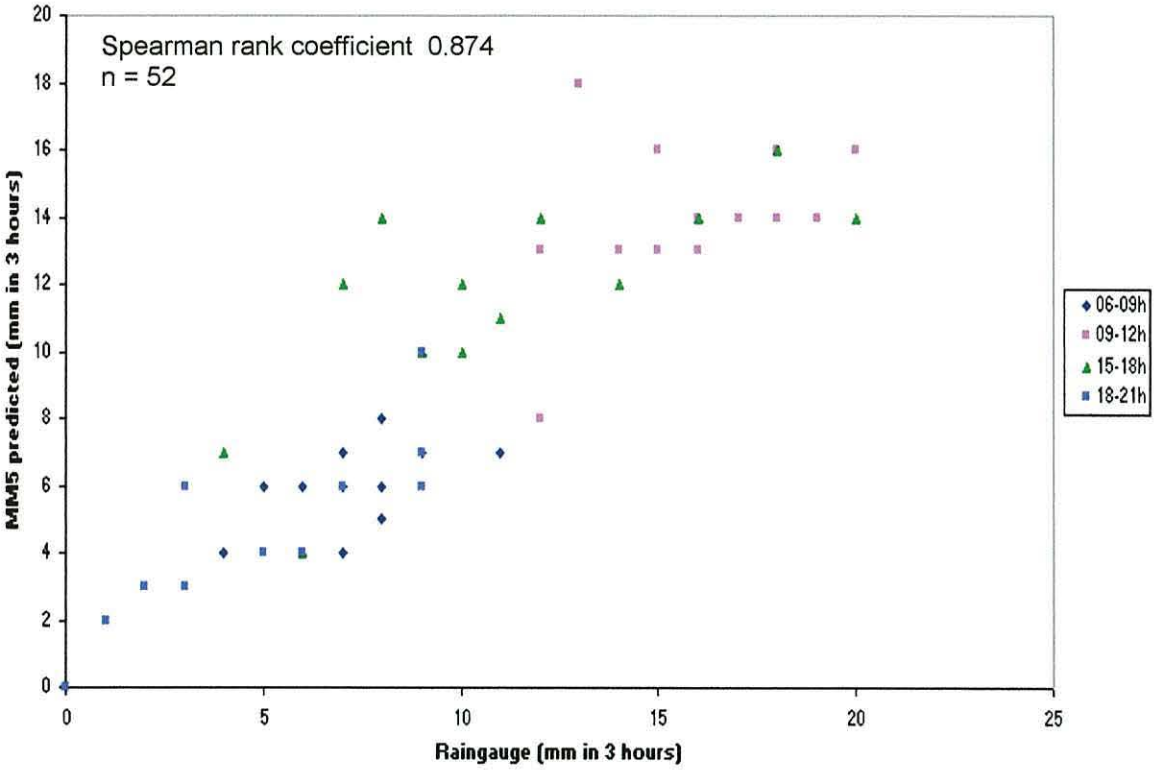

Figure 2.97: Storm event of 29 December 2002. Determination of Spearman rank correlation coefficient for MM5 rainfall forecast and observed rainfall

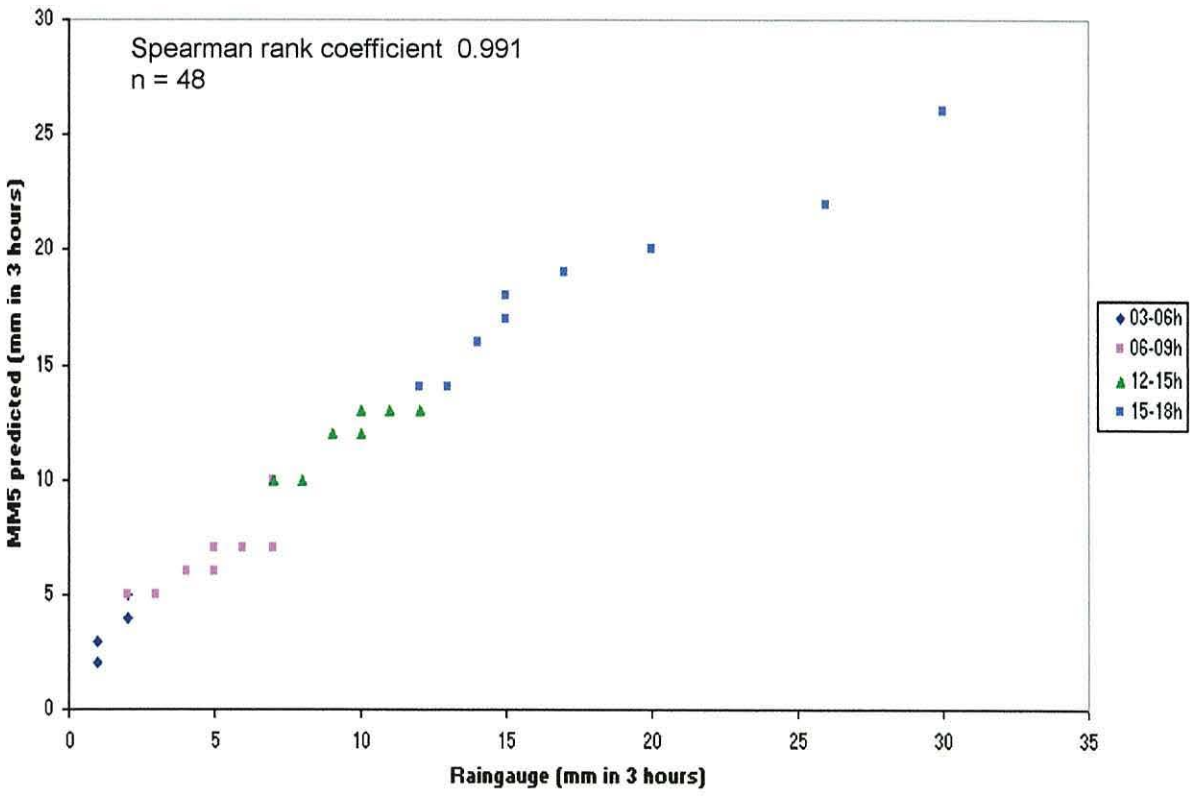

Figure 2.98: Storm event of 22 May 2003. Determination of Spearman rank correlation coefficient for MM5 rainfall forecast and observed rainfall

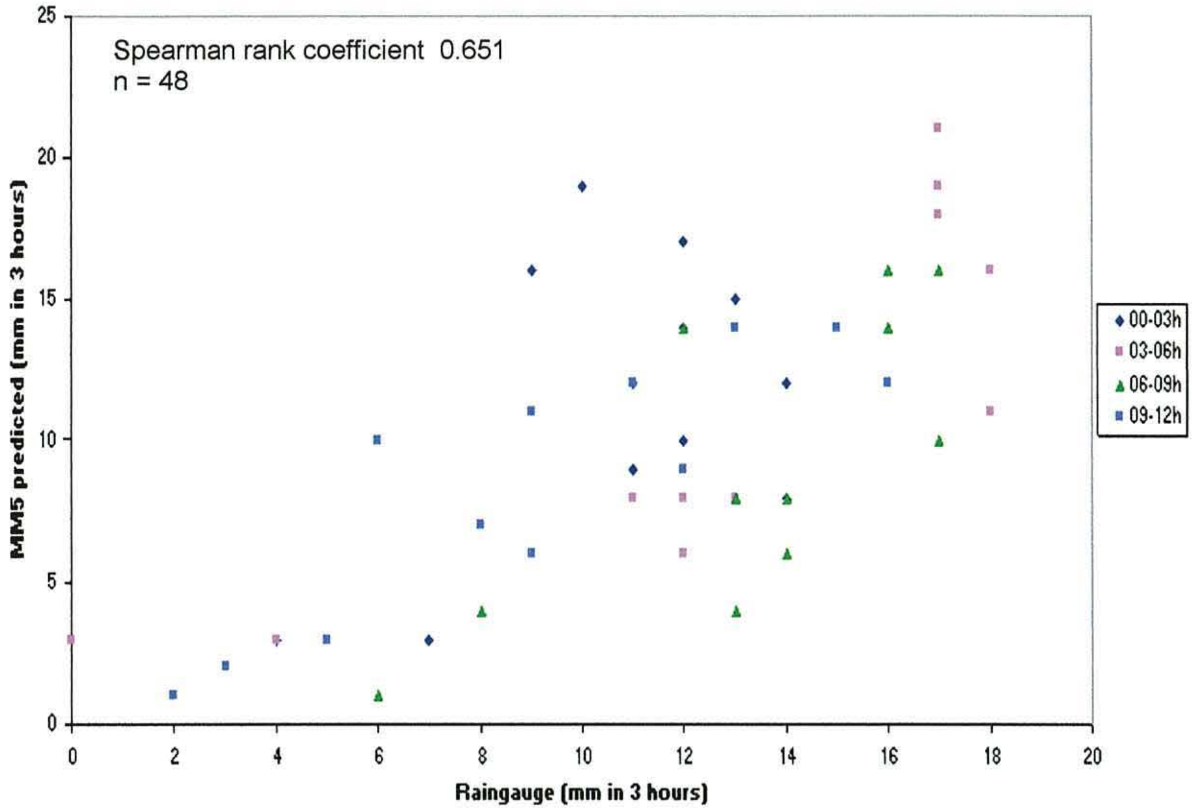

Figure 2.99: Storm event of 3 February 2004. Determination of Spearman rank correlation coefficient for MM5 rainfall forecast and observed rainfall

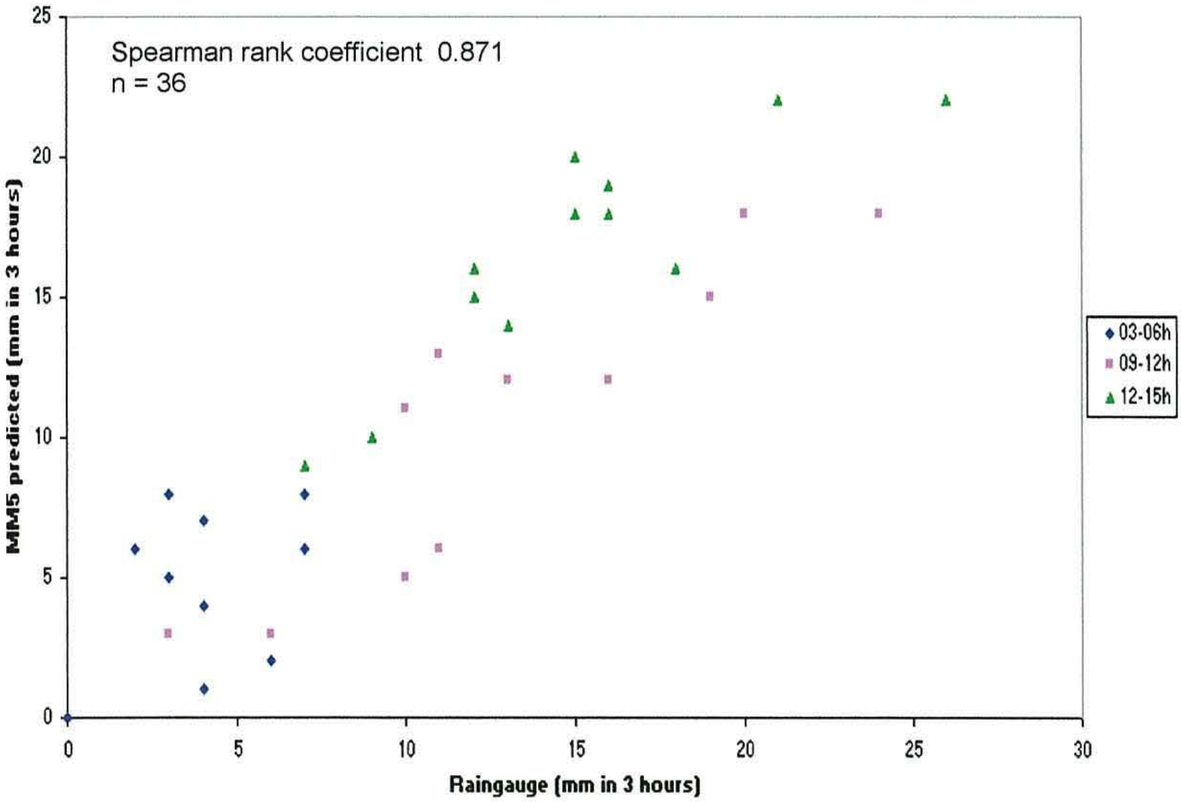

Figure 2.100: Storm event of 4 February 2004. Determination of Spearman rank correlation coefficient for MM5 rainfall forecast and observed rainfall

Rainfall radar

This chapter has examined the feasibility of computer modelling to provide rainfall input to a hydrological model. An alternative approach uses radar for rainfall estimation. The relative merits of the two methods should now be considered.

The tracking of storms by rainfall radar for is well developed in the USA, particularly in the mid-west and south-west where tornadoes and supercell thunderstorms are common (National Weather Service, 2005), and offshore in the Gulf of Mexico when hurricanes approach the coast. Cranston (2003) has examined the use of weather radar for flood forecasting in Scotland. Three weather radar installations cover the land area of Scotland and are producing promising results, but data suitable for use in operational flood warning systems is not yet being generated.

An essential difference exists between numerical weather modelling and rainfall radar observations. Modelling can provide a prediction of rainfall at a *future* point in time whilst radar patterns provide an estimate of rainfall rates at the *present* time. It is possible to make a forward extrapolation of rainfall radar patterns to predict rainfall at a future time, but this is dependant on knowledge of the manner in which weather systems move spatially and evolve chronologically within the forecasting region. As an example for discussion, a sequence of radar images at six-hourly intervals for 3 February 2004 are shown in fig.2.101, along with 3-hour MM5 rainfall predictions for corresponding times.

It is difficult to exactly compare the MM5 and rainfall radar images. MM5 integrates rainfall over a set time interval, in this case 3 hours, whilst the radar gives an estimate of rainfall rate at a particular instant. Some general observations can, however, be made.

Rainfall radar has a coarser resolution than the MM5 model. Radar uses an output grid of 5km or 10km squares, within which an average rainfall value is given. MM5 modelling may have an operational forecasting resolution down to 1km grid squares.

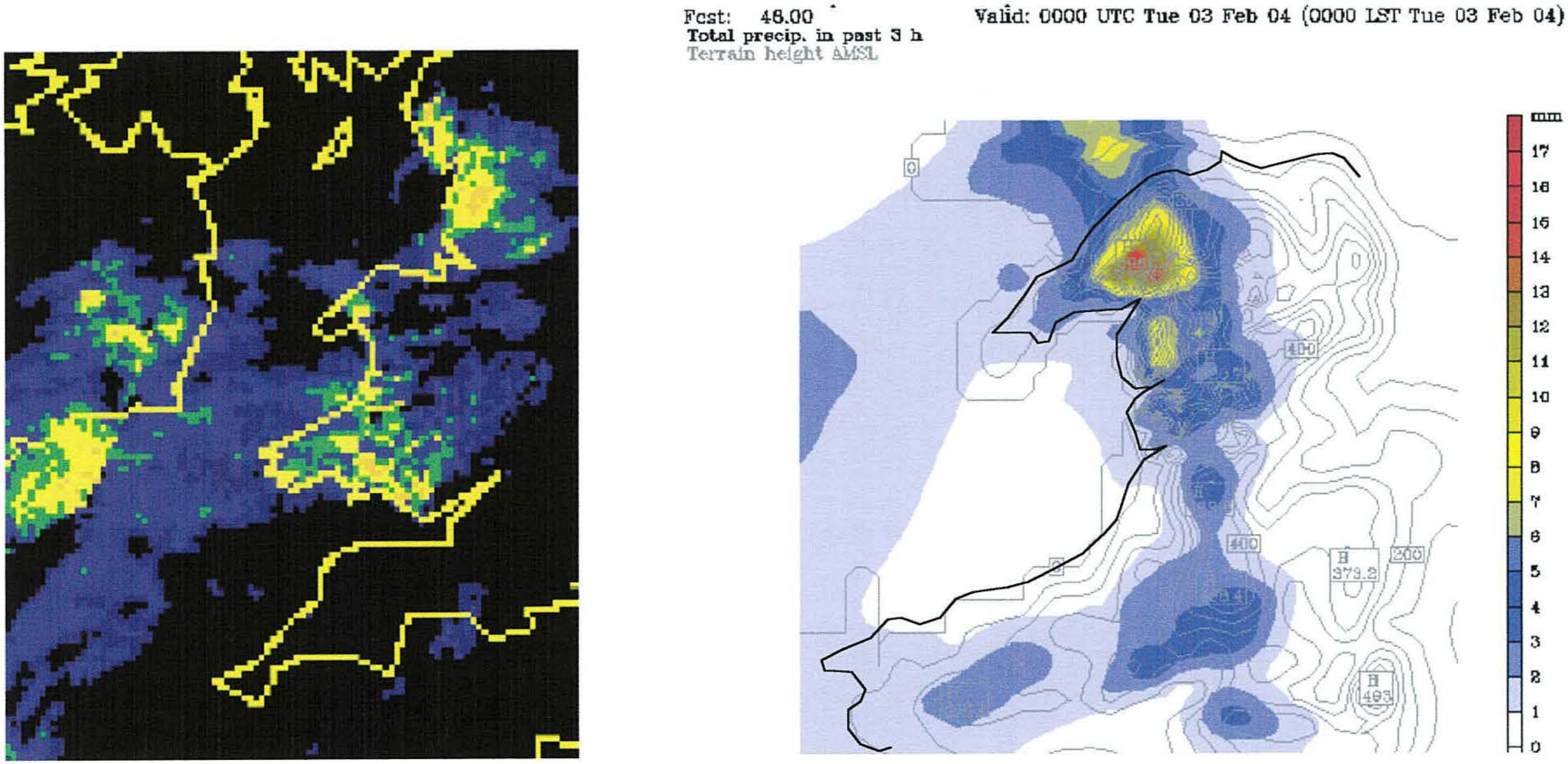

Figure 2-101: (left) Rainfall radar image for 00:00h 3 February 2004. Colour key (mm h^{-1}): blue<1 , green 1-2, yellow 2-4, orange 4-8, red >8.
(right) MM5 simulation for the 3-hour period 21:00h, 2 February to 00:00h, 3 February 2004.

Rainfall radar images must be calibrated for rainfall rate using raingauge data from rainfall events of known intensity. If calibration is based on lowland sites, inaccuracies may occur for mountain regions where rainfall generation mechanisms are more complex. Sibley (2005) discusses the accuracy of rainfall radar data for North Wales and comments that underestimation is common. He considers this to be due to the radar beam being angled upwards to clear the mountains, thereby missing lower layers of feeder cloud where much of the rainfall generation occurs. Underestimation may commonly exceed 50% for North Wales.

Flood forecasting based on current rainfall rates is limited to providing warnings of flood events a couple of hours in advance. For longer warning periods, advance predictions of storm rainfall will be needed. It is apparent that there would be difficulty in predicting the rainfall pattern of 6:00h on 3 February 2004 (fig.2.101), given only the information in the rainfall radar image of 0:00h on that day. Simple spatial translation of the rainfall pattern along a movement vector is insufficient.

Rainfall radar can play a valuable role in determining rainfall patterns as an alternative to telemetered rain gauge arrays, and will become more accurate with the development of the technology and improvement in coverage. There is a clear problem, however, in advance forecasting by means of rainfall radar images. This is particularly significant for mountain areas where weather systems can evolve rapidly and rainfall generation processes are complex.

Numerical weather forecasting is invaluable where advance warning of flooding is required on a timescale which exceeds the fast flow routing time of rain which has already fallen within the catchment . In the current state of the art, numerical weather forecasting is considered the most accurate method of generating rainfall input for the Mawddach hydrological model.

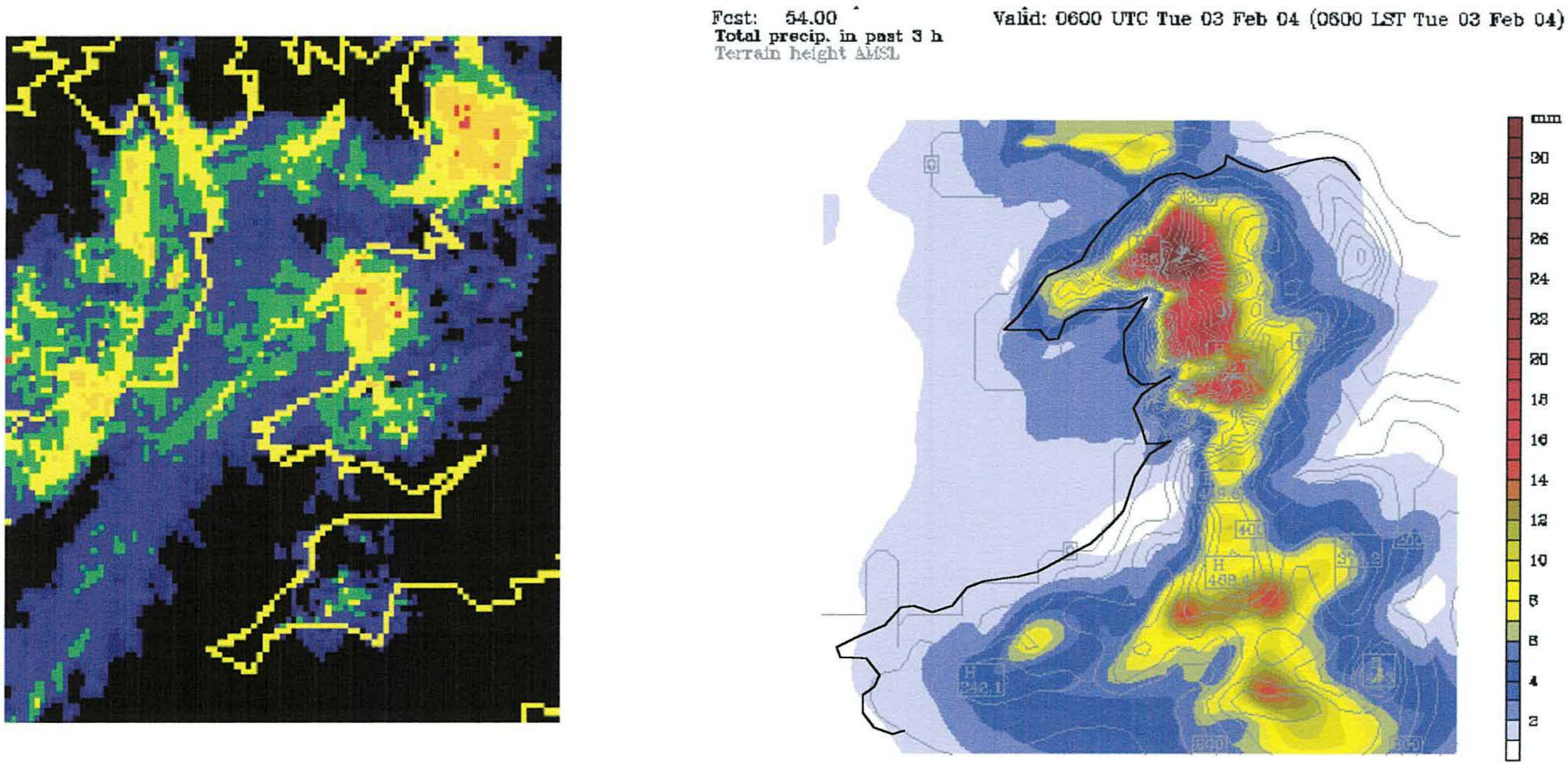

Figure 2.101 (cont.) (left) Rainfall radar image for 06:00h 3 February 2004. Colour key (mm h^{-1}): blue<1 , green 1-2, yellow 2-4, orange 4-8, red >8.
(right) MM5 simulation for the 3-hour period 03:00h - 06:00h, 3 February 2004.

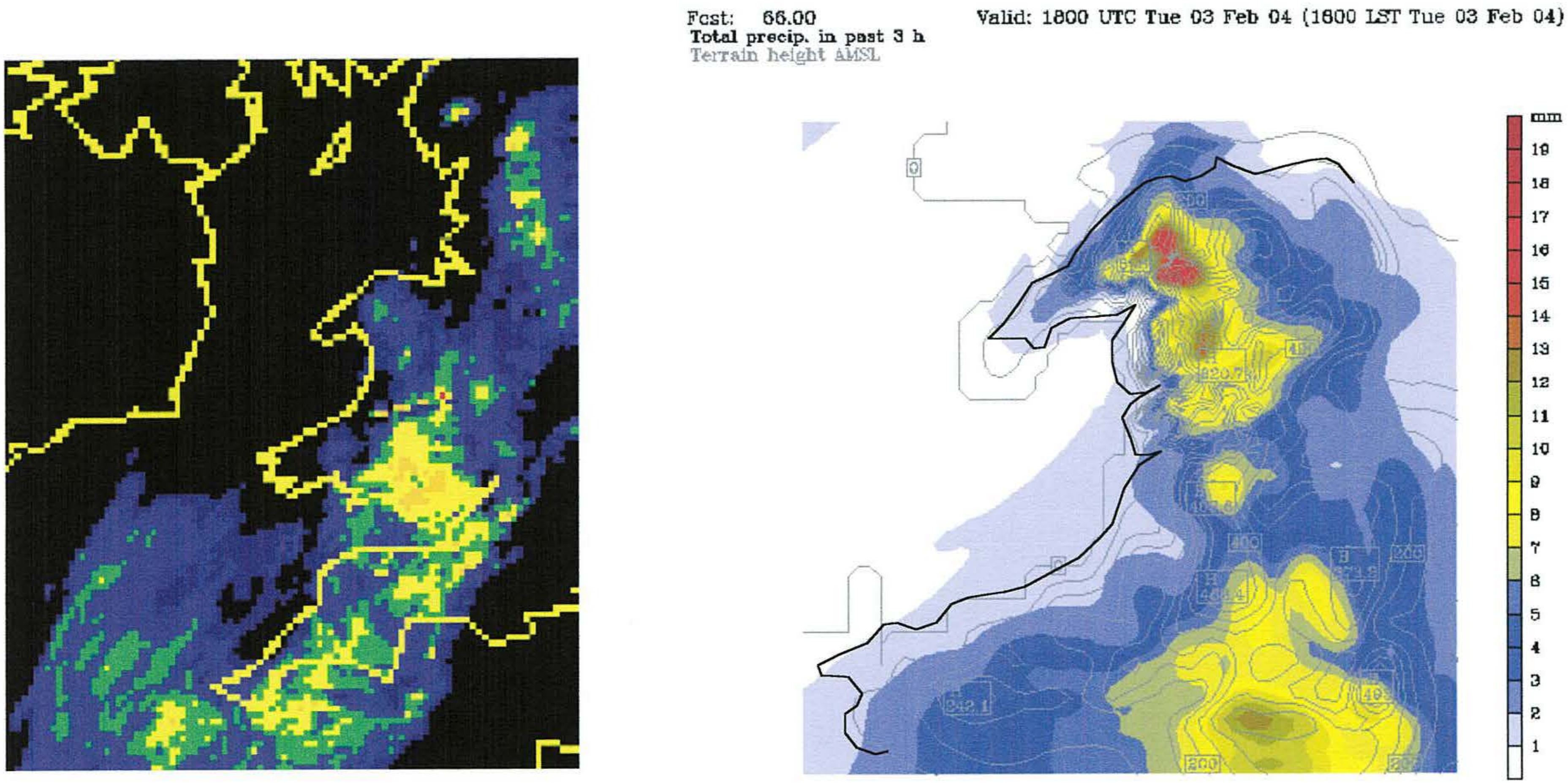

Figure 2.101 (cont.) (left) Rainfall radar image for 18:00h 3 February 2004. Colour key (mm h^{-1}): blue<1 , green 1-2, yellow 2-4, orange 4-8, red >8.
(right) MM5 simulation for the 3-hour period 15:00h - 18:00h, 3 February 2004.

Optimisation of MM5 models using a Neural Network

It was shown that inaccuracies may exist in rainfall predictions by the MM5 model, both in terms of the location and intensity of rainfall:

$$r_{ij} = R_{ij} + e_{ij}$$

where r is true rainfall, R is rainfall predicted by the model, and e is the error in prediction, for location i, j within the catchment. It is possible that e_{ij} is not randomly distributed, but is some systematic function of position and/or rainfall intensity resulting from imperfect modelling of meteorological processes:

$$e_{ij} = f(i, j, R)$$

If an error function f could be determined by comparison of predicted and actual rainfall, it would then be possible to apply this function to subsequent predictions in order to improve their accuracy.

Experiments have been carried out to determine whether MM5 rainfall predictions can be improved by application of an error function during post-processing with a neural network. For this work, the Neural Network Toolbox within the MATLAB mathematical software package has been used (Demuth and Beale, 2000).

The principle of a neural network is to apply mathematical transformations to input data in order to produce output which is, by some measure, a more accurate result. A variety of mathematical transformations are possible. After experimentation, it was found that best results for the MM5 problem are achieved by a combination of a pure linear function and a log-sigmoidal function:

The Pure Linear transfer function simply takes an input value and multiplies it by a weighting factor W:

purelin(n) = W * n

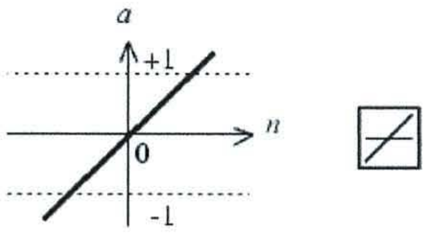

$a = purelin(n)$

Linear Transfer Function

A Log-Sigmoidal transfer function takes any value in the range from negative infinity to positive infinity and maps it to a value in the range 0-1. This is done by applying the formula:

logsig(n) = 1 / (1 + exp(-n))

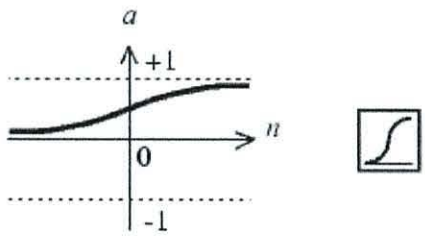

$a = logsig(n)$

Log-Sigmoid Transfer Function

The neural network set up for processing MM5 data is shown in fig.2.102. This consists of twelve processing channels termed *neurones* which are interconnected at several stages. The network accepts 12 input values, and each neuron will produce a revised output value which should be closer to the true solution for the problem:

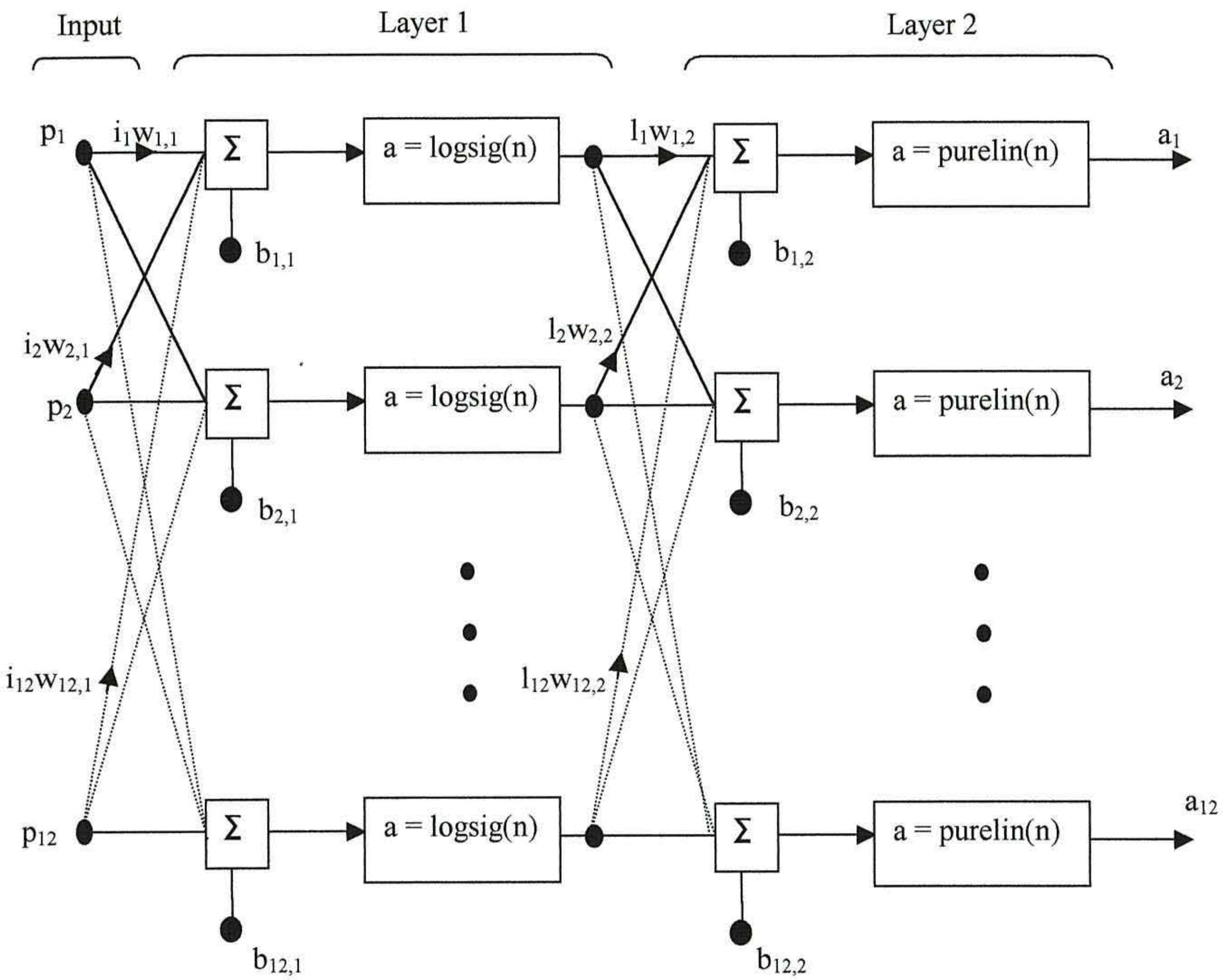

Figure 2.102: Diagrammatic representation of the neural network selected for post-processing of MM5 rainfall simulation data

Inputs to the system are MM5 rainfall forecasts for 12 raingauge sites, and it is hoped the neural network will generate a set of revised forecasts which will be closer to the actual rainfall totals recorded at the 12 sites.

The input values are subject to a sequence of mathematical operations:

- Each of the rainfall forecast values p_1 to p_{12} is multiplied by a weighting value $w_{1,1}$ to $w_{12,1}$ to provide an input to the first layer of the neural network. A multiple of every input value is supplied to each of the 12 neurones.
- Before the first transformation function is applied, a constant $b_{1,1}$ to $b_{12,1}$ is added to the inputs of the 12 neurones.
- The log-sigmoidal transformation is applied to each input n to provide an output a:

$$a = \frac{1}{1 + \exp(-n)}$$

- Each output is again multiplied by a weighting factor, and multiples of this value are transferred to each of the 12 neurones. A further constant $b_{1,2}$ to $b_{12,2}$ is added to the inputs.
- The pure linear transformation is finally applied using weights $w_{1,2}$ to $w_{12,2}$ as multipliers:

$$a = w.n$$

This algorithm provides opportunity to adjust a large number of parameters – multipliers and additive variables – in order to generate outputs which exactly match the true rainfall recordings. We then make an assumption that applying the same parameters to transform subsequent MM5 output values will generate improved predictions.

The purpose of the neural network software package is to provide automated learning for parameter optimisation. Sets of MM5 predictions and the subsequently recorded raingauge totals are supplied to the program in training mode. Progressive adjustment of parameters is carried out until an acceptable fit is achieved. Future MM5 output can then be processed by the neural network to hopefully enhance its accuracy.

Using the Neural Network software package

The first stage in running a neural network is to set up the configuration of neurones and transfer functions required (fig.2.103). The number of neurones is determined by the number of input data values to be processed. The number of layers within a neuron is determined by the complexity of the mathematical relationship which exists between the input estimates and the true values. A two layer neuron structure incorporating a linear and sinusoidal transfer function can exactly represent any non-linear continuous mapping between the predictions and true values.

The neural network structure is displayed diagrammatically by the software, using symbols to represent the chosen transfer functions at each neuron level.

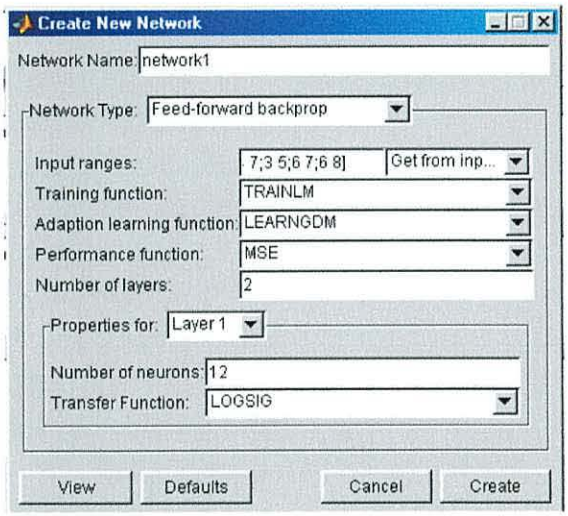

Figure 2.103: Configuration of the neural network. (Left) Specification of the numbers of neurones, number of layers for each neuron, and the transfer functions to be used. (Below) Diagrammatic representation of the neural network.

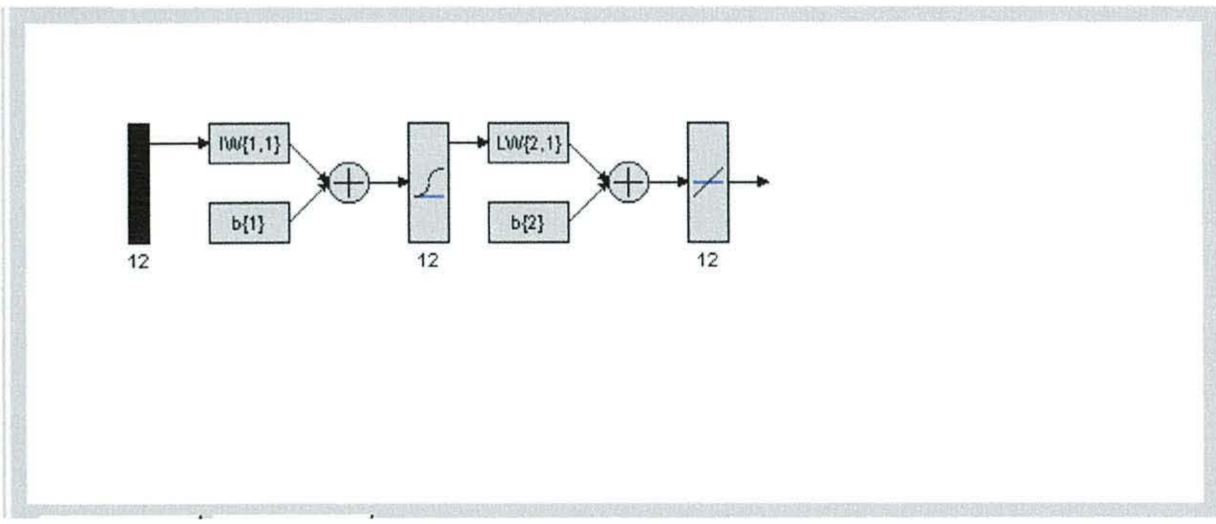

The next step is to train the neural network to correctly transform sets of MM5 forecast data to give outputs exactly matching the known field data from raingauges. Data sets for a number of time intervals may be input together to form a sequence at each gauge site (fig.2.104). The parameter optimisation procedure is run iteratively until a fit is achieved to the required degree of accuracy (fig.2.105).

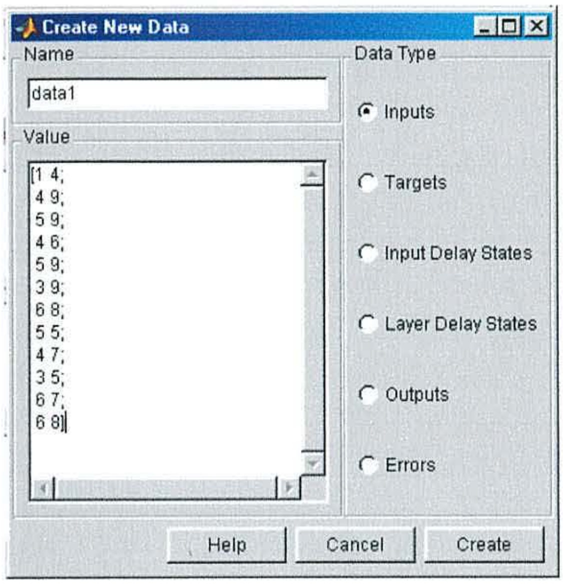

Figure 2.104: Entry of MM5 predicted rainfall values ('Inputs') and actual raingauge readings ('Targets'). This screen shows the input of predicted values for 12 raingauge sites at two time intervals.

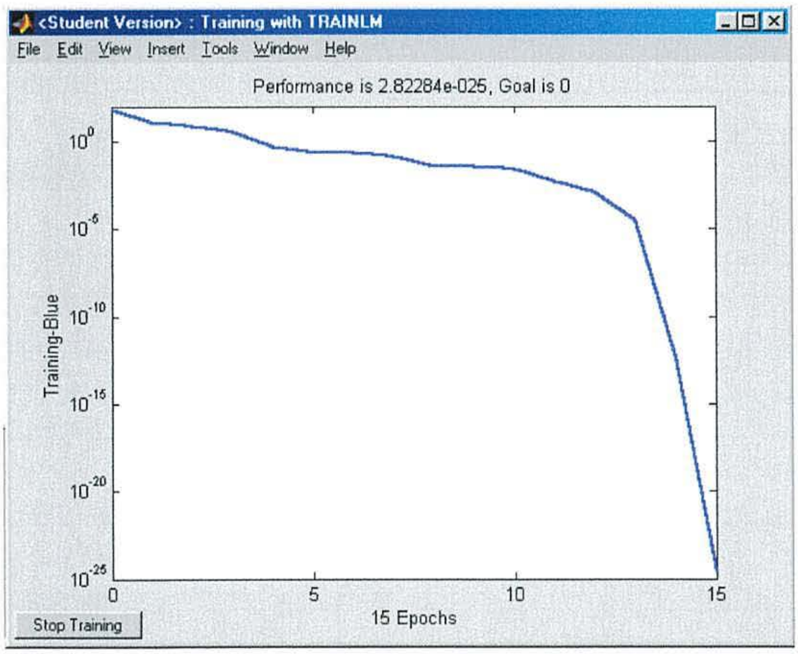

Figure 2.105: Neural Network software running in training mode to determine the optimum parameters for the transform functions. In this case, and exact fit has been found (to a tolerance of less than 10^{-24})

When training is complete, the neural network is run in simulation mode. New MM5 forecast data can be input, and output data generated which will hopefully give a more accurate rainfall forecast than the original estimate (fig.2.106).

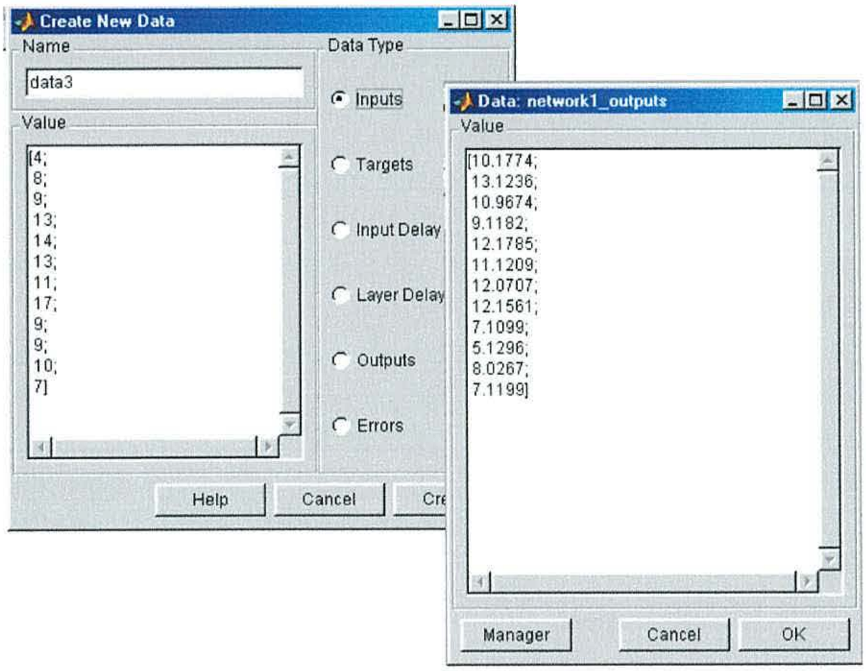

Figure 2.106: After training, sets of input data can be processed by the neural network to possibly provide output data of enhanced accuracy.

Evaluation of results from the Neural Network

Results of successful training and simulation cycles are shown in fig.2.107. Prior to achieving these results, various runs had been recorded where output data sets did not produce an improvement on the original MM5 rainfall predictions:

- A single layer pure linear neuron, and a two layer neuron using a combination of a tan-sinusoidal and pure linear transform gave unsatisfactory results.
- Training with one storm event did not produce improved forecasts when the neural network was applied directly to another storm event. Each storm appears to be mathematically unique, and training needs to take place progressively as an individual storm event develops.
- Training with an inadequate number of time interval data sets may lead to unsatisfactory results. An example is shown in the first block of fig.212 where only two time intervals were used in training with the 8 November 2002 storm

event. Neural network transformation for the third time interval lead to a signed deviation of 36%, which was a slightly poorer forecast than the 34% signed deviation of the original MM5 data.

Given adequate training, small but significant improvements to the forecast data can be consistently achieved. A comparison of accuracy with the original forecasts is given in table 2.2. It is perhaps worth observing that the greatest improvements are achieved in the case where the original MM5 forecast was least accurate. Use of neural network processing may therefore be a means of identifying and improving the least reliable forecasts.

Storm date	Training interval	Simulation interval	MM5 absolute deviation	MM5 signed deviation	Neural Net absolute deviation	Neural Net signed deviation
8 Nov 02	03-12h	12-15h	35.7	34.0	31.8	18.0
8 Nov 02	06-12h	12-15h	35.7	34.0	30.9	21.2
2-4 Feb 04	03h 2 Feb – 09h 3 Feb	09-12h	25.7	6.8	25.4	6.4
2-4 Feb 04	03h 2 Feb – 06h 4 Feb	09-12h	25.7	6.8	25.1	6.2

Table 2.2 Comparison of the accuracy of MM5 initial rainfall forecasts with forecasts after processing by neural network

		Llanbedr		Cwm Bychan		Caerdeon		Erw Wen		Cwm Mynach		Ganllwyd		Tir Penrhos		Trawsfynydd		Bronaber		Aran Hall		Rhobell Fawr		Allt Lwyd		Blaen Lliw		Pared yr Ychain		Dolgellau		Mean absolute difference	Mean signed difference	Total recorded rainfall	Mean absolute difference (mm/h)	% absolute deviation	% signed deviation
08-Nov-02	03-06	4	1	5	4	7	5	7	4			5	5	5	3	6	6	6	5			4	4	3	3	4	6	4	6			1.3	0.7	60			
	06-09	10	4	13	9	11	9	9	6			12	9	11	9	12	8	12	5			7	7	5	5	8	7	7	8			2.8	2.6	117			
	09-12	12	8.2	18	9	17	8.8	18	13			21	13	23	11	18	12	22	11			17	5	13	4	13	8.4	14	7			7.9	7.9	206			
	12-15	10	9	20	14	11	11	16	12			18	12	20	11	11	9	19	9			28	12	18	9	14	7	21	12			6.6	6.6	206			
																																			1.5	37.8	36.1
08-Nov-02	03-06	4	1	5	4	7	5	7	4			5	5	5	3	6	6	6	5			4	4	3	3	4	6	4	6			1.3	0.7	60			
	06-09	10	4	13	9	11	9	9	6			12	9	11	9	12	8	12	5			7	7	5	5	8	7	7	8			2.8	2.6	117			
	09-12	12	4	18	8	17	9	18	13			21	14	23	13	18	11	22	17			17	9	13	9	13	10	14	7			6.8	6.8	206			
	12-15	10	14	20	20	11	18	16	19			18	23	20	25	11	20	19	24			28	18	18	14	14	14	21	15			4.7	-1.2	206			
																																			1.3	31.8	18.0
08-Nov-02	03-06	4	1	5	4	7	5	7	4			5	5	5	3	6	6	6	5			4	4	3	3	4	6	4	6			1.3	0.7	60			
	06-09	10	4	13	9	11	9	9	6			12	9	11	9	12	8	12	5			7	7	5	5	8	7	7	8			2.8	2.6	117			
	09-12	12	4	18	8	17	9	18	13			21	14	23	13	18	11	22	17			17	9	13	9	13	10	14	7			6.8	6.8	206			
	12-15	10	12	20	18	11	17	16	18			18	21	20	23	11	18	19	22			28	17	18	13	14	13	21	14			4.3	0.3	206			
																																			1.3	30.9	21.2
02-Feb-04	03-06	2	7	13	12	13	11	13	11	18	17	12	13			12	11	11	10			11	12	8	10	8	9	12	10			1.7	0.0	133			
03-Feb-04	00-03	4	3	14	8	7	3	14	12	12	10	11	12			13	15	12	17			11	9	12	14	10	19	9	16			3.6	-0.8	129			
	03-06	0	3	12	6	4	3	13	8	12	8	11	8			18	11	17	18			11	8	18	16	17	21	17	19			3.4	1.8	150			
	06-09	6	1	13	4	8	4	14	8	14	6	13	8			17	10	16	14			12	14	16	14	16	16	17	16			4.3	3.9	162			
	09-12	2	1	5	6	3	3.1	9	8	8	7	6	9			11	13	9	11			12	8	13	14	15	13	16	14			1.7	0.2	109			
04-Feb-04	03-06	0	0	6	2	4	1	4	1	7	8	4	7			7	6	3	8			4	4	3	5	2	6	3	5			2.3	-0.5	47			
	09-12	3	3	10	5	6	3	11	6	10	11	11	13			16	12	13	12			24	18	20	18	19	15	16	12			3.1	2.6	159			
	12-15	7	9	12	15	9	10	13	14	12	16	15	20			16	19	15	18			26	22	21	22	16	18	18	16			2.6	-1.6	180			
																																			0.9	25.4	6.4
02-Feb-04	03-06	2	7	13	12	13	11	13	11	18	17	12	13			12	11	11	10			11	12	8	10	8	9	12	10			1.7	0.0	133			
03-Feb-04	00-03	4	3	14	8	7	3	14	12	12	10	11	12			13	15	12	17			11	9	12	14	10	19	9	16			3.6	-0.8	129			
	03-06	0	3	12	6	4	3	13	8	12	8	11	8			18	11	17	18			11	8	18	16	17	21	17	19			3.4	1.8	150			
	06-09	6	1	13	4	8	4	14	8	14	6	13	8			17	10	16	14			12	14	16	14	16	16	17	16			4.3	3.9	162			
	09-12	2	1	5	3	3	2	9	6	8	7	6	10			11	12	9	11			12	9	13	14	15	14	16	12			2.0	0.7	109			
04-Feb-04	03-06	0	0	6	2	4	1	4	1	7	8	4	7			7	6	3	8			4	4	3	5	2	6	3	5			2.3	-0.5	47			
	09-12	3	2.9	10	11	6	4.5	11	12	10	11	11	10			16	15	13	13			24	11	20	15	19	15	16	15			2.5	2.1	159			
	12-15	7	9	12	15	9	10	13	14	12	16	15	20			16	19	15	18			26	22	21	22	16	18	18	16			2.6	-1.6	180			
																																			0.9	25.1	6.2

Figure 2.107. Results of neural network processing of MM5 rainfall forecasts. Training intervals shown in dark blue, simulation interval in light blue.

Structure of frontal rainfall events

An important aspect of evaluating the MM5 model is to assess whether the simulation reasonably represents atmospheric patterns and processes predicted by meteorological theory. As a test of the system, an analysis has been carried out for the sample storm event of 29 December 2002. Output from MM5 is shown as figures 2.108-2.112:

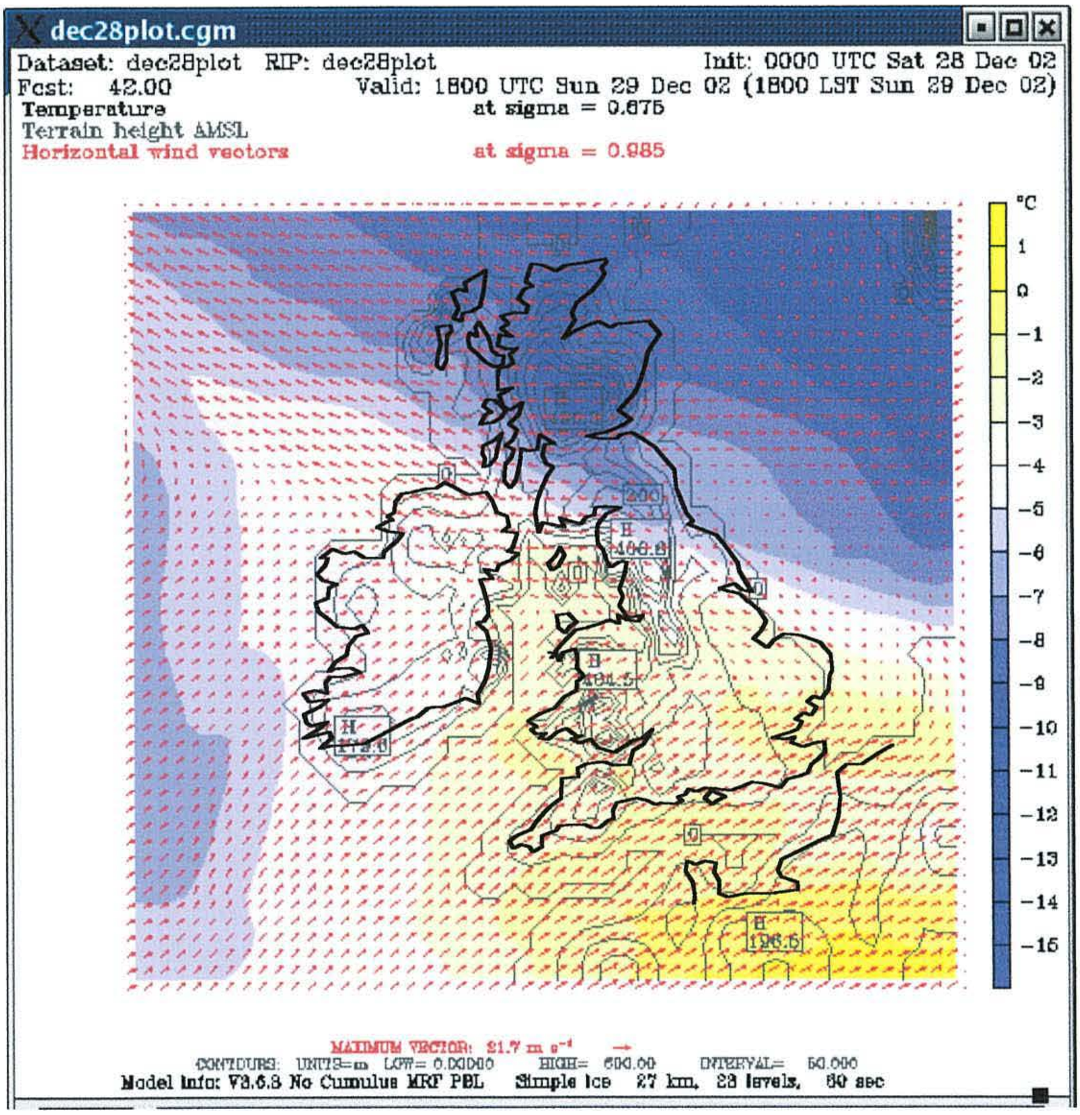

Figure 2.108: MM5 simulation of mid-troposphere temperatures at 18:00h, 29 December 2002. Low level wind vectors are shown as red arrows.

Fig.2.108 shows temperature distribution at mid-troposphere levels. A warm sector extends from Ireland into southern Britain. Low level air flow is towards the north-east across the warm sector, turning north westwards parallel to the warm front in the direction of the cyclonic low to the south of Greenland.

Fig.2.109 shows vertical air velocities at mid-troposphere levels. Uplift is firstly towards the north-east ahead of the cold front, then north westwards along the line of the warm front. These movements represent an ascending warm sector conveyor.

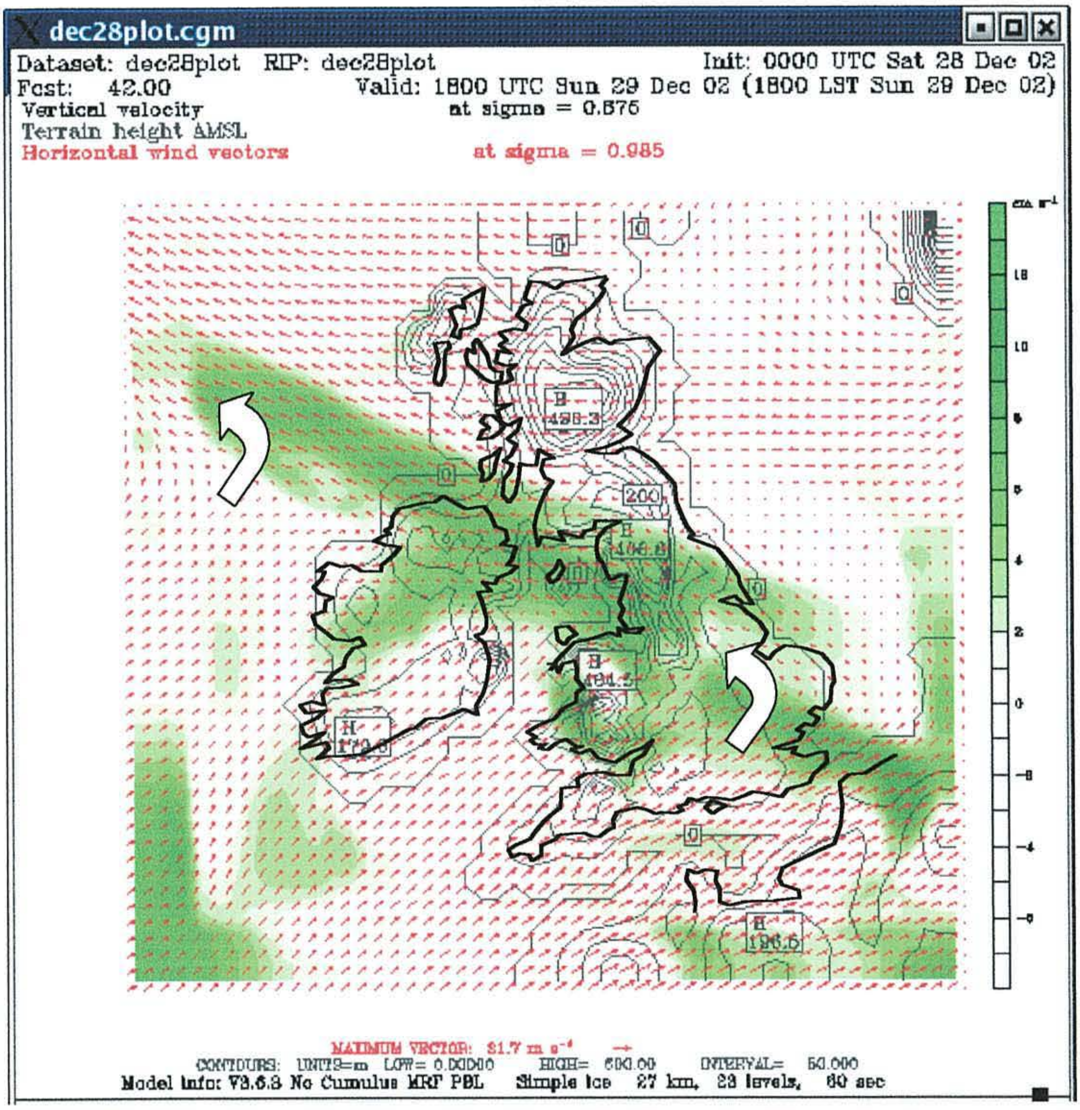

Figure 2.109: MM5 simulation of mid-troposphere vertical component of air flow at 18:00h, 29 December 2002. Low level wind vectors are shown as red arrows.

Fig.2.111 shows total rainfall for the six hour period to 18:00h. Rainfall is concentrated along the warm front conveyor, with subsidiary rain bands oriented north-south across the warm sector. This pattern is consistent with the instability model of Browning et al. (1973), with rainfall enhanced by gravity wave development over the Welsh mountains.

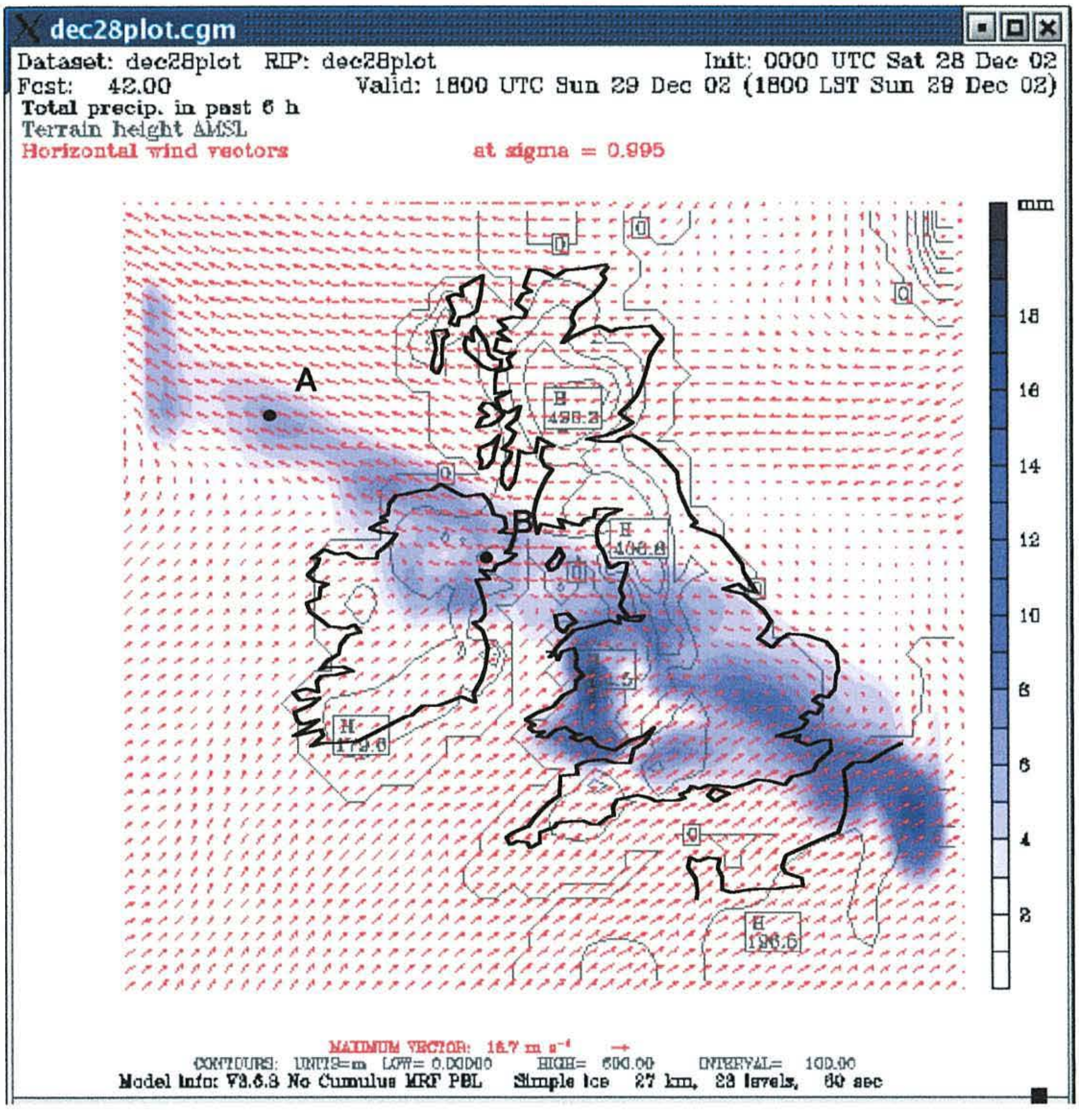

Figure 2.110: MM5 simulation of rainfall for the 6 hour period 12:00h to 18:00h, 29 December 2002. Low level wind vectors are shown as red arrows. A and B are the locations of the tephigrams displayed in fig. 2.112.

Fig.2.111 shows air flow at high troposphere level, with high velocity zones representing a jet stream pattern over eastern Britain and the North Sea. We should note that the upper air flow to the north-east over Wales is approximately perpendicular to the mid-troposphere warm air conveyor ascending to the north-west. This is similar to the situation recorded by Browning and Hill (1985) and represented here as fig.2.21.

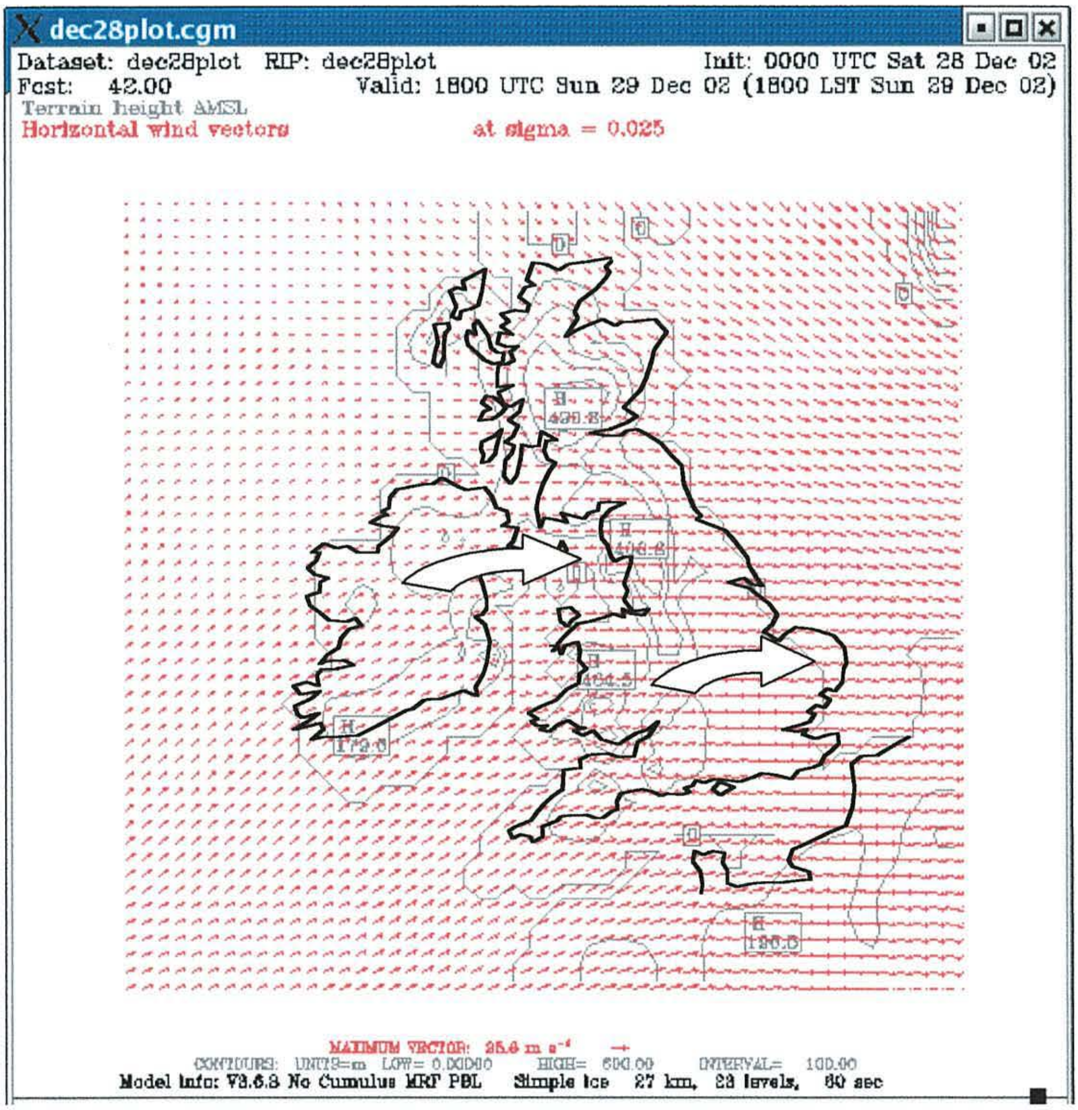

Figure 2.111: MM5 simulation of upper troposphere wind direction at 18:00h, 29 December 2002.

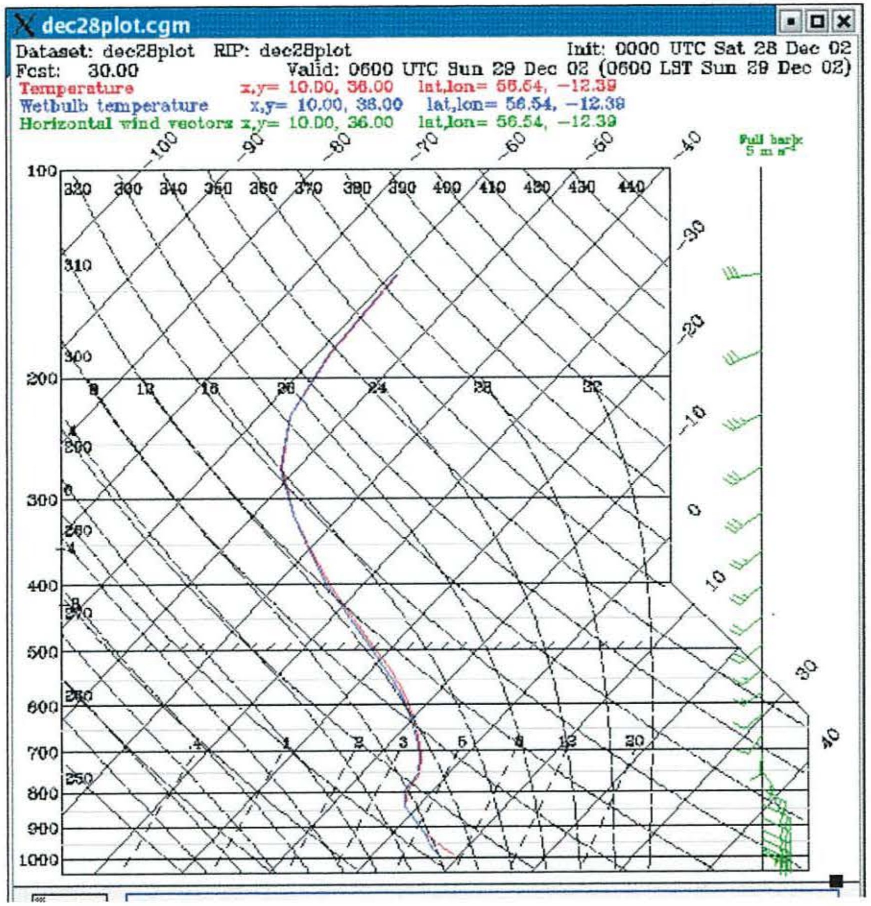

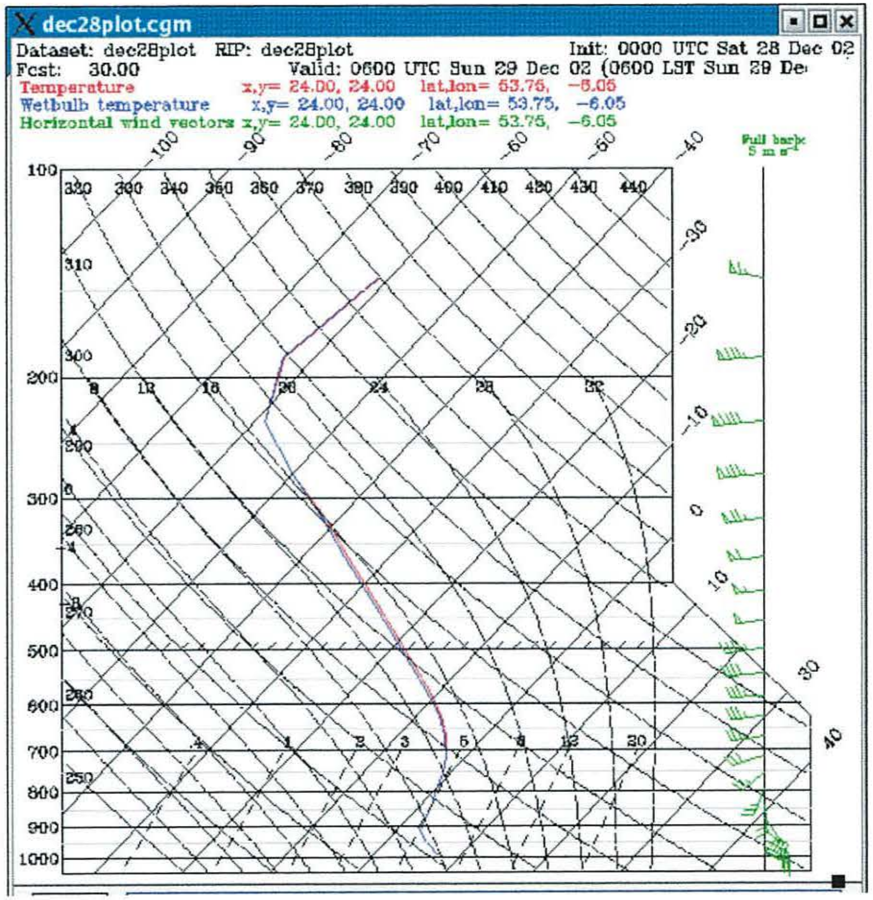

Figure 2.112: Tephigrams generated by the MM5 simulation for location A - off the north west of Ireland, and location B - Belfast, marked on fig. 2.110. 06:00h, 29 December 2002

Example tephigrams generated by MM5 are given in fig.2.112. Dry bulb temperature curves lie to the left of the lapse rate curve in the lower troposphere, indicating instability which can produce uplift within the warm sector conveyor. Maximum instability occurs at 900mb height at location A to the south-east, ascending to 850mb at location A towards the north-west. Temperatures fall rapidly above the conveyor at heights over 700mb.

Horizontal wind vectors are seen to change from a north-west directed airflow within the conveyor, towards the easterly airflow of the upper troposphere jet stream.

Squall line convection

Storms across Wales on 3 July 2001 were the result of intense convective thunder-storm activity along a squall line. The convective nature of the July 2001 event has provided an opportunity to compare the convective parameterisation schemes provided within the MM5 modelling system. The results for two schemes, Anthes-Kuo and Grell are discussed below.

Anthes-Kuo cumulus parameterisation

A rainfall distribution map using Anthes-Kuo parameterisation is given in Fig 2.113. This shows a close correspondence to observed rainfall patterns. The north-south orientation of the squall line is clearly defined, with several thunderstorm cells in observed locations over the mountain region. The only deficiency of the model is that the zone of intense rainfall (>25mm/hour) should extend some 5-10km further northwards along the squall line to account for extensive flood damage in the Arennig area.

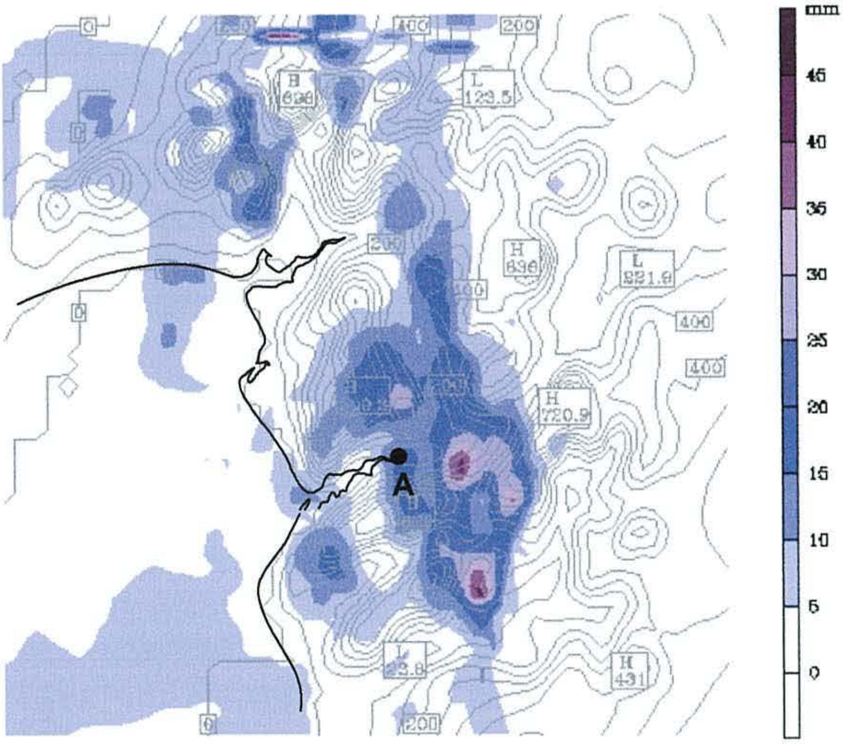

Figure 2.113: One hour rainfall total. 1800-1900, 3 July 2001. Anthes-Kuo model. A marks the location of the tephigram shown in fig. 2.116.

Examination of the MM5 model results shows the intense convective activity associated with the squall line (Figures 2.114-2.115).

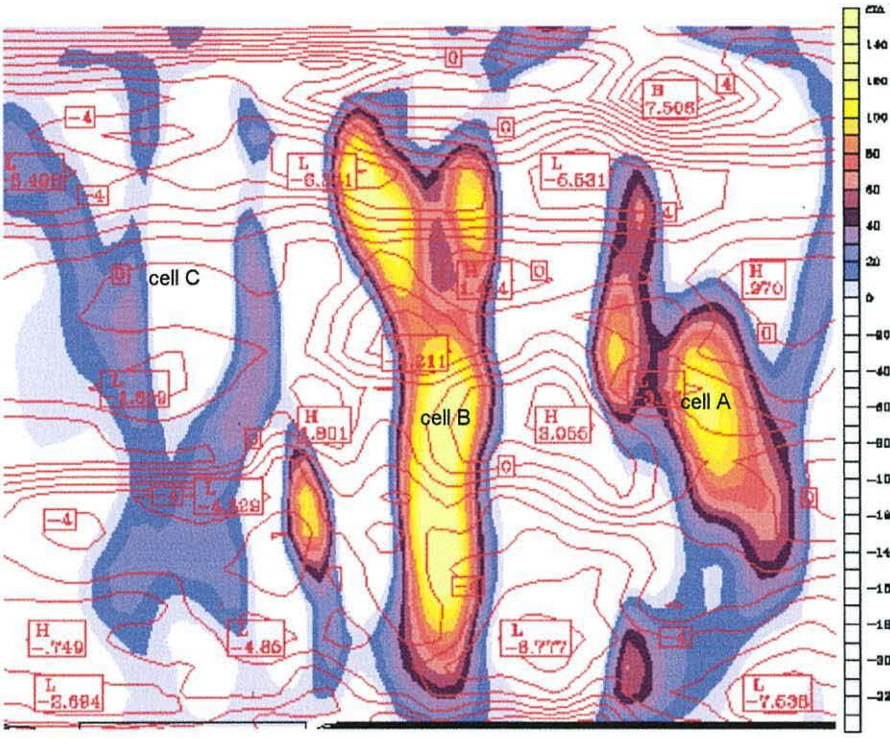

Figure 2.114: Vertical section from Cardigan Bay to the Arenig mountains. Shading indicates vertical air velocity. Contours indicate horizontal velocities. 18:00h, 3 July 2001. Anthes-Kuo model.

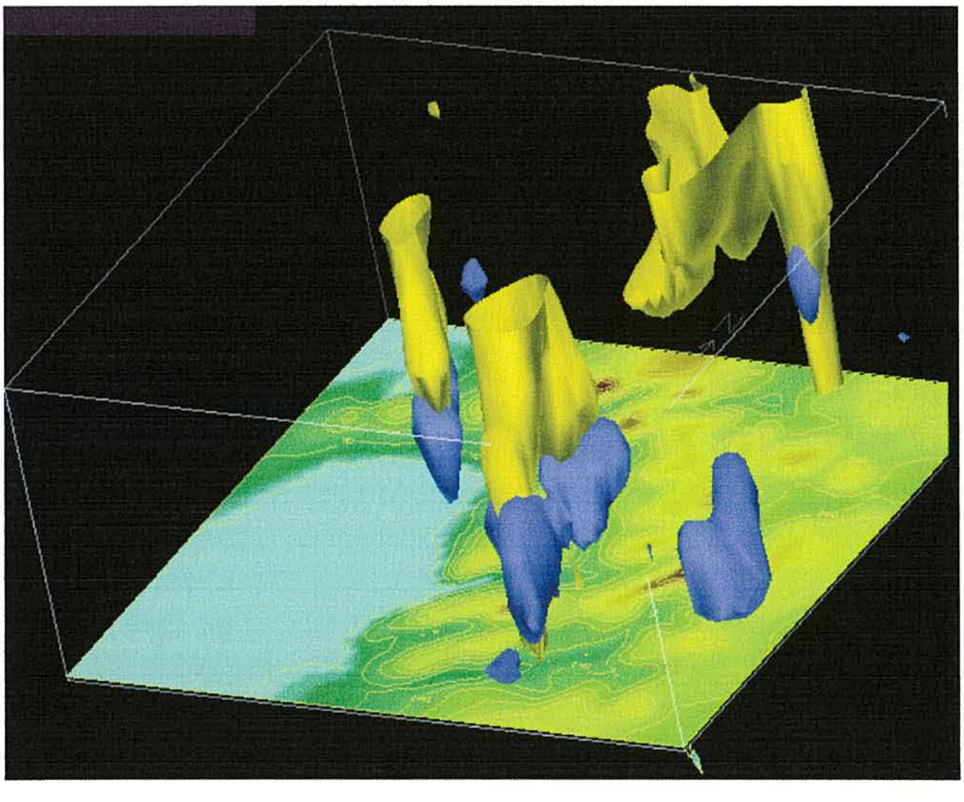

Figure 2.115: Isosurfaces for cloud mixing ratio>0.4 (yellow) and precipitation mixing ratio>0.4(blue). 1800, 3 July 2001. Anthes-Kuo model.

It is seen that the Anthes-Kuo physics scheme produces results in close agreement with the theoretical model of squall line propagation proposed by Fovell and Tan (1998, 2000). The cross section fig.2.114 shows a sequence of convection cell initiation at an advancing cold tongue (cell A), the vertical growth of a second cell (cell B), and evidence of the break-up of an earlier cell during advection towards the rear of the cold pool (cell C). Clear similarities exist with the simulations carried out by Fovell and Tan (cf. fig.2.32).

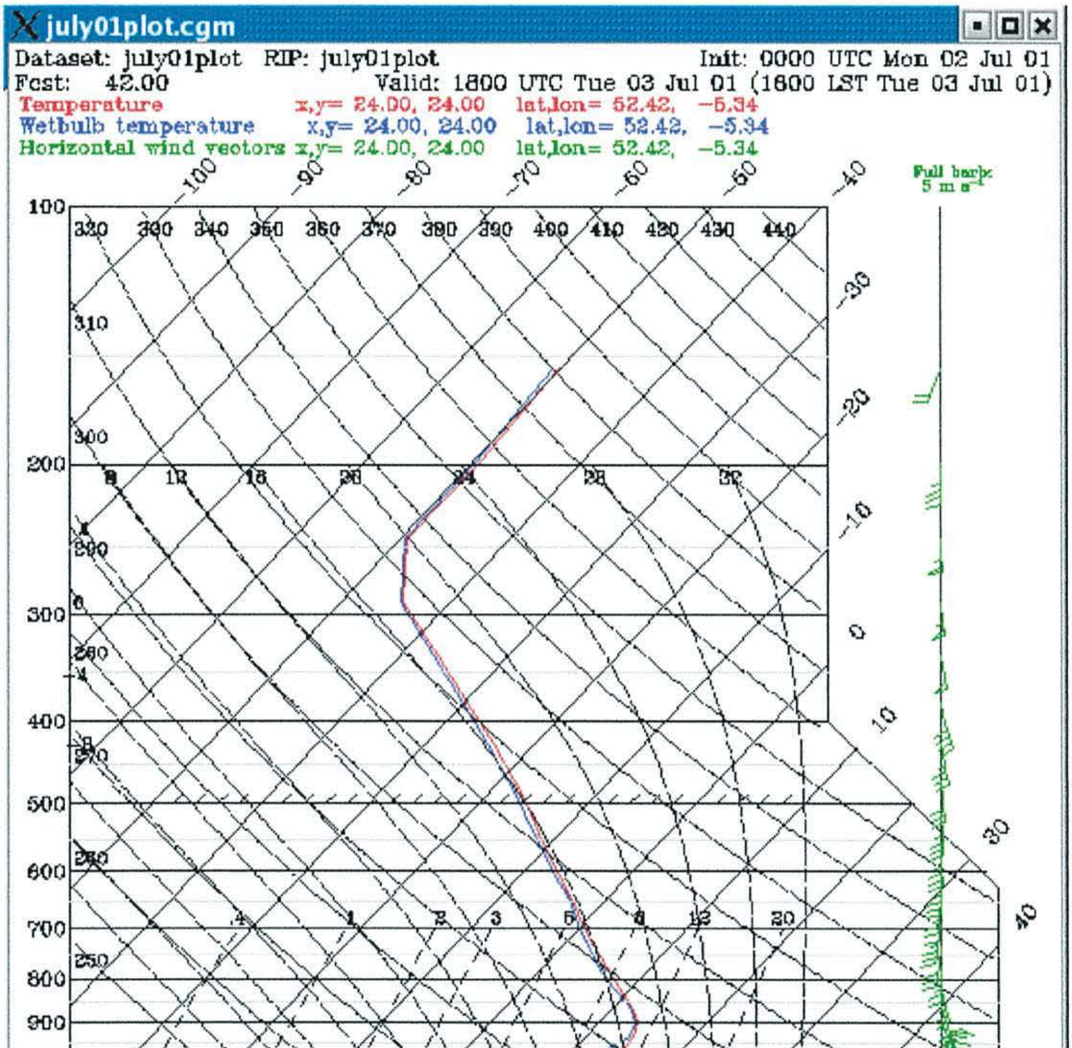

Figure 2.116: Tephigram generated by the MM5 simulation for location A – Dolgellau, shown on fig. 2.113, 18:00h, 3 July 2001

A tephigram is displayed in fig.2.116 for a location towards the rear of the squall line. This shows a fall in virtual temperature towards the ground, confirming the modelling of a pool of cool air below 950mb height. The dry bulb temperature curve lies to the left of the lapse rate curve for altitudes between 800mb and 500mb, indicating a wide vertical band of instability driving convection. Horizontal air flow vectors are towards the north, following the axis of the squall line.

Grell cumulus parameterisation

Results from the MM5 run using Grell cumulus parameterisation (cf. fig.2.89) are very different from those of the Anthes-Kuo model, and bear little resemblance to observed rainfall patterns during the storm event. Rainfall is modelled as occurring mainly over the sea, and is about half of the true intensity (fig.2.117).

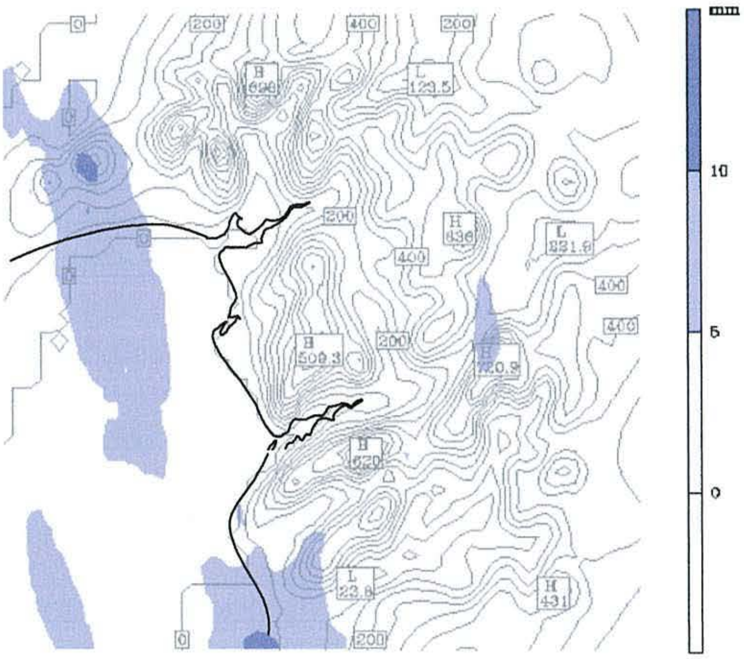

Figure 2.117: One hour rainfall total. 1800-1900, 3 July 2001. Grell model.

Patterns of vertical air motion produced by the Grell model (fig.2.118) indicate a number of small convective cells distributed over a broad belt, in contrast to the few very large cells of the Anthes-Kuo model. Little rainfall is shown as being generated by the convective system.

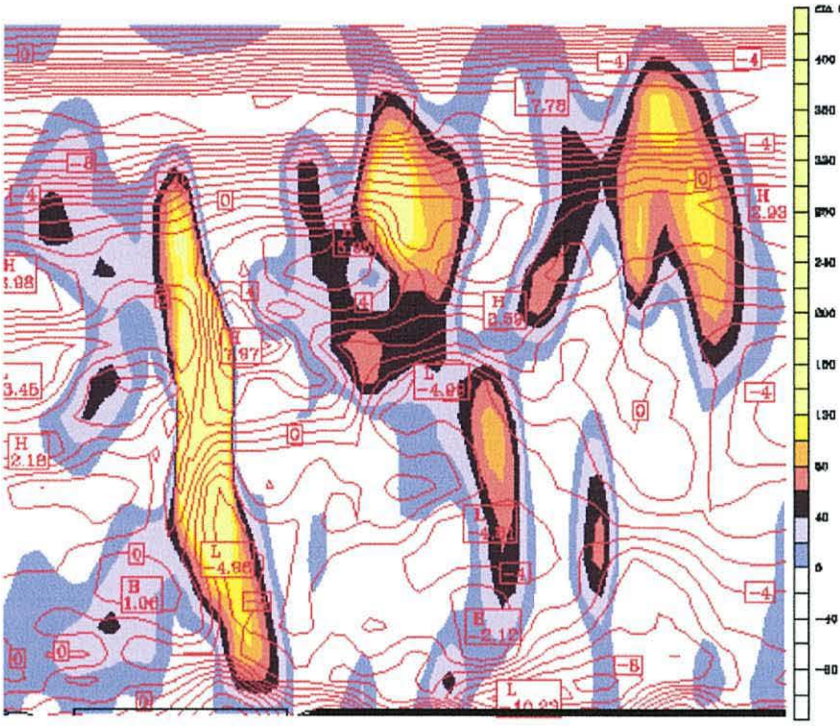

Figure 2.118: Vertical section from Cardigan Bay to the Arenig mountains. Shading indicates vertical air velocity. Contours indicate horizontal velocities. 18:00h, 3 July 2001. Grell model.

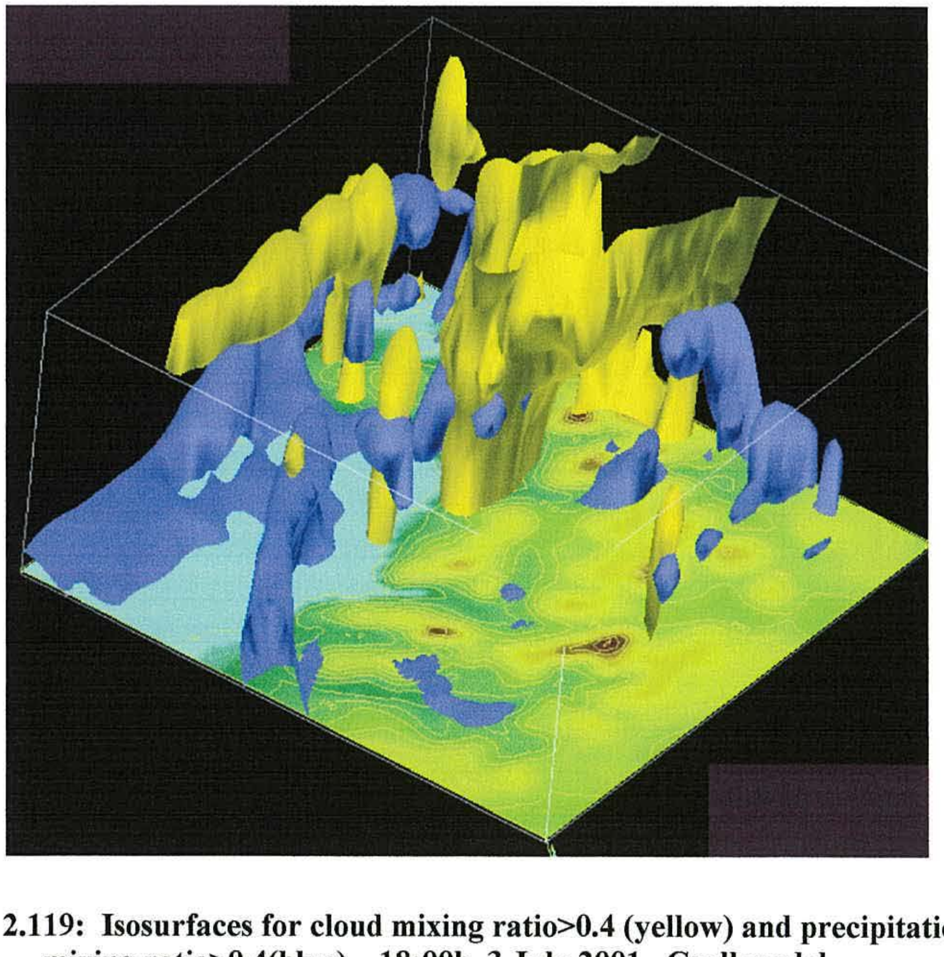

Figure 2.119: Isosurfaces for cloud mixing ratio>0.4 (yellow) and precipitation mixing ratio>0.4(blue). 18:00h, 3 July 2001. Grell model.

Summary

Analysis of frontal rainfall events simulated in the MM5 mesoscale model indicates:

- The general patterns of rainfall are reproduced well, both temporally and spatially. Rainfall distributions obtained from MM5 are in better agreement with field raingauge readings than rainfall radar over the North Wales area.
- Rainfall predictions using MM5 in a 6 hour forecasting mode are likely to be in the order of $\pm 30\%$ accuracy for individual point values, or $\pm$ 15% accuracy if rainfall averaging across the catchment is allowed.
- Some limited but useful improvement to forecast values can be achieved by neural network processing of initial MM5 output data. Retraining of the neural network needs to be carried out for each individual storm event.
- The MM5 model produces rainfall predictions from realistic simulations of atmospheric conditions within frontal systems, combined with appropriate rainfall enhancement by topographic forcing.

The July 2001 flood event was different in nature, resulting from intense convective thunderstorm activity along a squall line. Simulation of this event with MM5 has produced varied results with different cumulus parameterisations.

- The Anthes-Kuo scheme corresponds well to the sparse rain gauge data available, and gives a rainfall distribution which is largely consistent with field observations of flood damage and maximum river levels. Furthermore, it simulates atmospheric processes consistent with squall line theory.
- The Grell scheme considerably underestimated rainfall volumes. It may be the case that the Grell scheme is more suited to modelling isolated convective storms rather than structured pre-frontal squall line activity.

It may be necessary to carry out multiple runs of the MM5 model with different cumulus parameterisations if thunderstorm activity is expected, then make use of a weighted average of results in the integrated hydrology modelling system. Greater weight should be given to extreme conditions predicted by any of the cumulus schemes, since it seems likely that a severe convective event will be underestimated rather than overestimated by MM5.

3. Catchment Hydrology

3.1 Hydrological modelling systems

The main components of a hydrological model are summarised in fig.3.1 (Cornell University, 2003). Rainfall reaching the ground may enter the soil by *infiltration*, or may flow down the hillslope as *surface runoff*. Surface water can return to the atmosphere by *evaporation*. Water within the root zone may be taken up by plants and subsequently released into the atmosphere by *transpiration* from the plant leaves. Water within the soil may produce *lateral flow* downslope at shallow depth, or may percolate downwards to *groundwater store*. Water may also be drawn upwards from the subsoil by *capillary action* if the topsoil becomes dry. Surface runoff and shallow lateral flow may enter streams fairly quickly after the start of a storm event. Groundwater may be released to streams more slowly and over a longer period as *baseflow*. Once water has entered streams, it will be *routed* downstream.

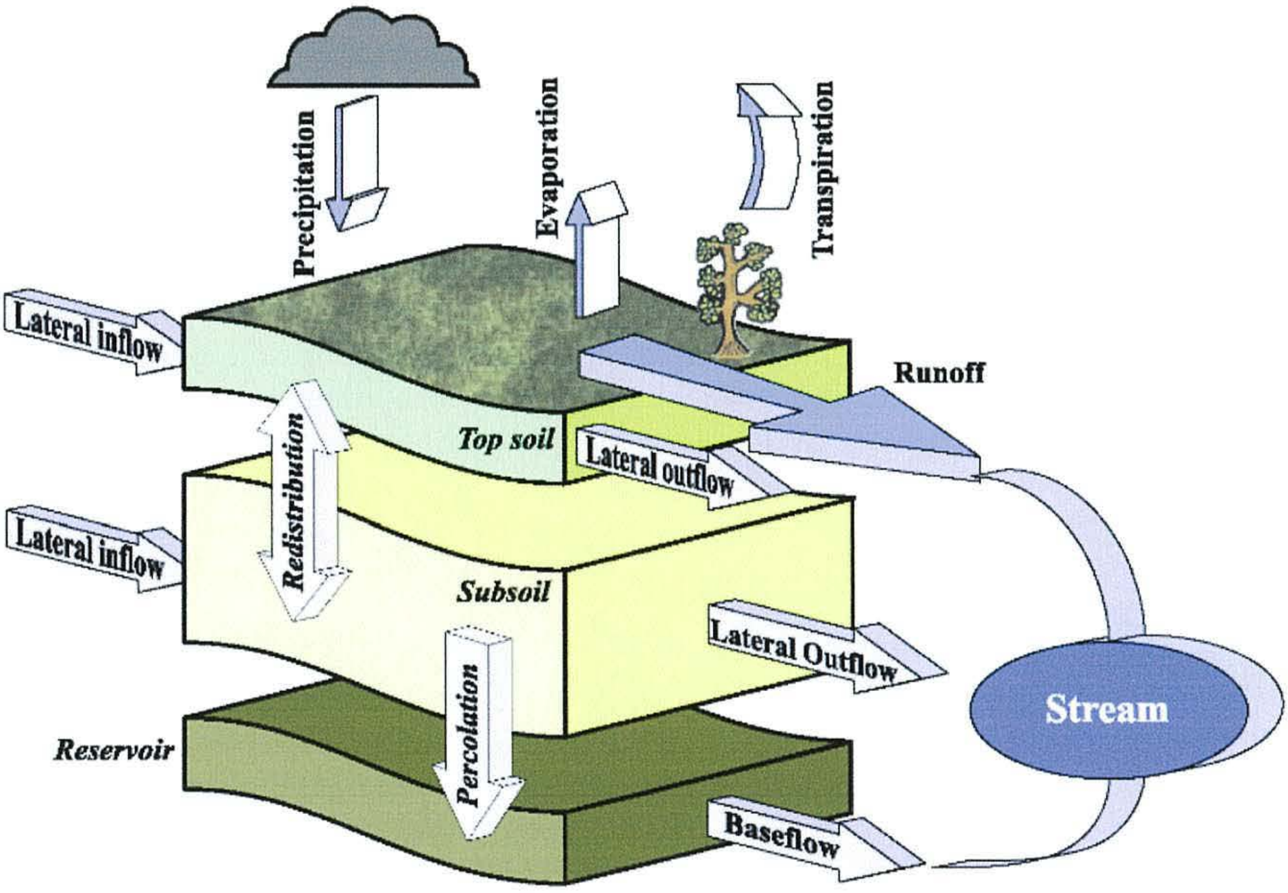

Figure 3.1: Main components of a hydrological model (Cornell University, 2003)

The conceptual model described above was first formulated mathematically in the 1960's as the Stanford Watershed Model. This system uses a series of water stores, with the rates of inflow and outflow to individual stores controlled by parameters representing physical properties of the hillslope environment. The system is illustrated in fig.3.2 (after Dawdy and O'Donnell, 1965).

Components of the Stanford Watershed Model may be divided into:

- precipitation input, generally representing the rainfall distribution across the catchment in space and time,
- volumes of water within the surface, soil, groundwater and river routing stores at any particular time, which may be controlled by soil depth and porosity,
- parameters controlling the rate at which water can pass between the different stores, which will be dependent on the hydrological properties of the soil and bedrock,
- parameters determining the rate of water loss through evaporation and transpiration, which will be determined by the nature of the ground surface and vegetation, and also by the prevailing climatic conditions,
- parameters determining the rate at which water released into rivers will be routed downstream through the river system.

Whilst the Stanford Model provides a good theoretical basis for hydrological modelling, a number of assumptions must be made in order to generate a workable computer simulation of a real watershed. The simplest approach is to assume that rainfall input and hydrological parameters are approximately uniform across the catchment, so that average catchment values can be used in the modelling equations. This leads to *lumped parameter models*, of which the Institute of Hydrology HYRROM model (fig.3.3) is an example.

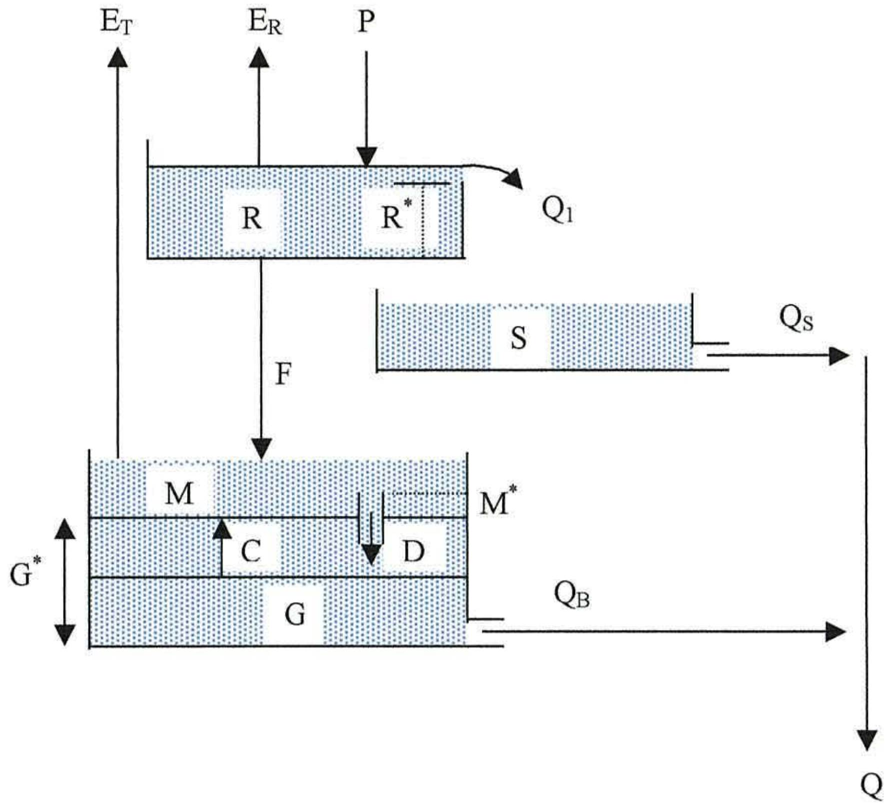

C	maximum rate of capillary rise
D	recharge to groundwater store
E_R	evaporation from surface water store
E_T	evapotranspiration from soil water store
F	infiltration to soil moisture store (parameters f_0,f_c,k)
G	groundwater store (parameter K_g)
G^*	groundwater storage threshold
M	soil moisture store
M^*	soil moisture storage threshold
P	precipitation input
Q	total stream discharge
Q_1	surface runoff
Q_B	outflow from groundwater store
Q_S	outflow from surface water routing store
R	surface water store
R^*	surface water storage threshold
S	surface water routing store (parameter K_S)

Figure 3.2. Stanford Watershed Model (after Dawdy and O'Donnell, 1965)

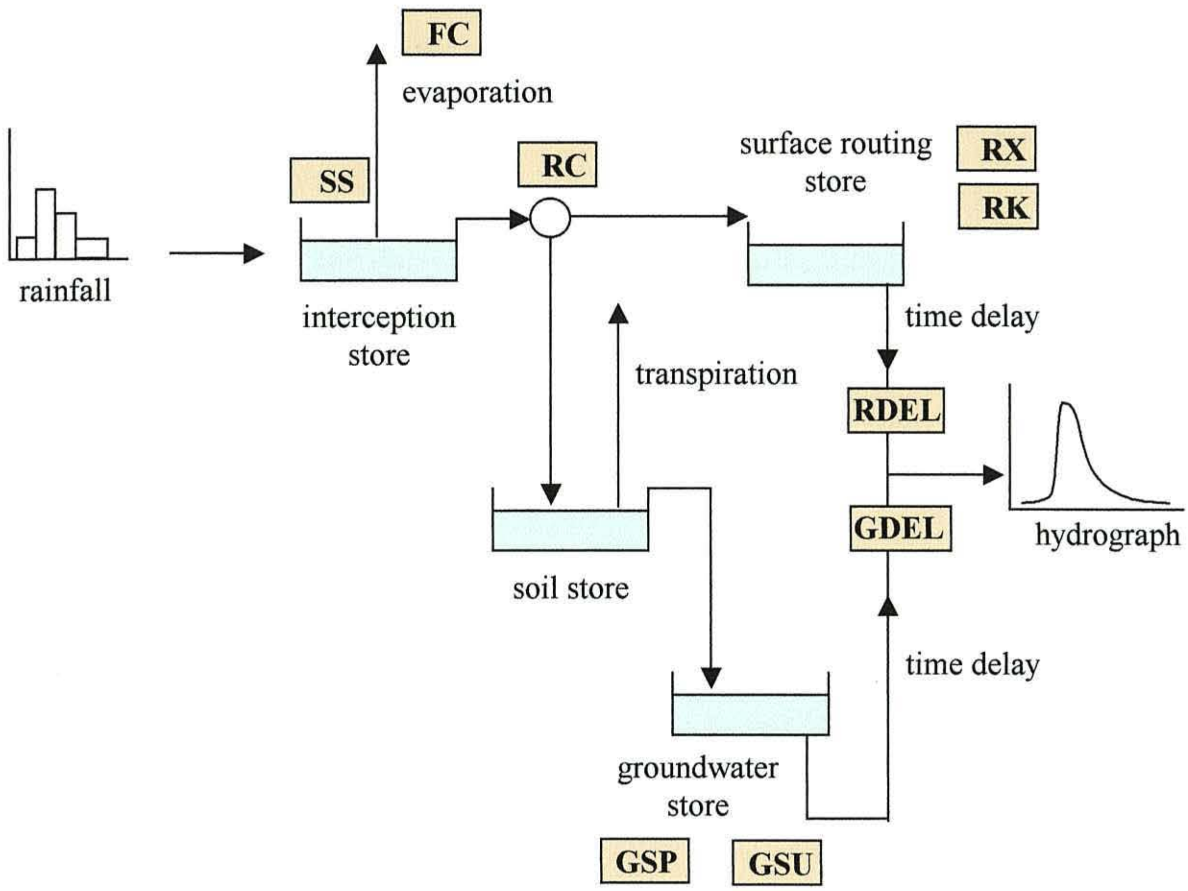

Figure 3.3: HYRROM model using nine parameters, identified by codes in the diagram above, to control the rates of input, output and transfer of water between the stores. (after Institute of Hydrology, 1988)

The lumped parameter approach can be very effective in predicting hydrograph responses at the output of a catchment. Although it may be difficult or impossible to accurately measure the required model parameters in the field, these can be optimised automatically by training the program with historical data. Parameters are adjusted to produce a best fit between the model output and real hydrographs recorded for the river.

The lumped parameter approach does, however, have some serious disadvantages:

- In a catchment of complex geology and varied vegetation, the assumption that parameters can be represented by average catchment values may not be valid.

- Reliance is often placed on automatic calibration of parameters. Optimisation algorithms work by systematically adjusting parameters in a direction which moves towards a lower overall error value, often the root mean square difference between the true and simulated hydrographs. It is possible that quite different sets of parameter values will produce an equally good optimisation. This situation is termed *equifinality.* An example is given in fig.3.4 for the simple case of two parameters, where combinations of the values A_1, B_1 and A_2, B_2 may represent similar minimums on a contoured error surface.

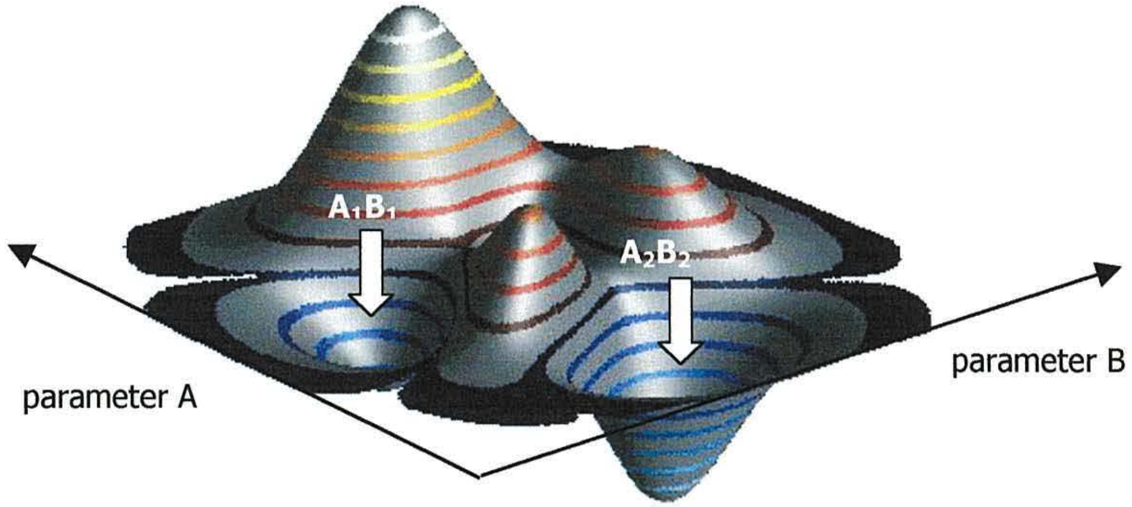

Figure 3.4: Two possible runs of an optimisation algorithm leading to different minima on the error surface

Equifinality may not be a problem if the prediction of river discharge is the sole objective of the model. There must be serious doubt, however, as to whether the parameter values chosen represent any true physical properties of the catchment.

- Lumped parameter models generally work well when predicting river discharges within the interpolation range of the data used for parameter calibration. Results may, however, become increasingly inaccurate when extrapolating beyond the known data to predict hydrographs for extreme storm events.

For these reasons and the considerations given below, a lumped parameter approach is considered unsuitable for meeting the objectives of the Mawddach research project:

- Wide variations in rainfall, geology, soils and vegetation are known to occur on a kilometre scale, so averaging of parameters across large areas is not appropriate.
- An objective of the research is to predict changes in river flows in response to changes in land management, so a clear link between model parameters and measurable catchment characteristics is necessary.
- A good understanding of the mathematical linkage between parameters measured in the field and model output should allow increased confidence in prediction beyond the limits of the historical records. This may be important for estimating the possible effects of a changing rainfall regime in future years.

An alternative mathematical approach which relates more closely to the physical characteristics of the catchment is the TOPMODEL concept of Bevan (1997). This makes use of the Kirkby topographic index γ:

$$\gamma = \frac{a}{\tan \beta}$$

where a is the land surface area draining to a unit contour length on the hillslope, and β is the slope angle at that point (fig.3.5).

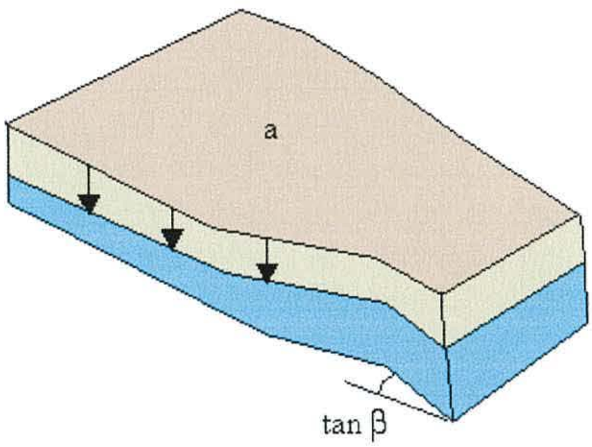

Figure 3.5: Determination of the Kirkby topographic index
(after Bevan, 2001)

A high value of topographic index represents a likelihood of saturated conditions, and occurs when a large upslope area drains onto gently sloping ground. By contrast, a low value of topographic index represents the likelihood of dry conditions, and may result from a small upslope area draining onto a steep slope. Areas of hillslope with similar values of topographic index would therefore be expected to behave similarly hydrologically. An advantage of the TOPMODEL approach is that the topographic index is an entirely geometrical concept, so can be computed automatically from a digital elevation model of the ground surface.

TOPMODEL makes a simplifying assumption that downslope hydraulic transmissivity T at any point on a hillslope can be expressed as a function of the water storage deficit at that point, measured as the depth to the water table.

$$T = T_0 e^{-D/m}$$

where T_0 is the lateral transmissivity when the soil is just saturated, D is the local depth to the saturated soil level, and m is a parameter controlling the rate of increase in transmissivity. With this assumption, the downslope saturated subsurface flow rate Q per unit contour length is given by:

$$Q = T_0 \tan \beta \exp(- D/m)$$

The saturated transmissivity parameter may be varied across the catchment to represent variations in soil type.

An alternative modelling approach is to subdivide the catchment into zones which might be expected to behave in a hydrologically similar manner. These zones are termed *hydrological response units*. Calculations of water storage and outflow are then carried out separately for each unit, with the outflow being routed to the next unit downslope or downstream. A hydrological response unit is likely to require:

- a relatively uniform slope angle, so that a representative value for downslope flow can be computed,
- relatively uniform soil and bedrock characteristics, so that representative values for hydraulic conductivity can be determined,
- relatively uniform surface characteristics and vegetation, so that representative values can be determined for evaporation and transpiration.

A model using hydrological response units is HEC-1, available within the Watershed Modelling System package (Goldman and Ely, 1990). HEC-1 has also been used in experiments for the Mawddach basin and will be discussed in detail in section 3.2.

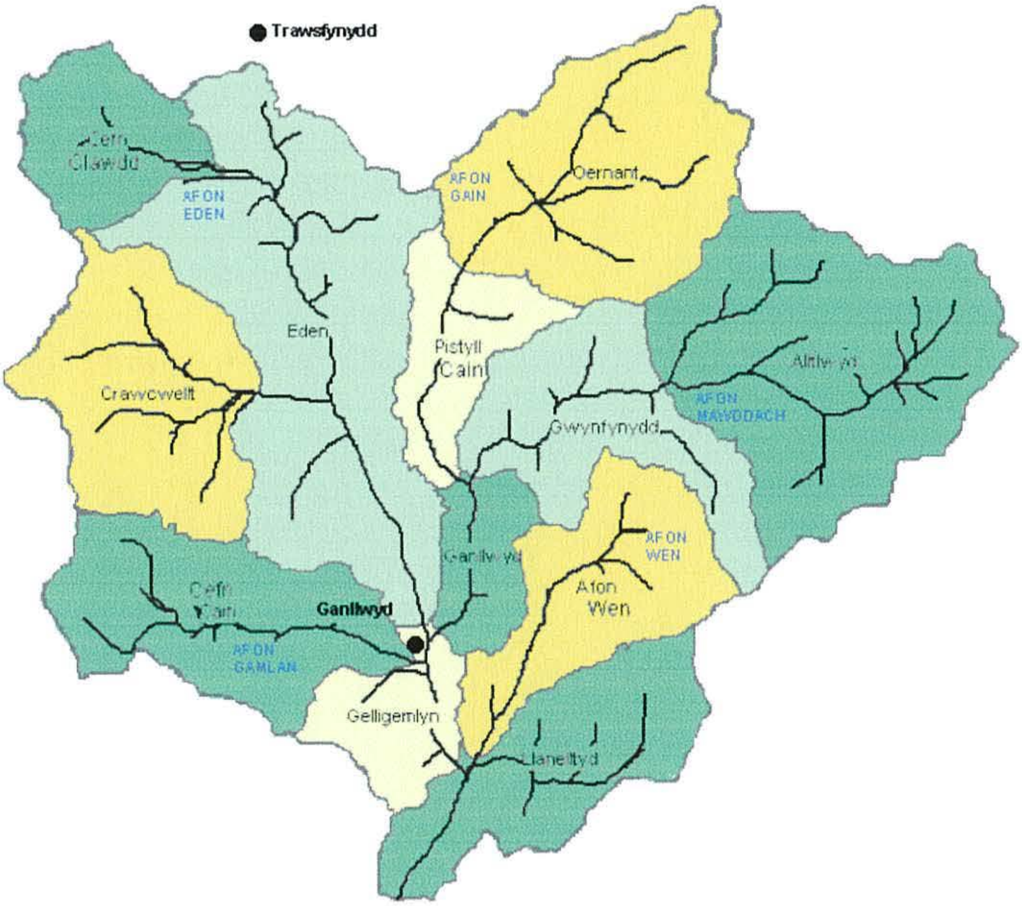

Figure 3.6: HEC-1 model for the Mawddach sub-catchments

HEC-1 requires the study area to be divided into sub-catchments (fig.3.6) which can be treated as having uniform properties of slope, soil runoff and infiltration characteristics. Additional sub-catchments can be defined as necessary, until the assumption of approximately uniform hydrological response units is achieved.

Within the HEC-1 package, several different methods of determining soil infiltration rate in response to rainfall are available. An option which has been employed in the Mawddach modelling is the US Soil Conservation Service curve numbers method (fig.3.7). This allocates a parameter on the basis of soil type and vegetation, which can then be used in the calculation of runoff generation.

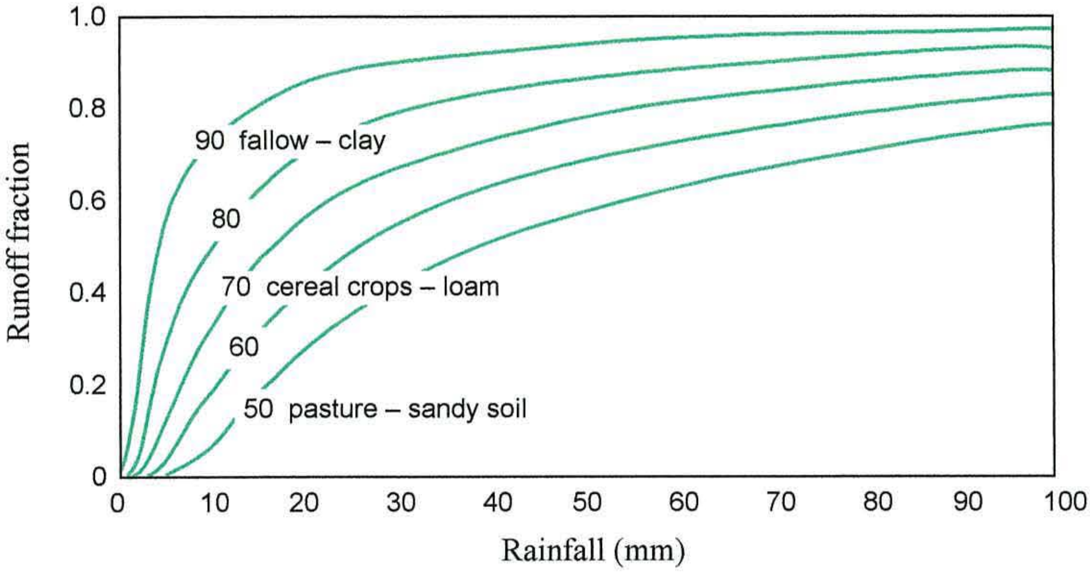

Figure 3.7: SCS curve number plots (after Bevan, 2001)

HEC-1 makes use of the kinematic wave equation for modelling the downslope flow of surface runoff:

$$\frac{\partial A}{\partial t} + \frac{\partial Q}{\partial x} = r$$

where:

$\frac{\partial A}{\partial t}$ is the rate of change of water depth on the hillslope surface,

$\frac{\partial Q}{\partial x}$ is the variation in discharge with distance down the hillslope,

r is water gained or lost per unit area.

The kinematic wave equation can be combined with Manning's equation:

$$Q = \frac{1.486}{n} AR^{2/3}S^{1/2}$$

which determines discharge Q in terms of slope S, hydraulic radius R, cross sectional area of the flow A, and a roughness factor n. This equation can be written in a simplified form by combining variables to give:

$$Q = \alpha A^m$$

where α and m are parameters related to flow geometry and surface roughness. This leads to the equation:

$$\frac{\partial A}{\partial t} + \alpha m A^{(m-1)} \frac{\partial A}{\partial x} = r$$

This equation can be solved to determine water movement down a hillslope over time, as a function of surface roughness and slope angle.

HEC-1 works well in simulating hydrographs from historical storm events, and meets the desired criterion of having parameters which link directly to measurable characteristics of the catchment. However, it is limited to the modelling of a single storm. Infiltration to the groundwater store is treated as a loss from the model, so long term base flow into rivers is not represented. This difficulty is illustrated in fig.3.8, which compares the recorded and simulated hydrographs at Tyddyn Gwladys on the River Mawddach for the July 3, 2001, flood event.

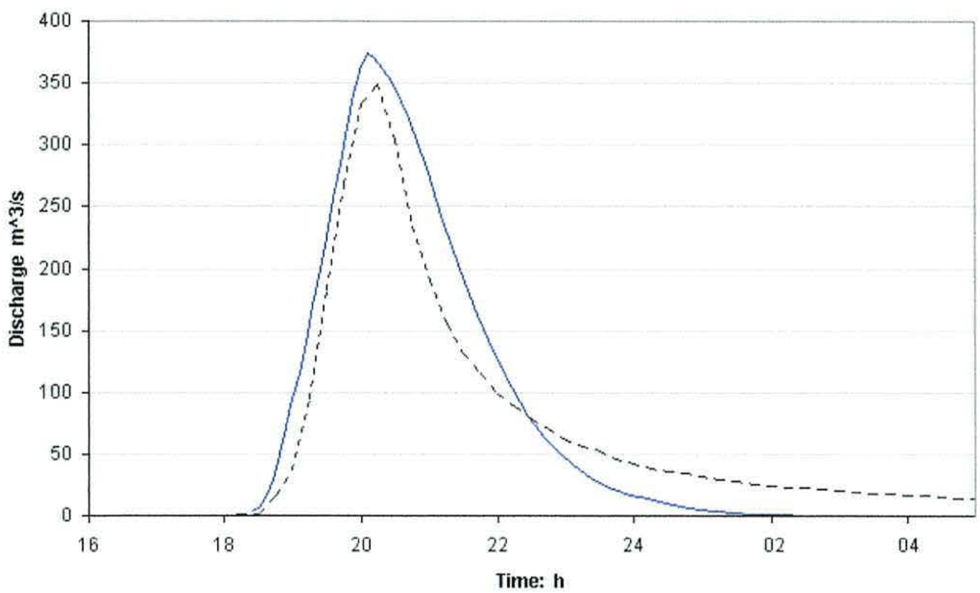

Figure 3.8: Synthetic hydrographs (solid line) and observed hydrograph (dotted line) for the July 3, 2001, flood event, Tyddyn Gwladys.

There is good agreement for the peak of the flood when hillslope runoff is the main contribution to the river flow. However, slower release of groundwater over the subsequent 12 – 24 hours is not represented by the model. The inability to handle groundwater flows adequately prevents HEC-1 being used in long term studies of the effects of antecedent conditions on flood generation.

A number of hydrological models have been developed which combine hillslope runoff simulation with groundwater baseflow. An alternative approach is to handle groundwater processes with a separate groundwater model MODFLOW (McDonald and Harbaugh, 1988) within the Groundwater Modelling System package.

The mathematical basis for MODFLOW is Darcy's equation for the flow of water through a porous medium (fig.3.9):

$$\frac{\partial}{\partial x}\left(K_x \frac{\partial h}{\partial x}\right) + \frac{\partial}{\partial y}\left(K_y \frac{\partial h}{\partial y}\right) + \frac{\partial}{\partial z}\left(K_z \frac{\partial h}{\partial z}\right) - W = S\frac{\partial h}{\partial t}$$

where K_x is hydraulic conductivity in the x-direction,

$\frac{\partial h}{\partial x}$ is the gradient of hydraulic head in the x-direction,

$\frac{\partial h}{\partial t}$ is the change in hydraulic head with time,

S is the water storage capacity of the porous medium, and

W represents water added as input, or lost as output from the system:

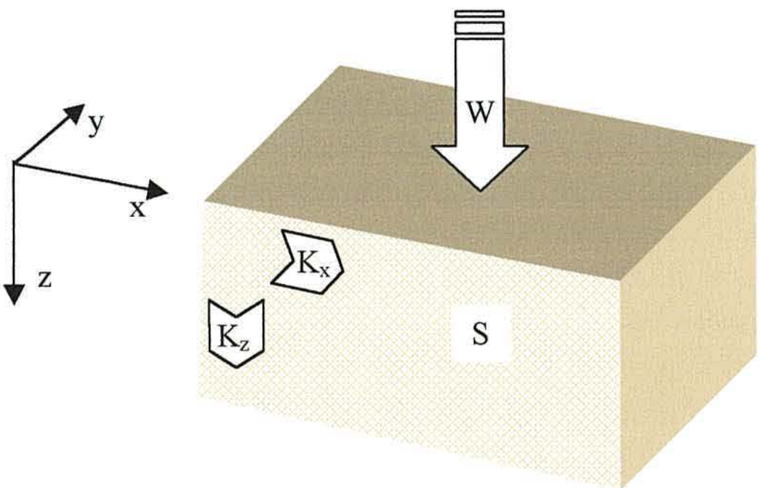

Figure 3.9: Components of Darcy's equation

If hydraulic conductivities can be estimated and starting values assigned for the hydraulic heads across the catchment, the directions and volumes of water flow through the bedrock can be computed. MODFLOW can determine water output to streams from groundwater baseflow, and can respond to recharge from rainfall events. River water can also be gained into groundwater storage where river channels cross unsaturated bedrock. Use of the MODFLOW package will be discussed in section 3.4.

A further component that is necessary for hydrological modelling is the simulation of surface water flows within the streams and rivers which make up the drainage system of the catchment. Many hydrological models have a river routing component in addition to hillslope runoff simulation, but again it was decided to use separate specialist packages for this aspect of the Mawddach project. Experiments have been carried out with the river routing packages HEC1 and GSTARS.

River channels of widely differing character make up the Mawddach system (fig.3.10). Flows occur under a mixture of critical and subcritical regimes, necessitating the modelling of varying water velocity-depth relations within individual reaches.

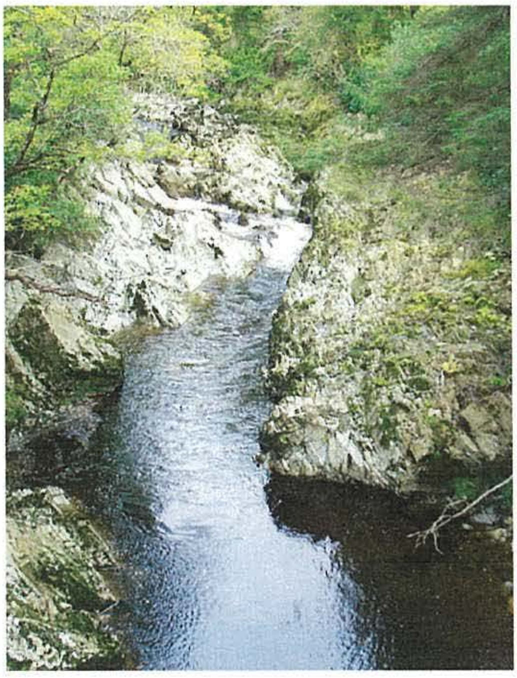

Figure 3.10: The River Mawddach in Coed Y Brenin, showing a transition from fast shallow supercritical flow in the middle distance, to slow deep sub-critical flow in the foreground.

For a given rate of river flow, it is possible that water may move downstream as either a deep slow moving body (sub-critical flow) or as a shallow fast moving body (super-critical flow). The nature of the flow will be determined by the bed slope and channel frictional resistance. A change from sub-critical to super-critical flow may inhibit the overall river flow, since frictional forces play a greater retarding role in shallow channels with fast moving water. It is also important to know which flow regime is operating if sediment transport modelling is to be carried out. Sediment may be readily transported through super-critical reaches but be redeposited in sub-critical reaches of the river.

The software package GSTARS (Generalized Stream Tube model for Alluvial River Simulation) produced by the US Bureau of Reclamation (Yang and Simões, 2000) has proved successful in handling mixed flow regimes. This program can be described as a one-and- a-half dimensional model, since river flow is determined from a finite number of specified cross sections (fig.3.11).

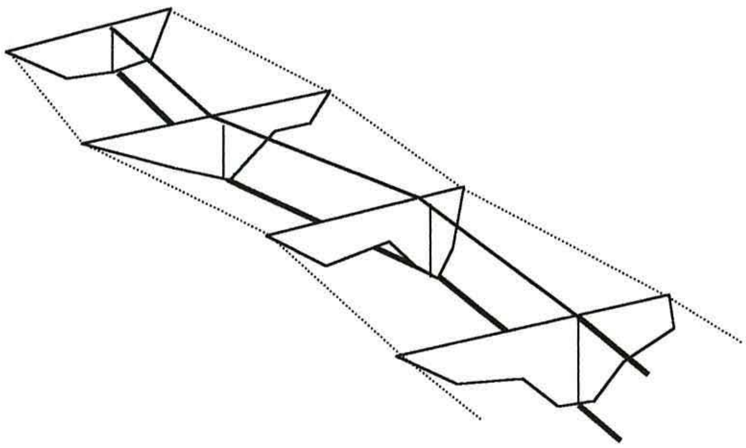

Figure 3.11: Schematic representation of the GSTARS model, with river flows determined from channel cross sections and river bed elevations at specified points

The river routing functions of HEC-1 and GSTARS are intended for modelling flows at discrete points along a river channel, so do not have the facility to map the extent of overbank flooding onto the floodplain area during storm events.

It was considered essential to predict overbank flood extent as an element of the flood prediction system for the Mawddach. To accomplish this, experiments have been carried out with the programs River2D (Steffler and Blackburn, 2002), and RMA2 (King et al.,1997) within the Surface Water Modelling System package. Both are finite element models which allow the channel and floodplain topography to be entered as an irregular triangulated grid (fig.3.12). The approach used by the programs is similar, employing the Navier-Stokes equation for turbulent flows, bed friction with Manning's equation, and eddy viscosity coefficients to define turbulence.

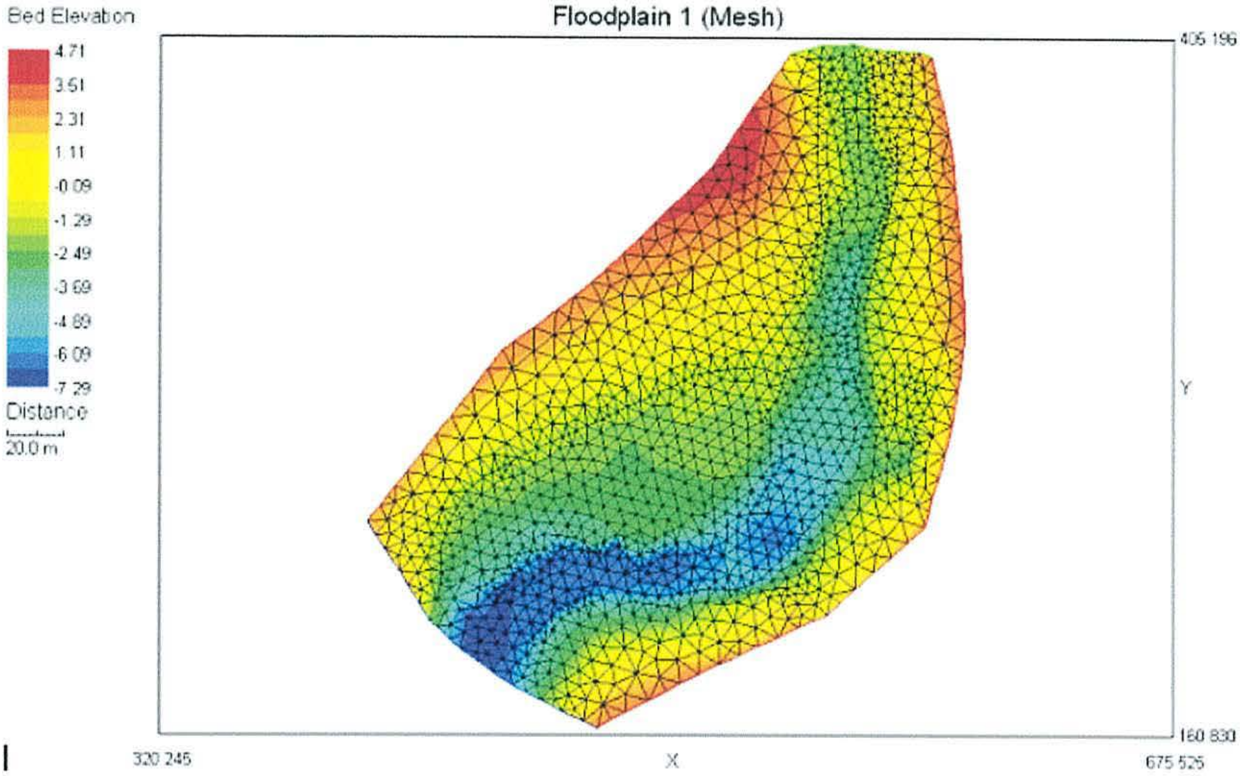

Figure 3.12: Finite element grid for the Mawddach floodplain at Tyddyn Gwladys, Coed y Brenin, developed with River2D

When simulating flood events, the software must be able to handle the wetting of additional surface elements as the water surface extends beyond the river banks and onto the flood plain. Changes to the boundary geometry of the river channel were found to produce mathematical instability in some RMA2 models, causing the model to fail without a solution. The River2D modelling code has a mechanism to link river levels to the groundwater profiles below adjacent hillslopes, and this has proved to produce more stable results.

The governing equation for the RIVER-2D program is the conservation of water mass:

$$\frac{\partial H}{\partial t}+\frac{\partial q_x}{\partial x}+\frac{\partial q_y}{\partial y}=0$$

where the term in H refers to the rate of change in hydraulic head as river level changes, and the terms in q are the discharge gradients in the coordinate directions x and y.

Beyond the channel margins, this equation is replaced by a groundwater equation

$$\frac{\partial H}{\partial t}=\frac{T}{S}\left(\frac{\partial^2}{\partial x^2}(H+z_b)+\frac{\partial^2}{\partial y^2}(H+z_b)\right)$$

in which T is transmissivity, a measure of the rate at which water can permeate through the geological formation, S is the storativity which determines the volume of water which can be held within a unit volume of the rock material, and zb is the ground surface elevation. Due to its mathematical stability, River2D is the preferred software option for modelling overbank flooding. Although intended for modelling river reaches of limited extent, River2D has also proved effective in modelling tidal flows within the Mawddach estuary.

An additional aspect of interest for the Mawddach river system is the movement of sediment during flood events, leading to accumulation around the town of Dolgellau and the head of the Mawddach estuary. Two software packages, GSTARS and CAESAR (Coulthard, 1999) for modelling sediment movement are discussed in section 3.3.

Summary

- The main components of a conceptual hydrological model for storm events in the Mawddach catchment are: surface runoff, lateral flow at shallow depth, transfer between surface water and groundwater stores, and river routing.
- Models will be required for hillslope hydrological processes, river routing and flow onto floodplains. Additionally, sediment transport during flood events is of importance to the study.
- Lumped parameter models are capable of predicting river discharge for different intensities and duration of storm rainfall. However, these models would not be adequate for modelling the areal extent of flooding within the catchment, and would be unsuitable for predictive studies which model changes in land use.
- The Kirkby topographic index can provide an effective way of predicting soil moisture content and the locations of surface runoff by using a digital elevation model for the catchment.
- Distributed models, in which hydrological parameters are specified for grid points across the catchment, provide a means of relating the mathematical model directly to aspects of topography, soil type and vegetation. The grid spacing possible for a distributed model will depend on the available computing capacity.
- Simple hillslope runoff-infiltration models will not adequately represent the short term storage and release of groundwater which occurs during and after storm events. Incorporation of a groundwater model may be necessary for adequate representation of flood processes.
- River routing within the Mawddach catchment must take account of variations in flow regimes of mountain streams.
- A floodplain model must be able to represent the changing boundary of the river channel as water spills over the river banks during flood events. This requires a stable system of differential equations within a finite element model.

3.2 Hillslope hydrology

In the following chapters, models are developed for different aspects of the hydrology of the Mawddach catchment. Instrumentation has been installed in six investigation areas within the catchment to provide data for calibration and verification of the models. The data collected may be split into two categories:

- Observations which directly provide parameter values for input to a model, for example: the river discharge at intervals during a storm event,
- Observations which do not directly link to model parameters but provide evidence against which model performance may be progressively refined, for example: the extent of surface saturation on a hillslope during a storm event.

The investigation areas, illustrated in fig.3.13, are:

1. **The upper basin of the Mawddach estuary**. Hydrographs have been recorded at the tidal limits of the rivers Mawddach and Wnion, and within the tidal estuary at Penmaenpool. These recordings are used to investigate river-tidal interactions and will be discussed further in *section 3.6: The Mawddach Estuary.*
2. **The central river system in Coed y Brenin**. A river gauging station is operated in Coed y Brenin by the Environment Agency, who have kindly made data available. The gauging station is at Tyddyn Gwladys, a short distance downstream from the confluence of the Afon Mawddach with its main tributary the Afon Gain. An additional river gauge was installed on the Afon Gain upstream of the confluence so that discharges for the Gain and upper Mawddach sub-catchments could be estimated separately.

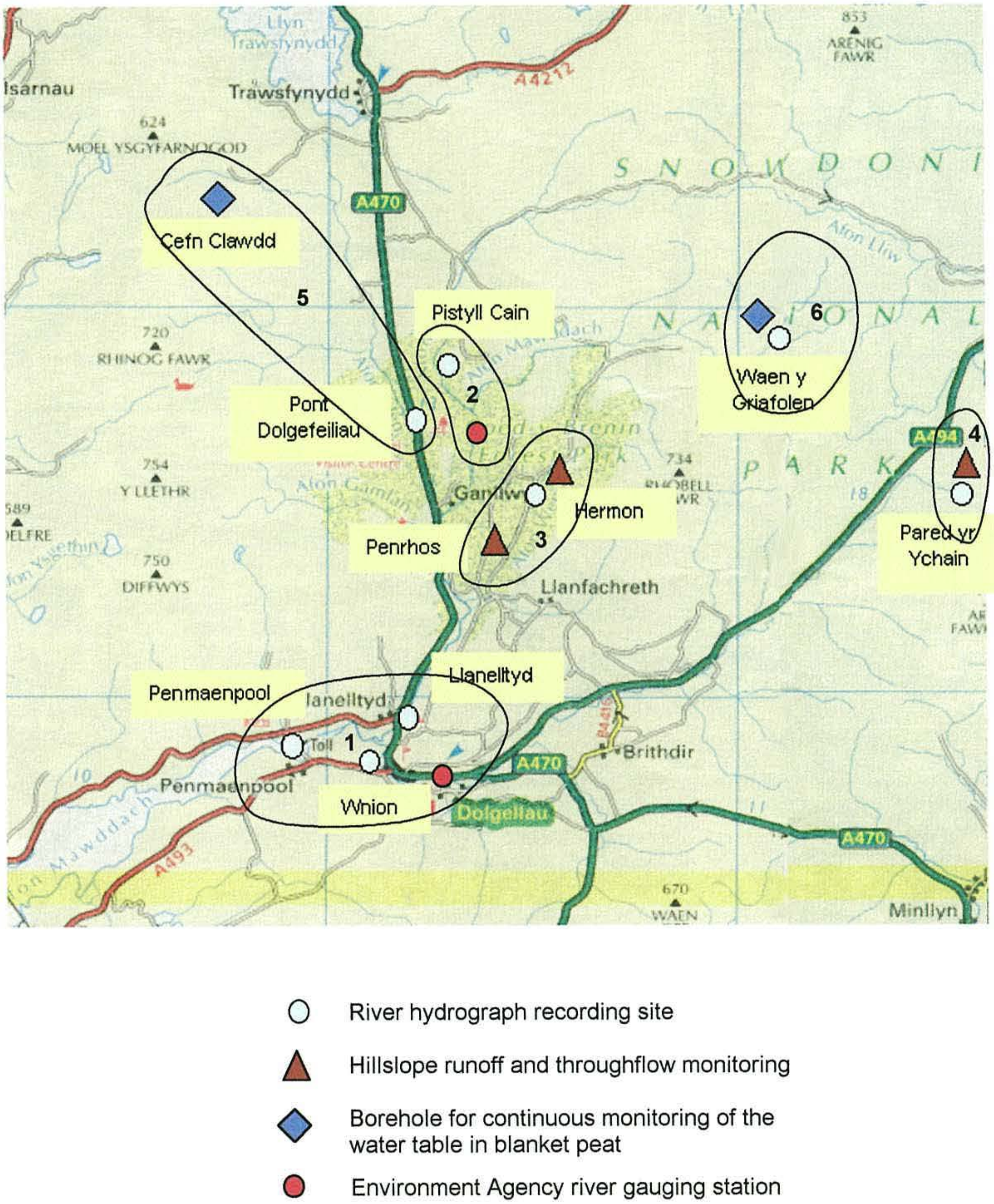

Figure 3.13: Experimental areas and hydrological recording sites

3. **The Afon Wen sub-catchment at Hermon**. The Afon Wen valley is typical of the deeply incised river gorges of Coed y Brenin which have extensive infill of glacial till and periglacial outwash and solifluction deposits. Surface runoff and soil throughflow monitoring sites have been established around the village of Hermon. Data is used to investigate the effects of antecedent drainage conditions on hillslope runoff during storm events . A river gauge has been operated at this location.
   River bed temperatures have also been monitored at Hermon to investigate river-groundwater interaction along the major fracture zone followed by the river. Results are discussed in *Section 3.4: River and floodplain processes.*
4. **Afon Wnion headwaters at Pared yr Ychain**. The Pared yr Ychain valley was selected as typifying the slopes of the Aran mountains which form the headwaters for the Afon Wnion. These slopes are largely covered by glacial till. Surface runoff and soil throughflow monitoring sites were established to investigate hillslope responses during storm events. A river gauge has been operated on the Afon Ty Cerrig at this location.
5. **Afon Eden headwaters at Cefn Clawdd**. The Cefn Clawdd valley was selected as typical of the Afon Eden headwaters of the Trawsfynydd plateau. This area is covered by blanket peat. A borehole was installed for water table monitoring; observations from the site are discussed in *Section 3.5: Peat blanket bogs.* A river gauge has been operated at Pont Dolgefeiliau where the Afon Eden flows south from the Trawsfynydd plateau.
6. **Source of the Mawddach at Waen y Griafolen**. The Mawddach has its source in an extensive peat basin which has been the subject of detailed hydrological monitoring. This work is also discussed in *Section 3.5: Peat blanket bogs.* A river gauge has been operated on the outlet stream from the peat basin.

Tyddyn Gwladys gauging station

A river gauging station is operated by the Environment Agency on the Afon Mawddach at Tyddyn Gwladys in the Coed y Brenin forest (fig.3.14). Flow is measured on a gravel plane-bed reach which has been artificially straightened to reduce turbulence and lateral variations in flow rate. Water depths are measured by float recorder in a stilling well. Calibration of river discharge against stage height is carried out by a propeller flow meter which traverses the river, suspended from a cable. A typical hydrograph of readings for the period September 2002 to July 2003 is shown in fig.3.15. Detailed data sets with 15min reading intervals have been provided by the Environment Agency for storm events of special interest:

- 3 July 2001
- 8 November 2002
- 29 December 2002
- 8 March 2003
- 22 May 2003
- 3-4 February 2004

These hydrographs are illustrated in fig.3.16(a)-(f).

Figure 3.14: Tyddyn Gwladys river gauging station

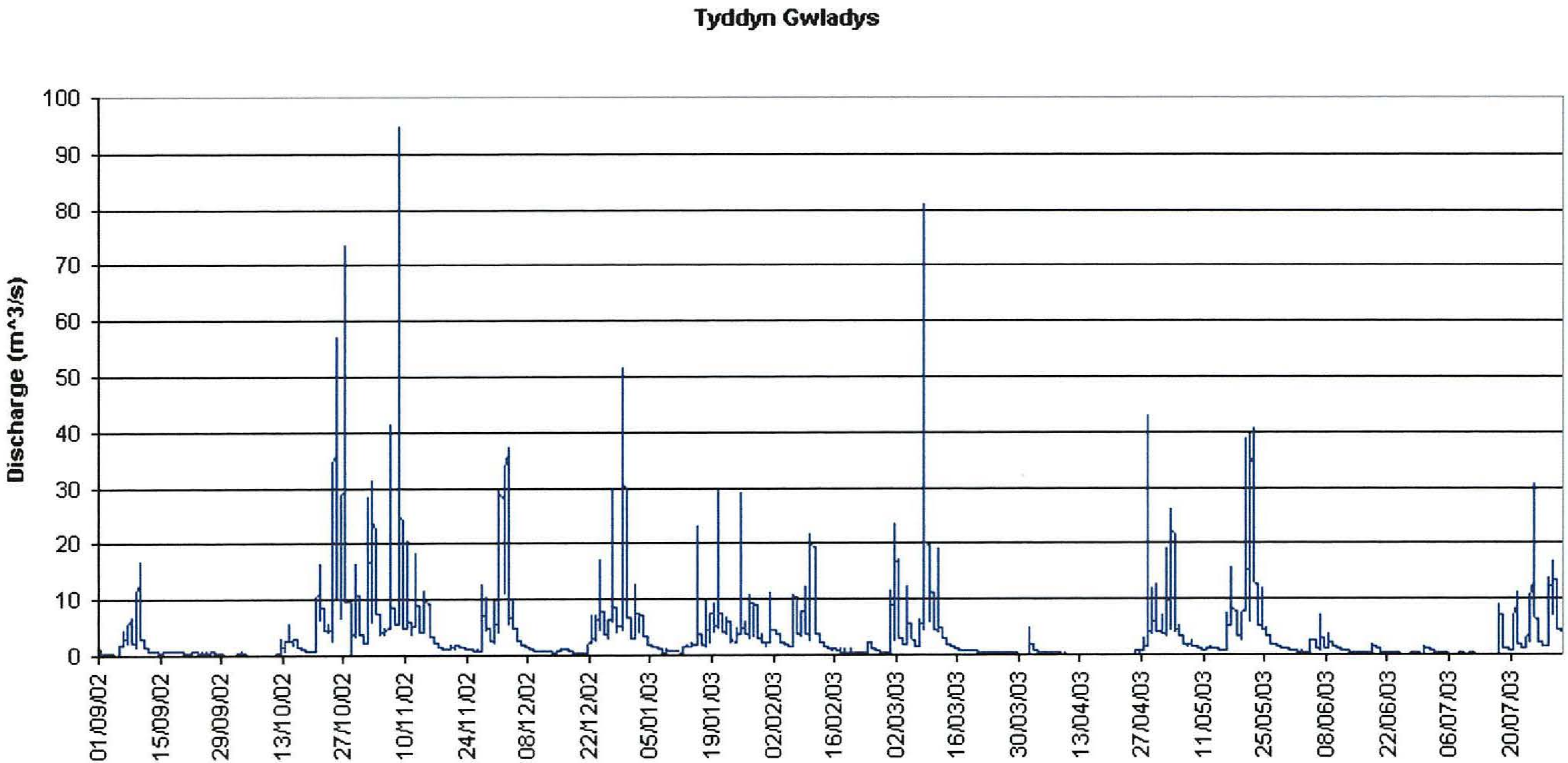

Figure 3.15: Readings for Tyddyn Gwladys river gauging station, Afon Mawddach, for the period September 2002 to July 2003

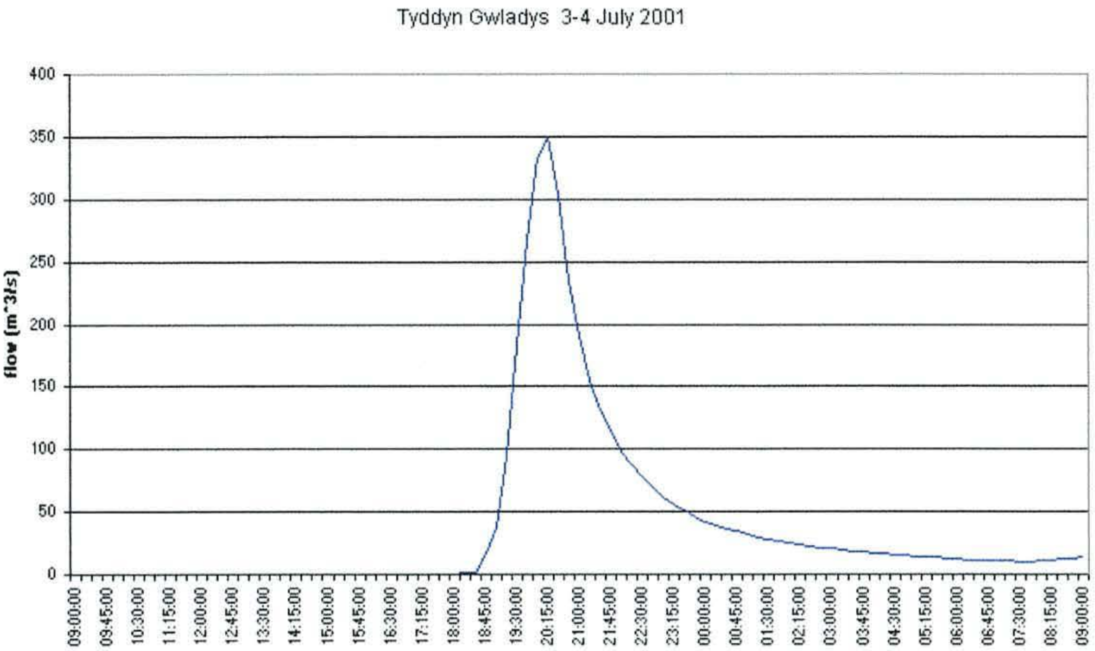

Figure 3.16(a). Hydrograph for the storm event of 3 July 2001, Tyddyn Gwladys

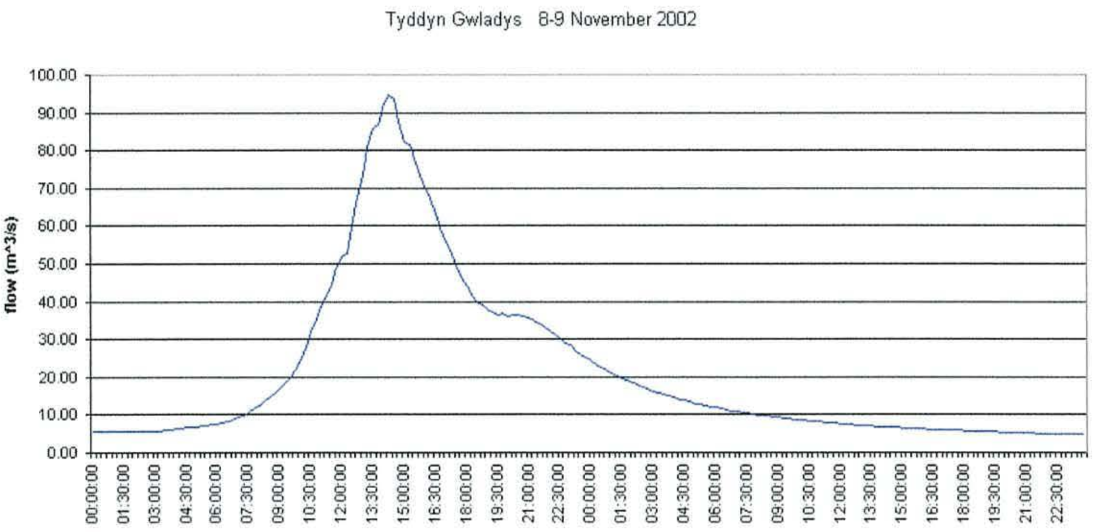

Figure 3.16(b). Hydrograph for the storm event of 8 November 2002, Tyddyn Gwladys

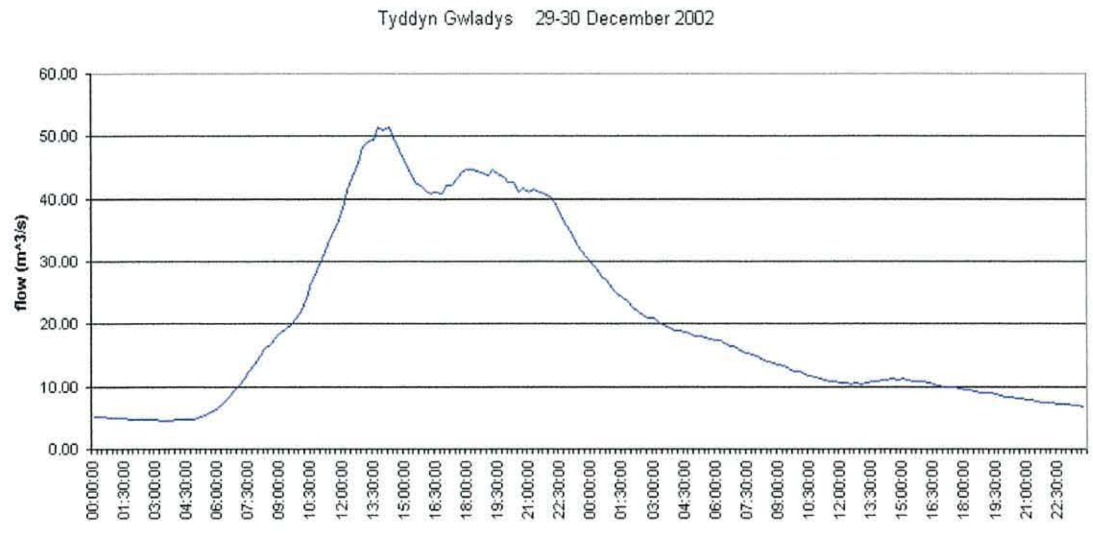

Figure 3.16(c). Hydrograph for the storm event of 29 December 2002, Tyddyn Gwladys

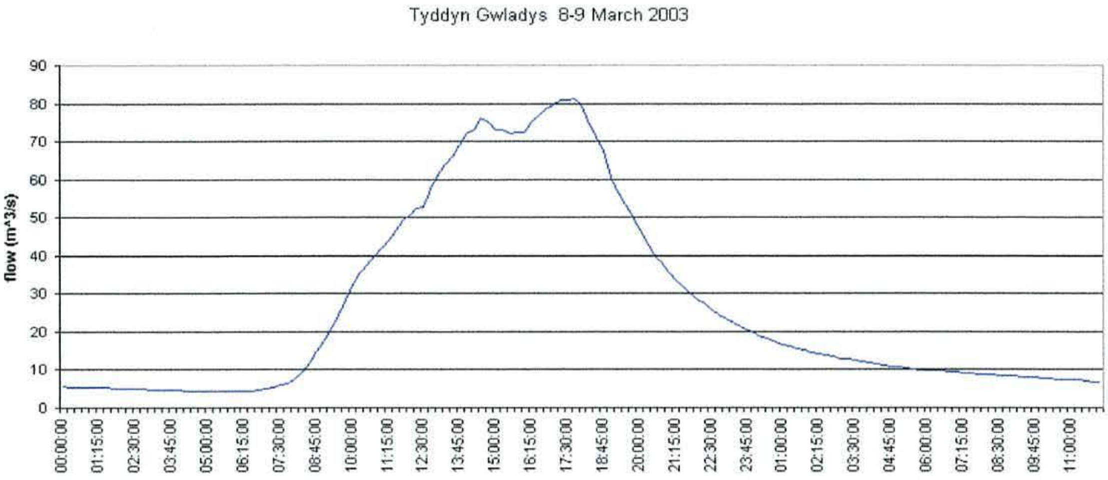

Figure 3.16(d). Hydrograph for the storm event of 8 March 2003, Tyddyn Gwladys

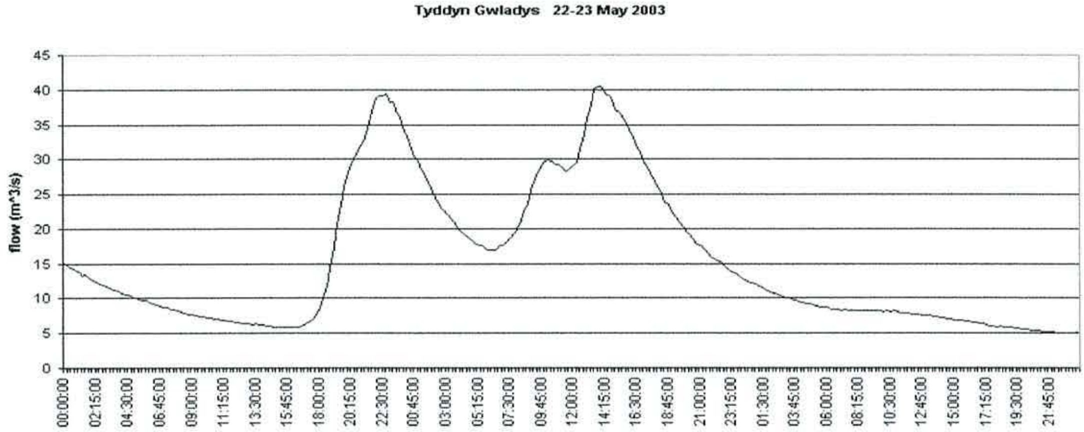

Figure 3.16(e). Hydrograph for the storm event of 22 May 2003, Tyddyn Gwladys

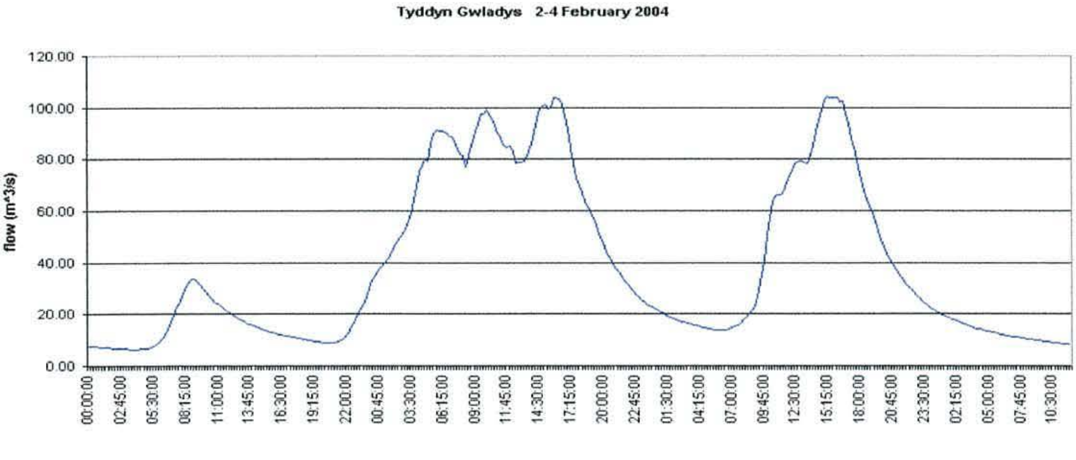

Figure 3.16(f). Hydrograph for the storm event of 3-4 February 2004, Tyddyn Gwladys

The July 2001, November 2002, December 2002 and March 2003 events represent isolated periods of intense rainfall, whereas the May 2003 and February 2004 events represent flooding at the culmination of a sequence of heavy rainfall periods.

Subcatchments and river reaches

For the purpose of hydrological modelling, the Mawddach and Wnion basins above the tidal limits have been divided into a number of subcatchments, each representing a reach of the trunk stream. The twelve reaches of the Mawddach are shown in fig.3.17, and the eight reaches of the Wnion are shown in fig.3.18. The hillslope hydrological characteristics and the nature of the river channels are described further in Appendix B.

Figure 3.17: Mawddach sub-catchments and river reaches

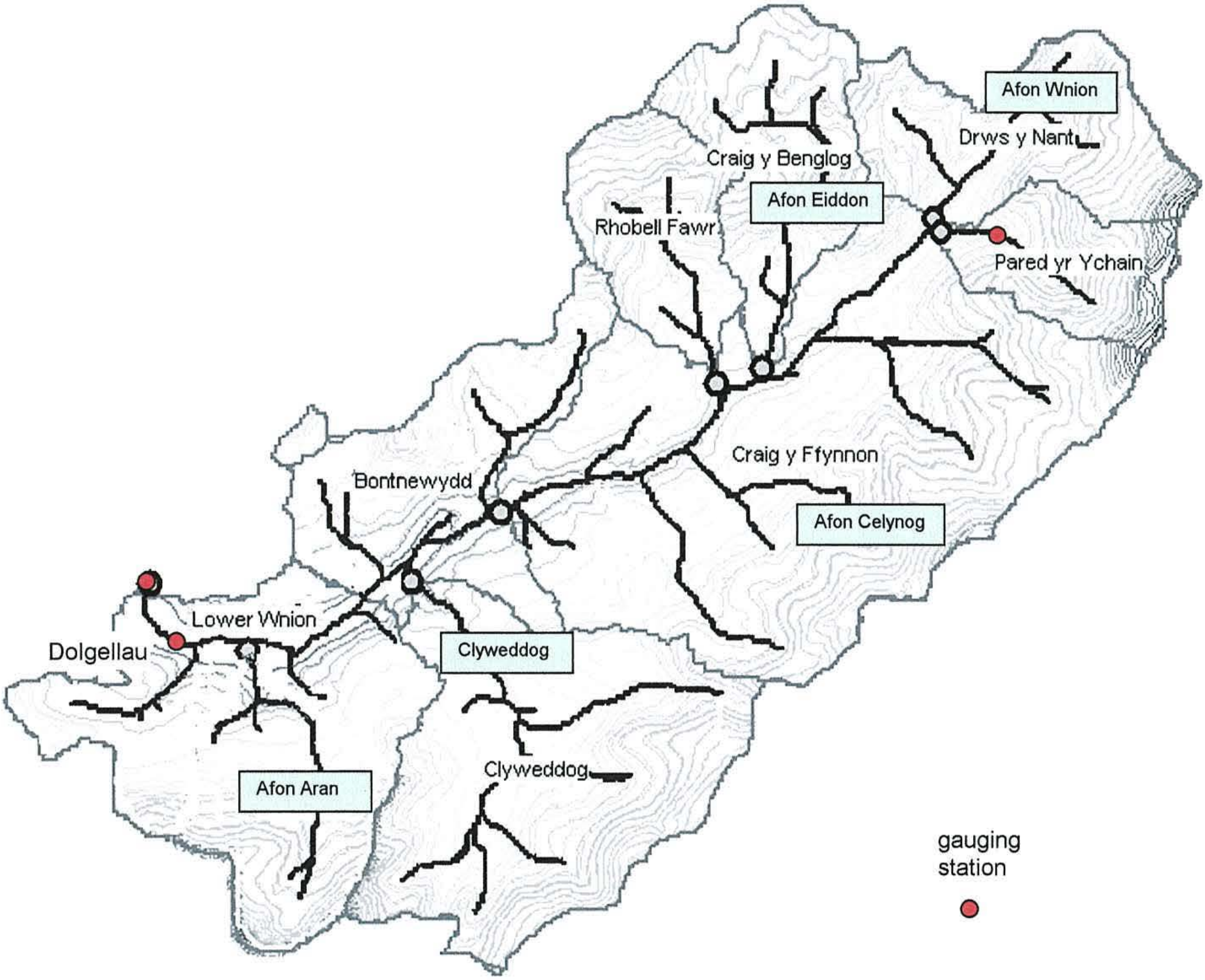

Figure 3.18: Wnion sub-catchments and river reaches

River channel surveying

Calibration of hydrograph sites and modelling of both river routing and sediment transport required the accurate surveying of channel cross profiles at many points throughout the river system. Between 3 and 9 cross-section sites were selected within each of the sub-catchments described in the previous section. The number of cross-sections needed to adequately record channel geometry over the whole river reach was determined by the variability in channel form. At each cross-section site, a survey was carried out by levelling up to points well above any expected flood stage. River bed and bank sediment characteristics were recorded. An estimate of water surface gradient at bankfull discharge was obtained by levelling between the highest points on the banks showing evidence of flood erosion or deposition along the river course.

Figure 3.19: Surveying the channel cross section, Afon Gain

Examples of surveyed sections for the Eden subcatchment, and the Llanelltyd subcatchment of the lower Mawddach, are shown in figs 3.20 and 3.21.

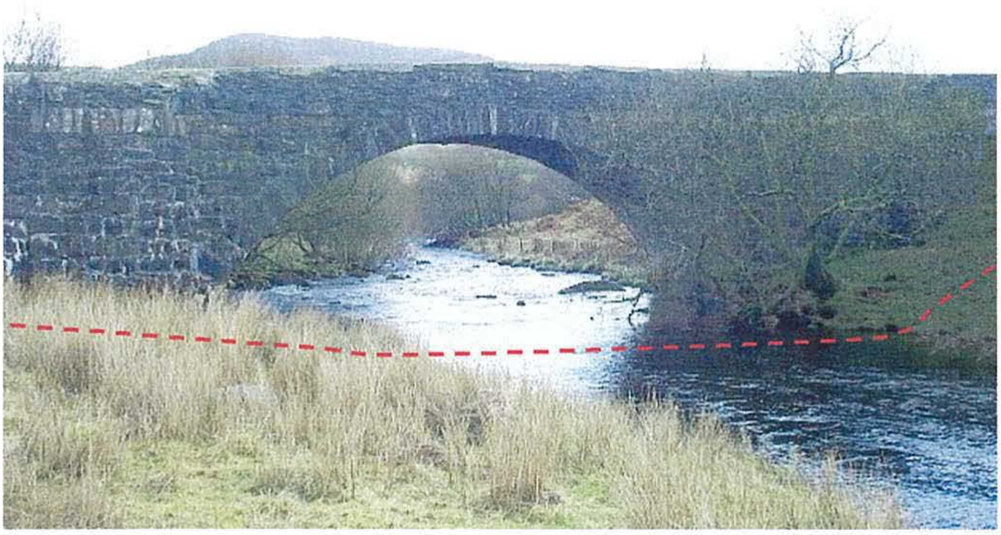

Figure 3.20(a)
(above)
Line of cross section surveyed at Pont y Grible, Afon Eden

(below)
Cross section at Pont y Grible

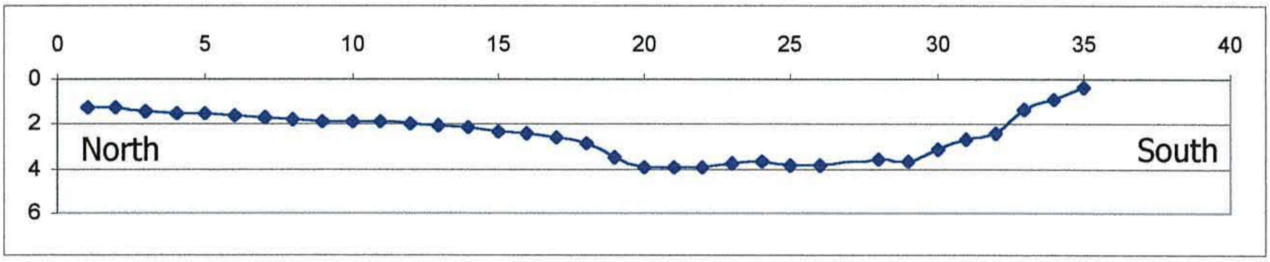

Figure 3.20(b)
(above)
Line of cross section surveyed at Pont Dolgefeiliau, Afon Eden

(below)
Cross section at Pont Dolgefeiliau

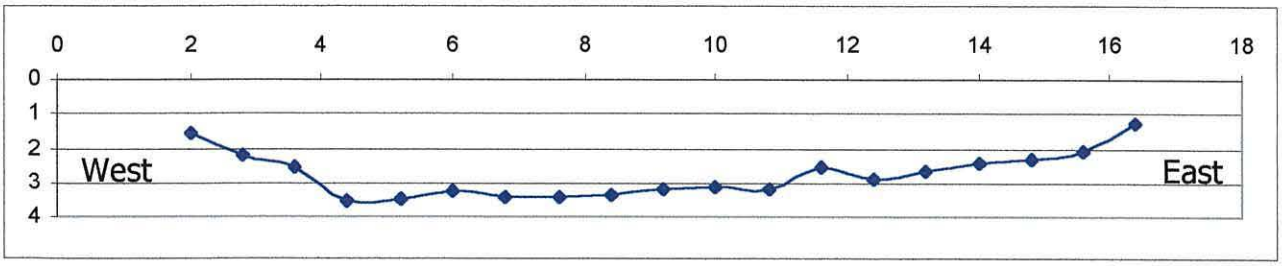

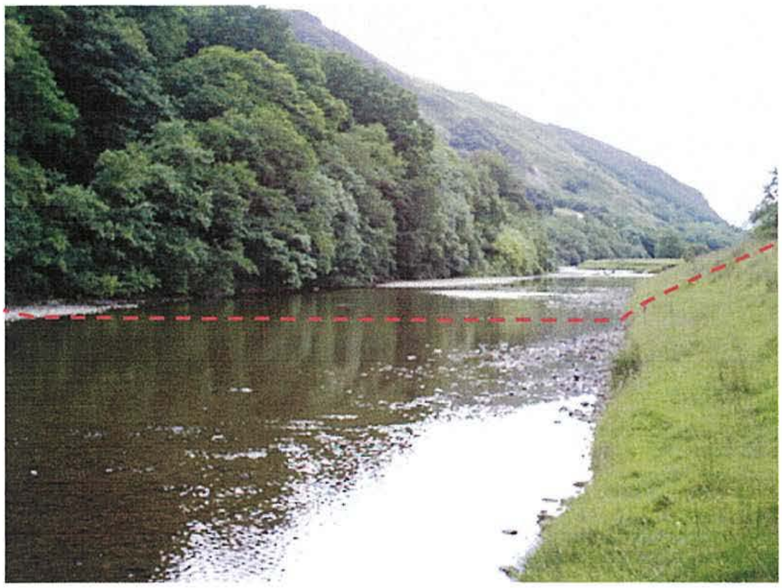

Figure 3.21(a)
(above)
Line of cross section surveyed on the Afon Mawddach north of Cymmer Abbey, Llanelltyd.
photo: Lydia Yates

(below)
Afon Mawddach cross section north of Cymmer Abbey.

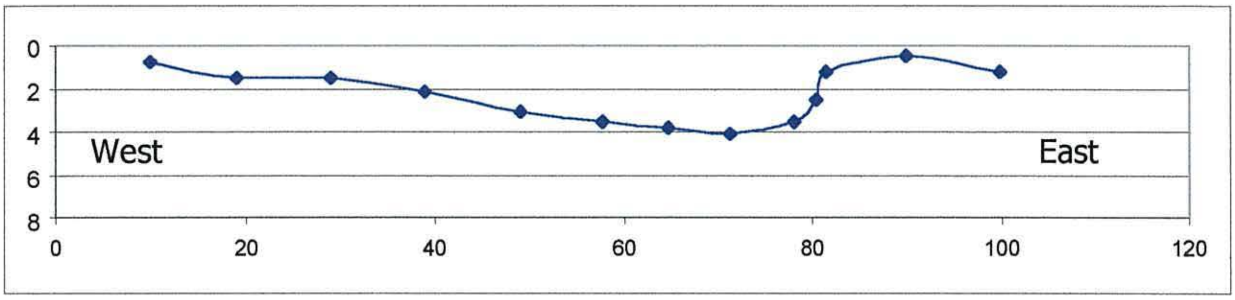

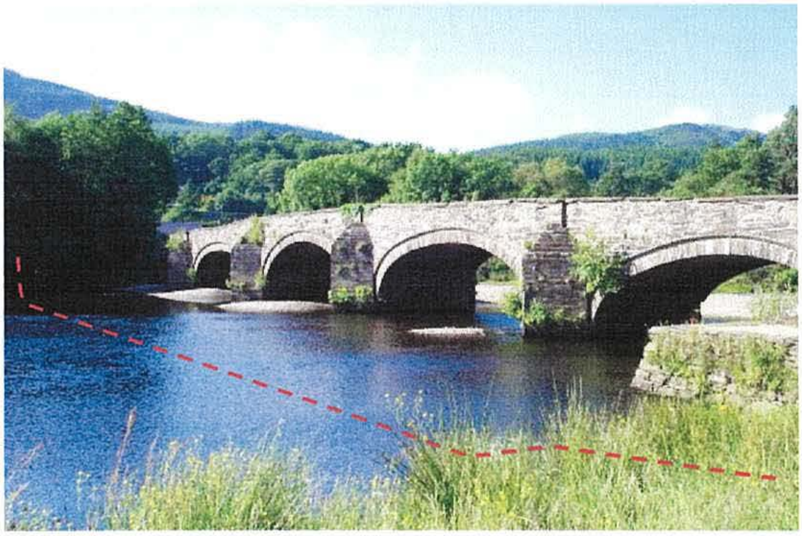

Figure 3.21(b)
(above)
Line of cross section surveyed at Llanelltyd Bridge, Afon Mawddach.

(below)
Cross section at Llanelltyd Bridge.

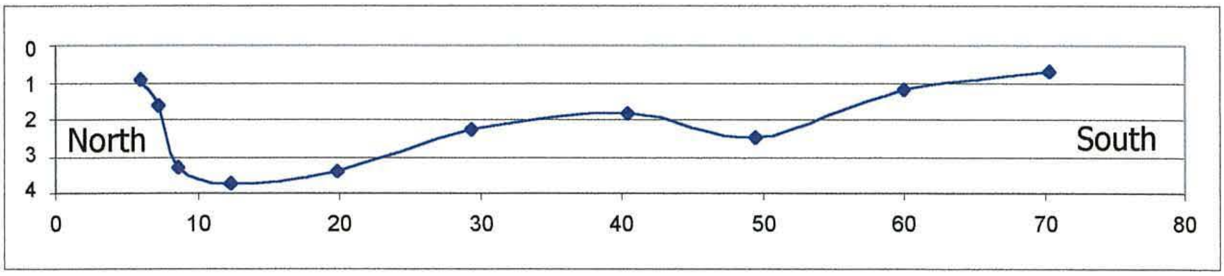

Hydrograph recording

Prior to this project, only one river gauging site existed at Tyddyn Gwladys on the Mawddach, run by the Environment Agency. Additional hydrograph recording sites were required for river flow data in the Mawddach and Wnion catchments.

The flash flood regimes of the Mawddach river system present severe problems for flow measurement. Binnie and Partners (1985) report that two gauging stations have operated for short periods on the Afon Eden, one upstream of Pont Dolgefeiliau and the other near Ganllwyd. The Pont Dolgefeiliau site was taken out of use after blockage of the stilling well by river sediment, and the data from the Ganllwyd site was considered too inaccurate for publication.

Figure 3.22: The Ganllwyd reach of the Afon Mawddach during low flow and flood conditions.

Practical difficulties in flow measurement may be appreciated by considering fig.3.22 which shows the Ganllwyd reach of the Afon Mawddach during low flow and flood conditions:

- Water levels may rise by 2m or more during flood flow, making it impossible to measure flows manually by entering the river.
- Even where river depths remain relatively shallow during flooding, the water flow can considerably exceed the $2ms^{-1}$ velocity considered to be a safe limit for working in the river.
- Overbank flooding is common, making access to the main channel hazardous during storm events.

Despite these problems, it was considered worthwhile to collect as much flow data as possible from different parts of the river system. Hydrographs were constructed as best-estimates for particular sites, ensuring that these were consistent with overall river flows within the catchment.

Gauges were installed at a series of sites on the Mawddach-Wnion system to provide continuous logging of water depth. Assistance was received from Malcolm Murgatroyd, electronics engineer in Dolgellau, who designed and constructed a number of portable instruments (fig.3.23). These use a pressure sensor, secured to the river bed and connected by heavy duty cable to a module on the river bank housing electronic circuitry, battery power supply and a data logger. Water depth is measured as a function of hydrostatic pressure, with the instrument design compensating for variations in water temperature and atmospheric pressure which might affect river bed readings. In tests at four different river sites under widely differing flow conditions, it was found that water depths were consistently recorded to an accuracy better than 1cm. This level of accuracy was considered adequate for recording on upland streams of steep gradient, where turbulence commonly produces surface oscillations of amplitude 1cm or more. These sites were operated as 'rated sections' and calibrated for river flow as described below.

Recorders were operated during the project (fig.3.13) at:

- Pont Dolgefeiliau, on the Afon Eden
- Pont Gwynfynydd, on the Afon Gain
- Hermon, on the Afon Wen
- Pared yr Ychain, on the Afon Ty Cerrig.
- Llanelltyd, at the tidal limit of the Afon Mawddach
- Pont y Wern Ddu, at the tidal limit of the Afon Wnion
- Penmaenpool bridge, in the upper estuary

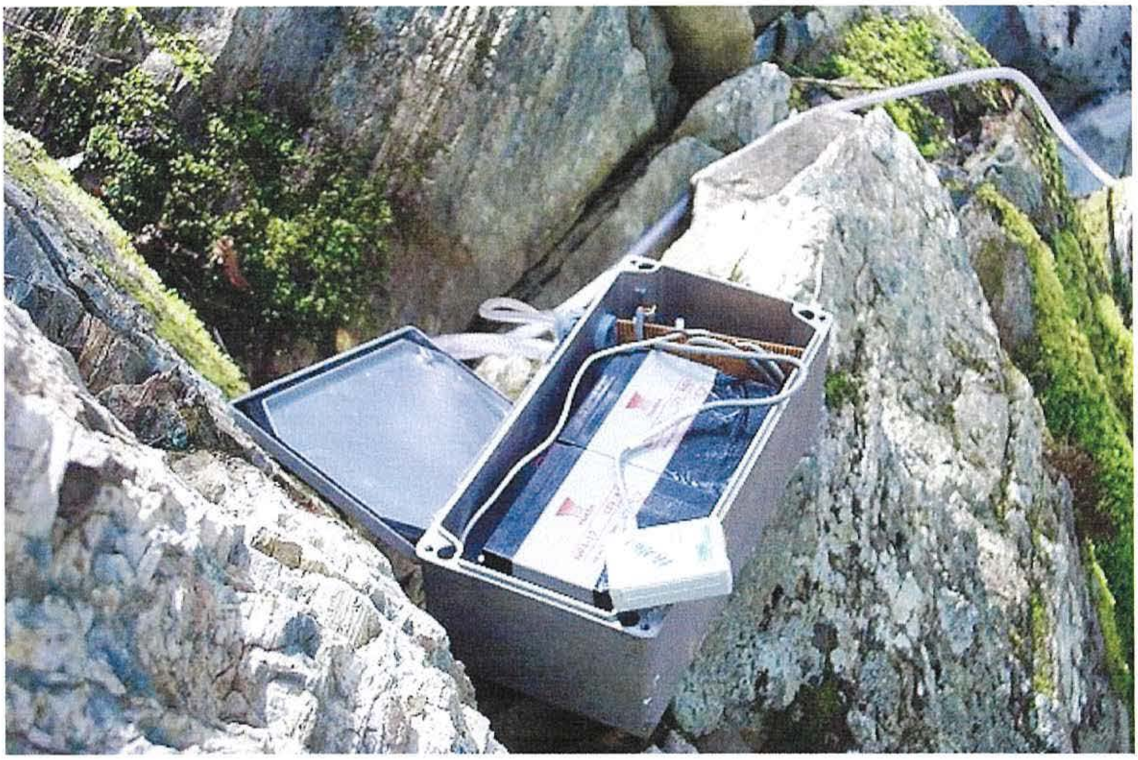

Figure 3.23: Barometric water depth recorder

An example set of water depth recordings is shown in fig.3.24 for the Pont Dolgefeiliau site over the period December 2002 to April 2003. This is based on measurements made at 5min intervals, so the timing of flood peaks may be considered precise.

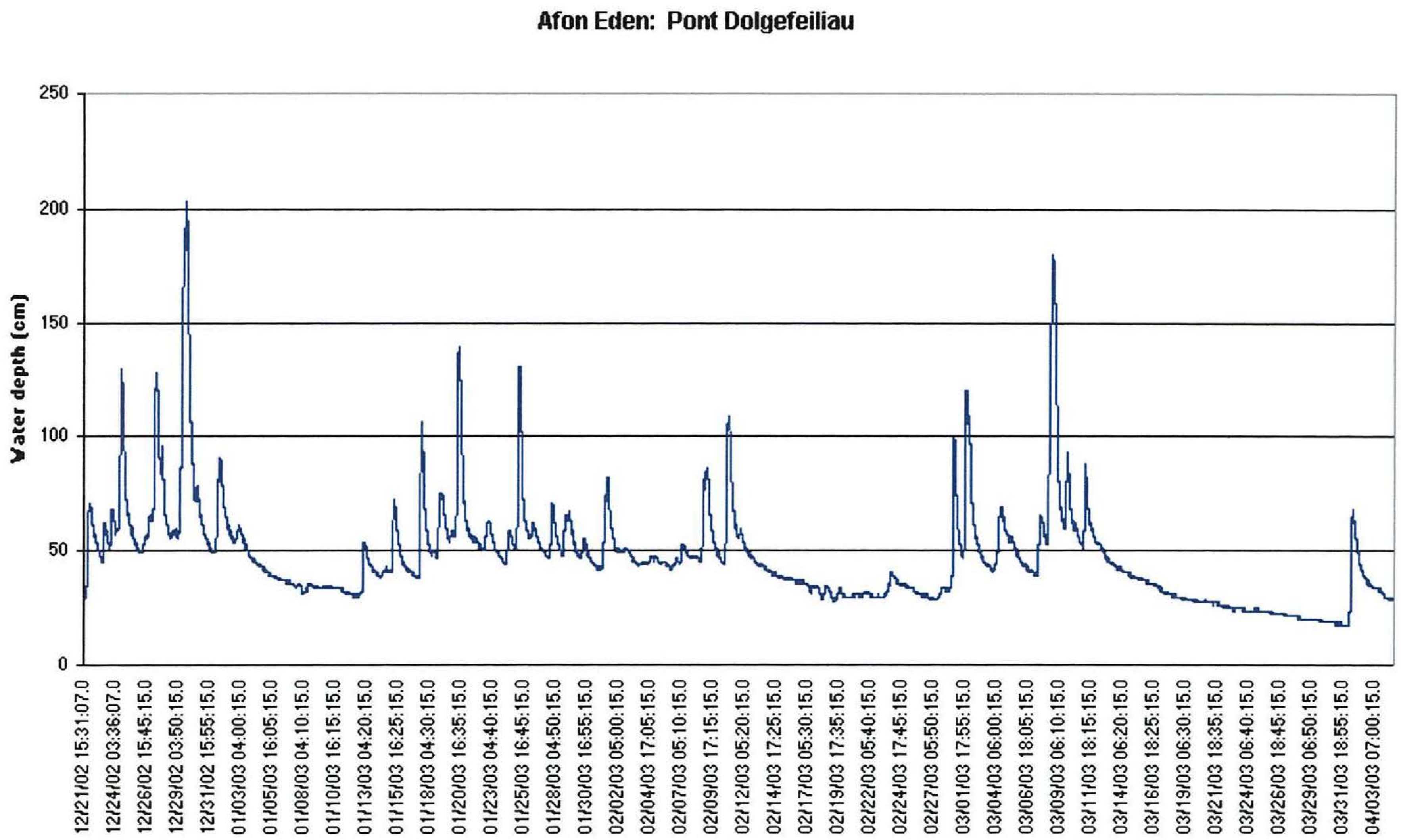

Figure 3.24: Water depth recordings for the Pont Dolgefeiliau site over the period December 2002 to April 2003.

Calibration of river discharge in terms of water depth was carried out by:

- Accurately surveying the channel cross section at the location of the depth recorder,
- Measuring water flow rates at points across the channel during different flow conditions, using a propeller flow meter (fig.3.25).
- Computing river discharge as a product of cross sectional area and flow rate.

Figure 3.25: Propeller flowmeter used in hydrograph site calibration

Under low flow conditions, it was possible to enter the river channel and make a series of flow measurements at measured positions across the channel.

Under flood conditions it was not safe to enter the rivers, so flow measurements were made with the propeller attached to a long metal pole extended from the bank (fig. 3.26). Flow rate was determined by integration over a 10 second interval to reduce perturbations due to turbulence. Three flow measuring points were chosen, which were measured as the centre and quarter-width points of the channel. Flow measurement made at an estimated quarter-depth from the surface. A mean flow velocity for the current river stage was obtained by averaging these values.

Figure 3.26:
(left) Flow meter in position above the river channel.
(below) Flow velocity measurement in progress

Calibration data for the hydrograph sites is given in Appendix D. The calibrations obtained from flow data are imprecise for a number of reasons:

- Velocity measurements were obtained mainly during low to moderate flow conditions. Adequate data for high flow conditions were difficult to obtain, due to problems in reaching hydrograph sites during the brief intervals of maximum flood discharge, and the difficulty of accessing central sections of the channel when river width was increased during flood conditions.

- Water surface gradient will be elevated upstream during the period of a rising hydrograph and depressed upstream during the period of a falling hydrograph. Flow velocities may therefore vary for the same river depth between the rising and falling limbs of the storm hydrograph due to water surface gradient.
- Sediment processes may significantly influence water velocities. Fig.3.27 illustrates the variability in suspended sediment between flood events on the Afon Eden at the Pont Dolgefeiliau gauging site. A first storm flow after an extended period of dry weather may pick up large quantities of silt and sand grade material from the channel bed and remove this from the river system, leaving a clean gravel bed with different frictional resistance characteristics during subsequent flood events.
- In a mountain stream regime with a predominantly gravel-cobble bedload, significant changes to bed profile may occur during individual flood events due to erosion or deposition.

To augment the measurements of high flow rate and to reduce the errors from field observations, additional theoretical calculations of flood discharge velocities were carried out using two methods, Manning's equation and the Relative Depth method.

Manning's equation:

Bankfull discharge Q is calculated from:

$$Q = \frac{1}{n} A r^{2/3} s^{1/2}$$

where A = cross sectional area at bankfull stage

r = cross sectional area / wetted perimeter

s = water surface downstream slope

n = Manning's roughness coefficient

Suitable values for roughness coefficient **n** can be obtained by comparison of the hydrograph sites with illustrations of calibrated mountain streams provided by Barnes (1967), and Arcement and Schneider(2003) .

8.30am, 07 August 2001

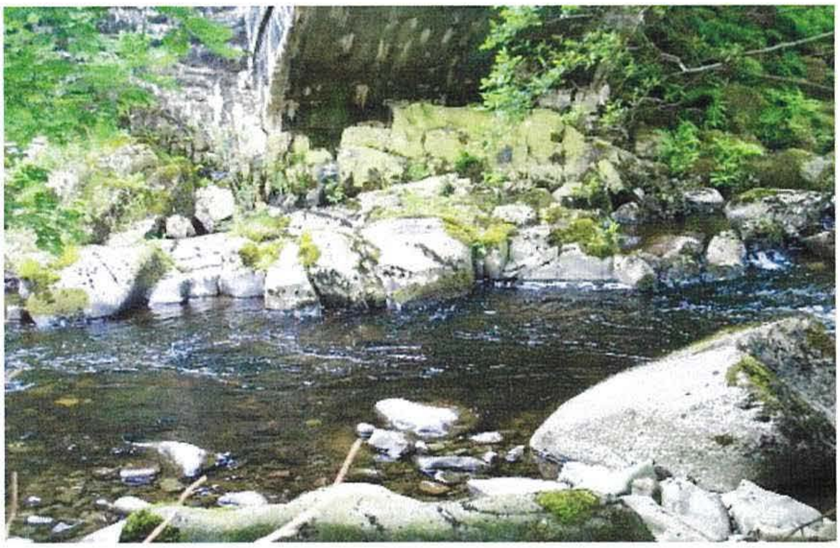

8.30am, 10 August 2001

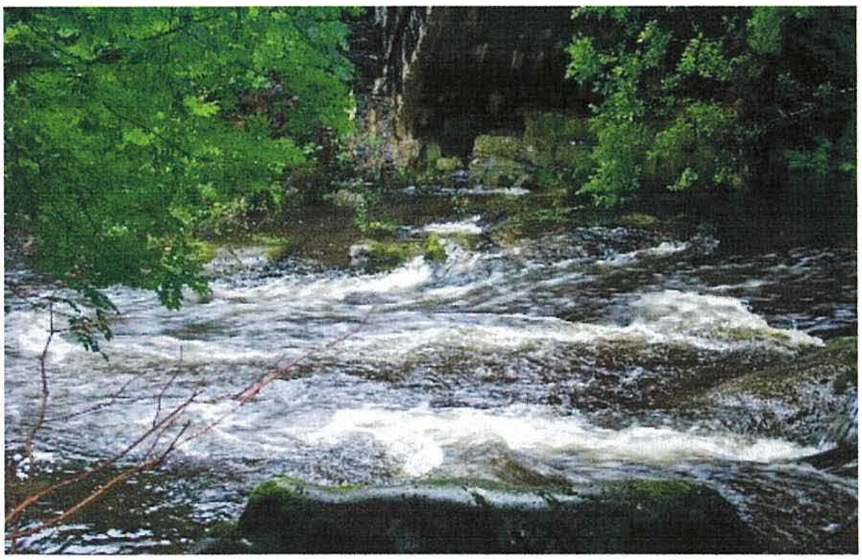

8.30am, 12 August 2001

Figure 3.27: Example water flows at different river stages, Pont Dolgefeiliau, Afon Eden

Relative depth method (Pethick, 1980):

The channel relative depth F is calculated as:

$$F = \frac{D}{B}$$

where D = average water depth at bankfull

B = average bedload size

A roughness factor R is obtained from the channel relative depth value, using the logarithmic relationship:

$$R = 0.95 \ln(F) + 0.95$$

Bankfull mean velocity is then calculated as

$$V = 8.86\sqrt{D.s.R}$$

where s = water surface downstream slope at bankfull

Determination of water surface downstream slope at bankfull has been relatively easy for the Mawddach river system, as evidence of maximum water levels during the 3 July 2001 flood event is extensively preserved. This evidence includes: debris accumulations (fig.3.28), deposition of sand and gravel on riverbank ledges, and scouring of moss, lichen and bark from trees adjacent to the channel.

Figure 3.28: Debris accumulations around trees, providing evidence of maximum water levels during the July 2001 flood, Afon Mawddach, Gwynfynydd

The methodology for calibration of the hydrograph recording sites equipped with portable water depth recorders was:

- Determine river discharge as a function of water depth under a range of flow conditions by field measurements. Between 9 and 12 sets of flow measurements were obtained at each hydrograph site.
- Determine bankfull depth and compute bankfull discharge using both Manning's equation and the Relative depth method. In practice, these methods were found to agree within 10%.
- Produce provisional calibration curves for the hydrograph sites as a best fit to the observed and calculated discharge values.
- Check the discharge values for consistency across the catchment during the six test flood events. There is a requirement that water volumes are conserved during passage through the river system, allowing for reasonable inflows and river/groundwater interactions.
- If anomalies were identified which appeared to contradict the conservation principle, then minimal adjustments to the calibration curves were allowed: The Environment Agency Tyddyn Gwladys gauging station was considered to be providing accurate discharge values. Storm hydrograph peak flows at sites using portable water depth recorders were required to be consistent with the flows at Tyddyn Gwladys.

After analysis of the test storm events, calibrations were achieved which were considered internally consistent and adequate for use in rainfall-runoff modelling.

Hydrograph sites

Afon Gain

Site description

A hydrograph recorder has been situated in the waterfall pool (fig.3.29) approximately 1km upstream from Pistyll Cain. Flow is measured at the outlet from the pool where the channel is constrained between rock outcrops. Access to the river is from the east bank, with flow measurement possible during low water and flood stages. The channel represents a bedrock reach, with isolated bed cover of cobbles and boulders of 0.5m to 1m median dimension.

Figure 3.29: Afon Gain hydrograph recording site. The recorder is located on the river bed at point A.

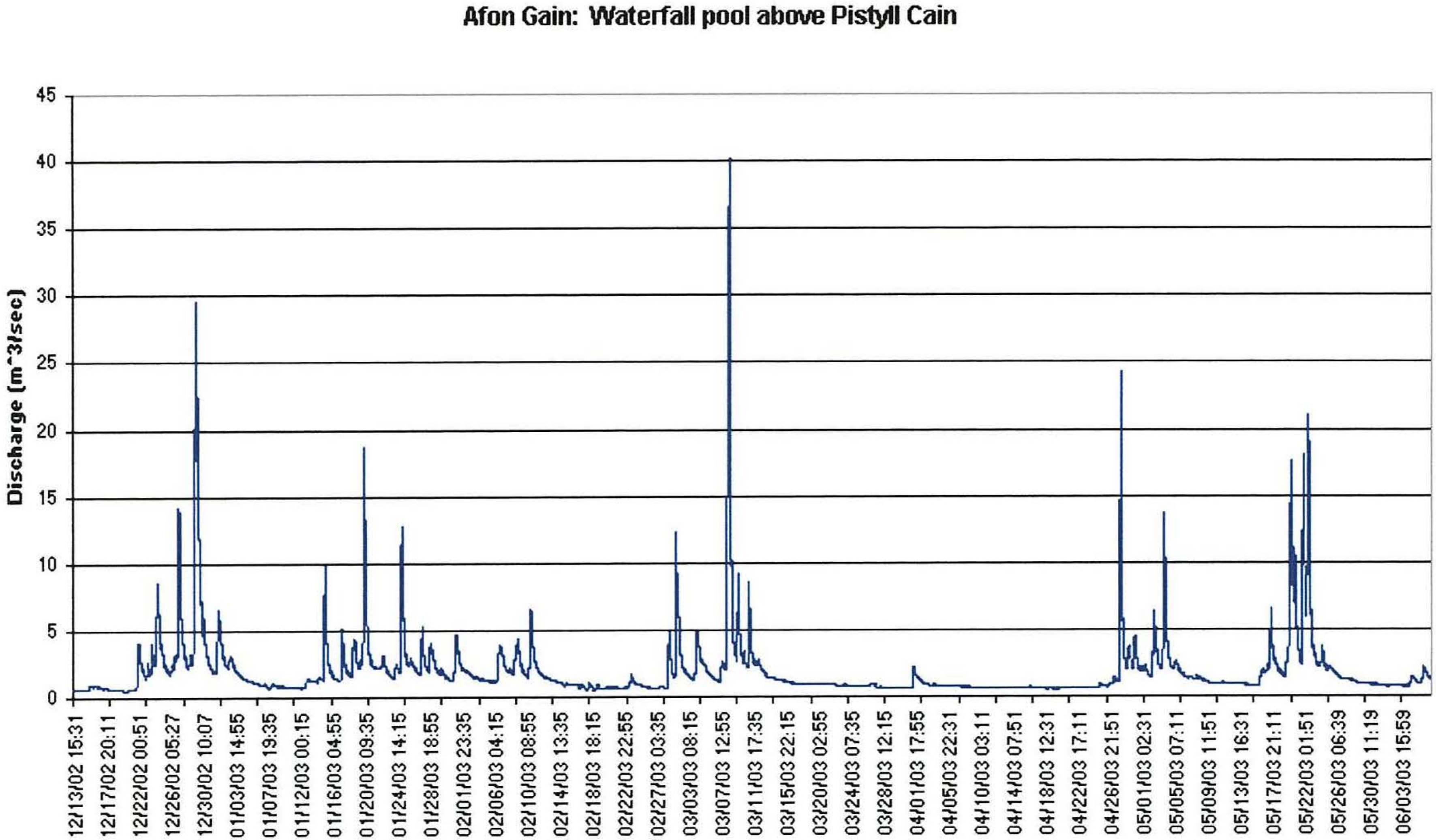

Figure 3.30: Example stage-discharge chart for the Afon Gain hydrograph recording site for the period December 2002 – May 2003.

Pont Dolgefeiliau, Afon Eden

Site description

A hydrograph recorder has been situated approximately 20m downstream from Pont Dolgefeiliau (fig.3.31). Access for the measurement of flow velocities is possible from either bank, except during high flood conditions when the river extends onto the flood plain on both sides. The channel forms a plane bed reach on bedrock, with more than 90% cover of coarse gravel and cobbles in the range 0.1m to 0.5m median dimension.

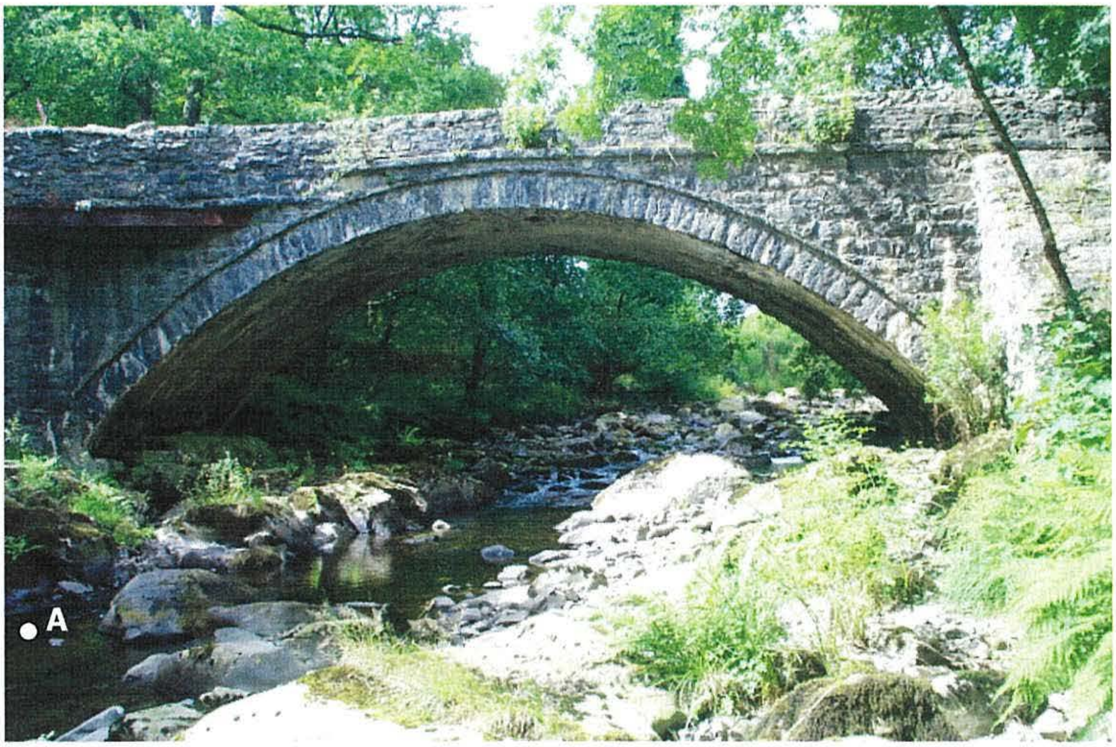

Figure 3.31: Afon Eden hydrograph recording site. The recorder is located on the river bed at point A.

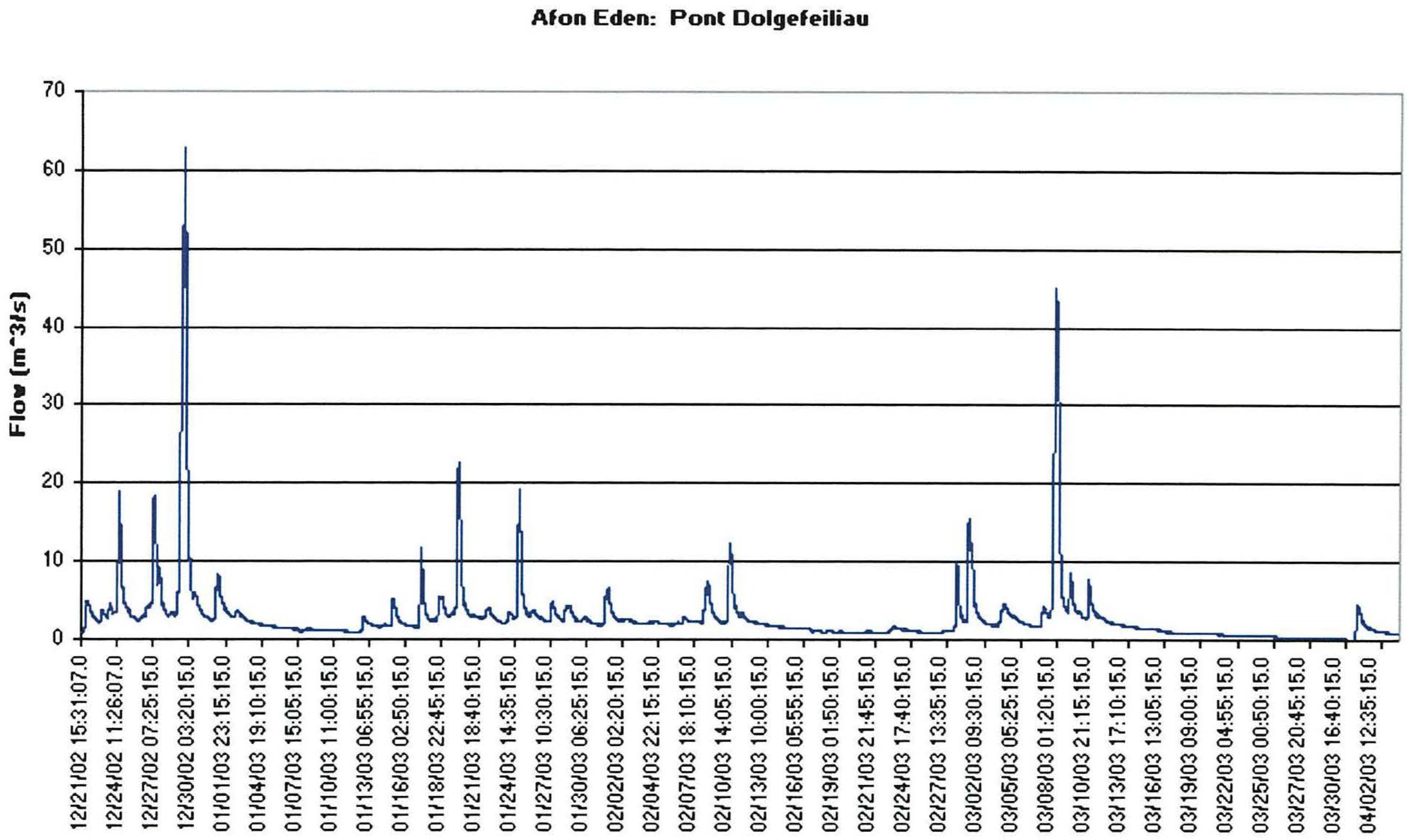

Figure 3.32: Example stage-discharge chart for the Afon Eden hydrograph recording site for the period December 2002 – April 2003

Afon Wen

Site description

A hydrograph recorder has been situated in the waterfall pool (fig.3.33) approximately 0.5km downstream from the village of Hermon. Flow is measured at the outlet from the pool where the channel is constrained between rock outcrops. Access to the river is from the east bank, with flow measurement possible during low water and flood stages. The channel represents a step pool reach, with bed cover of cobbles of 0.1m to 0.5m median dimension.

Figure 3.33: Afon Wen hydrograph recording site. The water depth recorder is located in the pool at location A. Flow is measured at the pool outlet along the section shown in red.

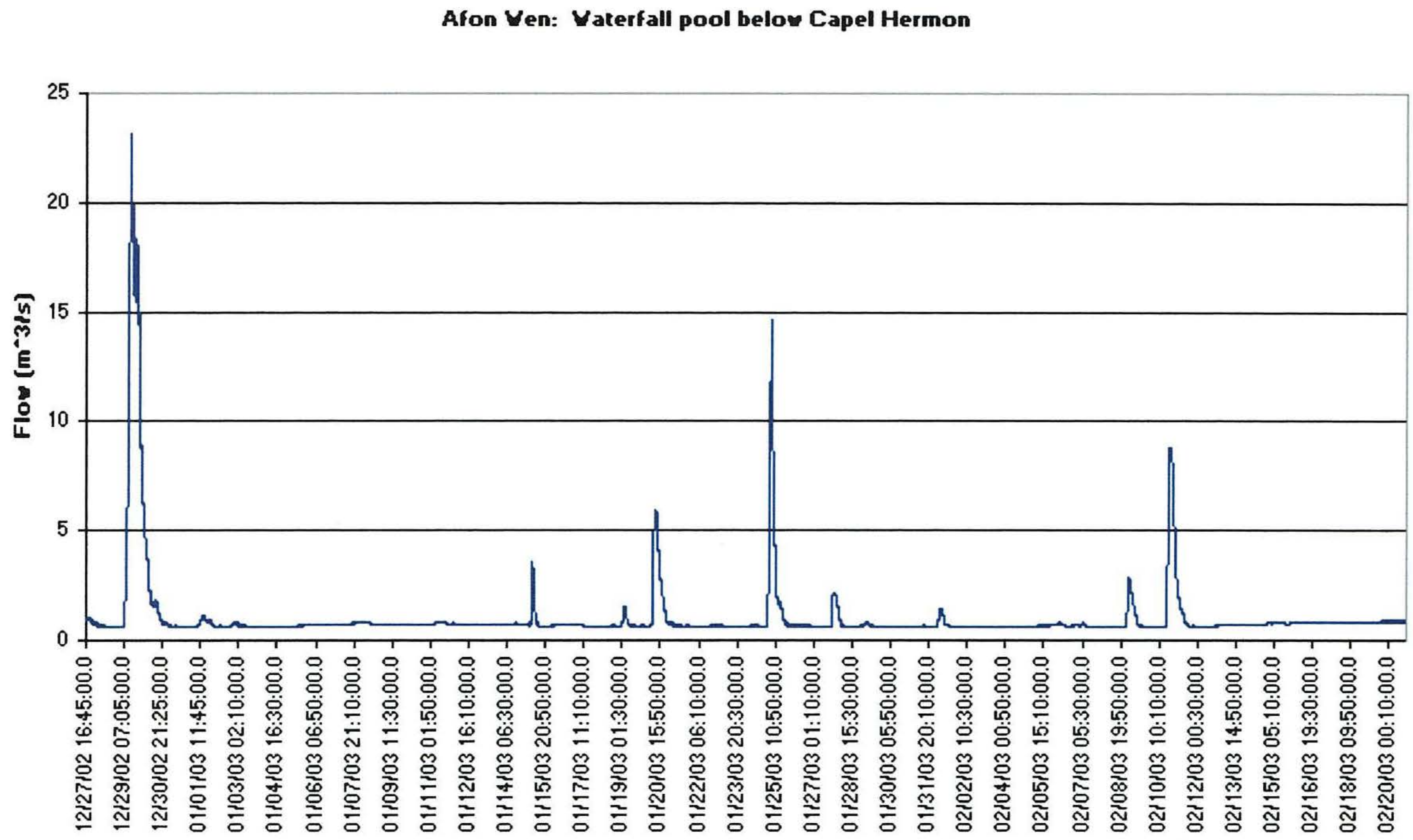

Figure 3.34: Example stage-discharge chart for the Afon Wen hydrograph recording site for the period December 2002 – February 2003

Afon Ty Cerrig

Site description

A hydrograph recorder has been situated in a pool on the Afon Ty Cerrig, a principal headwater stream of the Afon Wnion, at the location shown in fig.3.35. This lies within a forestry plantation at Pared yr Ychain on the slopes of Aran Fawddwy. The channel is composed of cobbles and boulders of 0.5m to 1m median dimension, with a high gradient producing characteristics of a cascade reach. The channel is relatively narrow and confined within incised banks, making it accessible for flow measurement during low flow and flood conditions.

Figure 3.35: Afon Ty Cerrig hydrograph recording site. The recorder is located on the river bed at point A.

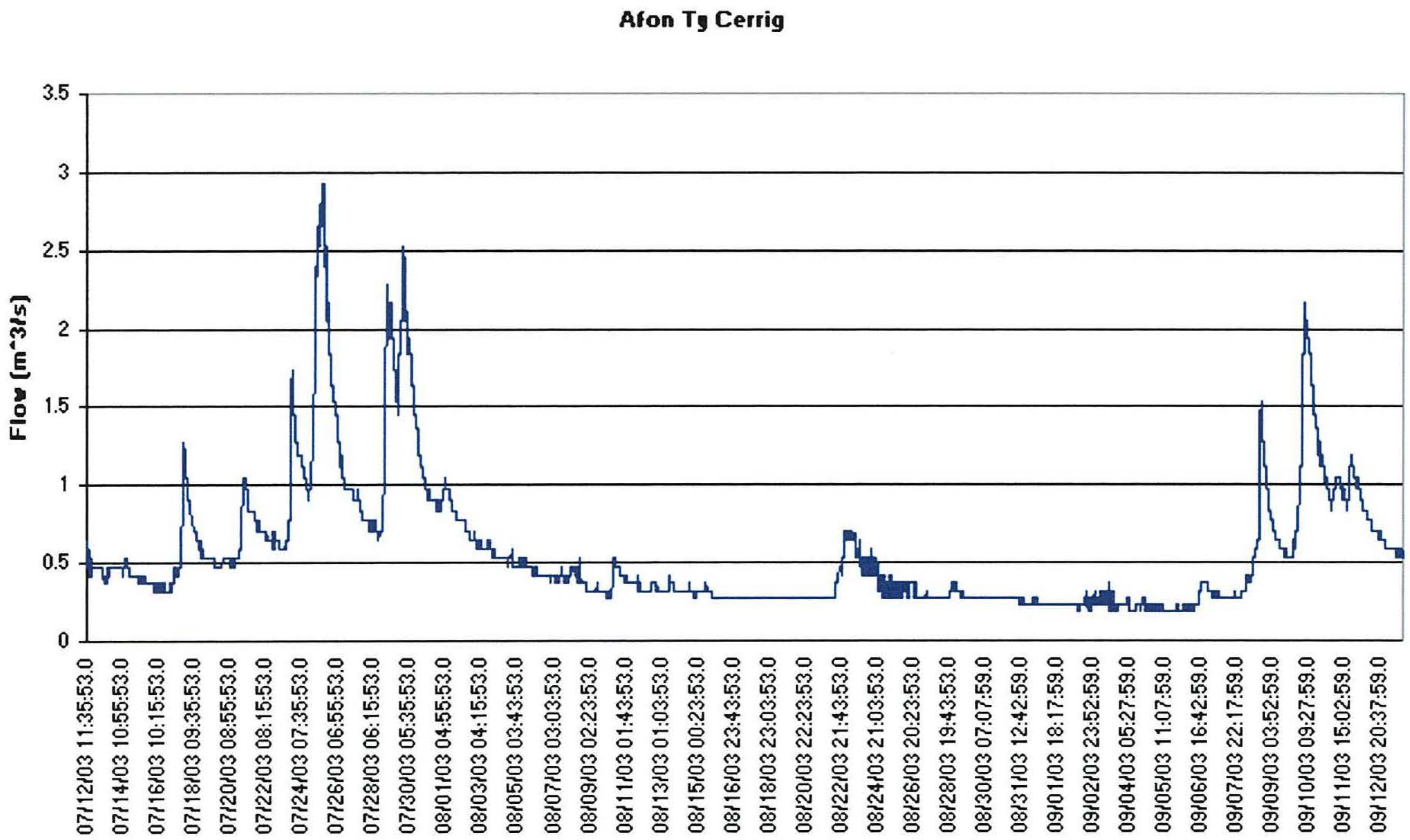

Figure 3.36: Example stage-discharge chart for the Afon Ty Cerrig hydrograph recording site for the period July 2003 – September 2003

Dolgellau

Site description

River stage height data has kindly been supplied by the Environment Agency for the gauging ststion on the Afon Wnion approximately 40m upstream from Bont Fawr, Dolgellau. The gauge is situated on a plane bed reach, with coarse gravel in the size range 0.05m to 0.30m making up most of the bed load.

Figure 3.37: Bont Fawr, Dolgellau, photographed from the Environment Agency river gauging station.

A calibration curve for conversion of river stage(m) to river discharge(m^3s^{-1}) was prepared in a similar manner to the calibration curves for the portable hydrograph recorder sites. The river cross profile was surveyed, and flows measured at points across the river under different stage heights (appendix C). Field measurements were augmented by calculated flow rates for flood conditions when measurement was impractical. The calibration curve function was then used to convert the stage height chart of fig.3.38 to the discharge chart of fig.3.39.

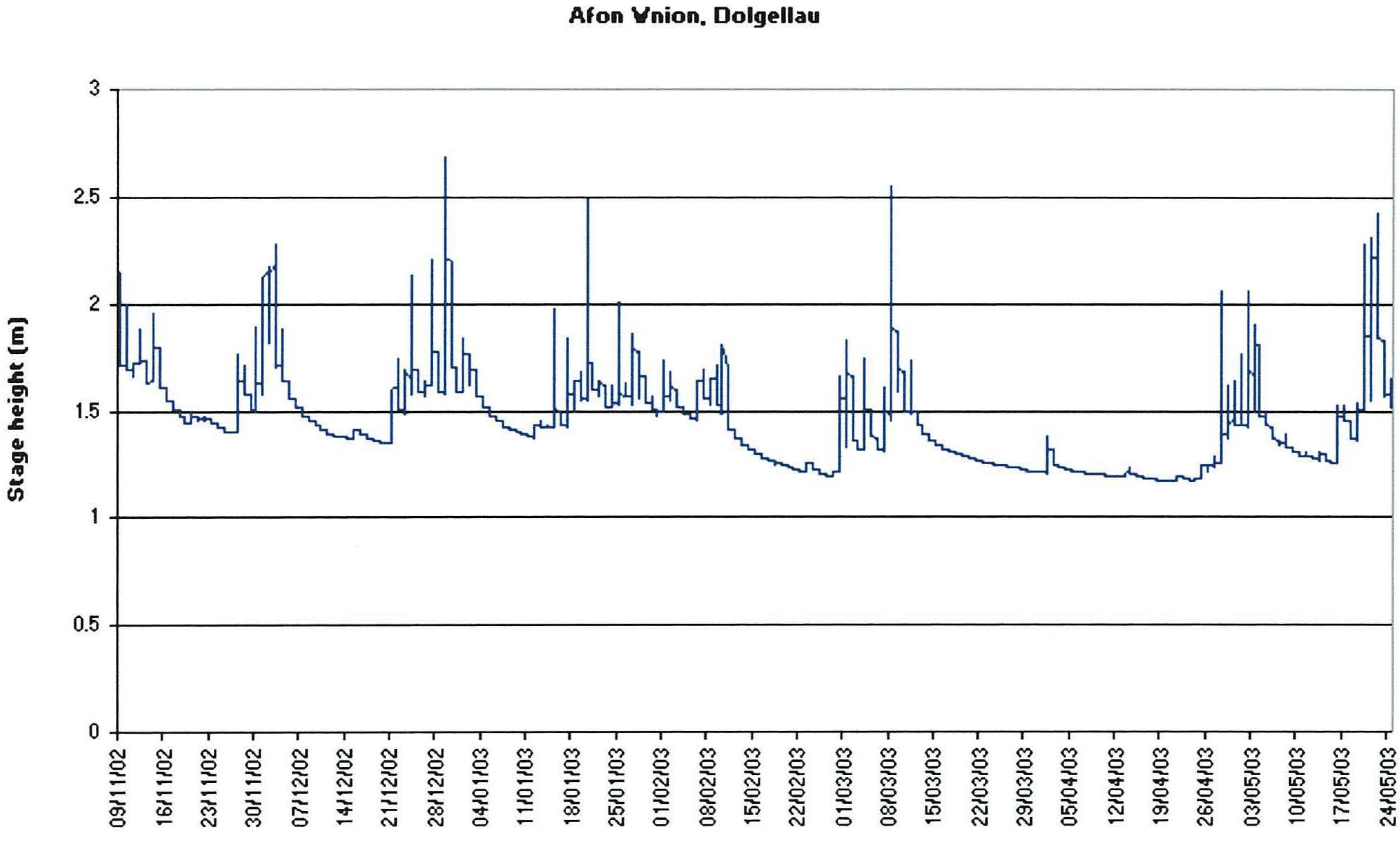

Figure 3.38: Example stage height chart for the Afon Wnion gauging station for the period November 2002 – May 2003

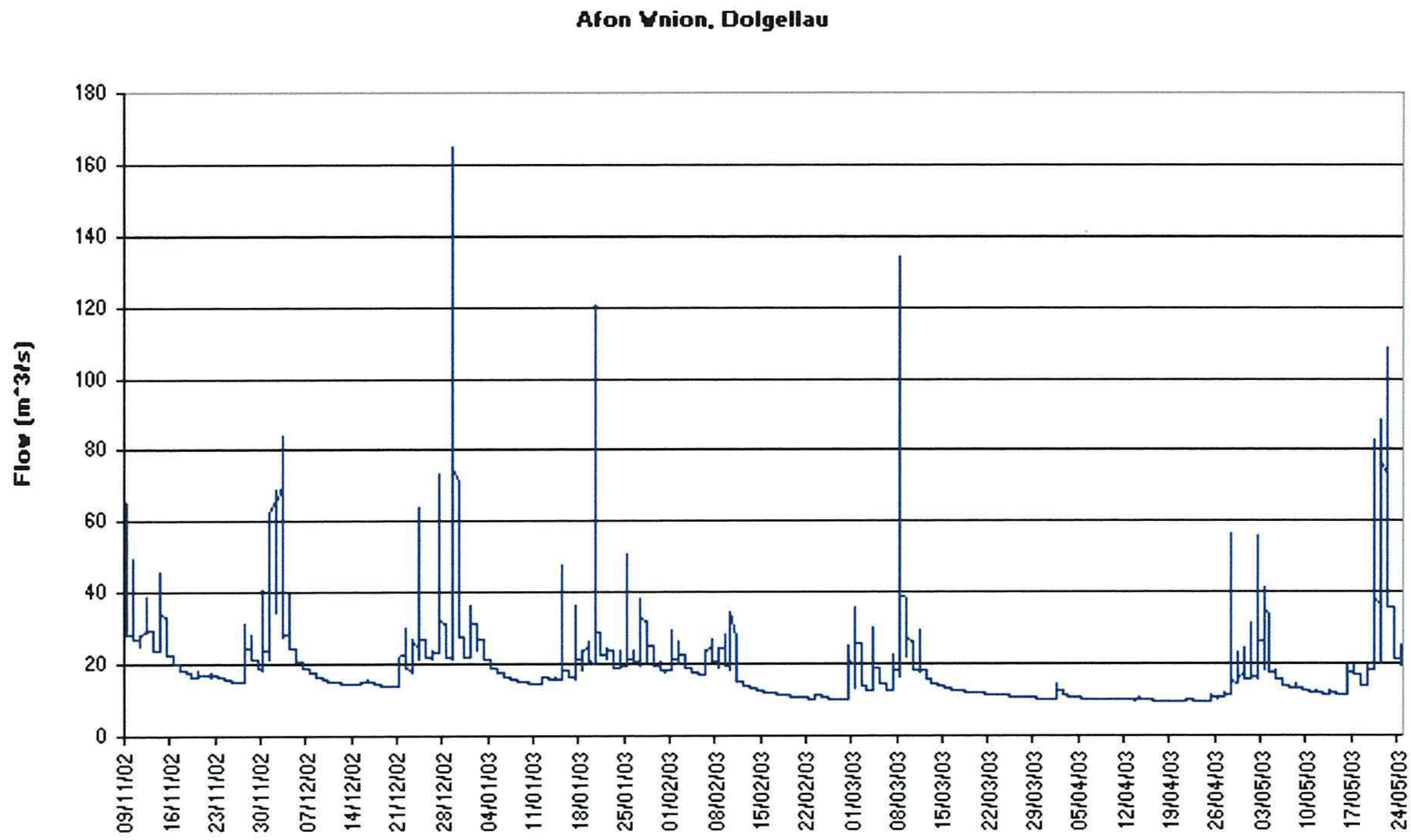

Figure 3.39: Example stage discharge chart for the Afon Wnion gauging station for the period November 2002 – May 2003

Hydrograph correlation

Whilst analysing hydrographs for consitency across the catchment, an interesting result was discovered. Hydrographs recorded at Pared yr Ychain in the source region of the Afon Wnion, and on the Afon Wnion 0.5km west of Dolgellau, can be closely linked by a simple mathematical transformation:

water depth in Dolgellau = **A** * exp(**B** * water depth at Pared yr Ychain) + **C**

using the empirically determined parameters: A = 0.05, B = 8.2, C = – 0.15, as shown in fig.3.40. Parameters were fitted manually by progressive refinement in an Excel spreadsheet and graph. This method was chosen in preference to the use of a statistical package, since tidal spikes present in the Dolgellau hydrograph had to be ignored during curve fitting.

The significance of this result is that the water depth predicted for Dolgellau is 3 hours 30 minutes after the time of the Pont Ty Cerrig hydrograph observation, providing a flood forecasting method of good accuracy. The success of the flood forecasting method appears to be due to two factors:

- Pared yr Ychain lies on the NW-SE axis of high rainfall which crosses the Mawddach catchment. Storm events at Pared yr Ychain therefore have a particularly significant effect on flood levels downstream on the Afon Wnion.
- The Afon Ty Cerrig which is gauged at Pared yr Ychain is typical of the streams draining the slopes of the Aran mountains. These slopes exhibit a high degree of hydrological uniformity over much of the course of the Wnion valley, with similar slope angles, cover by glacial deposits, and grassland vegetation. Hillslope runoff over this large area may therefore have a similar travel time to the Wnion trunk stream, and total flow in the Wnion is a simple scaling of the flow in the Afon Ty Cerrig tributary.

No similar simple relationship between hydrographs was found for the Mawddach sub-catchment. Contributions to total flow from the upper Mawddach, Gain, Eden and Afon Wen may vary greatly in volume and timing between storm events. This unpredicatability can be ascribed to: the variety of rainfall patterns, and local complexity of slopes, landuse and geology, and the different river routing times for flow along the different tributaries.

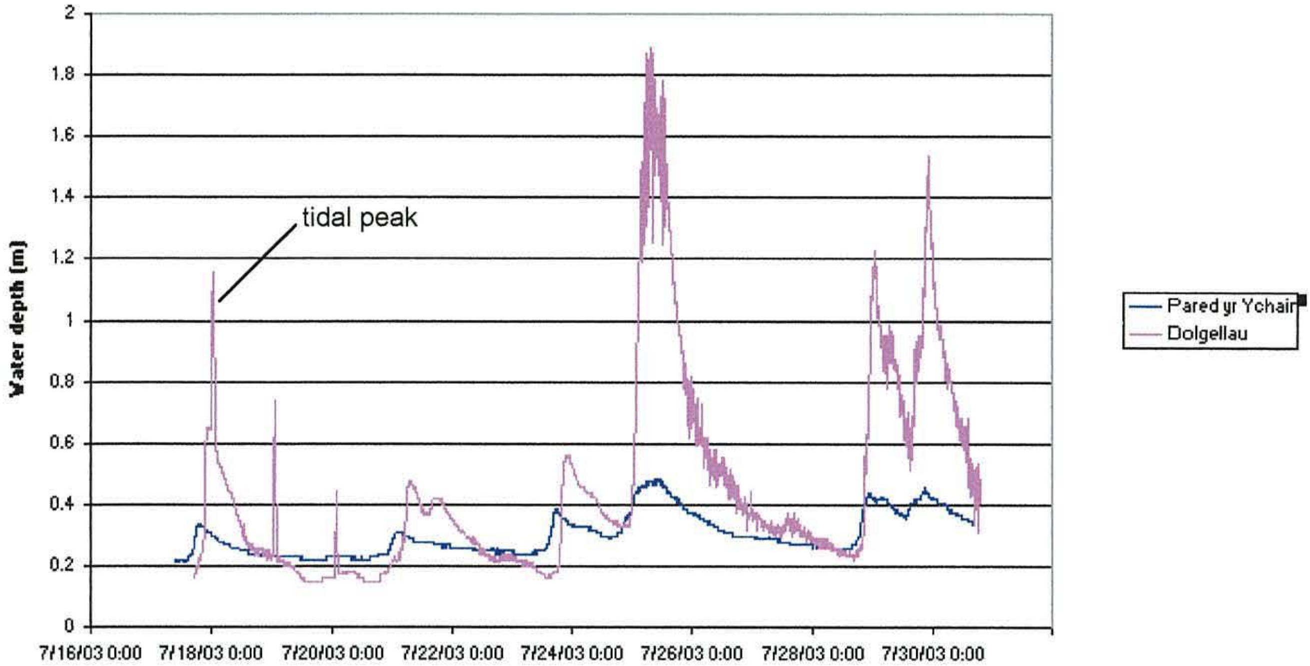

Figure 3.40(a). Original hydrographs recorded for the Afon Wnion

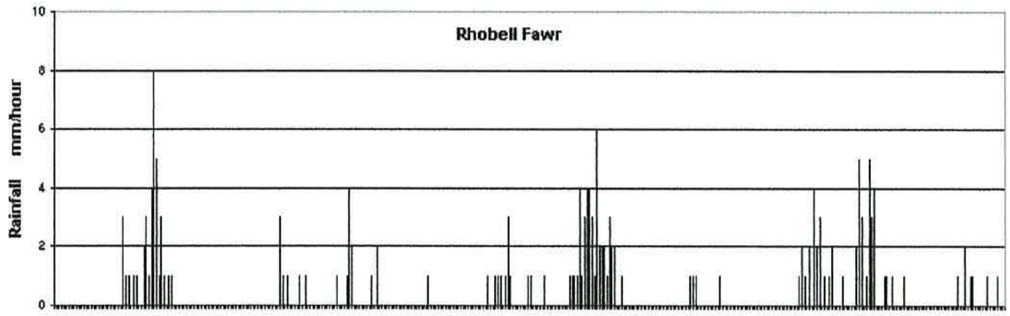

Figure 3.40(b). Rainfall for the period 16 July – 31 July 2003

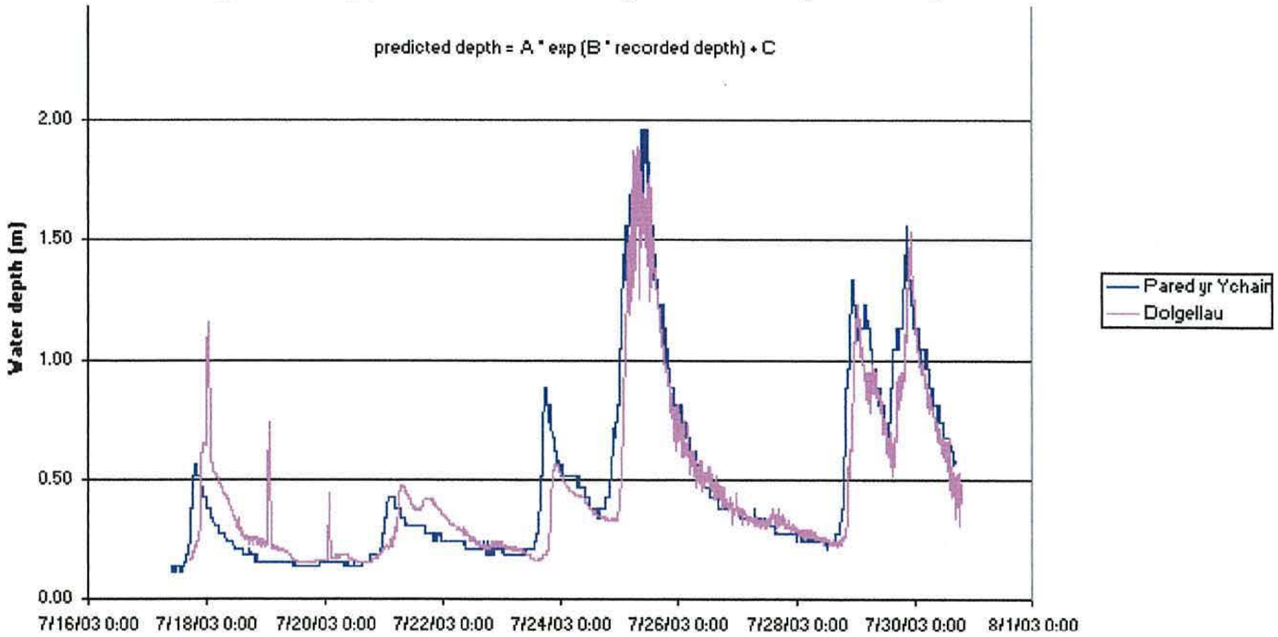

Figure 3.40(c). Hydrographs after transformation of the Pared yr Ychain data

Soil shallow stormflow

Weyman (1973) has studied the downslope flow of water in thick soils. Initial infiltration occurs vertically downwards, with lateral flow developing only within the saturated zone of the soil profile. Low permeability bedrock or low permeability soil horizons are considered essential for initiating lateral flow in the soil. Weyman observes that shallow flow may contribute to storm discharge, and may continue for several weeks after a storm event without further recharge. He states that lateral downslope flow appears to obey Darcy's law for fluid flow through porous media.

Hillslope water flow measurements have been carried out in the source area of the Afon Wnion at Pared yr Ychain, to investigate mechanisms of hillslope hydrology. Three sites have been instrumented to record surface runoff to a depth of 10cm and shallow stormflow (throughflow) at a depth of 1.5m, using a similar construction method to Atkinson (1978) as shown in fig.3.41.

Figure 3.41(a)
Site prepared for instrumentation, showing peat soil on glacial till, Pared yr Ychain

Figure 3.41(b)
Site after installation of water flow recorders and data loggers, Pared yr Ychain

The high rainfall of the area promotes prolific growth of ground vegetation – principally mosses, ferns and grasses amongst a young conifer plantation. An intermediate acidity peat soil is developed to a depth of 20 – 25cm on sandy clay glacial till derived from acid volcanic rocks. Typical results from flow measurements are shown in fig.3.42.

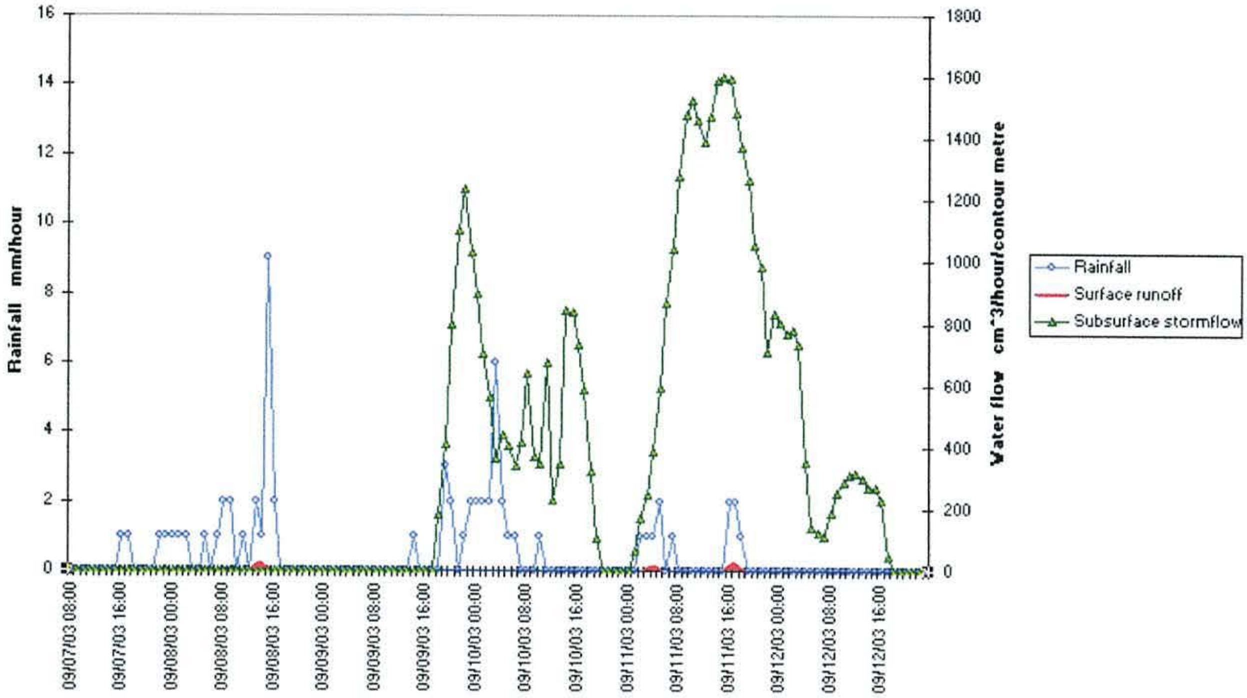

Figure 3.42: Hillslope water flows at Pared yr Ychain, 7 - 12 September 2003

It is found that volumes of hillslope water flow are strongly controlled by antecedent conditions. Nearly all downslope movement of water occurs as stormflow within the glacial till, with insignificant amounts of surface runoff recorded. This may be due to the absorbent effect of ground vegetation and ready availability of pathways for routing of water downwards through the thin peat layer. Streams are deeply incised into the glacial deposits of the Aran slopes, and shallow throughflow is discharged through the banks of channels during storm events.

It is significant that large volumes of sub-surface stormflow occur some four to six hours after the onset of heavy rainfall, which may be too late to directly influence flood peaks downstream. Stormflow can, however, continue for up to two days after rainfall and may control antecedent base flow levels for subsequent storm events. A series of rainfall events within a few days of one another in September 2003 are seen to produce progressively greater volumes of shallow stormflow, as the subsoil becomes saturated and the watertable is raised.

Further insight into the importance of antecedent conditions comes from another soil throughflow experimental site set up at Tir Penrhos, near Hermon in the Afon Wen valley (fig.3.43). This site is on a valley slope overlain by a thick succession of periglacial deposits in which 1.5m of scree overlies solifluction material and fluvial sands and gravels.

Figure 3.43: Surface runoff and soil throughflow monitoring site, Tir Penrhos, Hermon

Example data for surface runoff and soil throughflow is presented in fig.3.44. At Tir Penrhos, ground vegetation below mixed woodland is poorly developed. Surface runoff is relatively high in comparison to the Pared yr Ychain sites. Permeability of the periglacial scree at shallow depth is high, so throughflow is not recorded for the majority of rainfall events. At these times, the water table lies deep in the scree layer below the level of monitoring. A prolonged period of heavy rain can, however, cause the water table to rise, generating a very high volume of shallow throughflow for the discharge point at the base of the experimental site.

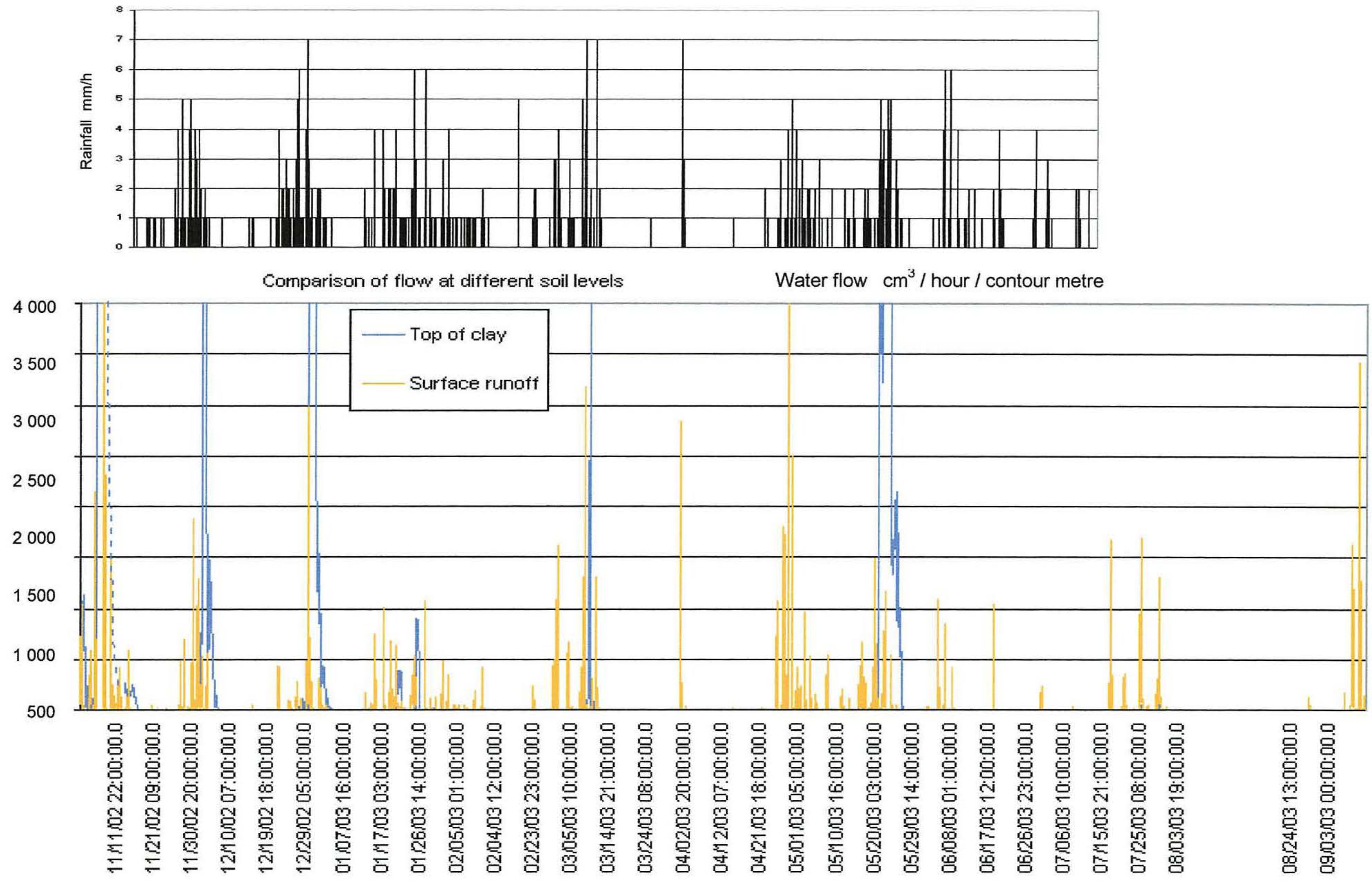

Figure 3.44: Surface runoff and soil throughflow monitoring at Tir Penrhos, November 2002 – September 2003

Results from the Tir Penrhos experiment are particularly interesting because the instances of high volumes of shallow throughflow correspond exactly with periods of extensive flooding of agicultural land around the head of the Mawddach estuary, some 5km downstream.

It is conjectured that under normal conditions:

- Glacial and periglacial deposits on the valley sides are unsaturated, and allow downwards percolation of soil water into groundwater storage.
- Due to the stepped profiles of the Mawddach and its tributaries, the water table lies below the river bed over a majority of reaches within the middle courses of the rivers in Coed y Brenin. Water may be lost through the river beds into groundwater storage.
- Groundwater is released into rivers over several days following rainfall. This timescale is too slow to affect the flood peak of a storm event.

After a prolonged period of heavy rainfall, hydrological conditions change:

- Glacial and periglacial deposits on the valley sides become saturated to a shallow depth. Downwards percolation into groundwater storage can no longer maintain drainage, and there is a rapid increase in downslope water transfer by shallow stormflow. Water is readily released through the banks of streams, and quickly enters the river routing system.
- The water table rises below the main channels, and groundwater is released through the streambed to increase river flow.
- Further rainfall follows fast surface runoff pathways, contributing to the buildup of a flood peak downstream.

Monitoring of subsurface throughflow below hillslopes in Coed y Brenin may provide early warning of the saturation conditions needed to initiate flooding downstream.

Watershed Modelling System

A first step in producing flood models for the Mawddach and Wnion subcatchments has been the use of the HEC-1 semi-distributed model, described previously in section 3.1 (fig.3.6). The model uses rainfall estimates to simulate infiltration, surface runoff and river routing processes. Synthetic hydrographs can be generated for selected points within the channel network.

Clear limitations of HEC-1 are:

- loss of infiltration water from the model completely,
- the modelling of sub-catchments with uniform hydrological properties, a situation which does not accurately represent the small scale variations in slope, geology, vegetation and soil types observed in the field.

Despite these simplifying factors, HEC-1 is found to produce acceptable hydrograph simulations for individual storm events. The hydrographs generated can provide input to sediment transport models as described in section 3.3, and to floodplain inundation models as described in section 3.4. HEC-1 may be taken as a baseline against which the performance of more sophisticated hydrological models should be judged.

Before running the HEC-1 model, data files must be generated to represent the hydrological properties of the catchment, the geometry of the river network, rainfall sequence, and the mathematical options selected to simulate infiltration, surface runoff and river routing (Goldman and Ely, 1990). These files may be prepared manually and input in alphanumeric format using a text editor, but the process is greatly simplified by the use of data preparation software based on GIS techniques. The Watershed Modelling System (Brigham Young University, 2004) has been used for this purpose in the current project. The WMS program additionally provides post-processing facilities for graphical display of the river network incorporating output hydrographs at selected points.

Setting up a hillslope runoff model

A HEC-1 model is developed by dividing the overall catchment into a series of basins which may be considered hydrologically homogeneous. Rainfall, infiltration and surface runoff will be averaged across each basin. Twelve sub-catchments were chosen above the tidal limit for the Mawddach, and eight sub-catchments were chosen for the Wnion. The sub-catchments are described in appendix B, and are outlined in figures 3.17 and 3.18.

A digital elevation model is first loaded into the program, then used to define the river channel network and sub-catchment boundaries (fig.3.45). For the Mawddach and Wnion catchments, a 50m gridded DEM provided by the Centre for Ecology and Hydrology has proved suitable.

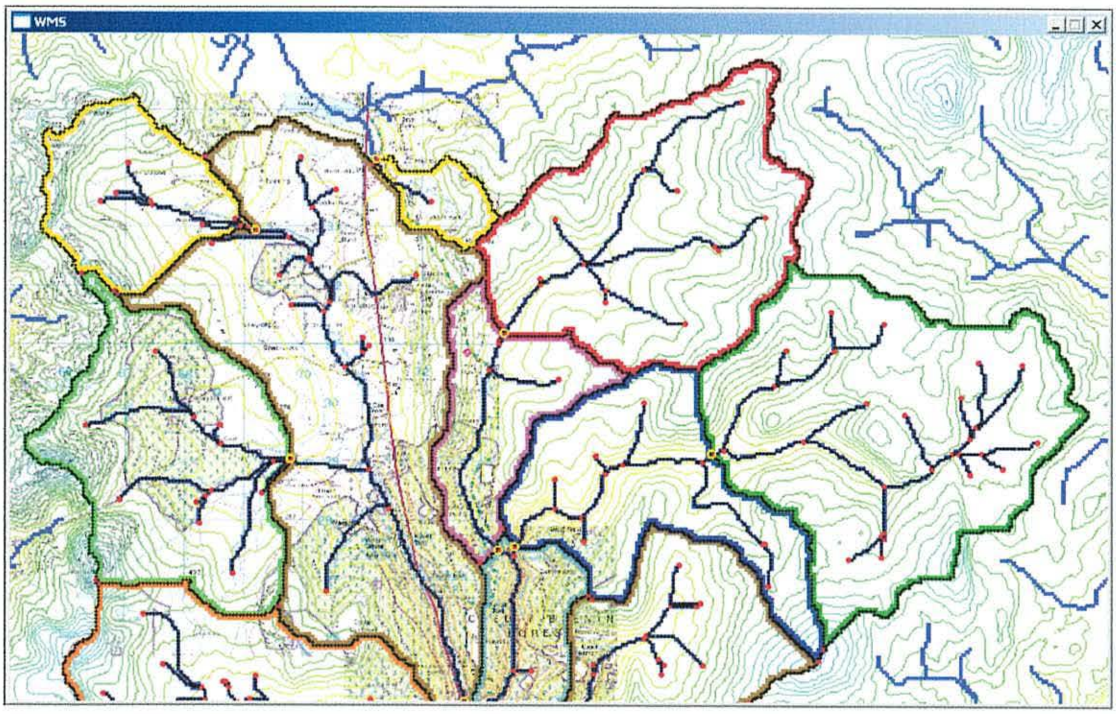

Figure 3.45: Construction of the Watershed Modelling System model for the upper Mawddach. Topographic contours, the stream network and sub-catchment boundaries and have been determined geometrically from the digital elevation model.

The digital elevation model is now converted to a Triangulated Irregular Network to simplify the calculation of the basin parameters required by the HEC-1 program. Triangles are constructed to conform with the stream courses and basin boundaries previously defined, in order to maximise the accuracy of the model (fig.3.46).

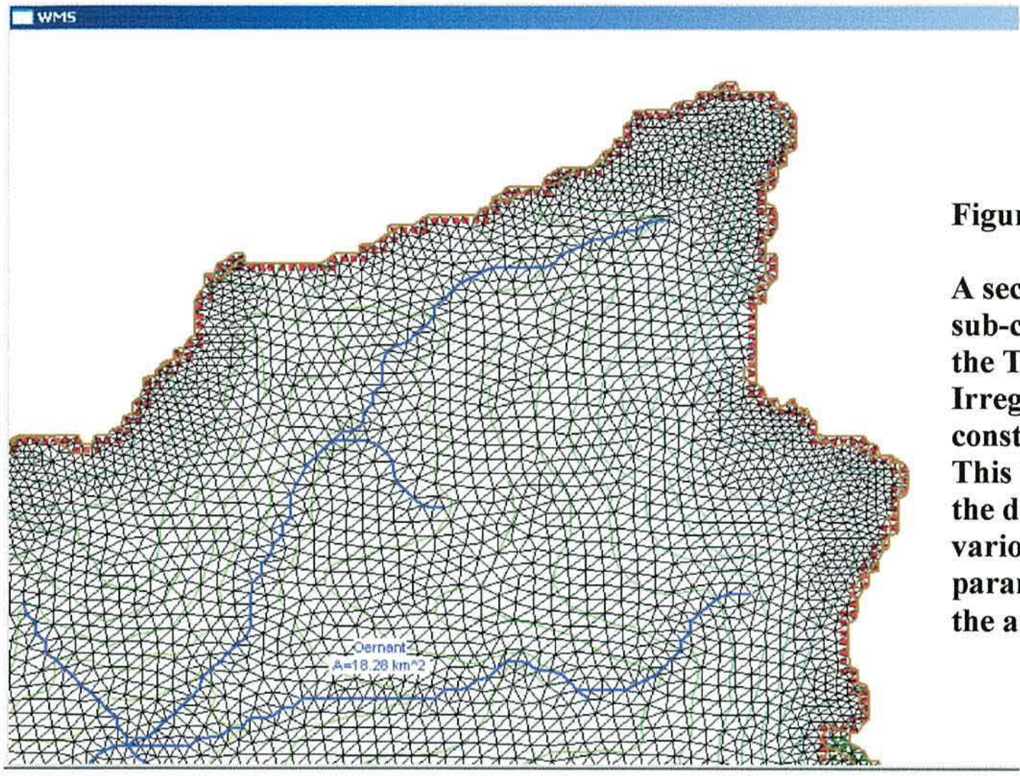

Figure 3.46:

A section of the Oernant sub-catchment, showing the Triangulated Irregular Network constructed by WMS. This network is used in the determination of various basin parameters, including the area value shown.

Soil and landuse overlays

An option available in HEC-1 is to determine infiltration rates by the SCS Curve Numbers method (fig.69). This option has proved successful when used in the Mawddach model.

Before using the Curve Numbers method, it is necessary to provide information on the types and distribution of soils and vegetation within the catchment. This is done by setting up separate overlays, as in the land use example of fig.3.48 below.

- Land use has been divided into the main categories of natural vegetation and agricultural use identified earlier in section 1.2 and displayed in fig.1.88.
- Soils are categorised on a four-point scale from: dry (type A) to wet (type D). Four curve numbers A to D are allocated to each land use category, as shown in Table 3.1. A curve number may then be selected from this group, depending on whether the soil is: dry, moderately dry, damp, or wet.
- Soils developed on well jointed Cambrian grit would belong to a drier group than those on poorly drained shales or basalts.
- The soils of the whole region belong to drier categories in the summer than in winter months.

The procedure for curve number allocation is illustrated in fig.3.47 for a hypothetical area of sub-catchment:

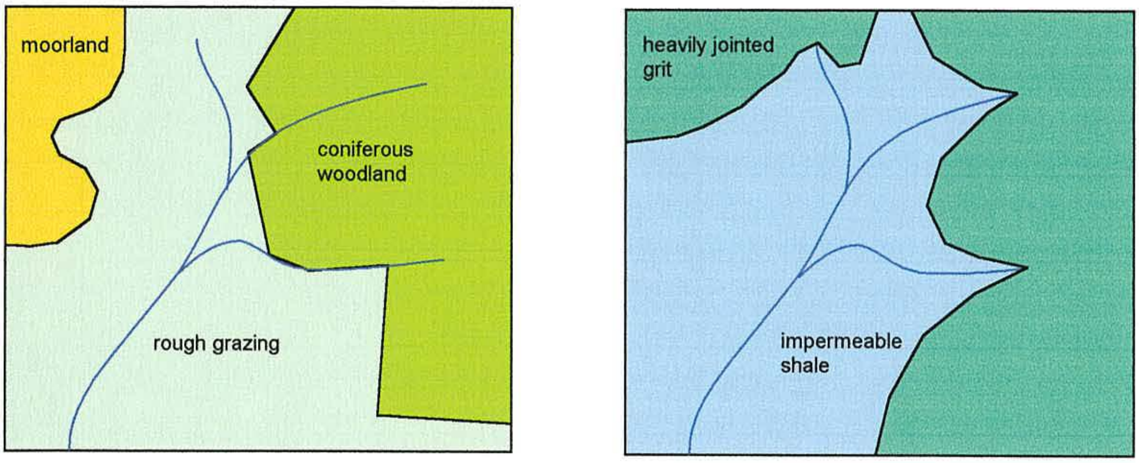

Figure 3.47(a). Land use and geology overlays.

Land use and geology overlays are superimposed in the model to identify zones with unique combinations of land use/geology. Curve Numbers are allocated according to the land use categories in Table 3.1. The soil moisture class (A-D) chosen depends partly on geology and partly on antecedent soil moisture conditions. For example, soils on freely draining grits are allocated class B during periods of low rainfall, but class C after a previous period of wet weather. Naturally damper soils on impermeable shales are allocated class C during periods of low rainfall, but class D after a previous period of wet weather.

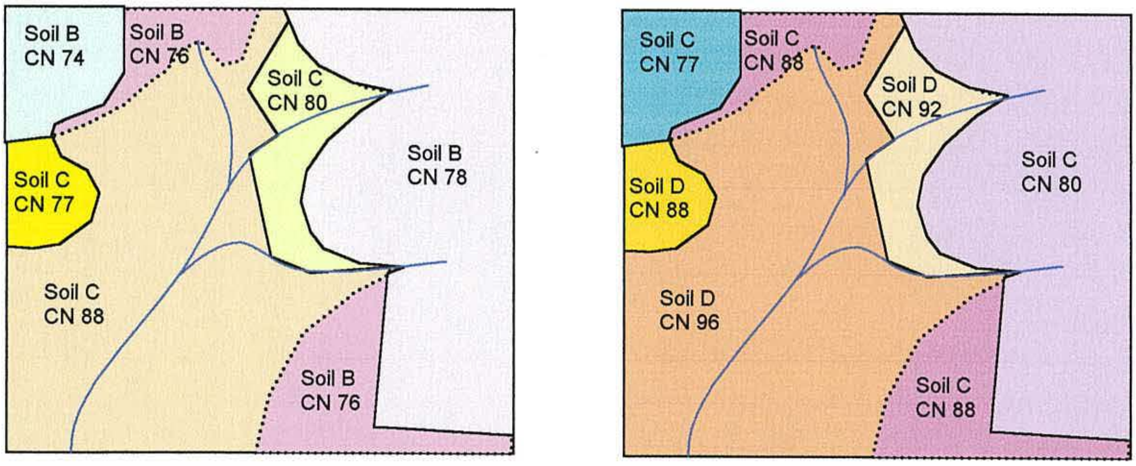

Figure 3.47(b). Allocation of Curve Numbers (left) dry antecedent conditions, (right) wet antecedent conditions

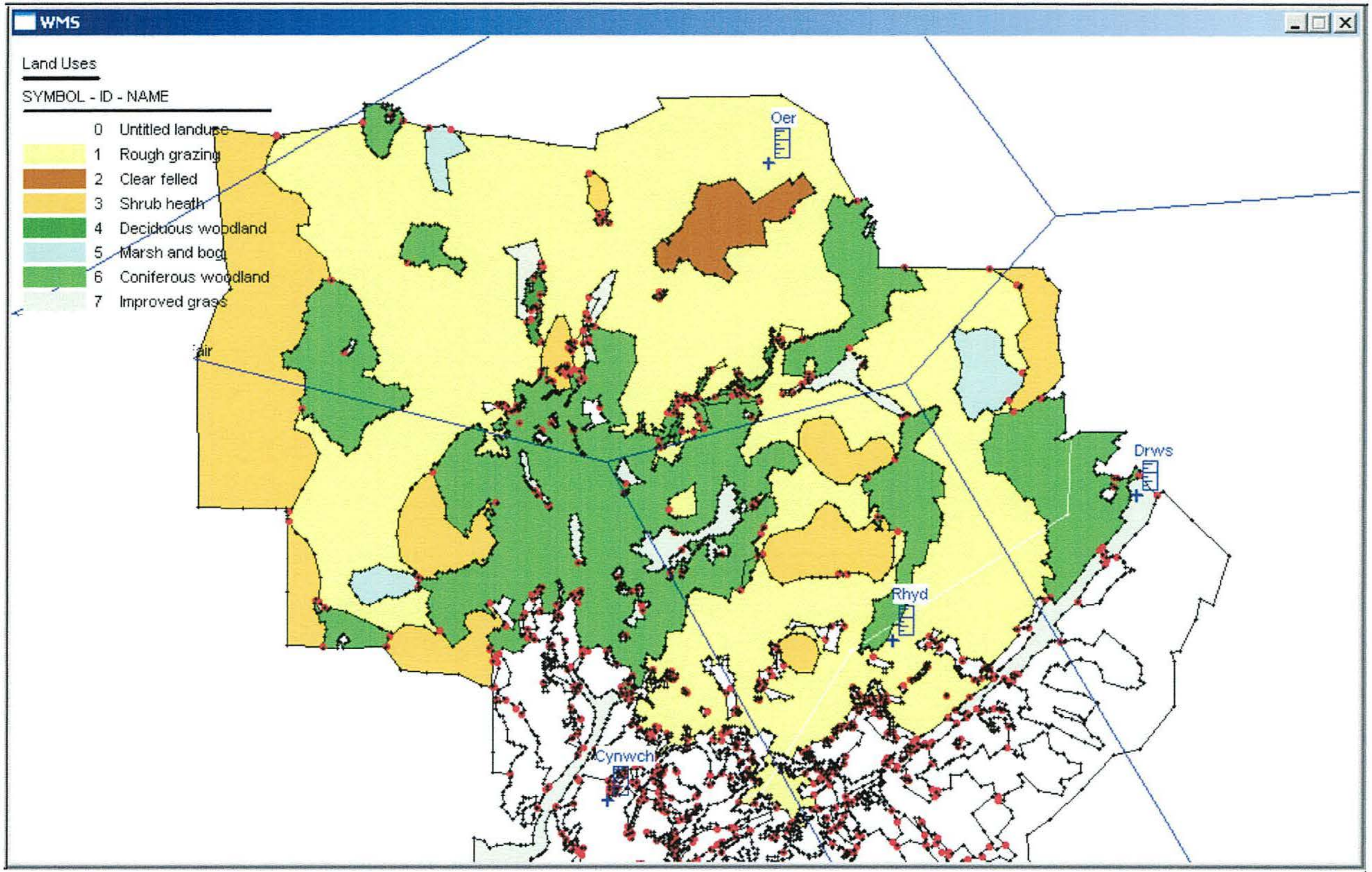

Figure 3.48: Land use overlay for the WMS Mawddach model

The partition of rainfall between infiltration and surface runoff is determined by the equation:

$$Q = \frac{(P - 0.2S)^2}{P + 0.8S}$$

using Imperial units, where Q is runoff (inches), P is cumulative rainfall during the storm event (inches), and S is the soil moisture deficit (inches). A parameter termed the *Curve Number,* CN, is related to S by the equation

$$S = \frac{1000 - 10CN}{CN}$$

Example graphs for different curve numbers are shown in fig.3.49. Qualitatively, this indicates that runoff increases during a storm event as the soil becomes increasingly saturated, and that zones of high curve number experience more runoff, and correspondingly less infiltration, than zones of low curve number.

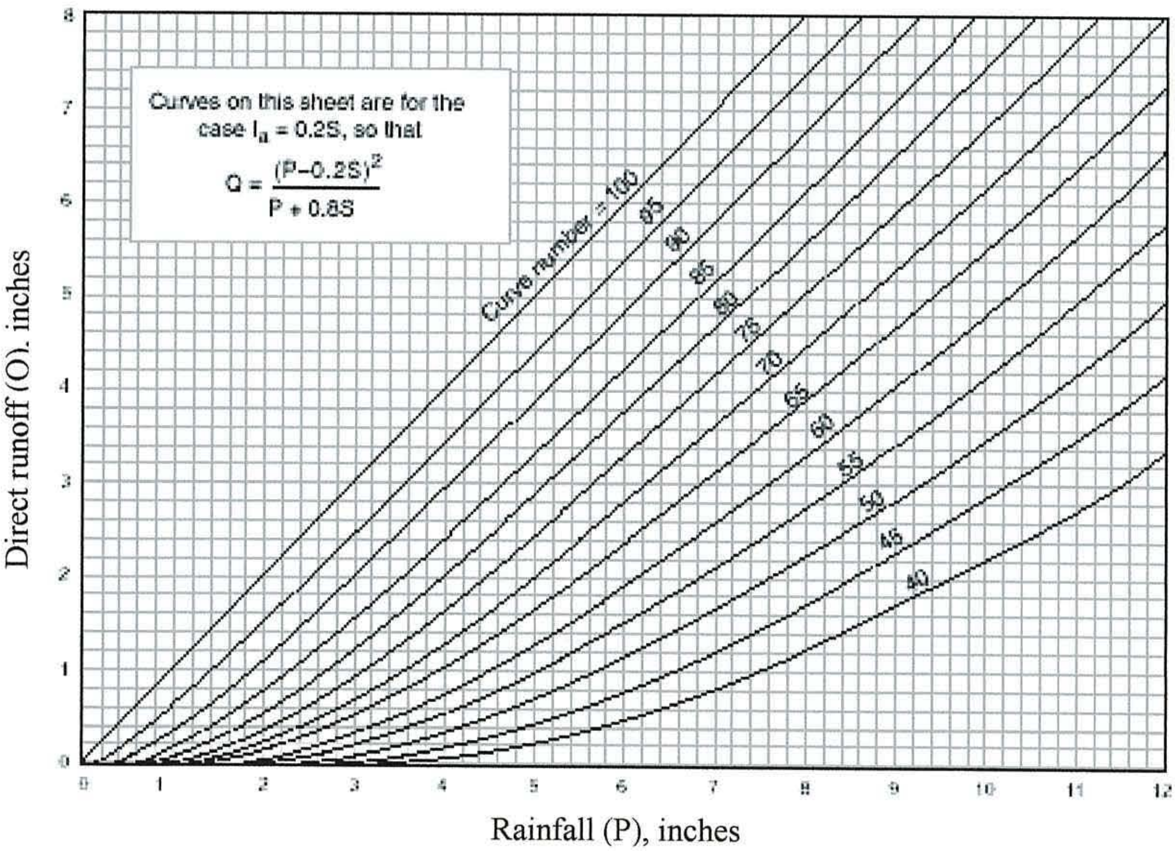

Figure 3.49: Soil Conservation Service curve number chart

Curve numbers are computed by superimposing vegetation and soil overlays, and using a table to determine values for different soil/vegetation combinations. Experimentation has led to the following values providing consistent results for storm events in the Mawddach catchment:

Land use category	Soil A	Soil B	Soil C	Soil D
Rough grazing	68	76	88	96
Heather moorland	70	74	77	88
Coniferous woodland	76	78	80	92
Deciduous woodland	76	78	83	92
Improved grassland	82	85	88	96
Clear felled	90	92	92	98
Bog and marsh	83	84	87	96

Table 3.1. SCS Curve Numbers used in the Mawddach catchment model

An alternative approach to computing soil infiltration in the HEC-1 model uses the Green-Ampt equation. Experiments have been carried with this method, but it was found that the SCS Curve Numbers approach provides more consistent results, with a simpler facility for incorporating antecedent soil moisture conditions.

Rainfall

To simulate water flows during a storm event, it is necessary to provide a time sequence of rainfall for one or more stations across the catchment. Where multiple raingauge stations are used, the program is able to construct interlocking Thiessen polygons around each station to represent the zones of applicability for each gauge. Rainfall values can be computed for each sub-basin by averaging adjacent raingauge readings, weighted in proportion to the Thiessen polygon coverage within the sub-basin. Fig.3.50 shows Thiessen polygons constructed for raingauge stations active around the Mawddach catchment at the time of the July 3, 2001 flood event.

Fig.3.51 illustrates the method of setting up a rainfall sequence to represent storm rainfall at a gauge site. The time interval between readings is chosen, in this case 15mins, and cumulative rainfall is entered for each specified time as a fraction of the total storm rainfall at that gauge site. It then just remains to enter the storm rainfall total for the gauge site.

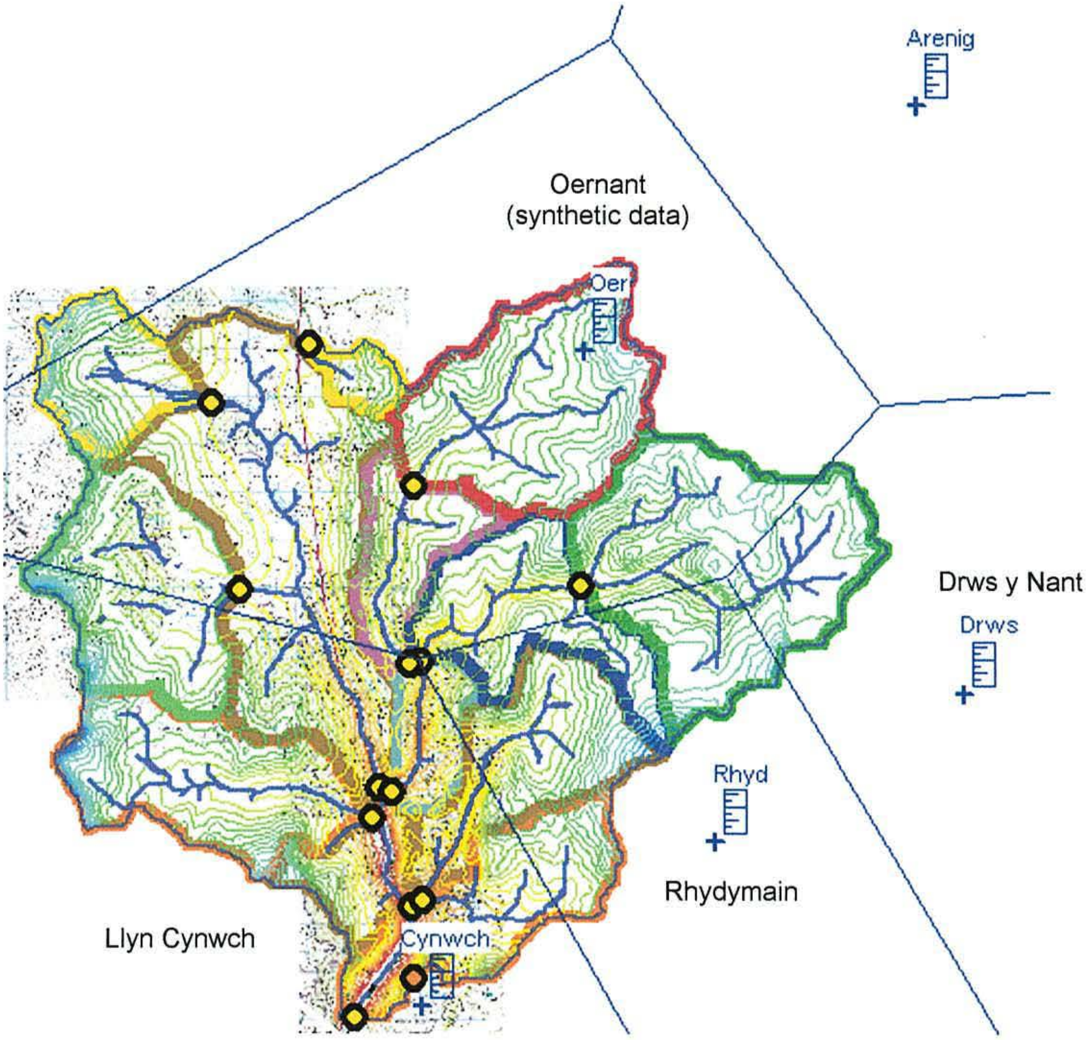

Figure 3.50: Construction of Thiessen polygons for the Mawddach sub-catchment

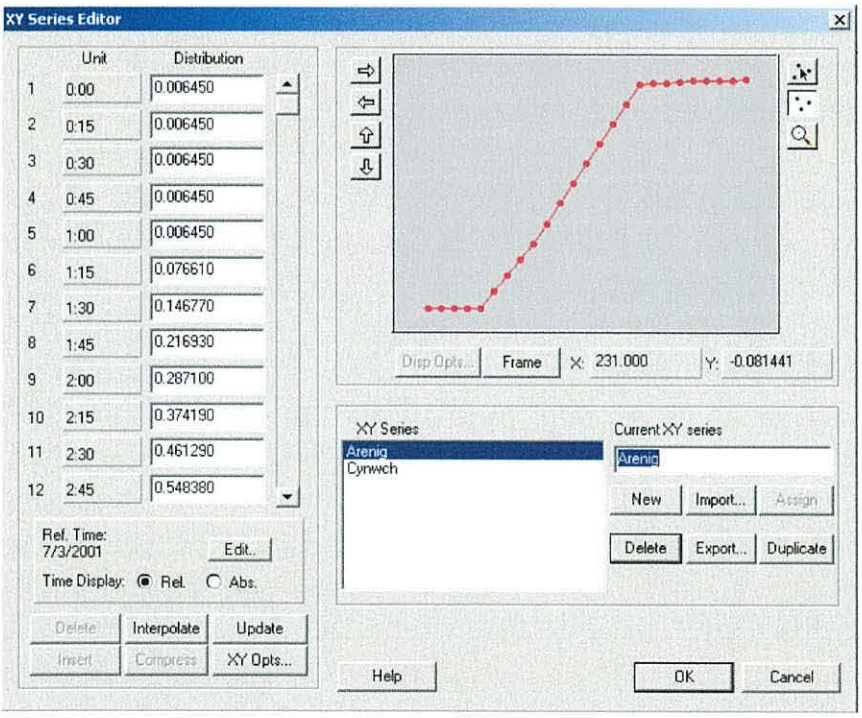

Figure 3.51: Setting up a storm rainfall sequence for a raingauge station

Overland flow

Rainfall not lost from the model as infiltration is treated as quickflow. This term may be taken to include both surface water sheet flow and shallow fast soil throughflow down hillslopes. Before running a HEC-1 model, the method to be used for computing overland flow must be chosen. The model provides both a Unit Hydrograph method and a Kinetic Wave method for overland flow.

The mathematical basis of the Kinematic wave method was outlined in section 3.1 above, and is discussed by Bevan (2001). The Kinetic Wave method treats the drainage system as composed of three orders of flow path:

- First order flow occurs across strips of hillslope, as at locations A. No permanent stream channels of this order are present.
- Second order flow occurs through feeder channels, as at locations B. Permanent channels are present, though they may be dry between storm events. These channels are too small to form part of the mapped river system.
- Third order flow occurs in river channels as at C. This flow is handled by river routing methods, and does not form part of the surface runoff calculation.

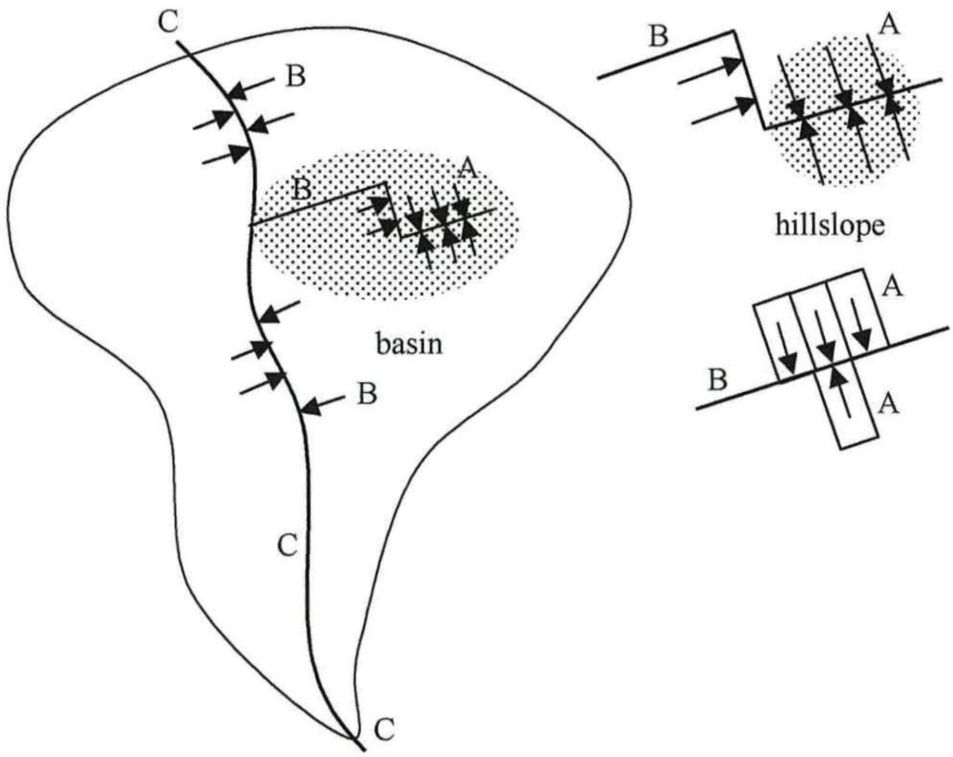

Figure 3.52: Orders of surface water flow modelled by WMS HEC-1

In order to determine flow volumes using the Kinetic Wave equations, the HEC-1 program carries out separate processing of the first order overland flow planes and the second order collector channels. In each case, the data required for calculations are:

- mean flow distance
- mean slope
- Manning roughness

Additionally, the mean cross section shape of the collector channels must be specified.

Experiments were carried out using the Kinetic Wave method for storm events in the Mawddach catchment. Whilst it was possible to produce results in close agreement with recorded hydrographs for single storm events, there was difficulty in obtaining a single set of hillslope parameters which produced consistent results for different storms. Consequently, the alternative method of Unit Hydrographs was selected for the Mawddach HEC-1 model.

Unit Hydrograph methods

The Unit Hydrograph methods operate on the principle that runoff during storms is additive. For a given area of hillslope,

- a storm of 20mm/h produces twice as much runoff as a storm of 10mm/h,
- a storm of duration 2 hours produces twice the runoff of a storm of 1 hour with the same rainfall intensity.

Runoff from different sub-catchments and time intervals can therefore be added in a simple way, allowing for the time of routing waterflows downstream between sub-catchments.

Unit Hydrograph methods depend on obtaining a mathematical relationship between the runoff produced by unit rainfall in one time interval, and geometric characteristics of the sub-catchment. From the various linking equations available, the Espey Rural method has proved successful for the Mawddach model. This equation makes use of the mean stream length and stream slope to compute the time for peak flow from the sub-catchment after the commencement of storm rainfall. The equation for the Espey Rural method is:

$$\text{time to peak flow} = 2.65 \times (\text{stream length})^{0.12} \times (\text{stream slope})^{-0.52} \text{ minutes}$$

The required measurements, amongst others, are determined automatically by the WMS software (fig.3.53).

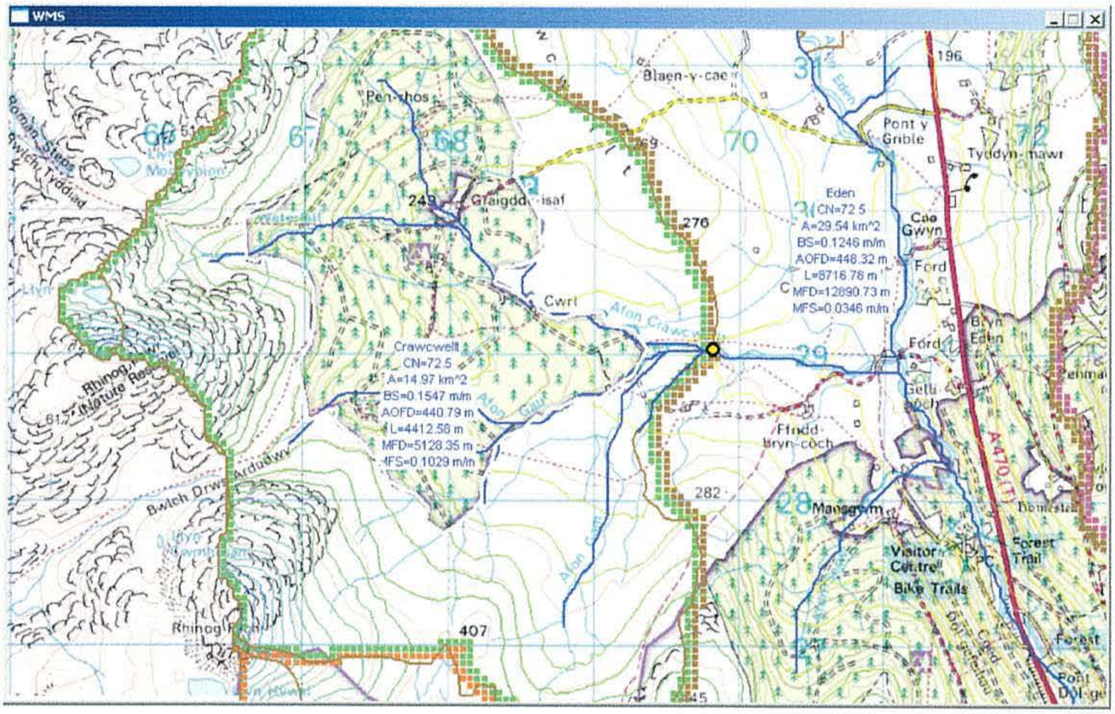

Figure 3.53: Illustration of basin parameters computed geometrically for two of the Mawddach sub-catchments: A area, BS basin mean slope, AOFD average overland flow distance, L basin length, MFD mean flow distance, MFS mean flow slope

River routing

River routing in the HEC-1 model can be carried out by various methods including the Muskingham and Muskingham-Cunge equations, and the Kinematic Wave equation. In each case, the downstream water flow volume is determined from the channel distance and flow velocity, with flow velocity being calculated as some function of channel slope, channel shape and Manning's roughness. In practice it was found that the model was relatively insensitive to the choice of routing method, with all giving similar routing times. The Muskingham method, requiring the least parameters, was therefore chosen for the Mawddach HEC-1 model.

Model output

After preparation of input data files is complete, the model may be run and output files are generated.

The HEC-1 model operates on a series of sub-catchments, linked upstream in a branching tree pattern (fig.3.54). When the model is run:

- hillslope flows are generated for each sub-catchment for each time interval,
- the hillslope flows are routed to the outflow of the sub-catchment,
- riverflows entering the head of the sub-catchment are routed downstream and combined with the hillslope flows at the outlet,
- the combined riverflow is then made available to the next sub-catchment downstream at the start of the next time interval,
- riverflows are combined at confluence points and routed downstream.

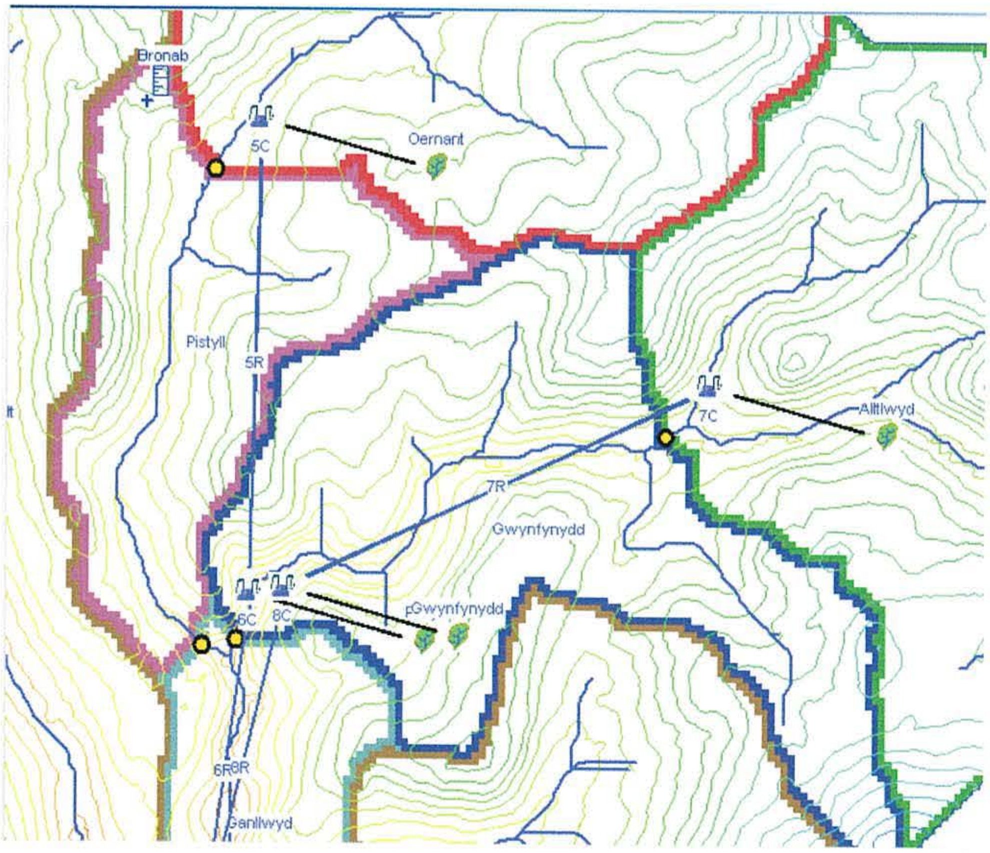

Figure 3.54: River routing diagram produced by WMS for the upper Mawddach. Green 'basin' symbols represent hillslope runoff from individual sub-catchments, Blue lines represent downstream routing directions, and 'flume' symbols represent points at which synthetic hydrographs have been generated by the model.

Results of model runs

Runs were carried out for the example rainfall events discussed earlier in section 2.4:

- Squall line convective storm: 3 July 2001
- Frontal storms: 8 November 2002, 29 December 2002, 8 March 2003, 21-22 May 2003, 3-4 February 2004

3 July 2001

The HEC-1 model was set up and configured to simulate the extreme storm event of 3 July 2001 associated with a squall line of convective thunderstorm cells across the Mawddach catchment. The storm was active between 16:00 h and 22:00 h.

At the time of the July 2001 storm, five raingauges were providing hourly totals within or close to the Mawddach catchment. From the pattern of river levels, it is likely that the zone of maximum storm rainfall lay within this ring of stations, over the mountainous terrain around Moel Oernant.

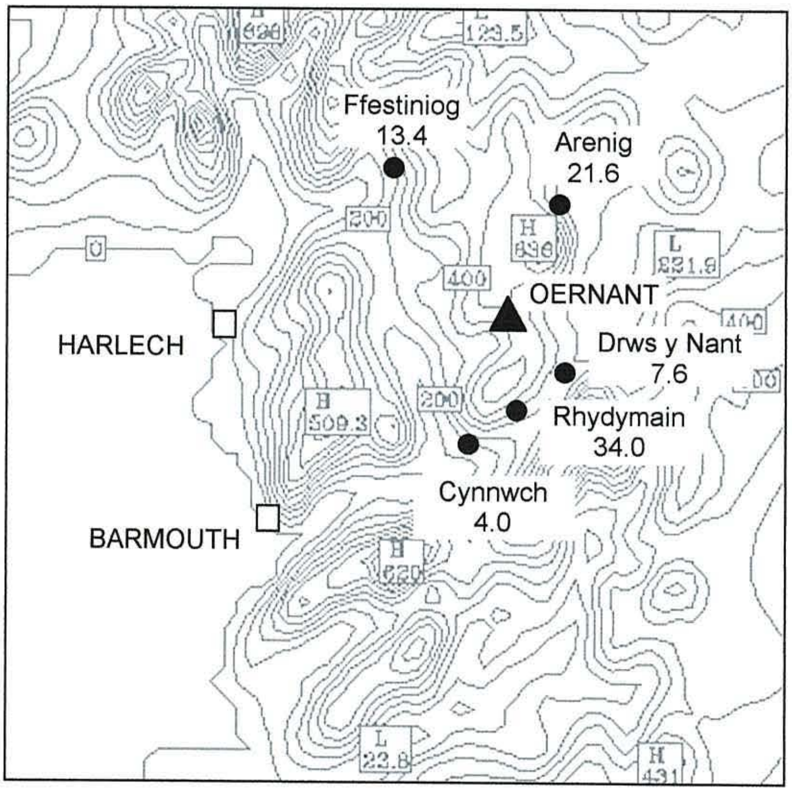

Fig. 3.55: Rain gauge sites, showing totals (mm) for the period 18:00–19:00 h, 3 July 2001

The MM5 mesoscale meteorological model has been used to obtain further insight into rainfall intensities and distribution during the storm (cf section 2.4). Modelling correctly identifies the north-south orientation of the squall line (fig.2.113). Localised convective cells with maximum rainfall intensities during the storm of between 45 and 70 mm h^{-1} are produced.

Inaccuracies in the model are likely to be positional, rather than in intensity. Random processes operating within a squall line make it difficult to predict the exact location where a convective cell will develop. On the basis of field evidence, the centres of convective cells should be displaced approximately 12 km northwards to lie over the southern Arenig plateau. A hypothetical rainfall distribution at Moel Oernant close to the centre of the storm can then be constructed (Table 3.2). The Moel Oernant synthetic data is included in the HEC-1 hydrological model which follows.

	Ffestiniog	Arenig	Drws y Nant	Rhydymain	Llyn Cynnwch	Oernant
15:00-16:00	0.2	0.4	0	0	5.6	0
16:00-17:00	23.6	0	0	6.2	21.6	20
17:00-18:00	7.4	17.4	11.4	19.8	13.6	25
18:00-19:00	13.4	21.6	7.6	34	4	40
19:00-20:00	16	21.4	29.4	25.8	1.2	35
20:00-21:00	0.6	0.8	0	0	0	0
21:00-22:00	0	0.4	0.2	0.2	1.8	0
storm total	61.2	62	48.6	86	47.8	120

Table 3.2. Hourly rainfall totals and total storm rainfall (mm) during the 3 July 2001 storm event.

The relative timing of rainfall is illustrated in fig.3.56. This shows the storm moving slowly across the catchment from Llyn Cynnwch in the west to Drws y Nant in the east, a distance of 15km in 3 hours. The cumulative rainfall curves, along with the storm rainfall totals for each location, were used to set up raingauge inputs for the HEC-1 model.

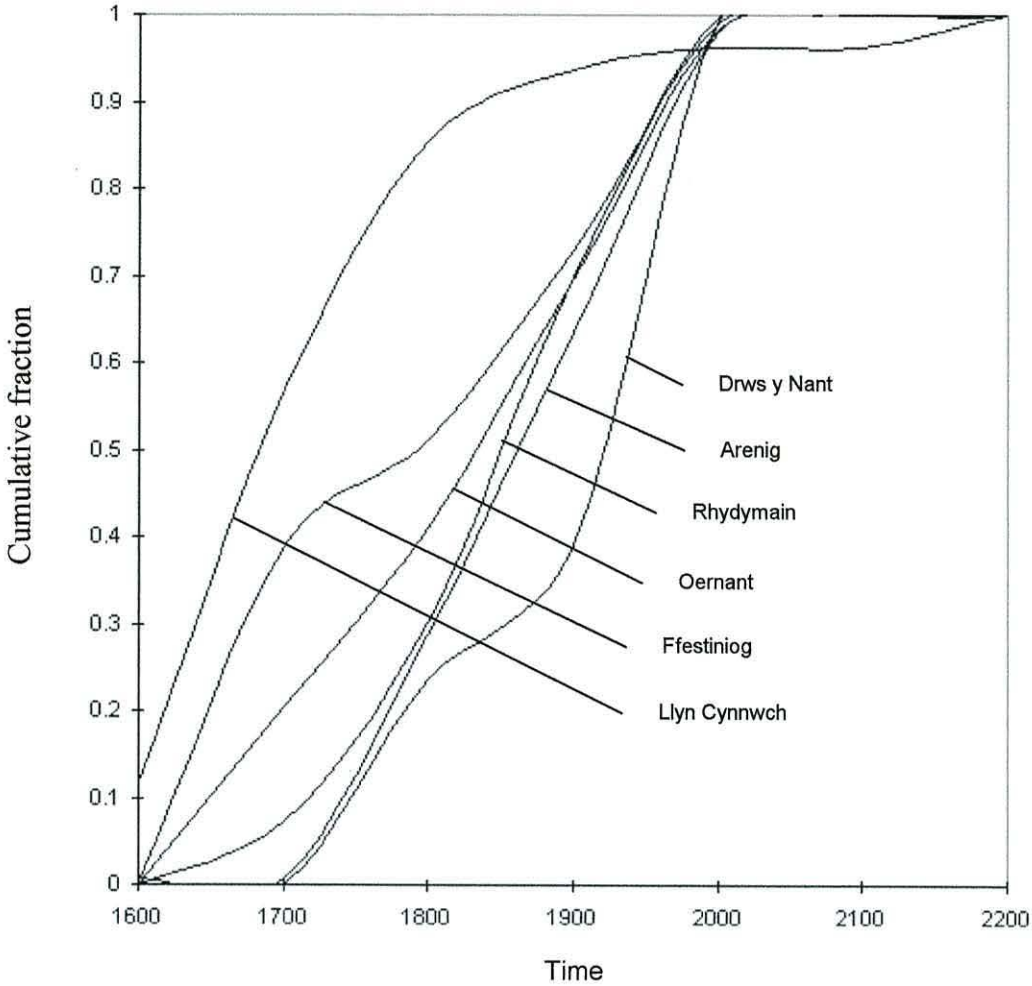

Figure 3.56: Cumulative curves for rainfall at gauge sites during the 3 July 2007 storm event

Runoff was determined in HEC-1 by the unit hydrograph Espey Rural method, with precipitation losses estimated by SCS curve numbers. This storm event occurred at the end of a dry summer period, so the model assumes soil moisture level A (dry) over the Cambrian grit outcrop and B (moderately dry) across the remaining Cambrian shales and Ordovician shales and volcanics. Rainfall was applied over the model area according to the Thiessen polygon method, weighted according to the area of the sub-catchment covered by each polygon, including estimated gauge totals for the Oernant site in Table 1. River routing then used the Muskingham equation.

Synthetic hydrograph results are presented for the Tyddyn Gwladys gauging station (fig.3.57) and the Bont Fawr gauging station, Dolgellau (fig.3.58), with recorded hydrographs for comparison.

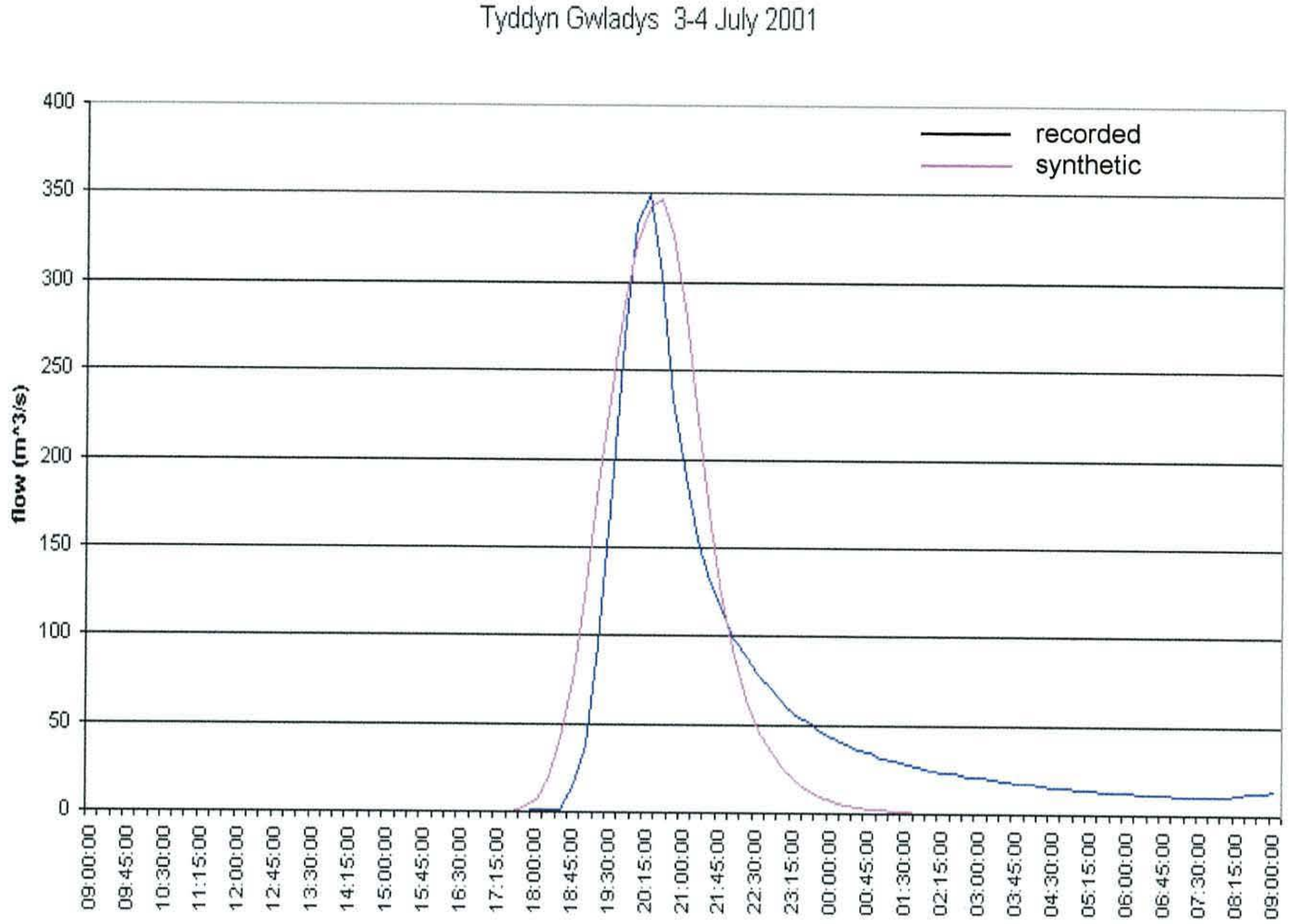

Figure 3.57: Comparison of recorded and synthetic hydrographs: Tyddyn Gwladys gauging station, 3 July 2001

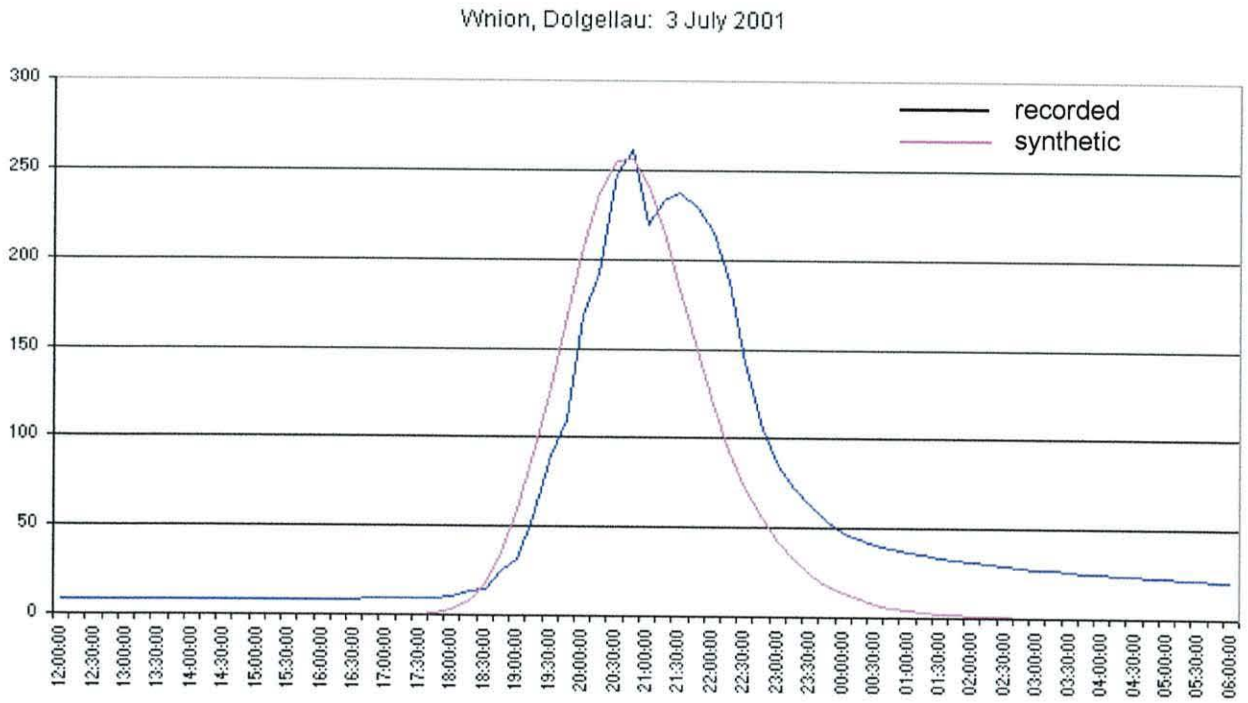

Figure 3.58: Comparison of recorded and synthetic hydrographs: Bont Fawr gauging station, Dolgellau, 3 July 2001

At Tyddyn Gwladys, a maximum flow of 340 $m^3 s^{-1}$ was recorded at 19:00 h. The modelled hydrograph has a rising limb in reasonable agreement, but the falling limb drops off too steeply at the end of the rainfall event. A likely explanation is the temporary groundwater storage of storm water which is released over the following 24 hours to produce the long tail of the recorded hydrograph. This flow is not represented in the simulation, since rainwater infiltrating to groundwater storage is lost from the HEC-1 model. The identification of fast storm runoff and slower base flow volumes from the hydrograph pattern is discussed by Linsley, Kohler and Paulhus (1988), and Wittenberg and Sivapalan (1999).

The hydrographs for the Wnion in Dolgellau show a similar relationship, with the simulated curve falling off too steeply and not representing the slow release of groundwater to the river system after the storm event. A further feature of note is the double peak present on the recorded hydrograph which is not produced by the model. Experience has shown that errors in hydrograph recording are most likely to occur around peak flows, when hydraulic pressures are greatest. If we assume, however, that the recording is accurate then a plausible explanation would be a sequence of two high intensity convection cells operating during the storm, sending successive waves of water down the river. The limited coverage of raingauges for the Wnion sub-catchment would have been insufficient to show the rainfall pattern in this amount of detail during the storm event. The operation of multiple convective cells within the squall line is consistent with both the Fovell and Tan theoretical model (figs 2.31-2.32), and the MM5 results from modelling the storm (fig.2.113).

One purpose of carrying out the HEC-1 simulation of the July 2001 flood event was to generate synthetic hydrographs for the ungauged outlets of the twelve Mawddach sub-catchments and eight Wnion sub-catchments. Results graphs are shown in figures 3.59 and 3.60. This hydrograph data is to be used as input to a GSTARS sediment transport model in section 3.3 below. It is appreciated that the tails of the synthetic hydrographs do not accurately represent the extended period during which the release of groundwater will affect river level. However, since a majority of sediment erosion and entrainment is likely to occur at high river discharges, the HEC-1 hydrographs were considered adequate for use in the sediment model. Subsequent evaluation of results of the sediment modelling indicates that this assumption was reasonable.

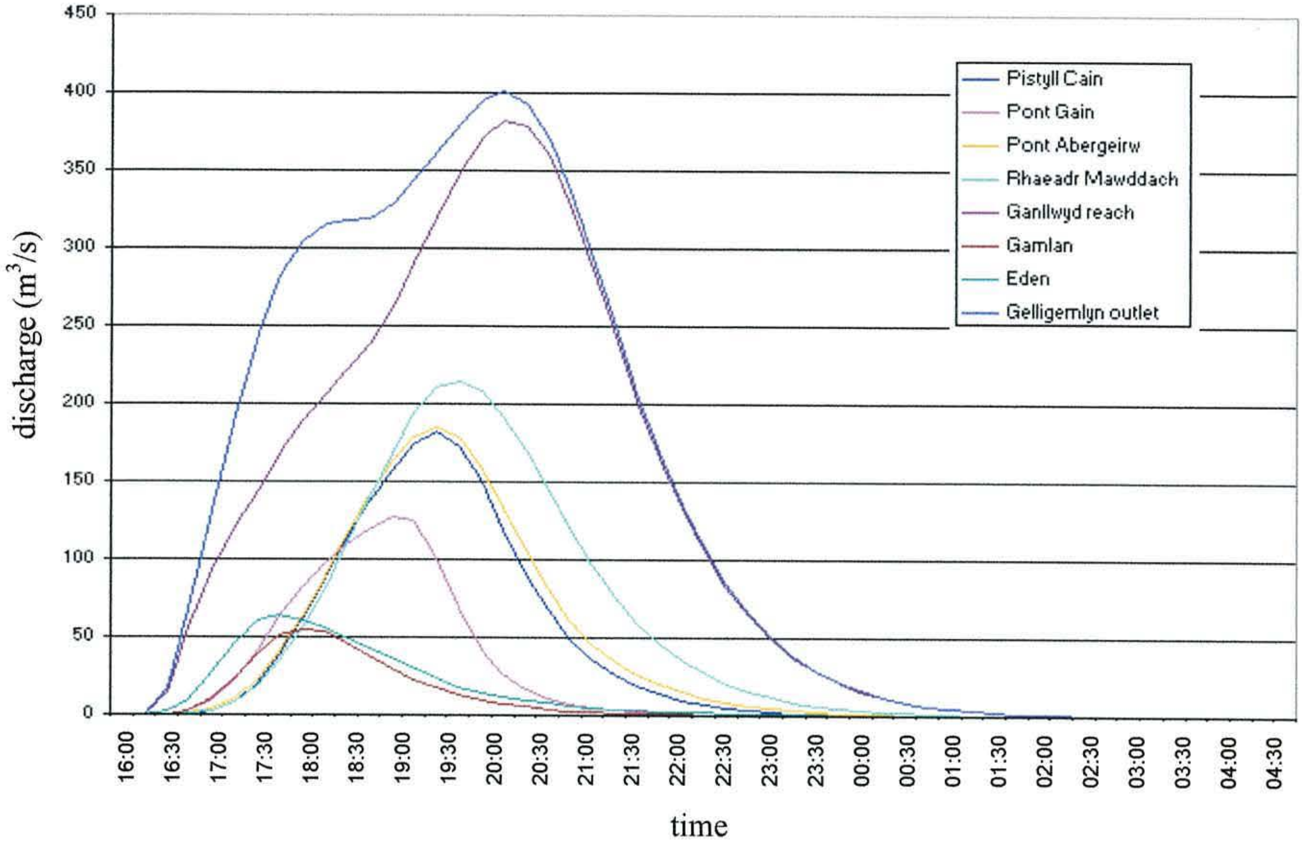

Figure 3.59: 3-4 July 2001 flood event: hydrographs for Mawddach sub-catchments

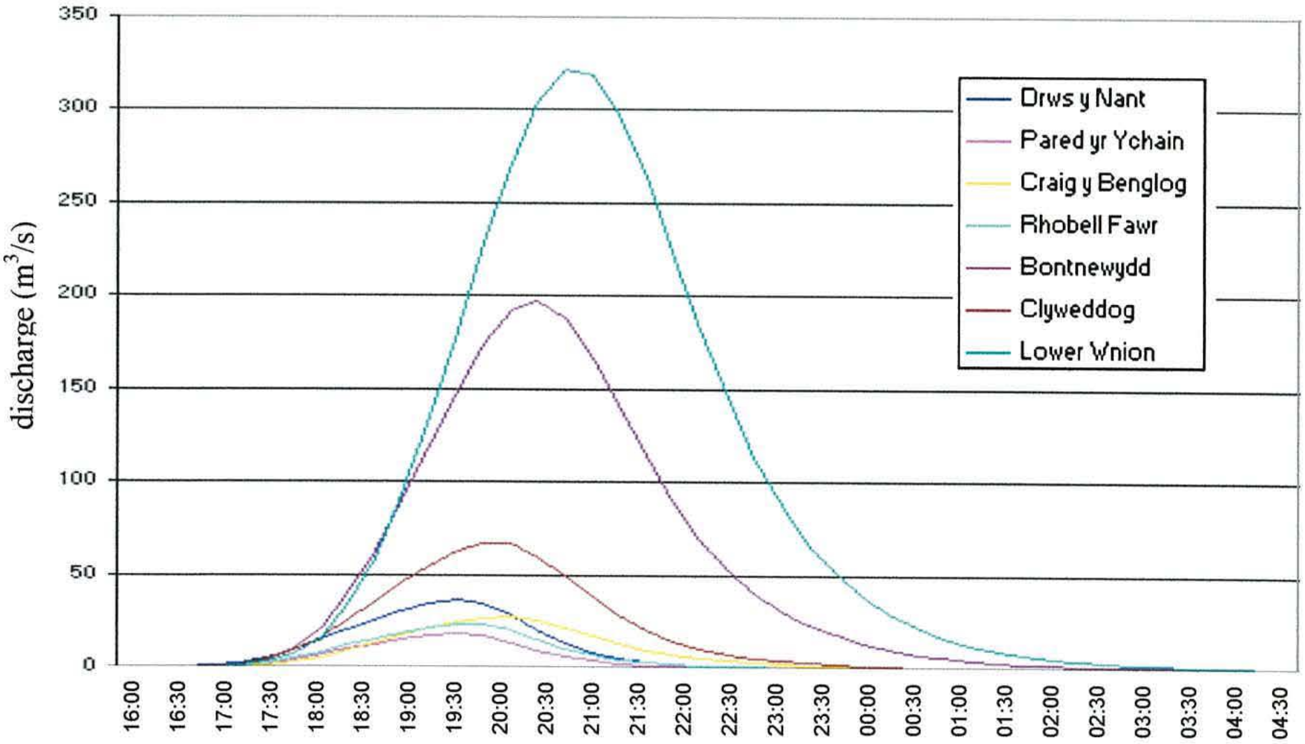

Figure 3.60: 3-4 July 2001 flood event: hydrographs for Wnion sub-catchments

Frontal storms

Runs of the HEC-1 Mawddach and Wnion sub-catchment models were carried out for a series of storms associated with frontal rainfall. With the exception of an event on 8 March 2003, these storms have all been analysed in section 2.2 and rainfall modelling carried out in section 2.4 above.

Simulation methods and parameters used in this set of HEC-1 models were identical to the 3 July 2001 case study, with the exception of:

- Rainfall: Data was available for a more numerous set of rain gauges, as shown in table 3.3. For each station, this table gives: three-hour rainfall totals(mm), cumulative storm rainfall(mm). In addition, cumulative rainfall fractions are calculated for use in the HEC-1 model.

- Soil characteristics: For the storms occurring during the wetter winter months between November and March, soil moisture level C (damp) was used for the Cambrian grit outcrop, and moisture level D (wet) was used for the Cambrian shale and Ordovician shale and volcanic outcrop areas. For the May storm event, the assumed soil moisture levels were reduced to B (moderately dry) for the Cambrian grit outcrop and moisture level C (damp) for the other areas of the catchment.

x coordinate		258800			264700			265000			268300			268200			272687			273982			270700		
y coordinate		327000			331500			318200			315600			322700			324518			323936			336000		
			Llanbedr			Cwm Bychan			Caerdeon			Erw Wen			Cwm Mynach			Ganllwyd			Tir Penrhos			Trawsfynydd	
08-Nov-02	03-06	4	4	0.11	5	5	0.08	7	7	0.13	7	7	0.11				5	5	0.07	5	5	0.07	6	6	0.11
	06-09	10	14	0.37	13	18	0.29	11	18	0.35	9	16	0.25				12	17	0.25	11	16	0.23	12	18	0.34
	09-12	12	26	0.68	18	36	0.57	17	35	0.67	18	34	0.53				21	38	0.56	23	39	0.56	18	36	0.68
	12-15	10	36	0.95	20	56	0.89	11	46	0.88	16	50	0.78				18	56	0.82	20	59	0.84	11	47	0.89
	15-18	1	37	0.97	2	58	0.92	2	48	0.92	3	53	0.83				6	62	0.91	7	66	0.94	2	49	0.92
	18-21	1	38	1.00	5	63	1.00	2	50	0.96	5	58	0.91				6	68	1.00	4	70	1.00	3	52	0.98
	21-00	0	38	1.00	0	63	1.00	2	52	1.00	6	64	1.00				0	68	1.00	0	70	1.00	1	53	1.00
29-Dec-02	00-03	1	1	0.03							1	1	0.02				0	0	0.00	1	1	0.02	2	2	0.03
	03-06	5	6	0.16							7	8	0.14				7	7	0.12	6	7	0.12	10	12	0.16
	06-09	4	10	0.27							7	15	0.27				9	16	0.28	7	14	0.23	8	20	0.27
	09-12	12	22	0.59							20	35	0.63				18	34	0.59	16	30	0.50	19	39	0.52
	12-15	9	31	0.84							9	44	0.79				9	43	0.74	10	40	0.67	9	48	0.64
	15-18	6	37	1.00							9	53	0.95				10	53	0.91	14	54	0.90	18	66	0.88
	18-21	0	37	1.00							3	56	1.00				5	58	1.00	6	60	1.00	9	75	1.00
21-May-03	09-12				1	1	0.01	0	0	0.00	0	0	0.00	1	1	0.01	0	0	0.00	1	1	0.02	0	0	0.00
	12-15				0	1	0.01	0	0	0.00	0	0	0.00	0	1	0.01	1	1	0.02	0	1	0.02	1	1	0.01
	15-18				12	13	0.13	10	10	0.14	10	10	0.14	16	17	0.11	6	7	0.11	5	6	0.10	8	9	0.13
	18-21				23	36	0.35	10	20	0.29	13	23	0.32	35	52	0.35	11	18	0.28	12	18	0.31	16	25	0.36
	21-00				8	44	0.42	8	28	0.41	12	35	0.49	18	70	0.47	11	29	0.45	8	26	0.45	6	31	0.44
22-May-03	00-03				2	46	0.44	1	29	0.42	1	36	0.51	2	72	0.49	1	30	0.47	1	27	0.47	1	32	0.46
	03-06				5	51	0.49	7	36	0.52	7	43	0.61	9	81	0.55	2	32	0.50	2	29	0.50	2	34	0.49
	06-09				26	77	0.74	14	50	0.72	12	55	0.77	20	101	0.68	9	41	0.64	7	36	0.62	11	45	0.64
	09-12				10	87	0.84	5	55	0.80	6	61	0.86	12	113	0.76	7	48	0.75	6	42	0.72	10	55	0.79
	12-15				15	102	0.98	12	67	0.97	6	67	0.94	30	143	0.97	14	62	0.97	13	55	0.95	13	68	0.97
	15-18				2	104	1.00	2	69	1.00	4	71	1.00	5	148	1.00	2	64	1.00	3	58	1.00	2	70	1.00
03-Feb-04	00-03	4	4	0.12	14	14	0.13	7	7	0.12	14	14	0.12	12	12	0.10	11	11	0.11				13	13	0.08
	03-06	0	4	0.12	12	26	0.25	4	11	0.18	13	27	0.23	12	24	0.21	11	22	0.21				18	31	0.20
	06-09	6	10	0.30	13	39	0.37	8	19	0.32	14	41	0.36	14	38	0.33	13	35	0.34				17	48	0.31
	09-12	2	12	0.36	5	44	0.42	3	22	0.37	9	50	0.43	8	46	0.40	6	41	0.39				11	59	0.38
	12-15	3	15	0.45	5	49	0.46	4	26	0.43	8	58	0.50	8	54	0.47	7	48	0.46				12	71	0.46
	15-18	0	15	0.45	4	53	0.50	1	27	0.45	8	66	0.57	8	62	0.54	7	55	0.53				13	84	0.55
	18-21	0	15	0.45	0	53	0.50	0	27	0.45	0	66	0.57	0	62	0.54	0	55	0.53				0	84	0.55
	21-00	0	15	0.45	1	54	0.51	0	27	0.45	0	66	0.57	0	62	0.54	0	55	0.53				2	86	0.56
04-Feb-04	00-03	0	15	0.45	0	54	0.51	0	27	0.45	0	66	0.57	0	62	0.54	0	55	0.53				0	86	0.56
	03-06	0	15	0.45	6	60	0.57	4	31	0.52	4	70	0.61	7	69	0.60	4	59	0.57				7	93	0.60
	06-09	6	21	0.64	17	77	0.73	10	41	0.68	12	82	0.71	16	85	0.74	12	71	0.68				18	111	0.72
	09-12	3	24	0.73	10	87	0.82	6	47	0.78	11	93	0.81	10	95	0.83	11	82	0.79				16	127	0.82
	12-15	7	31	0.94	12	99	0.93	9	56	0.93	13	106	0.92	12	107	0.93	15	97	0.93				16	143	0.93
	15-18	2	33	1.00	7	106	1.00	4	60	1.00	9	115	1.00	8	115	1.00	7	104	1.00				11	154	1.00
08-Mar-03	00-03	5	5	0.25	5	5	0.20	4	4	0.25	6	6	0.17	8	8	0.17	7	7	0.12	5	5	0.09	7	7	0.08
	03-06	4	9	0.45	4	9	0.36	3	7	0.44	7	13	0.36	9	17	0.36	11	18	0.32	10	15	0.26	20	27	0.29
	06-09	3	12	0.60	4	13	0.52	3	10	0.63	11	24	0.67	11	28	0.60	14	32	0.56	13	28	0.48	30	57	0.61
	09-12	3	15	0.75	5	18	0.72	3	13	0.81	5	29	0.81	9	37	0.79	14	46	0.81	17	45	0.78	19	76	0.82
	12-15	5	20	1.00	7	25	1.00	3	16	1.00	7	36	1.00	9	46	0.98	11	57	1.00	12	57	0.98	16	92	0.99
	15-18	0	20	1.00	0	25	1.00	0	16	1.00	0	36	1.00	0	46	0.98	0	57	1.00	0	57	0.98	0	92	0.99
	18-21	0	20	1.00	0	25	1.00	0	16	1.00	0	36	1.00	0	46	0.98	0	57	1.00	0	57	0.98	0	92	0.99
	21-00	0	20	1.00	0	25	1.00	0	16	1.00	0	36	1.00	0	46	0.98	0	57	1.00	0	57	0.98	0	92	0.99
09-Mar-03	00-03	0	20	1.00	0	25	1.00	0	16	1.00	0	36	1.00	1	47	1.00	0	57	1.00	0	57	0.98	1	93	1.00
	03-06	0	20	1.00	0	25	1.00	0	16	1.00	0	36	1.00	0	47	1.00	0	57	1.00	1	58	1.00	0	93	1.00
	06-09	0	20	1.00	0	25	1.00	0	16	1.00	0	36	1.00	0	47	1.00	0	57	1.00	0	58	1.00	0	93	1.00

Key

Station		
rainfall in 3 hours (mm)	cumulative storm rain (mm)	cumulative fraction of total storm rainfall at this station

Table 3.3: Storm event rainfall recorded at gauge sites in and around the Mawddach catchment

x coordinate		272864			279939			279843			279792			280650			284819			271999		
y coordinate		331732			321848			325367			328868			333400			323073			318021		
			Bronaber			Aran Hall			Rhobell Fawr			Allt Lwyd			Blaen Lliw			Pared yr Ychain			Dolgellau	
08-Nov-02	03-06	6	6	0.09				4	4	0.05	3	3	0.06	4	4	0.08	4	4	0.06			
	06-09	12	18	0.27				7	11	0.15	5	8	0.17	8	12	0.24	7	11	0.16			
	09-12	22	40	0.60				17	28	0.38	13	21	0.44	13	25	0.50	14	25	0.37			
	12-15	19	59	0.88				28	56	0.77	18	39	0.81	14	39	0.78	21	46	0.68			
	15-18	4	63	0.94				9	65	0.89	4	43	0.90	6	45	0.90	13	59	0.87			
	18-21	4	67	1.00				6	71	0.97	4	47	0.98	5	50	1.00	7	66	0.97			
	21-00	0	67	1.00				2	73	1.00	1	48	1.00	0	50	1.00	2	68	1.00			
29-Dec-02	00-03	1	1	0.02	0	0	0.00	1	1	0.01	1	1	0.02	2	2	0.04	1	1	0.01	0	0	0.00
	03-06	8	9	0.14	4	4	0.09	6	7	0.10	8	9	0.16	6	8	0.14	10	11	0.13	3	3	0.07
	06-09	8	17	0.26	8	12	0.27	7	14	0.20	8	17	0.30	6	14	0.25	11	22	0.26	8	11	0.26
	09-12	17	34	0.52	12	24	0.53	16	30	0.43	14	31	0.54	15	29	0.51	18	40	0.47	13	24	0.57
	12-15	10	44	0.68	11	35	0.78	14	44	0.64	8	39	0.68	9	38	0.67	16	56	0.66	8	32	0.76
	15-18	12	56	0.86	7	42	0.93	16	60	0.87	11	50	0.88	10	48	0.84	20	76	0.89	8	40	0.95
	18-21	9	65	1.00	3	45	1.00	9	69	1.00	7	57	1.00	9	57	1.00	9	85	1.00	2	42	1.00
21-May-03	09-12	0	0	0.00				0	0	0.00	0	0	0.00				1	1	0.01	0	0	0.00
	12-15	1	1	0.01				1	1	0.02	0	0	0.00				0	1	0.01	0	0	0.00
	15-18	14	15	0.15				7	8	0.12	7	7	0.14				8	9	0.12	10	10	0.16
	18-21	21	36	0.37				14	22	0.34	10	17	0.35				16	25	0.34	13	23	0.38
	21-00	10	46	0.47				10	32	0.49	8	25	0.51				7	32	0.44	6	29	0.48
22-May-03	00-03	1	47	0.48				1	33	0.51	2	27	0.55				1	33	0.45	1	30	0.49
	03-06	4	51	0.52				2	35	0.54	1	28	0.57				2	35	0.48	5	35	0.57
	06-09	15	66	0.67				8	43	0.66	7	35	0.71				8	43	0.59	10	45	0.74
	09-12	15	81	0.83				7	50	0.77	5	40	0.82				9	52	0.71	5	50	0.82
	12-15	15	96	0.98				12	62	0.95	8	48	0.98				17	69	0.95	10	60	0.98
	15-18	2	98	1.00				3	65	1.00	1	49	1.00				4	73	1.00	1	61	1.00
03-Feb-04	00-03	12	12	0.10				11	11	0.07	12	12	0.08	10	10	0.07	9	9	0.06			
	03-06	17	29	0.23				11	22	0.14	18	30	0.19	17	27	0.19	17	26	0.18			
	06-09	16	45	0.36				12	34	0.21	16	46	0.29	16	43	0.30	17	43	0.30			
	09-12	9	54	0.44				12	46	0.28	13	59	0.38	15	58	0.41	16	59	0.41			
	12-15	14	68	0.55				16	62	0.38	18	77	0.49	16	74	0.52	14	73	0.51			
	15-18	7	75	0.60				12	74	0.46	11	88	0.56	9	83	0.58	11	84	0.58			
	18-21	0	75	0.60				0	74	0.46	0	88	0.56	1	84	0.59	0	84	0.58			
	21-00	0	75	0.60				2	76	0.47	1	89	0.57	0	84	0.59	1	85	0.59			
04-Feb-04	00-03	0	75	0.60				0	76	0.47	0	89	0.57	0	84	0.59	0	85	0.59			
	03-06	3	78	0.63				4	80	0.49	3	92	0.59	2	86	0.61	3	88	0.61			
	06-09	11	89	0.72				17	97	0.60	15	107	0.68	12	98	0.69	9	97	0.67			
	09-12	13	102	0.82				24	121	0.75	20	127	0.81	19	117	0.82	16	113	0.78			
	12-15	15	117	0.94				26	147	0.91	21	148	0.94	16	133	0.94	18	131	0.91			
	15-18	7	124	1.00				15	162	1.00	9	157	1.00	9	142	1.00	13	144	1.00			
08-Mar-03	00-03	3	3	0.04	0	0	0.00	2	2	0.03	6	6	0.11	5	5	0.10	2	2	0.05	0	0	0.00
	03-06	15	18	0.23	3	3	0.10	15	17	0.24	11	17	0.30	8	13	0.26	10	12	0.28	3	3.4	0.15
	06-09	21	39	0.50	5	8	0.25	11	28	0.39	10	27	0.48	9	22	0.44	9	21	0.49	3	6.8	0.29
	09-12	20	59	0.76	7	15	0.48	23	51	0.72	15	42	0.75	14	36	0.72	11	32	0.74	7	13	0.58
	12-15	17	76	0.97	9	23	0.76	19	70	0.99	13	55	0.98	13	49	0.98	10	42	0.98	5	18	0.78
	15-18	1	77	0.99	7	30	0.99	1	71	1.00	0	55	0.98	0	49	0.98	0	42	0.98	5	23	0.99
	18-21	0	77	0.99	0	30	0.99	0	71	1.00	0	55	0.98	0	49	0.98	0	42	0.98	0	23	0.99
	21-00	0	77	0.99	0	30	0.99	0	71	1.00	0	55	0.98	0	49	0.98	0	42	0.98	0	23	0.99
09-Mar-03	00-03	1	78	1.00	0	30	0.99	0	71	1.00	1	56	1.00	0	49	0.98	1	43	1.00	0	23	0.99
	03-06	0	78	1.00	0	31	1.00	0	71	1.00	0	56	1.00	1	50	1.00	0	43	1.00	0	23	1.00
	06-09	0	78	1.00	0	31	1.00	0	71	1.00	0	56	1.00	0	50	1.00	0	43	1.00	0	23	1.00

Table 3.3: Storm event rainfall recorded at gauge sites in and around the Mawddach catchment

8 November 2002

A comparison between the recorded and modelled hydrograph for Tyddyn Gwladys is shown in fig.3.61. As in the case of the July 2001 convective storm, there is reasonable agreement in the ascending limb and peak of the hydrograph. The descending hydrograph limbs of both the field data and the model show a step. A second period of increased rainfall is not evident from the gauge data in table 3, so this feature is likely to represent the relative delays of waterflows on the upper Mawddach and Gain in reaching the Tyddyn Gwladys site. Although HEC-1 performs correctly qualitatively, the model again shows an excessively rapid fall in river level after the storm event because it ignores processes of groundwater storage and release.

The program provides a facility for entering a value of constant river base flow which will be added to the calculated storm discharge, offsetting the synthetic hydrograph upwards. Realistic base flows have been applied in the cases which follow.

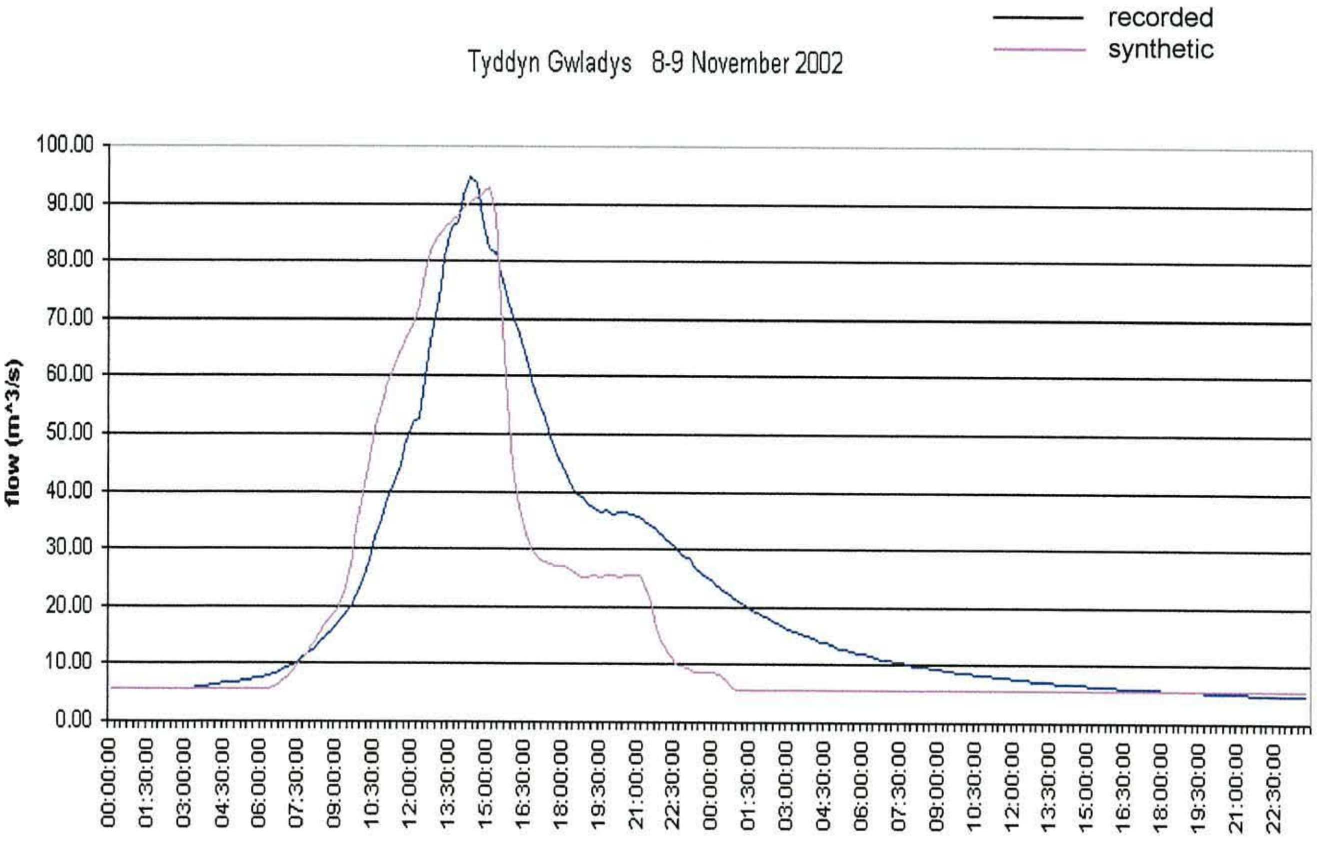

Figure 3.61: Comparison of modelled and recorded hydrographs for Tyddyn Gwladys, Afon Mawddach, 8 November 2002

29 December 2002

Hydrographs for four recording sites are given in figs 3.62-3.65, with HEC-1 synthetic hydrographs for comparison.

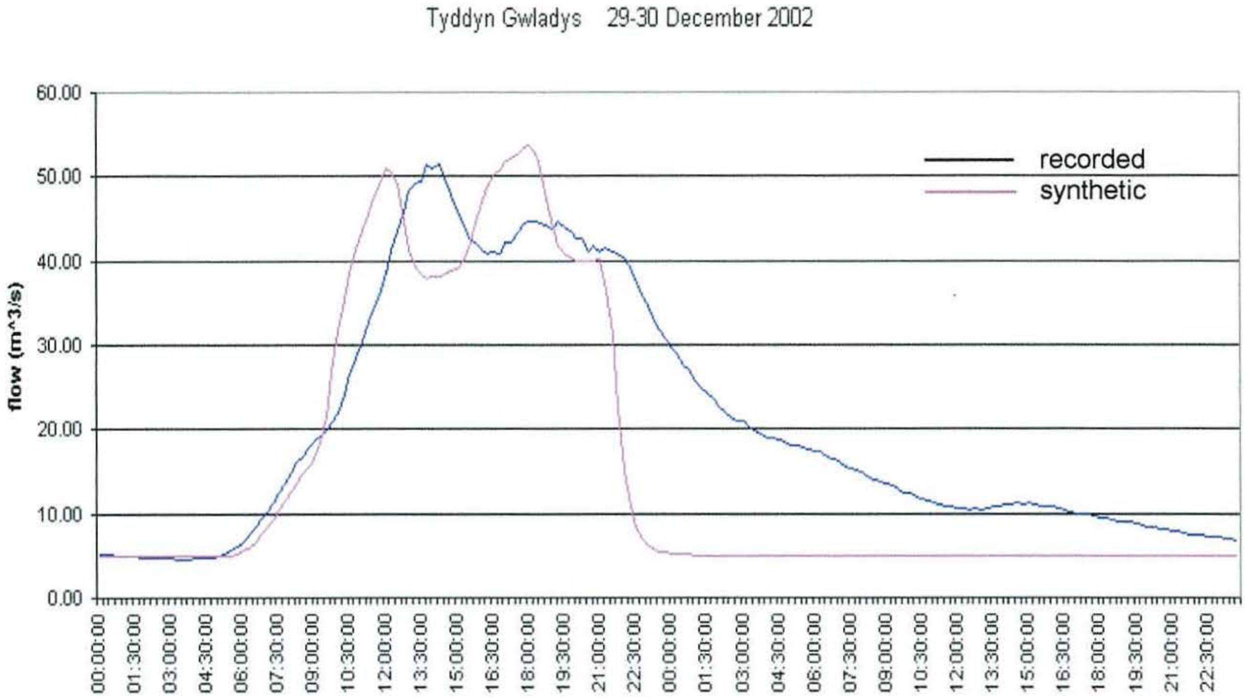

Figure 3.62: Comparison of modelled and recorded hydrographs for Tyddyn Gwladys, Afon Mawddach, 29 December 2002

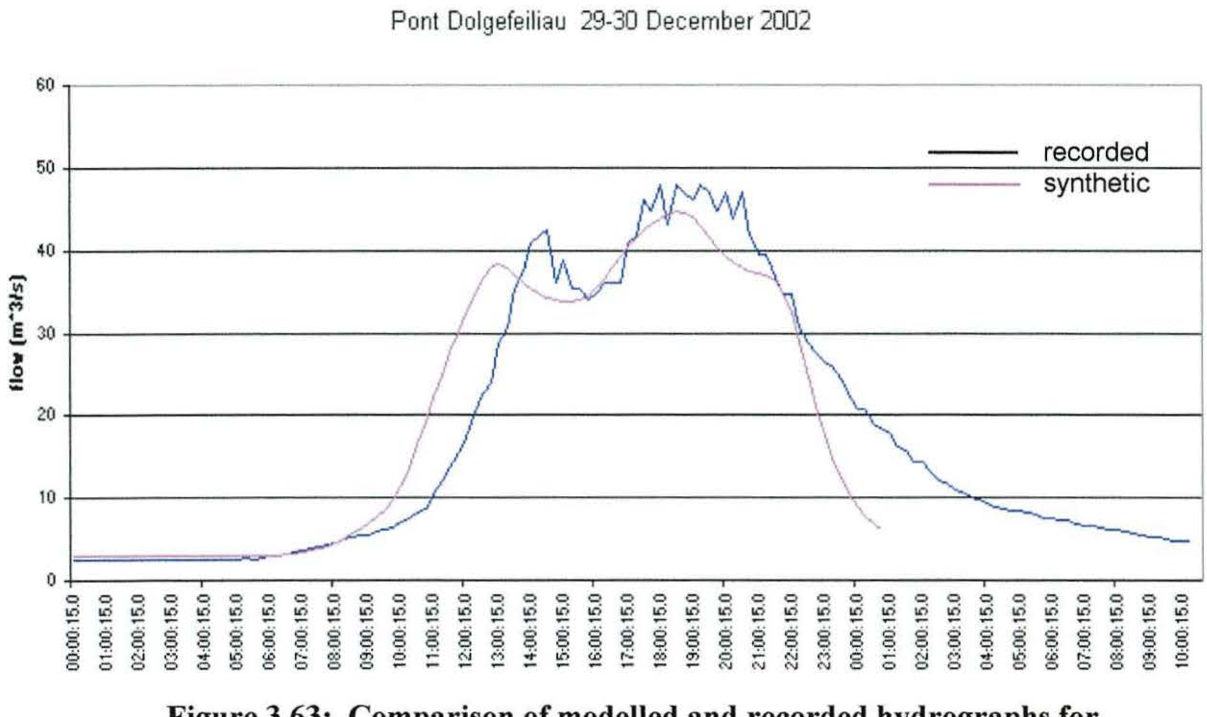

Figure 3.63: Comparison of modelled and recorded hydrographs for Pont Dolgefeiliau, Afon Eden, 29 December 2002

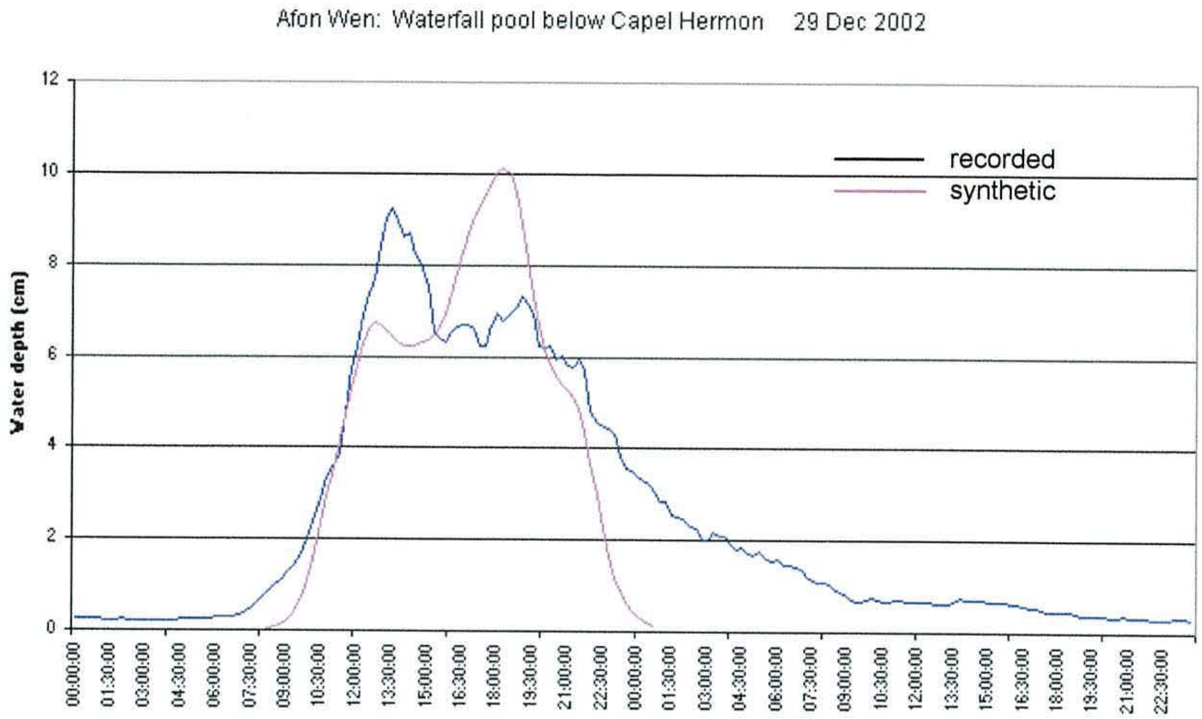

Figure 3.64: Comparison of modelled and recorded hydrographs for Hermon, Afon Wen, 29 December 2002

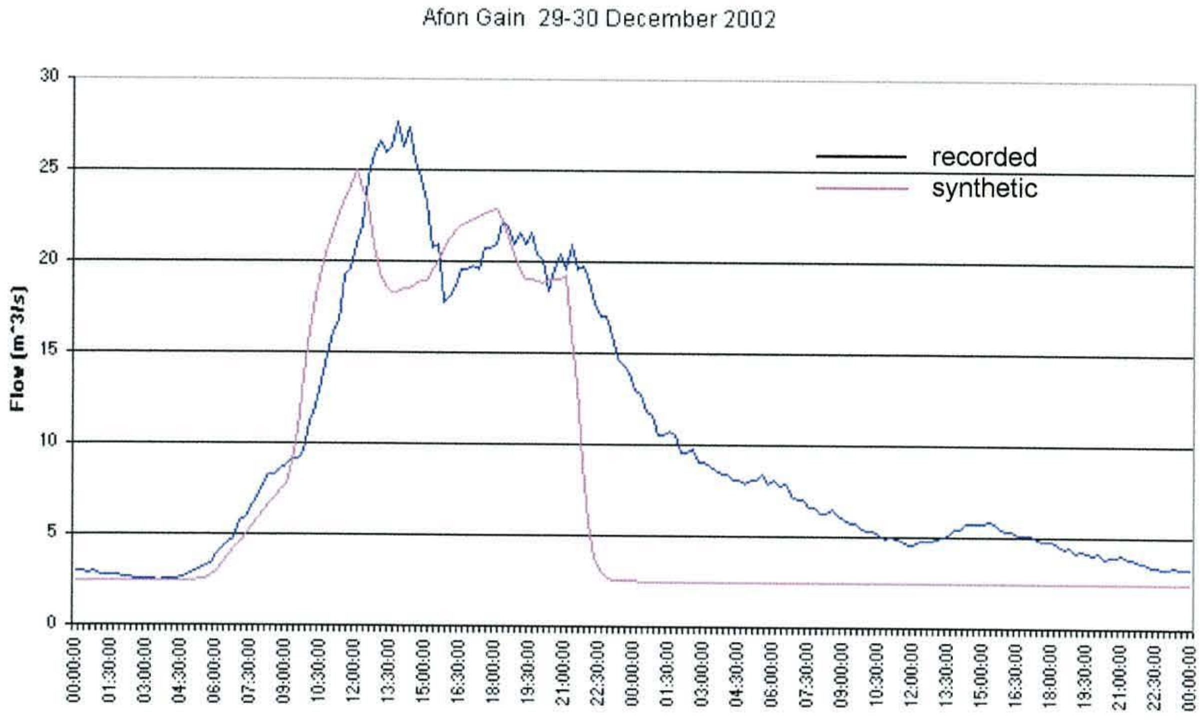

Figure 3.65: Comparison of modelled and recorded hydrographs for the Afon Gain near Pistyll Cain, 29 December 2002

The modelled hydrographs in each case show good correspondence with the rising limbs and time to peak of the field data but, as in previous examples, the falling limbs are excessively steep. It may be significant that this effect is most pronounced for hydrograph sites in the steeply descending gorge sections of the Mawddach, Gain and Afon Wen where resurgence of groundwater following the peak of a flood event might be expected. Field evidence of this process is presented in section 3.4 below. The discrepancy is less pronounced at Pont Dolgefeiliau in the wider floored Eden valley.

8 March 2003

The intense storm of 8 March 2003 was centred on the village of Trawsfynydd, with a band of heavy rainfall extending to the south east as shown in fig. 3.66. This represents a type A rainfall event in the classification of section 2.2.

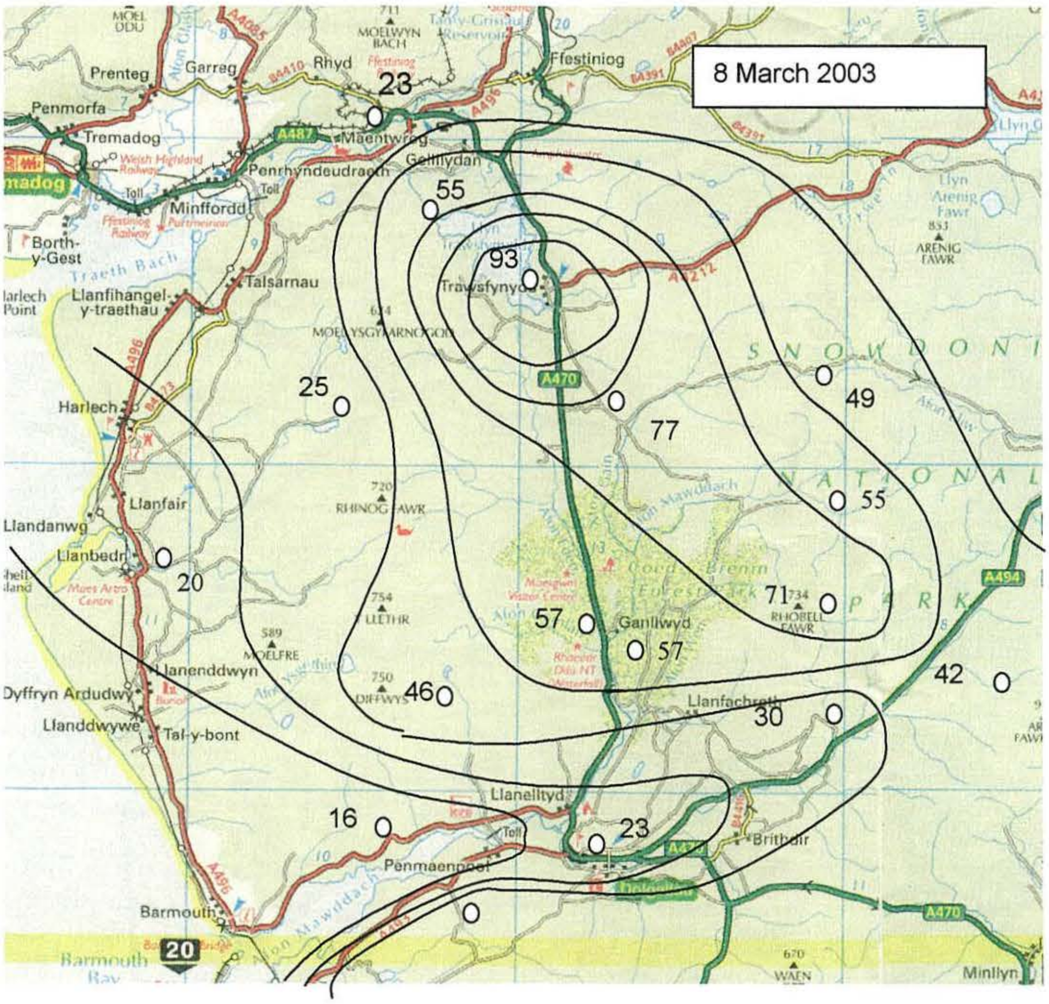

Figure 3.66: Total storm rainfall(mm), 8 March 2003

Hydrographs are available for three river sites for the 8 March 2003 storm, as shown in figs 3.67-3.69.

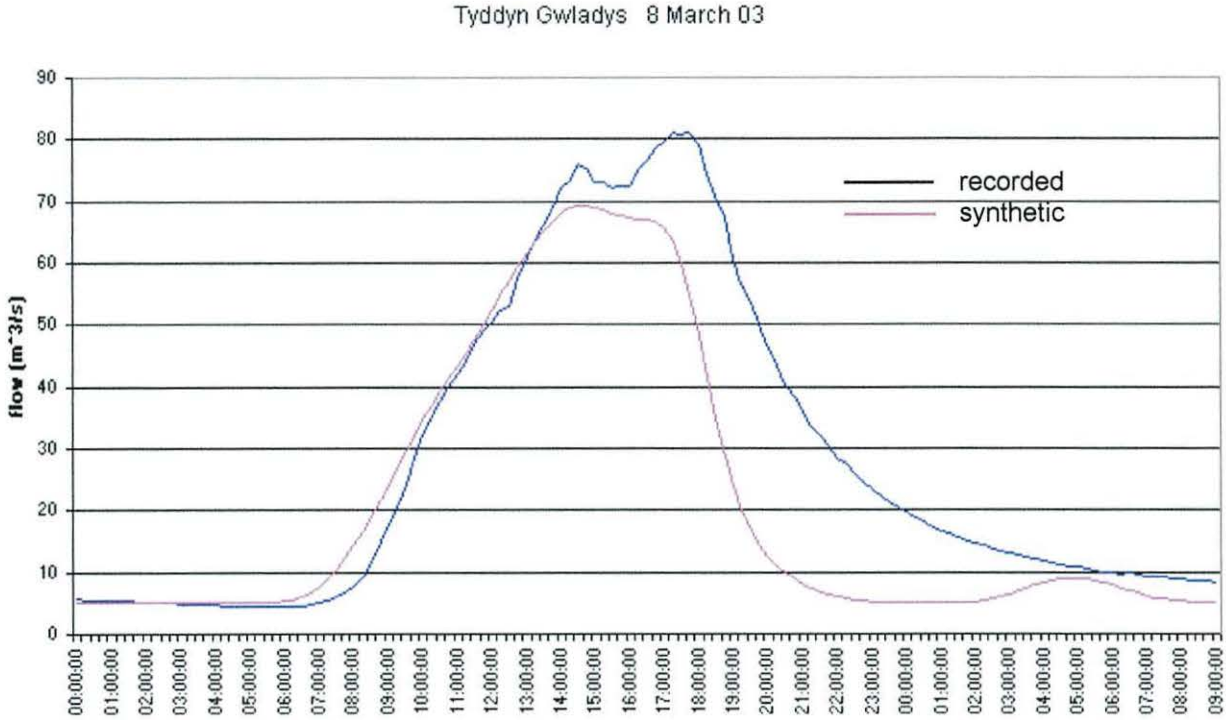

Figure 3.67: Comparison of modelled and recorded hydrographs for Tyddyn Gwladys, Afon Mawddach, 8 March 2003

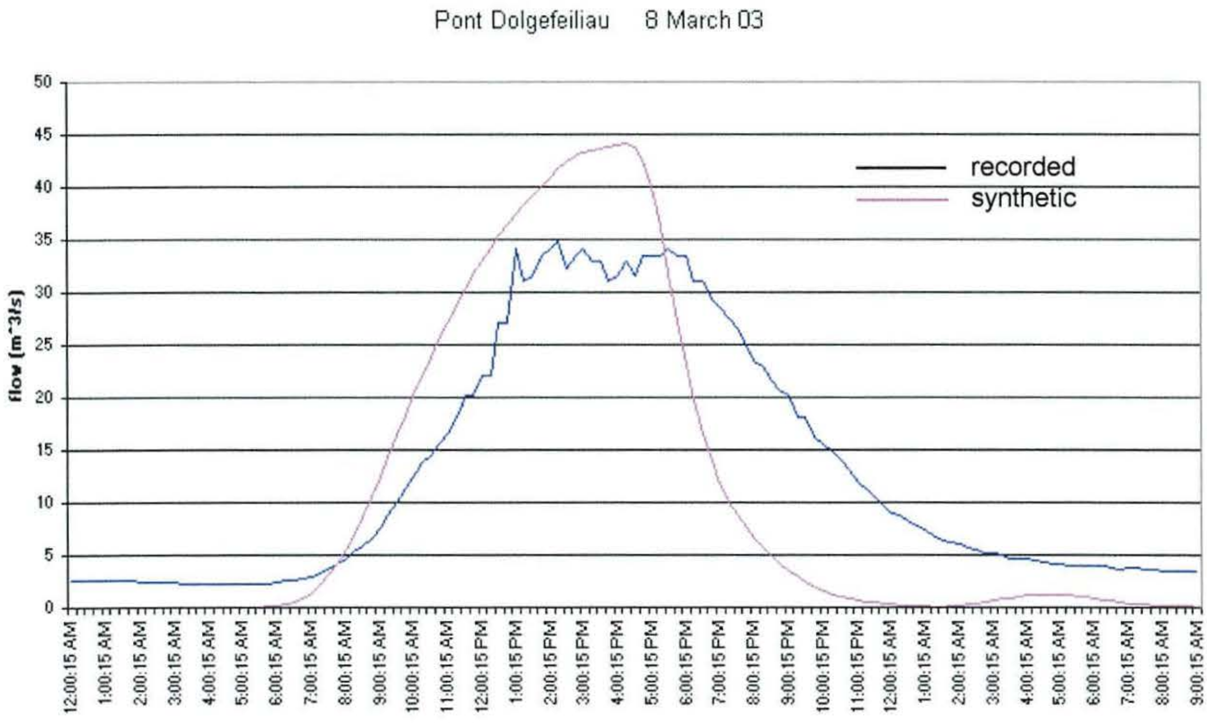

Figure 3.68: Comparison of modelled and recorded hydrographs for Pont Dolgefeiliau, Afon Eden, 8 March 2003

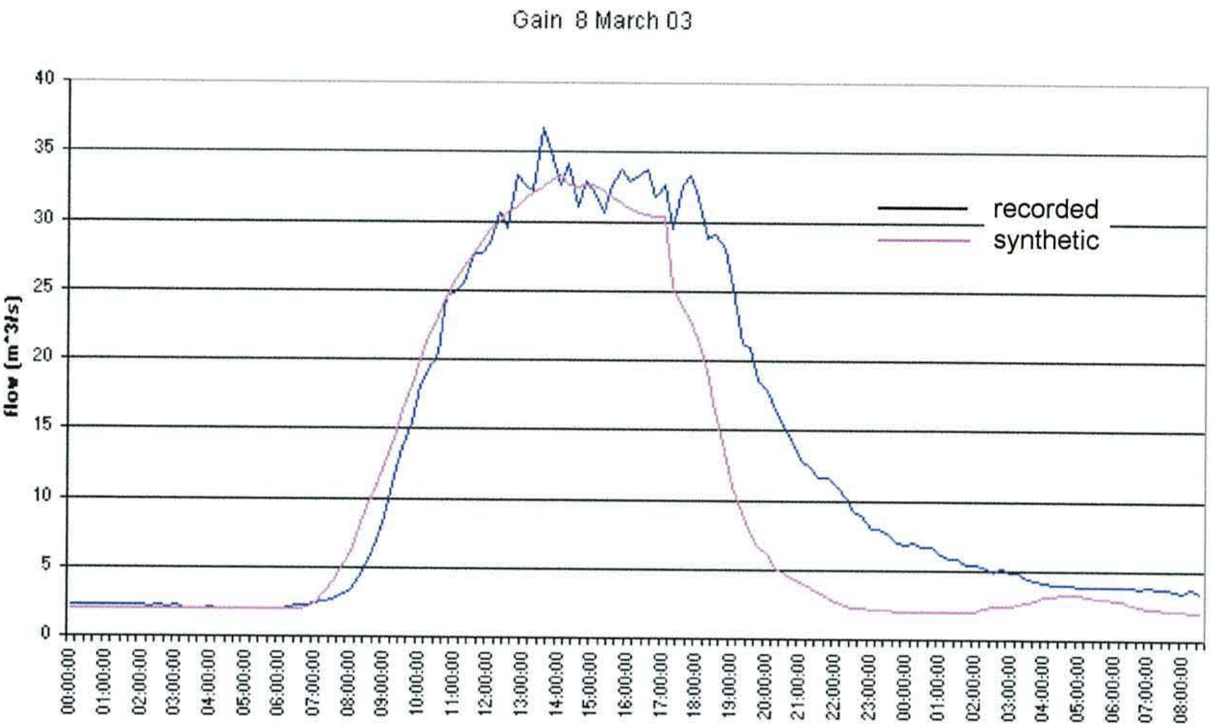

Figure 3.69: Comparison of modelled and recorded hydrographs for the Afon Gain near Pistyll Cain, 8 March 2003

Modelled hydrographs for Tyddyn Gwladys and Pistyll Cain give reasonable approximations for the rising hydrograph limbs and flow maxima. As expected, the falling limbs descend too rapidly due to lack of groundwater resurgence.

The model result for Pont Dolgefeiliau on the Afon Eden is unusual in significantly over-estimating the flood peak. This is the only occasion on which this type of error was observed during the modelling of simple storm events. A likely explanation lies in the very localised nature of the rainfall distribution. A rapid fall-off in rainfall total occurs over the Rhinog mountain range and the Crawcwellt plateau to the south of Trawsfynydd. It may be the case that the Thiessen polygon method has overestimated rainfall for the Eden sub-catchment. A distributed rainfall model such as MM5 which provides rainfall forecasts for each 1km grid square might be expected to provide a more accurate result than averaging rainfall between widely separated rain gauges.

21-23 May 2003

The rainfall event of 21-23 May 2003 differs from previous examples in being a pair of storms occurring on successive days. Three hydrograph records are available for this period, as shown in figs 3.70-3.72.

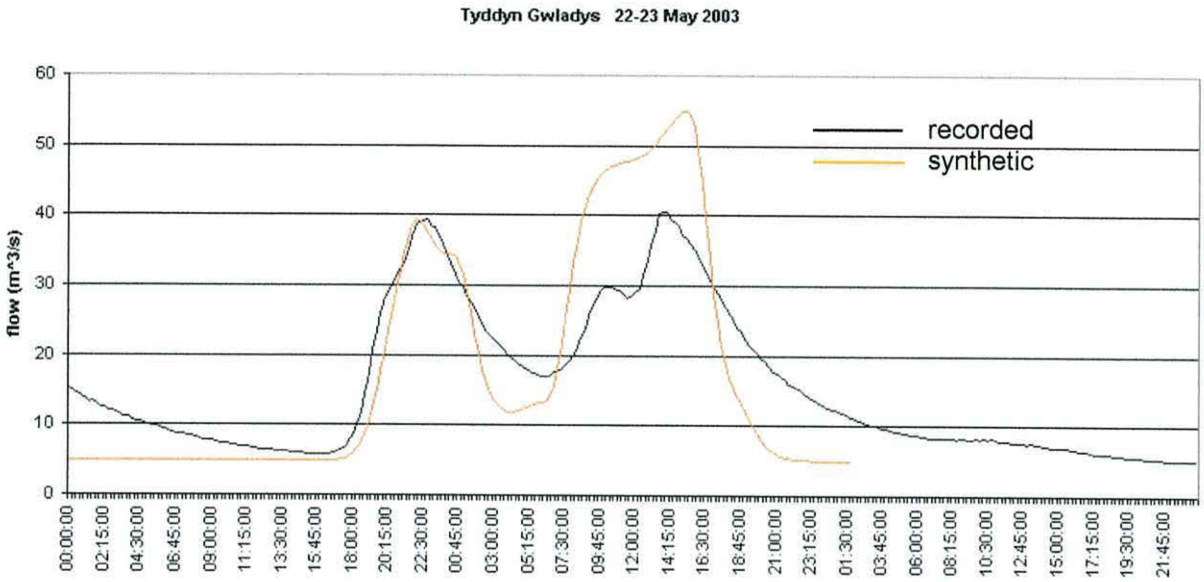

Figure 3.70: Comparison of modelled and recorded hydrographs for Tyddyn Gwladys, Afon Mawddach, 21-23 May 2003

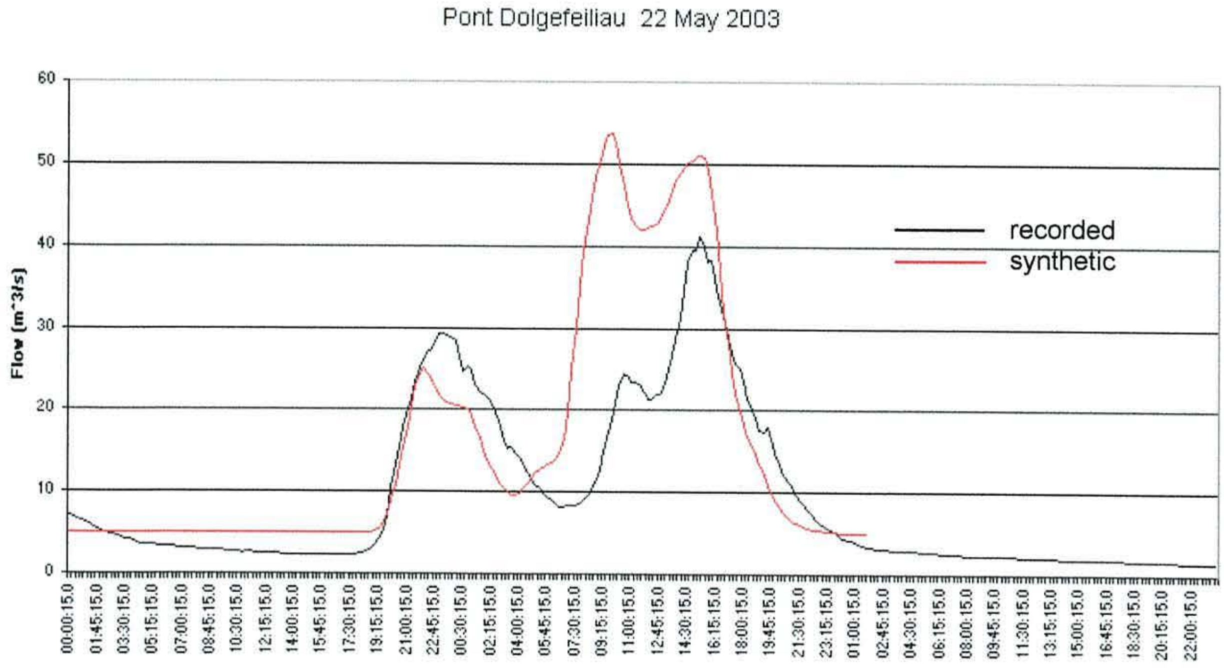

Figure 3.71: Comparison of modelled and recorded hydrographs for Pont Dolgefeiliau, Afon Eden, 21-23 May 2003

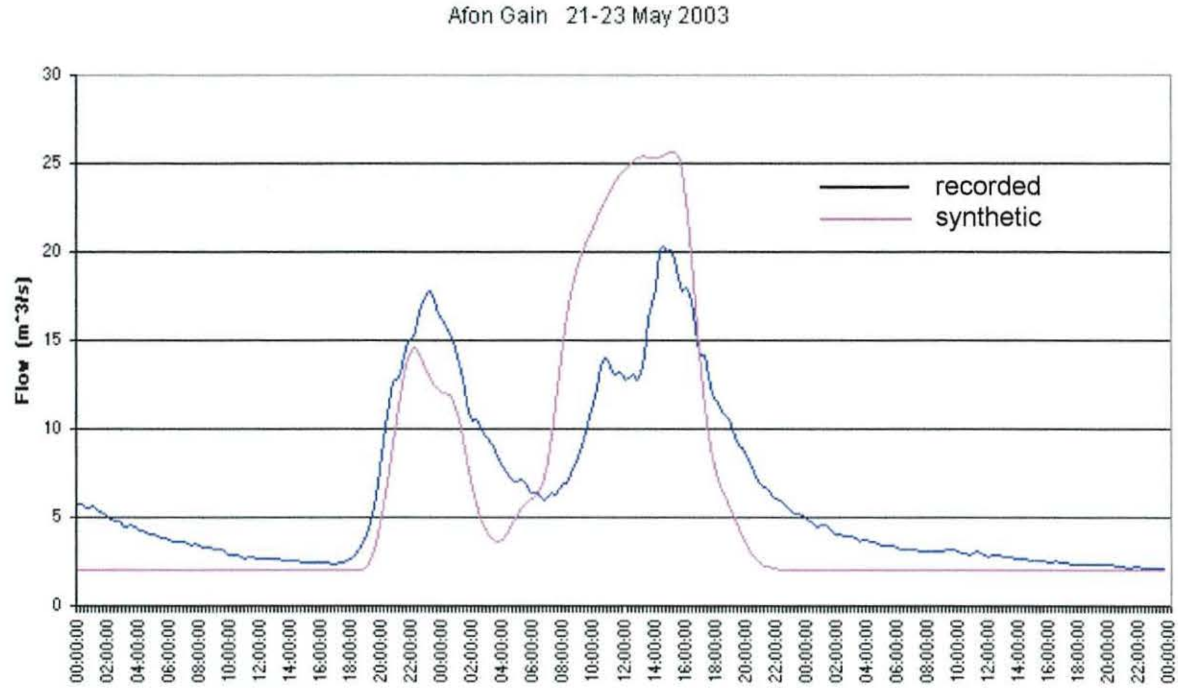

Figure 3.72: Comparison of modelled and recorded hydrographs for the Afon Gain near Pistyll Cain, 21-23 May 2003

A significant feature of each of the hydrographs is that the second storm peak is significantly overestimated by the HEC-1 model. This appears to be a result of the method used to determine infiltration rate based on total cumulative rainfall since the commencement of the rainfall event. The method assumes no recovery of soil water storage capacity during the interval between storms. The HEC-1 model appears to lose accuracy when modelling closely separated rainfall sequences.

3-4 February 2004

Another pair of closely spaced rainfall events occurred during the period 3-4 February 2004, as discussed previously in sections 2.2 and 2.4. A comparison of the recorded hydrograph at Tyddyn Gwladys and the HEC-1 modelled hydrograph is shown in fig.3.73. As in the May 2003 example, the second flood peak is overestimated by the model, but the extent of the error is less than in the May case. A likely explanation is that less recovery of storage capacity would occur during the colder and wetter February period, so the mathematical basis of the model is closer to reality.

The HEC-1 hydrographs generated for sub-catchments of the Mawddach and the Wnion (fig.3.74) are used in a sediment transport model in section 3.3 below.

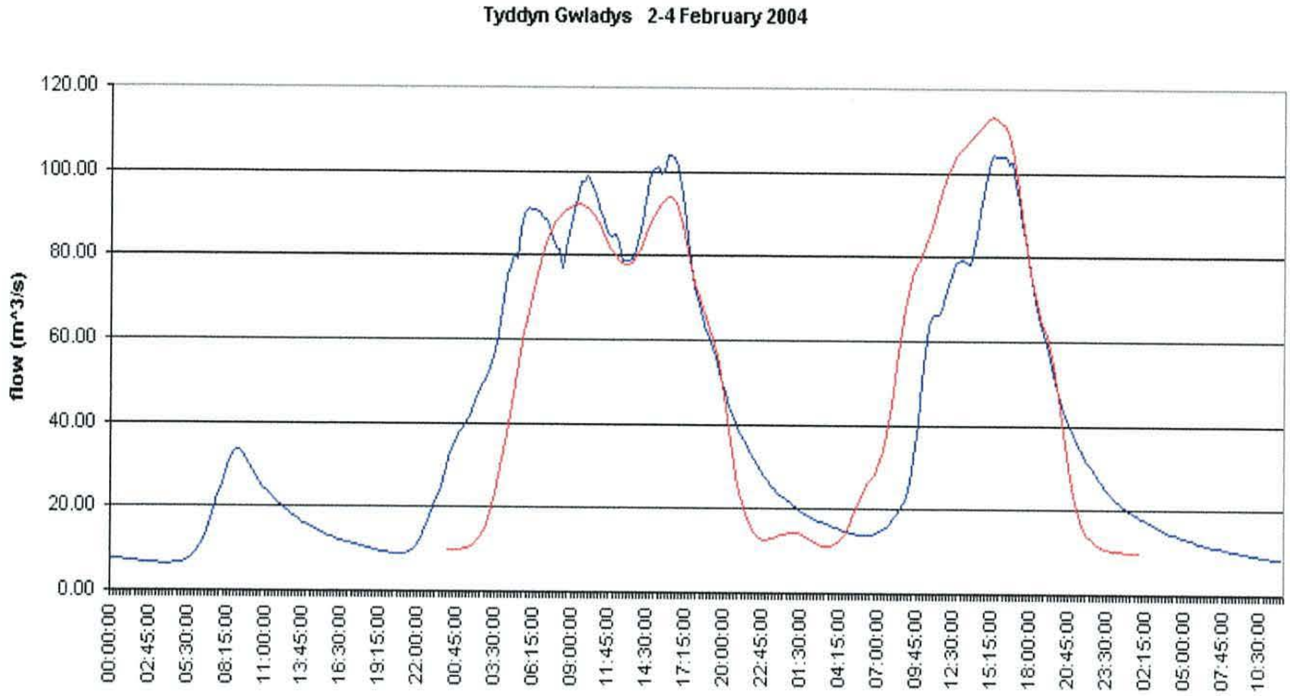

Figure 3.73: Comparison of modelled and recorded hydrographs for Tyddyn Gwladys, Afon Mawddach, 2-4 February 2004

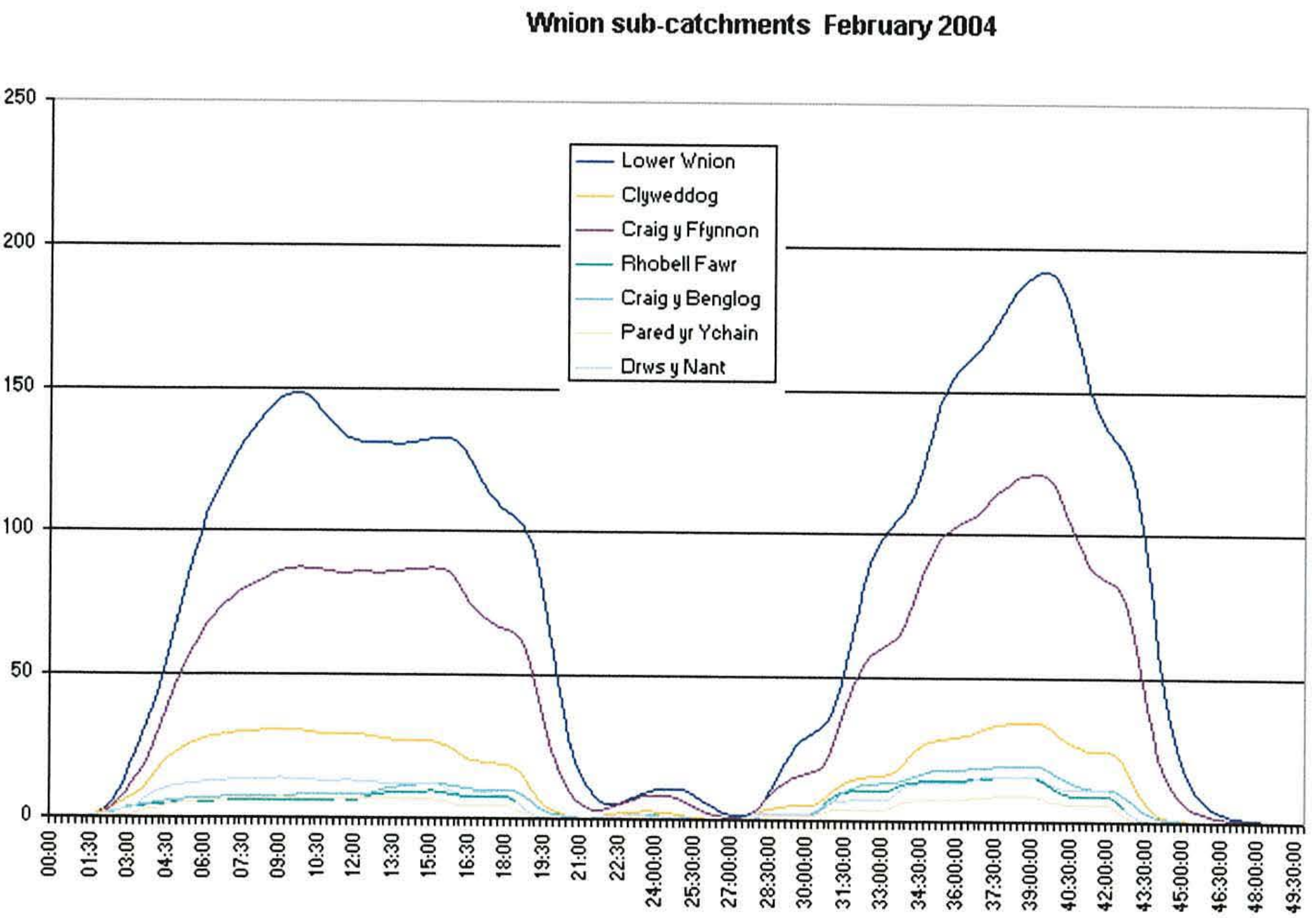

Figure 3.74: Hydrographs generated by theHEC-1 model for sub-catchments of the Afon Wnion, storm events of 2-4 February 2004

Summary

- Field data has been collected from sites within the Mawddach catchment for use in calibrating and validating hydrological models. This data includes measurements of river flows and hillslope runoff.
- Hydrograph data has also been made available by the Environment Agency for the Tyddyn Gwladys gauging station on the Afon Mawddach in Coed y Brenin.
- For the purpose of hydrological modelling, the Mawddach above the tidal limit has been divided into twelve sub-catchments and the Wnion has been divided into eight sub-catchments. A number of river cross-sections have been surveyed within each sub-catchment.
- Hydrographs have been produced for six sites within the river system by barometric water depth recording. Calibration for river discharge has been carried out by a combination of direct flow measurements and theoretical calculations using flow formulae.
- Within the Wnion sub-catchment, a relationship was found between the hydrograph for a headwater stream and the hydrograph at the river mouth with a time delay of 3 hours 30 minutes. No similar relationship could be found for hydrographs in the Mawddach sub-catchment.
- Hillslope runoff and shallow storm flow measurements were made at sites in the Wnion and Mawddach sub-catchments. During storm events, the volumes of shallow subsurface downslope flow greatly exceeded surface runoff. Periods of very high subsurface hillslope flow corresponded exactly with times of flooding downstream near the head of the Mawddach estuary.
- The HEC-1 hydrological model within the Watershed Modelling System has been used to model a variety of convective and frontal storms over the Mawddach catchment. Synthetic hydrographs produced by HEC-1 were evaluated against field recordings for each storm event. It was possible to select values for infiltration, hillslope runoff and river routing functions which give consistently accurate simulations of flood peak flows and times to flood peak for different storms.

- In order to model storm events at different times of the year with different soil antecedent moisture conditions, a simple adjustment of soil moisture categories can be made within the SCS curve number system.
- Limitations of HEC-1 have been demonstrated. The model assumes infiltration water is lost from the model, leading to an inability to model the slow release of stored groundwater back into rivers during the period following a storm. Consequently the receding limbs of the modelled hydrographs are found to be too steep.
- Where storm events follow in rapid succession, the model fails to recover soil moisture capacity. Saturation of increasingly large proportions of the catchment are assumed, and subsequent storm hydrograph peaks are overestimated.
- Notwithstanding the above limitations, HEC-1 could provide a basis for a reliable flood forecasting model for simple isolated storm events if provided with suitable rainfall forecasts from a model such as MM5. It would be necessary to specify the antecedent soil moisture condition through selecting an appropriate SCS Curve Numbers parameter: A (dry), B (moderately dry), C (damp) or D (wet). This could be chosen, for example, by examination of throughflow sites at key locations in the gorge sections of the Mawddach system in Coed y Brenin.
- The integrated meteorological/hydrological model to be developed in Chapter 5 addresses the limitations of HEC-1 identified above, and attempts to overcome these to allow the modelling of multiple-storm sequences.
- Limitations with the Curve Numbers method for specifying soil properties will be addressed by using a method based on the Hydrology of Soil Types (HOST) classification (cf. figs 1.65-66).

3.3 Sediment movement

Sediment accumulation around Dolgellau

The problem of sediment accumulation on the lower reaches of the Afon Wnion around the town of Dolgellau was introduced in section 1.1 (cf. figs 1.21-1.23). Gravel banks along the 2km stretch of the Wnion between Dolgellau and the estuary tidal limit have increased significantly in height and aerial extent over the period of this research project. Aggradation is reducing the effective height of flood defence walls protecting the centre of the town (figs 3.75-3.76).

Historical flood plain deposits are exposed in the banks of the Afon Wnion at times of low river flow. The photograph in fig.3.77, at a site near Coleg Meirion-Dwyfor in Dolgellau, exhibits a band of river gravel beneath flood plain sand and silt beds. The gravel has a mean grain size of 6 cm. This is significantly smaller than the gravel and cobbles accumulating nearby at the present day (fig.3.78) which may exceed 30cm in mean dimension. This suggests that there has been a significant increase in recent decades in either the supply or transport of coarse sediment in the Afon Wnion, or both of these factors.

Increases in coarse sediment deposition are also observed in the lower reaches of the Afon Mawddach, particularly around the tidal limit at Llanelltyd bridge (fig.3.79). The confluence of the Mawddach with the Wnion at the head of the estuary is marked by a large area of unstable gravel banks (fig.3.80), with the rivers changing their courses significantly in historical times. Large amounts of sediment deposition at the estuary head is likely to raise river base levels, reduce river gradients in the already gently graded lower reaches of the Mawddach and Wnion, and further promote gravel deposition upstream.

Sediment supply into the Mawddach and Wnion river systems is largely from the erosion of glacial and periglacial valley infill deposits of the types discussed in section 1.2 (cf. fig.1.50). This supply is significantly augmented in the Coed y Brenin area by the erosion of river bank spoil tips from metal mines (cf figs1.91-1.92). Mine tip erosion accounts for the popularity of gold panning amongst the sand and gravel deposits of rocky pools in the Mawddach and Afon Wen.

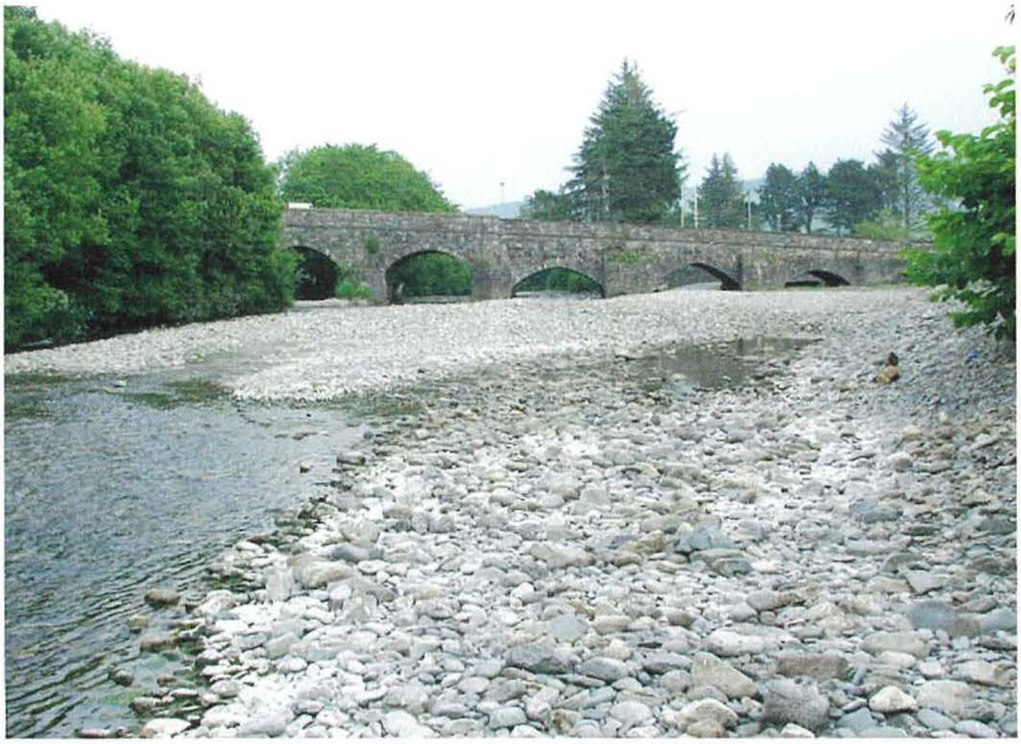

Figure 3.75: Recent sediment accumulation downstream from Bont Fawr, Dolgellau

Figure 3.76: Sediment accumulation alongside the Marian Mawr playing fields, Dolgellau, at Lower Wnion site 3

Figure 3.77: Historic river bed gravels exposed at low water level, Afon Wnion near Coleg Meirion-Dwyfor, Dolgellau

Figure 3.78: Present day gravel and cobble deposits in the Afon Wnion close to the site shown in figure 3.77 above.

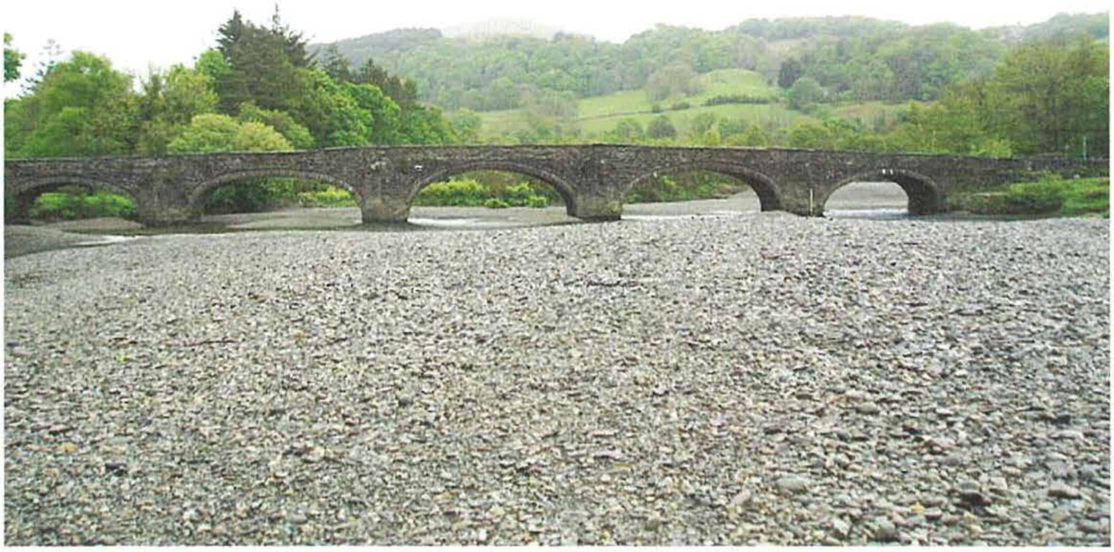

Figure 3.79: Gravel deposits around the tidal limit of the Afon Mawddach, Llanelltyd site 7

Figure 3.80: Area of unstable gravel deposits at the confluence of the rivers Mawddach and Wnion, Llanelltyd site 9

The Mawddach and Wnion are gravel-dominated streams for their entire courses from their headwaters to the tidal limits at the head of the estuary. Under low flow conditions, normally no gravel movement is observed. It is believed that almost all transport of gravel, cobbles and boulders occurs under flood conditions. Only sand and silt grade materials are in continuous movement within the river system throughout the year.

Effects of sediment movement are easily observed during and after flood events in the Mawddach and Wnion sub-catchments. Examples of severe erosion on the Afon Mawddach in Coed y Brenin are given in figs 1.16 and 1.17. Large amounts of sediment movement are likely to alter channel cross sections, affect channel base levels and modify river gradients. These effects, in turn, are likely to influence the locations and extent of flooding throughout the river system. It was therefore considered important to obtain some estimate of the extent of sediment movement and channel modification in response to individual flood events.

Approaches to sediment transport modelling

Two sediment transport models were examined for use in the Mawddach study: the CAESAR cellular automaton model (Coultard,1999), and the GSTARS stream tube model (Yang and Simões, 2000). These models have different starting points within the hydrological cycle, use different geometrical approaches, and employ different sedimentological formulae for erosion, transport and deposition processes.

CAESAR cellular automaton model

The CAESAR model uses a digital elevation model to create a representation of the catchment topography and river channel system. The model incorporates both hillslope runoff and river routing components, with sediment transport processes handled in addition to water flows (fig. 3.81):

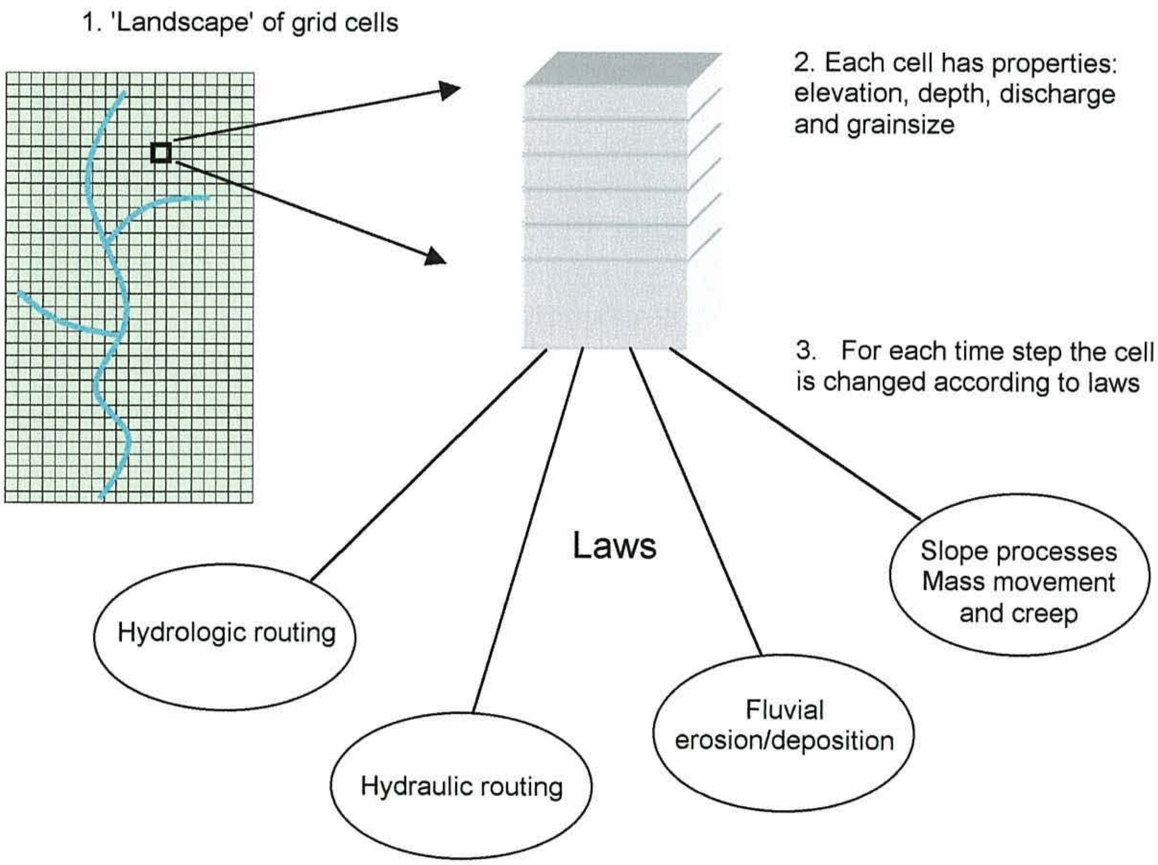

Figure 3.81: Schematic diagram of the key processes operating in the CAESAR cellular automaton model (after Coulthard, 1999)

Within each time step of the model, a sequence of operations are carried out:

- Soil saturation within each cell is calculated, based on rainfall input and infiltration,
- Hillslope surface runoff and subsurface water flows to downslope cells are calculated,
- Water flows are routed through surface channels,
- Sediment erosion within channels is calculated, depending on available sediment grain size and the available transporting capacity of the stream.
- Sediment deposition is calculated, as the excess of transported sediment over carrying capacity.
- Soil creep is determined according to slope angle.
- Mass movement is modelled whenever the slope value for a cell exceeds a critical angle. Material moves downslope until the stable angle of rest is restored.
- Vegetation growth can be modelled, and will stabilise slopes.

The CAESAR model has interesting features, particularly the ability to model sediment movement on hillslopes in addition to sediment transport in river channels. Mass movement is relatively common within the Mawddach catchment when soils and (peri)glacial deposits become saturated during storm events (fig.3.82). However, a detailed study of slope stability and erosion processes is beyond the scope of this project.

Figure 3.82: Mass movement at Oernant in the upper valley of the Afon Gain following the July 2001 storm event.

A drawback of the CAESAR model is the very large amount of parameter data needed to initialise hillslope cells for a mesoscale catchment on the scale of the Mawddach. It may be possible to run the overall simulation as a series of sub-catchment models on separate computers, but it is uncertain how sediment routing between sub-catchments would be handled. The CAESAR model seems more suited to detailed geomorphological studies of small catchments up to $10km^2$ with a single trunk stream.

GSTARS sediment transport model

The GSTARS model is essentially a river routing model (cf. section 3.1, fig.3.11) to which sediment erosion, transport and deposition functions have been added. The input to the model consists of hydrograph data for channel inflows, plus sedimentological data for the river channel and banks. Slope erosion and mass movement are only modelled within the flood plain.

A decision was taken to use GSTARS for sediment modelling within the Mawddach river system. It was apparent from initial experimentation with GSTARS models that measurable sediment erosion, transport and deposition processes were restricted to the period of flood events and the few days following these events. Two significant storms were chosen for analysis:

- the convective storm of 3 July 2001, which generated the highest river discharge values of any event recorded during this research project, although the event was of only a few hours duration. This magnitude of storm was estimated to have a return period of 200 years.
- the sequence of storms of 3-4 February 2004, which generated the longest period of continuous flooding around the head of the Mawddach estuary recorded during the project, although maximum river discharge values for any one hour period were significantly less than during the July 2001 extreme event. Storms of this magnitude are estimated to have a return period of 4 years.

In this way, it was hoped to compare the amounts of sediment erosion, transport and deposition generated by rare but extremely severe flash flooding, in comparison to the less severe flood events of longer duration which occur on an almost annual basis.

Mathematical basis of the GSTARS model

To carry out a sediment transport simulation, the river is divided into a series of reaches. The twelve reaches of the Mawddach sub-catchment and the eight reaches of the Wnion sub-catchment defined in section 3.2 are again used for this model.

Within each reach, the geometry of the river must be defined. Cross sections are surveyed at a series of points, and the elevation of each cross section above a datum is recorded. Channel roughness is specified for one or more zones across each section. The downstream channel distance between cross-sections is measured.

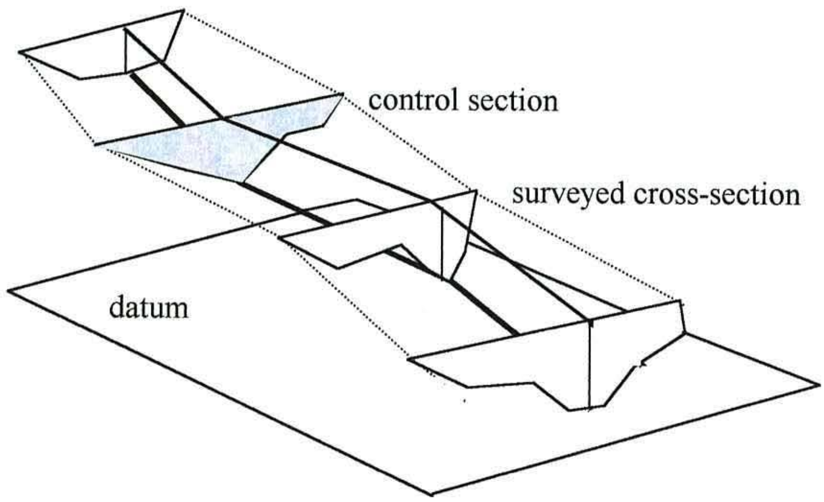

Figure 3.83: River reach data for input to the GSTARS model

One of the cross sections is chosen as a point at which river stage height and discharge will be specified for a sequence of time intervals during the flood event. The combination of channel geometrical and roughness characteristics, plus water flows at the control section, provide sufficient data to calculate water velocities and depths at the remaining points within the channel reach. This data will, in turn, be used in the calculation of sediment erosion rates, transport and deposition.

The method used by GSTARS to determine water depths and velocities through the river reach is based on the energy equation:

$$z_1 + y_1 + \alpha_1 \frac{V_1^2}{2g} = z_2 + y_2 + \alpha_2 \frac{V_2^2}{2g} + h_l$$

where: z is channel bed elevation, y is water depth, V is mean water velocity, and α is a correction factor (close to 1) which allows the approximation of discharge as the product of mean water velocity and channel cross sectional area. Subscripts 1 and 2 refer to locations at locations at each end of a river reach. The significance of the equation is shown in fig.3.84.

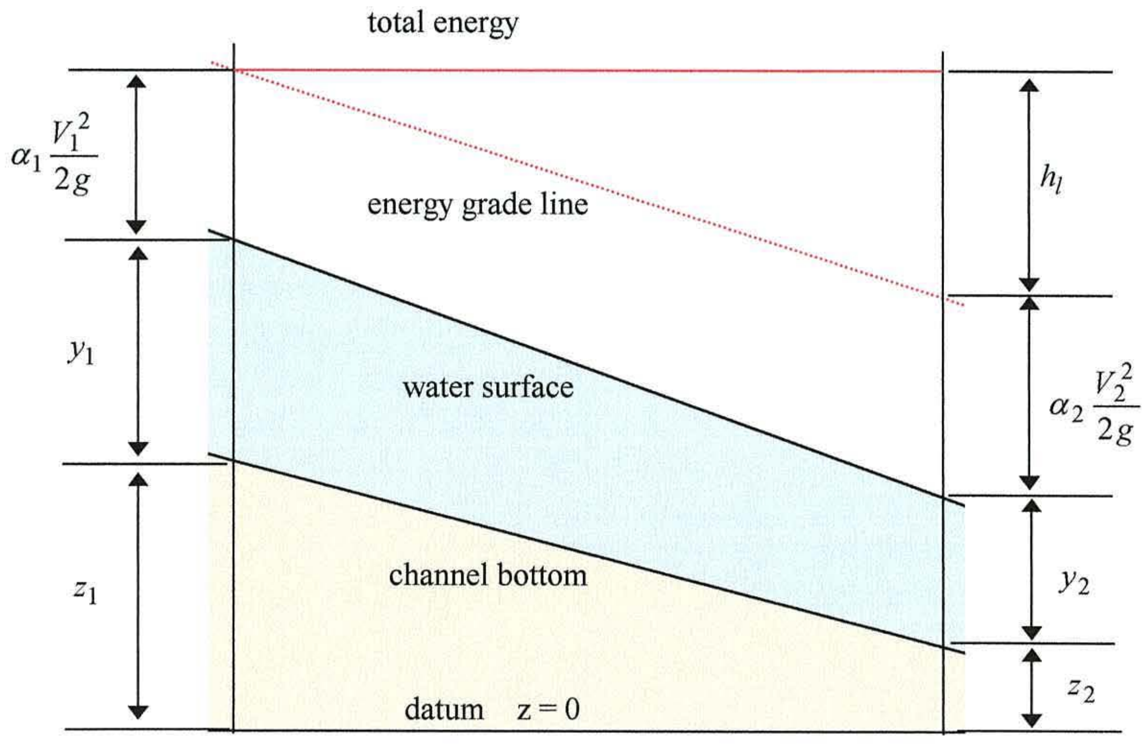

Figure 3.84: Calculation of total stream energy

The total energy of the stream flow at any point will be the sum of the potential energy and kinetic energy of the water.

- Potential energy at the water surface is determined by the surface elevation, which is in turn the total of the river bed elevation and the water depth.
- Kinetic energy of the water flow per unit area can be determined from the water velocity, allowing a correction α for channel shape.

The quantity h_l represents graphically the energy loss which occurs over the length of the river reach as a result of processes such as turbulence.

It is apparent from fig.3.84 that a stream could possess equal total energy under different flow conditions:

- shallow fast flow, where kinetic energy was increased but potential energy reduced,
- deep, slow flow, where potential energy was increased but kinetic energy reduced.

These two situations can indeed exist in nature, and are illustrated as points on a plot of kinetic energy E against water depth h under conditions of constant discharge (fig.3.85). The energy minimum occurs at a water depth known as *critical depth.* A shallow fast flow, such as point A, is said to be *super-critical,* whilst a deep, slow flow, as at point B, is said to be *sub-critical.* For example, it is common for a stream to change abruptly from super-critical to sub-critical flow where the river gradient is suddenly reduced, as at the base of a weir. This process is known as a *hydraulic jump.*

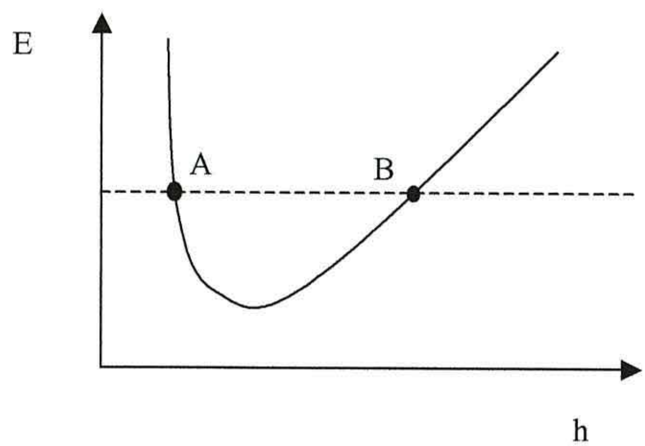

Figure 3.85: Kinetic energy – water depth curve for constant discharge

The GSTARS program is able to determine a continuous water surface profile where a change in flow regime occurs between two measured cross sections.

The determination of water depths is carried out by an iterative process using the relationship:

$$Z_{new} = Z_{old} - \frac{H_{old} - H_{new}}{1 - F_{old}^2\left(1 \mp 0.5C_L\right) \mp \left(\frac{3}{2}\right)\left(\frac{h_f}{R}\right)}$$

This equation involves six parameters:

Z	water surface elevation
H	total energy line
F	Froude number
R	hydraulic radius of the channel
C_L	energy loss coefficient
h_f	friction loss

The process begins by estimating values for Z and H at the channel cross-section, then progressively determining new values for Z and H until the difference between H_{old} and H_{new} falls below a specified tolerence. From the initial value of Z, an initial value for H can b determined using the relationship:

$$H = \frac{\alpha V^2}{2g} + y + z$$

where:

z	bed elevation
y	water depth
V	flow velocity
α	velocity distribution coefficient
H	elevation of the energy line above the datum.

Water velocity V can be determined by assuming that river discharge for the current time interval is equal to the discharge at the control section.

Hydraulic radius of the channel is the the ratio of its cross-sectional area to its wetted perimeter, and can be determined from the surveyed cross-section and specified water depth.

Froude number is the ratio of the inertial and gravitational forces operating within the stream, and is a measure of the resistance to water flow induced by the channel.

Froude number is computed by the equation:

$$F = \frac{Q}{A\left(\frac{g y_d \cos\theta}{\alpha}\right)^{1/2}}$$

where:

	Q	water discharge
	A	cross sectional area
	y_d	hydraulic depth = area/top width
	θ	angle of inclination of channel bed
	α	velocity distribution coefficient, approximately 1

The energy loss coefficient C_L depends on channel geometry. This is set to 0.1 for a contraction in the channel cross-section, and 0.3 for an expansion.

The friction loss h_f is computed from the values of the friction slope S_f at adjacent sections using the formula:

$$h_f = \frac{1}{2}\left(S_{f1} + S_{f2}\right)\Delta x$$

where Δx is the downstream separation of the sections. The friction slope can in turn be calculated by a choice of methods in the GSTARS program: Manning's formula, Chézy's formula or the Darcy-Weisbach formula. Manning's formula is:

$$Q = \left(\frac{1.49}{n} AR^{3/2}\right) S_f^{1/2}$$

where:

	A	cross sectional area
	R	hydraulic radius
	n	Manning roughness coefficient

A suitable value for Manning's roughness *n* can be selected by comparison with photographs of specimen river channels of known roughness (Arcement and Schneider, 2003; Barnes, 1967).

In order to determine suitable water surface profiles between channel cross-sections, it is necessary to identify situations where changes take place between *sub-critical*, *critical* or *super-critical* flows. To assist with this task, two quantities are calculated – the *critical depth* and the *normal depth* of the channel at each cross section.

For gentle or moderate downstream gradients, the *normal depth* is greater than the *critical depth.* If the water depth is greater than the *normal depth* at both ends of the section, then no change in flow regime occurs (fig.3.86, profile M1). If the water depth is less than the *normal depth,* the water surface will follow a parabolic path as it adjusts towards a *critical depth* downstream. The surface curve will follow M2 or M3, depending on whether the initial depth is above or below the *critical depth.*

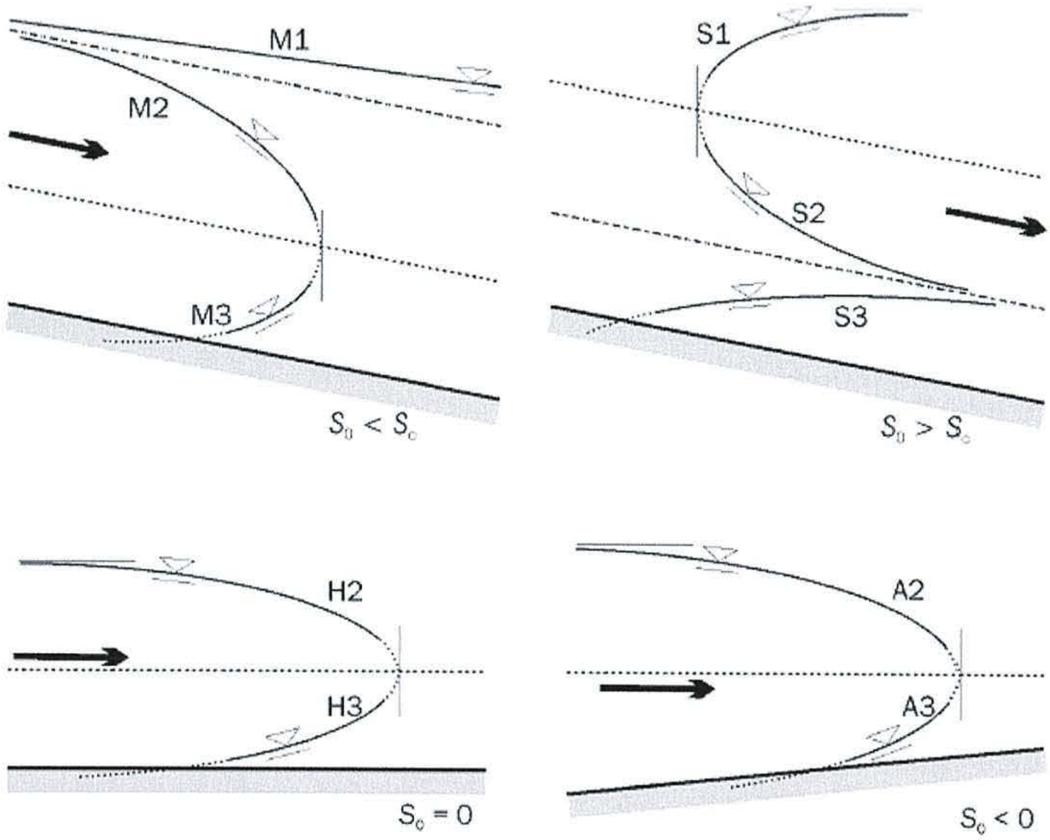

Figure 3.86: Water surface profiles in gradually varied flow (after Yang and Simões, 2000)

Normal depth may be less than *critical depth* for steep downstream slopes. If the initial water depth is above the *critical depth,* it will remain so (profile S1). If the initial water depth is below the *critical depth,* then it will trend towards the *normal depth* following parabolic profile S2 or S3.

In cases where the river channel is horizontal or slopes upwards in the downstream direction, the water profile will always trend towards the *critical depth,* following one of the paths H2,H3, A2 or A3.

The determination of Normal Depth *g(d)* is carried calculated by:

$$g(d) = Q - K(d)\sqrt{S_0} = 0$$

where: K(d) conveyance
S_0 bottom slope

Conveyance is related to friction slope S_f:

$$Q = KS_f^{1/2}$$

Critical depth is determined by setting the value of the Froude number to 1:

$$F = \frac{Q}{A\left(\frac{gy_{critical}\cos\theta}{\alpha}\right)^{1/2}} = 1$$

Sediment modelling

After determining water depths and flow velocities for a time interval of the simulation, the next stage is to determine the amounts of sediment erosion, transport and deposition for each section of the reach. Conservation laws are applied, as illustrated in fig. 3.87.

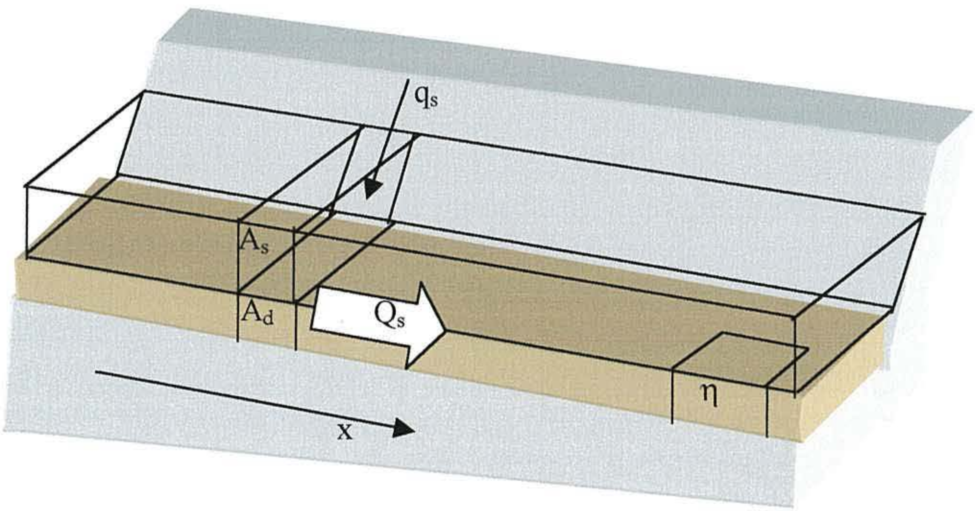

Figure 3.87: Components of the model for conservation of sediment mass

Conservation of sediment mass is determined by:

$$\frac{\partial Q_s}{\partial x} + \eta \frac{\partial A_d}{\partial t} + \frac{\partial A_s}{\partial t} - q_s = 0$$

where

η	volume of sediment in a unit bed layer volume
A_d	volume of bed sediment per unit length
A_s	volume of sediment in suspension at the cross section per unit length
Q_s	volumetric sediment discharge
q_s	lateral sediment inflow

Essentially this equation is stating that any change in the amount of sediment being transported at successive monitoring points downstream must be balanced by erosion of the river bed adding sediment to the transport stream, or deposition removing sediment from transport.

The expression may be simplified by making an assumption that the change in suspended sediment concentration in a cross section is much smaller than the change of the river bed during any time interval, ie.

$$\frac{\partial A_s}{\partial t} << \eta \frac{\partial A_d}{\partial t}$$

Assuming that the sediment transport function for a cross section remains constant during a time interval, then

$$\eta \frac{\partial A_d}{\partial t} + \frac{dQ_s}{dx} = q_s$$

The program routes sediment in stream tubes whose walls are defined by streamlines. Flow does not cross streamlines, so sediment remains within each stream tube as it is carried downstream. The number of streamtubes to be used by the model can be defined by the user. Sediment processes within each stream tube are modelled separately. Thus it is possible for GSTARS to model both erosion and deposition simultaneously on different sections of a channel cross section during a particular time interval.

Sediment transport is computed by size fraction. Particles of different size are transported at different rates. Depending on water velocity, some size fractions may be eroded whilst others are deposited. The model uses an *active layer*, which represents all the sediment which is available for transport during a time interval. Active layer thickness can be defined by the user. The program is able to model a situation known as *armouring* where all fine material is eroded from the surface of the active layer, leaving stable coarser sediment exposed. Deposited sediment during any time step is initially added to the active layer, but may be transferred to an inactive deposition layer when the thickness of the active layer is reset at the start of the next time interval (fig.3.88).

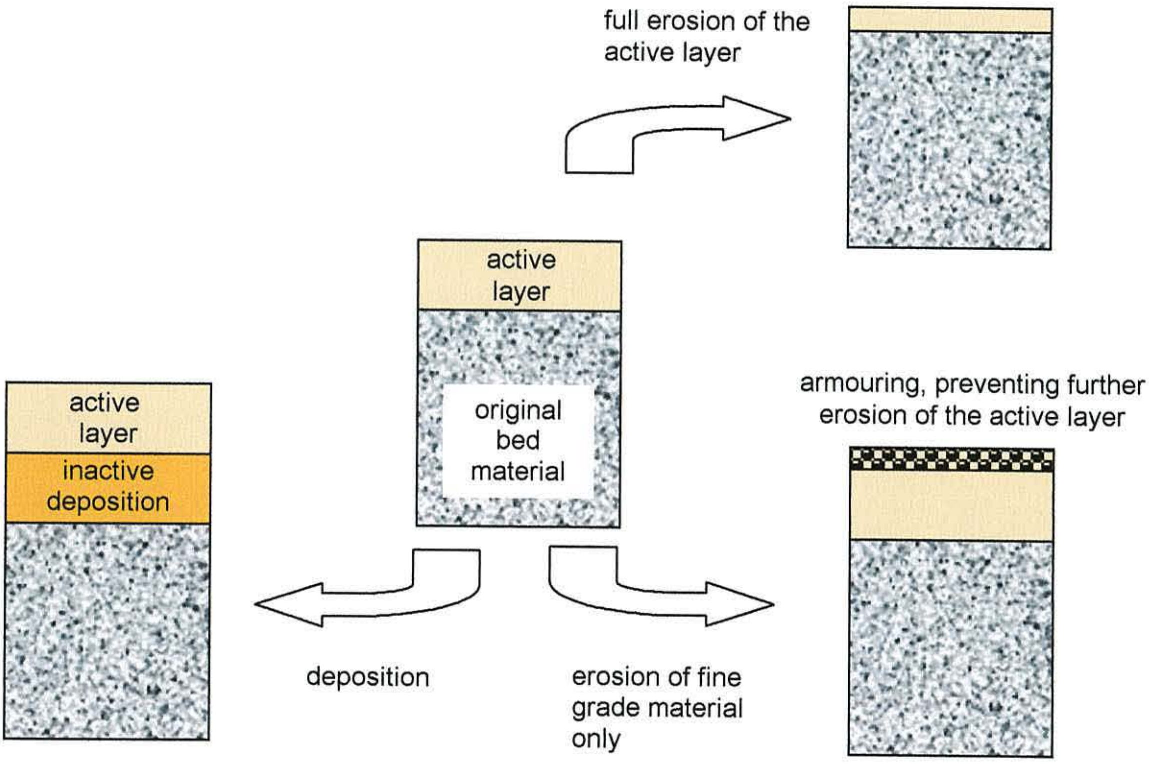

Figure 3.88: Sediment processes modelled by GSTARS

Initial sediment size distributions at each cross section must be specified when setting up a simulation.

For any time step, erosion may occur if the transport capacity of the stream at a cross section is greater than the incoming load from upstream. Various sediment transport functions are available within GSTARS. The method chosen for the Mawddach model is Yang's Sand (1973) and Gravel (1984) Transport Formulas, which is valid for the range of sediment sizes common within the river system:

Unit stream power formula for sand transport:

$$\log C_{ts} = 5.435 - 0.286 \log \frac{\omega d}{\nu} - 0.457 \log \frac{U^*}{\omega}$$
$$+ \left(1.799 - 0.409 \log \frac{\omega d}{\nu} - 0.314 \log \frac{U^*}{\omega}\right) \log\left(\frac{VS}{\omega} - \frac{V_{cr}S}{\omega}\right)$$

Unit stream power formula for gravel transport:

$$\log C_{tg} = 6.681 - 0.633 \log \frac{\omega d}{\nu} - 4.816 \log \frac{U^*}{\omega}$$
$$+ \left(2.784 - 0.305 \log \frac{\omega d}{\nu} - 0.282 \log \frac{U^*}{\omega}\right) \log\left(\frac{VS}{\omega} - \frac{V_{cr}S}{\omega}\right)$$

where:

C_{ts}	total sand concentration
C_{tg}	total gravel concentration
ω	sediment fall velocity
d	sediment particle diameter
U^*	shear velocity
VS	unit stream power
V	flow velocity
S	water surface slope
V_{cr}	critical flow velocity at incipient motion

The sand transport formula is used for grain sizes less than 2mm, whilst the gravel formula is used for grain sizes of 2mm or greater.

Channel width and depth adjustment

The GSTARS model uses minimum energy dissipation rate theory (Song and Yang, 1979) to determine the relative amounts of bed erosion in a vertical direction and bank erosion in a horizontal direction at each cross section. This theory specifies that when a closed and dissipative system reaches its state of dynamic equilibrium, its energy dissipation rate must be at its minimum value:

$$\Phi = \Phi_w + \Phi_s = \text{minimum}$$

where

Φ	total rate of energy dissipation
Φ_w	rate of energy dissipation due to water movement
Φ_s	rate of energy dissipation due to sediment movement.

The system will tend to adjust itself until the energy dissipation rate is a minimum. The program attempts to minimise the stream power:

$$\gamma QS$$

where

Q is discharge,

S is channel slope,

γ is the specific weight of water.

A consequence is that horizontal erosion is favoured where river gradient is gentle, but vertical bed erosion is favoured where channel gradient is steep.

GSTARS sediment models for the Mawddach catchment

Modelling has been carried out using twelve sub-catchments for the Afon Mawddach and eight sub-catchments of the Afon Wnion. The model treats discharge as uniform along each reach. To set up the model for a reach, the course of the river is entered on a base map. The position of cross section points are then chosen (fig.3.89).

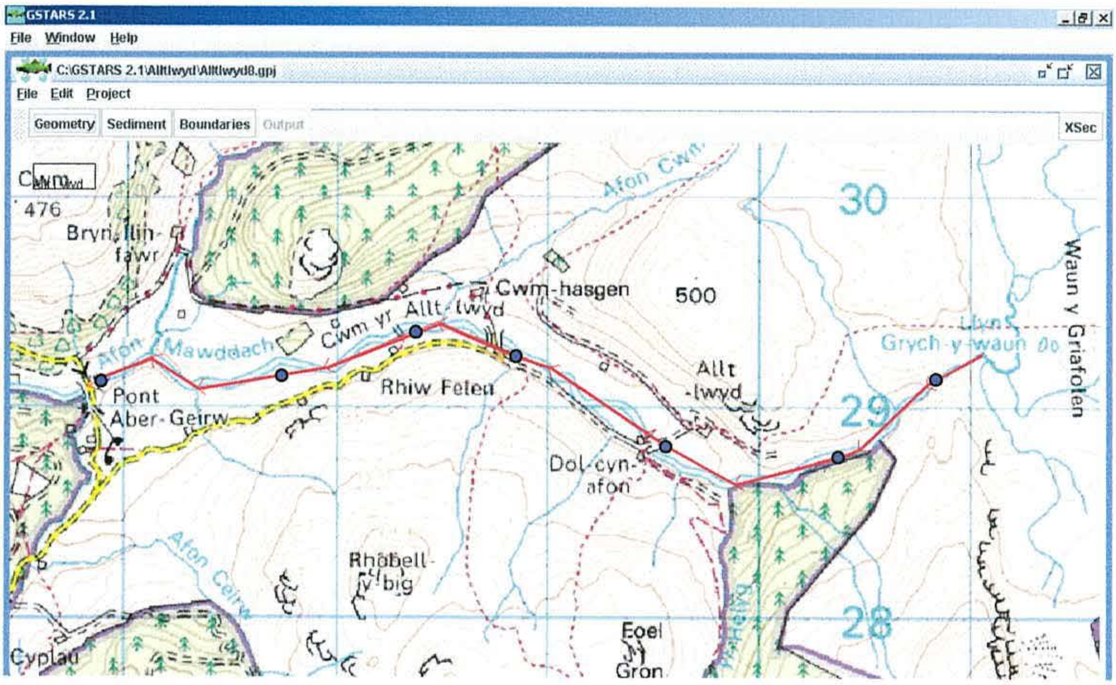

Figure 3.89: Entry of channel course and locations of surveyed cross-sections for the Alltlwyd reach, Afon Mawddach

Survey points for each cross-section are then entered, specifying distance across the section and elevation above Ordnance datum (fig.3.90). Cross-sections should extend to a level above maximum flood height on each bank of the stream. The collection of survey data for this purpose is described in chapter 3.2 above (cf fig.3.20). The GSTARS program displays the cross section, and allows Manning roughness values to be specified for different zones of the section.

Several choices of parameterisation and calculation method need to be made:

- options are available within GSTARS for the method of channel friction loss,
- the number of stream tubes should be specified for sediment transport,
- the sediment transport equation is selected,
- the depth of the active sediment layer is specified.

Figure 3.90: Input of river cross-section geometry and surface roughness

The size boundaries should be specified for each sediment class which is to be modelled separately in the transport model. For the Mawddach simulation, five size classes have been chosen to represent the range of grain sizes common within the river channels(fig.3.91):

1. silt – coarse sand
2. very coarse sand – fine gravel
3. medium gravel – coarse gravel
4. very coarse gravel – cobbles
5. boulders

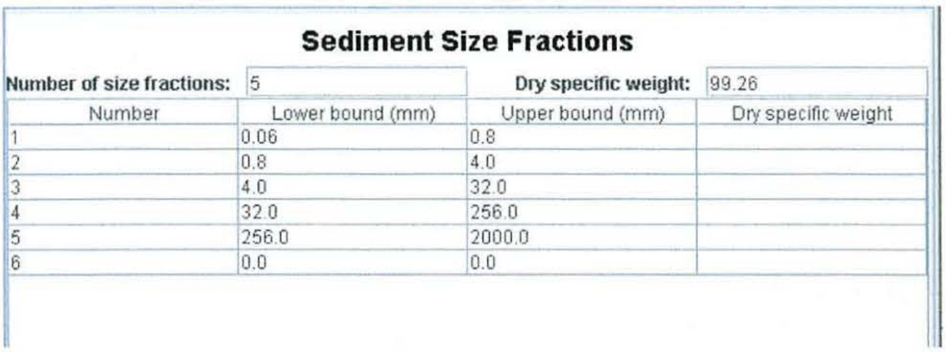

Number	Lower bound (mm)	Upper bound (mm)	Dry specific weight
1	0.06	0.8	
2	0.8	4.0	
3	4.0	32.0	
4	32.0	256.0	
5	256.0	2000.0	
6	0.0	0.0	

Figure 3.91: Specification of size fraction boundaries for the Mawddach model

For each cross-section, it is necessary to specify the fractions of each sediment class exposed within the channel bed and banks (fig.3.92). These fractions were estimated at the time that the cross-sections were surveyed in the field. The procedure involved:

- selection of a series of sampling points at intervals of 2m along the channel cross profile at bankfull level,
- estimation of the percentages of visible sediment within each of the five size grades, aided by the use of a 1m botanical quadrat frame divided with strings into 100 percentage squares.
- averageing of the results from each sample point to provide sediment size grade percentages for the overall cross section.

Fig.3.93 illustrates the typical wide variation in grain size observed within the bed and banks of upland reaches of the Mawddach and Wnion.

Sediment Size Distribution

☑ Include this record in input

X-sec #	0.06< % <0.8	% <4.0	% <32.0	% <256.0	% <2000.0
1	0.05	0.07	0.28	0.6	0.0
2	0.01	0.01	0.05	0.59	0.34
3	0.07	0.08	0.15	0.7	0.0
4	0.05	0.1	0.23	0.62	0.0
5	0.07	0.16	0.26	0.51	0.0
6	0.07	0.16	0.26	0.51	0.0
7	0.07	0.16	0.22	0.5	0.05

Figure 3.92: Specification of fractions of different sediment size grade at each cross-section site within a river reach

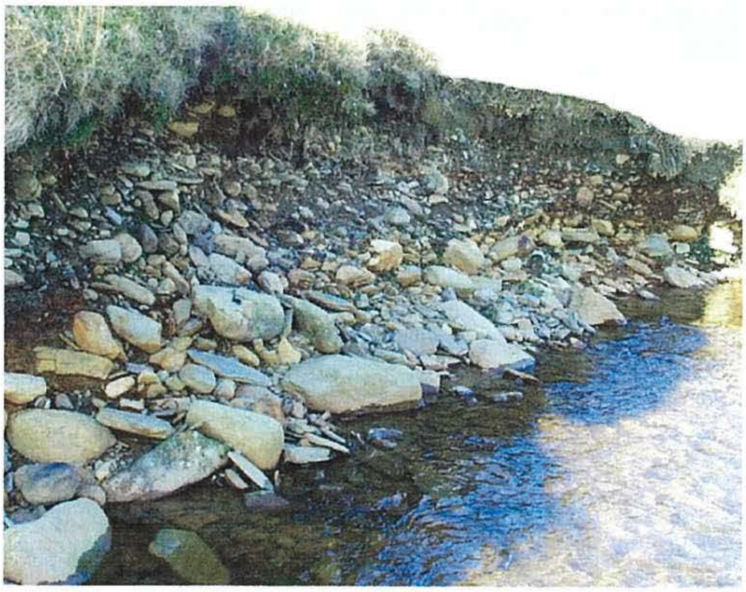

Figure 3.93: Sediment ranging from sand to cobble grade, exposed in the bed and banks of the Afon Gain, Oernant reach.

Limits can be specified for the maximum vertical or horizontal erosion permissible at any cross-section site (fig.3.94). This allows erosion to be limited where solid bedrock is present in the river bed or river banks, or where walls or bridge abutments stabilise the channel. The maximum permitted deposition may also be specified.

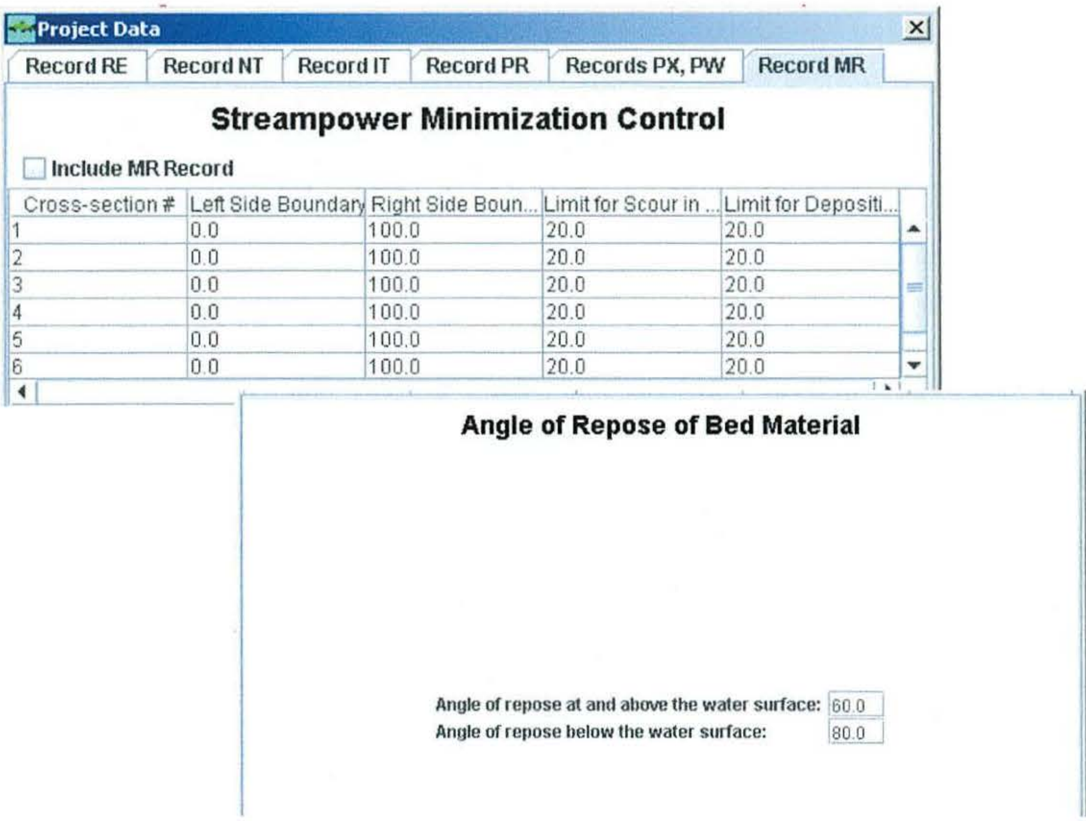

Figure 3.94: Specification of controls on bed and bank erosion and deposition

A further parameter required is the maximum stable slope angle allowed for the channel banks, above and below the water level. This which will depend on the cohesive properties of the exposed sediment .

Once the channel geometry and sediment characteristics have been specified, it is possible to simulate individual storm events. GSTARS requires discharge and water surface elevation data to be entered for a series of time steps during the simulation (fig.3.95). The actual length of a time step may be set by the user: 15 minute time steps have proved satisfactory for the Mawddach model.

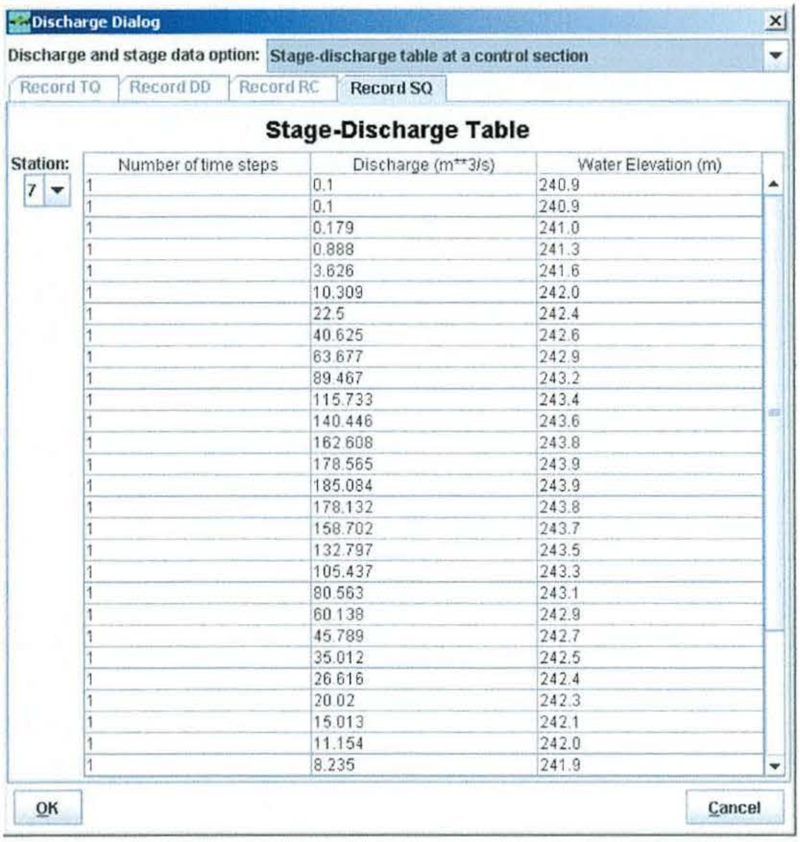

Number of time steps	Discharge (m**3/s)	Water Elevation (m)
1	0.1	240.9
1	0.1	240.9
1	0.179	241.0
1	0.888	241.3
1	3.626	241.6
1	10.309	242.0
1	22.5	242.4
1	40.625	242.6
1	63.677	242.9
1	89.467	243.2
1	115.733	243.4
1	140.446	243.6
1	162.608	243.8
1	178.565	243.9
1	185.084	243.9
1	178.132	243.8
1	158.702	243.7
1	132.797	243.5
1	105.437	243.3
1	80.563	243.1
1	60.138	242.9
1	45.789	242.7
1	35.012	242.5
1	26.616	242.4
1	20.02	242.3
1	15.013	242.1
1	11.154	242.0
1	8.235	241.9

Figure 3.95: Entry of discharge and water elevation data during a storm event on a reach of the Afon Mawddach.

Discharge data for storm events in July 2001 and February 2004 were determined by the HEC-1 hydrograph model within the Watershed Modelling System. Water depths were calculated from the discharge values and river cross-section calibrations described previously in section 3.2.

The final stage in setting up a GSTARS simulation is to specify the quantity and frequency of output data during the run of the model. Output may include water depth and velocity values for each cross-section, sediment volumes transported within each size class, the extent of bed and bank erosion or deposition, and data for plotting changes to channel cross-sections.

Sediment transport modelling has been carried out for two flood events over the Mawddach–Wnion catchment, the convective storm of 3 July 2001 and the sequence of frontal storms of 3-4 February 2004:

Flood event of July 3, 2001

The flash flooding caused by the squall line thunderstorms of 3 July 2001 has been described in chapter 1.1. A vast amount of erosion of valley-infill periglacial and glacial sediments occurred during the flood. Particularly significant changes to valley form have occurred within the gorge sections of the Mawddach and its tributaries in the Coed y Brenin forest (Mason, 2002).

A hydrological model was produced using HEC-1 software for the 12 sub-catchments of the Mawddach and 8 sub-catchments of the Wnion. The synthetic hydrographs generated (figs 3.59-3.60) provide river discharge data for input to the GSTARS sediment model.

The results of the run of the GSTARS model for the Mawddach sub-catchments are summarised in Appendix D Table 1, which illustrates the methodology for carrying out the simulation. Sediment movement is calculated over a 9 hour period following the commencement of storm rainfall:

- Calculations begin with the headwater streams of the Mawddach and Gain in the Alltlwyd and Oernant reaches respectively.
- Sediment quantities within each size category are passed downstream to the next reaches; the Gwynfynydd reach on the Mawddach and the Pistyll Cain reach on the Gain.
- Sediment from these converging headwaters is combined as input to the Ganllwyd reach.
- Sediment from the Eden and Gamlan is combined the output from the Ganllwyd reach of the Mawddach main stream, as input to the Gelligemlyn reach.
- Sediment from the Afon Wen is finally added to provide input to the Llanelltyd reach.

- Output from the Llanelltyd reach enters the tidal head of the Mawddach estuary.

Data from Appendix D Table 1 is summarised in the chart of fig.3.97. It is seen that both erosion and deposition occurred at different points within the Mawddach river system during the flood event. This is related to the polycyclic relief of the Mawddach catchment, producing a series of steep rejuvenated river reaches interspersed by reaches of gentle gradient (fig.3.96).

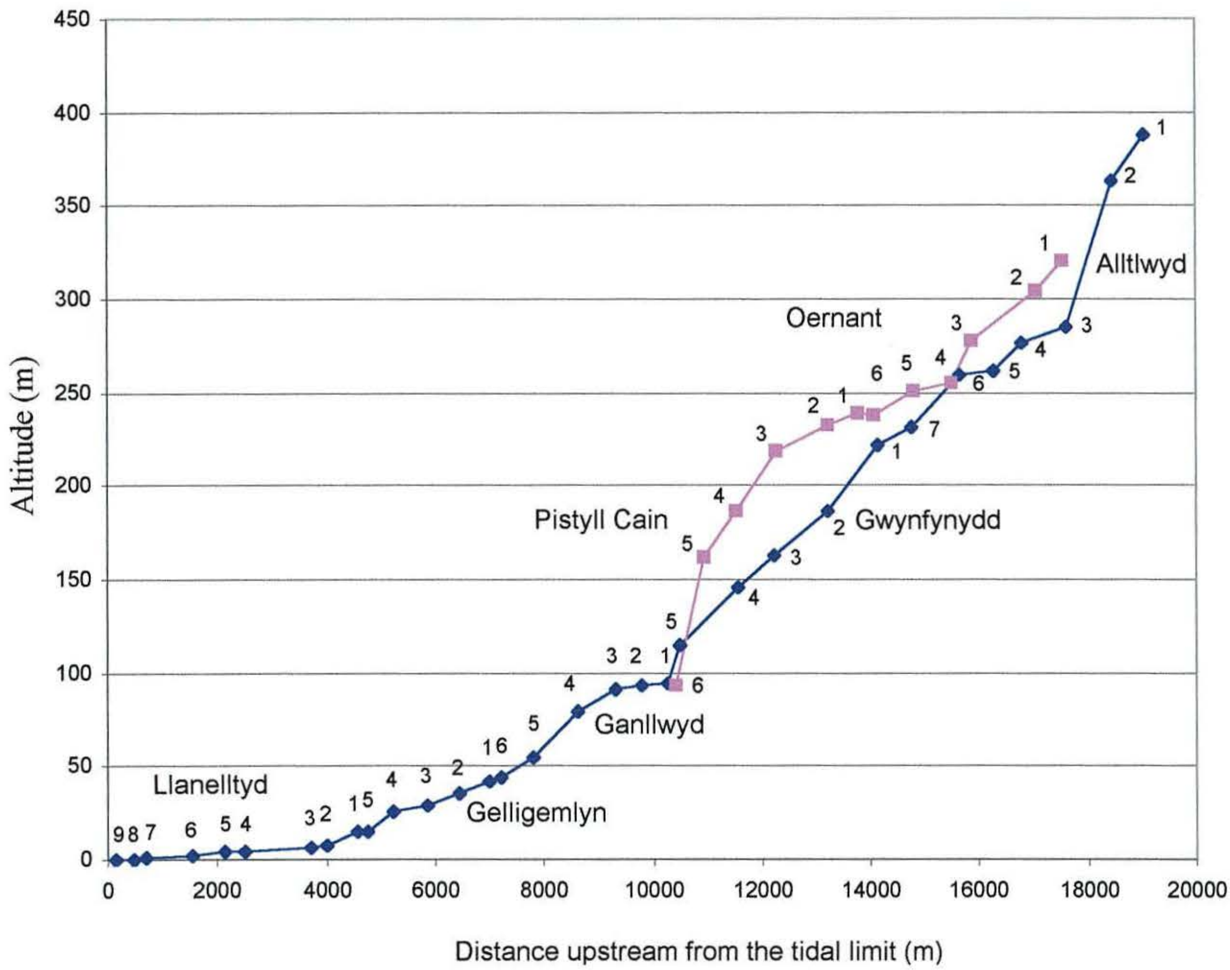

Figure 3.96: Reaches of the Mawddach sub-catchment.
Reach reference numbers refer to figs 3-97 and 3-100.

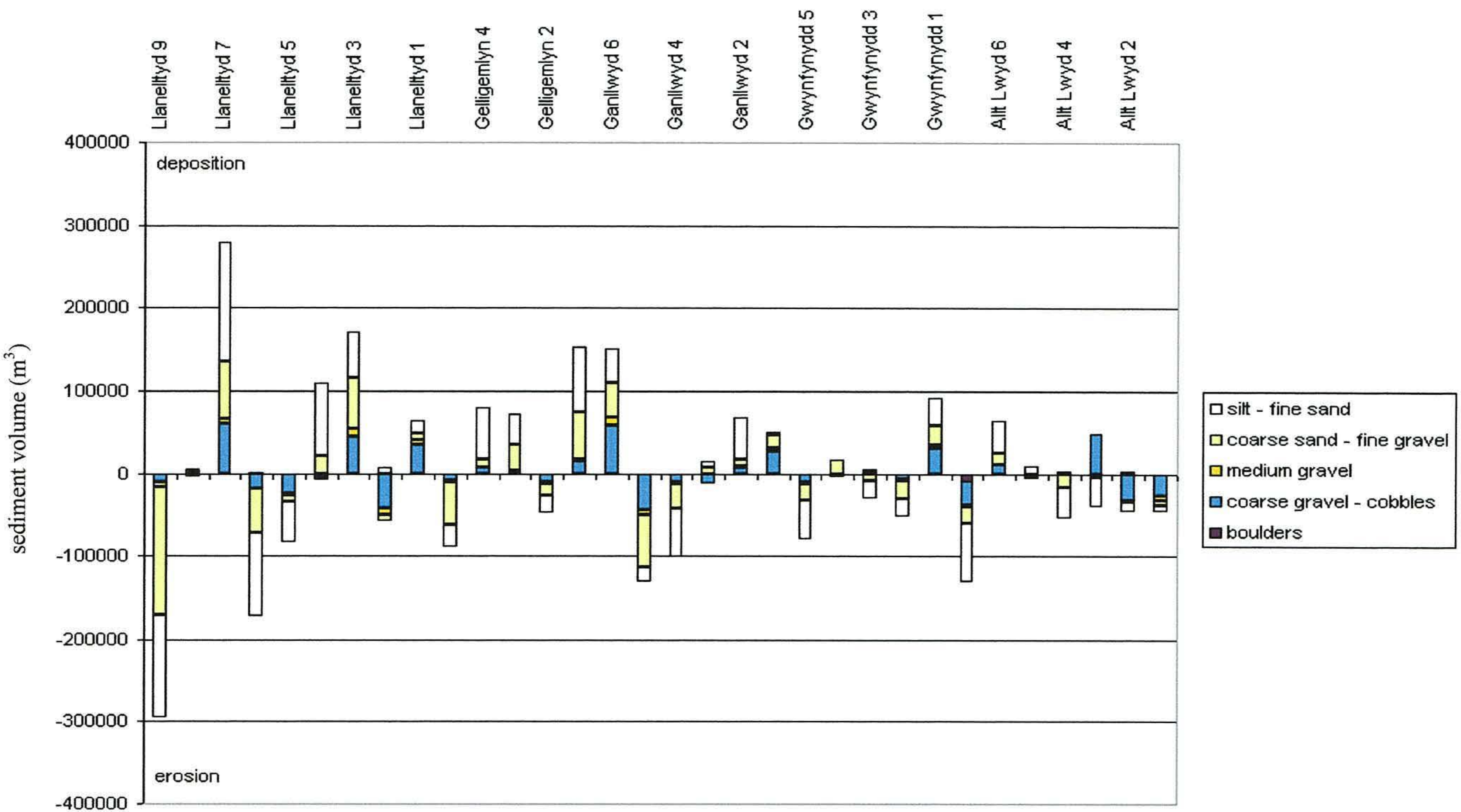

Figure 3.97: Sediment movement during the 3 July 2001 flood event: Mawddach sub-catchments

Valley cross-section plots produced by GSTARS appear consistent with profile changes which occurred during the 2001 flood event. An example is the erosion of a river cliff in glacial till at site 5 in the Oernant reach of the Afon Gain (fig. 3.99). Both vertical and lateral erosion have been simulated, along with deposition on the inner curve of a meander (fig. 3.98).

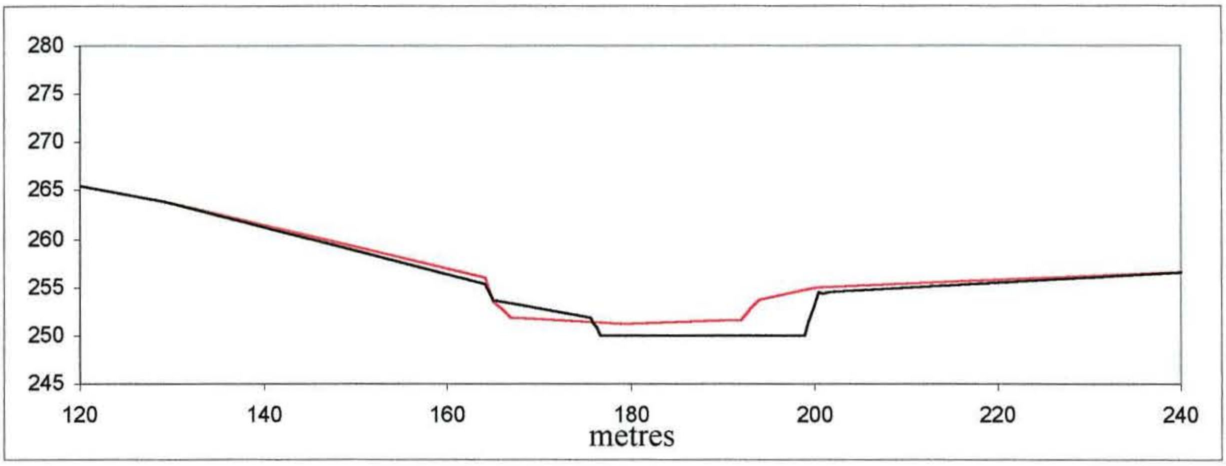

Figure 3.98: Modelling of channel profile change during the July 2001 flood event, Oernant reach of the Afon Gain. Initial pre-flood profile input to GSTARS is shown in red, with the modelled post-flood profile shown in black.

Figure 3.99: Photograph of the Oernant site depicted in the cross-profiles of fig.3.98. River cliff erosion occurred during the July 2001 flood, with gravel deposition on the meander slip-off slope opposite.

Details of sediment movement within the Oernant and Pistyll Cain reaches of the Afon Gain are given in fig.3.100.

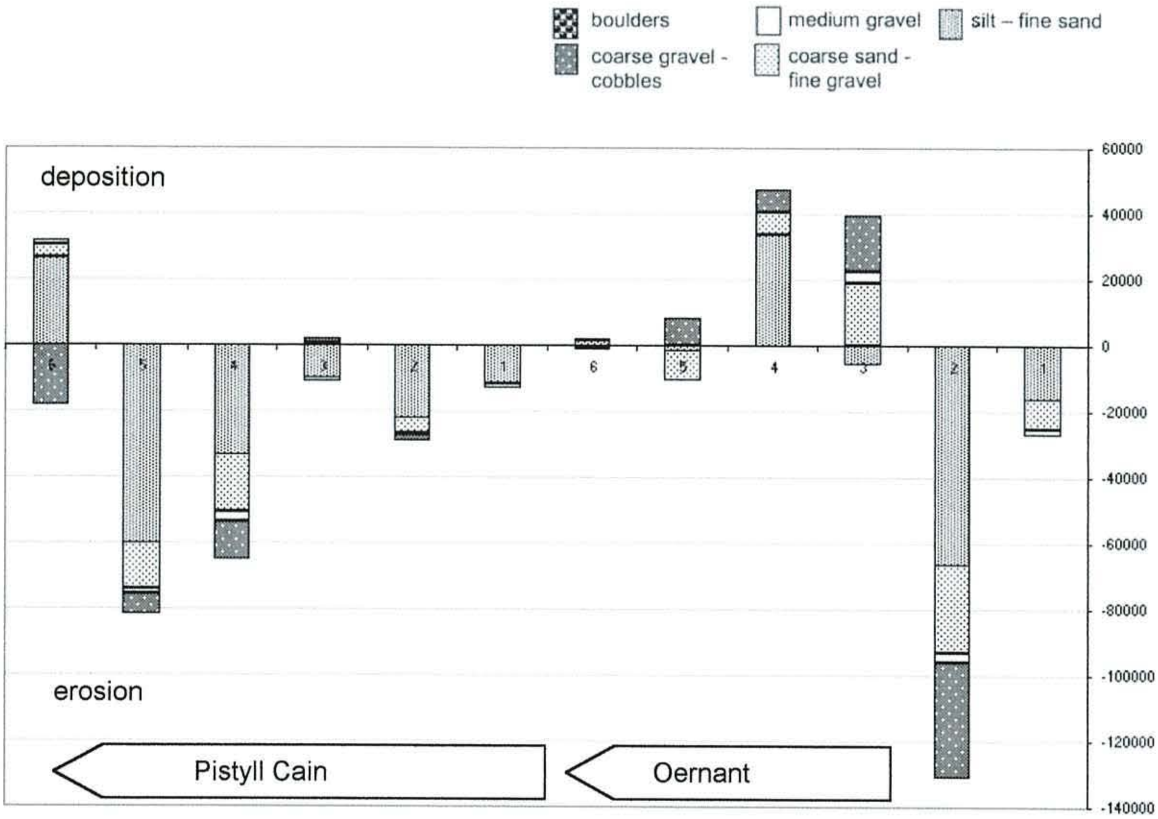

Figure 3.100: Erosion/deposition volumes (m^3) for river sections on the Afon Gain.

Sediment erosion and deposition volumes for modelled sections of the Afon Gain may be related to changes in river gradient. Erosion predominates, with a large sand fraction predicted at most erosional sites. This corresponds well with field observations of extensive erosion of glacial and periglacial valley infill, for example at Oernant sites 1–2 where the river has deeply incised a sheet of sandy glacial till (Fig. 3.101).

Sites of significant deposition, particularly of coarse grade material, may also be found within the upland reaches where valley gradients are reduced. An example is the deposition of gravel on grassland alongside the Afon Gain at Oernant sites 3–4 (Fig. 3.102).

Figure 3.101: Erosion of glacial till by the Afon Gain at Oernant sites 1–2 marked in figure 3.100

Figure 3.102: Gravel and sand deposition on grassland at Oernant site 4, along with tree debris washed down from forestry plantations bordering the river.

Movement of boulder-grade material is less common, but was predicted for the area of Pont Abergeirw on the upper Mawddach. This site (fig.1.15) has prominent boulder deposits within the channel, derived from glacial till. The simulated hydrograph for Pont Abergeirw indicates a rapid flash flood event close to the centre of the convective storm, where large water discharges from converging high-gradient streams were powerful enough to inflict considerable damage on the historic stone bridge.

The Mawddach flows through an area of disused metal mines, and considerable quantities of mine spoil were eroded from tips on the river banks (fig.1.91).
A section of forestry road along the Mawddach valley within Coed y Brenin was washed away by erosion on the outside of a meander, and has subsequently had to be rebuilt (fig.1.16). At these sites, erosion is modelled during the GSTARS simulation which is consistent with the field evidence. Large amounts of deposition and erosion are recorded for the lower Mawddach close to the tidal limit (fig.3.79), which is again consistent with field observations of the large unstabilised banks of poorly sorted sand-gravel-cobble sediment which accumulated in this area.

Fine sediment output is modelled as continuing at an exceptionally high rate for the day after the initial storm event, and was deposited on the floodplain of the lower Mawddach during overbank flow (fig.3.103). Twelve hours after the storm, the normal gravel bed of the Mawddach at Gelligemlyn was observed to be covered to a depth of several centimetres by coarse to fine sand. This sediment had been washed downstream by the following day and the clean gravel bed restored.

A feature of interest is the contrast in bed sediment grade at the confluence of the rivers Mawddach and Eden near the village of Ganllwyd (fig.3.104). Bedload of the Mawddach is predominantly of coarse gravel and cobble grade at this point, whilst the channel of the Eden is composed largely of boulders. From the sediment transport data presented in Appendix D Table 1, it is inferred that boulders within the Afon Eden are largely immobile residual deposits, left behind after the erosion of Boulder Clay valley infill. Any boulders reaching the more powerful River Mawddach may be rolled downstream as bedload and buried by large volumes of gravel during flood events.

Figure 3.103: Deposition of sand and silt on the Mawddach floodplain south of Gelligemlyn. Photograph: Chris Dixon

Figure 3.104: Confluence of the Afon Eden (approaching from the middle distance) with the Afon Mawddach (flowing towards the left in the foreground). Notice the contrast in bed sediment grade between the channels.

Modelling of sediment movement in the Afon Wnion sub-catchments during the 3 July 2001 flood event was carried out by a similar method to the Mawddach sub-catchment model.

- Sediment output is calculated separately for the Drws y Nant, Pared yr Ychain, Craig y Benglog and Rhobell Fawr reaches. These volumes are combined as input to the Craig y Ffynnon/Bontnewydd reach.
- Output from the Afon Clyweddog is combined with sediment from the Bontnewydd reach to provide input to the Lower Wnion reach.

Sediment transport data is summarised in Appendix D Table 2, and presented graphically in fig.3.105. Significant sediment erosion and deposition is restricted to the western part of the Wnion sub-catchment, particularly the Bontnewydd, Clyweddog and Lower Wnion reaches. This is constant with the raingauge data (cf fig.3.55). The maximum storm rainfall centre was located to the north over the Mawddach sub-catchment, but an additional convective cell of lesser magnitude appears to have been active over the Wnion valley between Dolgellau and Bontnewydd for part of the storm event.

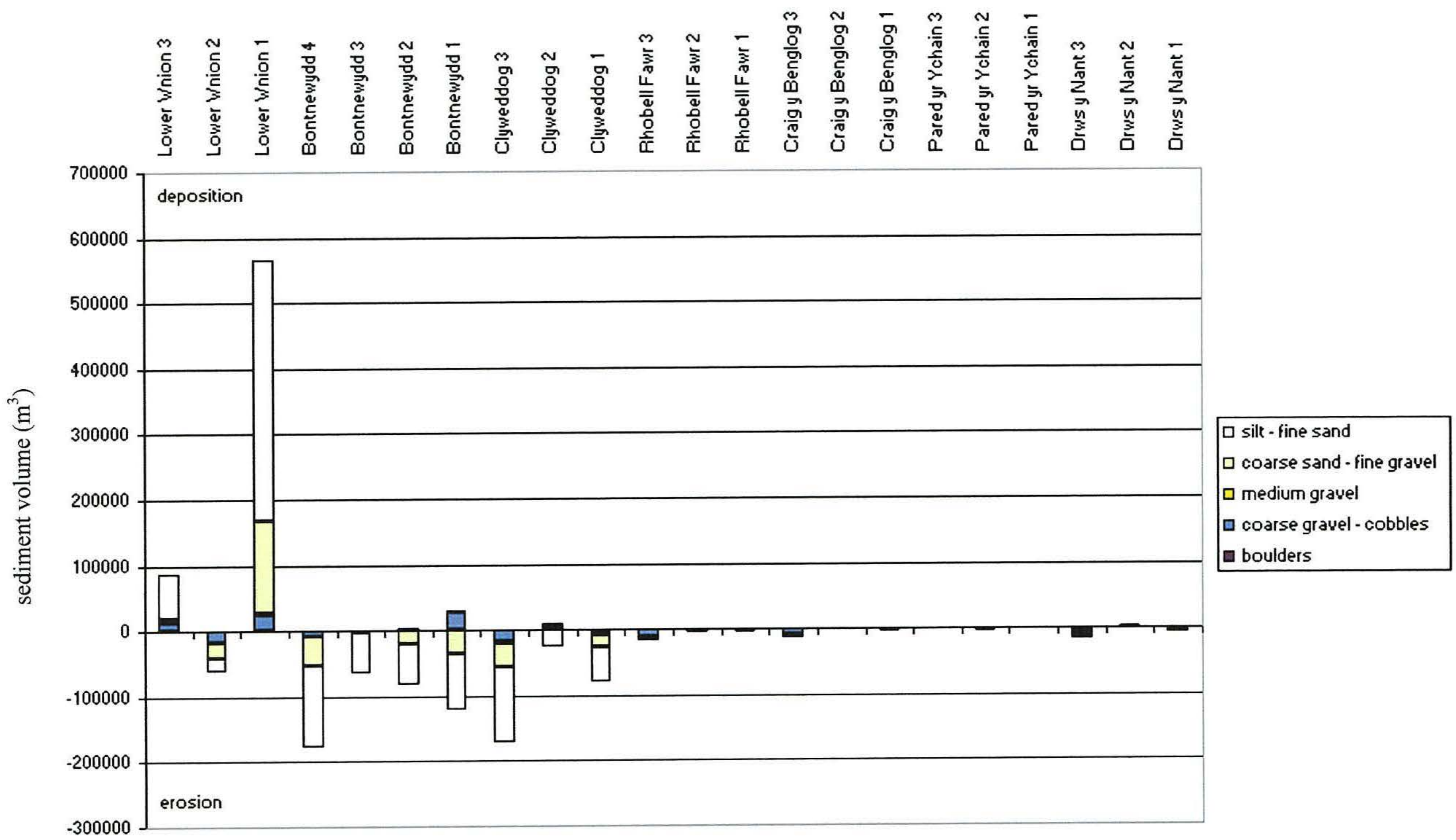

Figure 3.105: Sediment movement during the 3 July 2001 flood event: Wnion sub-catchments

Sediment ranging from coarse sand to coarse gravel grade is predicted to have been deposited around the town of Dolgellau (fig.3.105, Lower Wnion site 1). This is consistent with the large volumes of mixed sediment which accumulated at Bont Fawr (figs 3.106-3.107).

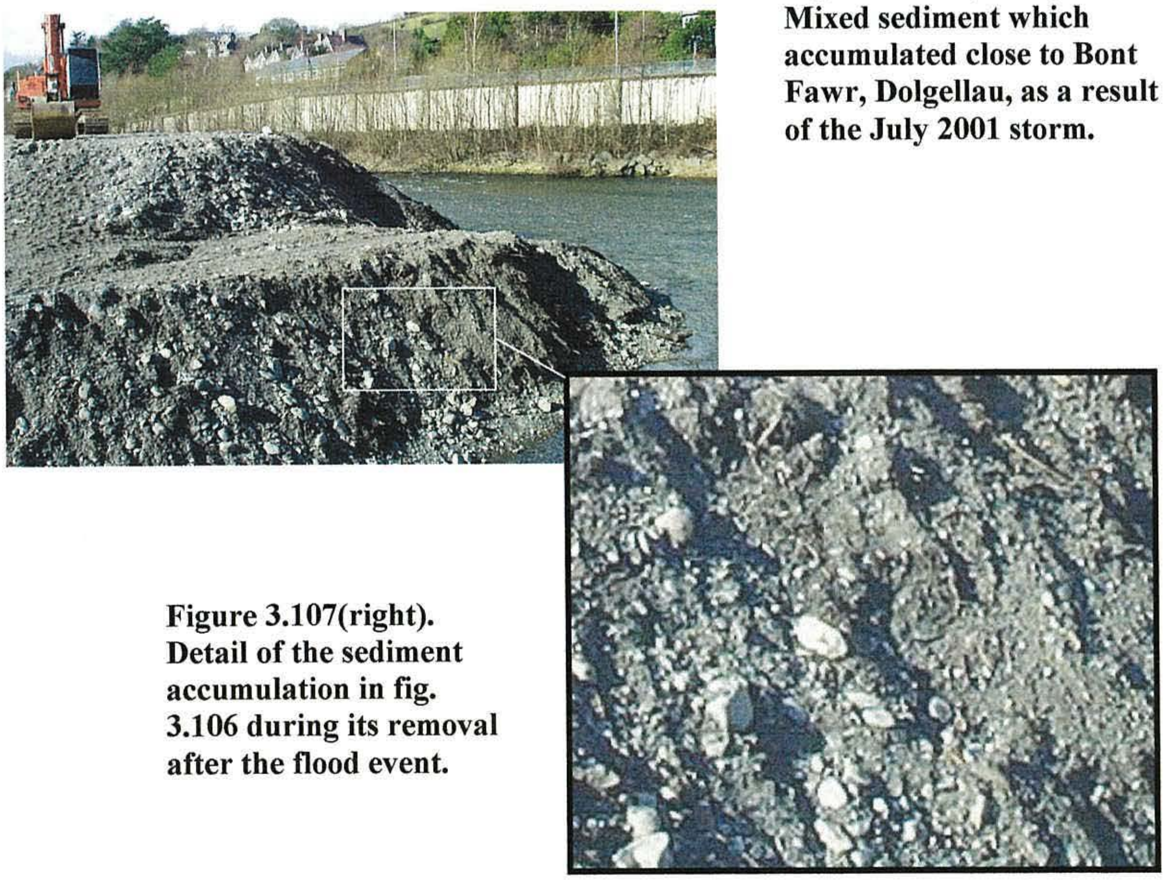

Figure 3.106 (above). Mixed sediment which accumulated close to Bont Fawr, Dolgellau, as a result of the July 2001 storm.

Figure 3.107(right). Detail of the sediment accumulation in fig. 3.106 during its removal after the flood event.

Output to the Mawddach estuary

Table 3.3 and figure 3.108 give GSTARS estimates of total output rates of sediment to the Mawddach estuary during each 1.5 hour time period within each sediment size grade. Sediment discharge data will be used in Section 3.4: River and Floodplain Processes, to provide input for flood scenario modelling for the Lower Wnion valley around Dolgellau.

	Sediment grade				
time (hours)	1	2	3	4	5
0	0	0	0	0	0
1.5	9476	4322	236	441	0
3	41580	39389	1447	4782	0
4.5	59634	53842	2027	5770	0
6	46960	52409	2308	4991	0
7.5	36867	32126	1859	707	0
9	26128	10676	965	0	0

Table 3.3. Sediment output rate (tonnes/hour) during each time interval of the 3 July 2001 flood event.

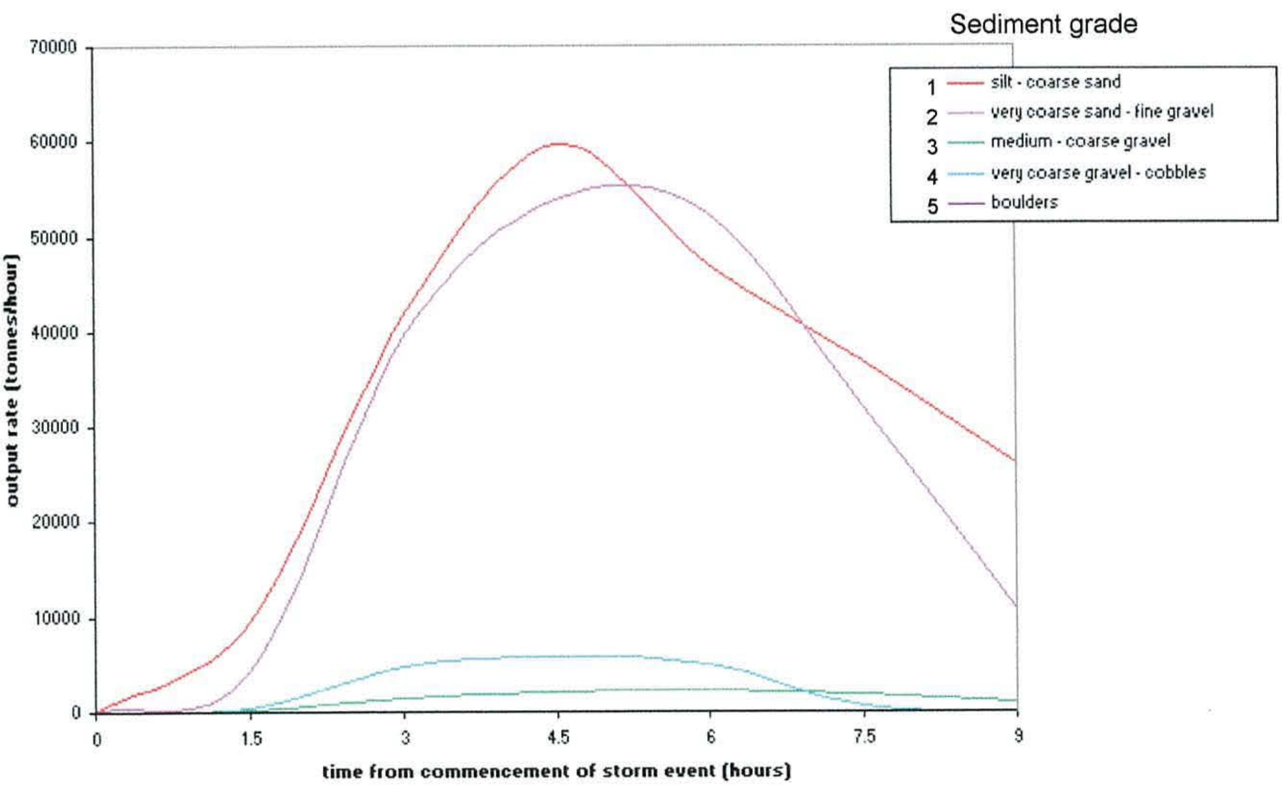

Figure 3.108: Sediment output rates for sediment size classes during each time interval of the 3 July 2001 flood event.

Flood event of 3-4 February 2004

Sediment modelling for the flood event of 3-4 February 2004 was carried out by the same methods described for the July 2001 model, with the exception that output was generated at intervals of 48 time steps of 15 minutes, i.e. each 12 hours, during the 2 day simulated period. Results for the Mawddach sub-catchments are shown in fig.3.110 and Appendix D Table 3, and results for the Wnion sub-catchments in fig.3.111 and Appendix D Table 4.

Sediment output to the estuary is shown in fig.3.109 and Table 3.4. A substantial silt and sand load is modelled for the whole period of the flood event. This is consistent with observations of high suspended sediment load for the Afon Mawddach as it discharged into the head of the estuary (fig.2.49).

	Sediment grade				
time (hours)	1	2	3	4	5
0	0	0	0	0	0
12	592	275	19	99	0
24	559	262	18	54	0
36	423	161	12	28	0
48	648	319	21	77	0
60	482	174	4	16	0

Table 3.4. Sediment output rate (tonnes/hour) during each time interval of the 3-4 February 2004 flood event.

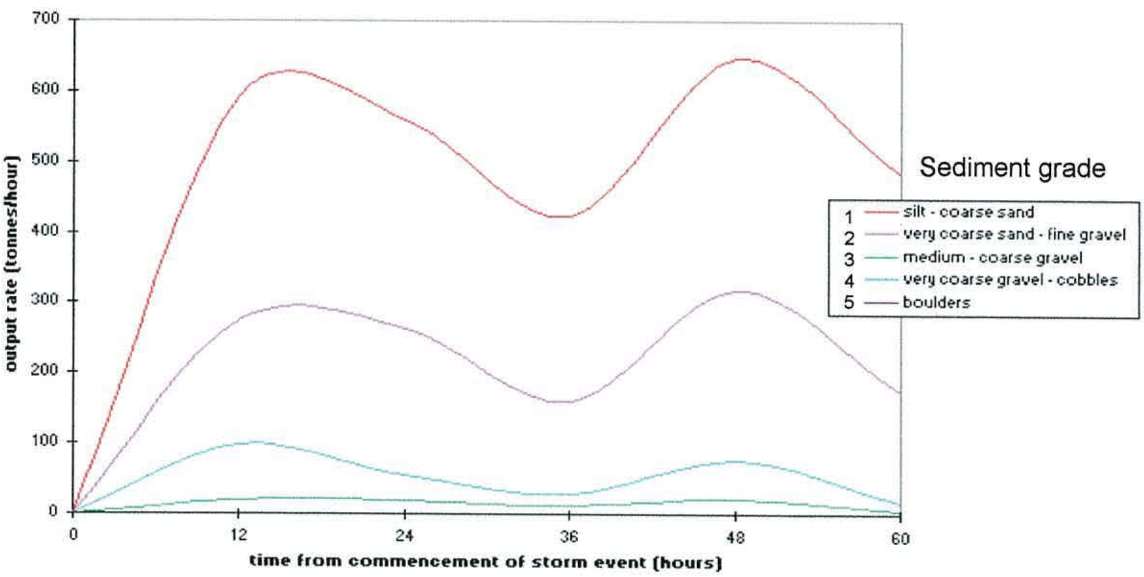

Figure 3.109: Sediment output rates for sediment size classes during each time interval of the 3-4 February 2004 flood event.

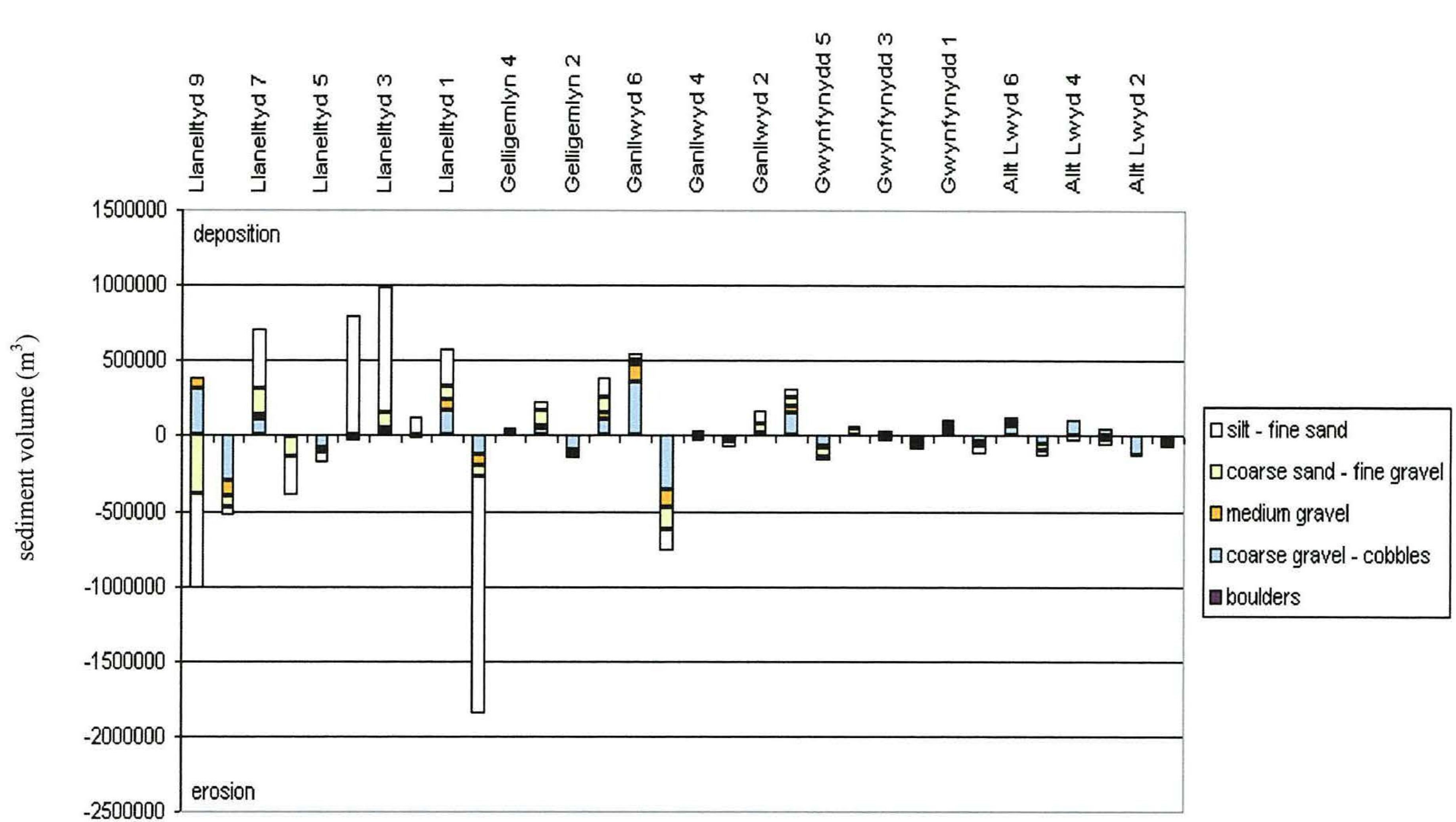

Figure 3.110: Sediment movement during the 3-4 February 2004 flood event: Mawddach sub-catchments

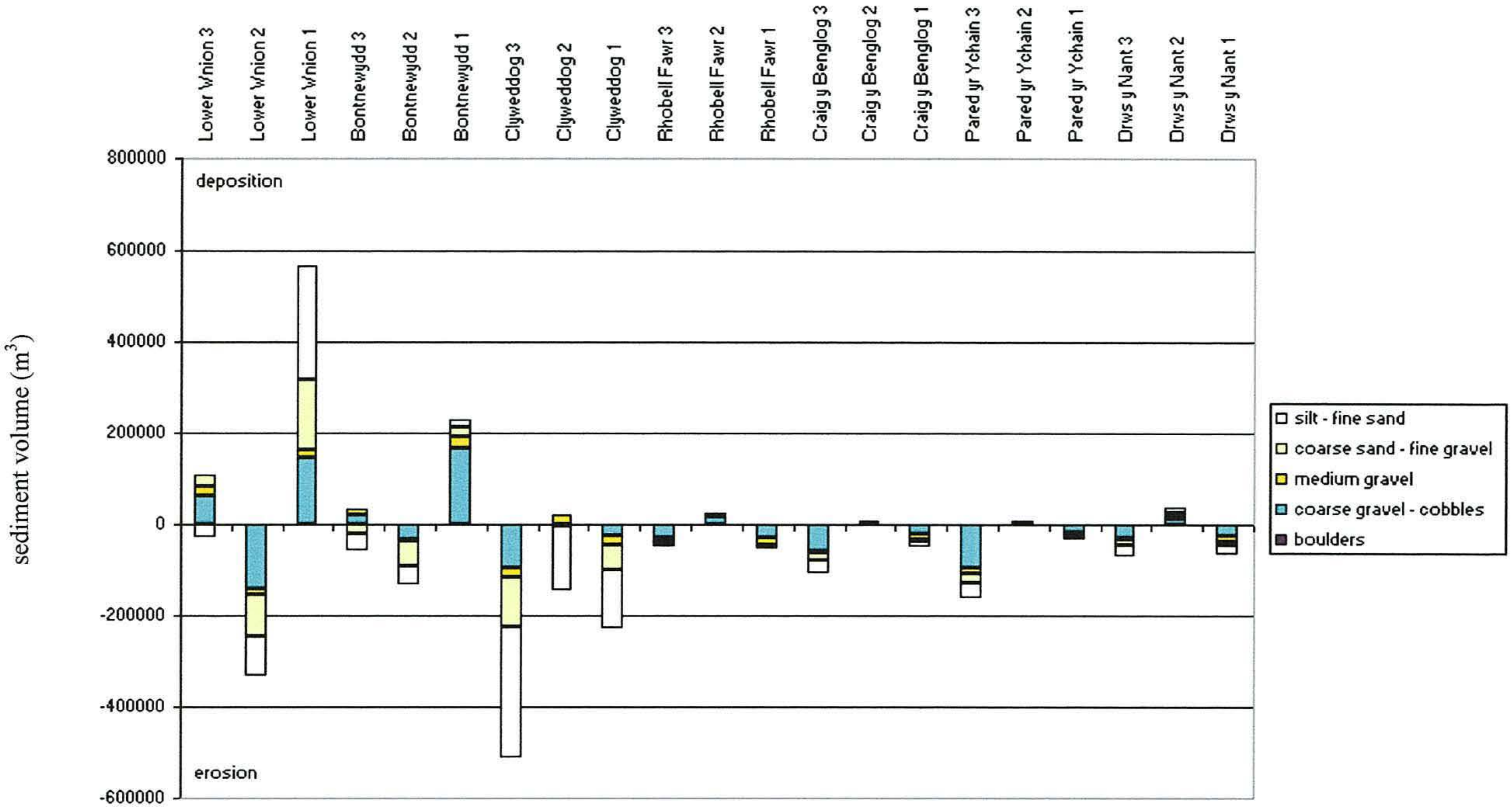

Figure 3.111: Sediment movement during the 3-4 February 2004 flood event: Wnion sub-catchments

Summary

- Modelling carried out by the GSTARS program for the July 2001 and February 2004 flood events provides results which appear consistent with field observations of erosion, sediment transport and deposition during these events. The program has been successful in predicting changes to channel cross- sections.
- Experience during the modelling activity has shown that accurate rainfall patterns and sub-catchment hydrographs are required for successful sediment modelling, with results particularly sensitive to the large localised variations which can occur within a mountain area.
- The peak rates of sediment discharge estimated by the GSTARS model for the July 2001 flood are approximately one hundred times greater then those for the February 2004 flood. This is consistent with field observations of exceptional river bank erosion to a height well above normal flood levels in the gorge section, and extensive deposition of fine sediment across agricultural land in the lower valley of the Mawddach.
- It must be taken into account that the February 2004 flood continued for approximately ten times the duration of the July 2001 flash flood, so the overall movement of sediment was considerable. Floods approaching the magnitude of the February 2004 event are an annual occurrence within the Mawddach catchment. Over a period of time, the volume of sediment redistributed by annual river processes may be equal to, or greater than, the volumes of sediment redistributed during rare extreme events.
- Estimates of coarse sediment deposition for the Lower Wnion and the head of the Mawddach estuary have been obtained for floods of different magnitude and duration, along with estimates of the volumes of coarse sediment transported downstream. This data will be used in Section 3.4: River and Floodplain Processes, to model flooding for the Lower Mawddach and Lower Wnion under different channel deposition scenarios.
- This preliminary evaluation of GSTARS has been qualitative. Further quantitative studies are needed, in which accurate field measurements of sediment erosion and deposition during flood events are compared to results generated by the sediment transport model.